frontiers | Research Topics

Traditional processing methods in ethnopharmacology: enhancing therapeutic effects and unveiling mechanisms of action

Edited by
Lingyun Zhong, José Carlos Tavares Carvalho and Bey Hing Goh

Published in
Frontiers in Pharmacology

ISSN 1664-8714
ISBN 978-2-8325-6099-0
DOI 10.3389/978-2-8325-6099-0

About Frontiers

Frontiers is more than just an open access publisher of scholarly articles: it is a pioneering approach to the world of academia, radically improving the way scholarly research is managed. The grand vision of Frontiers is a world where all people have an equal opportunity to seek, share and generate knowledge. Frontiers provides immediate and permanent online open access to all its publications, but this alone is not enough to realize our grand goals.

Frontiers journal series

The Frontiers journal series is a multi-tier and interdisciplinary set of open-access, online journals, promising a paradigm shift from the current review, selection and dissemination processes in academic publishing. All Frontiers journals are driven by researchers for researchers; therefore, they constitute a service to the scholarly community. At the same time, the *Frontiers journal series* operates on a revolutionary invention, the tiered publishing system, initially addressing specific communities of scholars, and gradually climbing up to broader public understanding, thus serving the interests of the lay society, too.

Dedication to quality

Each Frontiers article is a landmark of the highest quality, thanks to genuinely collaborative interactions between authors and review editors, who include some of the world's best academicians. Research must be certified by peers before entering a stream of knowledge that may eventually reach the public - and shape society; therefore, Frontiers only applies the most rigorous and unbiased reviews. Frontiers revolutionizes research publishing by freely delivering the most outstanding research, evaluated with no bias from both the academic and social point of view. By applying the most advanced information technologies, Frontiers is catapulting scholarly publishing into a new generation.

What are Frontiers Research Topics?

Frontiers Research Topics are very popular trademarks of the *Frontiers journals series*: they are collections of at least ten articles, all centered on a particular subject. With their unique mix of varied contributions from Original Research to Review Articles, Frontiers Research Topics unify the most influential researchers, the latest key findings and historical advances in a hot research area.

Find out more on how to host your own Frontiers Research Topic or contribute to one as an author by contacting the Frontiers editorial office: frontiersin.org/about/contact

Traditional processing methods in ethnopharmacology: enhancing therapeutic effects and unveiling mechanisms of action

Topic editors

Lingyun Zhong — Jiangxi University of Traditional Chinese Medicine, China
José Carlos Tavares Carvalho — Universidade Federal do Amapá, Brazil
Bey Hing Goh — Sunway University, Malaysia

Citation

Zhong, L., Carvalho, J. C. T., Goh, B. H., eds. (2025). *Traditional processing methods in ethnopharmacology: enhancing therapeutic effects and unveiling mechanisms of action*. Lausanne: Frontiers Media SA. doi: 10.3389/978-2-8325-6099-0

Table of contents

frontiers | Frontiers in Pharmacology

TYPE Original Research
PUBLISHED 04 March 2024
DOI 10.3389/fphar.2024.1367682

OPEN ACCESS

EDITED BY
Qianfeng Gong,
Jiangxi University of Traditional Chinese Medicine, China

REVIEWED BY
Zhipeng Qu,
University of Adelaide, Australia
Gang Fan,
Chengdu University of Traditional Chinese Medicine, China

*CORRESPONDENCE
Hong Du,
duhong@vip.163.com

RECEIVED 09 January 2024
ACCEPTED 19 February 2024
PUBLISHED 04 March 2024

CITATION
Song L, Mi S, Zhao Y, Liu Z, Wang J, Wang H, Li W, Wang J, Zu W and Du H (2024), Integrated virtual screening and *in vitro* studies for exploring the mechanism of triterpenoids in Chebulae Fructus alleviating mesaconitine-induced cardiotoxicity via TRPV1 channel. *Front. Pharmacol.* 15:1367682. doi: 10.3389/fphar.2024.1367682

Integrated virtual screening and *in vitro* studies for exploring the mechanism of triterpenoids in Chebulae Fructus alleviating mesaconitine-induced cardiotoxicity via TRPV1 channel

Liangliang Song, Shuo Mi, Ying Zhao, Ziqin Liu, Jing Wang, Hongyue Wang, Wenhui Li, Jiasheng Wang, Wenting Zu and Hong Du*

School of Chinese Materia Medica, Beijing University of Chinese Medicine, Beijing, China

Background: In traditional Mongolian or Tibetan medicine in China, Chebulae Fructus (CF) is widely used to process or combine with aconitums to decrease the severe toxicity of aconitums. Researches in this area have predominantly focused on tannins, with few research on other major CF components for cardiotoxicity mitigation. The present study aimed to clarify whether triterpenoids can attenuate the cardiotoxicity caused by mesaconitine (MA) and investigate the mechanism of cardiotoxicity attenuation.

Methods: Firstly, the pharmacophore model, molecular docking, and 3D-QSAR model were used to explore the mechanism of CF components in reducing the toxicity of MA mediated by the TRPV1 channel. Then three triterpenoids were selected to verify whether the triterpenoids had the effect of lowering the cardiotoxicity of MA using H9c2 cells combined with MTT, Hoechst 33258, and JC-1. Finally, Western blot, Fluo-3AM, and MTT assays combined with capsazepine were used to verify whether the triterpenoids reduced H9c2 cardiomyocyte toxicity induced by MA was related to the TRPV1 channel.

Results: Seven triterpenoids in CF have the potential to activate the TRPV1 channel. And they exhibited greater affinity for TRPV1 compared to other compounds and MA. However, their activity was relatively lower than that of MA. Cell experiments revealed that MA significantly reduced H9c2 cell viability, resulting in diminished mitochondrial membrane potential and nuclear pyknosis and damage. In contrast, the triterpenoids could improve the survival rate significantly and counteract the damage of MA to the cells. We found that MA, arjungenin (AR), and maslinic acid (MSA) except corosolic acid (CRA) upregulated

Abbreviation: AR, Arjungenin; CF, Chebulae Fructus; CRA, Corosolic acid; DDAs, Diesterditerpenoid alkaloids; DMEM, Dulbecco's modified eagle medium; DMSO, Dimethyl sulfoxide; EC50, Concentration for 50% of maximal effect; FBS, Fetal bovine serum; LD50, Median lethal dose; MA, Mesaconitine; MDAs, Monoester-diterpenoid alkaloids; MFI, Mean fluorescence indensity; MSA, Maslinic acid; MTT, 3-(4,5-Dimethylthiazol-2-yl)-2,5-diphenyltetrazolium bromide; NDAs, Non-esterified diterpene alkaloids; OD, Optical density; RMSD, Root-mean-square deviation; RTX, Resiniferatoxin; SD, Standard deviation; TRPV1, Transient receptor potential vanilloid type 1 channel; WB, Western blot.

the expression of TRPV1 protein. MA induced a significant influx of calcium, whereas all three triterpenoids alleviated this trend. Blocking the TRPV1 channel with capsazepine only increased the cell viability that had been simultaneously treated with MA, and AR, or MSA. However, there was no significant difference in the CRA groups treated with or without capsazepine.

Conclusion: The triterpenoids in CF can reduce the cardiotoxicity caused by MA. The MSA and AR function as TRPV1 agonists with comparatively reduced activity but a greater capacity to bind to TRPV1 receptors, thus antagonizing the excessive activation of TRPV1 by MA.

KEYWORDS

Chebulae Fructus triterpenoids, mesaconitine, TRPV1, cardiotoxicity, pharmacophore model, molecular docking, 3D-QSAR model

1 Introduction

According to traditional Mongolian medical theory, Chebulae Fructus (the fruits of *Terminalia chebula* Retz. or *Terminalia chebula* Retz, var. *Tomentella* Kurt., named Hezi in Chinese, CF) has a detoxifying function and may not only treat a variety of toxic diseases but also reconcile the drug properties and lessen the toxicity of poisonous medications (Nigam et al., 2020; Zhou et al., 2022; Ai et al., 2023). According to the records in the Tibetan medical classic "Jingzhu Materia Medica," CF has a therapeutic effect on various ailments and is the king of all remedies (Dimar, 1986). It can be inferred from the phenomenon that among the commonly used 200 prescriptions in the Ministry standards of Tibetan medicine, 125 prescriptions all contain the CF (Song et al., 2023). In the use habits of ethnic minorities, it is more commonly used together with the aconitum herbs, such as *Aconitum pendulum* Busch, *Aconiti kusnezoffii* radix. In order to reduce the toxicity or preservation effect, CF decoction processing aconitums or compatibility aconitums with CF are popular methods in clinical practice (Li et al., 2019; Li et al., 2021), and they are often used in the form of pills or powders, such as Naru Sanwei Wan (Guo et al., 2023). However, the mechanism behind the attenuation toxicity remains unclear and requires further exploration.

Diester diterpenoid alkaloids (DDAs), represented by mesaconitine ($C_{33}H_{45}NO_{11}$, CAS: 2752-64-9, MA), are the main toxic components of aconitums (Wei et al., 2019; Chen et al., 2023). The toxicity of MA is quite potent; the median lethal dose (LD_{50}) of oral administration, subcutaneous injection, intraperitoneal injection, and intravenous injection in mice is 1.9 mg/kg, 0.20 mg/kg ~ 0.38 mg/kg, 0.20 mg/kg ~ 0.30 mg/kg, 0.068 mg/kg ~ 0.13 mg/kg, respectively (Liu et al., 2016b; Yang et al., 2018; Chan et al., 2021). Cardiotoxicity is the main manifestation of aconitum herbs toxicity. It can lead to abnormal electrocardiogram changes, palpitations and arrhythmia, especially premature ventricular beats, which are the most common (Feng, 2019; Ye et al., 2021; Chen et al., 2023). For cells, it can lead to myocardial cell apoptosis, which is manifested in reducing the survival rate of rat H9c2 cardiomyocytes, causing cell nuclear condensation, damage and an increase in mitochondrial membrane potential (Li et al., 2020; Han et al., 2022c). There are multiple mechanisms of cardiotoxicity, including ion channels, protein expression, oxidative stress, energy metabolism damage, and so on (Sun et al., 2014; Zhou et al., 2021; Gao et al., 2022). Among them, ion channels are an important way to exert the efficacy and toxicity of diester alkaloids. When the function of ion channels is aberrant, the proportion of each channel in the myocardium will be destroyed, which will induce cardiac diseases such as arrhythmia (Fu et al., 2007; Yang et al., 2021).

The transient receptor potential vanilloid type 1 channel (TRPV1) is widely distributed in the heart (Peng and Li, 2010). It is a non-selective ion channel that dominates the influx of calcium ions. Activating the TRPV1 channel results in an influx of extracellular calcium and the release of intracellular calcium, causing an increase in intracellular calcium concentration (Sappington et al., 2009). Since calcium serves as the second messenger in many intracellular signaling pathways, TRPV1 can thus participate in various physiological processes of cells, including energy metabolism, cell proliferation, and apoptosis (Wu et al., 2015; Zhai et al., 2020). Researchers have discovered that TRPV1 channels are present in rat H9c2 cardiomyocytes and can be triggered in response to hypoxia/reoxygenation stimulation. The TRPV1 agonist capsaicin can dramatically worsen apoptosis, raise intracellular Ca^{2+} levels, increase mitochondrial superoxide release, and then lower mitochondrial membrane potential when mixed with it. However, the TRPV1 antagonist capsazepine can reverse this effect because it is a competitive small-molecule TRPV1 inhibitor and can block the activation of the TRPV1 channels by capsaicin or other agonists. Overactivation of TRPV1 channels in the heart induces apoptosis of cardiomyocytes, facilitating their death and contributing to ventricular tachycardia and fibrillation in individuals with myocardial infarction (Sun et al., 2014). This is a significant mechanism of cardiotoxicity and a notable pathway of cardiotoxicity as well. The TRPV1 channel is a significant pathway of cardiotoxicity induced by DDAs. The previous study found that the DDAs in aconitums caused intracellular calcium overload due to excessive activation of the TRPV1 channel in H9c2 cardiomyocytes. This led to damage to various organelles, resulting in a significant amount of apoptosis, which is one of the ways aconitum herbs produce cardiotoxicity (Han et al., 2022b; Han et al., 2022c).

CF is rich in tannins such as gallic acid and chebulic acid, as well as triterpenoids such as arjunolic acid, maslinic acid (MSA), corosolic acid (CRA), and chebulatriol. It also contains flavonoids, amino acids, and volatile compounds (Li et al., 2022). The components in CF might be involved in lowering toxicity, regardless of whether CF is compatibile with aconitum herbs or used

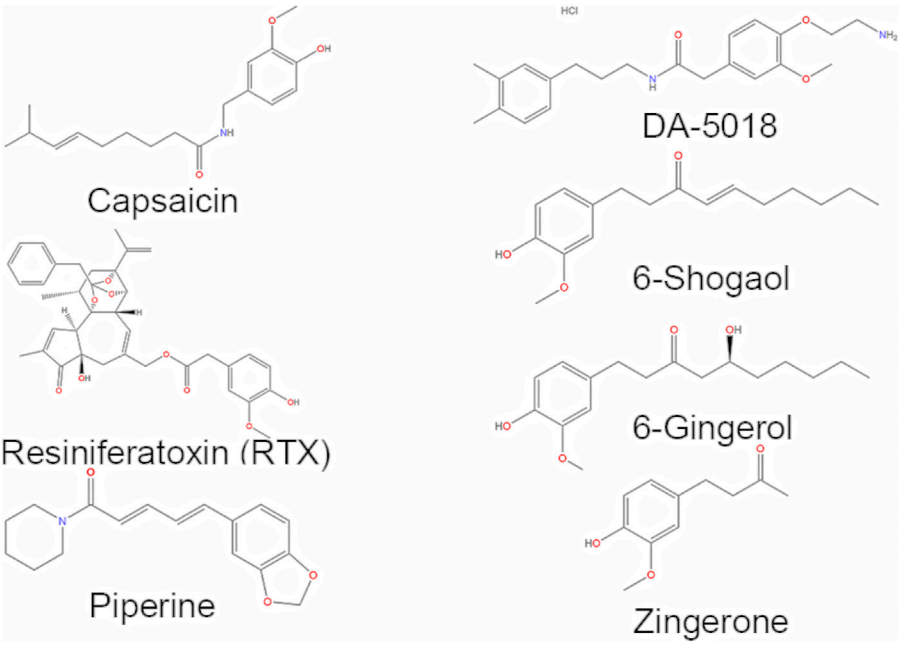

FIGURE 1
Structures of the TRPV1 agonists selected as the training set.

as an excipient to process aconitums (Liu et al., 2016a; Zhi et al., 2020a). Academics have conducted studies and found that the chemical constituents interactions between aconitums and the auxiliary substance CF can lower the cardiotoxicity of aconitums (Liu et al., 2013). Network pharmacology was employed to investigate how CF reduces the cardiac toxicity of aconitums. A total of 15 components in CF were screened, including seven tannins, five triterpenoids, and three alkaloids. They reduce cardiotoxicity by involving numerous protein functions, signaling pathways, and biological processes (Li et al., 2018). Our research group has verified that tannins and phenolic acids from CF can significantly reduce the mitochondrial membrane potential elevation and intracellular Ca^{2+} overload caused by aconitine and MA in rat H9c2 cardiomyocytes through the TRPV1 channel, thereby improving mitochondrial function and inhibiting the cardiotoxicity of aconitine (Han et al., 2020; Han et al., 2022b; Han et al., 2022c). When we were committed to the study of tannins, we accidentally found that triterpenoids in CF, while not as abundant as tannins, have a significant impact on antioxidant and cardioprotective properties. These effects were achieved through antioxidation, inhibition of intracellular calcium overload in cardiomyocytes, and prevention of oxidative stress damage in cardiomyocytes (Sumitra et al., 2001; Zou et al., 2017; Wang, 2019; An et al., 2020). Coincidentally, this aligns with the mechanism by which DDAs in aconitums exert cardiotoxicity. Furthermore, research has shown that the triterpenoids in CF have the potential to activate TRPV1, which may play a role in attenuating cardiotoxicity (Mi et al., 2023). Consequently, further research is vital to identify whether the triterpenoids present in CF possess the ability to alleviate the cardiotoxicity of MA and if the attenuation mechanism involves the TRPV1 channel.

In the present study, the pharmacophore model based on the common feature structure of ligands (TRPV1 agonists) was used to search for drug molecules that are identical or similar to the pharmacophore model screened in the database (Acharya et al., 2011; Qiao and Zhang, 2014). Then the binding ability of biological macromolecules and small molecules was evaluated according to the scoring function of molecular docking, and the molecules with reasonable binding modes and high prediction scores were selected (Yang, 2010). Subsequently, the 3D-QSAR model was used to investigate the structure-activity relationship and perform activity prediction afterward (Hansch et al., 1962), thereby screening out the components of CF that attenuate the cardiotoxicity of MA through the TRPV1 channel. The attenuation effect was then verified by cell experiments, and the chosen attenuation concentration was used to further verify whether the effect was related to the TRPV1 channel. This provided experimental support for the theoretical underpinnings and molecular mechanism of CF in reducing cardiotoxicity induced by aconitums.

2 Materials and methods

2.1 Virtual screening based on pharmacophore model

2.1.1 Preparation of ligands

The pharmacophore model is particularly useful when the receptor structure is unknown or the mechanism of action is unclear. Based on the common features of a series of small molecule ligands, the pharmacophore model is generated, and then the compound database is searched for active compounds. Pharmacophore model has become an important tool in drug

TABLE 1 Results of pharmacophore models construction.

No.	Features	Max fit	Rank value
01	HHAA	4	68.372
02	HHAA	4	67.154
03	HHAA	4	66.907
04	HHAA	4	66.849
05	HHAA	4	66.170
06	HHAA	4	66.168
07	HHAA	4	65.651
08	HHAA	4	65.077
09	HHAA	4	64.964
10	HHAA	4	64.007

The highest number of features is 4. H (hydrophobic features), A (Acceptor).
Max Fit represents the matching situation of the pharmacophore features.
Rank Value indicates the score of the pharmacophore, the higher the score, the better.

discovery, particularly for fast and effective screening of new bioactive molecules.

By searching the small molecule database PubChem (https://pubchem.ncbi.nlm.nih.gov/), TCMSP (http://tcmspw.com/tcmsp.php), TCMID (http://www.Megabionet.org/tcmid/) and relevant literature, we found 60 components in CF (Supplementary Table S1). And then, we searched for 10 TRPV1 agonists and 10 TRPV1 antagonists from the literature (Supplementary Table S2) and downloaded small molecule ligands (Gavva, 2008; Gunthorpe and Szallasi, 2008; Burgess and Williams, 2010; Li et al., 2011; Szolcsányi and Sándor, 2012; Sugimoto et al., 2013; Yin, 2019; Choi et al., 2020; Duarte et al., 2020; Mazeto et al., 2020; More et al., 2020; Nie, 2020). We also had to randomly download 90 compounds from the PubChem database that did not have well-defined TRPV1 agonist activity for later verification. All small molecular structures were reconstructed with energy minimization in the MMFF94 forcefield through Chem 3D (version 15.1.0) software. The obtained conformations were used for subsequent analysis.

2.1.2 Generation of pharmacophore model

Firstly, seven representative components were selected from the downloaded components with TRPV1 agonists to form a training set (Figure 1), including piperine, capsaicin, 6-gingerol, 6-shogaol, zingerone, resiniferatoxin (RTX), and DA-5018. And then the HipHop approach of the Common Feature Pharmacophore Generation module in Discovery Studio (version 4.0) was used to automatically generate the pharmacophore models based on the common structural features of the small molecules in the training set. The Principal value of the active compounds was set to 2, indicating that the small molecules are active, and the MaxOmitFeat value was set to 1, indicating that the number of characteristic elements in each molecule that allow not match to the pharmacophore model is 1. Then the Hydrophobe, Donor, Acceptor, Ionizable Positive and Ring Aromatic were selected as the characteristic elements of pharmacophore in the HipHop module. The best mode was adopted for superposition, and the Maximum Conformation was set to 255. Only the model whose energy difference with the lowest conformation was less than 20 kcal/mol was saved. Eventually, we would get the 10 pharmacophore models with the higher score.

2.1.3 Pharmacophore model validation

Using the Ligand Profiler module in Discovery Studio, the 10 generated pharmacophores were evaluated. The molecules in the test set consisted of 10 TRPV1 agonists (Supplementary Table S2) and 90 components with no reported TRPV1 agonist activity. According to the Rank value and the matching degree of the test set molecules, one pharmacophore was selected for subsequent screening, and the final selected pharmacophore was characterized by a high score, a high matching degree with the active ingredient, and a low matching degree with the inactive ingredient.

2.1.4 Virtual screening

The Search 3D Database module in Discovery Studio was used to screen components with potentially activated TRPV1 channel activity based on the generated pharmacophore model.

2.2 Virtual screening based on molecular docking

2.2.1 Preparations for molecular docking

Molecular docking is a method used to study the interaction between small molecules and target proteins. It can efficiently and accurately predict drug activity and selectivity, thus avoiding blind screening and reducing the cost of screening active compounds.

In the molecular docking experiment, the structure of MA also needed to be downloaded from PubChem (https://pubchem.ncbi.nlm.nih.gov/). We still use the small molecule ligands in Supplementary Table S1. Then we handled them with energy minimization and picked root and rotatable keys via Autodock Vina software (version 1.5.6), which was also used for the subsequent molecular docking calculations.

The two TRPV1 protein receptors that we selected for molecular docking were downloaded from the Protein Data Bank (PDB) database (http://www.ncbi.nlm.nih.gow/protein/). They are respectively the structure of TRPV1 in complex with DkTx and RTX (PDB ID code: 5IRX; Resolution: 2.95Å), and the structure of TRPV1 in complex with capsazepine (PDB ID code: 5IS0; Resolution: 3.43Å) (Gao et al., 2016).

To conduct virtual screening, firstly the active binding sites of molecular targets were determined by Discovery Studio. RTX is a TRPV1 agonist that interacts with residues: ARG557, LEU553, ALA566, ASN551, THR550, ILE569, MET547, ALA546, PHE591, LEU669, ALA665, TYR511, PHE543, LEU515, PHE507, ILE514, VAL518 of 5IRX (Supplementary Figures S1A, B). Capsazepine is a TRPV1 antagonist which interacts with residues: GLU570, LEU553, TYR554, TYR511, SER512, THR550, MET547, ALA665, PHE543, LEU662 of 5IS0 (Supplementary Figures S1C, D). The comparison shows that the TRPV1 agonist and the TRPV1 antagonist act on the same region of the TRPV1 protein, while the residues that act are not the same.

We needed to pretreat the protein receptors, including dehydration, hydrogenation, *etc.* The active sites of proteins also needs to be determined. What we obtained from the PDB database were the protein-ligand complexes. By analyzing the spatial position

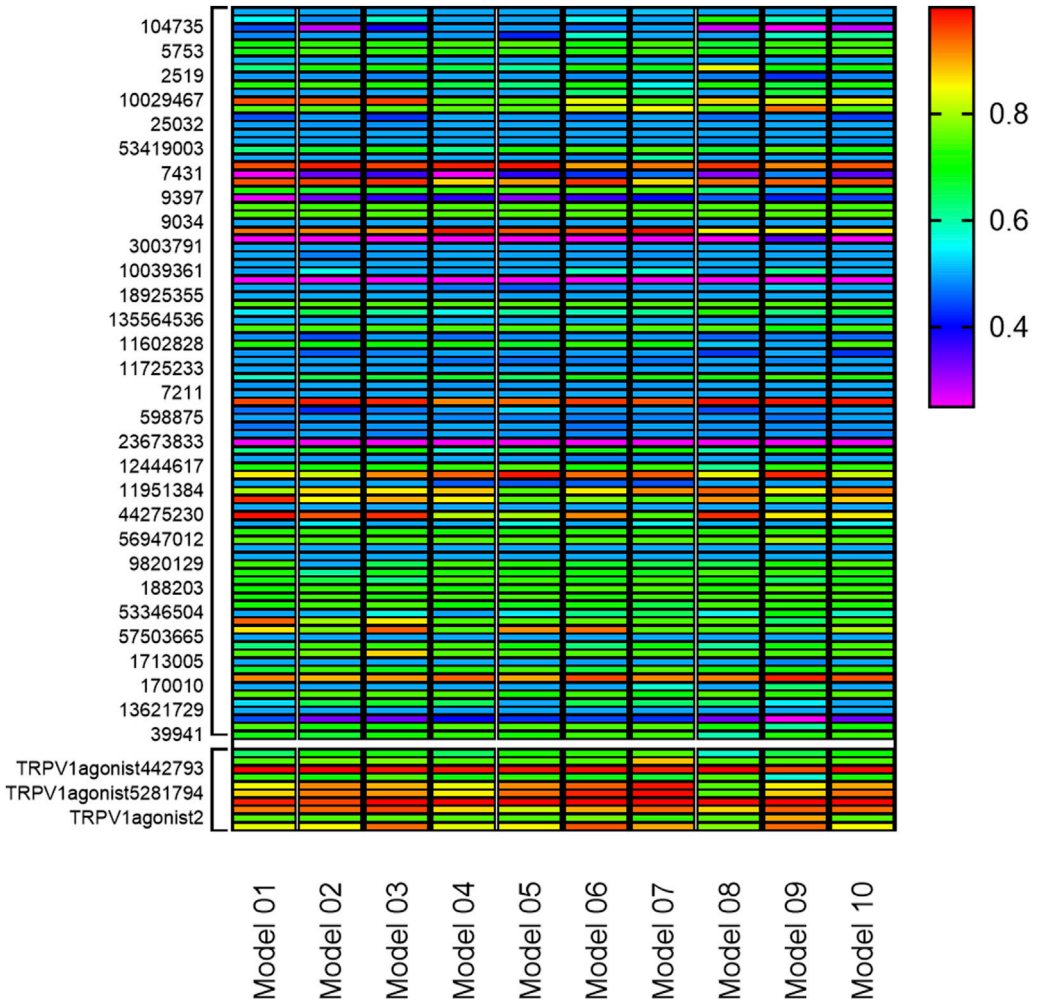

FIGURE 2
Validation of 10 pharmacophore models. (The bottom 10 color blocks in each column correspond to the TRPV1 agonists, and the rest 90 correspond to the components that have not been verified for activity. The ligands that depict higher responses to the pharmacophore models have a warm tone while those with lower responses have a cold tone.)

relationship between the receptor and the original ligand at the docking site, the information of the docking site can be obtained (Feinstein and Brylinski, 2015). The coordinates of RTX in 5IRX were (X = 93.69, Y = 114.04, Z = 129.88), and generated a square docking box with a side length of 21.275 centered on this site. The coordinates of capsazepine in 5IS0 were (X = 108.115, Y = 94.986, Z = 102.379), and generated a square docking box with a side length of 21.141 centered on this site. In addition, we researched the necessary literature to corroborate the location (Li and Yang, 2018).

2.2.2 Molecular docking

Molecular docking was carried out on Autodock Vina. During the procedure, the semi-flexible docking method was used, that is, the protein receptor was rigid and the partial bond of the small molecules ligand could rotate. The TRPV1 agonists were placed into the indicated cave of the 5IRX receptor, and the TRPV1 antagonists were placed in the specified box in the 5IRX receptor. And then the components of CF (Supplementary Table S1) and the MA were docked to the two receptors severally and evaluated their binding ability.

2.3 Virtual screening based on 3D-QSAR model

2.3.1 Construction of 3D-QSAR model

The 3D-QSAR model is a pharmacophore model with activity prediction ability based on a series of compounds with clear activity values for specific biological targets. The model was used to predict the related activities of new compounds that were not experimentally determined or even not synthesized. It is highly efficient, especially in the screening of compounds in large databases has an irreplaceable advantage.

Twelve TRPV1 agonists with the same EC_{50} data source were selected from the BindingDB database (https://www.bindingdb.org/). The corresponding small molecule ligands were downloaded from the PubChem database (https://pubchem.ncbi.nlm.nih.gov/) and the pEC_{50} data were added to the small molecule ligands (Supplementary Table S3). Chem 3D software was used to minimize the MMFF94 force field energy of all small molecule ligands. The first seven small molecules in the table were selected to

TABLE 2 Compounds of the CF selected by pharmacophore model 02 with potential activation of TRPV1.

NO.	Compound	Fit value
1	Catharanthamine	2.76795
2	Corosolic acid	2.28106
3	Chebupentol	1.86848
4	Arjungenin	1.79283
5	Arjunolic acid	1.78225
6	Maslinic acid	1.50544
7	Terminolic acid	1.46320
8	Chebuloside-II	1.29666

Fit Value indicates the matching status of the components to the pharmacophore, the larger the value, the better the matching degree.

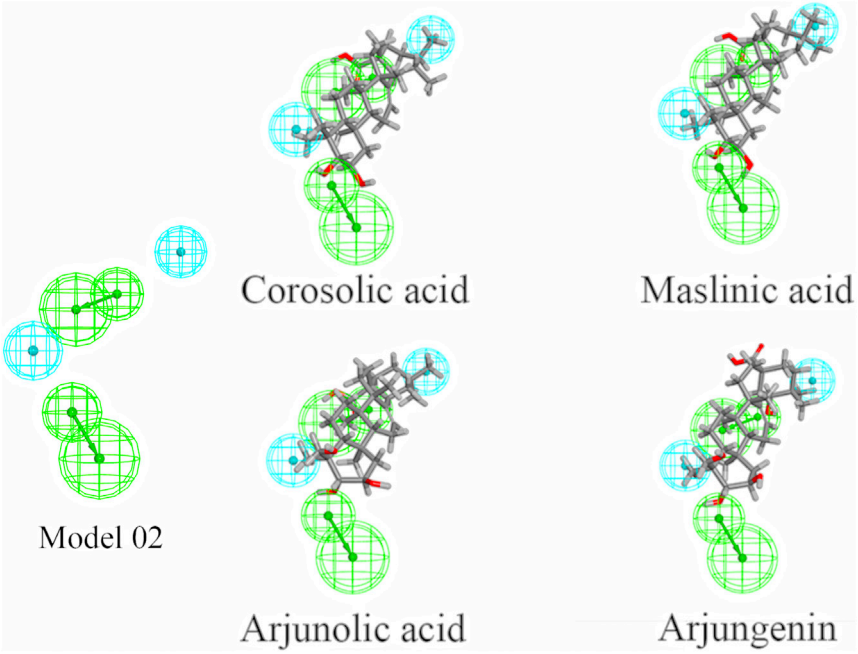

FIGURE 3
Pharmacophore model 02 and mapping with the selected triterpenoids. (The green spheres represent hydrophobic features, while blue spheres represent hydrogen bond acceptor features.)

form the training set, while all 12 TRPV1 agonists in Supplementary Table S3 will be used as the test set.

Using the Create 3D QSAR Model module in Discovery Studio, a 3D-QSAR model with activity prediction ability was constructed based on the common structural features and pEC_{50} values of small molecules selected in the training set, and the constructed model was verified by the test set. Representative components and a 3D-QSAR model were selected to generate visual contour maps of the electrostatic field coefficient and stereo field coefficient.

2.3.2 Prediction of activity based on 3D-QSAR model

The Calculate Molecular Properties module in Discovery Studio was used to predict the activity of prepared triterpenoids and MA using the already constructed 3D-QSAR model, and output the results.

2.4 Verification of triterpenoids alleviating the H9c2 cardiomyocyte toxicity caused by MA

2.4.1 Preparations of materials and cell culture

Rat cardiomyocyte H9c2 cells were purchased from the Cell Resource Center, IBMS, CAMS/PUMC (CRC/PUMC, Beijing, China). The H9c2 cells were cultured in high-glucose dulbecco's modified eagle medium (DMEM) medium (VivaCell Biosciences, China) supplemented with 10% fetal bovine serum (FBS) (VivaCell

TABLE 3 Docking scores of TRPV1 agonists and TRPV1 antagonists with 5IRX and 5IS0 respectively (Kcal/mol).

NO.	TRPV1 agonist	Scores (5IRX)	NO.	TRPV1 antagonist	Scores (5IS0)
1	Resiniferatoxin (RTX)	−9.8	1	MK-2295	−9.9
2	Compound 3	−7.9	2	AMG-517	−9.6
3	DA-5018	−6.1	3	SB-705498	−9.5
4	Compound 2	−8.4	4	K-685	−9.2
5	piperine	−8.3	5	ABT-102	−9.2
6	Compound 1	−8.1	6	Capsazepine	−9.1
7	capsaicin	−7.0	7	BCTC	−8.8
8	6-Gingerol	−7.0	8	PAC-14028	−8.4
9	zingerone	−6.5	9	SB-366791	−8.2
10	6-shogaol	−7.0	10	SC-0030	−7.4

The smaller binding affinity indicates a higher affinity for the TRPV1 receptor.

TABLE 4 Docking scores of mesaconitine and the selected triterpenoids by the pharmacophore with 5IRX and 5IS0 (Kcal/mol).

NO.	Compound	Scores (5IRX)	Scores (5IS0)
1	Corosolic acid	−8.5	−7.4
2	Chebuloside-II	−8.4	−7.1
3	Terminolic acid	−8.1	−7.1
4	Maslinic acid	−8.0	−7.3
5	Arjungenin	−7.7	−7.0
6	chebupentol	−7.5	−6.4
7	Arjunolic acid	−7.4	−7.0
8	Mesaconitine	−7.4	−6.5

Biosciences, China) and 1% penicillin-streptomycin (Lablead, China), and then incubated at 37°C with 5% CO_2.

Corosolic acid (CRA, >98%, DSTDX000501) Maslinic acid (MSA, >98%, DST220526-039) Arjungenin (AR, >98%, DST210106-442) Mesaconitine (MA, >98%, DSTDX002501) were purchased from DeSiTe (Chengdu, China). Capsazepine (>98%, D15O9F2190) was obtained from Yuanye Biochemical (Shanghai, China). All test samples were accurately weighed, and dissolved by dimethyl sulfoxide (DMSO) (Sigama-Aldrich, United States) to obtain concentrated solutions, and then preserved at 4°C. They were diluted to the corresponding concentration with medium prior to use and allowed the DMSO concentration less than 0.5%.

2.4.2 Cell viability of triterpenoids on H9c2 cardiomyocyte

Cell viability was assessed using the 3-(4,5-Dimethylthiazol-2-yl)-2,5-diphenyltetrazolium bromide (MTT) (Lablead, Beijing, China) assay. Initially, the MTT assay was utilized to identify a safe and non-toxic concentration range of triterpenoids to prevent the interference of triterpenoids with the survival rate of H9c2 cells and the subsequent experimental results. H9c2 cells were cultured with a medium containing various concentrations of triterpenoids for 24 h. The following grouping and dosages were used: 1) control group: H9c2 cells were cultured without any treatment; 2) CRA group: H9c2 cells were treated with different concentrations of CRA (8, 16, 32, 64, 128 μmol/L); 3) MSA group: H9c2 cells were treated with different concentrations of MSA (8, 16, 32, 64, 128 μmol/L); 4) AR group: H9c2 cells were treated with different concentrations of AR (8, 16, 32, 64, 128 μmol/L).

Upon incubation for 24 h, MTT (0.5 mg/mL) was added to each well, followed by a 4-h incubation period inside a light-protected incubator. Subsequently, DMSO was added and the optical density (OD) was measured at 490 nm wavelength. The cell survival was calculated using the relevant Formula 1.

$$\text{Cell survival}\ (\%) = (\text{experiment hole OD} / \text{blank hole OD}) \times 100\% \quad (1)$$

2.4.3 Cell viability of triterpenoids on MA-induced H9c2 cardiomyocyte

We conducted the MTT assay to evaluate the ability of triterpenoids from CF to attenuate cardiac toxicity induced by MA. The best-attenuated concentration was identified and used in subsequent experiments. The MTT assay was performed as described in Section 2.4.2. They were distributed into four groups as follows: 1) control group: H9c2 cells were cultured for 24 h without any treatment; 2) MA group: H9c2 cells were treated with 300 μmol/L of MA for 24 h; 3) MA+CRA group: H9c2 cells were treated with 300 μmol/L of MA and different concentrations of CRA (2, 4, 8, 16, 32 μmol/L) for 24 h; 4) MA+MSA group: H9c2 cells were treated with 300 μmol/L of MA and different concentrations of MSA (2, 4, 8, 16, 32, 64 μmol/L) for 24 h; 5) MA+AR group: H9c2 cells were treated with 300 μmol/L of MA and different concentrations of AR (2, 4, 8, 16, 32, 64, 128 μmol/L) for 24 h.

2.4.4 Nucleus morphology of triterpenoids on MA-induced H9c2 cardiomyocyte

Cell apoptosis was analyzed using Hoechst 33258 staining (Lablead, Beijing, China). H9c2 cells were treated with a medium containing MA or different concentrations of triterpenoids for 24 h.

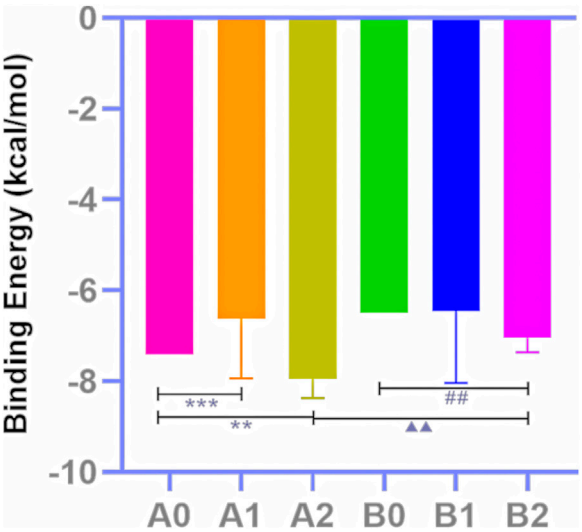

FIGURE 4
Docking score analysis. Molecular docking results of MA (A0), CF all components (A1), triterpenoids selected by the pharmacophore model 02 (A2) with 5IRX; molecular docking results of MA (B0), CF all components (B1), triterpenoids selected by the pharmacophore model 02 (B2) with 5IS0 (Compare A2 to A0, $^{**}p < 0.01$; compare A2 to A1, $^{\#\#}p < 0.01$; compare B2 to A2, $^{\triangle\triangle\triangle}p < 0.001$).

The grouping and dosages were as follows: 1) Control group: H9c2 cells were cultured without any treatment; 2) MA group: H9c2 cells were treated with 300 μmol/L of MA; 3) MA+CRA group: H9c2 cells were treated with 300 μmol/L of MA and different concentrations of CRA (28, 32, 36 μmol/L); 4) MA+MSA group: H9c2 cells were treated with 300 μmol/L of MA and different concentrations of MSA (12, 16, 20 μmol/L); 5) MA+AR group: H9c2 cells were treated with 300 μmol/L of MA and different concentrations of AR (60, 64, 68 μmol/L).

Following the treatment, the cells were stained with the Hoechst 33258 for 20 min in the absence of light. After then observed under a fluorescence microscope.

2.4.5 Mitochondrial membrane potential of triterpenoids on MA-induced H9c2 cardiomyocyte

We assessed changes in mitochondrial membrane potential in H9c2 cells by using JC-1 dye staining (Solarbio, Beijing, China) to confirm the mechanism by which triterpenoids from CF can reduce cardiac damage induced by mesaconitine. H9c2 cells were treated with a medium containing MA or triterpenoids for 24 h. The grouping and dosages were as follows: 1) control group: H9c2 cells were cultured without any treatment; 2) MA group: H9c2 cells were treated with 300 μmol/L of MA; 3) MA+CRA group: H9c2 cells were treated with 300 μmol/L of MA and 32 μmol/L of CRA; 4) MA+MSA group: H9c2 cells were treated with 300 μmol/L of MA and 20 μmol/L of MSA; 5) MA+AR group: H9c2 cells were treated with 300 μmol/L of MA and 64 μmol/L of AR.

Subsequently, the H9c2 cells were treated with JC-1 staining solution. And then incubated for 20 min in a 5% CO_2 incubator at 37°C. Apoptotic cells were directly visualized with inverted fluorescence microscopy.

2.5 Verification of triterpenoids reducing H9c2 cardiomyocyte toxicity induced by MA based on TRPV1 channel

2.5.1 TRPV1 expression in the triterpenoids or MA-treated H9c2 cardiomyocyte

The Western blot assay was performed to validate the results of the previous pharmacophore screening and molecular docking, which screened the triterpenoids with activation activity on the TRPV1 channel. This laid the groundwork for the subsequent confirmation of whether the effect of triterpenoids alleviating cardiotoxicity caused by MA was related to TRPV1.

H9c2 cells were treated with a medium containing MA or triterpenoids for 24 h. The grouping and dosages were as follows: 1) control group: H9c2 cells were cultured without any treatment; 2) MA group: H9c2 cells were treated with 300 μmol/L of MA; 3) CRA group: H9c2 cells were treated with 32 μmol/L of CRA; 4) MSA group: H9c2 cells were treated with 20 μmol/L of MSA; 5) AR group: H9c2 cells were treated with 64 μmol/L of AR.

Following treatment, the H9c2 cells were lysed with the total cell protein extraction reagent and then centrifuged at 13,000 g for 5 min at 4°C. The resulting supernatant collected was the total protein solution. The levels of proteins in the supernatant were determined using a BCA kit (Baiqiandu, Wuhan, China). Afterward, the total protein was separated by SDS-polyacrylamide gel electrophoresis (SDS-PAGE, Baiqiandu, Wuhan, China) and transferred onto polyvinylidene difluoride membranes (PVDF, Millipore, United States). The membranes were treated with the various primary antibodies (GAPDH, 1:6,000; TRPV1, 1:1,000) overnight after being blocked with 5% non-fat dry milk at 37°C for 2 h. After washing the membrane with TBST (Baiqiandu, Wuhan, China), the membranes were incubated with secondary antibodies for 30 min at room temperature. Finally, an ECL chemiluminescent (Baiqiandu, Wuhan, China) working buffer was treated with the protein bands. After that, the bands' quantitative grayscale analysis was done using the IPWIN60 program.

2.5.2 Intracellular calcium ions content of triterpenoids on MA-induced H9c2 cardiomyocyte

The TRPV1 channel is a calcium ion channel, and it plays a crucial role in the flow of calcium ions into cells. The effect of this channel on calcium ions in cardiomyocytes was detected by Fluo-3 AM fluorescent probe method. The H9c2 cells were treated with a medium containing MA or various doses of triterpenoids for 24 h. Groups allocation and dose were the same as in Section 2.4.5. Following the treatment, the Fluo-3 AM (Solarbio, Beijing, China) (5 μmol/L) was used to stain the cells. The cells were then rinsed with HBBS after being incubated for 60 min at 5% CO_2 at 37°C, and the fluorescent intensity was assessed using a fluorescence microscope.

2.5.3 Cell viability of triterpenoids on MA-induced H9c2 cardiomyocyte after TRPV1 channel blocked by the capsazepine

To further explore whether the attenuated effect is related to the TRPV1 channel, we observed the effect of triterpenoids on the survival rate of H9c2 cells treated with MA before and after the TRPV1 channel blockade by MTT assay. H9c2 cells were treated with a medium containing MA or triterpenoids for 24 h. The grouping and dosages were as follows: 1) control group:

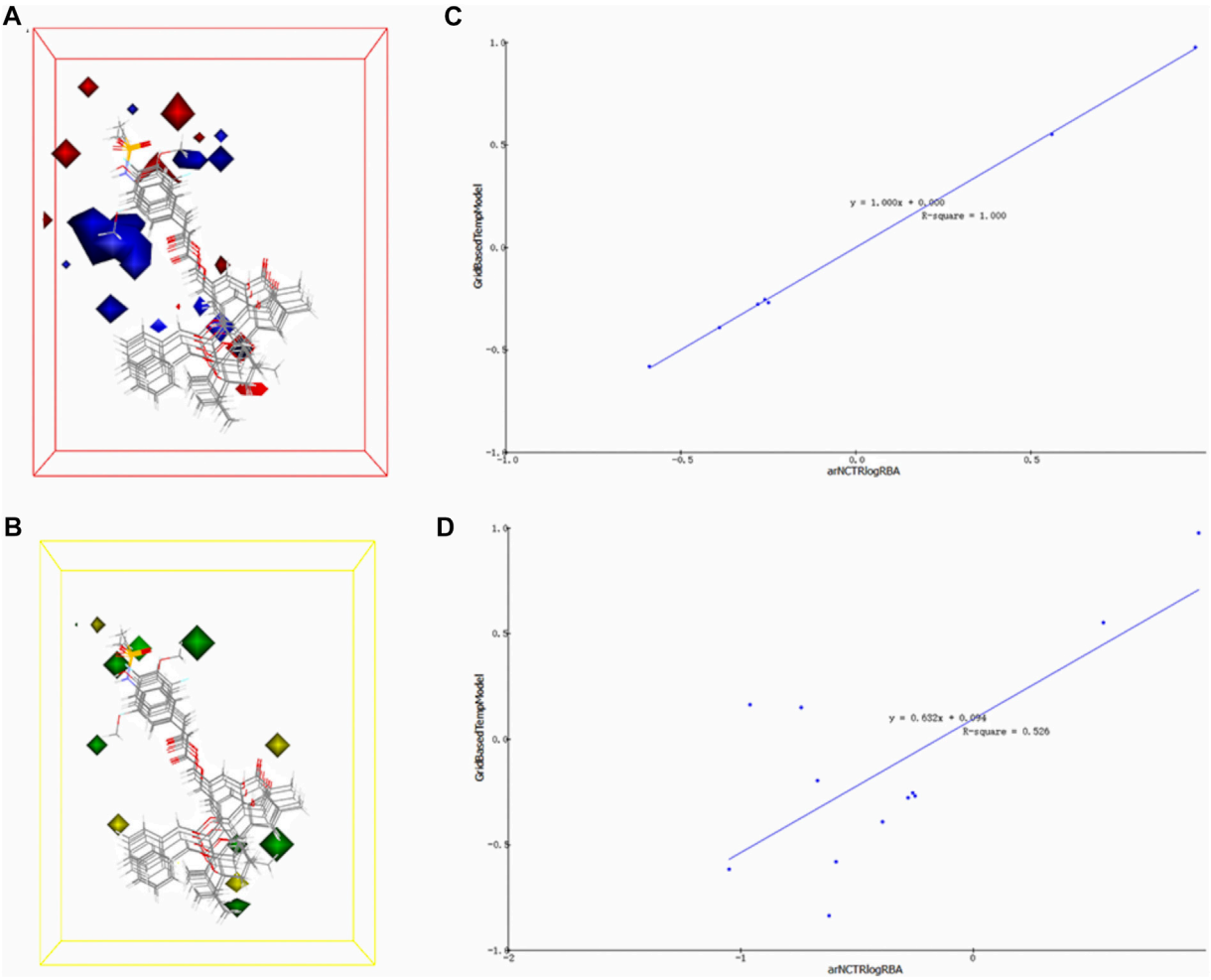

FIGURE 5
3D-QSAR model electrostatic and stereo field coefficient contour maps. **(A)** the high map of electrostatic field coefficient. **(B)** the high map of stereo field coefficient. **(C)** The fitting diagram of the prediction value of the 3D-QSAR model and the experimental value based on the training set. **(D)** The fitting diagram of the prediction value of the 3D-QSAR model and the experimental value based on the test set.

H9c2 cells were cultured without any treatment; 2) MA group: H9c2 cells were treated with 300 μmol/L of MA; 3) triterpenoid + MA group: H9c2 cells were treated with 300 μmol/L of MA and one of the triterpenoids (32 μmol/L of CRA; 20 μmol/L of MSA; 64 μmol/L of AR); 4) Capsazepine + triterpenoid + MA group: H9c2 cells were pretreated with capsazepine (10 μmol/L) for 30 min before 300 μmol/L of MA and one of the triterpenoids (32 μmol/L of CRA; 20 μmol/L of MSA; 64 μmol/L of AR).

2.6 Statistical analysis

All of the above cell experiments were independently repeated three times. The GraphPad Prism (version 8.0.1) was utilized to create all statistical calculations and graphs. Two-tailed Student's t-test was implemented to compare the two groups. ANOVA was used to compare three or more groups against one another. The mean and standard deviation (SD) were employed to express the results. When $p < 0.05$, the differences were deemed statistically significant.

3 Results

3.1 Pharmacophore model screening

3.1.1 Pharmacophore model establishment and validation

Based on the commonly shared features amongst seven agonists of TRPV1 selected from the training set, ten pharmacophoric models were constructed and their pharmacophoric characteristics along with Rank values were reported in Table 1. All the pharmacophores contained four features, namely, A: ACCEPTOR (Hydrogen bond acceptor) and H: HYDROPHOBIC had two each. The Rank values of these ten pharmacophoric models were greater than 60, signifying the prominence of the molecular common features while constructing the pharmacophores. Additionally, the differences among the top scores were extremely small. Hence, it was imperative to validate and screen the generated 10 pharmacophore models using a test set (Figure 2). The ligands that depict higher responses to the pharmacophore models have a warm tone and those with lower responses have a cold

TABLE 5 The prediction results of mesaconine and triterpenoids as TRPV1 agonist activity.

NO.	Compound	pEC_{50}
1	chebupentol	−0.356389
2	Mesaconitine	−0.446712
3	Terminolic acid	−0.503938
4	Arjunolic acid	−0.519541
5	Chebuloside-II	−0.528765
6	Arjungenin	−0.580258
7	Corosolic acid	−0.587511
8	Maslinic acid	−0.618522

tone. As seen, pharmacophore model 02 portrayed high responses against the active ingredients present in the test set and relatively lower responses to the inactive ingredients, thereby meeting the study requirements. Hence, pharmacophore model 02 was selected for virtual screening.

3.1.2 Virtual screening based on pharmacophore model 02

The 60 components in CF were virtually screened using the pharmacophore model 02 selected in Section 3.1.1, and eight components were finally selected (Table 2), comprising seven triterpenoids and one alkaloid. Furthermore, the matching diagram of the pharmacophore and some potential active components were shown in Figure 3. An observation from the figure depicted that the triterpenoids exhibited similar structural features as that of the pharmacophore model.

3.2 Molecular docking analysis

3.2.1 Molecular docking validation

When assessing the stability of the molecular docking model, re-docking the co-crystallized ligand into the empty binding pocket of the protein was employed. The calculated pose was then compared to the bioactive conformation from the crystal structure and the root mean square distance (RMSD) was calculated. Typically, RMSD values below 2 Å are considered acceptable (Temml and Kutil, 2021). Upon re-docking, the structural and spatial positions were fairly consistent with the native ligand. The RMSD (5IRX) = 1.2826 Å < 2 Å, RSMD (5IS0) = 1.7092 Å < 2 Å. Lower Score indicates higher affinity towards the TRPV1 receptor and greater propensity for interaction. The outcome (Table 3) exhibits that most of the other small molecule ligands displays high affinity and are in close proximity to the aforementioned ligands. This affirmed the high reliability of the molecular docking method utilized in this study. Meanwhile, The docking data also provides reference values for the subsequent molecular docking simultaneously.

3.2.2 Virtual screening based on molecular docking

The docking outcomes of CF components with TRPV1 receptors were presented in Supplementary Table S4. All of them and MA docking results were scrutinized and subsequently compared (Table 4; Figure 4). The results indicates that pharmacophore-selected triterpenoids exhibits higher affinity towards TRPV1 receptor 5IRX than MA ($^{**}p < 0.01$) as well as other CF components ($^{\#\#}p < 0.01$). Furthermore, these constituents demonstrates a higher affinity for the 5IRX receptor than the 5IS0 receptor ($^{\Delta\Delta\Delta}p < 0.001$).

3.3 Activity prediction of triterpenoids and MA based on 3D-QSAR model

3.3.1 3D-QSAR model construction and validation

The 3D-QSAR model is a pharmacophore model with activity prediction ability based on a series of compounds with clear activity values for specific biological targets. The model constructed in this section was based on the electrostatic field and steric field characteristics of TRPV1 agonists, which can be used to predict the activity of unknown compounds, thus providing a basis for subsequent experimental verification and mechanism exploration (Figures 5A, B). In the electrostatic map, the red area indicates that high negative charges enhance the compound's activity, while the blue area suggests high positive charges improve the compound activity. In the stereo field map, the yellow region denotes that expanding this area's volume does not enhance the compound activity, while the green area indicates that increasing the region's volume improves the compound activity.

The training set's predicted activity values were compared to experimental activity values (Figure 5C), with the R^2 value reflecting the accuracy of the curve. The curve's R^2 value of 1, indicating accurate prediction and closely matching experimental values.

To verify the accuracy of the 3D-QSAR model, the fitted curve based on the prediction and experimental values of the test set was created (Figure 5D). The R^2 value of 0.526 indicates that the model has some confidence, with the predicted values reflecting the experimental values to a reasonable extent. The model has the potential to predict the activity order of triterpenoids and MA's potential as a TRPV1 agonist.

3.3.2 Results of activity prediction based on the 3D-QSAR model

The developed 3D-QSAR model was utilized for predicting the activity of triterpenoids and MA, as shown in Table 5. All of the eight components in the table exhibited activity, among which MA had the strongest predicted activity with a predicted pEC_{50} of −0.446712. The triterpenoids exhibited relatively weak activity, with CRA, MSA, and AR exhibiting the weakest activity among them.

3.4 Verification of triterpenoids alleviating the H9c2 cardiomyocyte toxicity caused by MA

3.4.1 Effect of triterpenoids on H9c2 cell viability

The structures of the three triterpenoids were shown in Figure 6A. As shown in Figures 6B–D, the cell survival rate decreased when the CRA was in the range of 64 μmol/L to 128 μmol/L and MSA at 128 μmol/L ($^{\#\#}p < 0.01$, $^{\#\#\#}p < 0.001$). In contrast, AR not only exhibited safety and non-toxicity towards H9c2 cells in the concentration range of all 128 μmol/L, but also

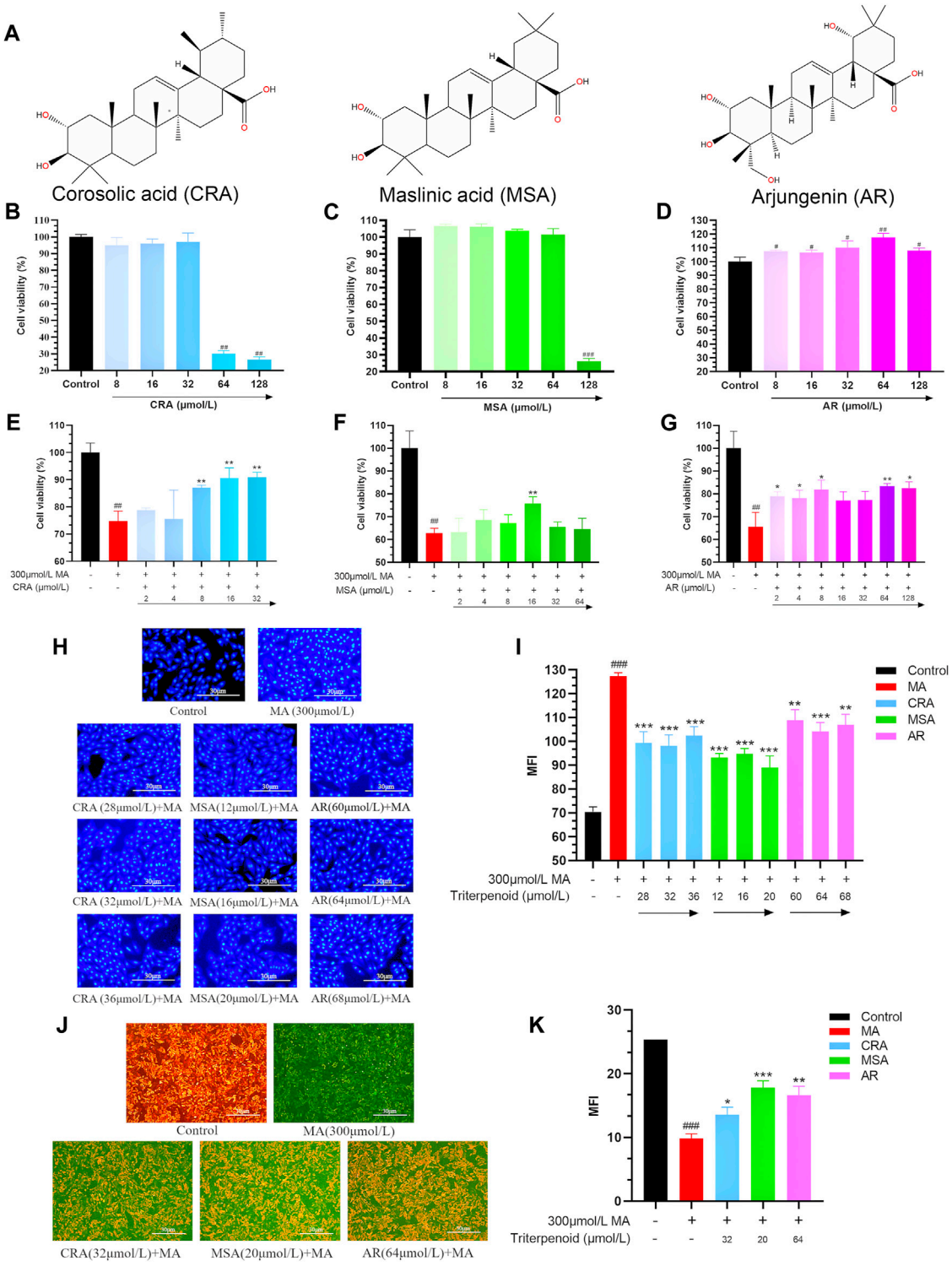

FIGURE 6
Triterpenoids attenuated cardiomyocyte toxicity caused by MA. **(A)** The structure of selected triterpenoids. Effect of CRA **(B)**, MSA **(C)**, and AR **(D)** on cell viability by MTT assay. The attenuating effect of CRA **(E)**, MSA **(F)**, and AR **(G)** on MA caused myocardial cytotoxicity by MTT assay. Effect of triterpenoids or MA on cell nucleus apoptosis in H9c2 cells by Hoechst 33258 staining, **(H)** fluorography (×100); **(I)** quantification is expressed as the Mean fluorescence indensity (MFI). Effect of triterpenoids or MA on mitochondrial membrane potential in H9c2 cells by JC-1 dye staining, **(J)** fluorography (×100); **(K)** quantification is expressed as the MFI. Data were presented as mean ± SD ($n = 3$. Compared with normal control group, $^{\#}p < 0.05$, $^{\#\#}p < 0.01$; compared with MA group, $^{*}p < 0.05$, $^{**}p < 0.01$, $^{***}p < 0.01$).

promoted cell growth ($^{\#}p < 0.05$), and the proliferation reached its maximum effect at 64 μmol/L of AR ($^{\#\#}p < 0.01$). For subsequent experimental verification, concentration ranges of 0 ~ 32 μmol/L, 0 ~64 μmol/L, and 0 ~ 128 μmol/L were selected for CRA, MSA, and AR, respectively.

3.4.2 Effect of triterpenoids on MA-induced cell viability in H9c2 cardiomyocyte

To confirm the triterpenoids can lessen the H9c2 cardiomyocyte toxicity brought on by MA, the survival rate of H9c2 cells was examined using the MTT assay (Figures 6E–G). MA (300 μmol/L) significantly decreased the survival rate of H9c2 cells as compared to the control group ($^{\#\#}p < 0.01$). All three triterpenoids have the potential to reduce the toxicity of MA on cardiomyocytes and increase cell survival (32 μmol/L of CRA, 16 μmol/L of MSA, 64 μmol/L of AR, $^{**}p < 0.01$). And the optimized attenuated concentration were selected for subsequent experiments.

3.4.3 Effect of triterpenoids on MA-induced nuclear apoptosis in H9c2 cardiomyocyte

The cells nuclear change was obtained by Hoechst 33258 staining (Figures 6H, I). Hoechst 33258 specifically stains the nucleus, and when the cell becomes apoptotic, its nuclei is colored blue and fragmented. The control group's nucleus displayed light blue fluorescence following staining and the nucleus shape were unaltered in the Hoechst 33258 staining results. Compared to the control group, the nucleus' apoptotic features became visible in the MA group. It was obviously that the nucleus' chromatin was compressed, and some fragments could be observed. The average fluorescence intensity was much higher than that of the control group on the entire, and it displayed dense and strong bright blue fluorescence ($^{\#\#\#}p < 0.001$). In comparison to the MA group, the addition of a small amount of CRA, MSA, and AR greatly enhanced cell apoptosis, dramatically enhanced nuclear chromatin condensation, and lowered fluorescence intensity ($^{***}p < 0.001$, $^{**}p < 0.01$).

3.4.4 Effect of triterpenoids on MA-induced mitochondrial membrane potential in H9c2 cardiomyocyte

The cells mitochondrial membrane potential change was measured by JC-1 staining (Figures 6J, K). During the JC-1 staining experiment, healthy cells produce red fluorescence due to their higher mitochondrial membrane potential. Conversely, apoptotic cells produce green fluorescence due to their lower membrane potential. A decrease in mitochondrial membrane potential is an early sign of apoptosis, and this decrease can be detected easily by the transition from red fluorescence to green fluorescence when cellular membrane potential drops. In the control group, orange-red fluorescence was predominantly observed, with only a small amount of green fluorescence indicating higher mitochondrial membrane potential. The MA group showed decreased mitochondrial membrane potential, as indicated by greater green fluorescence and weaker orange-red fluorescence ($^{\#\#\#}p < 0.001$). In comparison to the MA group, the inclusion of triterpenoids significantly increased mitochondrial membrane potential ($^{***}p < 0.001$, $^{*}p < 0.01$, $^{*}p < 0.05$).

Through this part of the experiment, we selected the concentrations of CRA, MSA, and AR as 32 μmol/L, 20 μmol/L, and 64 μmol/L for the subsequent exploration of the mechanism of triterpenoids reducing H9c2 cardiomyocyte toxicity induced by MA.

3.5 Verification of triterpenoids reducing MA-induced H9c2 cardiomyocyte toxicity via TRPV1 channel

3.5.1 Effect of triterpenoids or MA on TRPV1 expression in H9c2 cardiomyocyte

As depicted in Figures 7A, B, MA, MSA, and AR significantly increased the expression of the TRPV1 protein in H9c2 cells ($^{**}p < 0.01$, $^{***}p < 0.001$), although MSA and AR had a weaker effect when used in attenuated toxicity concentrations. CRA specifically failed to induce TRPV1 protein expression.

3.5.2 Effect of triterpenoids on MA-induced intracellular calcium ions content in H9c2 cardiomyocyte

The changes in calcium ion concentrations in H9c2 cells were estimated. As illustrated in Figures 7C, D, the intracellular Ca^{2+} level was lower in the control group, and only a trace of green fluorescence was observed. However, MA may greatly boost the green fluorescence intensity of H9c2 cells as well as the intracellular Ca^{2+} content ($^{\#\#\#}p < 0.001$). The addition of CRA, MSA, and AR significantly reduced both the green signal and intracellular Ca^{2+} levels compared to the MA group ($^{*}p < 0.05$, $^{**}p < 0.01$).

3.5.3 Effect of triterpenoids on MA-induced H9c2 cardiomyocyte toxicity after TRPV1 channel blocked by the capsazepine

MA dramatically decreased the H9c2 cells' survival rate as compared to the control group ($^{\#}p < 0.01$) (Figure 7E). Compared to the group without capsazepine, the AR and MSA groups that had previously received capsazepine were able to further improve the survival rate of the H9c2 cells ($^{\Delta}p < 0.05$, $^{\Delta\Delta\Delta}p < 0.001$), but the CRA group was not significantly different regardless of whether they had received capsazepine in advance treatment.

4 Discussion

Aconitum herbs have a long history of medication, such as *Aconitx kusnezoffll* radx., and *Aconitum pendulum* Busch. They have good anti-inflammatory and analgesic properties, but their toxicity is also extremely strong (Singhuber et al., 2009). It is necessary to study the measures and mechanism of toxicity reduction of aconitums, which is of great significance for safe drug use in clinical practice. In Mongolian and Tibetan medicine theory, CF is often used to process or combine aconitums to reduce their toxicity (Liu et al., 2017; Liet al., 2022b). Studies have shown that CF has the effect of reducing the toxicity of aconitums (Liu et al., 2015a; Zhang et al., 2017; Yuan et al., 2022), and the mechanism of the attenuation toxicity was not the same as the conventional heating and boiling to convert the toxic DDAs into less toxic and more powerful monoester-diterpenoid alkaloids (MDAs) or non-esterified diterpene alkaloids (NDAs) (Liu et al., 2013), involving multiple pathways *in vitro* and *in vivo*, such as material basis, internal absorption and metabolism, myocardial electrophysiology, etc. (Zhang,

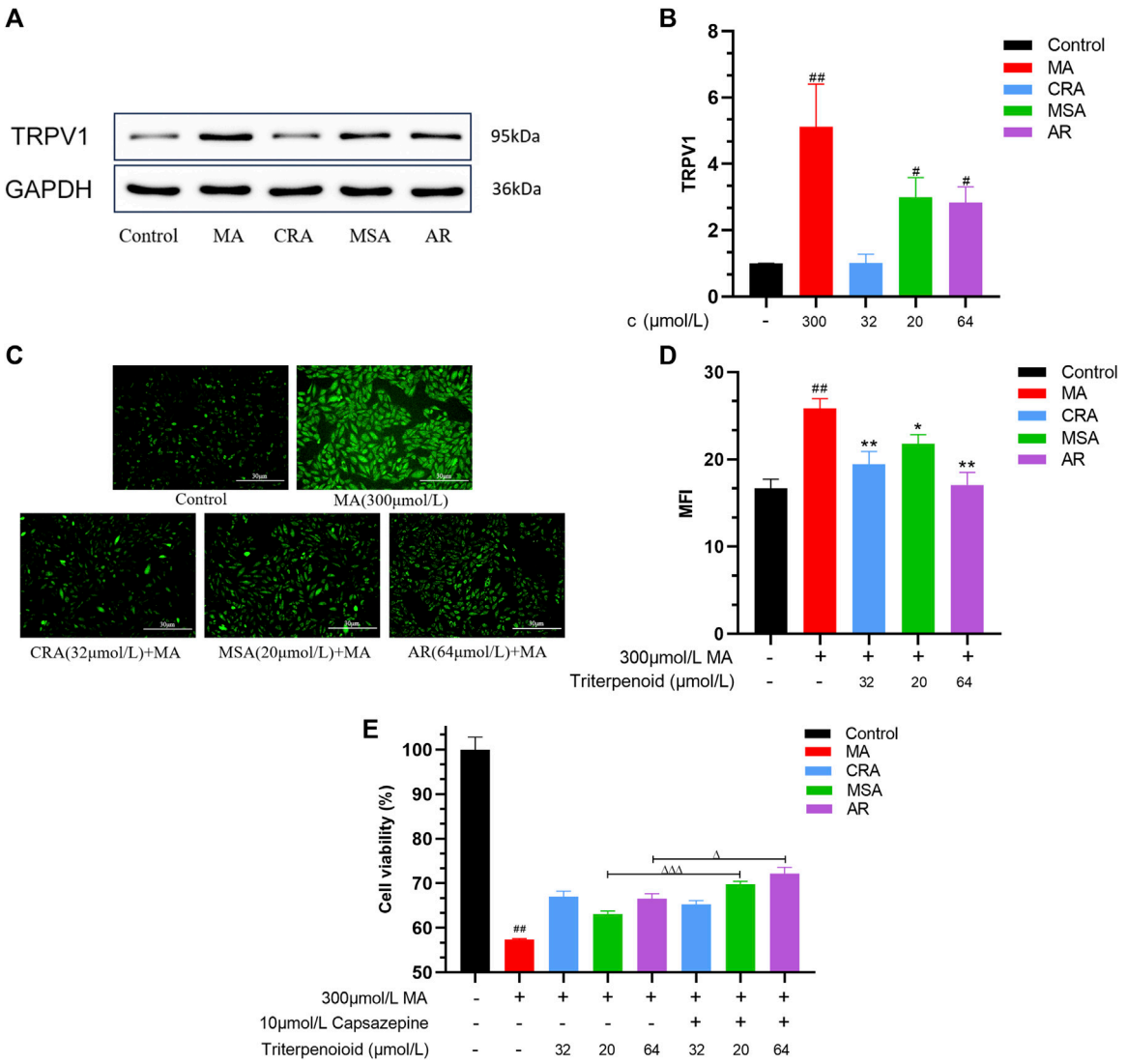

FIGURE 7
Triterpenoids attenuated cardiomyocyte toxicity caused by MA through TRPV1 channel. Effect of triterpenoids or MA on expression of TRPV1 in H9c2 cells detected by Western blot, **(A)** Western blot result, **(B)** the semiquantitative result of **(A)**. Effect of triterpenoids or MA on Ca^{2+} concentration in H9c2 cells by Fluo-3 AM, **(C)** fluorography (×100); **(D)** quantification is expressed as the MFI. **(E)** Effect of triterpenoids or MA on cell survival before and after TRPV1 channel blockade by MTT assay and capsazepine. Data were presented as mean ± SD (n = 3. Compared with normal control group, $^{\#}p < 0.05$, $^{\#\#}p < 0.01$; compared with MA group, $^{*}p < 0.05$, $^{**}p < 0.01$, $^{***}p < 0.001$; compared with the group of the TRPV1 channels that were not blocked, $^{\triangle}p < 0.05$, $^{\triangle\triangle\triangle}p < 0.001$).

2019; Tan et al., 2023). On the basis of the previous studies, we aimed to clarify the mechanism of reducing cardiotoxicity from the aspect of TRPV1 channel that DDAs induced cardiotoxicity in this study.

The pharmacophore model, molecular docking and 3D-QSAR model were used for virtual screening in this study. To screen for components in CF that may activate the TRPV1 channel, a pharmacophore model based on common features of TRPV1 agonists was constructed. However, the pharmacophore model can only identify components with activation potential; it cannot determine their relative activity or ability to bind to the TRPV1 protein. Furthermore, molecular docking was used to quantify each component's binding capacity to the TRPV1 protein receptor, which served as a confirmation and secondary screening of the pharmacophore results. However, further clarification of their activities is required. Consequently, a 3D-QSAR model based on TRPV1 agonists was developed to predict the activity of the screened chemical components. The pharmacophore model revealed seven triterpenoids in CF with TRPV1 agonistic effects. Subsequently, the molecular docking and 3D-QSAR model results indicated that the triterpenoids of CF, which were screened by pharmacophore, had a higher affinity to bind to the TRPV1 agonist receptor than MA. However, their relative activity was lower than that of MA, with CRA, MSA, and AR exhibiting the lowest predicted activity. Thus, we initially integrated the results of the virtual screening section and speculated that the triterpenoids in CF function as TRPV1 agonists. These compounds have a higher affinity for TRPV1 receptors and can competitively antagonize the binding of MA to TRPV1 receptors, whereas having lower activity. This

prevents the over-activation of TRPV1 channels and exerts an attenuated effect.

The rat H9c2 cardiomyocytes were then used to validate the results of the virtual screen. The administration concentration of MA was determined according to the previous pre-experiments. The concentrations of triterpenoids were selected step by step during the experiment. First, the triterpenoids were screened for safe and non-toxic ranges. Then the best attenuation was screened in the attenuated verification experiment section by degrees. Obviously, MA damaged the viability of H9c2 cardiomyocytes, seriously reduced the survival rate. It also caused nuclear damage and pyknosis, and decreased mitochondrial membrane potential. These are landmark events in the early stage of apoptosis and also prove the cardiotoxicity of MA. Moreover, MA promoted the expression of TRPV1 protein in cardiomyocytes, which in turn significantly increased the content of calcium ions in cardiomyocytes. This was consistent with the previous study that the MA had myocardial cytotoxicity, and the generation of toxicity was related to the excessive activation of TRPV1 channels. It was also established that the triterpenoids could reduce the myocardial cytotoxicity of MA to some extent, increase the mitochondrial membrane potential and relieve the damage to the nucleus caused by MA. In addition, MSA and AR can similarly stimulated TRPV1 protein expression in H9c2 cells, although their capacities were inferior to that of MA. In addition, the H9c2 cells survival rate increased when TRPV1 channels were blocked by capsazepine, indicating that the attenuated effects of MSA and AR were related to TRPV1 channels and acted as agonists of TRPV1 channels. Not only MSA and AR but also CRA, could attenuate this tendency for large calcium influx caused by MA and maintain homeostasis of intracellular calcium. These tests provided additional evidence that the TRPV1 channel played a role in reducing cardiotoxicity caused by MA, as the TRPV1 channel is a crucial channel for calcium ions to flow into cells.

So far, efforts have been devoted to the study of the mechanism of CF reducing the toxicity of aconitums, with the expectation of providing theoretical support for the safe application of aconitums. The mechanisms can be summarized in four categories: 1) The acidic components in the CF can inhibit the dissolution of DDAs and detoxify the aconitums (Liu et al., 2013; Yang et al., 2013; Xin et al., 2014). 2) Tannins in CF complexed with DDAs in aconitums to form insoluble substances, which slows down the dissolution rate of alkaloids in gastric and intestinal fluids and plays a certain role in reducing toxicity (Liu et al., 2015b). 3) CF can play a role in reducing toxicity by affecting the absorption, distribution and metabolic process of aconitums in the body. For absorption: the pharmacokinetics of alkaloids can be changed after the processing of aconitums or the compatibility with CF, and the absorption level and absorption rate of alkaloids are reduced, thus reducing the toxicity (Zhi et al., 2020b; Liu et al., 2023). For distribution: CF can reduce the distribution of DDAs in various organs and tissues, and the tannins can bind to DDAs and slowly distribute and eliminate them in the body to play a role in detoxification (Wang et al., 2002). Tannic acid in can reduce the plasma protein binding rate and bioavailability of DDAs (Zhang, 2019). For metabolism: CF can change the absorption and metabolism sites of toxic components, reduce its absorption in the intestinal wall, and increase intestinal bacteria and liver metabolism. This can prevent the absorption of toxic components from being too fast, and promote the metabolism, reduce the concentration of drugs in the blood and prevent poisoning (Celimuge et al., 2022). 4) The components in CF have myocardial protective effect, which can effectively inhibit the cardiotoxicity of aconitums. The use of CF can reduce the myocardial tissue damage caused by the single administration of aconitums in rats (Zhang et al., 2017). Scholars have proved that CF had a good intervention effect on arrhythmia caused by aconitine by Langendorff isolated heart perfusion technique (Liang et al., 2017). CF can resolve the toxicity of Aconitums and has a protective effect on the heart (Pan et al., 2011).

CF alleviates the cardiotoxicity of aconitums mainly due to the active ingredients in CF, such as tannins and triterpenoids, protect the heart from the serious toxicity of aconitums through various ways *in vivo*. Researchers have found that CF could regulate the contraction and relaxation of myocardial cells by multi-component, multi-target, multi-channel, further protect the normal function of the heart, and reduce the cardiac toxicity caused by aconitiums by using the method of network pharmacology (Li et al., 2018). Metabolomics technology was used to investigate the effect of CF on endogenous metabolites in rats. The results showed that glutamine and lysophosphatidylcholine may be the key to the detoxification and regulation efficacy of CF, and also have a certain role in improving cardiac function and acute myocardial infarction (Bilige et al., 2022). The combination of ellagic acid, liquiritin and aconitine can significantly increase the expression of cardiac metabolic enzyme CYP2J3, promote the metabolism of arachidonic acid to produce epoxyeicosatrienoic acids, and then reduce the cardiotoxicity (Li et al., 2023). The effective components of CF can inhibit the release of lactate dehydrogenase and creatine kinase isoenzyme and promote the release of superoxide dismutase to achieve the protective effect on aconitine-injured cardiomyocytes (Duolan, 2022). The compatibility of CF with aconitums can regulate the levels of FKBP1B and RyR2 genes in sarcoplasmic reticulum by affecting TRP gene, especially TRPM8, so as to protect myocardium from damage and play a role in reducing toxicity (Meng et al., 2023). Our research group found that Caowu could induce cardiotoxicity by activating the TRPV1 channel, while CF also played an attenuated role through the TRPV1 channel. The attenuated effect may be related to the synergistic effect of the acidic components in CF and the alkaloids in Caowu on the TRPV1 channel (Han et al., 2022c). Subsequently, we used the uniform design method to identify the primary components responsible in CF for the detoxification effect, and then gallic acid and ellagic acid were screened and the two a synergistic effect (Han et al., 2022a). We also demonstrated that chebulagic acid in CF has a protective effect on myocardial mitochondria, and can inhibit aconitine-induced Ca^{2+} overload in myocardial cells, thereby reducing the occurrence of arrhythmia (Han et al., 2020). In addition, we also found that the TRPV1 channel have an important role in exerting their attenuated effects, the gallic acid in CF may achieve the effect of detoxification by rapid desensitization of TRPV1 channel on the cells (Han et al., 2022b; Mi et al., 2023).

In summary, the research on the active ingredients reducing cardiotoxicity caused by aconitums mainly focused on tannins and phenolic acids. These components play a mitigating cardiotoxicity role by affecting the expression of relevant genes, enzyme activity, and ligand-receptor interactions to maintain a steady state within the cardiomyocyte and protect the organelles to maintain normal

cellular function. In addition to tannins, the triterpenoids in CF are also noteworthy, and most of them have cardiac and myocardial protective effects. MSA has a protective impact against cardiomyocyte damage by exerting both an anti-oxidative action and an ability to inhibit calcium overload in cardiomyocytes (Liu et al., 2008). The cardioprotective effect of arjunolic acid may lie in its protective potential against damage caused by myocardial necrosis (Sumitra et al., 2001). CRA not only upregulates antioxidant levels in cardiomyocytes and hence inhibits apoptosis and cardiomyocyte stress, but also effectively inhibits the development of fibrosis after myocardial infarction, thereby improving cardiac function (Wang, 2019; An et al., 2020). They are in line with how DDAs in Aconitum herbs exert cardiotoxicity. It was also discovered that the triterpenoids in CF showed a certain potential for TRPV1 activation, which may play an attenuated role (Mi et al., 2023).

Combined with the virtual screening and the attenuated validation experiment, the results preliminarily demonstrated that the triterpenoids in CF played a certain role in CF reducing aconitums cardiotoxicity. MSA and AR most likely acted as TPPV1 agonists with less potency that acted on the TRPV1 channel in cardiomyocytes like MA. Because of their high binding capacity, they can bind better to TRPV1 channels but exert weaker agonism, thus preventing MA from excessively stimulating the TRPV1 channel, inhibiting the large influx of calcium ions, keeping cells viable and achieving the purpose of attenuating cardiotoxicity. Besides, it was discovered that CRA failed to increase the expression of TRPV1 protein on its own, and its attenuating effect did not change before and after capsazepine blocked the TRPV1 channel. Nevertheless, CRA was still able to alleviate the calcium ion influx caused by MA. In this context, it is hypothesized that CRA did not achieve an attenuated effect through the TRPV1 channel, but it was likely through other channels related to calcium ions, such as the MAPK pathway (Schaub et al., 2006; Ai et al., 2016), and we will also explore this in depth next.

The toxicity and efficacy of aconitums are closely related to the TRPV1 channel, so reducing their cardiotoxicity through this channel while maintaining good efficacy is very meaningful. In this study, based on the theory of compatibility or processing in Traditional Chinese Medicine Science, the mechanism of reducing the toxicity of MA by triterpenoids of CF was elucidated from the perspective of antagonistic or synergistic effects of active components of drugs. At present, we have only explored the mechanism through computer simulation and at the cellular level. Next, we will further investigate the mechanism of attenuation at the animal level. Of course, other pathways also play a role in the reduction process, and the link and leading role between them are unclear. The DDAs toxicity is produced by the TRPV1 channel, and its analgesic anti-inflammatory effect is also related to TRPV1 channel. We only have evidence that triterpenoids can reduce MA toxicity at the cardiomyocyte level, but we are not clear about their treatment effect. So how can reduce the toxicity and at the same time show good treatment effects needs to further explored.

5 Conclusion

The triterpenoids in CF can reduce the H9c2 cardiomyocyte toxicity caused by MA. Through excessive TRPV1 channel activation, MA causes significant cardiomyocyte death, while MSA and AR also exert a detoxifying effect on cells via TRPV1 channels. Due to their higher affinity with TRPV1 protein receptors, they can competitively antagonize the binding of MA to TRPV1 channels, but at the same time, they have lower TRPV1 channel activation activity than MA, thus preventing MA from overactivating TRPV1 channels, thereby protecting cardiomyocytes and reducing toxicity. CRA may play an attenuated role through other pathways that affect intracellular calcium homeostasis. This paper provides ideas and credence to investigate the mechanism of CF alleviating the cardiotoxicity caused by aconitums *in vitro* experiments.

Data availability statement

The original contributions presented in the study are included in the article/Supplementary Material, further inquiries can be directed to the corresponding author.

Ethics statement

Ethical approval was not required for the studies on animals in accordance with the local legislation and institutional requirements because only commercially available established cell lines were used.

Author contributions

LS: Data curation, Software, Validation, Visualization, Writing–original draft, Writing–review and editing. SM: Software, Validation, Writing–review and editing. YZ: Formal Analysis, Methodology, Project administration, Validation, Visualization, Writing–review and editing. JnW: Conceptualization, Formal Analysis, Methodology, Validation, Writing–review and editing. ZL: Conceptualization, Data curation, Methodology, Writing–review and editing. HoW: Conceptualization, Data curation, Writing–review and editing. WL: Conceptualization, Data curation, Writing–review and editing. JaW: Conceptualization, Data curation, Writing–review and editing. WZ: Conceptualization, Data curation, Resources, Writing–review and editing. HD: Funding acquisition, Resources, Supervision, Writing–review and editing.

Funding

The authors declare financial support was received for the research, authorship, and/or publication of this article. National Natural Science Foundation of China (No. 82130113), and National Natural Science Foundation of China (No. 82274206).

Acknowledgments

This work is grateful to the above fundings.

Conflict of interest

The authors declare that the research was conducted in the absence of any commercial or financial relationships that could be construed as a potential conflict of interest.

Publisher's note

All claims expressed in this article are solely those of the authors and do not necessarily represent those of their affiliated organizations, or those of the publisher, the editors and the reviewers. Any product that may be evaluated in this article, or claim that may be made by its manufacturer, is not guaranteed or endorsed by the publisher.

Supplementary material

The Supplementary Material for this article can be found online at: https://www.frontiersin.org/articles/10.3389/fphar.2024.1367682/full#supplementary-material

References

Acharya, C., Coop, A., Polli, J. E., and Mackerell, A. D., Jr. (2011). Recent advances in ligand-based drug design: relevance and utility of the conformationally sampled pharmacophore approach. *Curr. Comput. Aided Drug Des.* 7 (1), 10–22. doi:10.2174/157340911793743547

Ai, L., Yang, F., Hu, W., Guo, L., Liu, W., Xue, X., et al. (2023). Hepatotoxic components effect of *Chebulae Fructus* and associated molecular mechanism by integrated transcriptome and molecular docking. *Mol. Basel, Switz.* 28 (8), 3427. doi:10.3390/molecules28083427

Ai, X., Yan, J., Carrillo, E., and Ding, W. (2016). The stress-response MAP kinase signaling in cardiac arrhythmias. *Rev. Physiol. Biochem. Pharmacol.* 172, 77–100. doi:10.1007/112_2016_8

An, C., Qi, Z., and Su, X. (2020). Research advance in Terminalia antioxidants. *Chem. Life* 40 (06), 925–932. doi:10.13488/j.smhx.20200109

Bilige, W., Li, L., Chen, H., Meng, X., and Bolor, R. (2022). Effect of Terminalia Chebula Retz on serum metabolites in rats. *Yunnan J. Traditional Chin. Med. Materia Medica* 43 (08), 85–88. doi:10.16254/j.cnki.53-1120/r.2022.08.008

Burgess, G., and Williams, D. (2010). The discovery and development of analgesics: new mechanisms, new modalities. *J. Clin. Invest.* 120 (11), 3753–3759. doi:10.1172/jci43195

Celimuge, S., Xu, L., Song, L., and Tu, Y. (2022). Study on the mechanism of processing Radix Aconiti with hezi decoction based on UPLC-Q-TOF/MS technology and sequential metabolism method. *Mod. Traditional Chin. Med. Materia Medica-World Sci. Technol.* 24 (08), 2995–3013. doi:10.11842/wst.20210817002

Chan, Y. T., Wang, N., and Feng, Y. (2021). The toxicology and detoxification of Aconitum: traditional and modern views. *Chin. Med.* 16 (1), 61. doi:10.1186/s13020-021-00472-9

Chen, Q., Deng, X., Zhang, K., Kang, Y., Jiao, M., Zhang, J., et al. (2023a). Changes to PUFA-PPAR pathway during mesaconitine induced myocardial coagulative necrosis. *Food Chem. Toxicol.* 177, 113831. doi:10.1016/j.fct.2023.113831

Chen, Y., Tang, Y., Yang, L., Xiong, A., and Wang, Z. (2023b). Advances on toxicity and metabolism of alkaloids from the "toxic" traditional Chinese medicines. *Acta Pharm. Sin.* 2023, 1–22. doi:10.16438/j.0513-4870.2023-0241

Choi, J. K., Cho, W., Lee, J. H., Choi, G., and Park, M. (2020). A TRPV1 antagonist, PAC-14028 does not increase the risk of tumorigenesis in chemically induced mouse skin carcinogenesis. *Regul. Toxicol. Pharmacol.* 112, 104613. doi:10.1016/j.yrtph.2020.104613

Dimar, D. (1986). *Jingzhu Materia Medica*. Shanghai, China: Shanghai Science and Technology Press.

Duarte, Y., Cáceres, J., Sepúlveda, R. V., Arriagada, D., Olivares, P., Díaz-Franulic, I., et al. (2020). Novel TRPV1 channel agonists with faster and more potent analgesic properties than capsaicin. *Front. Pharmacol.* 11, 1040. doi:10.3389/fphar.2020.01040

Duolan (2022). *Protective effect of Terminalia chebula extract on H9C2 myocardialcell injury induced by aconitine and its mechanism*. Inner Mongolia Medical University, 12–15.

Feinstein, W. P., and Brylinski, M. (2015). Calculating an optimal box size for ligand docking and virtual screening against experimental and predicted binding pockets. *J. Cheminformatics* 7 (1), 18. doi:10.1186/s13321-015-0067-5

Feng, A. (2019). Observation on the treatment of arrhythmia caused by severe acute aconitine poisoning. *World Latest Med. Inf.* 19 (94), 131–134. doi:10.19613/j.cnki.1671-3141.2019.94.082

Fu, M., Wu, M., Wang, J. F., Qiao, Y. J., and Wang, Z. (2007). Disruption of the intracellular Ca2+ homeostasis in the cardiac excitation-contraction coupling is a crucial mechanism of arrhythmic toxicity in aconitine-induced cardiomyocytes. *Biochem. Biophys. Res. Commun.* 354 (4), 929–936. doi:10.1016/j.bbrc.2007.01.082

Gao, Y., Cao, E., Julius, D., and Cheng, Y. (2016). TRPV1 structures in nanodiscs reveal mechanisms of ligand and lipid action. *Nature* 534 (7607), 347–351. doi:10.1038/nature17964

Gao, Y., Fan, H., Nie, A., Yang, K., Xing, H., Gao, Z., et al. (2022). Aconitine: a review of its pharmacokinetics, pharmacology, toxicology and detoxification. *J. Ethnopharmacol.* 293, 115270. doi:10.1016/j.jep.2022.115270

Gavva, N. R. (2008). Body-temperature maintenance as the predominant function of the vanilloid receptor TRPV1. *Trends Pharmacol. Sci.* 29 (11), 550–557. doi:10.1016/j.tips.2008.08.003

Gunthorpe, M. J., and Szallasi, A. (2008). Peripheral TRPV1 receptors as targets for drug development: new molecules and mechanisms. *Curr. Pharm. Des.* 14 (1), 32–41. doi:10.2174/138161208783330754

Guo, J., Xue, J., He, Z., Jia, H., and Yang, X. (2023). The mechanism by which Naru 3 pill protects against intervertebral disc cartilage endplate degeneration based on network pharmacology and experimental verification. *J. Orthop. Surg. Res.* 18 (1), 552. doi:10.1186/s13018-023-04014-x

Han, S., Bao, L., Han, X., Tang, Y., Liu, Z., Wang, H., et al. (2022a). Effects of characteristic components in Aconitii Kusnezoffii Radix processed with Chebulae Fructus on the cytotoxicity of H9c2 cardiomyocytes based on uniform design experiment. *China Pharm.* 25 (01). doi:10.19962/j.cnki.issn1008-049X.2022.01.005

Han, S., Bao, L., Li, W., Liu, K., Tang, Y., Han, X., et al. (2022b). Gallic acid inhibits mesaconitine-activated TRPV1-channel-induced cardiotoxicity. *Evid. Based Complement. Altern. Med.* 2022, 5731372. doi:10.1155/2022/5731372

Han, S., Bao, L., Liu, K., Han, X., Tang, Y., Liu, Z., et al. (2022c). Mechanism of Aconiti kusnezoffii radix processed with Chebulae Fructus against H9c2 cardiomyocyte toxicity based on TRPV1 channel. *Chin. J. Exp. Traditional Med. Formulae* 28 (01), 173–181. doi:10.13422/j.cnki.syfjx.20211748

Han, S., Liu, S., Zhang, Q., Zhi, M., Liu, K., Tang, Y., et al. (2020). Protective effect and mechanism of chebulagic acid on H9C2 cells injury induced by aconitine. *J. Beijing Univ. Traditional Chin. Med.* 43 (08), 645–652. doi:10.3969/j.issn.1006-2157.2020.08.006

Hansch, C. M., Peyton, P., Fujita, T., and Muir, R. M. (1962). Correlation of biological activity of phenoxyacetic acids with hammett substituent constants and partition coefficients. *Nature* 194 (4824), 178–180. doi:10.1038/194178b0

Li, C. Y., Zhou, Z., Xu, T., Wang, N. Y., Tang, C., Tan, X. Y., et al. (2022a). Aconitum pendulum and Aconitum flavum: a narrative review on traditional uses, phytochemistry, bioactivities and processing methods. *J. Ethnopharmacol.* 292, 115216. doi:10.1016/j.jep.2022.115216

Li, H., Liu, Y., Yang, H., and Liu, Y. (2022b). Research progress on chemical constituents, pharmacological mechanism, quality control and processing of Terminalia chebula Retz. *Nat. Prod. Res. Dev.* 34, 2130–2141. doi:10.16333/j.1001-6880.2022.12.017

Li, H., Song, L., Gao, Y., Chen, T., Hou, H., Peng, B., et al. (2023). Detoxification mechanism of combined Chebulae Fructus, Glycyrrhizae Radix et Rhizoma and prepared Aconiti Kusnezoffii Radix Cocta in regulating cardiac metabolic enzyme CYP2J3. *Chin. J. Exp. Traditional Med. Formulae* 29 (17), 88–95. doi:10.13422/j.cnki.syfjx.202202326

Li, H., Zhang, G., Chen, T., Gao, Y., Song, L., Hou, H., et al. (2021). Research progress on mechanism of reducing toxicity and increasing efficiency of compatibility of Mongolian medicinal materials Terminalia chebula and aconitum kusnezoffii. *Word Chin. Med.* 16 (24), 3701–3707. doi:10.3969/j.issn.1673-7202.2021.24.025

Li, H. Q., Xu, J. Y., Fan, X. H., and Wu, S. S. (2019). Optimization of the traditional processing method for precision detoxification of CaoWu through biomimetic linking kinetics and human toxicokinetics of aconitine as toxic target marker. *J. Ethnopharmacol.* 242, 112053. doi:10.1016/j.jep.2019.112053

Li, J., Liang, H., Cai, S., Li, Z., and Tu, Y. (2018). Mechanism of detoxification of Chebulae Fructus against Aconiti kusnezoffii radix toxicity based on network pharmacology. *Acta Pharm. Sin.* 53 (10), 1670–1679. doi:10.16438/j.0513-4870.2018-0506

Li, K., li, C., and Liu, X. (2011). Progress on the capsaicin receptor-TRPV1:Biological actions and as atherapeutic target for novel drugs. *J. Shenyang Pharm. Univ.* 28 (11), 917–927. doi:10.14066/j.cnki.cn21-1349/r.2011.11.014

Li, M., Xie, X., Chen, H., Xiong, Q., Tong, R., Peng, C., et al. (2020). Aconitine induces cardiotoxicity through regulation of calcium signaling pathway in zebrafish embryos and in H9c2 cells. *J. Appl. Toxicol.* 40 (6), 780–793. doi:10.1002/jat.3943

Li, X., and Yang, X. (2018). Study on the molecular targeting docking virtual screening of potential active components in tong-xie-yao-fang. *J. Nanjing Normal Univ. Sci. Ed.* 41 (03), 85–94. doi:10.3969/j.issn.1001-4616.2018.03.014

Liang, H., Li, J., Yang, Y., Tu, Y., and Song, L. (2017). Traditional Mongolian Medicine Chebulae Fructus protect arhythmiainduced by aconitine in rats. *J. Med. Pharm. Chin. Minorities* 23 (11), 75–77. doi:10.16041/j.cnki.cn15-1175.2017.11.036

Liu, J., Li, Y., Gong, X., Fang, W., and Sun, H. (2008). The protective effect of maslinic acid on the cardiac myocytes with ischemia *in vitro*. *Chin. J. New Drugs* 17 (09), 743–747. doi:10.3321/j.issn:1003-3734.2008.09.007

Liu, S., Li, F., Hou, Y., Yang, C., Tan, P., Li, X., et al. (2013). Influence of tannins from Chebulae Fructus on aconitum alkaloids of aconitum kusnezoffi processed with Chebulae fructus-principal of aconitum processed with Chebulae Fructus I. *Chin. J. Exp. Traditional Med. Formulae* 19 (05), 158–160. doi:10.13422/j.cnki.syfjx.2013.05.068

Liu, S., Li, F., Li, Y., Li, W., Xu, J., and Du, H. (2017). A review of traditional and current methods used to potentially reduce toxicity of Aconitum roots in Traditional Chinese Medicine. *J. Ethnopharmacol.* 207, 237–250. doi:10.1016/j.jep.2017.06.038

Liu, S., Li, W., Li, Y., Xu, j., Liu, X., Li, F., et al. (2016a). Lnfluence of Fructus Chebulae water solution on quality of Mongolian medicine Aconiti kusnezoffi radix praeparata. *J. Beijing Univ. Traditional Chin. Med.* 39 (11). doi:10.3969/j.issn.1006-2157.2016.11.012

Liu, S., li, Y., Li, W., Xu, J., Li, F., and Du, H. (2016b). Advances in studies on toxicity and modern toxicology of species in Aconitum L. *Chin. Traditional Herb. Drugs* 47 (22), 4095–4102. doi:10.7501/j.issn.0253-2670.2016.22.027

Liu, S., Liu, X., Li, Y., Yang, C., Liu, Q., Li, F., et al. (2015a). Experimental study on acute toxicity of the Aconiti kusnezo ffii radix and lts processed products. *Chin. J. Pharmacovigil.* 12 (09), 513–517. doi:10.19803/j.1672-8629.2015.09.001

Liu, S., Liu, X., Lin, S., Yang, C., Li, F., and Du, H. (2015b). Hydrolysis of simulation processing products of Aconitum kusnezoffii Processed with Terminalia chebula in simulated gastric fluid and intestinal fluid. *China Pharm.* 26 (13), 1752–1754. doi:10.6039/j.issn.1001-0408.2015.13.07

Liu, X., Tao, H., Tian, R., Huang, W., Zhang, T., Liu, Y., et al. (2023). Hezi inhibits Tiebangchui-induced cardiotoxicity and preserves its anti-rheumatoid arthritis effects by regulating the pharmacokinetics of aconitine and deoxyaconitine. *J. Ethnopharmacol.* 302, 115915. doi:10.1016/j.jep.2022.115915

Mazeto, T. K., Picada, J. N., Correa Á, P., Rebelo, I. N., Ribeiro, M. T., Gomez, M. V., et al. (2020). Antinociceptive and genotoxic assessments of the antagonist TRPV1 receptor SB-366791 on morphine-induced tolerance in mice. *Naunyn Schmiedeb. Arch. Pharmacol.* 393 (3), 481–490. doi:10.1007/s00210-019-01748-6

Meng, X., Huang, X., Dong, Y., Xu, X., Liu, S., Wu, Z., et al. (2023). Influence and mechanism of toxicity-efficacy relationship between the combination of Terminalia chebula Retz. and Aconitum pendulum Bush. On pentobarbital sodium-induced H9c2 myocardial cells. *Chin. J. Mod. Appl. Pharm.* 40 (08). doi:10.13748/j.cnki.issn1007-7693.20222649

Mi, S., Han, S., Liu, K., Bao, L., Zhang, F., Wang, H., et al. (2023). Mechanism of aconitum kusnezoffii processed with Terminalia chebula in reducing toxicity mediatedby TRPV1 based on pharmacophore and molecular docking. *World Chin. Med.* 18 (12), 1645–1652. doi:10.3969/j.issn.1673-7202.2023.12.001

More, K. N., Lee, Y. J., Kim, K. J., Suh, Y. G., Son, Y. J., and Chang, D. J. (2020). Effect of TRPV1 antagonist SC0030, a potent painkiller, on RANKL-mediated osteoclast differentiation involved in bone resorption. *Bull. Korean Chem. Soc.* 41 (4), 488–491. doi:10.1002/bkcs.11992

Nie, C. (2020). *Chemical modification and analgesic activity of TRPV1 antagonist N-(4-tert-butylphenyl)-4 -(3-chloropyridine-2-yl)piperazine-1-formamide*. Henan University, 22.

Nigam, M., Mishra, A. P., Adhikari-Devkota, A., Dirar, A. I., Hassan, M. M., Adhikari, A., et al. (2020). Fruits of Terminalia chebula Retz.: a review on traditional uses, bioactive chemical constituents and pharmacological activities. *Phytother. Res.* 34 (10), 2518–2533. doi:10.1002/ptr.6702

Pan, Y., Zhang, S., Li, F., Hou, J., and Zhou, X. (2011). Protective effects of decoction of Terminalia on myocardial cells damaged by Aconitine. *J. Med. Pharm. Chin. Minorities* 17 (01), 43–46. doi:10.16041/j.cnki.cn15-1175.2011.01.041

Peng, J., and Li, Y. (2010). The vanilloid receptor TRPV1: role in cardiovascular and gastrointestinal protection. *Eur. J. Pharmacol.* 627 (1-3), 1–7. doi:10.1016/j.ejphar.2009.10.053

Qiao, L., and Zhang, Y. (2014). Application of CADD on multi-target drug R&D in natural products. *China J. Chin. Materia Medica* 39 (11), 1951–1955. doi:10.4268/cjcmm20141101

Sappington, R. M., Sidorova, T., Long, D. J., and Calkins, D. J. (2009). TRPV1: contribution to retinal ganglion cell apoptosis and increased intracellular Ca2+ with exposure to hydrostatic pressure. *Invest. Ophthalmol. Vis. Sci.* 50 (2), 717–728. doi:10.1167/iovs.08-2321

Schaub, M. C., Hefti, M. A., and Zaugg, M. (2006). Integration of calcium with the signaling network in cardiac myocytes. *J. Mol. Cell Cardiol.* 41 (2), 183–214. doi:10.1016/j.yjmcc.2006.04.005

Singhuber, J., Zhu, M., Prinz, S., and Kopp, B. (2009). Aconitum in traditional Chinese medicine: a valuable drug or an unpredictable risk? *J. Ethnopharmacol.* 126 (1), 18–30. doi:10.1016/j.jep.2009.07.031

Song, Z., Chen, T., Wang, X., Wang, D., Shen, C., Wang, S., et al. (2023). Standardization of chebulagic acid as quality marker of Tibetan medicine Terminalia chebula. *Analysis Test. Technol. Instrum.* 29 (2), 140–148. doi:10.16495/j.1006-3757.2023.02.002

Sugimoto, Y., Kojima, Y., Inayoshi, A., Inoue, K., Miura-Kusaka, H., Mori, K., et al. (2013). K-685, a TRPV1 antagonist, blocks PKC-sensitized TRPV1 activation and improves the inflammatory pain in a rat complete Freund's adjuvant model. *J. Pharmacol. Sci.* 123 (3), 256–266. doi:10.1254/jphs.13088fp

Sumitra, M., Manikandan, P., Kumar, D. A., Arutselvan, N., Balakrishna, K., Manohar, B. M., et al. (2001). Experimental myocardial necrosis in rats: role of arjunolic acid on platelet aggregation, coagulation and antioxidant status. *Mol. Cell Biochem.* 224 (1-2), 135–142. doi:10.1023/a:1011927812753

Sun, G. B., Sun, H., Meng, X. B., Hu, J., Zhang, Q., Liu, B., et al. (2014a). Aconitine-induced Ca2+ overload causes arrhythmia and triggers apoptosis through p38 MAPK signaling pathway in rats. *Toxicol. Appl. Pharmacol.* 279 (1), 8–22. doi:10.1016/j.taap.2014.05.005

Sun, Z., Han, J., Zhao, W., Zhang, Y., Wang, S., Ye, L., et al. (2014b). TRPV1 activation exacerbates hypoxia/reoxygenation-induced apoptosis in H9C2 cells via calcium overload and mitochondrial dysfunction. *Int. J. Mol. Sci.* 15 (10), 18362–18380. doi:10.3390/ijms151018362

Szolcsányi, J., and Sándor, Z. (2012). Multisteric TRPV1 nocisensor: a target for analgesics. *Trends Pharmacol. Sci.* 33 (12), 646–655. doi:10.1016/j.tips.2012.09.002

Tan, X., He, Q., Pei, Z., Liu, Y., Feng, Z., Li, C., et al. (2023). Rapid visual characterization of alkaloid changes in traditional processing of Tibetan medicine Aconitum pendulum by high-performance thin-layer chromatography coupled with desorption electrospray ionization mass spectrometry imaging. *Front. Pharmacol.* 14, 1104473. doi:10.3389/fphar.2023.1104473

Temml, V., and Kutil, Z. (2021). Structure-based molecular modeling in SAR analysis and lead optimization. *Comput. Struct. Biotechnol. J.* 19, 1431–1444. doi:10.1016/j.csbj.2021.02.018

Wang, M., Zhang, S., and Zhai, H. (2002). The influence of terminalia on the toxicokinetics of aconitum decoction. *J. Inn. Mong. Med. Univ.* (04), 219–222. doi:10.16343/j.cnki.issn.2095-512x.2002.04.001

Wang, Z. (2019). *Effects of corosolic acid on post-myocardial infarction cardiac remodeling in mice*. Wuhan University, 27–30.

Wei, X., Qiu, Z., Chen, J., Sun, R., Huang, L., and Lai, C. (2019). Research advancement in mechanisms of processing and compatibility for detoxication of Aconitums. *China J. Chin. Materia Medica* 44 (17), 3695–3704. doi:10.19540/j.cnki.cjcmm.20190629.301

Wu, Z., He, E. Y., Scott, G. I., and Ren, J. (2015). α,β-Unsaturated aldehyde pollutant acrolein suppresses cardiomyocyte contractile function: role of TRPV1 and oxidative stress. *Environ. Toxicol.* 30 (6), 638–647. doi:10.1002/tox.21941

Xin, Y., Wang, S., Zhang, W., Lv, J., Zhang, Y., and Zhang, Z. (2014). Chemical detoxification of fruit of medicine Terminalia on Root of Kusnezoffii Monkshood by mass spectrometry. *Chin. J. Exp. Traditional Med. Formulae* 20 (23), 51–56. doi:10.13422/j.cnki.syfjx.2014230051

Yang, C., Li, F., hOU, y., Liu, S., Tan, P., Li, X., et al. (2013). Comparision of contents of aconitum alkaloids between the decoctions of aconitum processed with myrobalan and co-decoctions of aconitum and myrobalan - principal of aconitum processed with myrobalan II. *Chin. J. Exp. Traditional Med. Formulae* 19 (04), 130–132. doi:10.13422/j.cnki.syfjx.2013.04.051

Yang, C., Zeng, X., Cheng, Z., Zhu, J., and Fu, Y. (2021). Aconitine induces TRPV2-mediated Ca(2+) influx through the p38 MAPK signal and promotes cardiomyocyte apoptosis. *Evid. Based Complement. Altern. Med.* 2021, 9567056. doi:10.1155/2021/9567056

Yang, M., Ji, X., and Zuo, Z. (2018). Relationships between the toxicities of radix Aconiti lateralis preparata (fuzi) and the toxicokinetics of its main diester-diterpenoid alkaloids. *Toxins (Basel)* 10 (10), 391. doi:10.3390/toxins10100391

Yang, S. Y. (2010). Pharmacophore modeling and applications in drug discovery: challenges and recent advances. *Drug Discov. Today* 15 (11-12), 444–450. doi:10.1016/j.drudis.2010.03.013

Ye, Q., Liu, H., Fang, C., Liu, Y., Liu, X., Liu, J., et al. (2021). Cardiotoxicity evaluation and comparison of diterpene alkaloids on zebrafish. *Drug Chem. Toxicol.* 44 (3), 294–301. doi:10.1080/01480545.2019.1586916

Yin, Y. (2019). *Structural mechanism underlying TRPV1 activation by pungent compounds in gingers*. Qingdao University, 18–19.

Yuan, X., Gao, Y., Wang, Q., Wang, L., Zhang, C., Gu, C., et al. (2022). Study on the pharmacological effects of the compatibility of Mongolian medicine Aconiti kusnezoffii radix and Chebulae Fructus on the kidney and liver toxicity caused by Aconiti kusnezoffii radix. *J. Inn. Mong. Med. Univ.* 44 (06), 581–584+590. doi:10.16343/j.cnki.issn.2095-512x.2022.06.006

Zhai, K., Liskova, A., Kubatka, P., and Büsselberg, D. (2020). Calcium entry through TRPV1: a potential target for the regulation of proliferation and apoptosis in cancerous and healthy cells. *Int. J. Mol. Sci.* 21 (11), 4177. doi:10.3390/ijms21114177

Zhang, X. (2019). *The mechanism of detoxification and retention effect of Terminalia Chebula on Radix Aconiti Kusnezoffii based on pharmacokinetics*. Inner Mongolia Medical University, 45–46.

Zhang, X., Cui, Y., Miao, X., Liu, D., Ma, Z., and Li, G. (2017). Study on the protective effect of Mongolian medicine Chebulae Fructus on cardiac toxicity induced by Aconiti Kusnezoffii Radix in rats. *J. Chin. Med. Mater.* 40 (11), 2693–2696. doi:10.13863/j.issn1001-4454.2017.11.044

Zhi, M., Gu, X., Han, S., Liu, K., Liu, Z., Tang, Y., et al. (2020a). Chemical variation in aconti kusnezoffii radix before and after processing based on UPLC-orbitrap-MS. *China J. Chin. Materia Medica* 45 (05), 1082–1089. doi:10.19540/j.cnki.cjcmm.20191221.301

Zhi, M., Liu, K., Han, S., Xu, J., Li, W., Li, F., et al. (2020b). Influence of different dosage forms on pharmacokinetics of 6 alkaloids in raw Aconiti kusnezoffii radix (Caowu) and Chebulae Fructus- (hezi-) processed Caowu by UPLC-MS/MS. *Biomed. Res. Int.* 2020, 1942849. doi:10.1155/2020/1942849

Zhou, B., Qian, Z., Li, Q., Gao, Y., and Li, M. (2022). Assessment of pulmonary infectious disease treatment with Mongolian medicine formulae based on data mining, network pharmacology and molecular docking. *Chin. Herb. Med.* 14 (3), 432–448. doi:10.1016/j.chmed.2022.07.001

Zhou, W., Liu, H., Qiu, L. Z., Yue, L. X., Zhang, G. J., Deng, H. F., et al. (2021). Cardiac efficacy and toxicity of aconitine: a new frontier for the ancient poison. *Med. Res. Rev.* 41 (3), 1798–1811. doi:10.1002/med.21777

Zou, Y., Zhao, X., Sun, Y., and Wang, J. (2017). Effect and mechanism of maslinic acid on attenuating high glucose-induced myocardial cell injury and apoptosis. *Chin. Heart J.* 29 (03), 276–280. doi:10.13191/j.chj.2017.0071

frontiers | Frontiers in Pharmacology

TYPE Review
PUBLISHED 04 June 2024
DOI 10.3389/fphar.2024.1393209

OPEN ACCESS

EDITED BY
Michael Heinrich,
University College London, United Kingdom

REVIEWED BY
Bhuvnesh Kumar,
Sharda University, India
Eduardo Pena,
Arturo Prat University, Chile
Geng Wenye,
Fudan University, China

*CORRESPONDENCE
Yue Gao,
gaoyue@bmi.ac.cn
Maoxing Li,
limaox2020@aliyun.com

†These authors have contributed equally to this work and share first authorship

RECEIVED 28 February 2024
ACCEPTED 06 May 2024
PUBLISHED 04 June 2024

CITATION
Wu Z, Wang Y, Gao R, Chen J, Chen Y, Li M and Gao Y (2024), Potential therapeutic effects of traditional Chinese medicine in acute mountain sickness: pathogenesis, mechanisms and future directions.
Front. Pharmacol. 15:1393209.
doi: 10.3389/fphar.2024.1393209

Potential therapeutic effects of traditional Chinese medicine in acute mountain sickness: pathogenesis, mechanisms and future directions

Zhenhui Wu[1,2†], Yihao Wang[3†], Rong Gao[3], Junru Chen[3], Yingfan Chen[4], Maoxing Li[3*] and Yue Gao[1,3*]

[1]School of Pharmacy, Jiangxi University of Chinese Medicine, Nanchang, China, [2]Department of Hematology, Affiliated Hospital of Jiangxi University of Chinese Medicine, Nanchang, China, [3]Beijing Institute of Radiation Medicine, Beijing, China, [4]Department of Traditional Chinese Medicine, The Sixth Medical Center of Chinese People's Liberation Army General Hospital, Beijing, China

Background and objectives: Acute mountain sickness (AMS) is a pathology with different symptoms in which the organism is not adapted to the environment that occurs under the special environment of high altitude. Its main mechanism is the organism's tissue damage caused by acute hypobaric hypoxia. Traditional Chinese medicine (TCM) theory focuses on the holistic concept. TCM has made remarkable achievements in the treatment of many mountain sicknesses. This review outlines the pathogenesis of AMS in modern and traditional medicine, the progress of animal models of AMS, and summarizes the therapeutic effects of TCM on AMS.

Methods: Using the keywords "traditional Chinese medicine," "herbal medicine," "acute mountain sickness," "high-altitude pulmonary edema," "high-altitude cerebral edema," "acute hypobaric hypoxia," and "high-altitude," all relevant TCM literature published up to November 2023 were collected from Scopus, Web of Science, PubMed, and China National Knowledge Infrastructure databases, and the key information was analyzed.

Results: We systematically summarised the effects of acute hypobaric hypoxia on the tissues of the organism, the study of the methodology for the establishment of an animal model of AMS, and retrieved 18 proprietary Chinese medicines for the clinical treatment of AMS. The therapeutic principle of medicines is mainly invigorating qi, activating blood and removing stasis. The components of botanical drugs mainly include salidroside, ginsenoside Rg1, and tetrahydrocurcumin. The mechanism of action of TCM in the treatment of

Abbreviations: AMS, acute mountain sickness; TCM, traditional Chinese medicine; HACE, high altitude cerebral edema; HAPE, high altitude pulmonary edema; NF-κB, nuclear factor-κB; AMPK, AMP-activated protein kinase; ROS, Reactive oxygen species; SaO2, Blood oxygen saturation; Hb, Hemoglobin; RBC, Red blood cell; CDDP, Compound danshen dripping pill; TNF-α, Tumour necrosis factor-α; VEGF, Vascular endothelial-derived growth factor; MDA, malondialdehyde; SOD, Superoxide dismutase; GSH-Px, Glutathione peroxidase; mTOR, mammalian target of rapamycin; NLRP3, nod-like receptor protein 3; BBB, blood-brain barrier; LPS, lipopolysaccharide; Glu, Glucose; ATP, adenosine triphosphate; IL-6, interleukin 6.

AMS is mainly through the regulation of HIF-1α/NF-κB signaling pathway, inhibition of inflammatory response and oxidative stress, and enhancement of energy metabolism.

Conclusion: The main pathogenesis of AMS is unclear. Still, TCM formulas and components have been used to treat AMS through multifaceted interventions, such as compound danshen drip pills, Huangqi Baihe granules, salidroside, and ginsenoside Rg1. These components generally exert anti-AMS pharmacological effects by inhibiting the expression of VEGF, concentration of MDA and pro-inflammatory factors, down-regulating NF-κB/NLRP3 pathway, and promoting SOD and Na + -K + -ATPase activities, which attenuates acute hypobaric hypoxia-induced tissue injury. This review comprehensively analyses the application of TCM in AMS and makes suggestions for more in-depth studies in the future, aiming to provide some ideas and insights for subsequent studies.

KEYWORDS

traditional Chinese medicine, acute mountain sickness, hypobaric hypoxia, pathogenesis, mechanism

1 Introduction

China is the country with the largest plateau area in the world, and its area with an altitude greater than 2500 m accounts for more than a quarter of its land area. Compared with the plains, the high altitude condition has the characteristics of low air pressure, low oxygen partial pressure, coldness, strong ultraviolet rays, and dry climate. Among them, hypoxia has non-specific effects on the body's functions and metabolism and is the most important factor affecting the human body in the high altitude conditions (Richalet et al., 2023). Acute mountain sickness (AMS) refers to the condition that occurs due to low oxygen when people rush from plain areas or low-altitude areas to high-altitude areas. It is mainly headache, and may be accompanied by dizziness, loss of appetite, and nausea. A clinical syndrome with symptoms such as vomiting, palpitation, insomnia, fatigue, and fatigue (Burtscher et al., 2023). From the perspective of medical altitude (high altitude), 3,000 m above sea level was once used as the plateau limit. However, at the sixth International Conference on High Altitude Medicine held in Xining, Qinghai in 2004, 2,500 m above sea level was redefined as the medical altitude limit. Once one rushes from the mainland to an area above 2,500 m above sea level, AMS may occur (Wu, 2005; Luks et al., 2010). Although AMS is not fatal in most cases, in severe cases, it can progress to high altitude pulmonary edema (HAPE) and high altitude cerebral edema (HACE), both of which are also called acute severe mountain sickness. Generally not self-healing and can be life-threatening (West, 2012; Luks et al., 2017).

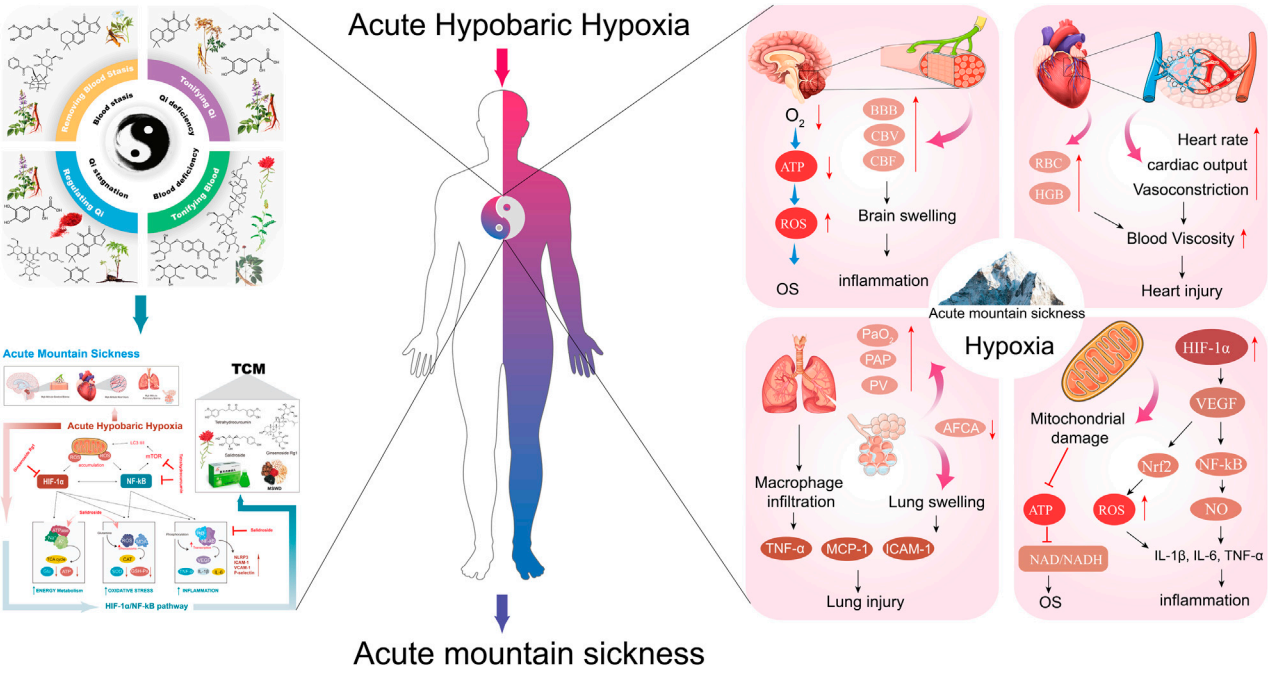

GRAPHICAL ABSTRACT

Currently, a large number of people travel from plain areas to high altitude areas for tourism, work, sports competitions and performing tasks. The incidence of AMS is closely related to altitude. According to statistics, the incidence rate of AMS in people who have not acclimated to hypobaric hypoxia is about 10%–25% after they quickly arrive at a high-altitude of 2500 m from the plains, and the symptoms are mild. The incidence rate of AMS after quickly reaching high altitude areas of 4500–5500 m is about 50%–85% and may affect mobility. In severe cases, it can cause severe altitude sickness such as HAPE and HACE (Norris et al., 2012; Garrido et al., 2021). Therefore, it is necessary to conduct in-depth research on the pathogenesis and drug treatment for AMS. The overall occurrence of AMS among participants was 73.5% (23.2% mild, 50.3% moderate–severe) (Cobb et al., 2021). Eleven of 21 volunteers had AMS and lower resting Blood oxygen saturation (SaO2) levels while ascending to high altitude (Fayazi et al., 2023).

Under acute hypobaric hypoxia, the body adapts to the external environment by changing a series of gene expressions, and hypoxia inducible factor-1 (HIF-1) is the most important transcription factor that regulates cellular adaptation to hypoxia, which plays a key role in cellular perception and acclimatation to the change of oxygen concentration (Li et al., 2020a). HIF-1 is a heterodimer consisting of two subunits: HIF-1α and HIF-1β. Under normoxia, HIF-1 was hydroxylated by oxygen and proline hydroxylase (PHD), and the hydroxylated modified HIF-1α was rapidly degraded after binding to oncoproteins, resulting in the inability of HIF-1α to be induced to be expressed (Bw et al., 2013). In hypobaric hypoxia, respiratory metabolism is enhanced, increasing reactive oxygen species (ROS) radicals in the electron transport chain complex III, which inactivates PHD, and the inactivated PHD can affect the stability of HIF-1α protein through the phosphorylation pathway (Bw et al., 2013). Additionally, under acute hypobaric hypoxia, degradation of HIF-1α is reduced, allowing it to stabilize and accumulate in the cell, where it then binds to HIF-1β and translocates to the nucleus, activating multiple downstream genes (Dzhalilova and Makarova, 2020). These genes are involved in promoting erythropoiesis (increased production of the erythropoietin EPO), increasing angiogenesis (upregulation of the vascular endothelial growth factor VEGF), and reprogramming cellular energy metabolism (increased expression of glycolytic enzymes) (Lappin and Lee, 2019). The mechanisms of HIF-1a involved in acute hypobaric hypoxia include the ROS pathway, the Toll-like receptor 4 (TLR4) signaling pathway, and the autophagy pathway (El Alam et al., 2022). Targeted inhibition on different pathways may be effective in attenuating acute hypobaric hypoxia-induced multiple tissue injuries.

With its multi-compounds and multi-target properties, traditional Chinese medicine (TCM) has been widely used as an alternative medical treatment for various diseases (Gan et al., 2023). Studies have shown that TCM has good clinical efficacy in treating AMS, and can significantly increase the levels of hemoglobin, hematocrit and antioxidant factors, and improve the ability to adapt to high altitude exposure (Li et al., 2020b). Therefore, this paper reviews the effects of acute hypobaric hypoxia on the organism, the pathogenesis of AMS, animal models of AMS, and the efficacy and mechanism of action of Chinese medicine in the treatment of AMS.

2 Methods

Literature searches were conducted through Scopus, Web of Science, PubMed, and China National Knowledge Infrastructure databases using the terms “traditional Chinese medicine,” “herbal medicine,” “acute mountain sickness,” “high-altitude pulmonary edema,” “high-altitude cerebral edema,” “acute hypobaric hypoxia,” and “high-altitude,” as well as various combinations of these keywords. We reviewed the retrieved literature for the pathogenesis of AMS and the efficacy and mechanism of action of TCM on AMS. Relevant studies on the mechanisms of AMS since the establishment of the repository up to November 2023 were selected to ensure completeness of the review and to provide support.

2.1 Inclusion criteria

1) Clinical and animal studies of TCM in relation to AMS, HAPE, HACE; 2) Studies on acute high altitude hypobaric hypoxia associated with TCM; 3) Clinical study of TCM for AMS.

2.2 Exclusion criteria

1) Studies related to simple hypoxia; 2) AMS-related questionnaire survey and Meta-analysis studies; 3) Clinical studies on non-Chinese medicine related drugs for AMS treatment.

3 The pathogenesis of AMS

3.1 Mechanisms of hemodynamic and hemorheological stress to acute hypobaric hypoxia

Under acute hypobaric hypoxia, the body will naturally increase cardiac output to ensure the supply of oxygen to vital organs, resulting in a faster heartbeat and higher blood pressure. At the same time, to increase the efficiency of oxygen transport, the red blood cells in the blood will increase, making the blood viscosity increase, leading to a decrease in the speed of blood flow, which in turn affects the delivery of oxygen (Richalet et al., 2023). The increased blood viscosity will also lead to a decrease in the deformation ability of red blood cells and impeded blood circulation. Particularly in the microvasculature, this may lead to microcirculatory disturbances that affect the supply of oxygen and nutrients to the tissues. In addition, cerebral vasodilatation occurs in hypobaric hypoxia environments to increase cerebral blood flow to compensate for the lack of oxygen, but this may lead to damage to the blood-brain barrier, resulting in elevated intracranial pressure, as shown in Figure 1. Elevated intracranial pressure, if not properly controlled, can further progress to HACE (Wilson et al., 2009; Turner et al., 2021). This increase in intracranial pressure is a key cause of major AMS symptoms such as headache, nausea, fatigue, and insomnia. In addition to this, due to the hypoxic environment, the pulmonary blood vessels also constrict, which can lead to an increase in

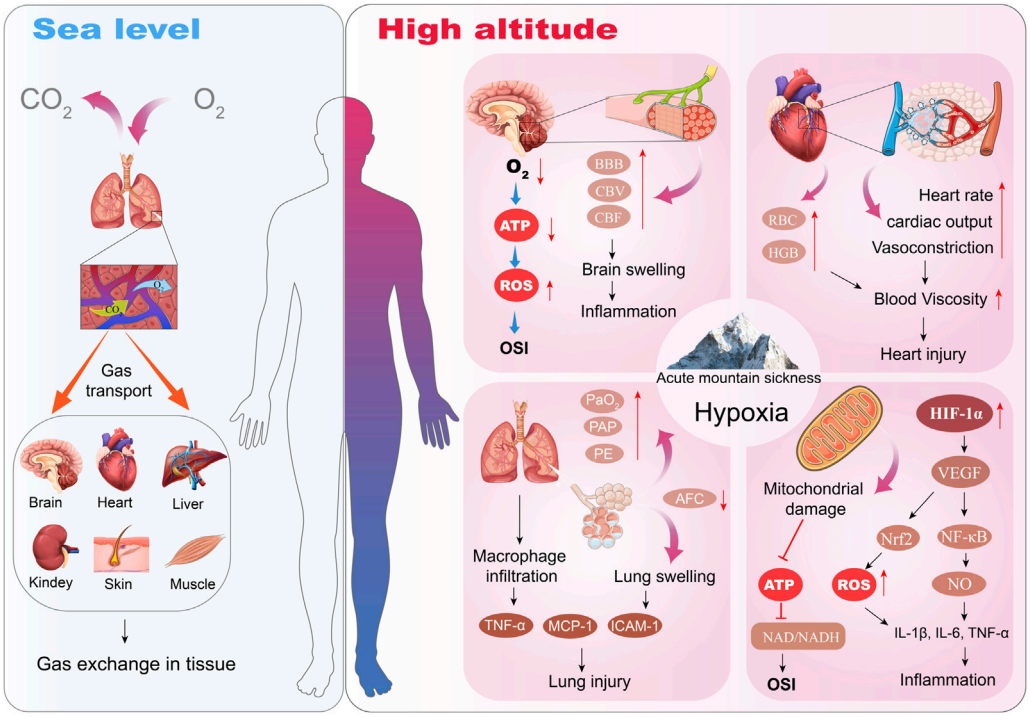

FIGURE 1
Effects of Acute Hypobaric Hypoxia in the development of AMS.

pulmonary blood pressure, and in the long term may result in the formation of HAPE (El Alam et al., 2022).

3.2 Changes in inflammatory cytokines

Hypobaric hypoxia is known to regulate inflammation (Bhattacharya et al., 2021). Inflammation is considered an important risk factor for the occurrence of AMS, and it plays a crucial role in the physiological response to hypoxia (El Alam et al., 2022; Pham et al., 2022). Hypobaric hypoxia exposure can lead to changes in the inflammatory profile (Pham et al., 2022). Studies have shown that the concentrations of pro-inflammatory cytokines and inflammatory markers such as C-reactive protein, interleukin-1β (IL-1β), IL-6, IL-17F, and CCL8 in acutely exposed individuals at high altitudes are significantly higher than at sea level, while the concentrations of the anti-inflammatory cytokine IL-10 are significantly lower than at sea level (Song et al., 2016; Liu et al., 2017). Meanwhile, in the HACE model induced by low-dose lipopolysaccharide (LPS, 0.5 mg/kg) combined with acute hypobaric hypoxia exposure (6000 m, exposure for 24 h), the level of TNF-α, IL-1β, and IL-6 in plasma and hippocampal tissue increased significantly, and the brain water content increased. These results demonstrate that hypobaric hypoxia augments LPS-induced inflammation and induces the occurrence and development of HACE in mice (Zhou et al., 2017).

In addition, Pham et al. showed that several inflammation-related genes were significantly upregulated in participants' peripheral blood after 1 day of hypobaric hypoxia exposure (3800 m), including HMGB1 (high mobility group box 1), calprotectin (S100A8), TLR4 and LY96 (Immunogenic cell death-related hub genes) (Pham et al., 2022). HMGB1 is a damage-associated molecular pattern (DAMP) molecule that amplifies immune responses during tissue damage (Pham et al., 2022). Additionally, hypobaric hypoxia can stimulate immune cells, such as macrophages and lymphocytes, to release a variety of inflammatory mediators, including tumor necrosis factor-alpha (TNF-α), IL-1, IL-6 and nitric oxide (NO), as shown in Figure 1. These inflammatory factors not only increase vascular permeability, leading to edema; they may also trigger systemic or local inflammatory responses (El Alam et al., 2022). The prolonged inflammatory response may also lead to tissue damage, further exacerbating the severity of acute mountain sickness. It has been shown that acute hypobaric hypoxia responders have higher levels of IL-1 receptor agonist (IL-1RA), heat-shock protein 70 (HSP-70), and adrenomedullin (Julian et al., 2011). In addition, macrophage inflammatory protein 1β (IL-1β) was higher in patients with acute hypobaric hypoxia response compared to the non-plateau-responsive population (Wang et al., 2018), suggesting that prevention of acute high altitude condition response may be aided by anti-inflammation. Bhattacharya et al. explored potential targets for regulating inflammation by genotyping the whole blood of Tibetan population in hypobaric hypoxia exposure areas, and proposed that enhancing PHD2 activity may be an important method to reduce inflammation caused by hypoxia (Bhattacharya et al., 2021). Therefore, inhibiting the inflammation caused by hypoxia may be used as a therapeutic strategy to reduce the occurrence of AMS disease.

3.3 Oxidative stress injury

Oxidative stress can cause an inflammatory response, and in turn, the inflammatory response itself can also trigger oxidative stress, and both promote and influence each other (Liao et al., 2023). Hypobaric hypoxia exposure-induced oxidative stress is a key pathological mechanism for AMS (Li et al., 2024). Oxidative stress injury is ubiquitous in the pathogenesis of AMS, HACE, and HAPE, and has become a hot topic of research in hypobaric hypoxic in recent years (Pena et al., 2022). Studies have shown that when exposed to acute hypobaric hypoxic (above 4500 m), the pO2 gradient decreases dramatically, and oxygen can activate the oxidative stress response by regulating the STAT3-RXR-Nrf2 signaling pathway, promoting reactive oxygen species (ROS) generation (Paul et al., 2018). Interestingly, high altitude hypoxia increases endoplasmic reticulum stress and oxidative stress (Hu et al., 2021). Whereas hypoxia-induced oxidative stress mediates endoplasmic reticulum dysfunction, which leads to the accumulation of unfolded proteins (Pena et al., 2022); this dysregulation contributes to the acceleration of multiple processes associated with hypoxic inflammatory pathways. Additionally, Himadri et al. found that rats exposed to a simulated altitude of 25,000 ft for 24 h developed HACE, with increased levels of ROS and MDA, decreased levels of SOD and GSH-Px, increased oxidative stress, and upregulation of NF-κB in brain tissues (Himadri et al., 2010). Moreover, oxidative stress and immune responses are rapidly initiated in rats under hypobaric hypoxic stress; however, with prolonged hypoxic stress, excessive oxidative stress further stimulates the immune system in the body and releases large amounts of inflammatory factors that accumulate in the body (Pu et al., 2022). This, in turn, may lead to an inflammatory storm and further damage to lung tissue resulting in AMS (Pu et al., 2022). Therefore, eliminating oxidative stress with an anti-oxidative and anti-inflammatory agent could be an important strategy to use as prophylaxis and in the treatment of AMS (Pena et al., 2020; Pena et al., 2022).

3.4 Autophagy

Hypoxia induces autophagy, which plays an important role in the protection of the body against tissue damage. Hu Y et al. found that prolonged high altitude hypoxia can lead to enhanced basal autophagy (Hu et al., 2021). Autophagy flux was increased in high altitude hypoxic environment, as evidenced by an increase in the ratio of microtubule-associated protein 1 light chain type 3 II/I (LC3-II/I) and an increase in the expression of LC3-II (Masschelein et al., 2014). In addition, Zhao Z et al. also found that prolonged exposure to high altitude hypoxia resulted in increased lung injury, formation of autophagosomes with a double-membrane structure, and increased levels of Beclin-1 and LC3-II in alveolar tissues compared with controls (Zhong et al., 2022). However, autophagy is a double activity. Acute hypobaric hypoxia may also inhibit levels of autophagy. Interestingly, using a hypoxic chamber (4000 m, 56.0 kPa, 6000 m, 47.0 kPa, and 8000 m, 36.0 kPa), Dai S et al. demonstrated that acute hypoxic exposure impaired autophagic activity in early and late stages of the mouse brain and partially contributed to hypoxia-induced oxidative stress, neuronal loss, and brain damage (Dai et al., 2024). This result confirms that enhanced autophagy activity attenuates neurological deficits after oxidative stress and exposure to hypobaric hypoxia (Dai et al., 2024). Therefore, whether to inhibit autophagy or to promote autophagy levels for the treatment of tissue damage induced by high altitude hypoxia requires an individualised comprehensive analysis.

3.5 Blood-brain barrier damage (increased cerebral vascular permeability)

The development of AMS is considered to be a multifactorial process, and blood-brain barrier (BBB) dysfunction caused by acute hypobaric hypoxia and the resulting vasogenic edema are considered to be one of the potential mechanisms. The BBB is a highly selective semipermeable membrane barrier that exists between the brain and blood and maintains homeostasis in the brain's internal environment (Neuwelt et al., 2011). The function of the BBB depends on the integrity of the neurovascular unit (NVU), which consists of endothelial cells, perivascular astrocytes, neurons, and microglia (Hourfar et al., 2023). These tight junctions between cells are essential for maintaining the integrity of the BBB and these tight junctions are regulated by several types of proteins such as intracellular occluder band-1 (ZO-1), occludin, claudins, and junctional adhesion molecules (Luo et al., 2024). Disruption of the tight junction induced by hypoxia is an important cause of BBB impairment and cerebral edema (Chen et al., 2020). Hypoxia-induced disruption of endothelial tight junctions triggers BBB injury and induces vasogenic edema (Xue et al., 2022). Studies have shown that hypoxia (1% O2 for 24 h) upregulates CAV-1 transcription through activation of NRF1 in endothelial cells, which induces internalization of claudin-5 and autophagic degradation, and accordingly, these effects lead to BBB disruption and trigger HACE (Xue et al., 2022). Moreover, hypoxia enhances lipopolysaccharide (LPS)-induced inflammatory responses and triggers HACE in mice (Zhou et al., 2017). LPS-induced systemic inflammatory responses rapidly exacerbated cerebral edema after acute hypobaric hypoxia exposure by disrupting the integrity of the blood-brain barrier and activating microglia, and by increasing water permeability through the accumulation of aquaporin-4 (AQP4) (Zhou et al., 2017). Furthermore, NB-3 (contactin-6) is a neural recognition molecule that also plays a key role in the development of HACE. Studies have shown that NB-3 is expressed in neurons and endothelial cells, and that deletion of NB-3 decreases levels of tight junction proteins, which disrupts BBB integrity and exacerbates HACE and BBB leakage (Zhou et al., 2017).

3.6 Regulation of related signaling pathways

3.6.1 Inflammatory signaling pathways

Hypobaric hypoxia also activates multiple inflammation-related signaling pathways. These include the nuclear factor-κB (NF-κB) pathway and the NOD-like receptor thermal protein domain associated protein 3 (NLRP3) pathway, which are commonly associated with stress and inflammatory responses (Jiang et al., 2022; Pu et al., 2022). NF-κB is an important intracellular

TABLE 1 Animal model construction of AMS, HACE, and HAPE.

Indication	Altitude	Ascent rate	Descent rate	Exposure time	Animal	Evaluation of indicators	Ref
AMS	5000 m	10 m/s	20 m/s	24 h	Male SD rats	SaO2 ↓, PaO2 ↓, heart Hematoxylin-eosin (HE) staining, RBC ↑, HGB ↑	Yan et al. (2022)
AMS	7000 m	10 m/s	10 m/s	7 days	Male SD rats	Heart water content ↑, heart HE staining	Shi et al. (2019)
AMS	5000 m, 6000 m	2 m/s	2 m/s	12, 24, 48 h	Male Wistar rats	PO2 ↓, brain and lung HE staining	Wang et al. (2015)
AMS	6000 m	10 m/s	20 m/s	6–12 h	Male BALB/C mice	Brain and heart HE staining	Ma et al. (2013)
AMS	7000 m	—	—	24 h	Male C57BL/6J mice	Recognition memory (discrimination ratio ↓), Open field test (total distance ↓, central distance ↓)	Wang et al. (2022)
AMS	6000 m	—	—	24 h	Male SD rats	Heart tissue HE staining	Ma et al. (2022)
AMS	6000 m	—	—	24, 48, 72 h	Male SD rats	Lung tissue HE staining	Pu et al. (2022)
AMS	8229.6 m	5 m/s	—	12 h	Male SD rats	Cerebral vascular leakage ↑, brain HE staining	Kumar et al. (2016b)
AMS	5000 m, 8000 m, 10000 m	16.67 m/s	—	5000 m and 8000 m maintained for 5 min, and 10,000 m maintained for 1 h	BALB/C mice	Survival time ↓, lactic acid ↑, lactate dehydrogenase content ↑	Ma et al. (2011)
AMS	3600 m, 5000 m	—	—	goats (3600 m); rabbits (5000 m)	goats (48 h); rabbits (4 h)	Blood Gases (SaO2 ↓, PaO2 ↓, lactic acid ↑), Brain and Lung water content ↑	Zhang et al. (2021)
HACE	6000 m	50 m/s	—	3 days	Male C57BL/6J mice	Brain water content ↑, BBB permeability ↓, brain HE staining	(Huang et al., 2015)
HACE	4000 m, 8000 m	—	—	4000 m (2days treadmill adaptation), 8000 m (3days)	Male SD rats	BBB permeability ↓, brain HE staining	(Guo et al., 2013)
HACE	7000 m	—	—	3 days	Male SD rats	Brain water content ↑, vascular leakage ↑, GSH ↓, SOD ↓, and MDA ↑	Su et al. (2021)
HACE	6000 m	50 m/s	—	6 h (LPS stimulation)	Male C57BL/6J mice	BBB integrity ↓, inflammatory factor ↑	(Geng et al., 2022)
HAPE	4700	20 m/s	—	48 h (exercise)	Male SD rats	Arterial blood gas (PaCO2 ↓, PaO2 ↓), bronchoalveolar lavage ↑, lung wet-to-dry weight ratio ↑, HE staining	(Bai et al., 2010)
HAPE	7000 m	10 m/s	—	48 h (cold)	Male SD rats	Lung water content ↑, lung HE staining, lung wet-to-dry weight ratio ↑	Yang et al. (2011)
HAPE	6000 m	10 m/s	—	72 h	Male SD rats	Lung water content ↑, lung HE staining, lung wet-to-dry weight ratio ↑	Yang et al. (2011)

Note: AMS, acute mountain sickness; BBB, blood brain barrier; GSH-PX, glutathione peroxidase; HE, Hematoxylin-eosin; HGB, hemoglobins; MDA, malondialdehyde; PaO_2, partial arterial oxygen pressure; $PaCO_2$, CO_2 partial pressure; RBC, red blood cell; SaO_2, blood oxygen saturation; SOD, Superoxide dismutase.

transcription factor that is essential for regulating inflammatory responses. Under hypobaric hypoxia conditions, NF-κB can be activated and translocated to the nucleus, activating a variety of inflammatory response genes, such as cytokines, chemokines, and adhesion molecules (Pena et al., 2020). An increase in these factors can lead to an inflammatory response in cells and tissues, promoting leukocyte infiltration and producing edema. Zeng et al. found that acute hypobaric hypoxia (6000 m, exposure for 3 days) induced a significant increase of TLR4, NLRP3, p-NF-κB p65, caspase-1 protein and gene expressions in lung tissue samples and induced acute lung injury (Zeng et al., 2024). Additionally, Jia et al. found that NLRP3, gasdermin D (GSDMD), cleaved caspase-1, and cleaved

IL-1β levels were upregulated in acute hypobaric hypoxia rats (6000 m, exposure for 3 days), suggesting that acute hypobaric hypoxia could activate the NLRP3/caspase-1 signaling pathway in heart tissue of acute hypobaric hypoxia-induced heart injury rats (Jia et al., 2023). Mechanistically, acute hypobaric hypoxia (6000 m, exposure for 3 days) aggravates oxidative stress and upregulates (pro)-inflammatory cytokines, activating NLRP3 inflammasome-mediated pyroptosis (Shen et al., 2023). Similaryly, hypobaric hypoxia (5000 m, exposure for 7 days) can induce retinal pyroptosis in rats by inducing activation of NLRP3 inflammasome and release of proinflammatory cytokines (Xin et al., 2022).

3.6.2 Hypoxia-sensing and hydrogen sulfide pathways

Cellular sensing and adaptation to changes in external oxygen concentration are important active processes in living organisms. Oxygen homeostasis is essential for the maintenance of body function. The disruption of oxygen homeostasis can lead to abnormal biological functions such as gene expression, energy metabolism, vascular regeneration, and stem cell proliferation and differentiation (Ghoneum et al., 2020). Carotid body is a sensory organ that monitors the concentration of oxygen in arterial blood. Decreased oxygen concentration in arterial blood stimulates neural activity in the carotid body, triggering reflex stimulation of respiration and blood pressure, which are essential for the maintenance of homeostasis in a hypoxia environment (Peng et al., 2023). Hydrogen sulfide (H2S) signaling is associated with hypoxic activation of carotid bodies (Peng et al., 2023). It is suggested that H2S is involved in sensing and response to hypoxia in multi-tissues that possess the ability to sense hypoxia (Wu et al., 2015). Using a hypobaric hypoxia animal model, it was demonstrated that exposure of animals to hypobaric hypoxia (7620 m, exposure for 1, 3, and 7 days) resulted in a significant decrease in H2S levels in the brain (Mishra et al., 2020). After exposure to acute hypobaric hypoxia (5260 m, for 1 day), H2S levels decreased significantly, while hypobaric hypoxia promoted glycolysis and dysregulated the pentose phosphate pathway, as well as purine catabolism, glutathione homeostasis, arginine/nitric oxide and sulfur/H2S metabolisms (D'Alessandro et al., 2016). Under hypobaric hypoxia exposure conditions (7620 m, 8% O2, for 7 days), increasing H2S levels inhibited hypobaric hypoxia-induced apoptosis in hippocampal neurons and also significantly protected glial vascular homeostasis and key neurophysiological functions (such as cerebral blood flow, functional congestion, and spatial memory) (Kumar et al., 2016a).

Mechanistically, H2S regulates intracellular O2 homeostasis and inhibits hypoxia-induced HIF-1 activation in a VHL- and mitochondria-dependent manner (Kai et al., 2012). Reduction of endogenous H2S increased pulmonary respiratory membrane permeability in HAPE rats and leads to increased protein exudation (Wang et al., 2017). This suggests that the reduction of H2S *in vivo* exacerbates the damage to lung respiratory membranes caused by acute hypobaric hypoxia. Moreover, Yang et al. found that in the early stage of exposure to acute hypobaric hypoxia, the stress of plasma H2S production was increased and pulmonary arterial pressure was elevated, suggesting that exogenous supplementation of H2S could delay acute hypobaric hypoxia-induced pulmonary arterial pressure elevation (Yang et al., 2011). Therefore, H2S can be used as a promising molecule to provide a reference for the development of AMS drugs.

4 Animal model construction of AMS, HACE, and HAPE

AMS is mainly caused by acute hypobaric hypoxia stimulation (Irarrázaval et al., 2017). Therefore, the animal model of AMS can be established in high altitude condition simulation chamber or plateau field. The model can be established by feeding in the hypobaric hypoxic chamber or animal treadmill-assisted sports training (Huo et al., 2021). Blood oxygen saturation (SaO2), blood gas, inflammatory factors, tissue water content, and pathological sections are commonly used to evaluate the success of the animal model (Wang et al., 2018; Huo et al., 2021; Peng et al., 2022).

Interestingly, some of the animal experimental conditions for high-altitude hypobaric hypoxia injury are consistent with the AMS animal model. The difference is the final detection index and evaluation method. Zeng Y et al. established an animal model of lung injury from hypobaric hypoxia in a high altitude condition, which involved exposing SD rats to hypoxia at an altitude of 6000 m, with an ascent rate of 10 m/s, and continuous exposure to hypoxia for 3 days (Zeng et al., 2024). Additionally, Zhang P et al. chose cynomolgus monkeys to establish an acute hypobaric hypoxia brain injury model, and the specific steps: altitude simulation was started at 320 m, then suspended at 3000 m, 4500 m, and 6000 m for 50 min each, and finally maintained at 7500 m for an initial 48 h, with a rate of ascent of 3 m/s (Zhang et al., 2021). Detailed AMS animal model construction methods and animal type information are shown in Table 1.

5 Traditional Chinese medicine in the treatment of AMS

5.1 Understanding AMS in traditional Chinese medicine theory

The body inhales insufficient pure air from the external high altitude conditions, which can easily lead to shortness of qi or qi deficiency in the body. In traditional Chinese medicine (TCM) theory, "qi" is an important concept, which refers to the manifestation of life activity and vitality and is one of the basic substances that make up everything in the universe. When stepping into the high altitude condition from the sea level, the body is suddenly stimulated by the cold and lack of oxygen, the body's zongqi is disordered, the spleen and stomach cannot be adequately moistened, nausea and vomiting easily. Insufficient qi in the high altitude condition results in insufficient zong qi, creating qi deficiency. Qi deficiency leads to blood stasis and insufficient blood supply to the brain, resulting in weakness and tiredness, and attacks of vertigo (Gao et al., 2023). TCM theory suggests that the etiology of this disease is a combination of qi deficiency, blood stasis, dampness stagnation, and phlegm and blood stasis obstruction (Feng et al., 2013). Most doctors believe that the cause of AMS is mainly divided into external and internal causes.

TABLE 2 The TCM pattern types of AMS and the rules of clinical application of TCM.

TCM pattern types	Therapeutic principle	TCM preparation	Compositions	Altitude (m)	Time	Treatment vs. control	Sample size (T/C)	Main clinical outcomes	Ref
Pattern of Qi deficiency	Benefiting Qi and nourishing Yin	Hongjingtian Oral-Solution (HOS)	Rhodiola rosea L. (Hongjingtian)	>3000	7 days	HOS + Dexamethasone vs. Dexamethasone	120 (60/60)	Reduced the levels of systolic pressure, diastolic pressure and Hb, and increase the level of SaO2	(Shen, 2019, p. 6)
				3600	7 days	HOS vs. Aminophylline	200 (100/100)	Increased the cure rate	Du et al. (2004)
		Taikong Yangxin Pill (TYP)	Panax ginseng C.A. Mey. (Renshen), Citrus reticulata Blanco (Chenpi), Crataegus pinnatifida Bge. (Shanzha), Acanthopanax gracilistylus W. W. Smith (Wujiapi)	3400	7 days	TYP vs. placebo	40 (20/20)	Increased the cure rate and the level of SaO2	Jiao et al. (2023)
		Huangqi Injection (HI)	Astragalus mongholicus Bunge (Huangqi)	>3000	3 days	HI vs. Routine treatment (RT)	400 (200/200)	Significantly effective (116 cases, 58.0%), effective (84 cases, 42.0%) in HI group	Xie and Guo (2004)
Pattern of blood stasis	Activating blood circulation and removing blood stasis	Compound Danshen Dripping Pill (CDDP) (复方丹参滴丸)	Salvia miltiorrhiza Bunge (Danshen), Panax notoginseng (Burkill) F.H. Chen (Sanqi), Cinnamomum camphora (L.) Presl (Bingpian)	4000	6 days	CDDP vs. placebo group	141 (71/70)	Decreased the heart rate, myocardial oxygen consumption	Li et al. (2020b)
				>3000	>2 days	CDDP + Aminophylline vs. CDDP	120 (64/56)	Reduced the incidence of AMS (25%), compare with CDDP (43%)	Ruan (2009)
		Rongshuang capsule (RC) (溶栓胶囊)	Pheretima aspergillum (E.Perrier) (Dilong)	4300	7 days	RC vs. placebo	72 (32/40)	Increased the level of SaO2	Cui et al. (2015)
		Danhong Injection (DI) (丹红注射液)	Salvia miltiorrhiza Bunge (Danshen), Carthamus tinctorius L. (Honghua)	>3000	5 days	(DI + RT) vs. RT	76 (39/37)	Increased the overall effective rate	Fang (2011)
Pattern of Qi deficiency with blood stasis	Benefiting Qi, activating blood circulation and removing blood stasis	Shengnaokang Pill (SP) (圣脑康丸)	Salvia miltiorrhiza Bunge (Danshen), Panax notoginseng (Burkill) F.H. Chen (Sanqi), Conioselinum anthriscoides (H.Boissieu) Pimenov & Kljuykov (Chuanxiong), Hirudo (Shuizhi), Codonopsis pilosula (Franch.) Nannf. (Dangshen)	4200	7 days	SP vs. placebo	41 (26/15)	Reduced heart rate; increase the level of SaO2; decreased the incidence of AMS	Tang et al. (2013)
		Danqijing granule (DQJ) (丹芪精颗粒)	Salvia miltiorrhiza Bunge (Danshen), Astragalus mongholicus Bunge (Huangqi), Polygonatum kingianum Coll.et Hemsl. (Huangjing)	>3000	7 days	DQJ vs. HJT	80 (40/40)	Reduced serum TNF-α and IL-6 levels and improve AMS clinical symptoms	Li et al. (2023a)
		Hongjingtian Capsule; Yinxingye Tablet	Rhodiola rosea L. (Hongjingtian), Ginkgo biloba L. (Yinxingye)	3650	7 days	Hongjingtian vs. Yinxingye vs. Acetazolamide	200 (67/65/68)	Increased the level of SaO2	Gongga et al. (2015)

(Continued on following page)

10.3389/fphar.2024.1393209

TABLE 2 (*Continued*) The TCM pattern types of AMS and the rules of clinical application of TCM.

TCM pattern types	Therapeutic principle	TCM preparation	Compositions	Altitude (m)	Time	Treatment vs. control	Sample size (T/C)	Main clinical outcomes	Ref
		Sankang Capsule (SK) (三康胶囊)	Astragalus mongholicus Bunge (Huangqi), Codonopsis pilosula (Franch.) Nannf. (Dangshen), Panax notoginseng (Burkill) F.H. Chen (Sanqi), Panax ginseng C.A. Mey. (Renshen), Cervus nippon Temminck (Lurong), Lycium barbarum L. (Gouqizi)	3200	15 days	SK vs. Danshen tablet	33 (18/15)	Increased the overall effective rate (83.3% in SC group; 46.7% in Danshen group)	Lin and Xiong (2008)
pattern of Qi stagnation and blood stasis	Activating Qi and activating blood circulation, resolving phlegm	Xingnaojing Injection (XNJ) (醒脑静注射液)	Moschus berezovskii Flerov (Shexiang), Cinnamomum camphora (L.) Presl (Bingpian), Curcuma wenyujin Y.H. Chen et C. Ling (Yujin), Gardenia jasminoides Ellis (Zhizi)	>3000	5 days	(XNJ + RT) vs. RT	78 (40/38)	Increased the overall effective rate	Fang (2008)
				>3000	7 days	(XNJ + RT) vs. RT	43 (21/22)	Increased the cure rate (66.7%) compare with the routine (22.7%)	Li and Qian (2011)
		Shulikang Capsule (SC) (舒理康胶囊)	Rosa rugosa Thunb. (Meiguihua), Juglans regia L. (Hetaoren), Lycium barbarum L. (Gouqizi), Rhodiola rosea L. (Hongjingtian), Prunus persica (L.) Batsch (Taohua), Astragalus mongholicus Bunge (Huangqi), Angelica sinensis (Oliv.) Diels (Danggui), Rheum palmatum L. (Dahuang)	3900	7 days	SC vs. placebo group	150 (50/50)	Slow the rapid heart rate, reduced the basal metabolic rate and the incidence of AMS	Niu et al., 2006b; 2006a
				>3000	15 days	SC vs. Compound Dangshen Tablet (CDT)	330 (180/150)	Total effective rate: 83.3% in SC group, 46.7% in CDT group	Lin et al. (2008)
	Benefiting Qi and protecting the heart	Shexiang Baoxin Pill (SBP)麝香保心丸	Moschus berezovskii Flerov (Shexiang), Panax ginseng C.A. Mey. (Renshen), *Bos taurus* domesticus Gmelin (Niuhuang), Cinnamomum cassia Presl (Rougui), Liquidambar orientalis Mill. (Suhexiang), *Bufo bufo* gargarizans Cantor (Chansu), Cinnamomum camphora (L.) Presl (Bingpian)	4200	4 days	SBP vs. Control	66 (26/40)	Improved headaches, panic attacks, chest tightness and shortness of breath	Yu et al. (2011)
Pattern of Qi and blood deficiency	Benefiting Qi, activating blood circulation, nourishing Yin	Compound Dangshen Capsule (CDC) (复方党参胶囊)	Codonopsis pilosula (Franch.) Nannf. (Dangshen), Glehnia littoralis Fr. Schmidtex Miq. (Beishashen), Salvia miltiorrhiza Bunge (Danshen)	5200	15 days	CDC vs. placebo	45 (30/15)	Decreased the AMS rate, improve lung ventilation function and finger motor ability	Zhang et al. (2010)
					7 days	CDC vs. placebo	45 (18/14)	Relieved headache and vomiting caused by altitude hypoxia	Zhang et al. (2005)
		Compound Dangshen Tablet (CDT) (复方党参片)	Codonopsis pilosula (Franch.) Nannf. (Dangshen), Panax quinquefolium L. (Xiyangshen),	>3000	7 days	CDT vs. RT	80 (40/40)	Total effective rate: 97.5% in CDT group, 65.0% in RT group	Li (2016)

(Continued on following page)

10.3389/fphar.2024.1393209

TABLE 2 (*Continued*) The TCM pattern types of AMS and the rules of clinical application of TCM.

TCM pattern types	Therapeutic principle	TCM preparation	Compositions	Altitude (m)	Time	Treatment vs. control	Sample size (T/C)	Main clinical outcomes	Ref
			Angelica sinensis (Oliv.) Diels (Danggui), Salvia miltiorrhiza Bunge (Danshen), Glehnia littoralis Fr. Schmidtex Miq. (Beishashen)						
Pattern of Qi deficiency and damp heat	Clearing heat and removing dampness, benefiting Qi for activating blood circulation	Gaoyuanan Capsule (GC)(高原安胶囊)	Panax quinquefolium L. (Xiyangshen), Astragalus mongholicus Bunge (Huangqi), Rhodiola rosea L. (Hongjingtian)	3700–4300	5 days	GC vs. placebo	50 (25/25)	Increased the level of SaO2	Cui et al. (2014)
Pattern of hyperactivity of liver-Yang	Suppressing hyperactive liver for calming endogenous wind, activating blood circulation and removing blood stasis	Xifengzhitong granule (XFZT) (息风止痛颗粒)	Uncaria macrophylla Wall. (Gouteng), Scorpio (Quanxie), Conioselinum anthriscoides (H.Boissieu) Pimenov & Kljuykov (Chuanxiong), Astragalus mongholicus Bunge (Huangqi)	4300	15 days	XFZT vs. placebo	118 (38/40)	Improved flustered, headache, and short breath	Cui et al. (2014)
N/A	N/A	Yinxingye Tablet	Ginkgo biloba L. (Yinxingye)	3696	3 days	Yinxingye vs. Acetazolamide vs. placebo	36 (12/12/12)	Reduced the rate of AMS, compare with the acetazolamide (36%)	Moraga et al. (2007)
N/A	N/A	EGb 761 Tablet	Ginko biloba L. extract (EGb 761)	5400	Twice a day	EGb 761 vs. placebo	44 (22/22)	Reduced the rate of AMS (13.6%), compare with the placebo (81.8%)	Roncin et al. (1996)
N/A	N/A	Acupuncture and moxibustion	Acupoints of Baihui, Zusanli, Qihai, Neiguan, and Zhongwan	3836	5 or 10 days	Acupuncture and moxibustion	56 (56/0)	Cured: 51 cases (91%); effective: 5 cases (9%)	Wang (1994)

Note: AMS, acute mountain sickness; CDC, compound dangshen capsule; CDDP, compound danshen dripping pill; CDT, compound dangshen tablet; DI, danhong injection; DQJ, danqijing granule; GC, gaoyuanan capsule; HI, huangqi injection; HOS, Hongjingtian oral-solution; RC, rongshuang capsule; SaO_2, blood oxygen saturation; SBP, shexiang baoxin pill; SC, shulikang capsule; SK, sankang capsule; SP, shengnaokang pill; TYP, taikong yangxin pill; XFZT, xifengzhitong granule; XNJ, Xingnaojing Injection.

10.3389/fphar.2024.1393209

TABLE 3 The information of top 10 botanical drugs with a relatively high frequency.

No.	Botanical drugs name	Latin name	Role in TCM	Flavor	Pharmacological effect	Frequency
1	Danshen	SALVIAE MILTIORRHIZAE RADIX ET RHIZOMA	Activating blood and removing stasis	Bitter	cardio-protector (Cheng, 2007)	6
2	Huangqi	ASTRAGALI RADIX	Invigorating Qi	Sweet	cardiovascular protective, immune modulatory (Chen et al., 2020; Su et al., 2021)	5
3	Dangshen	CODONOPSIS RADIX	Invigorating Qi	Sweet	anti-inflammatory, anti-tumor (Bailly, 2021; Yu et al., 2023)	4
4	Hongjingtian	RHODIOLAE CRENULATAE RADIX ET RHIZOMA	Invigorating Qi	Sweet	anti-aging, anti-hypobaric hypoxic (Zhuang et al., 2019; Hou et al., 2024)	3
5	Sanqi	NOTOGINSENG RADIX ET RHIZOMA	Hemostasis	Sweet; Bitter	inhibiting platelet aggregation (Liu et al., 2018b)	3
6	Bingpian	BORNEOLUM	Inducing resuscitation	Pungent; Bitter	neuroprotective effect and antipruritic effect (Ma et al., 2023; Luo et al., 2024)	3
7	Renshen	GINSENG RADIX ET RHIZOMA	Invigorating Qi	Sweet; Bitter	neuroprotective effect, improving markers related to blood glucose, blood pressure, and blood lipids (Chen et al., 2022; Park et al., 2022)	3
8	Beishashen	GLEHNIAE RADIX	Invigorating Qi, Nourishing Yin	Sweet; Bitter	anti-inflammatory, antioxidant, immunomodulatory (Li et al., 2023b)	2
9	Danggui	ANGELICAE SINENSIS RADIX	Blood tonification	Sweet	antifibrotic effect, anti-tumor, hematopoiesis (Qian et al., 2020)	2
10	Gouqizi	LYCII FRUCTUS	Nourishing Yin	Sweet	anti-oxidative stress and inflammatory effects (Zheng et al., 2023)	2

Note: The role in TCM, and flavors of botanical drugs are defined according to the 2020 edition of the Chinese Pharmacopoeia (Chinese Pharmacopoeia Commission Pharmacopoeia of the People's Republic of China, 2020).

The external causes are caused by the terrestrial qi and the celestial qi, which include lack of pure air, severe cold, and dry climate in the altitude. The internal causes are caused by the deficiency of qi in the human body (Zhang and Zhang, 1993; Li et al., 2012; Feng et al., 2013).

5.2 Understanding AMS in Tibetan medicine's theory

Although the concept of altitude diseases is not explicitly mentioned in the ancient books of Tibetan medicine, Tibetan medicine itself comes from the actual life of altitude people, so its essence is altitude medicine. Tibetan medicine is a great medical system formed by the people in the high-altitude hypoxia region in the struggle against various diseases and harsh natural environments (Liu et al., 2018a).

According to Tibetan medical theory and "Four Tantras"《四部医典》, there are three major factors in the human body ("Dragon", "Chiba", "Pegan"), seven major material bases (dietary essence, blood, meat, fat, bone, bone marrow, sperm), and three excretions (stool, urine, sweat), and the three major factors govern the movement of the seven major material bases and the three excretions (Zhong et al., 2022). The most essential cause of AMS is three major factors and seven major material dysfunctions (Zhang and Zhang, 1993; Feng et al., 2013).

5.3 Different TCM pattern types of AMS and the rules of clinical application of TCM

According to the theory of TCM and the principle of pattern differentiation and treatment, the main TCM pattern types of AMS are a pattern of Qi deficiency with blood stasis, and the main principle of treatment is activating Qi, activating blood circulation, and resolving phlegm (Feng et al., 2013; Wu et al., 2023). The clinical applications of TCM are based on compound danshen dripping pill (复方丹参滴丸), huangqi injection (黄芪注射液), shulikang capsule (舒理康胶囊), duoxuekang capsule (多血康胶囊), and xuefu zhuyu decoction (血府逐瘀汤). Commonly used botanical drugs are mainly Astragalus mongholicus Bunge (Huangqi), Salvia miltiorrhiza Bunge (Danshen), Panax ginseng C.A. Mey. (Renshen), and Rhodiola rosea L. (Hongjingtian). The TCM pattern types of AMS and the application of TCM are shown in Table 2.

In addition, the clinical evidence of TCM for several typical AMS is summarized in Table 2. A total of 18 representative TCMs, including 6 capsules, 3 injections, 3 pills, 2 tablets, 2 granules, 1 oral solution, and 1 acupuncture were compiled and summarized. TCM formulas can improve exercise tolerance and quality of life and relieve clinical symptoms. This provides a reference and basis for clinical use and further pharmacological studies based on the results of the analysis of TCM pattern types and TCM application in AMS.

TABLE 4 Mechanism of the effect of TCMs for AMS.

Type	Altitude	TCM	Compositions	Experimental model	Dose/kg andday	Hypoxic time	Pharmaceutical effects	Ref
Chinese patent drug	5000 m	Compound Danshen Dripping Pill (复方丹参滴丸)	Salvia miltiorrhiza Bunge (Danshen), Panax notoginseng (Burkill) F.H. Chen (Sanqi), Cinnamomum camphora (L.) Presl (Bingpian)	SD rat	72.9 mg/kg/d (i.g.)	7 days	Promoted high altitude acclimatization of rat by improving blood oxygen saturation, reduce myocardial enzymes and restore metabolic level	Yan et al. (2022)
Chinese patent drug	6000 m	Hongjingtian Capsule	Chinese medicine preparation	SD rat	0.63, 1.26, 2.52 g/kg/d (i.g.)	7 days	Ameliorated heart injury and decreased the heart levels of TNF, VEGFA and HIF-1α in acute hypoxia-induced rats	Ma et al. (2022)
Chinese patent drug	N/A	Dazhu Hongjingtian Capsule (大株红景天胶囊)	commercial product, Chinese medicine preparation composed of R. kirilowii (Regel) Maxim	UPLC/Q-TOF-MS/MS, network pharmacology	N/A	N/A	Regulate the inflammation pathway, apoptosis pathway, and HIF-1 signaling pathway	Ou et al. (2020)
botanical drugs	8000 m 10000 m	Saussurea involucrata (Kar. et Kir.) Sch.-Bip	Extract	BALB/C mice	12.5, 25, 50 mg/kg	20 min	Decreased the mortality of animals under acute decompression conditions, improve the changes in biochemical indicators for glycometabolism and energy metabolism	Ma et al. (2011)
botanical drugs	6000 m	Rhodiola crenulata	Extract	SD rats	0.63, 1.26, 2.52 g/kg/d (i.g.)	1 day	Ameliorated heart injury and decreased the heart levels of TNF, VEGFA and HIF-1α	Ma et al. (2022)
botanical drugs	8229.6 m	Terminalia arjuna	bark extract	SD rats	150 mg/kg (p.o.)	12 h	Prevented cerebral vascular leakage, attenuated oxidative stress	Kumar et al. (2016b)

Note: HIF-1α, Hypoxia-inducible factor-1α; TNF, Tumor necrosis factor.

5.4 Frequency of commonly used Chinese botanical drugs from clinical TCM formulas

According to the data in Table 2, among a total of 33 botanical drugs used clinically, and the top 10 botanical drugs ranked by their relatively high frequency of use are shown in Table 3. Table 3 shows that the most frequently used botanical drugs were Salvia miltiorrhiza Bunge (Danshen). The type of botanical drugs is mainly invigorating qi (huangqi, dangshen, hongjingtian, renshen), activating blood and removing stasis (danshen, chuanxiong) and nourishing Yin (Beishashen, Gouqizi), as shown in Supplementary Table S1. The properties of botanical drugs are mainly warm, calm, and cold. The flavor of botanical drugs is mainly sweet, bitter, and pungent. Specific botanical drugs information is shown in Table 3.

5.5 Mechanism of the effect of TCM for AMS

While many other TCM therapies, such as acupuncture and bloodletting, are effective in clinical applications for tissue damage caused by hypobaric hypoxia (Wang et al., 2022; Li et al., 2023a), this review focuses only on herbal treatments. Classical prescriptions or TCM formulas, as the main means of clinical treatment in modern TCM, are an important breakthrough point for the inheritance and innovative development of TCM (Xu et al., 2023). Currently, research on TCM formulas for the treatment of AMS is mainly based on the compound danshen drip pills (CDDP) (Yan et al., 2022). Several studies have confirmed that CDDP prevents hypobaric hypoxia induced tissue damage by reducing erythrocyte aggregation and hemorheology and promoting the expression of AQP1 and Nrf2 (Hu et al., 2021). Moreover, Fu et al. found that qi-long-tian formula extract attenuated the inflammatory response in AMS model rats (6000 m, exposed to a Fenglei hypobaric hypoxic chamber for 72 h) by inhibiting HIF-1a, VEGF, suppressing the expression of inflammation-associated effectors (MMP9 and TIMP1), inhibiting the expression of target genes downstream of IL-17 (Ccl2, MMP9, S100a9, and S100a8), and attenuating lung injury and immune cell infiltration (Fu et al., 2021). Our team also demonstrated that modified siwu decoction has a favorable protective effect against hypobaric hypoxia by down-regulating proteins associated with oxidative stress and the ubiquitin-proteasome system ((Superoxide dismutase 1, SOD1), (Catalase, CAT), GSTP1 and PRDX1), as well as by ameliorating hypoxia-induced upregulation of MDA and disturbances in energy and lipid metabolism (Tu et al., 2023). Meanwhile, Zeng Y et al. found that Huangqi Baihe Granules could significantly enhance lung function, reduce lung wet/dry ratio, alleviate lung tissue injury,

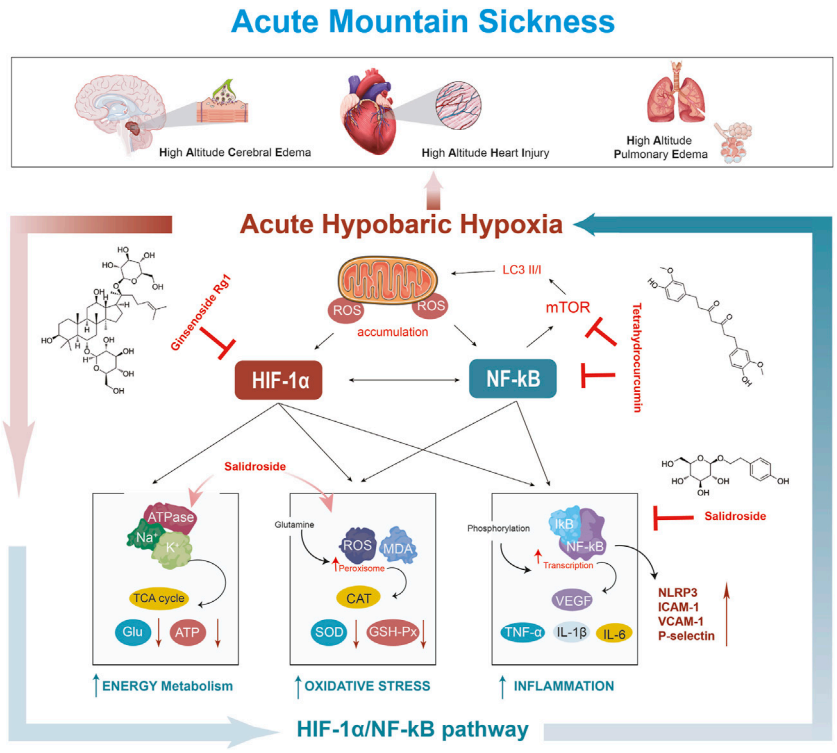

FIGURE 2
Mechanism of TCM on AMS.

inhibit the formation of ROS and MDA, and increase SOD activity and GSH expression, and its mechanism of action may be to inhibit the activation of TLR4/NF-κB p65/NLPR3 signaling pathway and reduce the release of downstream pro-inflammatory cytokines in lung tissue (Zeng et al., 2024).

In addition, studies on single TCMs for the treatment of AMS are mainly based on Rhodiola rosea L. (Hongjingtian), and it has been reported that chemical components salidroside can coordinate metabolic reprogramming by modulating the HIF-1α signaling pathway in AMS (Yan et al., 2021). Xie et al. found that Rhodiola rosea L. extract significantly increased SOD, GSH-Px, T-AO, and Na + -K + -ATPcase levels, decreased NF-α, IL-1β, IL-6, MDA, and LDH levels, and inhibited the NF-κB/NLRP3 signaling pathway, which further corrected the imbalance in energy metabolism and maintained the integrity of the BBB, thereby alleviates hypobaric hypoxia-induced brain injury (8000 m, exposed to a FLYDWC50-II C Fenglei hypobaric hypoxic chamber for 48 h) (Xie et al., 2022). Salidroside (Sal), the active chemical components of Rhodiola rosea L., has been reported to have potential protective effects against tissue damage caused by acute hypobaric hypoxia. Studies have shown that Sal attenuates acute hypobaric hypoxia-induced brain oxidative stress injury, inflammatory response, and BBB damage (Hou et al., 2024). Mechanically, Sal reduced the levels of ROS and MDA and the levels of TNF-α, IL-1β, and IL-6, and increased the activities of SOD and GSH-Px, thereby attenuating hypobaric hypoxia-induced pathological injury and oxidative stress (Jiang et al., 2022). In addition, Sal partially promoted energy metabolism and increased the activities of Na + -K + -ATPase and Ca2+-Mg2+-ATPase. The mechanism of action is related to inhibition of the NF-κB/NLRP3 pathway (Jiang et al., 2022).

Our team's previous study found that polysaccharide extracted from Potentilla anserina L could inhibit oxidative stress and inflammatory responses to treat and prevent HACE and HAPE, and its mechanism of action may be to block the activation of the NF-κB and HIF-1α signaling pathways, which inhibits the production of downstream pro-inflammatory cytokines (IL-1β, IL-6, TNF-α, and VEGF) (Shi et al., 2019; Shi et al., 2019). Meanwhile, Pan Y et al. showed that tetrahydrocurcumin significantly reduced the expression of VEGF (AMS biomarker), MMP-9 and NF-κB, and effectively attenuated cerebral edema and inflammation induced by acute high-altitude hypobaric hypoxia (Pan et al., 2020; Nourkami-Tutdibi et al., 2023). Moreover, Zha et al. established an animal model of AMS (6000 m, 10 m/s rate of ascent, continuous exposure to hypoxia for 24 h) and found that ginsenoside Rg1 reduced the wet-to-dry ratio of lung tissues, improved the pathological changes of lung tissues, decreased the MDA content and NOS viability, elevated the CAT and Na + -K + -ATPase viability, and decreased the IL-6 and TNF-α levels (Arriaza et al., 2022). As the main active chemical component of Panax notoginseng saponins, notoginsenoside R1 attenuated inflammation and oxidative stress, reduced lung dry-to-wet ratio, alleviated the lung tissue damage, and ameliorated arterial blood gas changes in acute hypobaric hypoxia-induced HAPE rats (6000 m, exposed to a ProOx-830 hypobaric hypoxic chamber for 48 h), and its mechanism of action may be that notoginsenoside R1 promoted the activation of the ERK1/2-P90rsk-BAD signaling pathway (Pei et al., 2023). Details of TCM formulas, the specific simple botanical

drugs, active components, modes of administration, experimental models, mimic altitudes, dosages, and pharmaceutical effects are shown in Table 4. The mechanism of action of TCM intervention for AMS is shown in Figure 2.

6 Scientific problems and considerations

AMS is a typical high altitude condition-specific hypoxic illness with a quick onset and progression. Even though fundamental and clinical research on AMS has advanced significantly, numerous scientific issues still need to be resolved. 1) Initial diagnosis of AMS is difficult and there is a lack of targeted treatment. Acetazolamide is currently the main drug used to treat AMS, but blind use of acetazolamide without a clear diagnosis of the disease can often lead to side effects. 2) The effects of different altitudes on the function of multiple tissues and organs of the body remain elusive. Studies have shown that different altitudes directly affect hepatic perfusion, with hepatic arterial perfusion increasing with altitude (Shi, 2011). 3) The basic experimental models of AMS are mainly animal-based, and the index parameters of model construction success are still not unified, so it is not possible to judge the success rate of the model effectively and quickly. In addition, animal experiments are time-consuming, so there is a need for cellular models for drug screening to facilitate rapid and effective drug screening.

7 Conclusion and perspectives

With the rapid development of tourism and mountaineering in the plateau and the construction of the plateau economy, more and more people from the plains will enter the high altitude conditions, which can cause AMS if no precautions are taken. This raises important questions about how to effectively prevent and treat AMS. Due to its multi-component, multi-target and multi-pathway action characteristics, TCM can better respond to the multi-system dysfunction caused by the complex hypobaric hypoxia environment. At the same time, TCM has long-term experience in human use, has better clinical safety, lower toxicity and side effects, and is often used in combination with chemical medicine to achieve synergistic effect. In addition, the research of TCM with both medicinal and edible values in the prevention and treatment of AMS diseases has also attracted much attention, such as Rhodiola rosea L., Tibetan Brassica rapa L., Tibetan Hippophae rhamnoides L. (HIPPOPHAE FRUCTUS) and so on. In the future, this will remain a hot spot in the research of TCM against AMS disease. According to TCM theory and practice, the etiology and pathogenesis of AMS are mainly "qi deficiency and blood stasis" and "qi stagnation and blood stasis". TCM for treating AMS is based on "invigorating qi botanical drugs" and "botanical drugs for activating blood circulation and removing blood stasis". At present, there is some efficacy in TCM formulas, active chemical components, and botanical drugs extracts in the treatment of AMS, and there is some research on the mechanism of action of related chemical components. Compound danshen dripping pill, Huangqi Baihe granules, salidroside, ginsenoside Rg1 and tetrahydrocurcumin have better ability in anti-AMS. These chemical components generally exert anti-AMS pharmacological effects by inhibiting the expression of VEGF (AMS marker), MDA, and pro-inflammatory factors (TNF-α, IL-1β, and IL-6), down-regulating NF-κB/NLRP3 pathway, and promoting SOD and Na + -K + -ATPase activities, which attenuates acute hypobaric hypoxia-induced tissue injury. This review focuses on the relationship between AMS and hemodynamic and hemorheological stress, changes in cytokines and inflammatory cytokines, regulation of related signaling pathways, blood-brain barrier damage, oxidative stress injury, autophagy, and summarises the establishment of AMS animal model methods. Although TCM has the potential to regulate AMS caused by hypobaric hypoxia, many studies still have some limitations. 1) The effective dose, maximum tolerated intake, and taking time for clinical treatment of TCM formulas are still uncertain. 2) In single-dose studies of TCM formula extracts or crude drugs, the pharmacological effects are still controversial. 3) As for the chemical components of TCM, except for in-depth research on components such as salidroside and ginsenoside, there are few studies on other effective chemical components of TCM. Subsequent screening and comparison of the anti-hypoxic activity of TCM chemical components is needed. 4) Due to the multi-component and multi-target characteristics of TCM, the research on TCM against acute hypobaric hypoxia in recent years has remained at the level of animal experiments, with few clinical studies. 5) There has been limited progress in translating research results into clinical applications. Future efforts should focus on exploring clinical treatment methods using TCM chemical components (salidroside, ginsenoside, etc.), such as exploring new drug delivery methods, which can improve drug targeting, stability, bioavailability, and exert its biological activity. In conclusion, this review summarizes the potential of TCM to treat AMS, but its specific mechanisms deserve further study. The solution to this problem will be beneficial to the long-term development of TCM in the treatment of body damage diseases induced by hypobaric hypoxia.

Author contributions

ZW: Writing–original draft, Writing–review and editing. YW: Funding acquisition, Writing–original draft, Writing–review and editing. RG: Investigation, Writing–original draft. JC: Conceptualization, Formal Analysis, Writing–original draft. YC: Data curation, Software, Writing–original draft. ML: Formal Analysis, Supervision, Writing–original draft. YG: Supervision, Writing–review and editing.

Funding

The author(s) declare that financial support was received for the research, authorship, and/or publication of this article. This work was supported by the Innovation Team and Talents Cultivation Program of National Administration of Traditional Chinese Medicine (ZYYCXTD-D-202207), the National Natural Science Foundation of China (82204774).

Conflict of interest

The authors declare that the research was conducted in the absence of any commercial or financial relationships that could be construed as a potential conflict of interest.

Publisher's note

All claims expressed in this article are solely those of the authors and do not necessarily represent those of their affiliated organizations, or those of the publisher, the editors and the reviewers. Any product that may be evaluated in this article, or claim that may be made by its manufacturer, is not guaranteed or endorsed by the publisher.

Supplementary material

The Supplementary Material for this article can be found online at: https://www.frontiersin.org/articles/10.3389/fphar.2024.1393209/full#supplementary-material

References

Arriaza, K., Cuevas, C., Pena, E., Siques, P., and Brito, J. (2022). Impact of zinc on oxidative signaling pathways in the development of pulmonary vasoconstriction induced by hypobaric hypoxia. *Int. J. Mol. Sci.* 23, 6974. doi:10.3390/ijms23136974

Bai, C., She, J., Goolaerts, A., Song, Y., Shen, C., Shen, J., et al. (2010). Stress failure plays a major role in the development of high-altitude pulmonary oedema in rats. *Eur. Respir. J.* 35, 584–591. doi:10.1183/09031936.00001709

Bailly, C. (2021). Anticancer properties of lobetyolin, an essential component of radix codonopsis (dangshen). *Nat. Prod. Bioprospect* 11, 143–153. doi:10.1007/s13659-020-00283-9

Bhattacharya, S., Shrimali, N. M., Mohammad, G., Koul, P. A., Prchal, J. T., and Guchhait, P. (2021). Gain-of-function Tibetan PHD2D4E;C127S variant suppresses monocyte function: a lesson in inflammatory response to inspired hypoxia. *EBioMedicine* 68, 103418. doi:10.1016/j.ebiom.2021.103418

Burtscher, J., Swenson, E. R., Hackett, P. H., Millet, G. P., and Burtscher, M. (2023). Flying to high-altitude destinations: is the risk of acute mountain sickness greater? *J. Travel Med.* 30, taad011. doi:10.1093/jtm/taad011

Bw, W., A, K., U, B., and P, C. (2013). Emerging novel functions of the oxygen-sensing prolyl hydroxylase domain enzymes. *Trends Biochem. Sci.* 38, 3–11. doi:10.1016/j.tibs.2012.10.004

Chen, Y. Y., Liu, Q. P., An, P., Jia, M., Luan, X., Tang, J. Y., et al. (2022). Ginsenoside Rd: a promising natural neuroprotective agent. *Phytomedicine* 95, 153883. doi:10.1016/j.phymed.2021.153883

Chen, Z., Liu, L., Gao, C., Chen, W., Vong, C. T., Yao, P., et al. (2020). Astragali Radix (Huangqi): a promising edible immunomodulatory herbal medicine. *J. Ethnopharmacol.* 258, 112895. doi:10.1016/j.jep.2020.112895

Cheng, T. O. (2007). Cardiovascular effects of danshen. *Int. J. Cardiol.* 121, 9–22. doi:10.1016/j.ijcard.2007.01.004

Chinese Pharmacopoeia Commission Pharmacopoeia of the People's Republic of China (2020) *Chinese Pharmacopoeia commission Pharmacopoeia of the People's Republic of China*, 1. Beijing: People's Medical Publishing House.

Cobb, A. B., Levett, D. Z. H., Mitchell, K., Aveling, W., Hurlbut, D., Gilbert-Kawai, E., et al. (2021). Physiological responses during ascent to high altitude and the incidence of acute mountain sickness. *Physiol. Rep.* 9, e14809. doi:10.14814/phy2.14809

Cui, J., Wu, P., Wang, F., Zhang, Y., Li, Q., Liu, Y., et al. (2014). Clinical observation of Xifengzhitong granule on Acute Mountain sickness. *J. High Alt. Med.* 24, 8–11.

Cui, J., Zhang, Y., Li, Q., Wu, P., Wang, F., and Li, B. (2015). Effect of thrombolytic capsule on prevention and treatment of Acute Mountain sickness. *Med. J. Natl. Defending Forces Southwest China* 25, 662–665. doi:10.3969/j.issn.1004-0188.2015.06.033

Dai, S., Feng, Y., Lu, C., Zhang, H., Ma, W., Xie, W., et al. (2024). Impairment of autophagic flux after hypobaric hypoxia potentiates oxidative stress and cognitive function disturbances in mice. *Neurosci. Bull.* 40, 35–49. doi:10.1007/s12264-023-01099-6

D'Alessandro, A., Nemkov, T., Sun, K., Liu, H., Song, A., Monte, A. A., et al. (2016). AltitudeOmics: red blood cell metabolic adaptation to high altitude hypoxia. *J. Proteome Res.* 15, 3883–3895. doi:10.1021/acs.jproteome.6b00733

Du, S., Miao, S., and Wang, K. (2004). Clinical efficacy analysis of Rhodiola rosea in the treatment of Acute Mountain sickness. *Med. J. Natl. Defending Forces Southwest China* 14, 615–616.

Dzhalilova, D., and Makarova, O. (2020). Differences in tolerance to hypoxia: physiological, biochemical, and molecular-biological characteristics. *Biomedicines* 8, 428. doi:10.3390/biomedicines8100428

El Alam, S., Pena, E., Aguilera, D., Siques, P., and Brito, J. (2022). Inflammation in pulmonary hypertension and edema induced by hypobaric hypoxia exposure. *Int. J. Mol. Sci.* 23, 12656. doi:10.3390/ijms232012656

Fang, Y. (2008). Study on the curative effect of xingnaojing injection for Acute Mountain sickness. *Sichuan Med. J.* 24, 853–854. doi:10.3969/j.issn.1004-0501.2008.07.023

Fang, Y. (2011). Clinical effictive observation of Danhong injection in treating Acute Mountain sickness. *J. Mod. Med. Health* 27, 2909–2910.

Fayazi, B., Tadibi, V., and Ranjbar, K. (2023). The role of hypoxia related hormones responses in acute mountain sickness susceptibility individuals unaccustomed to high altitude. *PLoS One* 18, e0292173. doi:10.1371/journal.pone.0292173

Feng, B., Liu, Z., Xing, Y., Gao, A., Huang, J., Zhu, H., et al. (2013). Traditional Chinese medical recognition on mountain sickness. *China J. Traditional Chin. Med. Pharm.* 28, 3475–3479.

Fu, X., Yang, C., Chen, B., Zeng, K., Chen, S., and Fu, Y. (2021). Qi-Long-Tian formula extract alleviates symptoms of acute high-altitude diseases via suppressing the inflammation responses in rat. *Respir. Res.* 22, 52. doi:10.1186/s12931-021-01645-8

Gan, X., Shu, Z., Wang, X., Yan, D., Li, J., Ofaim, S., et al. (2023). Network medicine framework reveals generic herb-symptom effectiveness of traditional Chinese medicine. *Sci. Adv.* 9, eadh0215. doi:10.1126/sciadv.adh0215

Gao, J., Zhang, Z., Yan, J., Ge, Y., Ma, Z., and Gao, Y. (2023). Evaluation of animal models of high altitude qi deficiency and blood stasis syndrome and research progress in therapeutic drugs. *Chin. J. Pharmacovigil.* 20, 1189–1194. doi:10.19803/j.1672-8629.20230120

Garrido, E., Botella de Maglia, J., and Castillo, O. (2021). Acute, subacute and chronic mountain sickness. *Rev. Clin. Esp.* 221, 481–490. doi:10.1016/j.rce.2019.12.013

Geng, Y., Yang, J., Cheng, X., Han, Y., Yan, F., Wang, C., et al. (2022). A bioactive gypenoside (GP-14) alleviates neuroinflammation and blood brain barrier (BBB) disruption by inhibiting the NF-κB signaling pathway in a mouse high-altitude cerebral edema (HACE) model. *Int. Immunopharmacol.* 107, 108675. doi:10.1016/j.intimp.2022.108675

Ghoneum, A., Abdulfattah, A. Y., Warren, B. O., Shu, J., and Said, N. (2020). Redox homeostasis and metabolism in cancer: a complex mechanism and potential targeted therapeutics. *Int. J. Mol. Sci.* 21, 3100. doi:10.3390/ijms21093100

Gongga, L., Ciren, W., Suolang, Y., Baima, D., and Duoji, Z. (2015). Clinical observation of Rhodiola rosea in the treatment of Acute Mountain sickness. *China Pharm.* 26, 2818–2820.

Guo, P., Luo, H., Fan, Y., Luo, Y., and Zhou, Q. (2013). Establishment and evaluation of an experimental animal model of high altitude cerebral edema. *Neurosci. Lett.* 547, 82–86. doi:10.1016/j.neulet.2013.05.008

Himadri, P., Kumari, S. S., Chitharanjan, M., and Dhananjay, S. (2010). Role of oxidative stress and inflammation in hypoxia-induced cerebral edema: a molecular approach. *High Alt. Med. Biol.* 11, 231–244. doi:10.1089/ham.2009.1057

Hou, Y., Fan, F., Xie, N., Zhang, Y., Wang, X., and Meng, X. (2024). Rhodiola crenulata alleviates hypobaric hypoxia-induced brain injury by maintaining BBB integrity and balancing energy metabolism dysfunction. *Phytomedicine* 128, 155529. doi:10.1016/j.phymed.2024.155529

Hourfar, H., Aliakbari, F., Aqdam, S. R., Nayeri, Z., Bardania, H., Otzen, D. E., et al. (2023). The impact of α-synuclein aggregates on blood-brain barrier integrity in the presence of neurovascular unit cells. *Int. J. Biol. Macromol.* 229, 305–320. doi:10.1016/j.ijbiomac.2022.12.134

Hu, Y., Sun, J., Wang, T., Wang, H., Zhao, C., Wang, W., et al. (2021). Compound Danshen Dripping Pill inhibits high altitude-induced hypoxic damage by suppressing oxidative stress and inflammatory responses. *Pharm. Bio* 59, 1585–1593. doi:10.1080/13880209.2021.1998139

Huang, X., Zhou, Y., Zhao, T., Han, X., Qiao, M., Ding, X., et al. (2015). A method for establishing the high-altitude cerebral edema (HACE) model by acute hypobaric hypoxia in adult mice. *J. Neurosci. Methods* 245, 178–181. doi:10.1016/j.jneumeth.2015.02.004

Huo, Y., Zhao, A., Li, X., Li, J., and Wang, R. (2021). Animal models of acute plateau disease. *Chin. Pharmacol. Bull.* 37, 26–30. doi:10.3969/j.issn.1001-1978.2021.01.006

Irarrázaval, S., Allard, C., Campodónico, J., Pérez, D., Strobel, P., Vásquez, L., et al. (2017). Oxidative stress in acute hypobaric hypoxia. *High Alt. Med. Biol.* 18, 128–134. doi:10.1089/ham.2016.0119

Jia, N., Shen, Z., Zhao, S., Wang, Y., Pei, C., Huang, D., et al. (2023). Eleutheroside E from pre-treatment of Acanthopanax senticosus (Rupr.etMaxim.) Harms ameliorates high-altitude-induced heart injury by regulating NLRP3 inflammasome-mediated pyroptosis via NLRP3/caspase-1 pathway. *Int. Immunopharmacol.* 121, 110423. doi:10.1016/j.intimp.2023.110423

Jiang, S., Fan, F., Yang, L., Chen, K., Sun, Z., Zhang, Y., et al. (2022). Salidroside attenuates high altitude hypobaric hypoxia-induced brain injury in mice via inhibiting NF-κB/NLRP3 pathway. *Eur. J. Pharmacol.* 925, 175015. doi:10.1016/j.ejphar.2022.175015

Jiao, L., Liu, Y., Xu, C., Wang, J., Liu, J., Tian, Y., et al. (2023). Protective effect of Taikong Yangxin pills against hypoxia when rush into plateau. *Manned Spacefl.* 29, 336–344. doi:10.16329/j.cnki.zrht.2023.03.006

Julian, C. G., Subudhi, A. W., Wilson, M. J., Dimmen, A. C., Pecha, T., and Roach, R. C. (2011). Acute mountain sickness, inflammation, and permeability: new insights from a blood biomarker study. *J. Appl. Physiology* 111, 392–399. doi:10.1152/japplphysiol.00391.2011

Kai, S., Tanaka, T., Daijo, H., Harada, H., Kishimoto, S., Suzuki, K., et al. (2012). Hydrogen sulfide inhibits hypoxia- but not anoxia-induced hypoxia-inducible factor 1 activation in a von hippel-lindau- and mitochondria-dependent manner. *Antioxid. Redox Signal* 16, 203–216. doi:10.1089/ars.2011.3882

Kumar, G., Chhabra, A., Mishra, S., Kalam, H., Kumar, D., Meena, R., et al. (2016a). H2S regulates hypobaric hypoxia-induced early glio-vascular dysfunction and neuro-pathophysiological effects. *EBioMedicine* 6, 171–189. doi:10.1016/j.ebiom.2016.03.002

Kumar, K., Sharma, S., Vashishtha, V., Bhardwaj, P., Kumar, A., Barhwal, K., et al. (2016b). Terminalia arjuna bark extract improves diuresis and attenuates acute hypobaric hypoxia induced cerebral vascular leakage. *J. Ethnopharmacol.* 180, 43–53. doi:10.1016/j.jep.2016.01.002

Lappin, T. R., and Lee, F. S. (2019). Update on mutations in the HIF: EPO pathway and their role in erythrocytosis. *Blood Rev.* 37, 100590. doi:10.1016/j.blre.2019.100590

Li, H., and Qian, D. (2011). Clinical observation of Xingnaojing injection in the treatment of high altitude cerebropathy. *Shaanxi J. Traditional Chin. Med.* 32, 162–163.

Li, M., Lu, B., Qi, X., Wang, P., and Qin, L. (2023a). Protective effect of Danqijing granules on acute high altitude exposure: a field cohort study on plateau. *Acad. J. Chin. PLA Med. Sch.*, 1–6.

Li, S., Xu, N., Fang, Q., Cheng, X., Chen, J., Liu, P., et al. (2023b). Glehnia littoralis Fr. Schmidtex Miq.: a systematic review on ethnopharmacology, chemical composition, pharmacology and quality control. *J. Ethnopharmacol.* 317, 116831. doi:10.1016/j.jep.2023.116831

Li, X., Zhang, J., Liu, G., Wu, G., Wang, R., and Zhang, J. (2024). High altitude hypoxia and oxidative stress: the new hope brought by free radical scavengers. *Life Sci.* 336, 122319. doi:10.1016/j.lfs.2023.122319

Li, X., Zhang, Q., Nasser, M. I., Xu, L., Zhang, X., Zhu, P., et al. (2020a). Oxygen homeostasis and cardiovascular disease: a role for HIF? *Biomed. Pharmacother.* 128, 110338. doi:10.1016/j.biopha.2020.110338

Li, Y. (2016). Observation on the therapeutic effect of compound dangshen tablet on Acute Mountain sickness. *Qinghai Med. J.* 46, 14–15.

Li, Y., Wang, D., Ma, H., and Bao, Q. (2012). Discussion on traditional Chinese medicine syndrome types of high altitude disease. *Liaoning J. Traditional Chin. Med.* 39, 653–656. doi:10.13192/j.ljtcm.2012.04.82.liyq.029

Li, Z., Guo, J., Liu, C., Shi, Y., Li, Y., Wang, J., et al. (2020b). Compound danshen dripping pill promotes adaptation to acute high-altitude exposure. *High. Alt. Med. Biol.* 21, 258–264. doi:10.1089/ham.2019.0126

Liao, Y., Chen, Z., Yang, Y., Shen, D., Chai, S., Ma, Y., et al. (2023). Antibiotic intervention exacerbated oxidative stress and inflammatory responses in SD rats under hypobaric hypoxia exposure. *Free Radic. Biol. Med.* 209, 70–83. doi:10.1016/j.freeradbiomed.2023.10.002

Lin, Y., and Xiong, J. (2008). Clinical observation of Sankang capsule on Acute Mountain reaction. *Clin. J. Med. Officers* 36, 831–832.

Lin, Y., Xiong, J., Zhang, H., Yin, T., Peng, Y., Zhang, Y., et al. (2008). Observation of curative effect of Shulikang capsule on acute mountain sickness. *J. Mil. Surg. Southwest China* 10, 45–46.

Liu, B., Chen, J., Zhang, L., Gao, Y., Cui, J., Zhang, E., et al. (2017). IL-10 dysregulation in Acute Mountain sickness revealed by transcriptome analysis. *Front. Immunol.* 8, 628. doi:10.3389/fimmu.2017.00628

Liu, H., Zhao, C., Zhang, W., Zhang, Y., and Nie, J. (2018a). Study on medication laws of Tibetan medicine in treatment of plateau diseases based on data mining technology. *China J. Chin. Materia Medica* 43, 1726–1731. doi:10.19540/j.cnki.cjcmm.20180112.001

Liu, Y., Liu, T., Ding, K., Liu, Z., Li, Y., He, T., et al. (2018b). Phospholipase Cγ2 signaling cascade contribute to the antiplatelet effect of notoginsenoside fc. *Front. Pharmacol.* 9, 1293. doi:10.3389/fphar.2018.01293

Luks, A. M., McIntosh, S. E., Grissom, C. K., Auerbach, P. S., Rodway, G. W., Schoene, R. B., et al. (2010). Wilderness medical society consensus guidelines for the prevention and treatment of acute altitude illness. *Wilderness & Environ. Med.* 21, 146–155. doi:10.1016/j.wem.2010.03.002

Luks, A. M., Swenson, E. R., and Bärtsch, P. (2017). Acute high-altitude sickness. *Eur. Respir. Rev.* 26, 160096. doi:10.1183/16000617.0096-2016

Luo, M., He, J., Yin, L., Zhan, P., Zhao, Z., Xiong, H., et al. (2024). Borneol exerts its antipruritic effects by inhibiting TRPA1 and activating TRPM8. *J. Ethnopharmacol.* 322, 117581. doi:10.1016/j.jep.2023.117581

Ma, D., Wang, L., Jin, Y., Gu, L., Yin, G., Wang, J., et al. (2022). Chemical characteristics of Rhodiola Crenulata and its mechanism in acute mountain sickness using UHPLC-Q-TOF-MS/MS combined with network pharmacology analysis. *J. Ethnopharmacol.* 294, 115345. doi:10.1016/j.jep.2022.115345

Ma, H., Fan, P., Jing, L., Yao, J., He, X., Yang, Y., et al. (2011). Anti-hypoxic activity at simulated high altitude was isolated in petroleum ether extract of Saussurea involucrata. *J. Ethnopharmacol.* 137, 1510–1515. doi:10.1016/j.jep.2011.08.037

Ma, H., Wu, J., Gao, R., Li, L., Fan, P., Jing, L., et al. (2013). Establishment of an animal model for Acute Mountain sickness with A decompression chamber. *Pharm. J. Chin. PLA* 29, 301–304.

Ma, R., Lu, D., Xie, Q., Yuan, J., Ren, M., Li, Y., et al. (2023). l-Borneol and d-Borneol promote transdifferentiation of astrocytes into neurons in rats by regulating Wnt/Notch pathway to exert neuroprotective effect during recovery from cerebral ischaemia. *Phytomedicine* 109, 154583. doi:10.1016/j.phymed.2022.154583

Masschelein, E., Van Thienen, R., D'Hulst, G., Hespel, P., Thomis, M., and Deldicque, L. (2014). Acute environmental hypoxia induces LC3 lipidation in a genotype-dependent manner. *FASEB J.* 28, 1022–1034. doi:10.1096/fj.13-239863

Mishra, S., Kumar, G., Chhabra, A., Sethy, N. K., Jain, N., Meena, R. N., et al. (2020). Cysteine becomes conditionally essential during hypobaric hypoxia and regulates adaptive neuro-physiological responses through CBS/H2S pathway. *Biochim. Biophys. Acta Mol. Basis Dis.* 1866, 165769. doi:10.1016/j.bbadis.2020.165769

Moraga, F. A., Flores, A., Serra, J., Esnaola, C., and Barriento, C. (2007). Ginkgo biloba decreases Acute Mountain sickness in people ascending to high altitude at ollagüe (3696m) in northern Chile. *Wilderness Environ. Med.* 18, 251–257. doi:10.1580/06-WEME-OR-062R2.1

Neuwelt, E. A., Bauer, B., Fahlke, C., Fricker, G., Iadecola, C., Janigro, D., et al. (2011). Engaging neuroscience to advance translational research in brain barrier biology. *Nat. Rev. Neurosci.* 12, 169–82. doi:10.1038/nrn2995

Niu, W., Wang, Y., Cao, Z., Yu, S., and Zhang, L. (2006a). Effects of Shulikang Capsule on heart rate of young men exposed rapidly to high altitude. *Med. J. Natl. Defending Forces Southwest China* 16, 493–495. doi:10.3969/j.issn.1004-0188.2006.05.011

Niu, W., Wang, Y., Cao, Z., Yu, S., and Zhang, L. (2006b). Experimental Effects of Shulikang capsule on prevention of acute high altitude reaction. *J. High Alt. Med.* 16, 2–4. doi:10.3969/j.issn.1007-3809.2006.03.002

Norris, J. N., Viirre, E., Aralis, H., Sracic, M. K., Thomas, D., and Gertsch, J. H. (2012). High altitude headache and Acute Mountain sickness at moderate elevations in a military population during battalion-level training exercises. *Mil. Med.* 177, 917–923. doi:10.7205/MILMED-D-12-00007

Nourkami-Tutdibi, N., Küllmer, J., Dietrich, S., Monz, D., Zemlin, M., and Tutdibi, E. (2023). Serum vascular endothelial growth factor is a potential biomarker for acute mountain sickness. *Front Physiol.* 14, 1083808. doi:10.3389/fphys.2023.1083808

Ou, C., Geng, T., Wang, J., Gao, X., Chen, X., Luo, X., et al. (2020). Systematically investigating the pharmacological mechanism of Dazhu Hongjingtian in the prevention and treatment of acute mountain sickness by integrating UPLC/Q-TOF-MS/MS analysis and network pharmacology. *J. Pharm. Biomed. Anal.* 179, 113028. doi:10.1016/j.jpba.2019.113028

Pan, Y., Zhang, Y., Yuan, J., Ma, X., Zhao, Y., Li, Y., et al. (2020). Tetrahydrocurcumin mitigates acute hypobaric hypoxia-induced cerebral oedema and inflammation through the NF-κB/VEGF/MMP-9 pathway. *Phytother. Res.* 34, 2963–2977. doi:10.1002/ptr.6724

Park, S. H., Chung, S., Chung, M.-Y., Choi, H.-K., Hwang, J.-T., and Park, J. H. (2022). Effects of Panax ginseng on hyperglycemia, hypertension, and hyperlipidemia: a systematic review and meta-analysis. *J. Ginseng Res.* 46, 188–205. doi:10.1016/j.jgr.2021.10.002

Paul, S., Gangwar, A., Bhargava, K., and Ahmad, Y. (2018). STAT3-RXR-Nrf2 activates systemic redox and energy homeostasis upon steep decline in pO2 gradient. *Redox Biol.* 14, 423–438. doi:10.1016/j.redox.2017.10.013

Pei, C., Jia, N., Wang, Y., Zhao, S., Shen, Z., Shi, S., et al. (2023). Notoginsenoside R1 protects against hypobaric hypoxia-induced high-altitude pulmonary edema by inhibiting apoptosis via ERK1/2-P90rsk-BAD ignaling pathway. *Eur. J. Pharmacol.* 959, 176065. doi:10.1016/j.ejphar.2023.176065

Pena, E., Brito, J., El Alam, S., and Siques, P. (2020). Oxidative stress, kinase activity and inflammatory implications in right ventricular hypertrophy and heart failure under hypobaric hypoxia. *Int. J. Mol. Sci.* 21, 6421. doi:10.3390/ijms21176421

Pena, E., El Alam, S., Siques, P., and Brito, J. (2022). Oxidative stress and diseases associated with high-altitude exposure. *Antioxidants* 11, 267. doi:10.3390/antiox11020267

Peng, Y., Yin, H., Li, S., and Yang, H. (2022). Transcriptome of pituitary function changes in rat model of high altitude cerebral edema. *Genomics* 114, 110519. doi:10.1016/j.ygeno.2022.110519

Peng, Y. J., Nanduri, J., Wang, N., Kumar, G. K., Bindokas, V., Paul, B. D., et al. (2023). Hypoxia sensing requires H2S-dependent persulfidation of olfactory receptor 78. *Sci. Adv.* 9, eadf3026. doi:10.1126/sciadv.adf3026

Pham, K., Frost, S., Parikh, K., Puvvula, N., Oeung, B., and Heinrich, E. C. (2022). Inflammatory gene expression during acute high-altitude exposure. *J. Physiol.* 600, 4169–4186. doi:10.1113/JP282772

Pu, X., Li, F., Lin, X., Wang, R., and Chen, Z. (2022). Oxidative stress and expression of inflammatory factors in lung tissue of acute mountain sickness rats. *Mol. Med. Rep.* 25, 49. doi:10.3892/mmr.2021.12565

Qian, W., Cai, X., Qian, Q., Wang, D., and Zhang, L. (2020). Angelica sinensis polysaccharide suppresses epithelial-mesenchymal transition and pulmonary fibrosis via a DANCR/AUF-1/FOXO3 regulatory Axis. *Aging Dis.* 11, 17–30. doi:10.14336/AD.2019.0512

Richalet, J.-P., Hermand, E., and Lhuissier, F. J. (2023). Cardiovascular physiology and pathophysiology at high altitude. *Nat. Rev. Cardiol.* 21, 75–88. doi:10.1038/s41569-023-00924-9

Roncin, J. P., Schwartz, F., and D'Arbigny, P. (1996). EGb 761 in control of acute mountain sickness and vascular reactivity to cold exposure. *Aviat. Space Environ. Med.* 67, 445–452.

Ruan, H. (2009). Compound Danshen Dripping Pill combined with aminophylline for prevention of acute mild altitude sickness. *Mod. J. Integr. Traditional Chin. West. Med.* 18, 4090–4091.

Shen, J. (2019). Hongjingtian combined with dexamethasone and albuterol aerosol in the treating 60 cases of Acute Mountain sickness. *West. J. Traditional Chin. Med.* 32, 80–82.

Shen, Z., Huang, D., Jia, N., Zhao, S., Pei, C., Wang, Y., et al. (2023). Protective effects of Eleutheroside E against high-altitude pulmonary edema by inhibiting NLRP3 inflammasome-mediated pyroptosis. *Biomed. Pharmacother.* 167, 115607. doi:10.1016/j.biopha.2023.115607

Shi, B., Cui, Q., Feng, Z., and Li, J. (2019). Mining potential drugs for prevention and treatment of acute mountain sickness based on bioinformatics approach. *Chin. J. Clin. Healthc.* 22, 503–507.

Shi, X. (2011) *MSCT study of liver hemodynamics and volume in normal adults at different altitudes*. China: Qinghai University.

Song, T.-T., Bi, Y.-H., Gao, Y.-Q., Huang, R., Hao, K., Xu, G., et al. (2016). Systemic pro-inflammatory response facilitates the development of cerebral edema during short hypoxia. *J. Neuroinflammation* 13, 63. doi:10.1186/s12974-016-0528-4

Su, H.-F., Shaker, S., Kuang, Y., Zhang, M., Ye, M., and Qiao, X. (2021). Phytochemistry and cardiovascular protective effects of huang-qi (astragali radix). *Med. Res. Rev.* 41, 1999–2038. doi:10.1002/med.21785

Tang, Y., Song, H., and Fei, J. (2013). Effect of Shengnaokang pills on prevention and treatment of Acute Mountain sickness. *People's Mil. Surg.* 56, 46–47.

Tu, B., Wang, Y., Wu, Z., Zhou, W., Tang, X., Zhang, C., et al. (2023). DIA-based serum proteomics revealed the protective effect of modified siwu decoction against hypobaric hypoxia. *J. Ethnopharmacol.* 319, 117303. doi:10.1016/j.jep.2023.117303

Turner, R. E. F., Gatterer, H., Falla, M., and Lawley, J. S. (2021). High-altitude cerebral edema: its own entity or end-stage acute mountain sickness? *J. Appl. Physiol.* 131, 313–325. doi:10.1152/japplphysiol.00861.2019

Wang, C., Jiang, H., Duan, J., Chen, J., Wang, Q., Liu, X., et al. (2018). Exploration of acute phase proteins and inflammatory cytokines in early stage diagnosis of Acute Mountain sickness. *High Alt. Med. Biol.* 19, 170–177. doi:10.1089/ham.2017.0126

Wang, C., Yan, M., Duan, J., Chen, J., and Huang, J. (2015). Reproduction of a rat model of acute high-altitude sickness and evaluation of its related indexes. *Med. J. Chin. PLA* 40, 716–721.

Wang, X., Liu, C., Zhang, H., Guo, X., and Zhang, W. (2017). Effect of hydrogen sulfide on pulmonary respiratory membrane permeability in rats with experimental high altitude pulmonary edema. *Chin. High Alt. Med. Biol.* 38, 86–90. doi:10.13452/j.cnki.jqmc.2017.02.003

Wang, X., Sun, H., Cui, L., Wang, X., Ren, C., Tong, Z., et al. (2022). Acute high-altitude hypoxia exposure causes neurological deficits via formaldehyde accumulation. *CNS Neurosci. Ther.* 28, 1183–1194. doi:10.1111/cns.13849

Wang, Z. (1994). Acupuncture for Acute Mountain sickness 56 cases. *Chin. Acupunct. Moxibustion*, 338–339.

West, J. (2012). High-altitude medicine. *Am. J. Respir. Crit. Care Med.* 186, 1229–1237. doi:10.1164/rccm.201207-1323CI

Wilson, M. H., Newman, S., and Imray, C. H. (2009). The cerebral effects of ascent to high altitudes. *Lancet Neurol.* 8, 175–191. doi:10.1016/S1474-4422(09)70014-6

Wu, B., Teng, H., Zhang, L., Li, H., Li, J., Wang, L., et al. (2015). Interaction of hydrogen sulfide with oxygen sensing under hypoxia. *Oxid. Med. Cell. Longev.* 2015, 758678. doi:10.1155/2015/758678

Wu, T. (2005). Chronic mountain sickness on the Qinghai-Tibetan plateau. *Chin. Med. J. Engl.* 118, 161–168.

Wu, Z., Xu, H., Wang, Y., Tu, B., Tang, X., Li, M., et al. (2023). Visual analysis of studies on traditional Chinese medicine for prevention and treatment of highaltitude disease. *J. Environ. Occup. Med.* 40, 1297–1306.

Xie, N., Fan, F., Jiang, S., Hou, Y., Zhang, Y., Cairang, N., et al. (2022). Rhodiola crenulate alleviates hypobaric hypoxia-induced brain injury via adjusting NF-κB/NLRP3-mediated inflammation. *Phytomedicine* 103, 154240. doi:10.1016/j.phymed.2022.154240

Xie, Y., and Guo, X. (2004). Treatment of Acute Mountain reaction with Astragalus injection in 200 cases. *Chin. J. Integr. Traditional West. Med.* 24, 1049.

Xin, X., Yang, K., Liu, H., and Li, Y. (2022). Hypobaric hypoxia triggers pyroptosis in the retina via NLRP3 inflammasome activation. *Apoptosis* 27, 222–232. doi:10.1007/s10495-022-01710-7

Xu, H., Li, S., Liu, J., Cheng, J., Kang, L., Li, W., et al. (2023). Bioactive compounds from Huashi Baidu decoction possess both antiviral and anti-inflammatory effects against COVID-19. *Proc. Natl. Acad. Sci. U.S.A.* 120, e2301775120. doi:10.1073/pnas.2301775120

Xue, Y., Wang, X., Wan, B., Wang, D., Li, M., Cheng, K., et al. (2022). Caveolin-1 accelerates hypoxia-induced endothelial dysfunction in high-altitude cerebral edema. *Cell. Commun. Signal* 20, 160. doi:10.1186/s12964-022-00976-3

Yan, J., Ruan, P., Zhang, Z., Ge, Y., Gao, J., Tan, H., et al. (2022). The effects and mechanism of compound Danshen driping pills on acute mountain sickness in rats. *Chin. J. Clin. Pharmacol.* 38, 2736–2740. doi:10.13699/j.cnki.1001-6821.2022.22.017

Yan, X., Liu, J., Zhu, M., Liu, L., Chen, Y., Zhang, Y., et al. (2021). Salidroside orchestrates metabolic reprogramming by regulating the Hif-1α signalling pathway in acute mountain sickness. *Pharm. Biol.* 59, 1540–1550. doi:10.1080/13880209.2021.1992449

Yang, H., Jin, G., Ma, Q., Liu, S., Li, S., and Ge, R. (2011). POTENTIAL ROLE OF EXOGENOUS HYDROGEN SULFIDE ON PULMONARY ARTERIAL PRESSURES IN RATS AT HIGH ALTITUDE. *J. Qinghai Med. Coll.* 32, 164–168+171. doi:10.13452/j.cnki.jqmc.2011.03.007

Yu, W., Yuan, J., Li, J., and Chen, Y. (2011). Observations on the efficacy of Shexiang Baoxin pill in the treatment of acute plateau reaction. *Chin. J. Health Care Med.* 13, 188+191.

Yu, Y., Ding, S., Xu, X., Yan, D., Fan, Y., Ruan, B., et al. (2023). Integrating network pharmacology and bioinformatics to explore the effects of dangshen (codonopsis pilosula) against hepatocellular carcinoma: validation based on the active compound luteolin. *Drug Des. Devel Ther.* 17, 659–673. doi:10.2147/DDDT.S386941

Zeng, Y., Cao, W., Huang, Y., Zhang, H., Li, C., He, J., et al. (2024). Huangqi Baihe Granules alleviate hypobaric hypoxia-induced acute lung injury in rats by suppressing oxidative stress and the TLR4/NF-κB/NLRP3 inflammatory pathway. *J. Ethnopharmacol.* 324, 117765. doi:10.1016/j.jep.2024.117765

Zhang, D., Zhang, Y., Nie, H., Zhang, R., Cui, J., Cheng, Y., et al. (2010). Protective effects of new compound codonopsis tablets against acute mountain sickness. *Chin. J. Appl. Physiology* 26, 148–152. doi:10.13459/j.cnki.cjap.2010.02.005

Zhang, D., Zhang, Y., Xie, Y., Ma, Y., Zhang, X., and Cui, J. (2005). Effect of Compound Dangshen capsule on prevention and treatment of acute mountain sickness. *J. Prev. Med. Chin. People's Liberation Army* 23, 271–272.

Zhang, J., Wu, Y., Peng, X.-Y., Li, Q.-H., Xiang, X.-M., Zhu, Y., et al. (2021). The protective effect of a novel cross-linked hemoglobin-based oxygen carrier on hypoxia injury of Acute Mountain sickness in rabbits and goats. *Front. Physiology* 12, 690190–690213. doi:10.3389/fphys.2021.690190

Zhang, J., and Zhang, X. (1993). Extrinsic factors of mechanism and characteristics on altitude sickness. *China J. Traditional Chin. Med. Pharm.* 8, 336–337.

Zheng, H. L., Li, M. T., Zhou, T., Wang, Y. Y., Shang, E. X., Hua, Y. Q., et al. (2023). Protective effects of Lycium barbarum L. berry extracts against oxidative stress-induced damage of the retina of aging mouse and ARPE-19 cells. *Food Funct.* 14, 399–412. doi:10.1039/d2fo02788g

Zhong, G., Mi, M., Ge, Z., Dang, Z., and Zongba, B. (2022). Preliminary study on tongue diagnosis in Tibetan medicine four Tantras. *China J. Traditional Chin. Med. Pharm.* 37, 2303–2305.

Zhou, Y., Huang, X., Zhao, T., Qiao, M., Zhao, X., Zhao, M., et al. (2017). Hypoxia augments LPS-induced inflammation and triggers high altitude cerebral edema in mice. *Brain Behav. Immun.* 64, 266–275. doi:10.1016/j.bbi.2017.04.013

Zhuang, W., Yue, L., Dang, X., Chen, F., Gong, Y., Lin, X., et al. (2019). Rosenroot (Rhodiola): potential applications in aging-related diseases. *Aging Dis.* 10, 134–146. doi:10.14336/AD.2018.0511

frontiers | Frontiers in Pharmacology

TYPE Review
PUBLISHED 17 June 2024
DOI 10.3389/fphar.2024.1427019

OPEN ACCESS

EDITED BY
Qianfeng Gong,
Jiangxi University of Traditional Chinese Medicine, China

REVIEWED BY
Bo Zhang,
Tsinghua University, China
Yuan Gao,
Capital Medical University, China
Songhong Yang,
Jiangxi University of Chinese Medicine, China

*CORRESPONDENCE
Yuancheng Gao,
gaoyuancheng@foxmail.com
Yang Liu,
liuyang311111@163.com

RECEIVED 02 May 2024
ACCEPTED 29 May 2024
PUBLISHED 17 June 2024

CITATION
Qian J, Feng C, Wu Z, Yang Y, Gao X, Zhu L, Liu Y and Gao Y (2024), Phytochemistry, pharmacology, toxicology and detoxification of *Polygonum multiflorum* Thunb.: a comprehensive review.
Front. Pharmacol. 15:1427019.
doi: 10.3389/fphar.2024.1427019

Phytochemistry, pharmacology, toxicology and detoxification of *Polygonum multiflorum* Thunb.: a comprehensive review

Jiawen Qian[1], Chenhang Feng[2], Ziyang Wu[1], Yuanmei Yang[3], Xiangfu Gao[1], Lingyan Zhu[4], Yang Liu[5]* and Yuancheng Gao[1]*

[1]Department of Nephrology, The First Affiliated Hospital of Zhejiang Chinese Medical University (Zhejiang Provincial Hospital of Chinese Medicine), Hangzhou, China, [2]The Third Affiliated Clinical Medical College, Zhejiang Chinese Medical University, Hangzhou, China, [3]School of Pharmacy, Fudan University, Shanghai, China, [4]Institute of Chinese Materia Medica, Shanghai University of Traditional Chinese Medicine, Shanghai, China, [5]Shaanxi Academy of Traditional Chinese Medicine, Xi'an, China

Background: Polygonum multiflorum Thunb. (PM), a kind of perennial plant, belongs to the genus *Polygonum* of the family polygonaceae.The dry root of PM (also called Heshouwu), is a traditional Chinese medicine, which has a series of functions and is widely used in clinic for hair lossing, aging, and insomnia. While, PM also has some toxicity, its clinical drug safety has been concerned. In this paper, the chemical components, toxic mechanisms and detoxification strategies of PM were reviewed in order to provide evidence for its clinical application.

Materials and methods: We conducted a systematic review of published literature of PM, including English and Chinese databases, such as PubMed, Web of Science, CNKI, and Wanfang.

Results: PM contains a variety of chemical compounds, including stilbenes, quinones, flavonoids, phospholipids, and has many pharmacological activities such as anti-aging, wound healing, antioxidant, and anti-inflammatory properties. The PE has certain therapeutic effect, and it has certain toxicity like hepatotoxicity, nephrotoxicity, and embryotoxicity at the same time, but.these toxic effects could be effectively reduced by processing and compatibility.

Conclusion: It is necessary to further explore the pharmacological and toxicological mechanisms of the main active compounds of PE.This article provides scientific basis for the safe clinical application of PM.

KEYWORDS

Polygonum multiflorum Thunb., toxicology, chemical components, processing, traditonal Chinese medicine

1 Introduction

Polygonum multiflorum Thunb. (PM), also known as He Shou Wu (HSW), is a perennial vine of the Polygonaceae family. First documented in "Kai Bao Ben Cao," HSW has been a staple in traditional Chinese medicine for centuries, treating a range of ailments including sores, age-related conditions, and anemia. Over 100 chemical constituents have been identified in PM, with variations in toxicity attributed to differences in these components. Both water and alcohol extracts of raw PM and processed ones have been studied, revealing distinct toxicological profiles. The primary

toxicity of PM is hepatotoxicity, with mechanisms involving intrinsic and idiosyncratic factors. Traditional Chinese Medicine (TCM) employs processing and compatibility techniques to reduce toxicity and enhance therapeutic effects, which are practical for daily use and deserve further research. This review aims to elucidate the traditional uses, chemical composition, toxicology, and detoxification methods of PM, providing a foundation for future research and therapeutic development.

2 Traditional application of PM

"He Shou Wu" has been an official entry in the Chinese Pharmacopoeia since the Tang dynasty, over 1200 years ago. It was first recorded in "Kai Bao Ben Cao," with pharmacological effects of anti-sores and anti-aging, treating anaemia and *postpartum* diseases. "Compendium of Materia Medica" stated that PM can treat the pain in the loins and knee, "Ben Cao Xin Bian," "Ben Cao Qiu Zhen" recorded that PM is used to treat headache, hemorrhoids, cutaneous pruritus, and immune related disease. "Zhong Hua Yao Dian" also stated that PM can be used to treat constipation and hyperlipidemia (Figure 1).

PM is often used in conjunction with other herbs in formulations that address age-related conditions. Processed PM is usually used in age-related diseases. "Shi Bu Zhai Yi Shu" mentioned a formula named "Shou Wu Yan Shou Pill," which can be used to treat hypertension and delaying the process of aging. There is another formula named "Qi Bao Mei Ran Pill," which was stated in "Ji Shan Tang Fang," it is used to treat hair losing. While raw PM is mainly used for treatment of *postpartum* fever, such as the formula of "He Ren Decoction" recorded in "Jing Yue Quan Shu".

In summary, PM is extensively used to nourish the liver and kidneys, nourish blood, and dispel wind, exhibiting a wide range of pharmacological effects that differ between its raw and processed forms. Processed PM is predominantly used for liver and kidney yin deficiency, including conditions like premature graying, weakness of the waist and knees, muscle and bone pain, limb numbness, tinnitus, neurasthenia, hyperlipidemia, and spermatozoa issues. It is also used to nourish blood, commonly treating anemia and dizziness. Raw PM is mostly used in dispel wind. Raw PM is mostly used in treatment of long-term malaria, long-term dysentery, chronic hepatitis, scrofula and hemorrhoids (Supplementary Table S1).

Clinical trials have validated these pharmacological effects. For instance, one study found that the PM group showed the most significant increase in black hair, with higher levels of total melanin, α-MSH, MC1R, and TYR—key targets in PM's use for hair graying. Chemical constituents other than TSG may contribute to the hair color regulation activity of PMR (Han et al., 2015). Another trial showed that the effect of PM extract on AD is superior to western medicine. The total effective rate of 93.33% in the PM extract treatment group was better than 73.33% in the Chinese herb control group and 68.97% in the western medicine control group ($p < 0.01$) (Chen et al., 2010). Additionally, Yadong Fan et al., 2021 investigated the anti-inflammatory activity of Tongmai Yangxin pill, a formula including PM, in treatment of coronary heart disease, and results showed that TMYX treatment showed reduced levels of apolipoprotein B, endothelin 1, nuclear factor κB (NF-κB) and homocysteine in CHD patients, suggesting the formula's effectiveness in attenuating macrophage foam cell formation and its anti-inflammatory activity through modulation of the ESR1 and NF-κB signaling pathways.

FIGURE 1
Polygonum multiflorum Thunb.: the plant, the medical section, the slices before and after processing.

TABLE 1 Toxic components and toxic mechanisms of water extract of PM.

Water extract	
toxic components	Toxic mechanisms
stilbene glycoside, emodin 8-O-β-D glucoside, emodin and emodin methyl ether	Inhibit the mRNA expression of various CYP450 enzymes in human hepatocytes, resulting in liver metabolic dysfunction and liver injury
cis-stilbene glycoside	Inhibit PPAR-γ pathway to induce idiotypic liver injury
emodin	Inhibit the function of UGTs and MRP2 transporters to induce liver injury
emodin methyl ether	The liver metabolites inhibit UGT1A1 enzyme
trans-stilbene glycoside	Metabolizing through UGTs mediated phase II pathway, inhibition of UGTs can lead to dysfunction of the metabolism, inducing liver injury

TABLE 2 Toxic components and toxic mechanisms of alcohol extract of PM.

Alcohol extract	
toxic components	Toxic mechanisms
aloe emodin	reduce the survival rate of L02 cells and causes S phase block of hepatocytes
chrysophanol	Inhibit bile salt export pump and multidrug resistance-associated protein 2 to accumulate endogenous BA in the liver, may be related to P450 1A2, P450 2B6 and P450 3A4 in hepatocytes
tetrahydroxy stilbene-O-(galloyl)-hex	Unknown, lead to apoptosis of rat hepatocytes

3 The chemical components of PM

The chemical components of PM varies between its water and alcohol extracts. The chief toxic compositions in water extract are stilbenes, while in alcohol extract are quinones. More than 103 components are isolated and characterized in PM, including flavonoids, phospholipids, quinones, stilbenes, etc. Stilbenes and quinones are the main characteristic components in PM, with cases of hepatotoxicity reported.

3.1 The effective ingredients are generally extracted from raw/processed PM using water and alcohol

While some studies suggest that the water extract is less toxic than the alcohol extract, this remains a topic of debate. Water extract of PM treated groups showed significant inhibitions in CYP2E1 enzymatic activities and mRNA expressions (Li et al., 2015). However, another study compared the toxicity of water extract and alcohol extract of PM, and the result indicated that alcohol extract had much stronger hepatotoxicity than water extract, the content of emodin-8-O-β-D-glucopyranoside, physcion-8-O-β-D-glucopyranoside, emodin and physcion was significantly higher in alcohol extract than in water extract, while the human hepatocytes extraction showed that 2,3,5,4′-tetrahydroxystilbene-2-O-β-D-glucopyranoside, emodin-8-O-β-D-glucopyranoside, physcion-8-O-β-D-glucopyranoside, emodin and physcion had interaction with human hepatocytes (Lv et al., 2015). Yang Xuehuan et al. showed a different result, they proved that the toxicity of water extract was greater than that of alcohol extract. Based on metabolomics technology, they found that the liver toxicity of alcohol extract and water extract of PM was mainly caused by one carbon unit metabolism, arachidonic acid metabolism and glycerophospholipid metabolism (Wang et al., 2021). Main toxic components and toxic mechanisms of water extract (Table 1) and alcohol extract (Table 2) are as follows.

Additional studies have explored other extracts of PM, scholars showed that ethyl acetate (EA) extract had close association with the idiosyncratic hepatotoxicity of PM. Co-treatment with non-toxic dose of lipopolysaccharide (LPS) and EA extract could result in evident liver injury, indicated by the significant elevation of plasma alanine aminotransferase (ALT) and aspartate aminotransferase (AST) activities, as well as obvious liver histologic damage (Li et al., 2016). Another study assessed in zebrafish embryos showed that the toxicity of 70% EtOH extract is considerably higher than that of other extracts (Yang et al., 2018).

In conclusion, both raw and processed PM pose risks to liver health, though the extent of toxicity varies among the different extracts. As a result, although the hepatotoxicity of processed product is reduced, caution should be taken in its clinical use.

3.2 The chemical components of PM are reported including flavonoids, phospholipids, quinones and stilbenes

PM is known for its diverse phytochemical composition, including flavonoids, phospholipids, quinones, and stilbenes. Notably, stilbenes and quinones stand out as key components due to their pharmacological properties and associated hepatotoxic risks, with compounds such as 2,3,5,4′-tetrahydroxystilbene-2-O-β-D-glucopyranoside and emodin dianthrones being particularly significant.

10.3389/fphar.2024.1427019

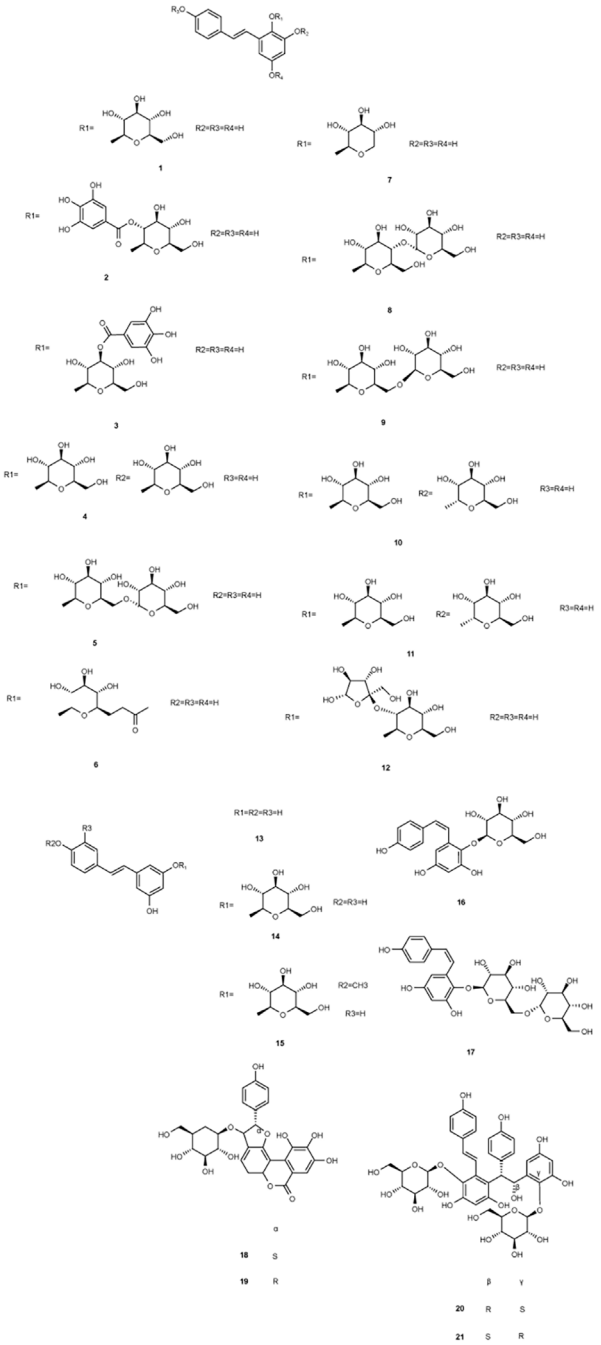

FIGURE 2
Structures of chemical components 1–21 in *Polygonum multiflorum* Thunb.

3.2.1 Stilbenes

Stilbenes, significant non-flavonoid phytochemicals with a polyphenolic structure, are prevalent in mosses and various plants. Stilbenes can be used as medicine for their anti-oxidant, anti-proliferation and anti-inflammatory properties. However, they may impair UDP-glucuronosyltransferases (UGTs), potentially leading to drug-induced liver injury (DILI).

The discovery of stilbenes in PM began in 1976 with the characterization of 2,3,5,4′-tetrahydroxystilbene-2-O-β-D-glucopyranoside. Since then, many stilbenes were found, such as 2,3,5,4′-tetrahydroxystilbene-2-O-β-D-glucopyranoside, rhaponticoside, physcion, emodin-8-O-glucoside etc. (Lin et al., 2015) From 2015 to 2020, most of the new compounds isolated are majorly dianthrones and stilbenes (Teka et al., 2021). In 2016, four new dianthrones were isolated by Yang et al., naming polygonumnolides C1-C4 from PM (Yang et al., 2016). After the isolation of polygonumosides A-D in 2014, a new type of stilbene, polygonumoside E was isolated and characterized in 2016 (Yan et al., 2014; Zhao et al., 2016). Zhang and Cui found a new stilbene with HPLC, and named it 2, 3,

10.3389/fphar.2024.1427019

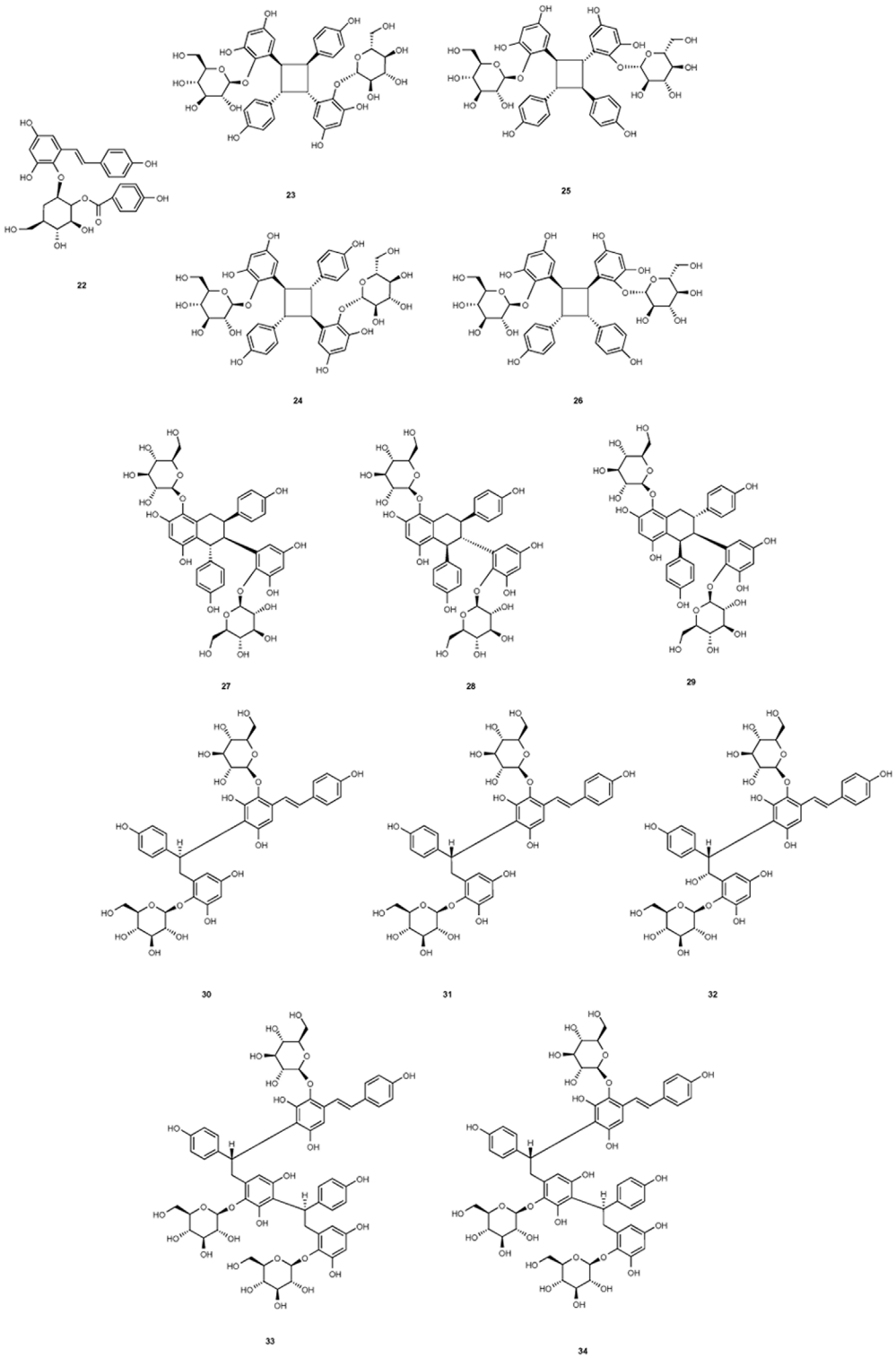

FIGURE 3
Structures of chemical components 22–34 in *Polygonum multiflorum* Thunb.

5, 4′-tetrahydroxystilbene-2-O-(2″O-p-Phydroxybenzoyl)-β-D-glucoside (Zhang and Cui, 2016). In 2017, a new type of polygonimitin was named as thunberginol-C-6-O-β-D-glucopyranoside. Moreover, polygonumnolide D and polygonumnolide E were found by Yang et al., 2017. The team of Yang continued their research and in 2018, they isolated seven new polygonumnolides, naming polygonumnolide A1, A2, A3, A4, B1, B2 and B3 (Yang J. et al., 2018). In 2018, Li et al. isolated seven new

dimeric stilbenes named as multiflorumisides A-G (Li et al., 2018). In the next year, they isolated 5 new oligomeric stilbenes naming multiflorumiside H-L, among which Multiflorumiside H and J showed moderate suppressive effect against nitric oxide production (Li et al., 2019). In 2020, Another research group isolated 9 new stilbenes, named them as polygonibene 1, polygonibene 2, polygonibene 2a, polygonibene 3, polygonibene 3a, and polygonibene 4, 5, 6, and 7 (Nguyen et al., 2020) (Figures 2–4).

3.2.2 Quinones

Quinones, which are abundant in nature, typically possess a basic structural pattern where ortho- or para-substituted diones are conjugated to an benzoquinone or to expanded polycyclic aromatic systems. These compounds exert antioxidant-related pharmacological actions including neuroprotective effects, anti-inflammation, anticancer, hepatoprotective effects and anti-aging, etc. (Zhao and Zheng, 2023) However, quinones can lead to an inhibition of cytochrome P450 enzymes (CYP450 enzymes) and UGTs, resulting in hepatotoxicity.

The first quinone identified in PM was 2-Methoxy-6-acethyl-7-methyliuglone, isolated in 1993. In subsequent research, Yang et al. isolated seven new polygonumnolides, including cis-emodin dianthrone, in 2018 (Yang et al., 2018). In 2021, Yang et al. first developed the UHPLC-QQQ-MS/MS method to simultaneously determine six dianthrones in PM, including trans-emodin dianthrones, and cis-emodin dianthrones (Yang et al., 2021), marking a significant advancement in analytical techniques (Figure 5).

3.2.3 Other components

In addition to quinones, PM also contains flavonoids and chromenones. Flavonoids, polyphenolic secondary metabolites found in various plants and diets, consist of a structural backbone of 15 carbon atoms and are composed of two benzene rings and heterocycles. These compounds exhibit multiple biological activities, including antioxidant, cardio-protective, hepatocyte-protective, and anti-cancer effects, and are primarily recognized for their liver-protective properties.

Two new types of chromenones, 2,5-dimethyl-7-hydroxychromone and 2-(2-hydroxylpropyl)-5-methylchromenone-7-O-β-D-glucopyranoside, and one new type of flavonoid, trycin-7-O-β-D-glucopyranoside, was isolated from PM in 2016 (Yan et al., 2014). With an effect of protecting liver, flavonoids may not be the toxic components in PM (Figure 6).

Although the above components cause liver injury when administrated in large quantities, the quantity of components is very low in the clinical dosage of PM. Therefore, *polygonum multiflorum*-induced liver injury (PM-DILI) may not be independently caused by the above components. The components may play a secondary or synergistic role in the occurrence of PM-DILI (Zhai et al., 2021). Recognition of this

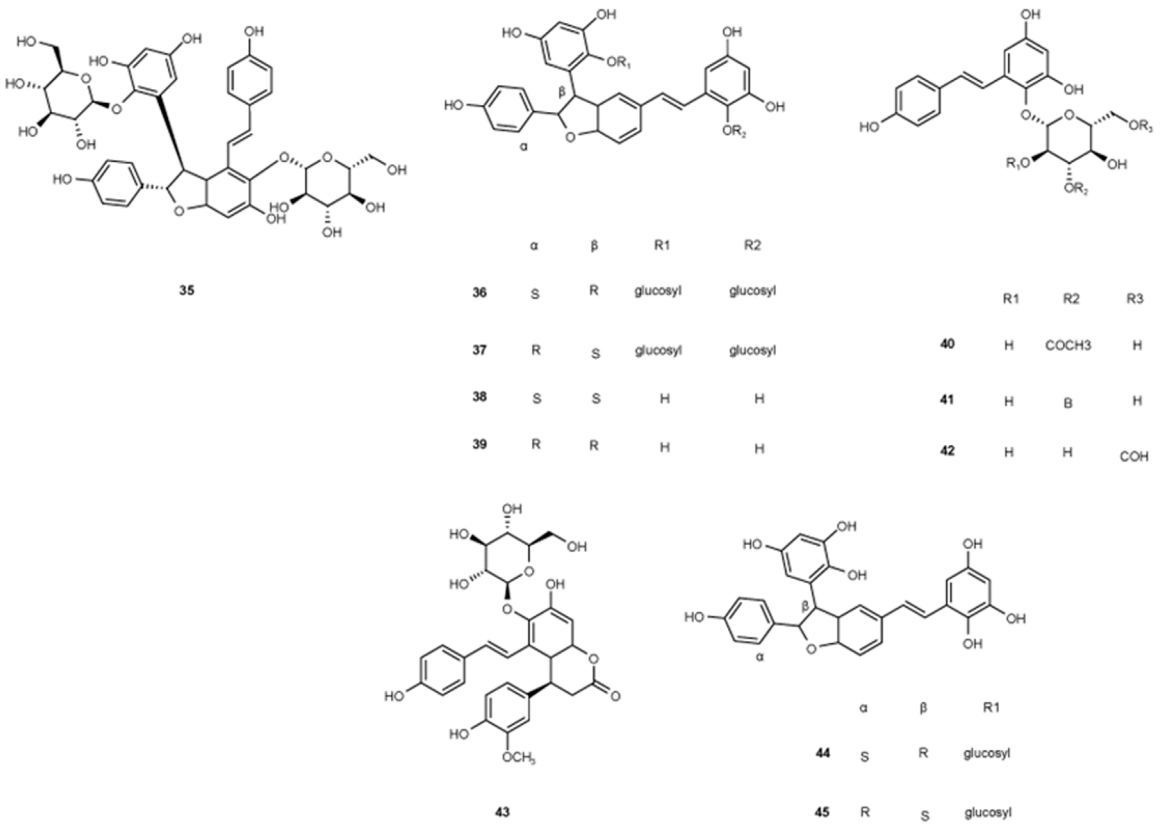

FIGURE 4
Structures of chemical components 35–43 in *Polygonum multiflorum* Thunb.

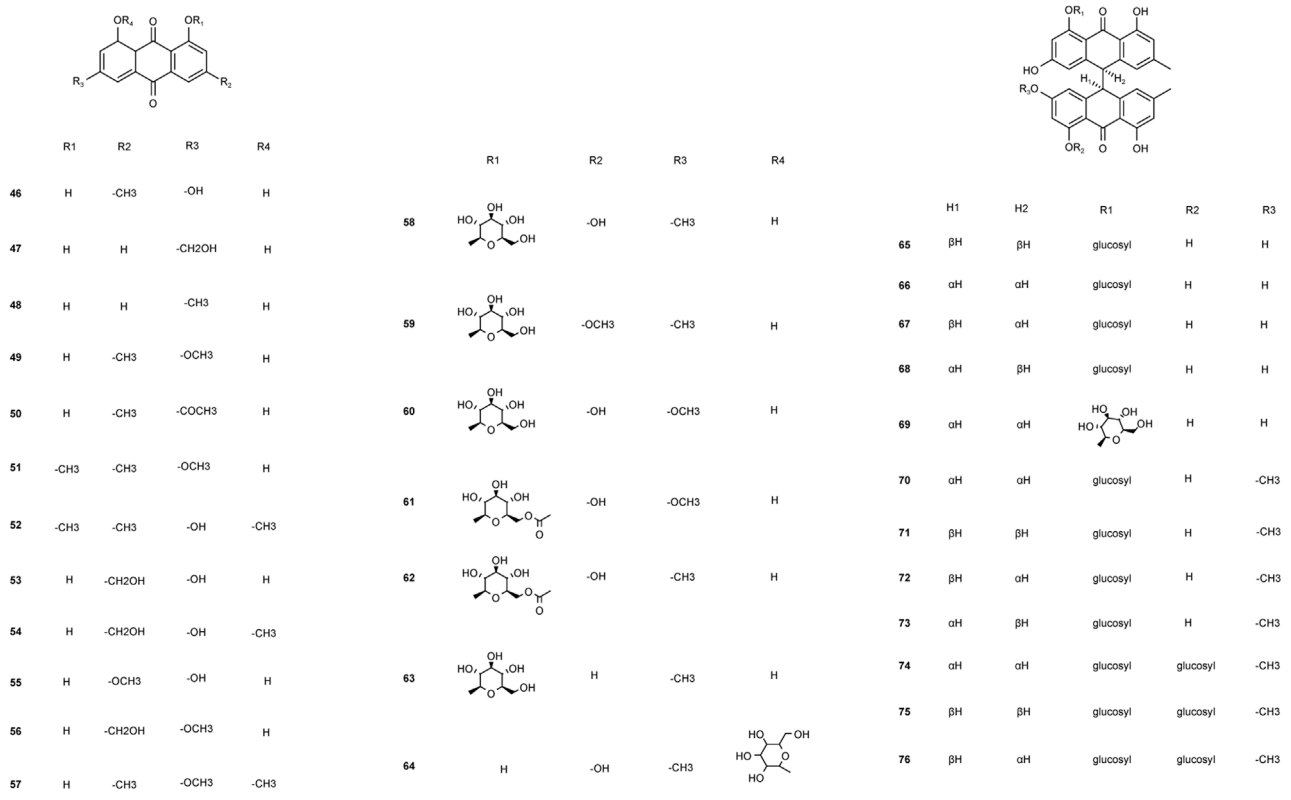

FIGURE 5
Chemical structures of quinones in *Polygonum multiflorum* Thunb.

may contribute to a more complete understanding of the complex multi-component mechanisms of PM-DILI.

4 The toxicity of PM

4.1 The toxicity of PM is mainly recognized as liver injury

PM has been recognized as a toxic herb since the toxicity was first reported by Hongkong scholars in 1996. The herb's toxicity encompasses hepatotoxicity, nephrotoxicity, and embryotoxicity. Hepatotoxicity is linked to stilbenes and quinones, nephrotoxicity and embryotoxicity are mostly linked to stilbenes. With hepatotoxicity being the most significant, it manifests in three forms: intrinsic, idiosyncratic, and indirect toxicity (Xiao et al., 2023).

Intrinsic toxicity refers to the predictable and dose-dependent effects caused by the inherent toxic substances in PM. This type of toxicity, which can be replicated in healthy animal models, is typical of traditional herbs and can often be mitigated through conventional processing methods. Idiosyncratic toxicity targets specific vulnerable populations and is linked to individual immune responses, metabolic processes, and genetic factors. This form of toxicity is less acknowledged in TCM, and its detoxification has not been extensively studied. Indirect toxicity arises from the pharmacological impact of biologically active compounds. It is challenging to replicate in animal models and remains an area of ongoing research (Table 3).

4.1.1 Intrinsic toxicity

Intrinsic toxicity, the most prevalent form of PM-DILI, is characterized by a dose-response relationship. This relationship suggests that within certain limits, the dosage of the drug correlates directly with its therapeutic effect, making the prediction and control of intrinsic toxicity more straightforward.

Two primary components of PM, 2,3,5,4′-tetrahydroxystilbene-2-O-β-D-glucoside and emodin (EMD), are chiefly responsible for this toxicity. Intrinsic toxicity is mainly caused by the toxicity of these two components, with a series of characteristics. A study found that different dose concentration of emodin can increase the expression of CYP2E1, 2B6, 1A2, 3A4, 2C9, 2D6, 7A1 mRNA, inducing the expression of CYP1A1 and CYP1B1 in a dose-dependent manner (Wang et al., 2016). And emodin intake can induce the enzymes of CYP1A, CYP2E1, and CYP2B (Wang et al., 2015). Emodin and emodin methyl ether have a strong inhibitory effect on CYP1A2, and a medium inhibitory effect on CYP2C9, CYP2D6 and CYP3A4 (Zheng et al., 2021).

While 2,3,5,4′-tetrahydroxystilbene-2-O-β-D-glucoside alone does not exhibit hepatotoxicity, it exacerbates liver damage when combined with sub-toxic doses of acetaminophen (APAP) in mice. 2,3,5,4′-tetrahydroxystilbene-2-O-β-D-glucoside aggravated hepatic reduced glutathione (GSH) depletion and APAP-cysteine adducts formation induced by APAP in mice (Xu et al., 2017), showing that 2,3,5,4′-

10.3389/fphar.2024.1427019

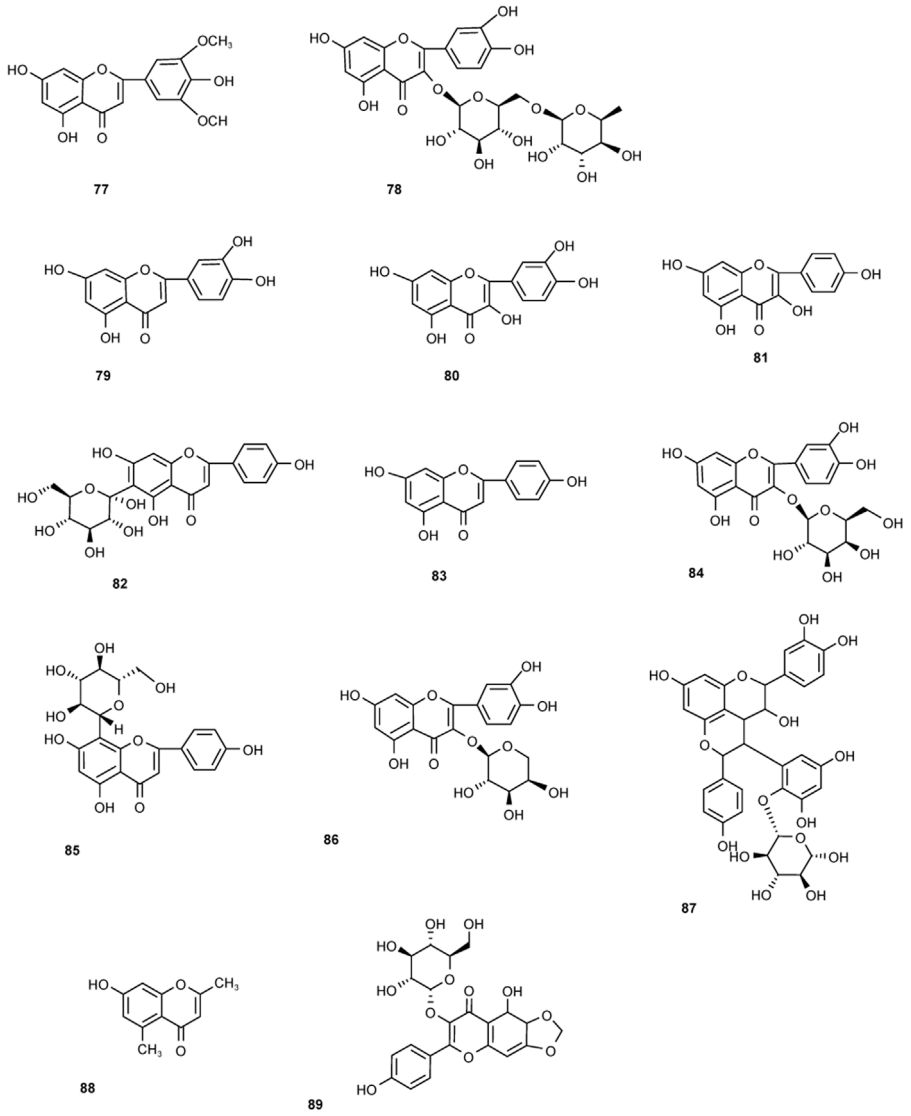

FIGURE 6
Chemical structures of other components in *Polygonum multiflorum* Thunb.

TABLE 3 Comparison of intrinsic toxicity and idiosyncratic toxicity.

	Intrinsic toxicity	Idiosyncratic toxicity
cause	Over-dose of usage	Immunity, metabolism and genes of specific patients
population affected	Affects all individuals	Affects only susceptible individuals
relationship with dose used	Dose-dependent	Not dependent on dose
clinically predictable	Predictable and can be avoided	Not predictable
courses after exposure	Predictable courses of disease after exposure	Variable courses of disease after exposure
liver characteristics	Distinctive liver toxicity	Variable liver pathology
animal models	Predictable and can be copied within animal models	Not able to be copied within animal models

tetrahydroxystilbene-2-O-β-D-glucoside may exacerbates the hepatotoxicity caused by APAP. Another study investigated effects of 2,3,5,4′-tetrahydroxystilbene-2-O-β-D-glucoside on the hepatotoxicity caused by DEN. 2,3,5,4′-tetrahydroxystilbene-2-O-β-D-glucoside inhibited liver injury and inflammatory cell infiltration in DEN-treated mice. Besides, 2,3,5,4′-tetrahydroxystilbene-2-O-β-D-glucoside

also attenuated DEN-induced accumulation of reactive oxygen species (ROS), pro-inflammatory cytokines, and DNA damage. Both the study indicated that 2,3,5,4′-tetrahydroxystilbene-2-O-β-D-glucoside exacerbates the hepatotoxicity induced by drugs in mice (Yu et al., 2020).

Clinical symptoms of liver toxicity caused by PM are mainly related to digestive system. Loss of appetite and oil aversion are two most emphasized symptoms. Growth of body mass is also reported in many studies. The liver fat growth may be more severe in female than male, indicated in a liver pathological section of rats fed with PM decoction for 3 months (Hu et al., 2009). Scholars found that transaminase and bilirubin (BIL) levels were higher in patients with liver injury caused by PM, and related jaundice is also detected in some patients. All the findings indicated that PM may disturb the metabolism of transaminase and BIL (Tang and Mei, 2017). BIL metabolism is related with UGT of phase II metabolism pathway, and among the isomers of UGT, the core enzyme related to BIL metabolism is UGT1A1 (Chang, 2020). Thus, PM may increase time of BIL metabolism by inhibiting enzyme UGT1A1 in phase II metabolism pathway (Zheng et al., 2021).

4.1.2 Idiosyncratic toxicity

Idiosyncratic drug-induced liver injury (IDILI) affects only a small subset of the population with specific predispositions, and does not exhibit a dose-response relationship, making it clinically unpredictable. Unlike other forms of toxicity, IDILI does not correlate directly with drug dosage, and its underlying pathophysiology remains poorly understood.

The exact pathophysiology of IDILI is multi-factorial involving drug or pharmacological factors (lipophilicity, dose, etc.), environmental factors, and host factors (genetics, immunity, possibly microbiome) (Chen et al., 2013; Stephens et al., 2014). Over the past decade, studies have found that polymorphisms in Human Leukocyte Antigen (HLA) molecules are associated with many drugs that cause IDILI, suggesting a role for the immune system in this pathology (Kaplowitz, 2013). HLA associations clearly point to the involvement of the adaptive immune system in IDILI (Dara et al., 2016).

Epidemiological and clinical data suggest that PM-DILI is an immune-mediated idiosyncratic liver injury. Results showed that 2,3,5,4′-tetrahydroxystilbene-2-O-β-D-glucoside isolated from PM could activate CD4+T and CD8+T in the liver, and could upregulate the levels of inflammatory cytokines including TNF-α, IFN-γ, IL-18, perforin and granzyme B in the liver tissues (Liu et al., 2024). Both PM water extract and cis-stilbene glucoside, the susceptibility component of hepatotoxicity, could cause hepatotoxicity in the mice pre-stimulated with TNF-α (Zhang et al., 2022). Dose of PM caused abnormal liver biochemical indicators and liver tissue damage in MIS model rats (Tu et al., 2019).

Recent attention has focused on IDILI triggered by LPS. Mice pretreated with a modest inflammatory dose of LPS became susceptible to intrinsic liver injury induced by nontoxic doses of APAP (Lai et al., 2018). With normal dose of PM engaged, HE staining of rats' liver showed mild swelling and local chronic inflammation. The results suggest that PM-DILI induced by LPS is related to inflammation, and this type of hepatotoxicity has no dose-dependence (Pang et al., 2015). Increased expression of cytokines and chemokines, activation of inflammatory cells, depression of PPAR-γ pathway, and stimulation of the TLR-NF-κB pathway, all indicated that the innate immune response may be involved with PM-DILI (Luyendyk et al., 2003; Deng et al., 2006; Zou et al., 2009; Maddox et al., 2010). Several drugs causing IDILI in humans also induce IDILI in animals with a normal dose of LPS, such as diclofenac, sulindac, ranitidine, amiodarone, halothane, and trovafloxacin (Zhu et al., 2019). Immunoinflammation may regulate the susceptibility to IDILI.

Additionally, TCM syndromes may influence PM-DILI susceptibility. After feeding water extract of processed PM, the serum inflammatory mediator TNF-α content of the rats with kidney-yang deficiency significantly increased. Processing of PM has certain liver damage to kidney-yang deficiency model (Bywpgxolgfy, 2016).

4.2 Central mechanisms of PM-DILI: Enzyme deficiency and inflammatory response interruption

Enzyme deficiency involves both CYP450 enzymes and UGTs, along with the presence of the HLA-B*35:01 gene in patients. In terms of drug effects, PM-DILI is characterized by disrupted inflammatory responses and impaired metabolism of BIL and bile acids (BA). As for the drugs, interrupting the inflammatory response, BIL and BA metabolism are the main aspects.

4.2.1 Deficiency of metabolism enzymes

Drug metabolism pathway *in vivo* can be divided into phase I and phase II (Ren et al., 2018). The metabolism of PM is mainly associated with CYP450 enzymes of the phase I metabolism, and UGT enzymes of the phase II metabolism (Figure 7).

4.2.1.1 Phase I metabolism pathway

CYP450 is an important enzyme in drug induced hepatotoxicity, vital for the process of phase I metabolism pathway. The main role of CYP450 is to make structural modifications to drug molecules, such as adding a hydroxyl group to the molecular structure to make it more hydrophilic. Many traditional Chinese medicine, PM included, induces or inhibits this enzyme, leading to the accumulation of active metabolic components of drugs, or leading to decreased drug efficacy, increased adverse reactions or toxicity (Mao et al., 2016).

Metabolism of many drugs depends on CYP1A2, such as phenacetin, caffeine, clozapine, tacrine, propranolol and mexiletine, etc. (Hou et al., 2016) PM extractions can significantly decrease the activity and mRNA expression of liver CYP1A2 enzyme (Guo et al., 2021). Another study found that genetic polymorphism of CYP1A2 in patients with PM-DILI is different from that of normal people (Ma et al., 2014). Thus, both the genetic polymorphism of CYP1A2 and the inhibition of PM on CYP1A2, leading to the accumulation of toxic components, may be the mechanism of PM-DILI. Besides, different processing methods of PM can lead to different regulation of mRNA expression levels of drug metabolizing enzymes CYP2E1, CYP3A4 and CYP1A2 (Li et al., 2021). As a result, processing may affect the regulation of CYP450 enzymes, leading to detoxification of PM.

4.2.1.2 Phase II metabolism pathway

UGTs is the main metabolic catalytic enzyme in the phase II metabolic reaction, metabolizing nearly 35% of drugs and inactivate them. UGTs can transfer the glucuronic acid group of the cofactor

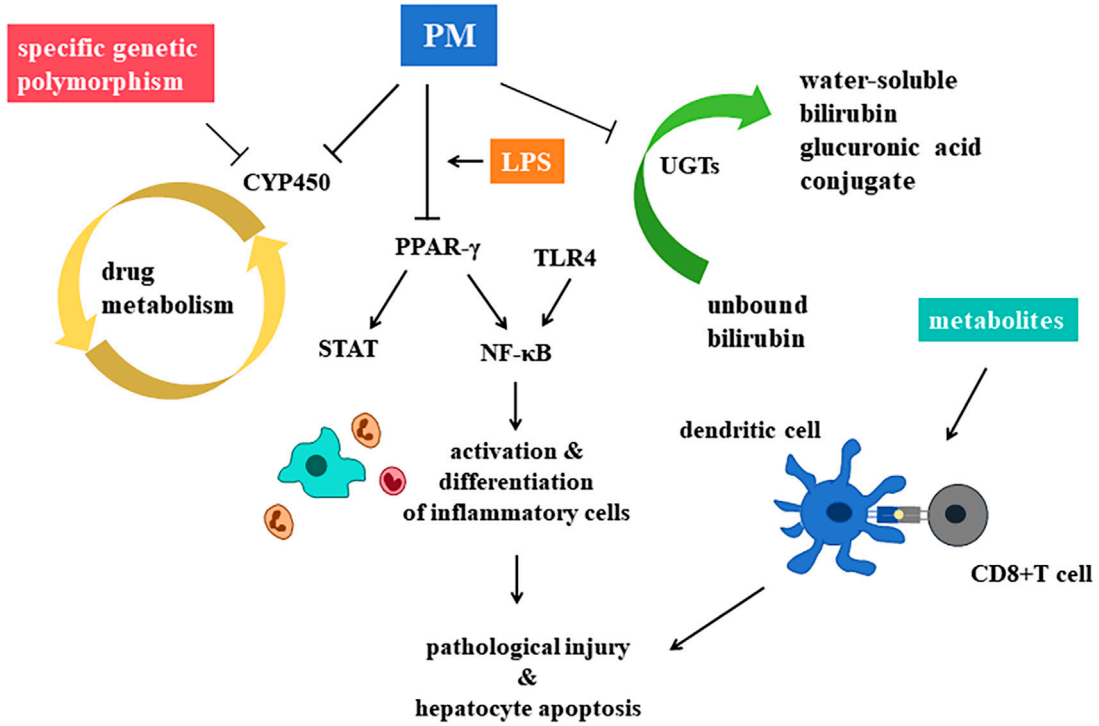

FIGURE 7
Central mechanisms of hepatotoxicity of *Polygonum multiflorum* Thunb. are recognized as the inhibition on CYP450 enzymes the decrease of PPAR-γ, and the inhibition of UGTs.

uridine diphosphate glucuronic acid (UDPGA) to the hydroxyl group of drug molecules, so as to improve the water solubility of drugs and facilitate their excretion through urine or bile, leading to the occurrence of PM-DILI (Yang et al., 2021).

Glucanosyltransferase 1 family polypeptide A1 (UGT1A1) is a phase II metabolic enzyme in the liver. It is related to the catalyze of unbound bilirubin (UCB), it can transform UCB into water-soluble BIL glucuronic acid conjugate, so that UCB can be secreted into bile for elimination. PM has been observed to inhibit UGT1A1, a key enzyme in BIL metabolism, thereby disrupting the conversion of UCB into its water-soluble form and promoting its accumulation, which could lead to hepatotoxicity (Wang Q. et al., 2022).

The toxicity of PM may result from more than one single pathway. Scholars found that the main components of PM such as emodin, rhein, emodin methyl ether, etc. had toxicity on liver cell through inhibiting the activity of CYP1A2 and CYP2C9 and competitively inhibiting the activity of BIL rate-limiting enzyme UGT1A1 (Zheng and Wang, 2019). Besides, there are studies demonstrated the mechanisms such as the induction of apoptosis and the inhibition of liver cell proliferation. Lipid metabolism, bile acid metabolism and energy metabolism are involved. Oxidative phosphorylation pathways is also related according to proteomics (Zhang et al., 2016). Functions of these pathways are still under cultivating (Zhu et al., 2019).

4.2.2 Interruption of inflammatory response

Interruption of the inflammatory response is a key mechanism underlying hepatotoxicity. Peroxisome proliferator activated receptor-γ (PPAR-γ), a member of the nuclear receptor superfamily, plays a critical role in modulating inflammatory and anti-inflammatory signaling pathways. PPAR-γ can inhibit NF-κB and STAT pathways, restraining inflammatory cells, retarding hepatotoxicity.

Based on the model of LPS induced IDILI, He Lanzhi et al. (He et al., 2017) explored the effects of PM's alcohol extract on hepatotoxicity. They discovered that toxicity might be linked to the over-expression of inflammatory factors and the suppression of the PPAR-γ pathway *in vivo*. PPAR-γ agonists can significantly reduce the levels of ALT and AST in rats plasma, alleviating pathological injury and hepatocyte apoptosis, significantly promote the expression of PPAR-γ and inhibit the expression of NF-κB p65 in liver tissue. Thus, the abnormal decrease of PPAR-γ and the over expression of inflammatory factors may lead to the hepatotoxicity, and PPAR-γ may be the target point of PM-DILI.

Furthermore, activation of the TLR4/IRF-3 signaling pathway has also been implicated in PM-DILI. Unlike dose-dependent mechanisms, hepatotoxicity here is associated with the expression levels of proteins in the TLR4/IRF-3 pathway (Xue et al., 2020).

4.2.3 Genetic risk factor

In the last decade, numerous genome-wide association studies (Kaliyaperumal et al., 2018) have linked human leukocyte antigens (HLAs) to IDILI susceptibility. Scholars found that the HLA-B*35: 01 allele is a genetic risk factor for PM-DILI and a potential biomarker for predicting PM-DILI in humans (Lin et al., 2017).

Three models have been put out for the possible mechanisms of T cell-mediated drug hypersensitivity regulated by HLA: the hapten/prohapten model, the pharmacological interaction model and the altered peptide repertoire model (Yun et al., 2012; Uetrecht and

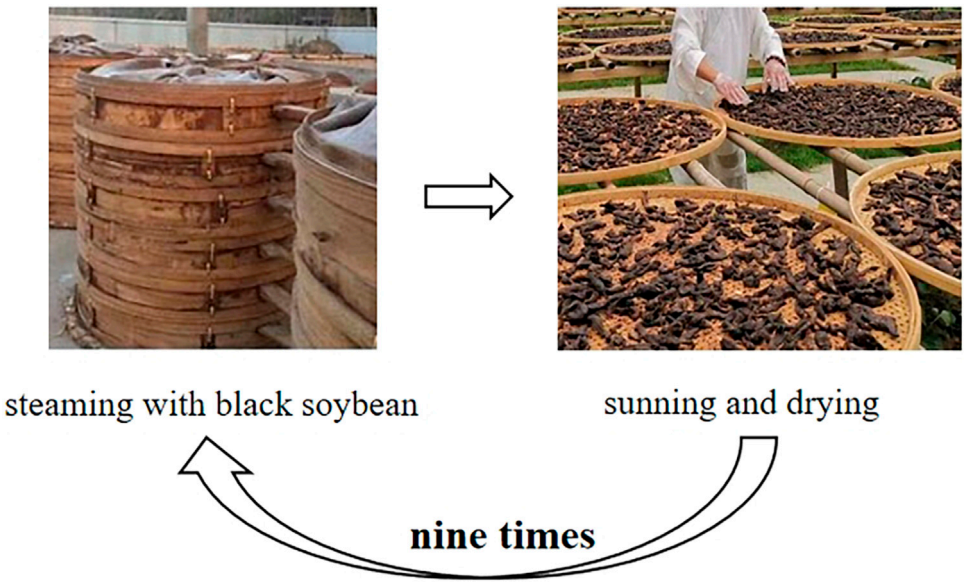

FIGURE 8
The most widely used processing method: nine times of steaming and sunning.

Naisbitt, 2013; Redwood et al., 2018). The hapten/prohapten model is the main hypothesis, and is widely studied. Other two hypothesis may act as an alteration to the hapten/prohapten model. As one of the HLA-associated forms of DILI, the mechanism of PM-DILI is associated with the interaction between antigen-presenting cells (APCs) and T cells. After the metabolism of toxic components in the liver, the metabolites can be taken by dendritic cells (DCs), forming adducts covalently with self-proteins, processing in the endoplasmic reticulum, triggering the maturation of DCs. HLA-B*35:01 molecules then present the adducts at the surface of cells, waiting for the activation of CD8+T cells by interacting with T cell receptors (TCRs) (Rodriguez-Pena et al., 2006; Megherbi et al., 2009; Qin et al., 2016; Jiang et al., 2017; Qin et al., 2018).

Besides, FXR gene may also be related to PM-DILI. Scholars screened and verified that the hepatotoxic components aloe emodin-8-O-β-D-glucoside and emodin-8-O-β-D-glucoside in PM could significantly inhibit FXR gene expression through molecular docking and *in vitro* cytotoxicity tests.

In conclusion, gene mechanisms of hepatotoxicity of PM varies a lot, most of the studies emphasize the alterations of drug-metabolizing enzymes as the main mechanism, Immune-Related Gene Polymorphism, BIL-BA metabolism pathway and HLA related T cell-mediated drug hypersensitivity are also important mechanisms.

5 Traditional processing and detoxification of PM

Traditional Chinese Medicine has utilized various processing methods for decades. There are many processing methods for PM: Wen PE, nine cycles of steaming and sunning, stewing, steaming, etc. Processing is often incorporating with various excipients to modify the herb's chemical profile and reduce toxicity. After processing, chemical components in PM changed, thus lead to a reduction in toxicity. What's more, both the methods of processing and excipients added can detoxify PM, as well as increase the effect of it (Figure 8).

5.1 Processing detoxification can detoxify PM by changing its chemical components

Processing significant increased content of polysaccharide in PM. Results showed that raw PM and processed PM both comprised Man, Rha, GlcA, GalA, Glc, Ara and Xyl, but markedly differed in polysaccharide yield, molar ratio of monosaccharide composition and Glc/GalA (Wang et al., 2023). The fingerprint of monosaccharide composition also demonstrated that Glc and GalA could be used as differential markers (Gu et al., 2022). It was found that the addition of black beans and steaming times would affect the content and composition of polysaccharide in PM significantly (Fan et al., 2024).

The content of 2,3,5,4′-tetrahydroxystilbene-2-O-β-D-glucoside decreased after processing. Researchers found that during the processing, maillard reaction occurred, producing a large number of compounds, including acetone alcohol, 2, 3-butanediol, succinic acid, 2, 3-dihydro-3, 5-dihydroxy-6-methyl-4H-pyranone (DDMP), 5-hydroxymethyl furfural (5-HMF) and its derivatives. 2,3,5,4′-tetrahydroxystilbene-2-O-β-D-glucoside was converted into a series of derivatives through the esterification reaction with small molecular compounds. Resveratrol was the intermediate product of 2,3,5,4′-tetrahydroxystilbene-2-O-β-D-glucoside, which was hydroxylated to form terahydroxystilbene, and then glycosylated to form 2,3,5,4′-tetrahydroxystilbene-2-O-β-D-glucoside. The representative herbal components trans-2,3,5,4′-tetrahydroxystilbene-2-O-β-D-glucopyranoside and cyanidin-3-O-β-glucoside from each herbal medicine were

selected to investigate the processing mechanism at the supramolecular level (Bai et al., 2022). The co-assembly of 2-O-β-D-glucopyranoside and cyanidin-3-O-β-glucoside that leads to supramolecular aggregates discovered here may imply the underlying mechanism of processing PM with black beans (Liu et al., 2023). After nine cycles of steaming, the amount of stilbenes and combined quinones decreased (Zheng et al., 2021).

There are some other components different in raw PM and processed PM. High-performance liquid chromatography studies on different processing methods reveal that stewing PM leads to the hydrolysis of combined quinones into their free forms, thereby diminishing the herb's toxicity (Ding et al., 2023). Main components of PM such as 2,3,5,4′-tetrahydroxystilbene-2-O-β-D-glucoside, emodin methyl ether and emodin increased significantly (Liu MJPJ. et al., 2020). Five compounds were different in raw and processed PM: α-arabinose, α-galactose, proline, isomer of daidzein and isomer of genistein, which may be potential active ingredients that affect the processing of PM (Chen et al., 2021). Quinones can be decomposed into gallic acid, resulting in an increase in the content after processing. After processing, gallic acid substances in PM increased, and the proportion of quinones decreased. Tannins in PM would be destructed with processing, and may be converted into gallic acid, which further increased the proportion of gallic acid in PM (Ke et al., 2021) (Table 4).

Wen PE, a unique method of PM processing, was first documented in "Pao Zhi Da Fa," and it was only passed down in Jianchangbang. The processing method is to take the PM slices, soak them, add black beans, put them in a boiled medicine jar, add warm water, cover them, simmer them for 48 h, take them out, dry them, and sieve them to remove the black bean dregs; Then mix well with yellow wine, wait for exhaustion, steam for 6 h, stop the fire and seal it overnight, take it out, and dry it. Researchers found that the amount of emodin-8-O-β-D-glucopyranoside、torachrysone-8-O-β-D-glucopyranoside、emodin 8-O-(6′-methylmalonyl)-glucopyranoside and physcion-8-O-β-D-monoglucoside decreased in Wen PE, and AST, ALT, LDH, GGT decreased *in vivo*, indicating that Wen processing decreased the hepatotoxicity in PM (Ding et al., 2022).

Processing detoxification can decrease the toxicity of PM with or without excipients. Black soybeans processing is the most widely used. With the excipients of black beans, 12 components changed significantly: Free quinones decreased first and increased as the steaming time extending. Quinones, cis-2,3,5,4′-tetrahydroxystilbene-2-O-β-D-glucoside, polydatin and hypericin increased first and then decreased. Amount of trans-2,3,5,4′-tetrahydroxystilbene-2-O-β-D-glucoside, resveratrol, epicatechin and rutin all decreased (Zhu et al., 2019). Li Yanyi et al. (Li et al., 2023) also found that the content of stilbene glycoside, quinone, flavonoid decreased after processing, while the amount of phenol increased. In a conclusion, steaming with black soybeans can not only decrease the hepatotoxicity, but also increase the medicinal value of PM.

Except for black soybean juice, there are some other excipients that have been investigated. Different processing excipients can lead to different levels of stilbene glycoside and free quinone. Processing of black soybean juice and ginger juice lead to the highest contents of stilbene glycoside and free quinone, the processing of rice swill with black soybean juice reflected the lowest level of stilbene glycoside, and the content of free quinone was the lowest in the procession of black soybean with *Rehmannia glutinosa* DC. juice (Li et al., 2020). Researchers also found that rice swill could be excipient for detoxification (BX, 2017; Liu et al., 2020), jujubes are also standard excipients for detoxification (Liu et al., 2020). The content of stilbene glycoside in boiled PM is the highest, meaning that the three methods of processing can all effectively retain the active ingredients of PM, while rice swill is the best (BX, 2017).

5.2 Processing detoxification can detoxify PM as well as increase its efficacy

Repeated processing, particularly through nine cycles of steaming and sunning, significantly alters the chemical composition of PM, thus lead to a decrease in toxicity and an increase in efficacy (Liang et al., 2018).

In vivo, results showed that raw PM and processed PM both exerted hepatoprotective effects by upregulating antioxidant enzymes and repressing lipid peroxidation, and that the polysaccharide yield of processed PM was seven-fold higher than that of raw PM, demonstrating that processed PM has better hepatoprotective effects at the same dose of decoction (Wang et al., 2023). Researchers also found that the immunomodulatory activity of processed PM was significantly better than that of raw PM (Gu et al., 2022).

In vitro, more cycles of steaming and sunning can lead to a lower serum ALT and AST in rats, due to lower percentage of stilbenes in processed PM (Zheng et al., 2021). The TBIL and DBIL levels decreased gradually with the increase of steaming and sunning times, suggesting that multiple steaming and sunning may result in a protection for the metabolism of transaminase and bilirubin (Gao et al., 2022). Moreover, it has been reported that processing could increase the amount of phenylethyl olefinic glycoside, increase the effects of protecting nerves, improving memory, anti-aging, decreasing

TABLE 4 Chemical components before and after processing.

Chemical components	Changes after processing
polysaccharides	The contents of monosaccharides and disaccharides decreased, the total content of carbohydrates increased, and the molecular weight of PM polysaccharides decreased
stilbene glycosides	The overall content of stilbene glycosides decreased, the proportion of trans/cis-stilbene glycosides decreased, and the amount of cis-stilbene glycosides increased
quinones	The content of emodin decreases, emodin methyl ether increases, gallic acid content increases

blood lipid and so on, thus stewing can not only decrease the toxicity, but can also increase the benefits of PM (Wang et al., 2022).

Mechanisms of processing is still under investigation. Processing PM with black beans could significantly decrease the apoptosis rate of L02 cells, indicating that the detoxification may related to apoptosis (Chen et al., 2021). Huang Chaowen et al. (Huang et al., 2023) explored the mechanism of PM detoxifying, and results showed that processing of PM can decrease the hepatotoxicity by decreasing autophagy, which may provide new interventions for the detoxification.

5.3 Compatible detoxification is a convenient way of detoxifying and is traditionally used in clinical practice

Compatible detoxification is one of the traditional Chinese medicine detoxification methods. It means that one kind of Chinese medicine is used together with another or more kinds of Chinese medicine, so as to achieve the purpose of inhibiting or eliminating the toxicity of Chinese medicine. This approach has been shown to alleviate PM-DILI when used with substances such as cistanche polysaccharides, brown algal oligosaccharides, and chito-oligosaccharides (Ren et al., 2021). *Ganoderma lucidum* (Curtis) P. Karst. was used for biological detoxification of tetrahydroxystilbene glucoside-induced idiosyncratic hepatotoxicity of PM (Lin et al., 2021). Scholars have also studied the compatibility of PM with *Poria cocos* (Schw.) Wolf and *Glycyrrhiza uralensis* Fisch., results showed that the compatibility of PM and *Poria cocos* (Schw.) Wolf is better in detoxification (Pang et al., 2015). Compatible detoxification is a convenient way of detoxifying, the two methods of detoxification is usually conducted together in clinical practice, while mechanism of them is worth investigation (Table 5).

6 Conclusion

Significant advancements have been made in understanding the pharmacology, toxicology, and processing detoxification of PM. Within the aspect of pharmacology, medications of PM have been cultivated since the usage by the ancient Chinese. It is widely used nowadays in the protection from aging, insomnia and hair-losing. Researcher found that PM is mainly consist of stilbenes, quinones and flavonoids. Stilbenes can lead to a dysfunction of UGTs, resulting in IDILI. Quinones can lead to an inhibition of CYP450 enzymes and UGTs, resulting in hepatotoxicity. As a dietary component, flavonoids are thought to have beneficial effects on human health. Their health-promoting properties are associated with antioxidant, anti-inflammatory, and anticancer properties (Serafini et al., 2010; Procházková et al., 2011; Kumar and Pandey, 2013; Gontijo et al., 2017; Dobrzynska et al., 2020). Flavonoids have a function of protecting liver, which means it may be the protecting components of PM. Within the aspect of toxicology, water extract and alcohol extract of raw and prepared PM have been explored, and more than 103 components, including flavonoids, phospholipids, quinones, stilbenes, have been isolated and characterized. Hepatotoxicity is the main aspect of toxicity of PM, intrinsic toxicity and idiosyncratic toxicity can affect the liver function through mechanisms of metabolism enzymes, inflammatory response and genetic risk factors. Within the aspect of processing detoxification, nine cycles of steaming and sunning, and different types of stewing can change the components in PM, resulting in decreased toxicity and enhanced efficiency. Compatible detoxification is also one of the specific ways of detoxification in TCM, with a convenience in usage, it is commonly applied in clinical practice.

In traditional Chinese medicine, PM is widely used for nourishing liver and kidney, tonifying blood, anti-aging and blackening hair. Ancient Chinese use raw PM to treat *postpartum* fever, and process PM with various excipients of Yellow Rice Wine, black soybean juice, swill, and jujube juice, etc. to treat hair losing, forgetfulness, headache, sores and ulcers. Processed PM is decreased in toxicity and is maximum in pharmacologic effects. However, with multi-targets and multi-components, the exact mechanism of processed PM and the pharmacokinetics *in vivo* are still worth investigating. Updating the research paradigm from the current "one target, one drug" mode to a new "network target, multi-components" mode, TCM network pharmacology approach provides a new research paradigm for translating TCM from an experience-based medicine to an evidence-based medicine system, which will accelerate TCM drug discovery, and also improve current drug discovery strategies (Li and Zhang, 2013; Wang et al., 2020; Wang et al., 2022c).

Different aspects of toxicity on PM have been reported, including hepatotoxicity, nephrotoxicity and embryotoxicity, of which hepatotoxicity is the most important. Based on an examination of the literature, we speculate that the possible

TABLE 5 Compatibility of PM and compatible effects.

Compatibility of PM	Compatible effects
poria cocos (Schw.) Wolf	Decreasing cytotoxicity and the detoxification effect is better than *Glycyrrhiza uralensis* Fisch
glycyrrhiza uralensis Fisch	Decreasing cytotoxicity
ganoderma lucidum (Curtis) P. Karst	P-hydroxybenzaldehyde was formed, decreasing cell toxicity
cistanche polysaccharides	Improving histopathological changes, reduce liver index and liver function index, inhibit the increase of spleen index, and inhibit TNFα, IL-1β, MCP-1, MIP-1α
brown algal oligosaccharides	Decreasing inflammatory cell infiltration and hepatocyte necrosis, decreasing serum ALT and AST, and decreasing MIP-1α, TNFα, IL-1α
chito-oligosaccharides	Improving histopathological changes, decreasing liver index and liver function index

reasons are as follows. Firstly, the over-dose of usage may lead to intrinsic toxicity, resulting in the binding of drugs and their RM to host proteins, the depletion of antioxidant systems such as GSH, the activation of stress kinases, the release of strong oxidizing groups such as ROS from mitochondrial stress and mitochondrial dysfunction, endoplasmic reticulum stress, as well as the activation of the innate immune system and local inflammatory response of the liver. Secondly, immunity, metabolism and genes of specific patients affects susceptible individuals, leading to idiosyncratic toxicity, resulting in increased expression of cytokines and chemokines, activation of inflammatory cells, depression of PPAR-γ pathway, and stimulation of the TLR-NF-κB pathway.

Indirect liver injury is a kind of drug liver injury caused by the action of the drug rather than by its toxic or idiosyncratic properties, the mechanism of injury is that drugs indirectly cause liver injury by changing the patient's original liver disease or immune status (Hoofnagle and Björnsson, 2019), which can be caused by immune checkpoint inhibitors (ICIs), glucocorticoids, monoclonal antibodies, etc. At present, there have been no reports of indirect liver injury caused by PM, and it is worth exploring whether PM can cause indirect liver injury.

Therefore, proper dosage, extractions and components of PM, effects as well as toxicity of PM are still need to be verified. Given the diverse toxicological profiles observed, including hepatotoxicity, nephrotoxicity, and embryotoxicity, further research is essential. Mechanisms of traditional processing and compatible detoxification are worth explored. Changes of chemical components before and after processing, as well as changes of chemical components before and after compatibility are need to be deeply researched.

Author contributions

JQ: Investigation, Methodology, Writing–original draft, Writing–review and editing. CF: Investigation, Methodology, Writing–original draft. ZW: Investigation, Methodology, Writing–original draft. YY: Conceptualization, Methodology, Software, Writing–review and editing. XG: Writing–review and editing, Conceptualization. LZ: Conceptualization, Methodology, Software, Writing–review and editing. YL: Conceptualization, Writing–review and editing. YG: Conceptualization, Methodology, Writing–review and editing.

Funding

The author(s) declare that no financial support was received for the research, authorship, and/or publication of this article.

Conflict of interest

The authors declare that the research was conducted in the absence of any commercial or financial relationships that could be construed as a potential conflict of interest.

Publisher's note

Supplementary material

The Supplementary Material for this article can be found online at: https://www.frontiersin.org/articles/10.3389/fphar.2024.1427019/full#supplementary-material

References

Bai, J., Chen, W., Huang, J., Su, H., Zhang, D., Xu, W., et al. (2022). Transformation of stilbene glucosides from reynoutria multiflora during processing. *Front. Pharmacol.* 13, 757490. doi:10.3389/fphar.2022.757490

Bx, G. (2017). Analysis of the influence of different processing methods on the active ingredient content of Polygonum multiflorum. *Inn. Mong. Tradit. Chin. Med.* 36 (09), 143–144. doi:10.16040/j.cnki.cn15-1101.2017.09.128

Bywpgxolgfy, J. H. (2016). Study on the mechanism of liver toxicity induced by polygoni multiflori radix (PMR) and polygoni multiflori praeparata radix decoction in rats. *Her. Traditional Chin. Med.* 22 (06), 21–23.

Chang, Y. L. L. N. (2020). Systematic review of drug - induced liver injury caused by polygonum multiflorum and its preparations. *China Pharm.* 29 (19), 81–86.

Chen, L., Huang, J., Fau - Xue, L., and Xue, L. (2010). Effect of compound Polygonum multiflorum extract on Alzheimer's disease. *Control. Clin. Trial* 35 (6), 612–615. doi:10.3969/j.issn.1672-7347.2010.06.012

Chen, M., Borlak, J., and Tong, W. (2013). High lipophilicity and high daily dose of oral medications are associated with significant risk for drug-induced liver injury. *Hepatology* 58 (1), 388–396. doi:10.1002/hep.26208

Chen, W., Wang, P., Chen, H., Xing, Y., Liu, C., Pan, G., et al. (2021). The composition differences between small black beans and big black beans from different habitats and its effects on the processing of Polygonum multiflorum. *Phytochem. Anal.* 32 (5), 767–779. doi:10.1002/pca.3022

Dara, L., Liu, Z.-X., and Kaplowitz, N. (2016). Mechanisms of adaptation and progression in idiosyncratic drug induced liver injury, clinical implications. *Liver Int.* 36 (2), 158–165. doi:10.1111/liv.12988

Deng, X., Stachlewitz, R. F., Liguori, M. J., Blomme, E. A. G., Waring, J. F., Luyendyk, J. P., et al. (2006). Modest inflammation enhances diclofenac hepatotoxicity in rats: role of neutrophils and bacterial translocation. *J. Pharmacol. Exp. Ther.* 319 (3), 1191–1199. doi:10.1124/jpet.106.110247

Ding, P. P. Y. B., Chen, H. S., Chen, M. X., Lu, S., Zhang, Q., Chen, X. Y., et al. (2023). Changes of anthraquinone glycosides and detoxificatio effect in decoction pieces of stewed polygoni multiflori radix. *Chin. J. Mod. Appl. Pharm.* 40 (9), 1180–1186. doi:10.13748/j.cnki.issn1007-7693.20220692

Ding, P. Y. B., Yang, H., Chen, H., Chen, X., Zhang, Q., Rao, Y., et al. (2022). Influence of simmering on anthraquinone glycosides of polygonum multiflora radix and its attenuation effect. Traditional Chinese drug research & clinical. *Pharmacology* 33 (10), 1400–1406.

Dobrzynska, M., Napierala, M., and Florek, E. (2020). Flavonoid nanoparticles: a promising approach for cancer therapy. *Biomolecules* 10 (9), 1268. doi:10.3390/biom10091268

Fan, X., Zhou, L., Xing, Y., Wang, L., Choi, S. S., Zhang, Z., et al. (2024). A comprehensive investigation on the chemical changes of traditional Chinese medicine with classic processing technology: polygonum multiflorum under nine cycles of steaming and sunning as a case study. *Anal. Bioanal. Chem.* 416 (7), 1733–1744. doi:10.1007/s00216-024-05177-0

Fan, Y., Liu, J., Miao, J., Zhang, X., Yan, Y., Bai, L., et al. (2021). Anti-inflammatory activity of the Tongmai Yangxin pill in the treatment of coronary heart disease is associated with estrogen receptor and NF-κB signaling pathway. *J. Ethnopharmacol.* 276, 114106. doi:10.1016/j.jep.2021.114106

Gao, F. T. Y., Zhang, Y. N., Zou, Y. R., Qiao, J. X., and Wei, P. F. (2022). Discussion and experimental verification of hepatotoxicity mechanism of Polygonum multiflorum processed by different methods based on network pharmacology. *Drug Eval. Res.* 45 (8), 1522–1530. doi:10.7501/j.issn.1674-6376.2022.08.009

Gontijo, V. S., Dos Santos, M. H., and Viegas, C. (2017). Biological and chemical aspects of natural biflavonoids from plants: a brief review. *Mini Rev. Med. Chem.* 17 (10), 834–862. doi:10.2174/1389557517666161104130026

Gu, D., Wang, Y., Jin, H., Kang, S., Liu, Y., Zan, K., et al. (2022). Changes of physicochemical properties and immunomodulatory activity of polysaccharides during processing of polygonum multiflorum Thunb. *Front. Pharmacol.* 13, 934710. doi:10.3389/fphar.2022.934710

Guo, J., Zhu, X., Badawy, S., Ihsan, A., Liu, Z., Xie, C., et al. (2021). Metabolism and mechanism of human cytochrome P450 enzyme 1A2. *Curr. Drug Metab.* 22 (1), 40–49. doi:10.2174/1389200221999210101233135

Han, M. N., Lu, J. M., Zhang, G. Y., Yu, J., and Zhao, R. H. (2015). Mechanistic studies on the use of polygonum multiflorum for the treatment of hair graying. *Randomized Control. Trial* 2015, 651048. doi:10.1155/2015/651048

He, L. Z. Y. P., Meng, Y. K., Zhang, Z. F., Liu, H. M., Cui, H. R., Ni, H. T., et al. (2017). Study on the mechanism of PPAR-γ dependent immunological idiosyncrasy liver injury induced by Polygonum multiflorum. *Acta Pharm. Sin.* 52 (7). doi:10.16438/j.0513-4870.2016-0774

Hoofnagle, J. H., and Björnsson, E. S. (2019). Drug-induced liver injury - types and phenotypes. *N. Engl. J. Med.* 381 (3), 264–273. doi:10.1056/NEJMra1816149

Hou, J. S. E., Song, J., Yang, L., Zhang, Z. H., Ning, Q., Jia, X. B., et al. (2016). Relationship between hepatic drug-metabolizing enzymes CYP450 and traditional Chinese medicine-induced hepatotoxicity. *China J. Chin. Materia Medica* 41 (15), 2774–2780. doi:10.4268/cjcmm20161505

Hu, X. Q. L. F., Li, Y., Zhuo, J., and Wang, J. S. (2009). Effects of Polygonum multiflorum, its production and Poria cocos compatibility on rat liver microsomal cytochrome P450. *Shaanxi Tradit. Chin. Med.* 30 (02), 240–241.

Huang, C. W. L. Y., Wang, L., Bao, Q., Jiang, Y., and Yang, L. (2023). Hepatocytotoxic mechanism of different processing products of Heshouwu (Polygonum Multiflorum) based on transcriptomics. *J. Hunan Univ. Chin. Med.* 43 (6), 1028–1034. doi:10.3969/j.issn.1674-070X.2023.06.010

Jiang, L.-L., Zhao, D.-S., Fan, Y.-X., Yu, Q., Li, P., and Li, H.-J. (2017). Detection of emodin derived glutathione adduct in normal rats administered with large dosage of polygoni multiflori radix. *Front. Pharmacol.* 8, 446. doi:10.3389/fphar.2017.00446

Kaliyaperumal, K., Grove, J. I., Delahay, R. M., Griffiths, W. J. H., Duckworth, A., and Aithal, G. P. (2018). Pharmacogenomics of drug-induced liver injury (DILI): molecular biology to clinical applications. *J. Hepatol.* 69 (4), 948–957. doi:10.1016/j.jhep.2018.05.013

Kaplowitz, N. (2013). Avoiding idiosyncratic DILI: two is better than one. *Hepatology* 58 (1), 15–17. doi:10.1002/hep.26295

Ke, Y. C. C. J., Chen, X. P., and Liang, Y. L. A qualitative and quantitative analysis of the chemical constituents of polygonum multiflorum after processing. 2021;13(22): 42–45.

Kumar, S., and Pandey, A. K. (2013). Chemistry and biological activities of flavonoids: an overview. *Scientific World Journal* 2013, 162750. doi:10.1155/2013/162750

Lai, X.-X., Wu, J.-B., Chen, S., Lai, P., Wang, X.-H., Wang, Y.-Y., et al. (2018). Risk factors analysis and security application discussion of Polygonum multiflorum based on retrospective study. *Zhongguo Zhong Yao Za Zhi* 43 (15), 3205–3210. doi:10.19540/j.cnki.cjcmm.20180529.002

Li, C.-Y., Tu, C., Gao, D., Wang, R.-L., Zhang, H.-Z., Niu, M., et al. (2016). Metabolomic study on idiosyncratic liver injury induced by different extracts of polygonum multiflorum in rats integrated with pattern recognition and enriched pathways analysis. *Front. Pharmacol.* 7, 483. doi:10.3389/fphar.2016.00483

Li, H., Yang, H.-I., Li, D.-K., Feng, G.-Y., Wei, B.-H., Zhang, Y.-Y., et al. (2015). Study on inhibitory effect of water extract of Polygonum multiflorum on CYP1A2 and CYP2E1 enzymatic activities and mRNA expressions in rat liver. *Zhongguo Zhong Yao Za Zhi* 40 (7), 1370–1375.

Li, J. X. G. Y., Liu, Q., Gao, F., Dong, T. W., Chen, L., Li, R., et al. (2021). Study on the change law of"Time-toxicity-effect"for polygonum multiflorum based on drug metabolic enzyme pathway. *J. Sichuan Traditional Chin. Med.* 39 (11).

Li, R. H. G. G., Long, G. B., Xiang, Y. F., and Zhu, W. X. (2020). Effects of different processing excipients on contents of effective components in polygonum multiflorum Thunb. *Pharm. Today* 30 (4), 255–258. doi:10.19803/j.1672-8629.20230146

Li, S., and Zhang, B. (2013). Traditional Chinese medicine network pharmacology: theory, methodology and application. *Chin. J. Nat. Med.* 11 (2), 110–120. doi:10.1016/S1875-5364(13)60037-0

Li, S.-G., Huang, X.-J., Li, M.-M., Liu, Q., Liu, H., Wang, Y., et al. (2018). Multiflorumisides A-G, dimeric stilbene glucosides with rare coupling patterns from the roots of polygonum multiflorum. *J. Nat. Prod.* 81 (2), 254–263. doi:10.1021/acs.jnatprod.7b00540

Li, S.-G., Huang, X.-J., Zhong, Y.-L., Li, M.-M., Li, Y.-L., Wang, Y., et al. (2019). Stilbene glycoside oligomers from the roots of polygonum multiflorum. *Chem. Biodivers.* 16 (6), e1900192. doi:10.1002/cbdv.201900192

Li, Y. Y. W. H., Wang, Y., Yang, J. B., Liu, Y., Wang, Q., Zhang, Y. J., et al. (2023). Influences of continuous steaming with black bean decoction on contents of 24 components of Polygoni Multiflori Radix. *Chin. J. Pharmacovigil.* 20 (6), 609–615.

Liang, L., Xu, J., Zhou, W.-W., Brand, E., Chen, H.-B., and Zhao, Z.-Z. (2018). Integrating targeted and untargeted metabolomics to investigate the processing chemistry of polygoni multiflori radix. *Front. Pharmacol.* 9, 934. doi:10.3389/fphar.2018.00934

Lin, L., Li, H., Lin, H., Zhang, M., Qu, C., Yan, L., et al. (2017). Application of iTRAQ-based quantitative proteomics approach to identify deregulated proteins associated with liver toxicity induced by polygonum multiflorum in rats. *Cell Physiol. Biochem.* 43 (5), 2102–2116. doi:10.1159/000484229

Lin, L., Ni, B., Lin, H., Zhang, M., Li, X., Yin, X., et al. (2015). Traditional usages, botany, phytochemistry, pharmacology and toxicology of Polygonum multiflorum Thunb.: a review. *J. Ethnopharmacol.* 159, 158–183. doi:10.1016/j.jep.2014.11.009

Lin, Y., Peng, X., Xia, B., Zhang, Z., Li, C., Wu, P., et al. (2021). Investigation of toxicity attenuation mechanism of tetrahydroxy stilbene glucoside in Polygonum multiflorum Thunb. by Ganoderma lucidum. *J. Ethnopharmacol.* 280, 114421. doi:10.1016/j.jep.2021.114421

Liu, M. J. P. J., Dai, B., Yang, Q. W., Zhang, Z. G., and Yang, L. (2020a). Optimization of processing technology of "nine-time repeat steaming and sun-drying process" of polygoni multiflori radix and effects on L02 hepatocytes. *Chin. J. Inf. TCM* 27 (04), 70–73. doi:10.3969/j.issn.1005-5304.201904391

Liu, W., Zeng, X., Wang, X., Hu, Y., Chen, L., Luo, N., et al. (2024). 2,3,5,4'-tetrahydroxystilbene-2-O-β-D- glucopyranoside (TSG)-Driven immune response in the hepatotoxicity of Polygonum multiflorum. *J. Ethnopharmacol.* 326, 117865. doi:10.1016/j.jep.2024.117865

Liu, Y., Wang, S., Qin, Y., Wang, Y., Yang, J., Zhang, L., et al. (2023). Enhanced TSG stability through co-assembly with C3G: the mechanism behind processing Polygonum multiflorum Thunb with black beans via supramolecular analysis. *Food Funct.* 14 (9), 4204–4212. doi:10.1039/d2fo03402f

Liu, Y. L. G. D., Li, X. F., Xiao, X. H., and Wang, J. B. (2020b). Preliminary study on hepatotoxic components in Polygoni Multiflori Radix based on different adjuvants processing for detoxification. *Chin. Traditional Herb. Drugs* 51 (2), 330–337. doi:10.7501/j.issn.0253-2670.2020.02.008

Luyendyk, J. P., Maddox, J. F., Cosma, G. N., Ganey, P. E., Cockerell, G. L., and Roth, R. A. (2003). Ranitidine treatment during a modest inflammatory response precipitates idiosyncrasy-like liver injury in rats. *J. Pharmacol. Exp. Ther.* 307 (1), 9–16. doi:10.1124/jpet.103.054288

Lv, G. P., Meng, L. Z., Han, D. Q., Li, H. Y., Zhao, J., and Li, S. P. (2015). Effect of sample preparation on components and liver toxicity of Polygonum multiflorum. *J. Pharm. Biomed. Anal.* 109, 105–111. doi:10.1016/j.jpba.2015.02.029

Ma, K. F., Zhang, X. G., and Jia, H. Y. (2014). CYP1A2 polymorphism in Chinese patients with acute liver injury induced by Polygonum multiflorum. *Genet. Mol. Res.* 13 (3), 5637–5643. doi:10.4238/2014.July.25.19

Maddox, J. F., Amuzie, C. J., Li, M., Newport, S. W., Sparkenbaugh, E., Cuff, C. F., et al. (2010). Bacterial- and viral-induced inflammation increases sensitivity to acetaminophen hepatotoxicity. *J. Toxicol. Environ. Health A* 73 (1), 58–73. doi:10.1080/15287390903249057

Mao, H. M. X. L., Fan, X., Wu, C. Q., Wang, X. S., and Wang, Q. J. (2016). Effect of ethanol extracts from Polygonum multiflorum Thunb on expressions of signal pathway TLR4/TRIF/IRF-3 in LPS induced rats liver. *J. Int. Pharm. Res.* 43 (3). doi:10.13220/j.cnki.jipr.2016.03.018

Megherbi, R., Kiorpelidou, E., Foster, B., Rowe, C., Naisbitt, D. J., Goldring, C. E., et al. (2009). Role of protein haptenation in triggering maturation events in the dendritic cell surrogate cell line THP-1. *Toxicol. Appl. Pharmacol.* 238 (2), 120–132. doi:10.1016/j.taap.2009.05.001

Nguyen, T.-T. A., Ha, M. T., Park, S.-E., Choi, J. S., Min, B. S., and Kim, J. A. (2020). Stilbenes with potent protein tyrosine phosphatase-1B inhibitory activity from the roots of polygonum multiflorum. *J. Nat. Prod.* 83 (2), 323–332. doi:10.1021/acs.jnatprod.9b00777

Pang, J. L. Y., Bai, Z., Zhao, Y., Zhao, K., Ma, Z., Wang, J., et al. (2015). Compatibility attenuated detoxification study on radix polygoni multiflori-caused hepatic sinus endothelial cell injury based on high content analysis. *Mod. Chin. Med.* 17 (4), 331–334. doi:10.13313/j.issn.1673-4890.2015.4.008

Procházková, D., Boušová, I., and Wilhelmová, N. (2011). Antioxidant and prooxidant properties of flavonoids. *Fitoterapia* 82 (4), 513–523. doi:10.1016/j.fitote.2011.01.018

Qin, B., Xu, Y., Chen, J., Huang, W., Peng, Y., and Zheng, J. (2016). Chemical reactivity of emodin and its oxidative metabolites to thiols. *Chem. Res. Toxicol.* 29 (12), 2114–2124. doi:10.1021/acs.chemrestox.6b00191

Qin, X., Peng, Y., and Zheng, J. (2018). *In vitro* and *in vivo* studies of the electrophilicity of physcion and its oxidative metabolites. *Chem. Res. Toxicol.* 31 (5), 340–349. doi:10.1021/acs.chemrestox.8b00026

Redwood, A. J., Pavlos, R. K., White, K. D., and Phillips, E. J. (2018). HLAs: key regulators of T-cell-mediated drug hypersensitivity. *HLA* 91 (1), 3–16. doi:10.1111/tan.13183

Ren, H. W. P. W., Wei, J., Han, L. F., Fu, Z. F., Su, Y. F., Chang, Y. X., et al. (2021). Hepatotoxic components and attenuation of polygoni multiflori radix praeparata induced idiosyncratic liver injury. *Biomed. Transform.* 2 (3), 62–73. doi:10.12287/j.issn.2096-8965.20210310

Ren, H. W. W. J., Gao, X. M., and Shi, J. W. (2018). Research Progress on pharmacological action and mechanism of Polygonum Multiflorum and its main chemical components. *Drug Eval. Res.* 41 (07), 1357–1362. doi:10.7501/j.issn.1674-6376.2018.07.038

Rodriguez-Pena, R., Lopez, S., Mayorga, C., Antunez, C., Fernandez, T. D., Torres, M. J., et al. (2006). Potential involvement of dendritic cells in delayed-type hypersensitivity reactions to beta-lactams. *J. Allergy Clin. Immunol.* 118 (4), 949–956. doi:10.1016/j.jaci.2006.07.013

Serafini, M., Peluso, I., and Raguzzini, A. (2010). Flavonoids as anti-inflammatory agents. *Proc. Nutr. Soc.* 69 (3), 273–278. doi:10.1017/S002966511000162X

Stephens, C., Andrade, R. J., and Lucena, M. I. (2014). Mechanisms of drug-induced liver injury. *Curr. Opin. Allergy Clin. Immunol.* 14 (4), 286–292. doi:10.1097/ACI.0000000000000070

Tang, Z. F. M. G., and Mei, Q. X. Research progress on the hepatotoxicity of Polygonummultiflorum. 2017;28(07):1722–1725.

Teka, T., Wang, L., Gao, J., Mou, J., Pan, G., Yu, H., et al. (2021). Polygonum multiflorum: recent updates on newly isolated compounds, potential hepatotoxic compounds and their mechanisms. *J. Ethnopharmacol.* 271, 113864. doi:10.1016/j.jep.2021.113864

Tu, C., He, Q., Li, C.-Y., Niu, M., Han, Z.-X., Ge, F.-L., et al. (2019). Susceptibility-related factor and biomarkers of dietary supplement polygonum multiflorum-induced liver injury in rats. *Front. Pharmacol.* 10, 335. doi:10.3389/fphar.2019.00335

Uetrecht, J., and Naisbitt, D. J. (2013). Idiosyncratic adverse drug reactions: current concepts. *Pharmacol. Rev.* 65 (2), 779–808. doi:10.1124/pr.113.007450

Wang, L., Wang, Z., Xing, Y., Liu, E., Gao, X., Wang, L., et al. (2021). Biomarkers and mechanism analysis for polygoni multiflori radix preparata-induced liver injury by UHPLC-Q-TOF-MS-based metabolomics. *Evid. Based Complement. Altern. Med.* 2021, 7677392. doi:10.1155/2021/7677392

Wang, M. X. W. Y., Xu, H. H., Zhang, Z. Y., Ma, Z. C., Xiao, C. R., Tan, H. L., et al. (2016). Effect of emodin on the expression of CYP subenzyme and cytotoxicity in hepatocytes. *Chin. Pharmacol. Bull.* 32 (11), 1543–1548. doi:10.3969/jissn.1001-1978.2016.11.013

Wang, Q., Wen, H., Ma, S., and Zhang, Y. (2022a). Polygonum multiflorum Thunb. Induces hepatotoxicity in SD rats and hepatocyte spheroids by Disrupting the metabolism of bilirubin and bile acid. *J. Ethnopharmacol.* 296, 115461. doi:10.1016/j.jep.2022.115461

Wang, Q. X. L. R., Wu, C. Q., Liao, M. Y., Xiao, X. H., and Wang, Q. J. (2015). Induction of cytochrome P450 enzymes by emodin in liver tissue of rats. *Drug Eval. Res.* 38 (02), 147–150. doi:10.7501/j.issn.1674-6376.2015.02.006

Wang, X., Wu, M., Lai, X. A.-O., Zheng, J., Hu, M., Li, Y., et al. (2020). Network pharmacology to uncover the biological basis of spleen qi deficiency syndrome and herbal treatment. *Oxid. Med. Cell Longev.* 2020, 2974268. doi:10.1155/2020/2974268

Wang, Y., Yang, J., Jin, H., Gu, D., Wang, Q., Liu, Y., et al. (2023). Comparisons of physicochemical features and hepatoprotective potentials of unprocessed and processed polysaccharides from Polygonum multiflorum Thunb. *Int. J. Biol. Macromol.* 235, 123901. doi:10.1016/j.ijbiomac.2023.123901

Wang, Y. N. Z. H., Luo, L. P., Bai, L., Cai, J. Y., Li, S. Y., Lv, Q., et al. (2022b). Principal components of stewed Polygonum multiflorum with"Jianchangbang"based on UPLC-Q/TOF-MS. *Cent. South Pharm.* 20 (9), 2052–2058. doi:10.7539/j.issn.1672-2981.2022.09.015

Wang, Z. Y., Wang, X., Zhang, D. Y., Hu, Y. J., and Li, S. (2022c). Traditional Chinese medicine network pharmacology: development in new era under guidance of network pharmacology evaluation method guidance. *Zhongguo Zhong Yao Za Zhi* 47 (1), 7–17. doi:10.19540/j.cnki.cjcmm.20210914.702

Xiao, X. H. Z. X., Bai, Z. F., Wang, J. B., and Song, H. B. (2023). New outlook on safety of traditional Chinese medicine: concept and practice. *China J. Chin. Materia Medica* 48 (10), 2557–2564. doi:10.19540/j.cnki.cjcmm.20230309.601

Xu, S., Liu, J., Shi, J., Wang, Z., and Ji, L. (2017). 2,3,4',5-tetrahydroxystilbene-2-O-β-D-glucoside exacerbates acetaminophen-induced hepatotoxicity by inducing hepatic expression of CYP2E1, CYP3A4 and CYP1A2. *Sci. Rep.* 7 (1), 16511. doi:10.1038/s41598-017-16688-5

Xue, X., Quan, Y., Gong, L., Gong, X., and Li, Y. (2020). A review of the processed Polygonum multiflorum (Thunb.) for hepatoprotection: clinical use, pharmacology and toxicology. *J. Ethnopharmacol.* 261, 113121. doi:10.1016/j.jep.2020.113121

Yan, S.-L., Su, Y.-F., Chen, L., Que, M., Gao, X.-M., and Chang, J.-B. (2014). Polygonumosides A-D, stilbene derivatives from processed roots of Polygonum multiflorum. *J. Nat. Prod.* 77 (2), 397–401. doi:10.1021/np400720y

Yang, J., Yan, Z., Ren, J., Dai, Z., Ma, S., Wang, A., et al. (2018b). Polygonumnolides A1-B3, minor dianthrone derivatives from the roots of Polygonum multiflorum Thunb. *Arch. Pharm. Res.* 41 (6), 617–624. doi:10.1007/s12272-016-0816-7

Yang, J.-B., Li, L., Dai, Z., Wu, Y., Geng, X.-C., Li, B., et al. (2016). Polygonumnolides C1-C4; minor dianthrone glycosides from the roots of Polygonum multiflorum Thunb. *J. Asian Nat. Prod. Res.* 18 (9), 813–822. doi:10.1080/10286020.2016.1171758

Yang, J.-B., Li, W.-F., Liu, Y., Wang, Q., Cheng, X.-L., Wei, F., et al. (2018a). Acute toxicity screening of different extractions, components and constituents of Polygonum multiflorum Thunb. on zebrafish (*Danio rerio*) embryos *in vivo*. *Biomed. Pharmacother.* 99, 205–213. doi:10.1016/j.biopha.2018.01.033

Yang, J.-B., Song, Y.-F., Liu, Y., Gao, H.-Y., Wang, Q., Wang, Y., et al. (2021). UHPLC-QQQ-MS/MS assay for the quantification of dianthrones as potential toxic markers of Polygonum multiflorum Thunb: applications for the standardization of traditional Chinese medicines (TCMs) with endogenous toxicity. *Chin. Med.* 16 (1), 51. doi:10.1186/s13020-021-00463-w

Yang, J.-B., Tian, J.-Y., Dai, Z., Ye, F., Ma, S.-C., and Wang, A.-G. (2017). a-Glucosidase inhibitors extracted from the roots of Polygonum multiflorum Thunb. *Fitoterapia* 117, 65–70. doi:10.1016/j.fitote.2016.11.009

Yu, W., Zhao, J., Li, W., Zheng, Y., Zhu, J., Liu, J., et al. (2020). 2,3,5,4'-Tetrahydroxystilbene-2-O-β-d-glucoside alleviated the acute hepatotoxicity and DNA damage in diethylnitrosamine-contaminated mice. *Life Sci.* 243, 117274. doi:10.1016/j.lfs.2020.117274

Yun, J., Adam, J., Yerly, D., and Pichler, W. J. (2012). Human leukocyte antigens (HLA) associated drug hypersensitivity: consequences of drug binding to HLA. *Allergy* 67 (11), 1338–1346. doi:10.1111/all.12008

Zhai, X.-R., Zou, Z.-S., Wang, J.-B., and Xiao, X.-H. (2021). Herb-induced liver injury related to reynoutria multiflora (Thunb.) moldenke: risk factors, molecular and mechanistic specifics. *Front. Pharmacol.* 12, 738577. doi:10.3389/fphar.2021.738577

Zhang, C.-E., Niu, M., Li, Q., Zhao, Y.-L., Ma, Z.-J., Xiong, Y., et al. (2016). Urine metabolomics study on the liver injury in rats induced by raw and processed Polygonum multiflorum integrated with pattern recognition and pathways analysis. *J. Ethnopharmacol.* 194, 299–306. doi:10.1016/j.jep.2016.09.011

Zhang, J.-X., and Cui, Y.-M. (2016). Chemical constituents from Polygonum multiflorum. *Zhongguo Zhong Yao Za Zhi* 41 (17), 3252–3255. doi:10.4268/cjcmm20161721

Zhang, L., Niu, M., Wei, A.-W., Tang, J.-F., Li, P.-Y., Song, D., et al. (2022). Clinical correlation between serum cytokines and the susceptibility to Polygonum multiflorum-induced liver injury and an experimental study. *Food Funct.* 13 (2), 825–833. doi:10.1039/d1fo03489h

Zhao, L., and Zheng, L. (2023). A review on bioactive anthraquinone and derivatives as the regulators for ROS. *Molecules* 28 (24), 8139. doi:10.3390/molecules28248139

Zhao, Z., Su, Y., Yan, S., Li, T., Li, J., and Gao, X. (2016). Chromenone derivatives from processed roots of polygonum multiflorum. *Chem. Nat. Compd.* 52, 838–840. doi:10.1007/s10600-016-1791-4

Zheng, X. Y. Y. Z., and Wang, X. (2019). Hepatotoxicity of main components of PM and their effects on drug metabolism enzymes. *Chin. Pharm.* 32 (21), 2619–2623. doi:10.6039/j.issn.1001-0408.2021.21.10

Zheng, X. Y. Y. Z., Wang, X., and Zhou, S. W. (2021). Hepatotoxicity of main components of polygonum multiflorum and its effects on drug metabolism enzyme. *China Pharm.* 32 (21), 2619–2623.

Zhu, Y. L. C., Li, H. L., and Wang, X. B. (2019). Anti-cancer effect of anthraquinones in polygoni multiflori radix. *Chin. J. Exp. Traditional Med. Formulae* 25 (18), 196–205. doi:10.13422/j.cnki.syfjx.20191228

Zou, W., Devi, S. S., Sparkenbaugh, E., Younis, H. S., Roth, R. A., and Ganey, P. E. (2009). Hepatotoxic interaction of sulindac with lipopolysaccharide: role of the hemostatic system. *Toxicol. Sci.* 108 (1), 184–193. doi:10.1093/toxsci/kfn259

frontiers | Frontiers in Pharmacology

TYPE Review
PUBLISHED 03 July 2024
DOI 10.3389/fphar.2024.1427333

OPEN ACCESS

EDITED BY
Qianfeng Gong,
Jiangxi University of Traditional Chinese Medicine, China

REVIEWED BY
Kelei Su,
Nanjing University of Chinese Medicine, China
Junping Zheng,
Hubei University of Chinese Medicine, China
Fengyang Duan,
First Affiliated Hospital of Henan University of Traditional Chinese Medicine, China

*CORRESPONDENCE
Yuancheng Gao,
gaoyuancheng@foxmail.com
Yang Liu,
liuyang311111@163.com

RECEIVED 03 May 2024
ACCEPTED 11 June 2024
PUBLISHED 03 July 2024

CITATION
Wu Z, Qian J, Feng C, Chen Z, Gao X, Liu Y and Gao Y (2024), A review of Aconiti Lateralis Radix Praeparata (Fuzi) for kidney disease: phytochemistry, toxicology, herbal processing, and pharmacology.
Front. Pharmacol. 15:1427333.
doi: 10.3389/fphar.2024.1427333

A review of Aconiti Lateralis Radix Praeparata (Fuzi) for kidney disease: phytochemistry, toxicology, herbal processing, and pharmacology

Ziyang Wu[1], Jiawen Qian[1], Chenhang Feng[2], Zhouqi Chen[1], Xiangfu Gao[1], Yang Liu[3]* and Yuancheng Gao[1]*

[1]Department of Nephrology, The First Affiliated Hospital of Zhejiang Chinese Medical University (Zhejiang Provincial Hospital of Chinese Medicine), Hangzhou, China, [2]The Third Affiliated Clinical Medical College, Zhejiang Chinese Medical University, Hangzhou, China, [3]Shaanxi Academy of Traditional Chinese Medicine, Xi'an, China

Background: Aconiti Lateralis Radix Praeparata, commonly known as Fuzi in. traditional Chinese medicine (TCM), is widely utilized in clinical practice despite its inherent toxicity. Since ancient times, TCM practitioners have explored various processing techniques to broaden its clinical applications and enhance its safety profile. This review aims to summarize the effects of processing on the chemical composition, toxicity, and pharmacological properties of Fuzi, as well as investigate potential underlying mechanisms.

Methods: Data on phytochemistry, toxicology, pharmacology, and processing methods of Fuzi were gathered from the literature of electronic databases, including Web of Science, PubMed, and CNKI.

Results: Fuzi contains over 100 kinds of chemical compounds, including alkaloids, flavonoids, and polysaccharides, among which alkaloids are the main active compounds. Diester-diterpenoid alkaloids are the main contributors to Fuzi's toxicity and have side effects on some organs, such as the heart, liver, kidneys, nervous system, and reproductive system. The chemical composition of aconite, particularly its alkaloid content, was changed by hydrolysis or substitution reaction during processing to enhance its efficacy and reduce its toxicity. Salted aconite could enhance the therapeutic efficacy of Fuzi in treating kidney diseases and influence its pharmacokinetics.

Conclusion: Processing plays an important role in increasing the efficiency and decreasing toxicity of aconite. Further studies are needed to elucidate the changes of aconite before and after processing and the underlying mechanisms of these changes, thereby providing evidence for the clinical safety of drug use.

KEYWORDS

Aconiti Lateralis Radix Praeparata (Fuzi), processing, kidney disease, pharmacology, toxicology, phytochemistry

1 Introduction

Aconiti Lateralis Radix Praeparata, the lateral root of *Aconitum carmichaelii* Debeaux, is a traditional Chinese medicine (TCM), renowned for its significant bioactivities and high toxicity. This herb, known as "Fuzi" in Chinese, "Bushi" in Japanese, and "Kyeong-Po Buja" in Korean, is prevalent across many Asian countries and is frequently cited in traditional medical classics (Kondo et al., 2022; Wu et al., 2022).

Historically, as detailed in Shennong's *Classic of Materia Medica* from the Han Dynasty, Fuzi was used for its warming property and pungent taste. It was prescribed for wind-cold dispersal, cough with dyspnea from pathogenic qi, warming the spleen and lungs, healing trauma, resolving abdominal masses and circulatory disorders, and alleviating limb spasms and pain caused by cold-damp conditions (Li et al., 2023; Yuan and Yuan, 2023).

Recent pharmacological studies have explored Fuzi's active compounds, which have shown potential in anti-inflammatory and anti-tumor activities, cardiovascular and renal protection, and immune enhancement.

Despite its therapeutic benefits, the pronounced toxicity of Fuzi limits its clinical application compared to other TCM herbs. Therefore, optimizing the balance between efficacy and toxicity through various processing methods has emerged as a critical area of research. This review examines the different processing techniques applied to Fuzi, focusing on how these methods enhance its pharmacological effects and reduce its toxicity, such as salt processing to improve renal benefits. Moreover, it discusses the outcomes in terms of phytochemistry, toxicity, herbal processing, and pharmacology. It concludes by summarizing the changes in Fuzi's compounds, toxicity, and pharmacological properties after processing.

By summarizing and analyzing the relevant literature, this review enriches the knowledge related to the processing of Fuzi and organizes the content related to the influence of processing methods on its pharmacological properties. Emphasizing the enhancement of Fuzi's renal pharmacological effects through salt processing, the review thoroughly explores the mechanisms by which various processing methods affect its pharmacological effects.

2 Phytochemistry

In review, 122 compounds have been extracted and identified from *Aconitum carmichaelii* Debeaux (Zhang et al., 2022). Among these compounds, alkaloids are the principal active compounds responsible for the pharmacological activity, clinical efficacy, and even the toxicity of Fuzi. Consequently, these Fuzi alkaloids serve as indicator compounds in their quality evaluation. Based on the carbon atom count in their skeleton, these alkaloids are categorized as C_{18}, C_{19}, and C_{20} diterpenoid alkaloids (Wu et al., 2018; Gu et al., 2022) (Figure 1).

2.1 Fuzi's alkaloids

Prior studies have demonstrated that Fuzi's alkaloids possess a broad spectrum of pharmacological effects, including anti-inflammatory, anticancer, immunoregulatory, analgesic, and nephroprotective properties (Xu et al., 2021).

2.1.1 C_{19} diterpenoid alkaloids

The primary bioactive and toxic compounds in Fuzi are the C19-diester-diterpenoid alkaloids (DDAs), predominantly comprising aconitine (AC), mesaconitine (MA), and hypaconitine (HA). C_{19} diterpenoid alkaloids are subdivided into various types, such as aconitine, lycoctonine, pyro-type, lactone-type, 7,17-seco-type, and rearranged-type, based on the specific oxygen-containing groups and structures at the C-7 position. *A. carmichaelii* primarily features alkaloids of the aconitine skeleton type, which exhibit diverse chemical properties due to different substituents at various positions within their fundamental skeleton (Wang et al., 2023). The structures of these C_{19} diterpenoid alkaloids in Fuzi are detailed in Table 1. Hydrolyzing the esters in Fuzi transforms DDAs into either monoester-diterpenoid alkaloids (MDAs) or ester-free amine-diterpenoid alkaloids (ADAs), significantly reducing their toxicity. For instance, the toxicity of MDA in rats decreases by 64–180 times compared to DDAs post-hydrolysis, without diminishing their pharmacological effects (Zhao et al., 2018). This reduction is why Chinese physicians have traditionally used decoctions and other processing methods to mitigate Fuzi's toxicity, thus enabling its safer clinical application (Yang et al., 2023).

2.1.2 C_{20} diterpenoid alkaloids

C_{20} diterpenoid alkaloids represent the foundational diterpenoid alkaloids and are crucial as precursors for synthesizing various other diterpenoid alkaloids. These include atisine, denudatine, hetidine, hetisine, veatchine, napelline, and anopterine groups (Ren et al., 2017). Within Fuzi, the primary C_{20} diterpenoid alkaloids are songorine, ignavine, napelline, hetisine, *etc.*, (Figure 2).

2.1.3 Other alkaloids

Beyond diterpenoid alkaloids, other alkaloids such as yokonoside, higenamine, fuzitine, and aconicaramide have been identified. Their chemical structures are depicted in Figure 3.

2.2 Other compounds

In addition to alkaloids, Fuzi contains other compounds extracted from various plant parts, including flavonoids, polysaccharides, fatty acids, and ceramides. Fuzi's polysaccharides, primarily comprising glucose, galacturonic acid, galactose, arabinose, and mannose, are noted for their anti-inflammatory effects, anticancer potential, immunomodulation, and cholesterol-reducing properties (Liu et al., 2019).

Fuzi flavonoids, mainly comprising flavanones and chalcones, are recognized for their antioxidant capabilities, inflammation reduction, cardiovascular health support, immune system modulation, and antibacterial, antiviral, and antifungal properties (Fu et al., 2022).

3 Toxicology

Despite its significant multi-systemic therapeutic effects, Fuzi's narrow therapeutic window often yields severe

10.3389/fphar.2024.1427333

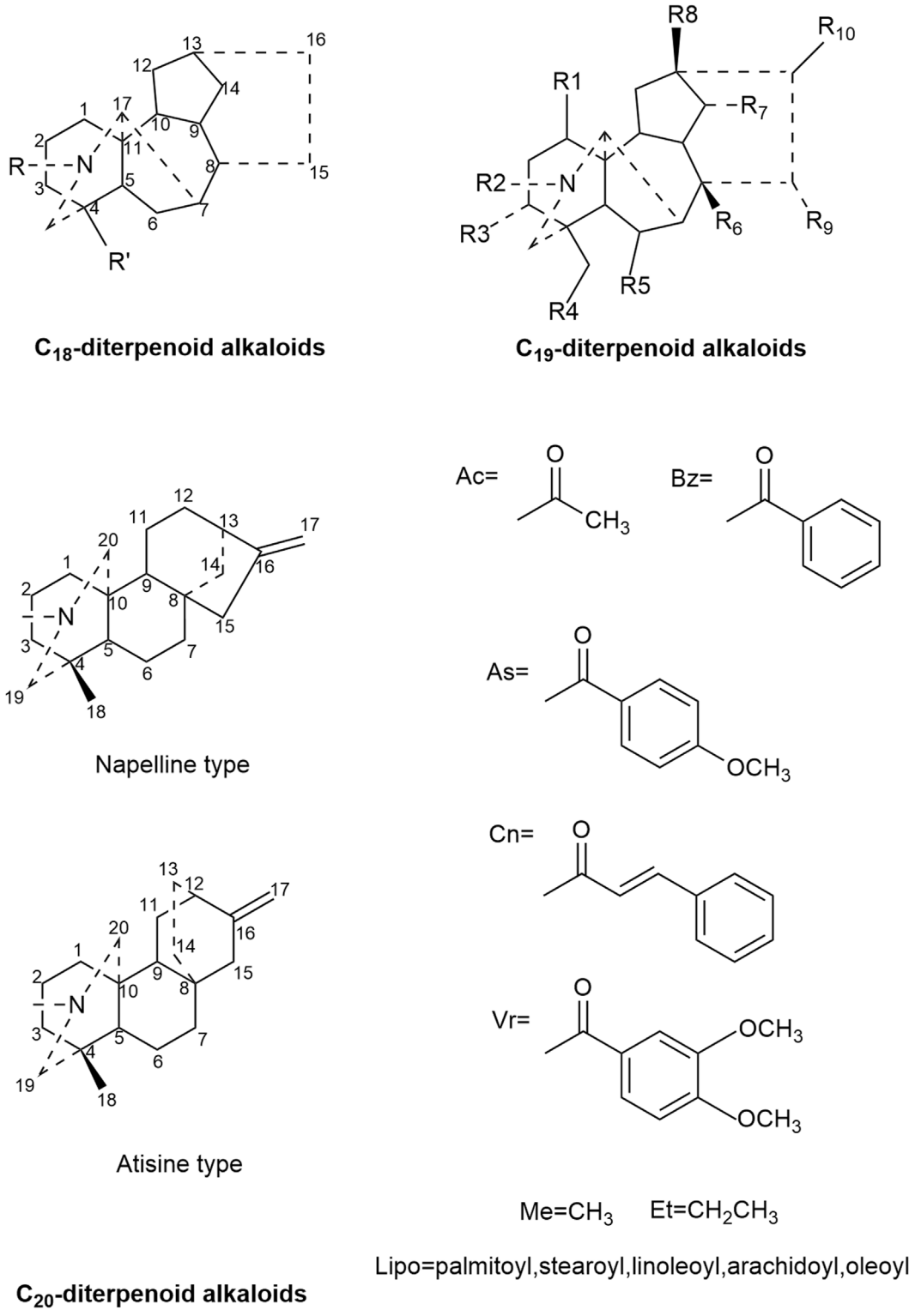

FIGURE 1
Three diterpenoid alkaloids' skeleton and certain particluar groups.

toxicity in clinical practice, particularly affecting the heart, liver, and kidneys. To ensure drug safety, clinicians strictly regulate Fuzi's dosage. This section examines the toxic compounds, symptoms, and mechanisms of Fuzi's toxicity across different systems.

3.1 Toxic ingredients and clinical symptoms of poisoning

The primary toxic compounds in Fuzi are the DDAs, mainly including aconitine (AC), mesaconitine (MC), and hypaconitine

TABLE 1 Structures and names of the C_{19}-diterpenoid alkaloids from Fuzi.

NO.	Chemical component	Molecular formula	R1	R2	R3	R4	R5	R6	R7	R8	R9	R10
1	Aconitine	$C_{34}H_{47}NO_{11}$	OMe	Et	OH	OMe	OMe	OAc	OBz	OH	OH	OMe
2	Mesaconitine	$C_{33}H_{45}NO_{11}$	OMe	CH3	OH	OMe	OMe	OAc	OBz	OH	OH	OMe
3	Hypaconitine	$C_{33}H_{45}NO_{10}$	OMe	CH3	H	OMe	OMe	OAc	OBz	OH	OH	OMe
4	Talatizamine	$C_{24}H_{39}NO_5$	OMe	Et	H	OMe	H	OH	OH	H	H	OMe
5	Isotalatizidine	$C_{23}H_{37}NO_5$	OH	Et	H	OMe	H	OH	OH	H	H	OMe
6	Karacoline (Carmichaeline)	$C_{22}H_{35}NO_4$	OH	Et	H	H	H	OH	OH	H	H	OMe
7	Neoline	$C_{24}H_{39}NO_6$	OH	Et	H	OMe	OMe	OH	OH	H	H	OMe
8	Fuziline	$C_{24}H_{39}NO_7$	OH	Et	H	OMe	OMe	OH	OH	H	OH	OMe
9	Isodelphinine	$C_{33}H_{45}NO_9$	OMe	Me	H	OMe	OMe	OAc	OBz	H	OH	OMe
10	Benzoylmesaconine	$C_{31}H_{43}NO_{10}$	OMe	Me	OH	OMe	OMe	OH	OBz	OH	OH	OMe
11	14-Acetyltalatisamine	$C_{26}H_{41}NO_6$	OMe	Et	H	OMe	H	OH	OAc	H	H	OMe
12	Lipoaconitine	$C_{29}H_{54}NO_7$	OMe	Et	OH	OMe	OMe	O-lipo	OBz	OH	OH	OMe
13	Lipomesaconitine	$C_{34}H_{54}NO_7$	OMe	Me	OH	OMe	OMe	O-lipo	OBz	OH	OH	OMe
14	Lipohypaconitine	$C_{34}H_{54}NO_7$	OMe	Me	H	OMe	OMe	O-lipo	OBz	OH	OH	OMe
15	Lipodeoxyaconitine	$C_{35}H_{56}NO_7$	OMe	Et	H	OMe	OMe	O-lipo	OBz	OH	OH	OMe
16	Monoacetyltalizamine	$C_{26}H_{41}NO_6$	OMe	Et	H	OMe	H	OH	OAc	H	H	OMe
17	Senbusine A	$C_{23}H_{37}NO_6$	OH	Et	H	OMe	OH	OH	OH	H	H	OMe
18	Senbusine B	$C_{23}H_{37}NO_6$	OH	Et	H	OMe	H	OH	OH	H	OH	OMe
19	Senbusine C	$C_{24}H_{39}NO_7$	OH	Et	H	OMe	OMe	OH	OH	H	OH	OMe
20	Hokbusine A	$C_{36}H_{59}NO_{10}$	OMe	Me	OH	OMe	OMe	OMe	OBz	OH	OH	OMe
21	Hokbusine B	$C_{34}H_{55}NO_{10}$	OH	H	H	H	H	OH	OAc	H	H	OMe
22	Benzoylaconine	$C_{32}H_{45}NO_{10}$	OMe	Et	OH	OMe	OMe	OH	OBz	OH	OH	OMe
23	Benzoylhypaconine	$C_{31}H_{43}NO_9$	OMe	Me	H	OMe	OMe	OH	OBz	OH	OH	OMe
24	Neojiangyouaconitine	$C_{33}H_{47}NO_9$	OMe	Et	H	OMe	OMe	Ome	OBz	OH	OH	OMe
25	Aldohypaconitine	$C_{33}H_{43}NO_{11}$	OMe	CHO	H	OMe	OMe	OAc	OBz	OH	OH	OMe
26	Deoxyaconitine	$C_{34}H_{47}NO_{10}$	OMe	Et	H	OMe	OMe	OAc	OBz	OH	OH	OMe
27	Beiwutine	$C_{33}H_{45}NO_{12}$	OMe	Me	OH	OMe	OMe	OAc	OH	OBz	OH	OH
28	8-O-Cinnamoylneoline	$C_{33}H_{45}NO_7$	OH	Et	H	OMe	OMe	OCn	OH	H	H	OMe
29	Karakanine	$C_{22}H_{33}NO_4$	OMe	Et	H	H	H	OH	OH	H	H	OMe
30	14-O-Cinnamoylneoline	$C_{33}H_{45}NO_7$	OH	Et	H	OMe	OMe	OH	OCn	H	H	OMe
31	14-O-Anisoylneoline	$C_{32}H_{45}NO_8$	OH	Et	H	OMe	OMe	OH	OAs	H	H	OMe
32	14-O-Veratroylneoline	$C_{33}H_{47}O_9N$	OH	Et	H	OMe	OMe	OH	OVr	H	H	OMe
33	Lipo-14-O-Anisoylbikhaconine	$C_{51}H_{81}NO_{10}$	OMe	Et	H	Et	Et	O-lipo	OAs	OH	H	OMe
34	Lipoforesaconitine	$C_{28}H_{51}AsNO_6$	OMe	Et	H	OMe	OMe	O-lipo	OAs	H	H	OMe
35	14-O-Acetyneoline	$C_{26}H_{41}NO_7$	OH	Et	H	OMe	OMe	OH	OAc	H	H	OMe
36	Foresaconitine	$C_{35}H_{49}NO_9$	OMe	Et	H	OMe	OMe	OAc	OAs	H	H	OMe
37	Crassicauline A	$C_{35}H_{49}NO_{10}$	OMe	Et	H	OMe	OMe	OAc	OAs	OH	H	OMe
38	Lipoyunanaconitine	$C_{30}H_{57}AsNO_6$	OMe	Et	OH	OMe	OMe	O-lipo	OAs	OH	H	OMe

(Continued on following page)

TABLE 1 (*Continued*) Structures and names of the C_{19}-diterpenoid alkaloids from Fuzi.

NO.	Chemical component	Molecular formula	R1	R2	R3	R4	R5	R6	R7	R8	R9	R10
39	8-Oet-14-Benzoylmesaconitine	$C_{36}H_{59}NO_9$	OMe	Me	OH	OMe	OMe	OEt	OBz	OH	OH	OMe
40	Aconifine	$C_{34}H_{47}NO_{12}$	OMe	H	OH	OMe	OMe	OH	OAc	OBz	OH	OMe
41	Aconine	$C_{25}H_{41}NO_9$	OMe	Et	OH	OMe	OMe	OH	OH	OH	OH	OMe
42	Yunaconitine	$C_{35}H_{49}NO_{11}$	OMe	Et	OH	OMe	OMe	OAc	OAs	OH	H	OMe
43	Chasmanine	$C_{25}H_{41}NO_6$	OMe	Et	H	OMe	OMe	OH	OH	H	H	OMe
44	Foresticine	$C_{24}H_{39}NO_7$	OMe	Et	H	OMe	OH	OH	OH	H	H	OMe
45	N-deethylaconine	$C_{25}H_{44}NO_9$	OMe	H	OH	OMe	OMe	OH	OH	OH	OH	OMe
46	Beiwutinine	$C_{23}H_{37}NO_9$	OMe	Me	OH	OMe	OMe	OH	OH	OH	OH	OH
47	Hypaconine	$C_{24}H_{39}NO_8$	OMe	Me	H	OMe	OMe	OH	OH	OH	OH	OMe
48	Mesaconine	$C_{24}H_{39}NO_9$	OMe	Me	OH	OMe	OMe	OH	OH	OH	OH	OMe
49	N-Ethylhokbusine B	$C_{24}H_{37}NO_5$	OH	Et	H	H	H	OH	OAc	H	H	OMe
50	8-O-Ethylyunaconitine	$C_{35}H_{51}NO_{10}$	OMe	Et	OH	OMe	OMe	OEt	OAs	OH	H	OMe
51	Oxonitine	$C_{33}H_{43}NO_{12}$	OMe	CHO	H	OMe	OMe	OAc	OBz	OH	OH	OMe
52	(−)-(A-b)-8β-acetoxy-14α-benzoyloxy-N-Ethyl-13β,15α-dihydroxy-1α,6α,16β,18-tetramethoxy-19-oxo-aconitane	$C_{34}H_{45}NO_{11}$	OMe	Et	CHO	OMe	OMe	OAc	H	OBz	OH	OH
53	(−)-(A-b)-8β-acetoxy-14α-benzoyloxy-N-ethyl-3α,10β,13β,15α-tetrahydroxy-1α,6α,16β,18-tetramethoxyaconitane	$C_{37}H_{59}NO_{11}$	OMe	Et	OH	OMe	OMe	OAc	OH	OBz	OH	OH
54	(−)-(A-b)-14α-benzoyloxy-3α,10β,13β,15α-tetrahydroxy-1α,6α,8β,16β,18-pentamethoxy-N-methylaconitane	$C_{31}H_{44}NO_{11}$	OMe	Me	OH	OMe	OMe	OH	OMe	OBz	OH	OMe
55	(−)-(A-c)-14α-benzoyloxy-3α,10β,13β,15α-tetrahydroxy-1α,6α,8β,16β,18-pentamethoxy-N-methylaconitane	$C_{25}H_{42}NO_7$	OMe	H	H	H	H	OH	OAc	OH	OH	OMe
56	(−)-(A-b)-14α-benzoyloxy-N-ethyl-3α,10β,13β,15α-tetrahydroxy-1α,6α,8β,16β,18-pentamethoxyaconitane	$C_{34}H_{48}NO_{11}$	OMe	Et	OH	OMe	OMe	OAc	OH	OBz	OH	OH
57	(−)-(A-b)-14α-Benzoyloxy-3α,10β,8β,13β,15α-Pentahydroxy-1α,6α,16β,18-Tetramethoxy-N-Methylaconitane	$C_{31}H_{43}NO_{11}$	OMe	Me	OH	OMe	OMe	OH	OMe	OBz	OH	OMe
58	(−)-(A-b)-8β-acetoxy-14α-benzoyloxy-N-ethyl-3α,10β,13β-trihydroxy-1α,6α,16β,18-tetramethoxyaconitane	$C_{34}H_{48}NO_{11}$	OMe	Et	OH	OMe	OMe	OH	OMe	OBz	OH	OMe
59	(−)-(A-b)-8β-acetoxy-14α-benzoyloxy-10β,13β,15α-trihydroxy-1α,6α,16β,18-tetramethoxy-N-methylaconitane	$C_{33}H_{46}NO_{11}$	OMe	Me	H	OMe	OMe	OAc	OH	OBz	OH	OH
60	(−)-(A-b)-8β-Acetoxy-14α-benzoyloxy-N-ethyl-13β,15α-dihydroxy-1α,6α,16β,18-tetramethoxyaconitane	$C_{34}H_{48}NO_{10}$	OMe	Et	H	OMe	OMe	OAc	H	OBz	OH	OH
61	(−)-(A-b)-14α-benzoyloxy-N-ethyl-8β,13β-dihydroxy-1α,6α,16β,18-tetramethoxyaconitane	$C_{32}H_{46}NO_8$	OMe	Et	H	OMe	OMe	OH	OBz	OH	H	OMe
62	(−)-(A-b)-14α-benzoyloxy-N-ethyl-3α,8β,13β,15α-tetrahydroxy-1α,6α,16β,18-tetramethoxyaconitane	$C_{32}H_{46}NO_{10}$	OMe	Et	OH	OMe	OMe	OH	OBz	OH	OH	OMe
63	(−)-(A-b)-8β,14α-dibenzoyloxy-N-ethyl-3α,13β,15α-trihydroxy-1α,6α,16β,18-tetramethoxyaconitane	$C_{38}H_{48}NO_{11}$	OMe	Me	OH	OMe	OMe	OBz	H	OBz	OH	OH
64	(−)-(A-b)-14α-benzoyloxy-N-ethyl-13β,15α-dihydroxy-1α,6α,8β,16β,18-tetramethoxyaconitane	$C_{33}H_{48}NO_9$	OMe	Et	H	OMe	OMe	OMe	OBz	OH	OH	OMe

(Continued on following page)

TABLE 1 (*Continued*) Structures and names of the C_{19}-diterpenoid alkaloids from Fuzi.

NO.	Chemical component	Molecular formula	R1	R2	R3	R4	R5	R6	R7	R8	R9	R10
65	(−)-(A-b)-14α-benzoyloxy-N-ethyl-8β,13β,15α-trihydroxy-1α,16β,18-trimethoxyaconitane	$C_{31}H_{44}NO_8$	OMe	Et	H	OMe	H	OH	OBz	OH	OH	OMe
66	(−)-(A-b)-14α-benzoyloxy-N-ethyl-6α,8β,15α-trihydroxy-1α,16β,18-trimethoxyaconitane	$C_{31}H_{44}NO_8$	OMe	Et	H	H	OMe	OH	OH	H	OBz	OH
67	(−)-(A-b)-14α-benzoyloxy-8β-ethoxy-N-ethyl-6α,15α-dihydroxy-1α,16β,18-trimethoxyaconitane	$C_{33}H_{48}NO_8$	OMe	Et	H	H	OMe	OH	OEt	H	OBz	OH
68	(−)-(A-b)-14α-benzoyloxy-N-ethyl-8β,15α-dihydroxy-1α,16β,18-trimethoxyaconitane	$C_{31}H_{44}NO_7$	OMe	Et	H	H	OMe	H	OH	H	OBz	OH
69	(−)-(A-b)-14α-benzoyloxy-N-ethyl-1α,8β,15α-trihydroxy-16β,18-dimethoxyaconitane	$C_{30}H_{42}NO_7$	OH	Et	H	H	OMe	H	OH	H	OBz	OH
70	(−)-(A-b)-14α-benzoyloxy-N-ethyl-1α,8β,15α-trihydroxy-6α,16β,18-trimethoxyaconitane	$C_{31}H_{44}NO_8$	OH	Et	H	H	OMe	OMe	OH	H	OBz	OH
71	(−)-(A-b)-14α-cinnamoyloxy-N-ethyl-1α,8β,15α-trihydroxy-6α,16β,18-trimethoxyaconitane	$C_{33}H_{46}NO_8$	OH	Et	H	H	OMe	OMe	OH	H	OCn	OH
72	(−)-(A-b)-8β-acetoxy-14α-benzoyloxy-N-ethyl-15α-hydroxy-1α,6α,16β,18-tetramethoxyaconitane	$C_{34}H_{48}NO_9$	OMe	Et	H	OMe	OMe	OAc	H	OBz	H	OH
73	Bullatine B	$C_{24}H_{39}NO_6$	OH	Et	H	OMe	OMe	OH	OH	H	H	OMe

(HC), with AC being exceptionally lethal at doses as low as 2 mg. HC, while being the most toxic, is present in the smallest quantity (Strzelecki et al., 2010). Symptoms of Fuzi's poisoning include nausea, vomiting, palpitations, arrhythmias, muscle dysfunction, perioral paresthesia, respiratory distress, convulsions, gastrointestinal disturbances, and in severe cases, shock or coma. Death can occur due to ventricular arrhythmias. Currently, there is no direct antidote for Fuzi poisoning; treatment is primarily supportive and symptomatic (Chan et al., 2021).

3.2 Toxicity in various systems

3.2.1 Cardiotoxicity

While being moderately beneficial for heart health, Fuzi could be cardiotoxic in high doses. AC affects cardiomyocytes by shortening the arrhythmic phase through enhancing intracellular Na^+ flow and hastening cardiac membrane depolarization. At toxic levels, AC disrupts ion channels, promotes myocardial apoptosis, and may cause severe ventricular arrhythmias and myocardial damage (Zhou et al., 2021). Studies searching for potential tissue-specific biomarkers of Fuzi's poisoning by myocardial lipidomics have identified alterations in lipid metabolites that participate in various metabolic pathways. Additionally, Cai et al. emphasized Fuzi's dose-dependent cardiotoxic effects. These effects have been observed in histological cardiac damage and arrhythmias following overdose (Cai et al., 2013). Several studies have shown that AC induces Ca^{2+} overload and apoptosis in myocardial H9c2 cells by promoting the release and plasma membrane translocation of transient receptor potential cation channel subfamily V member 2 through the p38 MAPK signaling pathway (Yang et al., 2021). In an *in vitro* study on Fuzi's cardiotoxic effects on zebrafish embryos and H9c2 cells, Li et al. exposed fertilized zebrafish embryos to AC. They confirmed that AC-induced cardiac dysfunction and apoptosis with an LD_{50} value of 7.92 μM and a 95% confidence interval ranging from 6.49 to 9.83 μM. Simultaneously, AC-induced intracellular Ca^{2+} oscillations increased the rate of apoptosis, inhibited the levels of TnT and Bcl-2 proteins, and promoted the upregulation of caspase 3 and Bax proteins in H9c2 cells after a 30-min treatment at a suitable concentration. These data confirmed that cardiac insufficiency and apoptosis induced by AC are related to the Ca^{2+} signaling pathway (Li et al., 2020). Furthermore, Fuzi water extracts and ethanol extracts exhibited cardiotoxicity by inducing apoptosis in cardiomyocytes by activating the PI3K/Akt/mTOR signaling pathway in rat myocardium tissue (Huang et al., 2018).

3.2.2 Liver and kidney toxicity

Fuzi and its metabolites, when processed through the liver and kidneys, can induce liver and kidney damage. Studies using ultra-performance liquid chromatography-tandem mass spectrometry have noted a predominant distribution of toxic alkaloids in the liver and kidneys after long-term feeding of Fuzi preparations to mice, causing notable hepatic and renal damage. Conversely, these alkaloids were present at relatively low levels in the heart, brain, and blood (Ji et al., 2019). Hepatic and renal injury has been reported in some toxicity studies on rodents after single or long-term oral administration of Fuzi's extracts. Symptoms of liver damage include elevated serum alanine aminotransferase and aspartate aminotransferase levels, edema, and necrosis, while kidney damage is characterized by increased serum creatinine (SCr) and blood urea nitrogen (BUN) levels, with histological evidence of lymphocyte infiltration and tissue atrophy (Zhou et al., 2016). Zhang et al. injected water extracts of Heishunpian (HSP) (a form of prepared Fuzi) intraperitoneally into mice; the results showed that these extracts could cause liver injury. Upon further

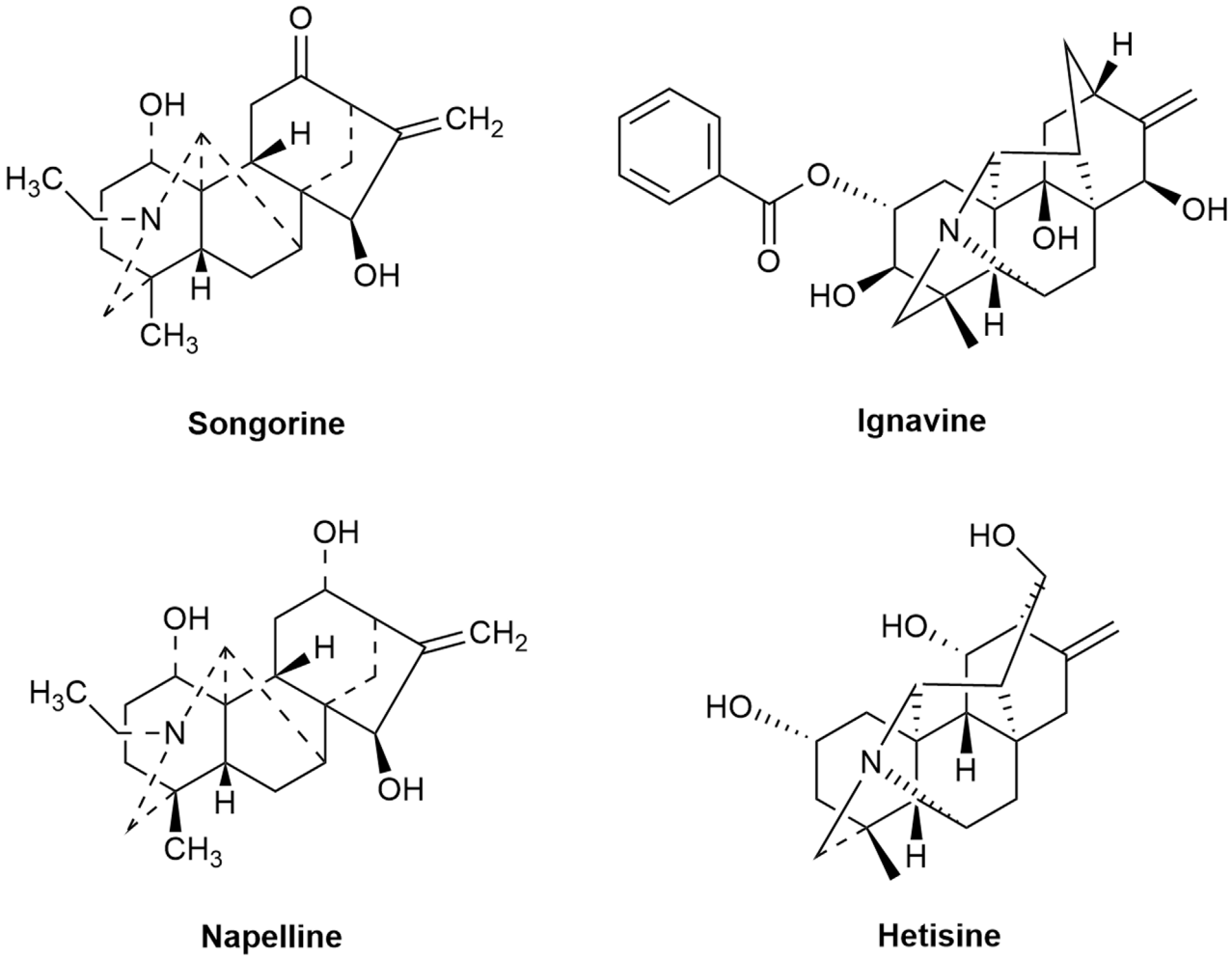

FIGURE 2
A part of C_{20}-diterpenoid alkaloids from Fuzi.

investigation, the generation of hepatotoxic events can be attributed to the influence of toxic components on Th17 cell differentiation, Jak-STAT signaling pathway, and glutathione metabolism by modulating important targets such as AKT1, IL2, F2, GSR, and EGFR (Zhang et al., 2020). Sun et al. used metabolomics analysis to study the metabolic changes caused by toxic alkaloids of Fuzi in Wistar rats. The results showed that the maximum metabolic changes occurred six h after alkaloid treatment, leading to perturbations in renal tubular function. These changes lasted for about 24 h and tapered off after that time point (Sun et al., 2009). According to a TCM theory, Fuzi could be used to treat patients with the TCM "kidney-yang" deficiency pattern; modern research has also indicated that Fuzi has a nephroprotective effect that allows it to be used clinically in chronic kidney disease. A study on the different toxic responses of Baifupian (a form of prepared Fuzi) administration in healthy and hydrocortisone-exposed (mimicking the state of the kidney-yang deficiency pattern) rats showed that drug-induced toxic reactions were greatly attenuated in hydrocortisone-pretreated animals. Additionally, altered metabolic profiles involving oxidative phosphorylation, amino acid, and lipid metabolism featured alterations in phosphate, betaine, and phosphatidylcholine and may be associated with different toxic response profiles (Tan et al., 2013).

3.2.3 Neurotoxicity

The central nervous system, susceptible to damage from toxins like AC, can exhibit acute neurotoxic effects, including motor blockade, cyanosis, asthenia, abdominal respiration, locomotor difficulty, and flaccid paralysis, often culminating in death (Li T. F. et al., 2016). The total fat-soluble alkaloids of Fuzi are neurotoxic to zebrafish; some researchers found that the toxicity may be related to the promotion of apoptosis and the effect on acetylcholinesterase activity through further experiments (Li et al., 2019). The potential mechanism of neurotoxicity resulting from Fuzi was initially elucidated by network pharmacology and molecular docking techniques. The results indicate that the neurotoxic mechanisms of Fuzi involve multiple targets and pathways. Notably, the MAPK signaling pathway and Akt protein-related pathway emerge as pivotal, significantly influencing cell membrane integrity, mitochondrial function, and neuronal apoptosis (An et al., 2022; Wang and Li, 2022).

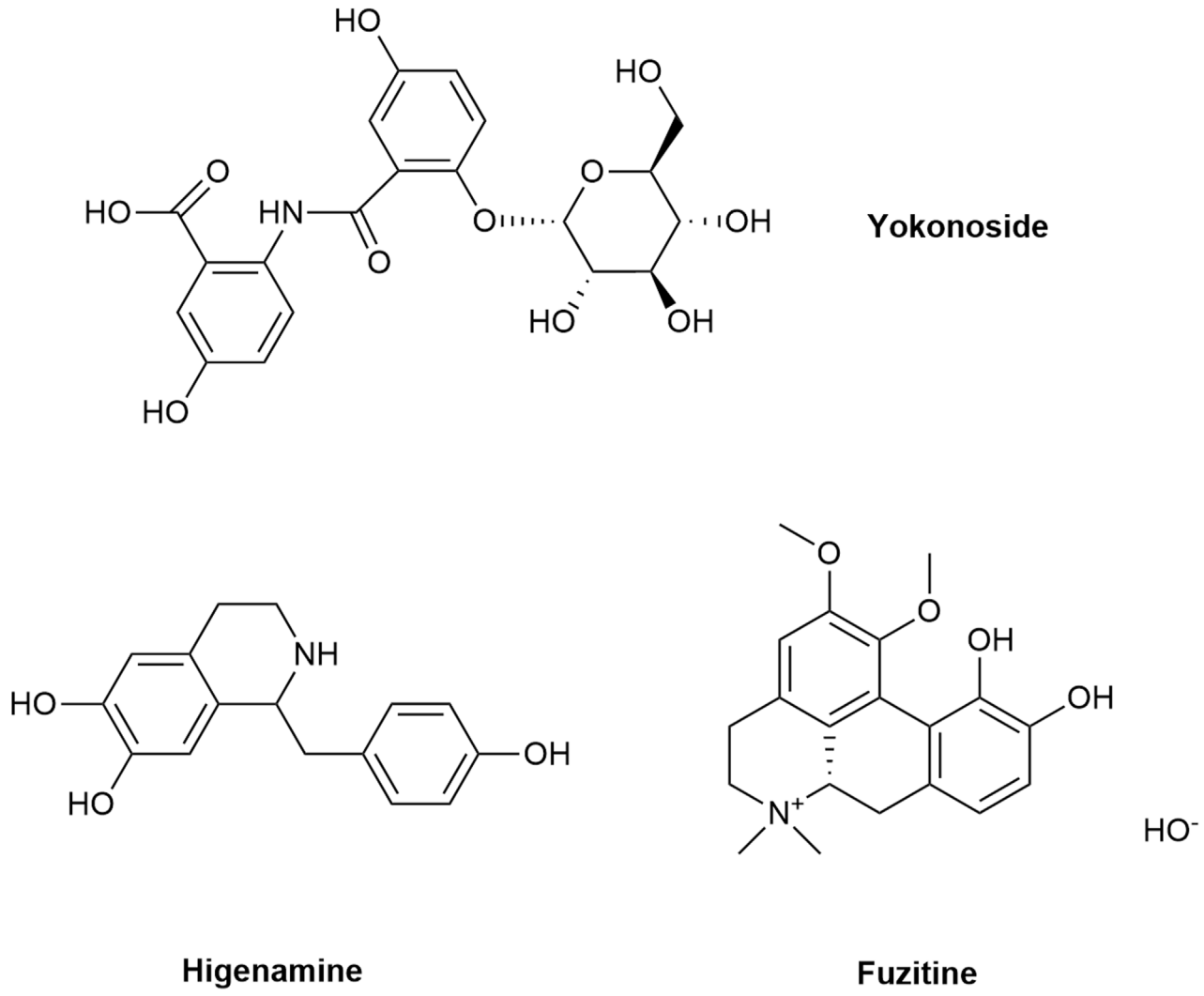

FIGURE 3
The main alkaloids contained in Fuzi, except for diterpenoid alkaloids.

3.2.4 Embryotoxicity and reproductive toxicity

High doses of AC in zebrafish embryos induce malformations such as shortened body length, body curvature, pericardial edema, and impaired organ development, mediated by oxidative stress and mitochondrial apoptosis pathways (Xia et al., 2021). In male mice, Fuzi and its products have shown significant reproductive toxicity, evidenced by pathological changes in testicular tissue, reduced sperm count and viability, increased sperm abnormalities, and DNA damage, likely due to oxidative stress (Zhang et al., 2021).

4 Herbal processing

Given its unique pharmacological properties, Fuzi is extensively used in TCM. However, its narrow therapeutic window and significant toxicity often limit its clinical utility. Traditional processing techniques, honed over millennia, moderately mitigate these issues by altering the herb's properties, flavor, and therapeutic channels, thus enhancing efficacy and reducing toxicity to ensure clinical safety. Additionally, the salt processing could particularly enhance the effect of Fuzi in kidney disease treatment.

4.1 Processing methods

4.1.1 Thermal processing (called *huozhi* in Chinese)

Huozhi, or thermal processing, involves heat treatment of herbs without liquid adjuvants. This method, which includes stir-frying, roasting, and baking, varies by temperature, duration, and technique specifics. Historically, during the Han and Tang dynasties, this was the predominant method for preparing herbs (Liu et al., 2017).

Research by Deng et al. demonstrated that oven baking could decrease the concentration of toxic DDAs in Fuzi while preserving or increasing the levels of beneficial compounds, minimizing alkaloid loss compared to aqueous processing (Deng et al., 2012). Stir-frying with inert materials, like river sand, a common adjuvant, has been shown to preserve more active alkaloids and offer a simpler, more effective alternative to traditional methods (Peng et al., 2018).

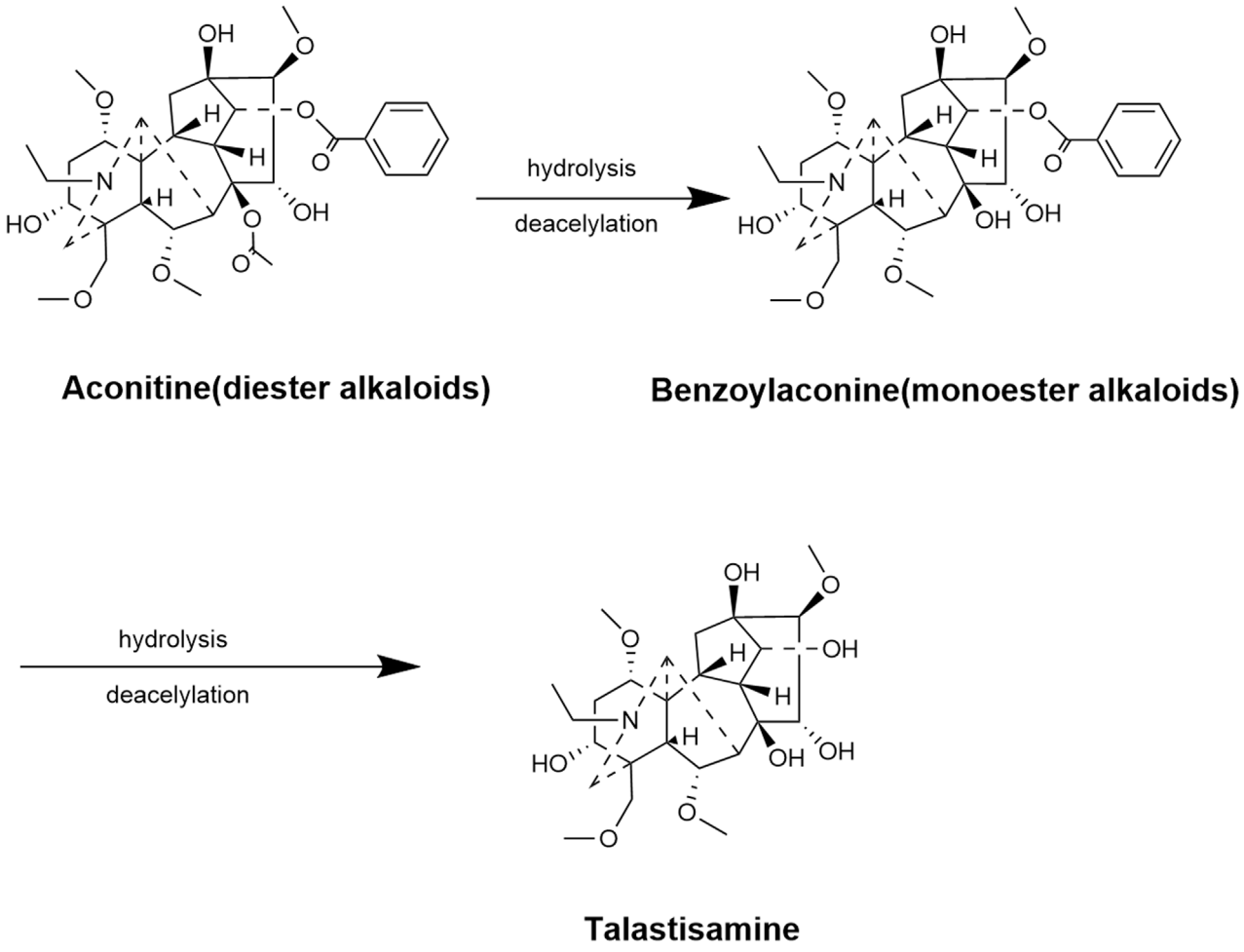

FIGURE 4
Hydrolysis reaction of aconitine.

4.1.2 Aqueous processing (called *shuizhi* in Chinese)

Shuizhi involves processing herbs with water or liquid adjuvants (like salt water, vinegar, and wine), with or without heat. Zhang et al. noted that soaking Fuzi reduces its DDA content by 36.8% and MDAs by 25.5%, decreasing toxicity but potentially impacting therapeutic effectiveness (Zhang et al., 2017). Advanced techniques like pressurized steaming have been shown to maintain safety even at dosages of processed Fuzi much higher than typical clinical levels, underscoring the method's reliability (Zhang, 2008). Furthermore, innovations like treatment with a saturated solution of $Ca(OH)_2$, extended cooking times, and high-pressure cooking have been effective in reducing toxic diterpenoid alkaloid content significantly while enhancing the concentrations of less toxic forms, thus optimizing the safety and effectiveness of processed Fuzi (Yu et al., 2023).

4.1.3 Innovative methods

In addition to the two previously mentioned commonly used processing methods of Fuzi, the integration of modern technology with traditional processes has introduced novel methods such as microwave processing, high-pressure treatment, and microbial fermentation (Yang et al., 2019). Microwave processing, characterized by high temperature, rapid heating, and a sterilizing effect, efficiently hydrolyzes toxic alkaloids in raw Fuzi, enhancing the solubility and stability of its active compounds, which improves the safety, efficacy, and medicinal value of the herb (Li et al., 2022).

4.2 Mechanisms of enhanced efficacy and reduced toxicity

4.2.1 Hydrolysis reaction

At the appropriate temperature, the alkaloids in Fuzi react with water, undergoing hydrolysis to produce new components that modify the efficacy and toxicity of the drug. Modern pharmacological studies have identified a significant number of DDAs in Fuzi, which are pivotal to its therapeutic effects and toxicity. Structurally, Fuzi contains DDAs, MDAs, and non-esterolamine alkaloids. DDAs, such as AC, exhibit substantial pharmacological activity but high toxicity, constituting the primary toxic compounds. MDAs display reduced toxicity (1/50 to 1/500 of AC) and significant pharmacological effects,

making them crucial in clinical applications. Non-esterolamine alkaloids possess even lower toxicity (1/2,000 to 1/4,000 of AC) but weaker pharmacological activity (Wei et al., 2019). AC, a highly toxic DDA, becomes unstable at high temperatures, with two ester bonds undergoing hydrolysis to form benzoyl monomer alkaloid (benzoylaconine), which has approximately 1/200 the toxicity of AC. Further heating leads to the hydrolysis of benzoylaconine into the alcoholamine AC alkaloid with the loss of the benzoyl group (Sun et al., 2016) (Figure 4). Herbal processing techniques, including decoction, steaming, and microwave processing, are employed to mitigate Fuzi's toxicity through hydrolysis, thereby enhancing its clinical safety and efficacy. A study by Zhang et al. showed that the concentration of DDAs in crude Fuzi's aqueous extract decreased rapidly during the initial decoction phase and stabilized at a lower level after 4 h, while MDA levels initially increased, peaking between 4 and 6 h. This pattern aligns with the traditional processing principle of boiling Fuzi for 4–6 h (Zhang et al., 2015).

4.2.2 Replacement reaction

A replacement reaction typically involves a simple substance reacting with a specific compound to yield new elements and compounds. Similar substitution reactions occur during the herbal processing of Fuzi, where certain groups in the herb's main compounds are substituted by other small organic molecules, ultimately altering the drug's therapeutic efficacy (Li et al., 2021). Concocting Fuzi with Radix Glycyrrhiza (RG) involves the replacement reaction; *Jing Yue's complete work* published in the Ming Dynasty summarized the detoxifying principles of concocting Fuzi with RG using Chinese medicine theories. It introduced the specific method of utilizing RG to concoct Fuzi, "If you want to use prepared Fuzi urgently, wrap crude Fuzi with thick paper, pour RG soup over it, then simmer or bake, until it is soft, cut, then wrap with paper and pour RG soup, bake it again, repeat the above steps when it's cooked thoroughly" (Chen et al., 2014). Fatty acids in RG undergo a lipid exchange reaction with the DDAs in Fuzi and their degradation products. This reaction ultimately produces less toxic lipid alkaloids; simultaneously, a small amount of DDAs forms an insoluble precipitate together with glycyrrhizinic acids in RG, which reduces the DDA content, thus diminishing toxicity (Cai et al., 2012). Processing Fuzi with RG significantly alters its chemical profile, decreasing the concentration of DDAs by about 98%, while increasing MDAs by approximately 0.6 times. HPLC-MS analyses have tentatively identified new components in the processed product, such as liquiritin and ononin (Guo et al., 2015).

4.2.3 Destruction and loss of alkaloids

The processing of Fuzi often involves washing, soaking, moistening, and rinsing. Despite not involving chemical reactions, the processing effectively reduces toxicity by causing the destruction and loss of alkaloids. These steps are crucial in Fuzi's concoction as long as they do not cause excessive alkaloid loss.

4.3 Detoxifying effects of different processing methods

Advancements in processing technology have diversified the methods applied to Fuzi, extending beyond traditional techniques. While different methods can reduce Fuzi's toxicity to varying extents, a key consideration is their ability to diminish toxic substances without compromising the retention of active pharmacological compounds.

According to the 2015 edition of the Chinese Pharmacopoeia, the allowable content of DDAs (the sum of AC, MC, and HC) in Heishunpian and Baifupian—two common forms of processed Fuzi—should not exceed 0.020%. Similarly, the content of monoester alkaloids (the sum of benzoylaconine, benzoylmesaconine, and benzoylhypaconine) should not be less than 0.010%. Additionally, regulations in Sichuan Province mandate that the content of DDAs in raw sliced Fuzi should be 0.10%–0.20% (Zan et al., 2019; Gu et al., 2022). Table 2 illustrates the variations in toxic and active components of Fuzi following different processing methods (Su et al., 2010; Yang et al., 2014; Xu et al., 2017; Ye et al., 2019; Xia et al., 2021; He et al., 2023).

4.4 Various changes in Fuzi after processing

4.4.1 The changes in compounds

The processing initially induces alterations in the compounds of Fuzi; these compounds serve as the foundation for its toxicity and pharmacological effects. Using HPLC measurements to analyze the changes in the chemical composition of Fuzi after sand scalding, the results indicated a decrease in the content of DDAs from 0.0675% to 0.0015%, representing a reduction of approximately 98%. Conversely, the content of MDAs increased approximately threefold from 0.0141% to 0.0382% (Chen et al., 2016). In a separate study, the UPLC-Q-TOF-MS/MS method was employed to identify compounds that exhibited variations before and after low-temperature baking of raw Fuzi. By utilizing variable importance in the projection (VIP), 44 potentially differentiated compounds were identified (Ye et al., 2021). Through employing the UHPLC-Q-TOF/MS technique to gather data on the chemical compound groups during the decoction of Fuzi, Li et al. discovered that the compositional changes during decocting primarily involved the conversion of DDAs to MDAs, and subsequently to aconine alkaloids. Notably, the transformation of MDAs to aconine alkaloids was predominant. Furthermore, ester alkaloids such as karakoline, songorine, and fuziline exhibited negligible changes during prolonged heating, attributed to their excellent thermal stability (Li R et al., 2016).

In addition to studies on compositional changes following a single processing method, research involving multiple processing techniques has been conducted. Heishunpian and Baifupian, two common forms of processed Fuzi involving thermal and aqueous treatments, were utilized for compositional comparisons with unprocessed Fuzi using chemical UPLC-MS profiling and multivariate classification techniques. A total of 18 compounds, including one veatchine alkaloid, seven ADAs, six DDAs, three MDAs, and one lipo-diterpenoid alkaloid (LDA), were identified in this study. While the two processed products exhibited a significant decrease in the content of highly compounded DDAs compared to raw Fuzi, there was an increase in the content of catabolized low-toxicity derivatives such as MDAs, ADAs, and LDA (Sun et al., 2019).

TABLE 2 Detoxifying effects of different processing methods.

Processing method	Ingredient	Processing time	Unit (content)	Aconitine		Mesaconitine		Hypaconitine		Diester alkaloids	
				Unprocessed	Processed	Unprocessed	Processed	Unprocessed	Processed	Unprocessed	Processed
Steaming	raw Fuzi	90 min	mg/kg	184.03	0.45	736.29	0.47	829.53	3.84	1749.85	4.77
Baking	raw Fuzi	60 min	mg/kg	184.03	9.07	736.29	27.46	829.53	48.25	1749.85	84.78
Decocting	raw Fuzi	8 h	mg/kg	184.03	0.39	736.29	0.52	829.53	2.00	1749.85	2.91
Stir-frying (with sand)	raw Fuzi	—	mg/mL	0.0195	0.0048	0.0649	0.0059	0.1872	0.0268	0.0863% (proportion of sample content)	0.0119% (proportion of sample content)
Fermenting Processing with adjuvants	raw Fuzi	—	mass fraction (%)	0.0670%	0.0522%	0.2750%	0.0633%	0.0550%	0.0291%	0.3970%	0.1446%
Processing with Radix Glycyrrhizae and Black Soya Bean	salt-processing Fuzi	—	mass fraction (%)	0.0038%	—	0.018%	—	0.017%	0.0013%	0.039%	0.0013%
Processing with ginger juice	raw Fuzi	—	mg/g	142.4926	50.1496	298.5440	27.0973	473.6812	109.2593	914.7178	186.5062
Processing by microwave	raw Fuzi	—	mass fraction (%)	—	—	—	—	—	—	—	0.004%–0.016%

Benzoylaconine		Benzoylmesaconine		Benzoylhypaconine		Monoester alkaloids		References
Unprocessed	Processed	Unprocessed	Processed	Unprocessed	Processed	Unprocessed	Processed	
15.67	145.25	137.02	878.91	22.79	632.14	175.48	1,656.30	Yang et al. (2014a)
15.67	92.61	137.02	594.39	22.79	335.99	175.48	1,022.99	Yang et al. (2014a)
15.67	145.86	137.02	807.34	22.79	584.59	175.48	1,537.79	Zhang et al. (2015a)
0.0344	0.0735	0.0934	0.1641	0.0310	0.0970	0.0415% (proportion of sample content)	0.0785% (proportion of sample content)	Ye et al. (2019)
—	—	—	—	—	—	—	—	Su et al. (2010)
0.00032%	0.0013%	0.0046%	0.00820%	0.00070%	0.0035%	0.0053%	0.013%	Guo et al. (2015)
194.2307	16.2768	17.4816	42.0960	68.8040	22.1509	280.5163	80.5237	Xu et al. (2017)
—	—	—	—	—	—	—	0.071–0.166%	He et al. (2023)

10.3389/fphar.2024.1427333

4.4.2 The changes in toxicity

Processing-induced changes in toxic alkaloids within raw Fuzi undoubtedly impact the toxicity of the processed Fuzi. Ren et al. investigated the alterations in the content of Aconitum alkaloids in Fuzi following various processing methods using DESI-MSI and UHPLC-QTOF MS. The results revealed that the content of less toxic MDAs and NAs, converted from the more toxic DDAs, increased in all processed products. Additionally, the content of benzoylaconine increased post-processing, indicating enhanced pharmacological activity and reduced toxicity (Ren et al., 2023). Furthermore, processed Fuzi can elevate testosterone, superoxide dismutase (SOD), glutathione (GSH), and catalase (CAT) levels while decreasing malondialdehyde levels in serum compared to raw Fuzi, thereby mitigating the reproductive toxicity and genotoxicity of Fuzi. The protective mechanism of processing to alleviate Fuzi toxicity may be associated with increased testosterone levels and reduced oxidative stress (Zhang et al., 2021). The processing of Fuzi with RG represents a classical method capable of reducing the toxicity of raw Fuzi. The detoxification principle of this method involves decreasing the content of DDAs through replacement reactions. However, a study found that co-administration of Fuzi and RG could attenuate significant metabolic changes in several amino acids, organic acids, and ketone bodies induced by Fuzi alone in rats. This suggests that reducing toxicity at the metabolic level through various pathways, including energy metabolism and the synthesis and degradation of ketone bodies, may represent another potential detoxification mechanism of Fuzi processed with RG (Sun et al., 2016).

4.4.3 The changes in pharmacological effects

Processing alters the composition of Fuzi, leading to variations in pharmacological effects. Heishunpian is a processed Fuzi product involving multiple complex processing steps. To investigate the impact of each step on its anti-inflammatory and analgesic effects, a study employed a "step knockout" strategy to assess the efficacy of different samples. The findings revealed that ibuprofen and Heishunpian exhibited the highest efficacy in the hot plate test, while ibuprofen and the sample without rinsing were the most effective in the acetic acid torsion test. The differences in efficacy may be attributed to the varying effects of different steps on the content of active analgesic components, such as mesaconine, aconine, 3-deoxyaconine, delbruine, and asperglaucide (Xue et al., 2024). Processing influences the pharmacological effects of Fuzi and its therapeutic mechanism in specific diseases. Tong et al. compared the differences in expressed proteins between unprocessed Fuzi and its processed product (Yinfupian, characteristic decoction pieces for the Yang deficiency syndrome) inducing Yang deficiency syndrome in rats. They found that raw Fuzi primarily targeted muscle contraction-related proteins, closely linked to inflammation and myocardial injury. Conversely, the processed products primarily affected mitochondrial proteins, closely associated with adenosine triphosphate energy metabolism (Tong et al., 2021).

4.5 The theory of "salt processing leading drug into kidney"

The 2020 edition of the Chinese Pharmacopoeia highlights that treating crude Fuzi with a salt solution is essential. This standard draws on the extensive experience of TCM practitioners developed through long-term clinical practice. The exact mechanism behind Fuzi's salt processing remains elusive; however, the theory of "salt processing directing drugs to the kidney" provides a partial explanation.

4.5.1 Salt processing

Salt processing, a classical pharmaceutical technique in TCM, involves using salt as an auxiliary ingredient. Salt, characterized by its flavor and cold nature, is known for clearing heat, cooling blood, softening and dispersing masses, and moistening dryness. After salting the Chinese medicine, it will mainly enter the kidney meridian. Historically, *Leigong's Treatise on Preparations* from the Northern and Southern Dynasties first documented the use of salt to process various medicines (Liu et al., 2023). Modern medical theory acknowledges that salt, primarily composed of NaCl along with traces of $MgCl_2$, $CaCl_2$, KCl, and NaI, is crucial for maintaining normal osmotic pressure in human tissues. Salt enhances gastric juice secretion and protein absorption and has a diuretic effect (Zhou et al., 2021). Initially, during the Sui Dynasty, salt processing was used to enhance the curative effect and reduce the toxicity of Fuzi, with its antiseptic and preservative qualities being significant under less advanced conditions. Presently, salt processing comprises salt washing, salt infiltration, salt infiltration heating, and salt stir-frying, with saltwater frying and steaming being the most common (Hou et al., 2023).

4.5.2 Influence of salt processing on the renal action of drugs

Rooted in the foundational TCM five-phase theory, which posits that "five flavors enter the five viscera," saltiness is associated with the kidney. Despite the differing definitions of internal organs in TCM and modern medicine, certain references can still be drawn. The physiological characteristics of the kidney, particularly its role in Na^+ reabsorption, enable many active ingredients in salt-processed drugs to be absorbed by the kidneys along with Na^+ reabsorption in clinical application (Wei et al., 2019).

Although many scholars have mentioned in their studies that salt processing enhances the effects of drugs on the kidney, there is a lack of research on the effects of salt-processed Fuzi on the kidney. However, insights might be drawn from studies on other salt-processed drugs or compound medicines (Bai et al., 2023). For instance, research using NMR techniques has shown that salt processing significantly alters the chemical composition of Alismatis rhizoma (ALR), commonly used for treating kidney diseases, by promoting dehydration, deacetylation, and oxidation (Han et al., 2016). HPLC studies conducted by Cao et al. have confirmed increases in specific bioactive components in salt-processed ALR, enhancing its diuretic effect (Cao et al., 2016).Suoquan pill composed of salt-processed Yizhiren (*Alpiniae oxyphyllae*) could significantly reduce the serum levels of BUN and creatinine in the kidney-yang deficiency model mice compared with Suoquan pill composed of crude Yizhiren and have a more pronounced effect on the repair of renal injury in model mice. The result validates the science and correctness of using salt-processed Yizhiren instead of raw Yizhiren in the Suoquan pill (Shuai et al., 2018).

TABLE 3 Pharmacological effects of Fuzi on the kidney.

Pharmacology	Extract/Chemical components/ Decoction	Experimental animals/cells	Model establishment	Experimental dose	Time of administration	Effects	References
Nephroprotective effect							
Antioxidant effect	Fuzi water extract	mouse	Intragastric administration of aristolochic acid	5 g/kg/d	2 weeks	↓renal index, ↓SCr, ↓BUN, ↓UA ↑γ-GT	Du et al. (2012)
	modified Fuzi Lizhong Decoction	rat	Gavage administration of aristolochic acid	10 mL/kg	3 weeks	↑SOD ↓MDA	Shi et al. (2011)
	Fuzi polysaccharides	NRK-52E cells, rat	Treated with H2O2, Intraperitoneal injection of cisplatin	5000, 2,500, 1,250 μg/mL 200, 400, 800 mg/kg	24 h, 10 days	↓cell apoptotic rate ↑GSH, ↑GPX-4, ↓MDA, ↓4-HNE	Tian et al. (2022)
Interventional effect on apoptosis and autophagy	Fuzi water extract Fuzi polysaccharides	HMCs	Treated with 10 μg lipopolysaccharides	100 μL	24 h	↑ Bax, ↑ caspase-8, ↑caspase-3 ↓Cyclin E, ↓CDK2	Li et al. (2022b)
	modified Fuzi Lizhong Decoction	rat	Blocked left and right renal arteries with arterial clips	10 mL/kg	7 days	↓SCr, ↓BUN, ↓MDA, ↓caspase-3, ↓PARP, ↓Bax ↑SOD	Lan et al. (2020)
	Mahuang Fuzi and Shenzhuo Decoction	rat	Injected with anti-Fx1A Serum	1 mL/100 g	12 weeks	↓24 hUTP, ↓CHO, ↓TG, ↓nephrin, ↓IgG, ↓LC3-II, ↓p62, ↓β-catenin, ↓GSK-3β	Gao et al. (2022)
	Dahuang Fuzi Decoction	rat	Administered 2% adenine	2.5 g/kg	3 weeks	↓proteinuria, ↓NAG, ↓BUN, ↓SCr, ↓Bax, ↓caspase-3, ↓TGF-β1, ↓p-JNK ↑ Bcl-2	Tu et al. (2014)
Promotion of metabolic waste excretion	Fuzi water extract	mouse	Gavage administration of aristolochic acid Gavage administration of adenine	3,10 g/kg	5 weeks 4 weeks	↓BUN, ↓LD, ↓LDH, ↓kidney coefficient ↑sperm counts, ↑renal protein contents	Fan et al. (2011)
	Fuzi water extract	rat	Intravenous injection of adriamycin	3, 6, 9 g/kg	8 weeks	↓urinary protein, ↓TC, ↓TG, ↓BUN, ↓SCr ↑TP, ↑ALB	Yang and Wang (2010)
Anti-inflammatory and antifibrotic effects	Fuzi water extract	mouse	administered adenine by oral gavage	1 g/kg	5 days	↓Scr, ↓BUN, ↓NAG, ↓IL-1β, ↓IL-6 ↓TNF-α, ↓Ccl2, ↓Tgfb1, ↓Col1a1	Yang et al. (2021b)
	Fuzi and Ganjiang extraction	BV2 cells	Treated with LPS	400 μg/mL	—	↓IL-6, ↓TNF-α, ↓ROS, ↓NO ↓PGE2, ↓iNOS, ↓COX2	Yang et al. (2021a)
	ShenFu Decoction	rat	Administered 2.5% adenine	7.56 g, 3.78, 1.89 g/kg	4 weeks	↓TGF-β1, ↓CTGF, ↓TNF-α ↑Smad7	Yuan (2020)
Immunomodulatory effect	Aconitine	mouse	Intraperitoneal injection of 0.5 mL pristane	25, 75 μg/kg	9 weeks	↓blood leukocyte counts ↓serum anti-dsDNA antibody ↓IgG deposit, ↓PGE2, ↓IL-17a, ↓ IL-6	Li et al. (2017)

(Continued on following page)

10.3389/fphar.2024.1427333

10.3389/fphar.2024.1427333

TABLE 3 (*Continued*) Pharmacological effects of Fuzi on the kidney.

Pharmacology	Extract/Chemical components/ Decoction	Experimental animals/cells	Model establishment	Experimental dose	Time of administration	Effects	References
	Fuzi water extract	rat	Injected with hydrocortisone sodium succinate	12 g/kg	7 days	↓IFN-γ ↑Na^+-K^+-ATPase ↑Mg^{2+}-ATPase, ↑SDH	Li et al. (2021b)
	Fuzi polysaccharides	mouse	Intraperitoneal injections of cyclophosphamide	200, 100, 50 mg/kg	7 days	↑NO, ↑IFN-γ, ↑spleen index, ↑thymus index, ↑proliferation of spleen cells and peritoneal macrophages	Fu et al. (2018)
	Fuzi neutral polysaccharide	mouse	Inoculated subcutaneously with H22 liver cancer cells	100, 200 mg/kg	7 days	↓IL-10, ↓TNF-α ↑IL-1β, ↑IL-6	Hu et al. (2023)

5 Pharmacology

5.1 Pharmacodynamics of Fuzi on the kidney

Fuzi, a TCM, is known for its pungent and sweet flavors, extreme heat nature, and toxicity. It is associated with the heart, kidney, and spleen meridians. Clinically, Fuzi is a primary ingredient in treatments for various kidney ailments, such as acute and chronic glomerulonephritis and nephrotic syndrome (Jiang et al., 2023). Modern pharmacological research suggests that its nephroprotective, anti-inflammatory, and immunomodulatory properties contribute to these effects (Table 3).

5.1.1 Nephroprotective effects

Various animal models of nephropathy have elucidated potential mechanisms behind Fuzi's renal protective effects. These include antioxidative stress, regulation of apoptosis and autophagy, and enhancement of metabolic waste excretion.

5.1.1.1 Antioxidant effects

Aristolochic acid nephropathy (AAN), characterized by acute and chronic tubulointerstitial lesions, results in acute and chronic renal failure and tubular acidosis. Previous studies have suggested that the nephrotoxicity of aristolochic acid may be related to lipid peroxidation and DNA oxidative damage which result from elevated levels of reactive oxygen species *in vivo* (Du et al., 2012). A Study on the AAN rat model has shown that the modified Fuzi Lizhong Decoction (mFLD) increases SOD activity in renal tissues, reduces malondialdehyde (MDA) levels, and alleviates renal pathology, underscoring Fuzi's antioxidant properties (Shi et al., 2011). Refined fucose polysaccharide (RFP), extracted from Aconitum carmichaelii's lateral root, exhibits antioxidant activity by enhancing the clearance rates of various free radicals and reducing lipid peroxidation. Taking it a step further, Tian et al. uncovered that RFP could reduce cell membrane lipid peroxidation in mice with cisplatin-induced acute kidney injury by increasing the levels of GSH and glutathione peroxidase-4 and lowering the levels of malondialdehyde (MDA) and 4-hydroxynonenal (Chen et al., 2022; Tian et al., 2022).

5.1.1.2 Interventional effects on apoptosis and autophagy

Apoptosis and autophagy are both forms of programmed cell death; many studies indicate that Fuzi and its components have an intervening effect on them. For example, aqueous extracts of Aconiti Lateralis Radix and its polysaccharides inhibit mesangial cell proliferation via the PI3K/AKT/mTOR pathway and induce apoptosis by modulating key proteins (such as Cyclin E/CDK2, Bax, caspase-8, and caspase-3) involved in the cell cycle and death pathways in a study discussing the underlying therapeutic mechanisms of mesangial proliferative glomerulonephritis (MesPGN) (Li et al., 2022). Ischemia-reperfusion is one of the most common causes of acute kidney injury; current research suggests that the underlying mechanism is the massive production of oxygen free radicals after reperfusion, which leads to extensive oxidative stress injury and then induces apoptosis. Lan et al. explored the protective effect of the prophylactic administration of mFLD on the ischemia-reperfusion injury rat model; the results suggested that it may be related to the antioxidant

stress response, modulation of apoptotic pathways through inhibiting the expression of Caspase-3, PARP, and Bax proteins (Lan et al., 2020). During the investigation into potential mechanisms of Mahuang Fuzi and Shenzhuo Decoction (MFSD) in treating membranous nephropathy (MN), researchers observed significant reductions in proteinuria and podocyte injury in passive Heymann nephritis rats (a classical MN model) following MFSD treatment. This corresponded with improvements in renal pathology. Analysis of the study suggests that modulation of autophagy in podocytes and inhibition of the Wnt/β-catenin pathway could be potential targets (Gao et al., 2022). Furthermore, given that Dahuang Fuzi Decoction (DFD) is a traditional formula clinically proven for treating chronic kidney disease (CKD) in China, Tu et al. investigated its therapeutic effects on the adenine-induced renal injury rat model to elucidate the *in vivo* therapeutic mechanism. The findings revealed that DFD mitigated apoptosis by downregulating the expression of Bax and cleaved caspase-3 proteins while enhancing Bcl-2 protein expression. Furthermore, it attenuated renal tubular epithelial apoptosis by suppressing the activation of the TGF-β1-JNK pathway (Tu et al., 2014; Ta et al., 2023).

5.1.1.3 Promotion of metabolic waste excretion

Fan et al. investigated the impact of Fuzi on lactic acid (LD) metabolism in two different mouse models of CKD. Both groups of mice exhibited varying degrees of LD acidosis. Following the administration of Fuzi's aqueous decoction, serum or organ LD levels decreased, while the activity of lactate dehydrogenase (LDH) significantly increased in both groups. These findings suggest that Fuzi exerts a nephroprotective effect by modulating LD metabolism. The underlying mechanism may involve Fuzi's ability to reduce LD production or enhance LD excretion, consequently diminishing LD accumulation, correcting acidosis, and improving energy metabolism (Fan et al., 2011). Moreover, in a study on the therapeutic effect of Fuzi on adriamycin-induced nephropathy in rats, significant reductions in SCr and BUN were observed in the treatment group compared to the model group, reflecting Fuzi's ability to promote the excretion of serum urea nitrogen and creatinine (Yang and Wang, 2010).

5.1.2 Anti-inflammatory and antifibrotic effects

Renal damage typically involves inflammatory and fibrotic responses. When various factors damage renal intrinsic cells, endothelial cytokines (such as TNF-α and IL-1) become activated. This activation prompts the recruitment of diverse inflammatory cells from the bloodstream, which infiltrate the membranes, capillaries, and renal mesangial area, subsequently releasing a plethora of inflammatory mediators. Following a cascade of inflammatory reactions and cytokine activity, renal intrinsic cells release fibrogenic factors, transforming into myofibroblasts. These myofibroblasts synthesize and secrete substantial amounts of collagen fibers that resist degradation, yielding an imbalance in extracellular matrix formation and degradation, ultimately forming a scar. These alterations culminate in renal histoarchitectural damage, renal interstitial fibrosis, and a progressive decline in renal function.

Yang et al. found that the main active ingredients of Fuzi, such as AC, HC, and neoconitine, could reduce SCr, BUN, and urinary N-acetyl-β-D-glucosidase levels and decrease inflammatory and fibrotic factors (IL-1β, IL-6, TNF-α, Ccl2, Tgfb 1, and Col1a1) in mice with adenine-induced CKD (Yang et al., 2021). Another study also showed that the Chinese herb couple, Fuzi and Ganjiang, effectively reduced the production of pro-inflammatory mediators (IL-6, TNF-α, ROS, NO, and PGE2) and inhibited the expression of iNOS and COX2, which was associated with the inhibition of NF-κB/activation of the Nrf2/HO-1 signaling pathways (Yang et al., 2021). After comparing renal histopathological changes in an adenine-induced CKD rat model treated with Shenfu Decoction (SD), Yuan et al. hypothesized that SD might inhibit the irregular release of fibrogenic factors and reduce inflammatory cell infiltration and fibrous tissue proliferation through the TGF-β1/Smads signaling pathway, thus exerting an anti-fibrotic effect on renal interstitium (Yuan, 2020).

5.1.3 Immunomodulatory effect

Immunoregulatory mechanisms are a driving force in the pathogenesis of many kidney diseases. Moreover, immunosuppressants are commonly used in the treatment of kidney diseases (Wang and Zhang, 2017). One of the common syndrome types of low immune function in TCM is kidney-yang deficiency. Therefore, warming and tonifying kidney yang is an important rule to improve human immune function; Fuzi is one of the prime choices for reinforcing kidney yang (Yuan, 2018).

Many secondary kidney diseases are caused by autoimmune disorders. For instance, lupus nephritis is one of the most serious complications of systemic lupus erythematosus (SLE). Li et al. observed the pathological lesions of lupus nephritis induced by phytane in mice; the results showed that AC reduced the blood leukocyte count, lowered the serum anti-dsDNA antibody level, and improved the health status, thus reducing the damage to the organism. In conclusion, AC has a strong immunosuppressive effect and may inhibit the activity and progression of SLE (Li et al., 2017). Hydrocortisone sodium succinate injection-induced cold immunocompromise and energy metabolism disorders in rats are significantly ameliorated via Fuzi aqueous extract (Li et al., 2021).

Fuzi's impact on immune functions is particularly significant in conditions where immunity influences kidney disease progression. Recent research has increasingly attributed the immunomodulatory effects of Fuzi to Fuzi's polysaccharides. At a dosage of 200 mg/kg, HSP polysaccharide notably elevated the serum levels of NO and IFN-γ in cyclophosphamide-induced immunocompromised mice. IFN-γ, a Th1 cytokine, can activate macrophages, while NO is produced by macrophages to eliminate pathogens (Fu et al., 2018). In another study, water-soluble polysaccharides derived from Fuzi showed significant antioxidant and immunomodulatory activities and promoted macrophage phagocytosis, which increased the secretion of macrophage-derived biofactors in RAW 264.7 cells (Yang et al., 2020). In a recent study, 200 mg mL^{-1} Fuzi neutral polysaccharide attenuated the suppression of immune organs and immune cells caused by cyclophosphamide (CTX) treatment by activating immune cells and promoting inflammation (Hu et al., 2023). In conclusion, Fuzi's polysaccharides have shown potential in modulating immune responses, enhancing macrophage activity, and promoting cytokine production, thereby supporting its use in immunocompromised cases.

5.2 Pharmacokinetics

Unlike single-compound drugs, herbal extracts such as Aconiti Lateralis Radix Praeparata (Fuzi) exhibit a complex composition, which complicates their clinical use, particularly given Fuzi's narrow therapeutic window due to its inherent toxicity. Understanding the pharmacokinetics of Fuzi and its primary chemical compounds—encompassing absorption, distribution, metabolism, and excretion—enables optimization of dosage, timing, and administration routes to maximize clinical efficacy and minimize toxicity (Zhang et al., 2014). Fuzi's key components are diterpene alkaloids such as AC, MC, and HC, which also include less toxic derivatives like benzoylaconitine (BAC), benzoylmesaconitine (BMC), and benzoylhypaconitine (BHC).

5.2.1 Absorption

5.2.1.1 Fuzi extracts

AC shows low bioavailability (4.72% ± 2.66%) in rats, to which Fuzi extract (0.118 mg/kg AC) was administered intragastrically; however, its absorption is rapid, with a T_{max} of 58.00 ± 21.68 min. Pharmacokinetic parameters do not significantly change with repeated administration, although absorption rates increase. These findings suggest that other components in Fuzi may influence AC's pharmacokinetic profile after prolonged exposure (Tang et al., 2012). Furthermore, the low bioavailability of Fuzi's alkaloids is attributed to efflux transporter proteins, such as P-glycoprotein (P-gp), multidrug resistance protein 2 (MRP2), and breast cancer resistance protein (BCRP). These proteins serve as barriers by ejecting xenobiotic substances from the bloodstream back into the intestinal lumen, thus mitigating Fuzi's toxicity. Studies have demonstrated that efflux transporter proteins mediate the uptake and transport of Fuzi active ingredients with the rule that the greater the toxicity of the alkaloids, the more efflux occurs, namely, AC, MA, HA > BAC, BMA, BHA (Yang et al., 2014).

5.2.1.2 Monomer compounds of Fuzi

Research by Zhang et al. on three representative alkaloids—AC, benzoylaconitine (BAC), and aconine (ACN)—demonstrates that while all are rapidly absorbed, BAC shows the fastest absorption with a T_{max} of 0.31 ± 0.17 h. The C_{max} of the three were 10.99, 3.99, and 4.29 ngmL−1, respectively, reflecting that AC could be better absorbed compared to BAC and ACN. Despite their rapid uptake, these alkaloids are poorly absorbed overall, with P-gp inhibiting the uptake of AC and BAC, whereas ACN is absorbed passively (Zhang et al., 2015). Additionally, an *in vitro* intestinal absorption study of MC found that the absorption rate of MC was associated with concentration differences across the intestinal wall, indicating passive transport as its primary absorption mechanism (Yun et al., 2018).

5.2.2 Distribution

Alkaloids are the primary active ingredients in Fuzi; understanding their tissue distribution is vital for elucidating Fuzi's pharmacokinetics.

Wang et al. used HPLC-MS to study the distribution of AC in rats, finding the highest concentrations in the liver and lungs, followed by the heart, kidneys, and spleen, with notable individual variability (Wang et al., 2005). Another study on mice showed that AC was predominantly distributed in the liver and kidney, followed by the heart, blood, and brain. However, the results show significant alterations in distribution patterns in Mdr 1a −/− mice, with increased AC levels in all organs, especially the brain (Wu J. J. et al., 2018). A study about the Aconitum alkaloids' distribution in the cadaver of a patient with acute aconite poisoning revealed the highest levels in urine, followed by bile, stomach, heart, and blood. Therefore, urine, blood, and bile can be used as the preferred bioassay in case of aconite poisoning (Liu et al., 2009). Niistu et al. found that Aconitum alkaloids were higher in the liver and kidney and lower in the heart and brain in autopsies of three suicide cases involving aconite poisoning. Moreover, the Aconitum alkaloid content was higher in the blood than in brain tissues (Niitsu et al., 2013).

ADAs, among the active ingredients of Fuzi, are considered less toxic alkaloids. According to available studies, ADAs are widely distributed in the heart, liver, lung, and kidney after entering the human body but less prevalent in the brain (Tao et al., 2023).

5.2.3 Metabolism

5.2.3.1 Drug-metabolizing enzymes (DMEs)

Cytochrome P450 enzymes (CYPs) are found in all organs and tissues, except for skeletal muscles and mature erythrocytes, with the highest abundance in the liver, gastrointestinal tract, lung, and kidney. These enzymes are crucial in metabolizing endogenous substances and exogenous compounds, including drugs and environmental chemicals. Notably, at least nine human hepatic cytochrome P450 enzymes are integral to drug metabolism, primarily through hydroxylation or oxidation processes that enhance solubility and facilitate excretion.

Tang et al. examined the cytochrome P450 isozyme changes during AC metabolism using human liver microsomes (HLMs) and recombinant CYPs, identifying six CYP-mediated metabolites in HLMs and eight recombinant CYP isoforms. Additionally, they found significant inhibition of AC metabolism by CYP 3A inhibitors, with moderate inhibition by CYP 2C9, 2C8, and 2D6, whereas CYP 2C19, 1A2, and 2E1 showed negligible effects. Aconitine is mainly transformed by CYP 3A4/5 and 2D6 into various metabolites, indicating the importance of these isoforms in its biotransformation (Tang et al., 2011; Jin et al., 2022). Since AC, MA, and HA have similar structures, studies have shown that the metabolic mechanisms of MA and HA are similar to those of AC. Ye et al. demonstrated that MA generates at least nine metabolites in the presence of HLMs. The main metabolic pathways include demethylation, dehydrogenation, hydroxylation, and dehydrodemethylation (Ye et al., 2010). Conversely, HA generates at least 11 metabolites, metabolized by demethylation, dehydrogenation, hydroxylation, dehydrodemethylation, and desdimethylation (Ye et al., 2011). In addition to DDAs, CYPs are involved in the metabolic reactions of MDAs. A total of 7, 8, and 9 metabolites of BAC, BMA, and BHA were found, respectively, in HLMs (Ye et al., 2013a).

Zhang et al. also investigated the inhibitory effects of aconitine on different isoforms of the CYP450 enzyme in rat liver microsomes *in vitro*. They concluded that aconitine inhibited the activities of CYP2C9 and CYP2D6 to a certain extent. Given that CYP2C9 and CYP2D6 are involved in the metabolism of commonly used clinical

drugs, attention should be paid to the occurrence of drug metabolic interactions in the clinical use of Chinese medicines rich in aconitine alkaloids (Zhang, 2016).

5.2.3.2 Efflux transporters

Efflux transporters (ETs), containing ATP-binding cassette proteins, mainly include P-gp, MRP2, and BCRP. These transporters are widely expressed in intestinal, hepatic, renal, and cerebral tissues and are involved in drug absorption, distribution, and excretion.

The role of efflux transporter proteins in alkaloid transport has received the attention of many researchers. Ye et al. performed bidirectional translocation assays of Aconitum alkaloids in the presence or absence of P-gp, BCRP, and MRP 2 inhibitors (cyclosporin A and verapamil, Ko 143, MK 571). Ultimately, they concluded that P-gp and BCRP are involved in the transport of AC, MA, and HA, while MRP2 may be implicated in the transport of several forms of these alkaloids (Ye et al., 2013b). While ETs are involved in Aconitum alkaloid transport, Aconitum alkaloids simultaneously affect ETs. AC increased the expression of P-gp, MRP 2, and BCRP in mouse jejunum, ileum, and colon. Diterpene alkaloids such as AC and benzoylglycyrrhetinic acid significantly increased MRP 2 and BCRP expression through activation of Nrf 2-mediated signaling pathways (Wu X. et al., 2018).

5.2.4 Excretion

The kidney is the most important organ involved in the excretion of Aconitum alkaloids. In a case involving a 45-year-old male who ingested approximately 11 mg of DDAs, AC, MA, HA, and their hydrolyzed products were detected in the serum on the first day, with some alkaloids detectable in the urine even 6 days after intoxication. This suggests that Aconitum alkaloids undergo metabolism *in vivo*, and their hydrolysis products are excreted time-dependently in the urine (Mizugaki et al., 1998). Additionally, in a 40-year-old woman who died of aconite poisoning, higher levels of alkaloids were detectable in the kidneys, liver, and bile compared to other organs or serum, suggesting primary elimination of these alkaloids by the liver and kidneys. Meanwhile, the concentration of astragalus alkaloids in the ileum was also notably high., demonstrating that Aconitum alkaloids are eliminated through urine and feces (Ito et al., 2000).

6 Conclusion

Fuzi is a widely utilized herbal medicine in TCM. Recent studies have highlighted its potent pharmacological benefits coupled with significant toxicity. Processing Fuzi is recognized as an effective way to enhance its therapeutic effects while reducing its toxicity. This review addresses this topic through a wide range of Chinese and English research articles. Although Fuzi contains diverse chemical components, alkaloids, particularly DDAs, are its most active and toxic compounds. Improper clinical use of Fuzi can cause severe cardiotoxicity, hepatotoxicity, nephrotoxicity, and neurotoxicity, potentially leading to patient mortality. Consequently, traditional clinical practices have developed numerous processing methods to further influence the toxicity and pharmacological effects of Fuzi by altering the composition of its chemical components. Among these, salt processing particularly improves the pharmacological effects of Fuzi on the kidney (mainly including nephroprotective, anti-inflammatory, and immunomodulatory effects). However, research on processed Fuzi remains insufficient; further studies are urgently needed to explore its medicinal potential, particularly to understand its mechanism of action after processing.

7 Discussion

This review overviews the primary compounds, toxicity characteristics, kidney-related pharmacological effects, and processing methods of Fuzi. It outlines various processing techniques and introduces discussions on the mechanisms through which these methods enhance therapeutic effects and minimize toxicity. Notably, salt processing stands out for its unique ability to amplify Fuzi's benefits for kidney health. However, this review does not exhaustively detail the changes in Fuzi's chemical composition, toxicity, and pharmacological effects following processing, nor does it deeply explore the potential mechanisms by which different processing methods influence Fuzi. Current research on the chemical composition, toxicity, and pharmacological effects of processed Fuzi remains inadequate; the mechanisms underlying specific processing methods, such as salt processing, are poorly understood. Therefore, further investigations are essential to evaluate the impact of these processing techniques on the physicochemical properties of Fuzi and to elucidate their mechanisms. Additionally, future research should focus on clinical studies evaluating the safety and efficacy of Fuzi preparations for treating kidney disease. Through these studies, we can determine how far processing methods can extend the boundaries of Fuzi's clinical applications, thereby supporting the identification of new methods and standards for Fuzi processing. In brief, the role and mechanisms of processing in improving the clinical efficacy and reducing the adverse effects of Fuzi and other Chinese herbal medicines hold significant potential for future research.

Author contributions

ZW: Writing–review and editing, Writing–original draft. JQ: Writing–original draft. CF: Writing–review and editing. ZC: Writing–original draft. XG: Writing–review and editing, Project administration, Funding acquisition. YL: Supervision, Writing–review and editing. YG: Writing–review and editing, Supervision, Project administration, Methodology, Funding acquisition.

Funding

The author(s) declare that no financial support was received for the research, authorship, and/or publication of this article.

Conflict of interest

The authors declare that the research was conducted in the absence of any commercial or financial relationships that could be construed as a potential conflict of interest.

Publisher's note

References

An, J., Fan, H., Han, M., Peng, C., Xie, J., and Peng, F. (2022). Exploring the mechanisms of neurotoxicity caused by fuzi using network pharmacology and molecular docking. *Front. Pharmacol.* 13, 961012. doi:10.3389/fphar.2022.961012

Bai, R., Fan, J., Wang, Y., Wang, Y., Li, X., and Hu, F. (2023). Protective effect of Cistanche deserticola on gentamicin-induced nephrotoxicity in rats. *Chin. Herb. Med.* 15 (1), 102–109. doi:10.1016/j.chmed.2022.03.008

Cai, B., Qin, K., Wu, H., Cai, H., Lu, T., and Zhang, X. (2012). Chemical mechanism during Chinese medicine processing. *Prog. Chem.* 24 (4), 637–649.

Cai, Y., Gao, Y., Tan, G., Wu, S., Dong, X., Lou, Z., et al. (2013). Myocardial lipidomics profiling delineate the toxicity of traditional Chinese medicine Aconiti Lateralis radix praeparata. *J. Ethnopharmacol.* 147 (2), 349–356. doi:10.1016/j.jep.2013.03.017

Cao, L., Li, Q. M., Fang, Q. M., Wang, X. Y., Zhou, X. J., and Yang, Y. X. (2016). Effects of three processing methods on four triterpenoids in Alismatis Rhizoma. *Chin. Tradit. Pat. Med.* 38 (9), 1994–1998. doi:10.3969/j.issn.1001-1528.2016.09.025

Chan, Y. T., Wang, N., and Feng, Y. (2021). The toxicology and detoxification of Aconitum: traditional and modern views. *Chin. Med.* 16 (1), 61. doi:10.1186/s13020-021-00472-9

Chen, J., Tan, P., Wu, Y. J., Qin, Y. X., Wang, L., and Li, F. (2016). Variations of six alkaloids in Shengfupian heated with sand and Paofupian before and after preparation. *Chin. Tradit. Pat. Med.* 38 (6), 1342–1345. doi:10.3969/j.issn.1001-1528.2016.06.028

Chen, R. C., Sun, G. B., Zhang, Q., and Sun, X. B. (2014). Advances in research on processing and toxicology reduction of aconiti lateralis radix praeparata. *Chin. J. Exp. Traditional Med. Formulae* 20 (15), 237–241. doi:10.13422/j.cnki.syfjx.2014150237

Chen, X., Liang, X., Kong, X., Ji, M., Naeem, A., Li, C., et al. (2022). Effect and molecular mechanism research of Astragalus membranaceus on inhibiting intestinal absorption of six alkaloids of Aconitum carmichaelii in spleen deficiency rats. *Chin. Herb. Med.* 14 (1), 117–124. doi:10.1016/j.chmed.2021.07.001

Deng, W. W., Hou, D. B., and Jiang, D. (2012). Effect of oven baking on ester alkaloids from Aconitum carmichaeli. *Chin. J. Exp. Traditional Med. Formulae* 18 (19), 44–46. doi:10.13422/j.cnki.syfjx.2012.19.020

Du, S., Shi, H., Wu, Q., Yi, Y., and Wang, Y. (2012). The effects of Fuzi combination with three common drugs on chronic renal failure mice induced by aristolochic acid. *Asia-Pacific Tradit. Med.* 8 (6), 23–26. doi:10.3969/j.issn.1673-2197.2012.06.011

Fan, J. P., Yang, J., and Wang, Y. Q. (2011). The effects of the prepared aconite root on lactic acid metabolism in two kinds of chronic renal diseases mice models. *Prog. Pharm. Sci.* 35 (7), 323–329.

Fu, Y. P., Du, B. X., Fan, S. S., Li, C., Rong, R., and Zhang, Y. Y. (2018). Study on the extraction of polysaccharides from Heishunpian and its immune activity. *China J. Traditional Chin. Med. Pharm.* 33 (9), 4147–4150.

Fu, Y. P., Zou, Y. F., Lei, F. Y., Wangensteen, H., and Inngjerdingen, K. T. (2022). Aconitum carmichaelii Debeaux: a systematic review on traditional use, and the chemical structures and pharmacological properties of polysaccharides and phenolic compounds in the roots. *J. Ethnopharmacol.* 291, 115148. doi:10.1016/j.jep.2022.115148

Gao, Y., Dai, H., Zhang, N., Jiang, H., Zhang, Z., Feng, Z., et al. (2022). The ameliorative effect of Mahuang fuzi and Shenzhuo decoction on membranous nephropathy of rodent model is associated with autophagy and wnt/β-catenin pathway. *Front. Pharmacol.* 13. doi:10.3389/fphar.2022.820130

Gu, S., Lin, P., Ou, R., Guo, J., and Gong, X. (2022b). Discussion on several statistical problems in establishing quality standards of standard decoctions. *Chin. Herb. Med.* 14 (1), 36–47. doi:10.1016/j.chmed.2021.09.012

Gu, X., Hao, D., and Xiao, P. (2022a). Research progress of Chinese herbal medicine compounds and their bioactivities: fruitful 2020. *Chin. Herb. Med.* 14 (2), 171–186. doi:10.1016/j.chmed.2022.03.004

Guo, W., Tan, P., Wu, Y. J., Qin, Y. X., Zhao, L. L., and Li, F. (2015). Effect of adjuvants on trait and the ester alkaloid from salt-Fuzi. *Chin. Tradit. Pat. Med.* 37 (6), 1289–1293. doi:10.3969/j.issn.1001-1528.2015.06.028

Han, W. J., Lin, X. T., Guo, N., Chen, Q., Zhang, T. T., and Xu, N. (2016). Changes of chemical constitution in Alismatis rhizoma after saline processing as revealed by 1H NMR analysis Chinese. *J. Magnetic Reson.* 33 (1), 117–124. doi:10.11938/cjmr20160111

He, Y. N., Yang, X., Wu, J., Hou, Y. S., Hu, Q., Xu, R. C., et al. (2023). "Liquid seal to detoxification – drying and puffing" of two stage processing technology design and pharmacodynamic study of aconite(Aconiti Lateralis Radix Praeparata) processed by microwave. *Acta Pharm. Sin.* 58 (5), 1328–1337. doi:10.16438/j.0513-4870.2022-1229

Hou, A., Lv, J., Zhang, S., Zhang, J., Yang, L., Jiang, H., et al. (2023). Salt processing: a unique and classic technology for Chinese medicine processing. *Front. Pharmacol.* 14, 1116047. doi:10.3389/fphar.2023.1116047

Hu, Q., Liu, Y., Yu, J., Yang, X., Yang, M., He, Y., et al. (2023). The protective effect and antitumor activity of Aconiti Lateralis Radix Praeparata (Fuzi) polysaccharide on cyclophosphamide-induced immunosuppression in H22 tumor-bearing mice. *Front. Pharmacol.* 14, 1151092. doi:10.3389/fphar.2023.1151092

Huang, G., Yang, L., Zhou, W., Tang, X., Wang, Y., Ma, Z., et al. (2018). Study on cardiotoxicity and mechanism of "fuzi" extracts based on metabonomics. *Int. J. Mol. Sci.* 19 (11), 3506. doi:10.3390/ijms19113506

Ito, K., Tanaka, S., Funayama, M., and Mizugaki, M. (2000). Distribution of Aconitum alkaloids in body fluids and tissues in a suicidal case of aconite ingestion. *J. Anal. Toxicol.* 24 (5), 348–353. doi:10.1093/jat/24.5.348

Ji, X., Yang, M., Or, K. H., Yim, W. S., and Zuo, Z. (2019). Tissue accumulations of toxic Aconitum alkaloids after short-term and long-term oral administrations of clinically used radix aconiti lateralis preparations in rats. *Toxins (Basel).* 11 (6), 353. doi:10.3390/toxins11060353

Jiang, C., Wang, L., Wang, Y., Xu, R., Yang, H., and Peng, J. (2023). Therapeutic effects of Chinese herbal medicines for treatment of urolithiasis: a review. *Chin. Herb. Med.* 15 (4), 526–532. doi:10.1016/j.chmed.2023.09.001

Jin, W., Bi, J., Xu, S., Rao, M., Wang, Q., Yuan, Y., et al. (2022). Metabolic regulation mechanism of Aconiti Radix Cocta extract in rats based on 1H-NMR metabonomics. *Chin. Herb. Med.* 14 (4), 602–611. doi:10.1016/j.chmed.2022.07.002

Kondo, T., Ishida, T., Ye, K., Muraguchi, M., Tanimura, Y., Yoshida, M., et al. (2022). Suppressive effects of processed aconite root on dexamethasone-induced muscle ring finger protein-1 expression and its active ingredients. *J. Nat. Med.* 76 (3), 594–604. doi:10.1007/s11418-022-01606-5

Lan, F., Xie, Y., Meng, L., Shi, W., and Zhao, J. (2020). Effect and mechanism of modified Fuzi Lizhong Decoction in rats with acute renal injury after ischemia reperfusion. *Mod. J. Integr. Traditional Chin. West. Med.* 29 (31), 3432–3435. doi:10.3969/j.issn.1008-8849.2020.31.003

Li, D., Guo, H., Niu, L., Yin, Q., Zhang, Y., and Zhuang, P. (2023). Clinical value-oriented research paradigm about inheritance and innovation development of TCM dominant diseases. *Chin. Herb. Med.* 15 (4), 476–484. doi:10.1016/j.chmed.2023.09.002

Li, L., Chai, Y., Xue, C., and Zhang, B. (2021b). Effects of fuzi(aconm lateralis radix praeparaia),rougui(cinnamomi cortex) and xianmao (curculiginis rhizoma) on immune function and energy metabolism of rats in different state. *Chin. Archives Traditional Chin. Med.* 39 (5), 32–36. doi:10.13193/j.issn.1673-7717.2021.05.009

Li, M., Xie, X., Chen, H., Xiong, Q., Tong, R., Peng, C., et al. (2020). Aconitine induces cardiotoxicity through regulation of calcium signaling pathway in zebrafish embryos and in H9c2 cells. *J. Appl. Toxicol.* 40 (6), 780–793. doi:10.1002/jat.3943

Li, M., Zhang, H., Wen, R., Xiang, Y., Peng, C., and Xie, X. (2019). Study on the neurotoxicity of fat-soluble alkaloids from radix aconiti lateralis based on zebrafish. *Pharmacol. Clin. Chin. Materia Medica* 35 (6), 63–66. doi:10.13412/j.cnki.zyyl.2019.06.014

Li, R. L., Zhang, Q., Liu, J., He, L. Y., Huang, Q. W., Peng, W., et al. (2021a). Processing methods and mechanisms for alkaloid-rich Chinese herbal medicines: a review. *J. Integr. Med.* 19 (2), 89–103. doi:10.1016/j.joim.2020.12.003

Li, R. Y., Zhang, D. K., Han, X., Lin, J. Z., and Yang, M. (2016b). Chemical constituent change regulation of processed aconite during decoction and discussion on time limit of decoction based on metabolomics. *Chin. Traditional Herb. Drugs* 47 (1), 38–45. doi:10.7501/j.issn.0253-2670.2016.01.007

Li, T. F., Gong, N., and Wang, Y. X. (2016a). Ester hydrolysis differentially reduces aconitine-induced anti-hypersensitivity and acute neurotoxicity: involvement of spinal microglial dynorphin expression and implications for Aconitum processing. *Front. Pharmacol.* 7, 367. doi:10.3389/fphar.2016.00367

Li, X., An, P., Zhao, Y., Cai, Z., Ye, B., Wang, Y., et al. (2022b). Aqueous extract and polysaccharide of aconiti lateralis radix induce apoptosis and G0/G1 phase cell cycle arrest by PI3K/AKT/mTOR signaling pathway in mesangial cells. *Evidence-Based Complementary Altern. Med.* 2022, 3664696–3664715. doi:10.1155/2022/3664696

Li, X., Gu, L., Yang, L., Zhang, D., and Shen, J. (2017). Aconitine: a potential novel treatment for systemic lupus erythematosus. *J. Pharmacol. Sci.* 133 (3), 115–121. doi:10.1016/j.jphs.2017.01.007

Li, Z. L., Wu, C. L., and Cao, Y. C. (2022a). Research progress on different processing methods of poisonous traditional Chinese medicine aconite. *China J. Pharm. Econ.* 17 (9), 126–129. doi:10.12010/j.issn.1673-5846.2022.09.025

Liu, S., Li, F., Li, Y., Li, W., Xu, J., and Du, H. (2017). A review of traditional and current methods used to potentially reduce toxicity of Aconitum roots in Traditional Chinese Medicine. *J. Ethnopharmacol.* 207, 237–250. doi:10.1016/j.jep.2017.06.038

Liu, S., Zhang, X., Wang, H., Zeng, Z., Zhang, J., and Zuo, A. (2019). Research progress on polysaccharides of Aconitum medico-plants. *China Pharm.* 28 (3), 1–6. doi:10.3969/j.issn.1006-4931.2019.03.001

Liu, W., Shen, M., and Qin, Z. Q. (2009). Distribution of Aconitum alkaloids in the corpse died of acute aconite intoxication. *J. Forensic Med.* 25 (3), 176–178. doi:10.3969/j.issn.1004-5619.2009.03.007

Liu, X., Chen, L., Sun, P., Zhan, Z., and Wang, J. (2023). Research progress on processing theory of Chinese medicine "salt into the kidney. *J. Basic Chin. Med.* 29 (7), 1224–1229. doi:10.19945/j.cnki.issn.1006-3250.2023.07.027

Mizugaki, M., Ito, K., Ohyama, Y., Konishi, Y., Tanaka, S., and Kurasawa, K. (1998). Quantitative analysis of Aconitum alkaloids in the urine and serum of a male attempting suicide by oral intake of aconite extract. *J. Anal. Toxicol.* 22 (4), 336–340. doi:10.1093/jat/22.4.336

Niitsu, H., Fujita, Y., Fujita, S., Kumagai, R., Takamiya, M., Aoki, Y., et al. (2013). Distribution of Aconitum alkaloids in autopsy cases of aconite poisoning. *Forensic Sci. Int.* 227 (1-3), 111–117. doi:10.1016/j.forsciint.2012.10.021

Peng, S., Zhang, X., Yuan, J., Zhang, Y., Wang, X., Sun, M., et al. (2018). A comparative study on 4 kinds of processing methods of paofuzi based on Zhang zhongjing's academic thoughts. *World Sci. Technology/Modernization Traditional Chin. Med. Materia Medica* 20 (5), 716–721. doi:10.11842/wst.2018.05.016

Ren, M. Y., Yu, Q. T., Shi, C. Y., and Luo, J. B. (2017). Anticancer activities of C18-C19-C20-and bis-diterpenoid alkaloids derived from genus Aconitum. *Molecules* 22 (2), 267. doi:10.3390/molecules22020267

Ren, Z., Zhang, H., Yang, L., Chen, X., Zhang, S., Chen, S., et al. (2023). Spatial distribution and comparative analysis of Aconitum alkaloids in Fuzi using DESI-MSI and UHPLC-QTOF-MS. *Analyst* 148 (7), 1603–1610. doi:10.1039/d2an02051c

Shi, W., Huang, R. F., Lan, F., and Chen, Y. Q. (2011). Study on the antioxidant effect of flavored fried-free aconite particles on acute aristolochic acid nephropathy rats. *Yunnan J. Traditional Chin. Med. Materia Medica* 32 (7), 61–64. doi:10.3969/j.issn.1007-2349.2011.07.041

Shuai, X. C., Hu, C. J., and Shan, S. (2018). The influence of suoquan wan formulated by yizhiren (alpiniae oxyphyllae) processed by salt on serum bun, crea, etc. and renal morphology of the kidney yang deficiency model mice. *Guid. J. Traditional Chin. Med. Pharm.* 24 (13), 15–18. doi:10.13862/j.cnki.cn43-1446/r.2018.13.003

Strzelecki, A., Pichon, N., Gaulier, J. M., Amiel, J. B., Champy, P., and Clavel, M. (2010). Acute toxic herbal intake in a suicide attempt and fatal refractory ventricular arrhythmia. *Basic Clin. Pharmacol. Toxicol.* 107 (2), 698–699. doi:10.1111/j.1742-7843.2010.00566.x

Su, J., Liu, B., Tian, P., Lin, Q., Zhao, Y., and Ge, X. (2010). Effect of microbial fermentation on the extraction of alkaloids from radix aconiti and aconite. *J. Beijing Univ. Chem. Technol.* 37 (3), 97–101. doi:10.3969/j.issn.1671-4628.2010.03.020

Sun, B., Li, L., Wu, S., Zhang, Q., Li, H., Chen, H., et al. (2009). Metabolomic analysis of biofluids from rats treated with Aconitum alkaloids using nuclear magnetic resonance and gas chromatography/time-of-flight mass spectrometry. *Anal. Biochem.* 395 (2), 125–133. doi:10.1016/j.ab.2009.08.014

Sun, B., Wang, X., Cao, R., Zhang, Q., Liu, Q., Xu, M., et al. (2016). NMR-based metabonomics study on the effect of Gancao in the attenuation of toxicity in rats induced by Fuzi. *J. Ethnopharmacol.* 193, 617–626. doi:10.1016/j.jep.2016.10.042

Sun, L., You, G., Cao, X., Wang, M., and Ren, X. (2019). Comparative investigation for raw and processed Aconiti Lateralis Radix using chemical UPLC-MS profiling and multivariate classification techniques. *J. Food Drug Anal.* 27 (1), 365–372. doi:10.1016/j.jfda.2018.10.006

Ta, W., Yang, X., Wang, J., Han, C., Hua, R., and Lu, W. (2023). Comparison of intestinal absorption characteristics between rhubarb traditional Chinese medicine preparation and activity ingredients using *in situ* and *in vitro* model. *Chin. Herb. Med.* 15 (1), 117–122. doi:10.1016/j.chmed.2022.09.004

Tan, Y., Li, J., Liu, X., Ko, J., He, X., Lu, C., et al. (2013). Deciphering the differential toxic responses of Radix aconiti lateralis praeparata in healthy and hydrocortisone-pretreated rats based on serum metabolic profiles. *J. Proteome Res.* 12 (1), 513–524. doi:10.1021/pr300965d

Tang, L., Gong, Y., Lv, C., Ye, L., Liu, L., and Liu, Z. (2012). Pharmacokinetics of aconitine as the targeted marker of Fuzi (Aconitum carmichaeli) following single and multiple oral administrations of Fuzi extracts in rat by UPLC/MS/MS. *J. Ethnopharmacol.* 141 (2), 736–741. doi:10.1016/j.jep.2011.08.070

Tang, L., Ye, L., Lv, C., Zheng, Z., Gong, Y., and Liu, Z. (2011). Involvement of CYP3A4/5 and CYP2D6 in the metabolism of aconitine using human liver microsomes and recombinant CYP450 enzymes. *Toxicol. Lett.* 202 (1), 47–54. doi:10.1016/j.toxlet.2011.01.019

Tao, H., Liu, X., Tian, R., Liu, Y., Zeng, Y., Meng, X., et al. (2023). A review: pharmacokinetics and pharmacology of aminoalcohol-diterpenoid alkaloids from Aconitum species. *J. Ethnopharmacol.* 301, 115726. doi:10.1016/j.jep.2022.115726

Tian, M., Wang, L., Dong, Z., Wang, X., Qin, X., Wang, C., et al. (2022). Preparation, structural characterization, antioxidant activity and protection against cisplatin-induced acute kidney injury by polysaccharides from the lateral root of Aconitum carmichaelii. *Front. Pharmacol.* 13, 1002774. doi:10.3389/fphar.2022.1002774

Tong, H. L., Chen, H., Gong, F. P., Zhong, L. Y., Zhu, J., and Yang, S. H. (2021). Components and pharmacodynamical mechanism of yinfupian based on liquid chromatography-mass spectrometry and proteomics analyses. *Front. Pharmacol.* 12, 680640. doi:10.3389/fphar.2021.680640

Tu, Y., Sun, W., Wan, Y. G., Gao, K., Liu, H., Yu, B. Y., et al. (2014). Dahuang Fuzi Decoction ameliorates tubular epithelial apoptosis and renal damage via inhibiting TGF-β1-JNK signaling pathway activation *in vivo*. *J. Ethnopharmacol.* 156, 115–124. doi:10.1016/j.jep.2014.08.035

Wang, C., Ye, M., Xing, J., He, Y., and Guo, D. (2005). Determination of aconitine distribution in acute toxic rats by HPLC-MS. *Chin. J. Chromatogr.* 23 (3), 316. doi:10.3321/j.issn:1000-8713.2005.03.029

Wang, M., Hu, W. J., Zhou, X., Yu, K., Wang, Y., Yang, B. Y., et al. (2023). Ethnopharmacological use, pharmacology, toxicology, phytochemistry, and progress in Chinese crude drug processing of the lateral root of Aconitum carmichaelii Debeaux. (Fuzi): a review. *J. Ethnopharmacol.* 301, 115838. doi:10.1016/j.jep.2022.115838

Wang, Y. H., and Zhang, Y. G. (2017). Kidney and innate immunity. *Immunol. Lett.* 183, 73–78. doi:10.1016/j.imlet.2017.01.011

Wang, Z., and Li, S. (2022). Network pharmacology in quality control of traditional Chinese medicines. *Chin. Herb. Med.* 14 (4), 477–478. doi:10.1016/j.chmed.2022.09.001

Wei, X. Y., Qiu, Z. D., Chen, J. L., Sun, R. Q., Huang, L. Q., and Lai, C. J. S. (2019). Research advancement in mechanisms of processing and compatibility for detoxication of Aconitums. *China J. Chin. Materia Medica* 44 (17), 3695–3704. doi:10.19540/j.cnki.cjcmm.20190629.301

Wu, J. J., Guo, Z. Z., Zhu, Y. F., Huang, Z. J., Gong, X., Li, Y. H., et al. (2018a). A systematic review of pharmacokinetic studies on herbal drug Fuzi: implications for Fuzi as personalized medicine. *Phytomedicine* 44, 187–203. doi:10.1016/j.phymed.2018.03.001

Wu, X., Wang, S., Lu, J., Jing, Y., Li, M., Cao, J., et al. (2018b). Seeing the unseen of Chinese herbal medicine processing (Paozhi): advances in new perspectives. *Chin. Med.* 13 (1), 4. doi:10.1186/s13020-018-0163-3

Wu, X., Wu, P., Gu, M., and Xue, J. (2022). Trace heavy metals and harmful elements in roots and rhizomes of herbs: screening level analysis and health risk assessment. *Chin. Herb. Med.* 14 (4), 622–629. doi:10.1016/j.chmed.2021.11.004

Xia, F., Cao, J. J., Feng, J., Wang, M. W., Liu, Z. C., and Cui, L. J. (2021b). Study on the processing technology development and antioxidant activity of Aconite. *J. Shaanxi Univ. Sci. Technol.* 39 (3), 54–60. doi:10.3969/j.issn.1000-5811.2021.03.009

Xia, Q., Gao, S., Rapael Gnanamuthu, S. R., Zhuang, K., Song, Z., Zhang, Y., et al. (2021a). Involvement of nrf2-HO-1/JNK-erk signaling pathways in aconitine-induced developmental toxicity, oxidative stress, and ROS-mitochondrial apoptosis in zebrafish embryos. *Front. Pharmacol.* 12, 642480. doi:10.3389/fphar.2021.642480

Xu, T., Zhong, L. Y., and Luo, Y. H. (2017). Content comparsion of six alkaloids in different Zingiber-processed Aconiti lateralis Radix Praeparata. *Chin. Tradit. Pat. Med.* 39 (12), 2555–2559.

Xu, X., Li, G., Sun, C., Chen, J., Peng, C., Xie, X., et al. (2021). Research progress on water-soluble alkaloids from fuzi and their pharmacological effects. *Pharmacol. Clin. Chin. Materia Medica* 37 (5), 213–219. doi:10.1016/j.chmed.2022.03.004

Xue, R., Ji, D., Gong, J., Qu, L., Zhang, Q., Xu, R., et al. (2024). Research on the effects of processing Heishunpian from Aconiti lateralis radix praeparata on components and efficacy using the "step knockout" strategy. *Fitoterapia* 172, 105747. doi:10.1016/j.fitote.2023.105747

Yang, C. L., Huang, Z. F., Zhang, Y. H., Liu, Y. H., Liu, Y. H., Chen, Y., et al. (2014a). Effects of steaming and baking on content of alkaloids in aconite lateralis radix (fuzi). *China J. Chin. Materia Medica* 39 (24), 4798–4803.

Yang, J., and Wang, C. (2010). Experimental study of prepared commonot on adriamycin-induced nephropathy in rats. *Shanxi J. Traditional Chin. Med.* 26 (2), 39–41. doi:10.3969/j.issn.1000-7156.2010.02.025

Yang, S., Yang, Y., Chen, C., Wang, H., Ai, Q., Lin, M., et al. (2021a). The anti-neuroinflammatory effect of fuzi and Ganjiang extraction on LPS-induced BV2 microglia and its intervention function on depression-like behavior of cancer-related fatigue model mice. *Front. Pharmacol.* 12, 670586. doi:10.3389/fphar.2021.670586

Yang, X., Wu, J., Lu, L., Zhu, L., and Liu, Z. (2014b). Progress of pharmacokinetic study on fuzi. *World Chin. Med.* 9 (2), 171–174. doi:10.3969/j.issn.1673-7202.2014.02.010

Yang, Y., Wei, W., Wu, G., Wang, X., Ying, F., and He, S. (2023). *Modern research progress of aconite*. Research of Zhuang and Yao Ethnic Medicine, 19–22.

Yang, Y., Yang, G., Feng, G., Huang, R., and Mei, Q. (2019). Chemical composition and pharmacotoxicology of aconiti lateralis radix praeparata before and after processing. *Lishizhen Med. Materia Medica Res.* 30 (11), 2724–2727. doi:10.3969/j.issn.1008-0805.2019.11.057

Yang, Z., Lin, Y., Gao, L., Zhou, Z., Wang, S., Dong, D., et al. (2020). Circadian clock regulates metabolism and toxicity of Fuzi(lateral root of Aconitum carmichaeli Debx) in mice. *Phytomedicine* 67, 153161. doi:10.1016/j.phymed.2019.153161

Yang, Z., Lin, Y., Su, C., Wang, S., Gao, L., Lin, J., et al. (2021b). Pharmacokinetics-based chronoefficacy of Fuzi against chronic kidney disease. *J. Pharm. Pharmacol.* 73 (4), 535–544. doi:10.1093/jpp/rgaa060

Ye, L., Tang, L., Gong, Y., Lv, C., Zheng, Z., Jiang, Z., et al. (2010). Characterization of metabolites and human P450 isoforms involved in the microsomal metabolism of mesaconitine. *Xenobiotica* 41 (1), 46–58. doi:10.3109/00498254.2010.524950

Ye, L., Wang, T., Yang, C., Tang, L., Zhou, J., Lv, C., et al. (2011). Microsomal cytochrome P450-mediated metabolism of hypaconitine, an active and highly toxic constituent derived from Aconitum species. *Toxicol. Lett.* 204 (1), 81–91. doi:10.1016/j.toxlet.2011.04.015

Ye, L., Yang, X., Yang, Z., Gao, S., Yin, T., Liu, W., et al. (2013b). The role of efflux transporters on the transport of highly toxic aconitine, mesaconitine, hypaconitine, and their hydrolysates, as determined in cultured Caco-2 and transfected MDCKII cells. *Toxicol. Lett.* 216 (2-3), 86–99. doi:10.1016/j.toxlet.2012.11.011

Ye, L., Yang, X. S., Lu, L. L., Chen, W. Y., Zeng, S., Yan, T. M., et al. (2013a). Monoester-DiterpeneAconitumAlkaloid metabolism in human liver microsomes: predominant role of CYP3A4 and CYP3A5. *Evidence-Based Complementary Altern. Med.* 2013, 941093–941124. doi:10.1155/2013/941093

Ye, Q., Liu, Y. S., Liu, H. M., Liu, J. R., Tang, X. M., and Guo, L. (2019). Effects of different processing technology on contents of alkaloids in Aconiti Lateralis Radix Praeparata. *Chin. Tradit. Pat. Med.* 41 (3), 601–607. doi:10.3969/j.issn.1001-1528.2019.03.024

Ye, X. W., Xia, L. T., Zhang, J. L., Ren, H. M., Deng, Y. L., Liu, M. M., et al. (2021). Study on the differences in chemical constituents before and after the processing of simmering Fuzi slices of "Jianchang Gang" based on UPLC-Q-TOF-MS/MS. *Lishizhen Med. Materia Medica Res.* 32 (9), 2159–2164. doi:10.3969/j.issn.1008-0805.2021.09.30

Yu, Y., Yao, C., Zhang, J., Bi, Q., Wei, W., Li, Z., et al. (2023). Comprehensive quality evaluation of Aconiti Lateralis Radix Praeparata based on pseudotargeted metabolomics and simultaneous determination of fifteen components, and development of new processed products of black slices with less toxicity. *J. Pharm. Biomed. Analysis* 228, 115295. doi:10.1016/j.jpba.2023.115295

Yuan, T. (2020). *Study on the effect of Shenfu Decoctoin on renal interstitial fibrosis in CKD rats based on TGF-β1/Smads signaling pathway*. Harbin: Heilongjiang University of Chinese Medicine. [dissertation/doctor's thesis].

Yuan, W. (2018). A research on the pharmacological action of Fuzi. *Clin. J. Chin. Med.* 10 (4), 145–147. doi:10.3969/j.issn.1674-7860.2018.04.073

Yuan, X., and Yuan, H. (2023). Fuzi(Aconti lateralis radix praeparaia) in Shennong's classic of Materia Medica and its application in classical formulas. *J. Shandong Univ. traditional Chin. Med.* 47 (3), 261–265. doi:10.16294/j.cnki.1007-659x.2023.03.001

Yun, W. J., Yao, Z. H., Fan, C. L., Qin, Z. F., Tang, X. Y., Gao, M. X., et al. (2018). Systematic screening and characterization of Qi-Li-Qiang-Xin capsule-related xenobiotics in rats by ultra-performance liquid chromatography coupled with quadrupole time-of-flight tandem mass spectrometry. *J. Chromatogr. B* 1090, 56–64. doi:10.1016/j.jchromb.2018.05.014

Zan, K., Guo, L., Ma, S., Liu, J., Zheng, J., and Gao, Y. (2019). Research progress in quality control of radix aconiti lateralis praeparata. *Chin. Pharm. Aff.* 33 (7), 767–773. doi:10.16153/j.1002-7777.2019.07.008

Zhang, D. K., Han, X., Tan, P., Li, R. Y., Niu, M., Zhang, C. E., et al. (2017). Establishment of one-step approach to detoxification of hypertoxic aconite based on the evaluation of alkaloids contents and quality. *Chin. J. Nat. Med.* 15 (1), 49–61. doi:10.1016/s1875-5364(17)30008-0

Zhang, H., Sun, S., Zhang, W., Xie, X., Zhu, Z., Chai, Y., et al. (2015b). Biological activities and pharmacokinetics of aconitine, benzoylaconine, and aconine after oral administration in rats. *Drug Test. Analysis* 8 (8), 839–846. doi:10.1002/dta.1858

Zhang, K., Liu, C., Yang, T., Li, X., Wei, L., Chen, D., et al. (2020). Systematically explore the potential hepatotoxic material basis and molecular mechanism of Radix Aconiti Lateralis based on the concept of toxicological evidence chain (TEC). *Ecotoxicol. Environ. Saf.* 205, 111342. doi:10.1016/j.ecoenv.2020.111342

Zhang, K., Liu, Y., Lin, X., Yang, J., and Wu, C. (2021b). Assessment of reproductive toxicity and genotoxicity of Aconiti Lateralis Radix Praeparata and its processed products in male mice. *J. Ethnopharmacol.* 275, 114102. doi:10.1016/j.jep.2021.114102

Zhang, L. (2008). Experimental study on the acute toxicity of pressurized processed Radix aconite lateralis preparata. *World Health Dig.* 5 (6), 401–402.

Zhang, L., Siyiti, M., Zhang, J., Yao, M., and Zhao, F. (2021a). Anti-inflammatory and anti-rheumatic activities *in vitro* of alkaloids separated from Aconitum soongoricum Stapf. *Exp. Ther. Med.* 21 (5), 493. doi:10.3892/etm.2021.9924

Zhang, P. P. (2016). *Metabolism and drug-drug interaction profile of aconitine in rat liver microsomes and* in vivo *of rat[dissertation/doctor's thesis]*. Shijiazhuang: Hebei Medical University.

Zhang, W., Lu, C., Cai, S., Feng, Y., Shan, J., and Di, L. (2022). Aconiti lateralis radix praeparata as potential anticancer herb: bioactive compounds and molecular mechanisms. *Front. Pharmacol.* 13, 870282. doi:10.3389/fphar.2022.870282

Zhang, Y. H., Yang, C. L., Huang, Z. F., Liu, Y. H., Chen, Y., Liu, Y. H., et al. (2015a). Study on dynamic variation patterns of 13 alkaloids in Aconiti Lateralis Radix Praeparata during decocting process. *Chin. J. Pharm. Anal.* 35 (1), 16–23. doi:10.16155/j.0254-1793.2015.01.003

Zhang, Z., Jia, P., Zhang, X., Zhang, Q., Yang, H., Shi, H., et al. (2014). LC–MS/MS determination and pharmacokinetic study of seven flavonoids in rat plasma after oral administration of Cirsium japonicum DC. extract. *J. Ethnopharmacol.* 158, 66–75. doi:10.1016/j.jep.2014.10.022

Zhao, D., Shen, Y., Shi, Y., Shi, X., Qiao, Q., Zi, S., et al. (2018). Probing the transcriptome of Aconitum carmichaelii reveals the candidate genes associated with the biosynthesis of the toxic aconitine-type C19-diterpenoid alkaloids. *Phytochemistry* 152, 113–124. doi:10.1016/j.phytochem.2018.04.022

Zhou, H., Zhang, P., Hou, Z., Xie, J., Wang, Y., Yang, B., et al. (2016). Research on the relationships between endogenous biomarkers and exogenous toxic substances of acute toxicity in radix aconiti. *Molecules* 21 (12), 1623. doi:10.3390/molecules21121623

Zhou, W., Liu, H., Qiu, L. Z., Yue, L. X., Zhang, G. J., Deng, H. F., et al. (2021a). Cardiac efficacy and toxicity of aconitine: a new frontier for the ancient poison. *Med. Res. Rev.* 41 (3), 1798–1811. doi:10.1002/med.21777

Zhou, Y., Shi, L., Lin, S., Xie, H., Xia, C., Qin, K., et al. (2021b). Progress of modern research on the mechanism of salti-processing of Traditional Chinese Medicines. *Chin. Tradit. Pat. Med.* 43 (10), 2774–2778. doi:10.3969/j.issn.1001-1528.2021.10.031

frontiers | Frontiers in Pharmacology

TYPE Review
PUBLISHED 03 July 2024
DOI 10.3389/fphar.2024.1426972

OPEN ACCESS

EDITED BY
Qianfeng Gong,
Jiangxi University of Traditional Chinese Medicine, China

REVIEWED BY
Bo Zhang,
Tsinghua University, China
Yuan Gao,
Capital Medical University, China
Li Long Mei,
Guangzhou University of Traditional Chinese Medicine, China

*CORRESPONDENCE
Shao-Bin Wei,
weishaobin5620@163.com
Mao-Ya Li,
lmy941027@163.com

†These authors have contributed equally to this work and share first authorship

RECEIVED 02 May 2024
ACCEPTED 06 June 2024
PUBLISHED 03 July 2024

CITATION
Zhong H-Z, Mo J, Li Y-X, Li M-Y and Wei S-B (2024), Changes in Rehmanniae Radix processing and their impact on ovarian hypofunction: potential mechanisms of action. *Front. Pharmacol.* 15:1426972. doi: 10.3389/fphar.2024.1426972

Changes in Rehmanniae Radix processing and their impact on ovarian hypofunction: potential mechanisms of action

Han-Zhi Zhong[1†], Jing Mo[1†], Yan-Xin Li[1], Mao-Ya Li[2*] and Shao-Bin Wei[2*]

[1]School of Clinical Medicine, Chengdu University of Traditional Chinese Medicine, Chengdu, China, [2]Department of Gynecology, Hospital of Chengdu University of Traditional Chinese Medicine, Chengdu, China

Objective: This study evaluates the research developments concerning Rehmanniae Radix in ovarian hypofunction diseases. It explores the processing methods of Rehmanniae Radix, the variations in its compounds before and after processing, the mechanism of Rehmanniae Radix and its active compounds in improving ovarian function, and the advancements in clinical applications of traditional Chinese medicine (TCM) compound that include Rehmanniae Radix.

Methods: Comprehensive literature search was conducted using databases such as China National Knowledge Infrastructure (CNKI), China Science and Technology Journal Database, National Science and Technology Library, the Pharmacopoeia of the People's Republic of China, Pubmed, and the Web of Science Database. The search utilized the following Medical Subject Headings (MeSH) and keywords: "Rehmanniae Radix," "Drying Rehmannia Root," "Rehmannia glutinosa," "Rehmanniae Radix Praeparata," "Traditional Chinese Medicine Processing," "Pharmacological Effects," "Ovarian Aging," "Diminished ovarian reserve," "Premature ovarian insufficiency," "Premature Ovarian Failure," "Ovarian hypofunction diseases".

Results: The ancient Chinese medical books document various processing techniques for Rehmanniae Radix. Contemporary research has identified changes in its compounds processing and the resultant diverse therapeutic effects. When processed into Rehmanniae Radix Praeparata, it is noted for its ability to invigorate the kidney. TCM compound containing Rehmanniae Radix is frequently used to treat ovarian hypofunction diseases, demonstrating significant clinical effectiveness. The key changes in its compounds processing include cyclic dilute ether terpene glycosides, phenylethanol glycosides, sugars, and 5-hydroxymethylfurfural. Its pharmacological action is primarily linked to the improvement of granulosa cell proliferation, antioxidative and anti-aging properties, and modulation of the immune and inflammatory microenvironment. Furthermore, Rehmanniae Radix also offers therapeutic benefits for cardiovascular and cerebrovascular diseases, osteoporosis and cognitive dysfunction caused by low estrogen levels. Thereby Rehmanniae Radix mitigates both the short-term and long-term health risks associated with ovarian hypofunction diseases.

Conclusion: Processed Rehmanniae Radix has shown potential to improve ovarian function, and its compound prescriptions have a definite effect on

ovarian dysfunction diseases. Therefore Rehmanniae Radix was garnering interest for both basic and clinical research, with promising application prospects as a future therapeutic agent for ovarian hypofunction diseases. However, further studies on its toxicology and the design of standardized clinical trials are necessary to fully establish its efficacy and safety.

KEYWORDS

Rehmanniae Radix, medicine processing, pharmacology, traditional Chinese medicine, ovarian hypofunction diseases

1 Introduction

Ovarian hypofunction diseases primarily encompass conditions such as diminished ovarian reserve (DOR), premature ovarian insufficiency (POI), and premature ovarian failure (POF) (Chen et al., 2017). These represent a progressive, gradual decline in ovarian function. DOR primarily highlights the decline in ovarian responsiveness and reproductive function in women of childbearing age, while POI and POF are more focused on the progressive changes associated with age and ovarian aging. Short-term clinical manifestations include menstrual irregularities, reduced fertility and reproductive quality, and perimenopausal symptoms due to low estrogen levels. Menstrual irregularities commonly present as shorter menstrual cycles, prolonged menstrual cycles, reduced menstrual flow, and potentially amenorrhea. A reduction in fertility stems from the progressive decrease in the number of ovarian follicles and a decline in follicle quality, culminating in lower pregnancy rates, higher miscarriage rates, and reduced live birth rates. A decline in reproductive quality is evident in the increased rate of aneuploidy in offspring. The incidence of these conditions is increasingly affecting younger women, significantly impacting female fertility. Reports indicate that the prevalence of DOR ranges from 10% to 32% (Pastore et al., 2018), POI affects about 3.5% (Li M. et al., 2023) of the population, and only approximately 5%–10% (Rebar, 2009) of women diagnosed with POI can conceive spontaneously. However, the impact of ovarian function decline is systemic, posing long-term risks of cardiovascular disease, osteoporosis, and neurological disorders. Estrogen acts as a protective factor for the cardiovascular system, whereas premature ovarian aging markedly elevates the risk of cardiovascular events. Reduced estrogen and elevated FSH levels cause abnormal bone metabolism, leading to osteoporosis and fractures. Furthermore, a decline in ovarian function and changes in HPO axis activity can lead to emotional disturbances, vascular dysfunction, cognitive impairment, and sleep disorders, severely affecting the quality of life for women.

Current treatments primarily involve hormone replacement therapy (HRT) and assisted reproductive technology (ART), with emerging methods such as stem cell therapy still under research. HRT is the primary treatment for alleviating symptoms of low estrogen and providing primary prevention against cardiovascular diseases and osteoporosis. However, HRT cannot restore ovarian function, and its long-term use is associated with risks of thromboembolic diseases, breast tumors, and other adverse effects, prompting concerns regarding the occurrence of adverse reactions (Ewertz et al., 2005; Canonico et al., 2014; Gu et al., 2014). The 2016 European Society of Human Reproduction and Embryology (ESHRE) Guideline advised POI patients with fertility needs to actively pursue ART for conception. Women with a family history of POI or those without current fertility needs may choose to freeze and preserve oocytes or embryos to mitigate age-related fertility decline, thus preserving part of their reproductive potential. Despite advancements in ART, its efficacy is limited in cases of ovarian aging (Leridon, 2004). Meanwhile, as international research on traditional Chinese medicine (TCM) progresses and cross-cultural communication between the East and West deepens, TCM has gained attention due to its natural compounds, multi-target effects, minimal adverse events, and the concept of medicinal and edible use (Heinrich et al., 2021).

Rehmanniae Radix (RR) is either the fresh or dried root of *Rehmannia glutinosa* Libosch., harvested in autumn, cleaned of reeds and fibrous roots, and either used fresh or slow-roasted until it is about 80% dry. Freshly processed RR is termed "Fresh RR (FRR)," and the partially dried form is known as "Raw RR (RRR)." RR has been a staple of TCM for millennia, classed among the "Four Great Medicines," and is widely used in clinical settings. The processing of RR, which includes methods like steaming and nine steaming and nine drying, transforms it into "RR Praeparata (RRP)." This process alters RR's medicinal properties from cold to warm and its flavor from bitter to sweet, the function changes from clearing heat to nourishing (Qianfeng, 2005). RR contains various bioactive compounds including iridoid glycosides, polysaccharides, amino acids, and small amounts of β-sitosterol, which undergo changes after processing. RR's pharmacological actions span multiple systems, offering antioxidant, immune-modulating, anti-inflammatory, and anti-aging benefits, and are principally applied in the treatment of gynecological and diabetic metabolic disorders, cardiovascular diseases, and osteoporosis. This reflects the advantages of TCM in treating complex, multi-system diseases, and functional disorders. It not only fundamentally improves patients' condition but also offers multi-target synergy and additive effects (Li D. et al., 2023; Zhang, 2023). RR has become a common treatment in clinical settings due to its protective effects on ovary. In recent years, studies on RR's role in ovarian hypofunction have proliferated, mainly focusing on the mechanism of RR to improve reproductive hormones and increase the number of follicles. At the same time, basic and clinical studies were conducted on the TCM compound containing RR to observe its efficacy, safety and potential mechanism in the treatment of ovarian dysfunction diseases. These studies also seek to explore the long-term health benefits of RR, aiming for synergistic and enhancing effects.

This article reviewed the changes in the compounds of RR before and after processing, its mechanism of action in treating ovarian

hypofunction diseases, and the clinical use of related compound prescriptions. It also elaborates on the scientific implications of its transformed medicinal effects to better leverage RR's therapeutic potential.

2 The protective effect of RR on ovary according to TCM theory

RR was first documented in "*Shennong's Classic Materia Medica*" as "Drying Rehmannia Root" and later appeared as "RRR" in Zhang Zhongjing's "*Jin Kui Yao Lue*" during the Han Dynasty. The term "RRP" was officially introduced in the Song Dynasty's "*Bencao Tujing*". Initially classified as cold, RR's properties shift to warm after processing, transitioning from an effect of clearing heat to nourishing. This change significantly alters its therapeutic impact on diseases. RRP is the core drug for tonifying the kidney, known for its mild medicinal power and is frequently employed in treating various kidney deficiency diseases in clinical settings. Ancient Chinese medical books extensively describe the clinical signs of ovarian hypofunction diseases, such as menstrual irregularities or amenorrhea and reduced fertility, attributing these conditions to kidney deficiency. According to TCM, the kidney is vital for growth, development, and reproduction, and both menstruation and pregnancy are closely linked to kidney health. The belief that "menstruation originates from the kidney" and "the person who appears amenorrhea before age 49″are supported in "*Fu Qingzhu's Gynecology,*" aligning with the pathophysiology of these conditions. RRP is acclaimed for its abilities to nourish blood, nourish yin, nourish kidney and invigorate essence. "*Compendium of Materia Medica*" notes that RR has the efficacy in treating "irregular menstruation and long-term infertility." Furthermore, TCM prescriptions commonly used to treat ovarian hypofunction diseases, such as Guishen Pill, Liuwei Dihuang Pill, Siwu Tang, and Yijing Tang, all incorporate RRP. It can be seen that the clinical treatment of this type of disease is inseparable from the use of RRP.

3 Changes in the compounds of RR before and after processing

3.1 Methods of processing

Archaeological research has revealed that processed RR found in the Haihunhou tomb from the Western Han Dynasty is the earliest Chinese medicine excipient concoction product found in ancient China so far, which involved excipients of starch and sucrose, suggesting that these samples were processed by rice steaming (Peng et al., 2019; Zhu et al., 2021). The history of RR processing involves a variety of methods. Traditional methods include steaming and boiling without excipients, as well as the excipients of ingredients such as alcohol, Amomi Fructus and ginger (Xie et al., 2022). In contemporary practice, processed RR varieties with region-specific characteristics have developed, such as Wenzhi RR with Jiangxi Jianchang Band and Salt RR from Yunnan.

Historically, RR has been known by various names depending on the processing method employed. However, the 2020 edition of *The Pharmacopoeia of the People's Republic of China* recognizes only two designations: RR and RRP. RR encompasses Fresh RR and RRR, with RRP defined as the processed product of RRR, the specific two processing methods are steaming and wine stewing. In addition, "nine steamed and nine sun-dried" is also a traditional processing method of RR.

Steamed refers to the method of heating the raw productswithout excipients and separating water to a certain extent. The description of the 2020 edition of *The Pharmacopoeia of the People's Republic of China* is more precise, which points that "steamed with water involves heating the raw medicinal botanical drug by placing it over boiling water until it achieves a black and moist state. It is then removed and dried to about eighty percent dryness before being cut into thick slices or chunks and fully dried to produce RRP" (National Pharmacopoeia Committee, 2020).

The method of stewing with wine, widely used today, was first documented in *Shennong Bencao Jing Jizhu* during the Liang Dynasty. *Leigong Paozhi Lun* during the Northern and Southern Dynasties mentioned for the first time that wine was used as an auxiliary material to mix and steam. This method entails mixing RR with wine prior to steaming (Wang et al., 2019). The pharmacopeia (National Pharmacopoeia Committee, 2020) details that for every 100 kg of RRR, 30–50 kg of yellow rice wine is used. The operational steps include stewing the RR with wine until it fully absorbs the wine, followed by air drying until the sticky fluid on its surface slightly dries. It is then processed further into thick slices or chunks to finally obtain RRP.

The "nine steamed and nine sun-dried" method, with a long historical lineage, first appeared in the Tang Dynasty's *Qianjin Yi Fang* and was subsequently referenced in later texts such as the Song Dynasty's *Bencao Tujing*, the Yuan Dynasty's *Tangye Bencao*, the Ming Dynasty's *Bencao Gangmu*. While the exact number of steaming and sun-drying cycles described in these books may vary, the overall goal is to control the quality of RRP, indicating that the number of cycles is not rigidly fixed (Yan et al., 2020; Wu et al., 2022). It is theorized that the number "nine" in "nine steamed and nine sun-dried" reflects a traditional practice where some Chinese medicines are often processed this way multiple times, thus giving rise to the collective term (Peng et al., 2018).

3.2 Active compounds before processing

The Pharmacopoeia of the People's Republic of China identifies rehmannioside D and catalpol, both iridoid glycosides, as the key indicators for assessing the quality of RRR. Currently, 75 compounds have been extracted from RRR, which are categorized into classes such as iridoid glycosides, phenylethanoid glycosides, flavonoids, ionones, phenolic acids, and carbohydrates. The structures of these compounds are illustrated in Figure 1. Among these, iridoid glycosides, phenylethanoid glycosides, carbohydrates, and nucleosides are frequently used as reference compounds for selecting quality markers for RR (Zhu J. et al., 2022). These compounds are consolidated into Table 1 (Li et al., 2020; Gu et al., 2021; Chen SQ. et al., 2023; Lu et al., 2023; Xue et al., 2023; Zhu et al., 2023).

10.3389/fphar.2024.1426972

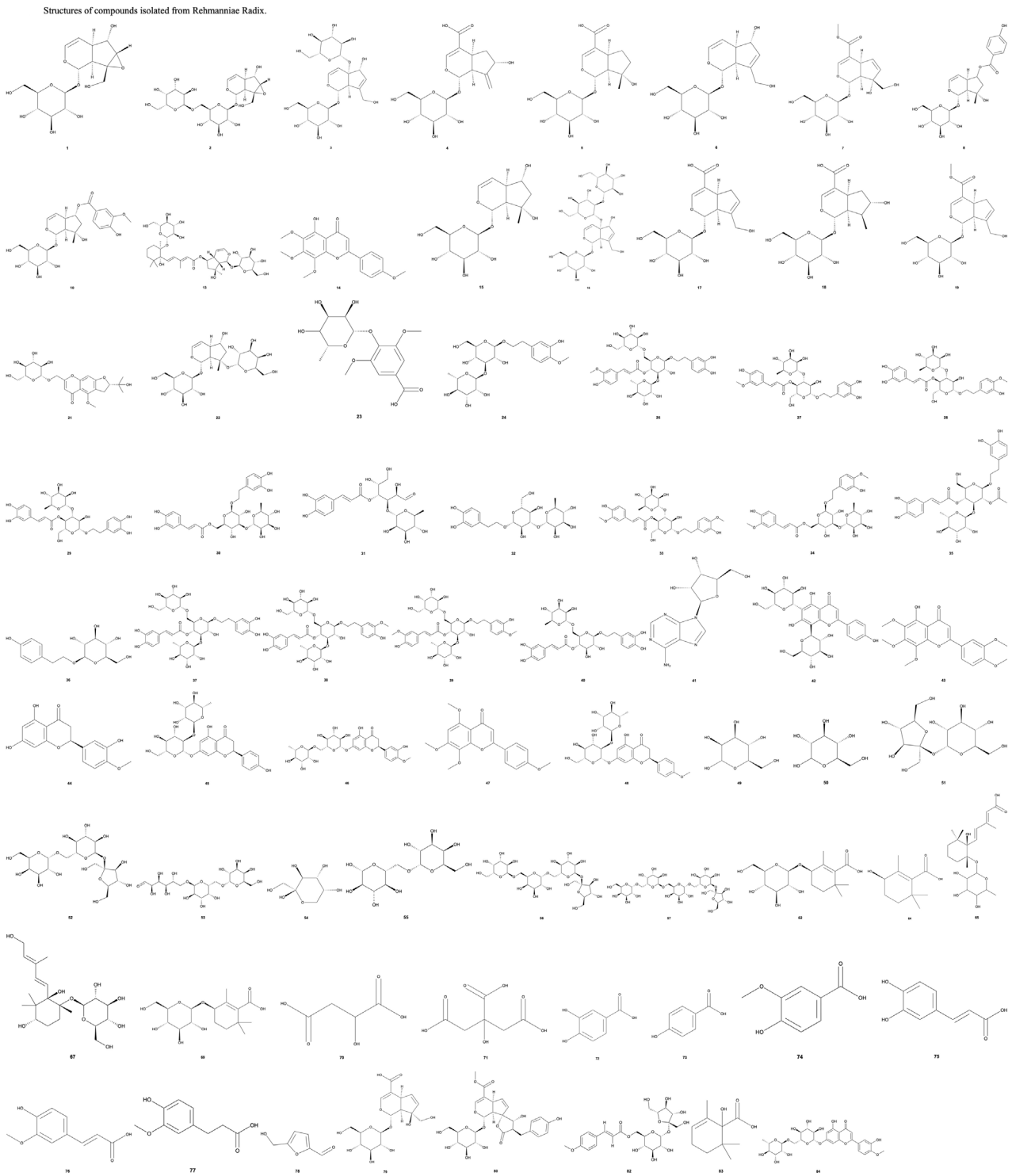

FIGURE 1
Structures of compounds isolated from Rehmanniae Radix. P.S: The structures in this article were referenced from the PubChem database. Structures not displayed were not found in the database. The bold Arabic numbers below the structures in Figure 1 correspond to the compounds numbered in Table 1.

10.3389/fphar.2024.1426972

TABLE 1 Compounds in raw Rehmanniae Radix and Rehmanniae Radix praeparata.

No.	Category	Compound	Molecular formulas	Extraction method	Raw	Steamed	Wine stewed	Repeatedly steamed and sundried	References
1	iridoid glycosides	Catalpol	$C_{15}H_{22}O_{10}$	methanol, by ultrasonication	+	NR	NR	+	Gu et al. (2021), Chen et al. (2023a)
2	iridoid glycosides	rehmannioside A	$C_{21}H_{32}O_{15}$	methanol, by ultrasonication	+	+	+	-	Li et al. (2020), Gu et al. (2021)
3	iridoid glycosides	Melittoside	$C_{21}H_{32}O_{15}$	methanol, by ultrasonication	+	+	+	-	Lu et al. (2023)
4	iridoid glycosides	Gardoside	$C_{16}H_{22}O_{10}$	methanol, by ultrasonication	+	+	+	+	Lu et al. (2023)
5	iridoid glycosides	mussaenosidic acid	$C_{16}H_{24}O_{10}$	methanol, by ultrasonication	+	+	+	+	Lu et al. (2023)
6	iridoid glycosides	Rhinanthin	$C_{15}H_{22}O_{9}$	methanol, by ultrasonication	+	+	+	+	Lu et al. (2023)
7	iridoid glycosides	Gardenoside	$C_{17}H_{24}O_{11}$	methanol, by ultrasonication	+	+	+	+	Lu et al. (2023)
8	iridoid glycosides	6-O-p-hydroxybenzoyl ajugol	$C_{22}H_{28}O_{11}$	methanol, by ultrasonication	+	-	-	-	Lu et al. (2023)
9	iridoid glycosides	6-O-E-caffeoyl ajugol	$C_{24}H_{30}O_{12}$	methanol, by ultrasonication	+	+	+	-	Lu et al. (2023)
10	iridoid glycosides	6-O-Vanilloylajugol	$C_{23}H_{30}O_{12}$	methanol, by ultrasonication	+	+	+	-	Lu et al. (2023)
11	iridoid glycosides	6-O-p-Vanillyl Ajugaol	$C_{24}H_{30}O_{11}$	methanol, by ultrasonication	+	+	+	+	Lu et al. (2023)
12	iridoid glycosides	6-O-E-feruloyl Ajugaol	$C_{25}H_{32}O_{12}$	methanol, by ultrasonication	+	+	+	+	Lu et al. (2023)
13	iridoid glycosides	rehmaglutoside I	$C_{36}H_{56}O_{17}$	methanol, by ultrasonication	+	-	-	-	Lu et al. (2023)
14	iridoid glycosides	gardenin B	$C_{19}H_{18}O_{7}$	methanol, by ultrasonication	-	-	-	-	Lu et al. (2023)
15	iridoid glycosides	Leonuride	$C_{15}H_{24}O_{9}$	methanol, by ultrasonication	+	+	+	+	Gu et al. (2021), Chen et al. (2023a), Lu et al. (2023)
16	iridoid glycosides	rehmannioside D	$C_{27}H_{42}O_{20}$	methanol, by ultrasonication	+	+	+	+	Gu et al. (2021), Chen et al. (2023a), Lu et al. (2023)
17	iridoid glycosides	geniposidic acid	$C_{16}H_{22}O_{10}$	methanol, by ultrasonication	+	+	+	+	Lu et al. (2023), Zhu et al. (2023)
18	iridoid glycosides	8-epiloganic acid	$C_{16}H_{24}O_{10}$	methanol, by ultrasonication	+	+	+	+	Lu et al. (2023), Zhu et al. (2023)
19	iridoid glycosides	Geniposide	$C_{17}H_{24}O_{10}$	methanol, by ultrasonication	+	NR	+	+	Zhu et al. (2023)
20	iridoid glycosides	Acetylcatalpol	$C_{17}H_{24}O_{11}$	methanol, by ultrasonication	+	NR	+	+	Zhu et al. (2023)
21	iridoid glycosides	prim-o-glucosylcimifugin	$C_{22}H_{28}O_{11}$	methanol, by ultrasonication	+	NR	+	+	Zhu et al. (2023)
22	iridoid glycosides	rehmannioside C	$C_{19}H_{32}O_{8}$	methanol, by ultrasonication	+	NR	+	+	Zhu et al. (2023)

(Continued on following page)

TABLE 1 (*Continued*) Compounds in raw Rehmanniae Radix and Rehmanniae Radix praeparata.

No.	Category	Compound	Molecular formulas	Extraction method	Raw	Steamed	Wine stewed	Repeatedly steamed and sundried	References
23	phenylethanoid glycosides	syringic acid-4-O-α-L rhamnoside	$C_{15}H_{20}O_9$	methanol, by ultrasonication	+	+	+	-	Lu et al. (2023)
24	phenylethanoid glycosides	darendoside B	$C_{21}H_{32}O_{12}$	methanol, by ultrasonication	+	+	+	+	Lu et al. (2023)
25	phenylethanoid glycosides	2-phenylethyl-O-β-D xylopyranosyl-(1→6)-β-D-glucopyranoside	$C_{19}H_{28}O_{10}$	methanol, by ultrasonication	+	+	+	+	Lu et al. (2023)
26	phenylethanoid glycosides	jionoside A_1/A_2	$C_{36}H_{48}O_{20}$	methanol, by ultrasonication	+	+	+	+	Lu et al. (2023)
27	phenylethanoid glycosides	leucosceptoside A	$C_{30}H_{38}O_{15}$	methanol, by ultrasonication	+	+	+	+	Lu et al. (2023)
28	phenylethanoid glycosides	jionoside D	$C_{30}H_{38}O_{15}$	methanol, by ultrasonication	+	+	+	+	Lu et al. (2023)
29	phenylethanoid glycosides	Verbascoside	$C_{29}H_{36}O_{15}$	methanol, by ultrasonication	+	+	+	+	Gu et al. (2021), Chen et al. (2023a), Lu et al. (2023)
30	phenylethanoid glycosides	Isoverbascoside	$C_{29}H_{36}O_{15}$	methanol, by ultrasonication	+	+	+	+	Chen et al. (2023a), Lu et al. (2023), Zhu et al. (2023)
31	phenylethanoid glycosides	cistanoside F	$C_{21}H_{28}O_{13}$	methanol, by ultrasonication	+	+	+	+	Lu et al. (2023), Zhu et al. (2023)
32	phenylethanoid glycosides	Verbasoside	$C_{20}H_{30}O_{12}$	methanol, by ultrasonication	+	+	+	+	Lu et al. (2023), Zhu et al. (2023)
33	phenylethanoid glycosides	Martynoside	$C_{31}H_{40}O_{15}$	methanol, by ultrasonication	+	+	+	+	Lu et al. (2023), Zhu et al. (2023)
34	phenylethanoid glycosides	Isomartynoside	$C_{31}H_{40}O_{15}$	methanol, by ultrasonication	+	+	+	+	Lu et al. (2023), Zhu et al. (2023)
35	phenylethanoid glycosides	2′-acetylacteoside	$C_{31}H_{38}O_{16}$	methanol, by ultrasonication	+	NR	+	+	Zhu et al. (2023)
36	phenylethanoid glycosides	Rhodioloside	$C_{14}H_{20}O_7$	methanol, by ultrasonication	+	NR	+	+	Zhu et al. (2023)
37	phenylethanoid glycosides	Echinacoside	$C_{35}H_{46}O_{20}$	methanol, by ultrasonication	+	NR	+	+	Zhu et al. (2023)
38	phenylethanoid glycosides	cistanoside a	$C_{36}H_{48}O_{20}$	methanol, by ultrasonication	+	NR	+	+	Zhu et al. (2023)
39	phenylethanoid glycosides	jionoside b1	$C_{37}H_{50}O_{20}$	methanol, by ultrasonication	+	NR	+	+	Zhu et al. (2023)
40	phenylethanoid glycosides	forsythiaside A	$C_{29}H_{36}O_{15}$	methanol, by ultrasonication	+	NR	+	+	Zhu et al. (2023)
41	nucleosides	Adenosine	$C_{10}H_{13}N_5O_4$	methanol, by ultrasonication	+	NR	+	+	Zhu et al. (2023)
42	flavonoids	vicenin II	$C_{27}H_{30}O_{15}$	methanol, by ultrasonication	-	-	-	-	Lu et al. (2023)
43	flavonoids	Demethylnobiletin	$C_{20}H_{20}O_8$	methanol, by ultrasonication	-	-	-	-	Lu et al. (2023)
44	flavonoids	Hesperetin	$C_{16}H_{14}O_6$	methanol, by ultrasonication	-	-	-	-	Lu et al. (2023)

(Continued on following page)

TABLE 1 (*Continued*) Compounds in raw Rehmanniae Radix and Rehmanniae Radix praeparata.

No.	Category	Compound	Molecular formulas	Extraction method	Raw	Steamed	Wine stewed	Repeatedly steamed and sundried	References
45	flavonoids	Naringin	$C_{27}H_{32}O_{14}$	methanol, by ultrasonication	-	-	-	-	Lu et al. (2023)
46	flavonoids	hesperidin/ neohesperidin	$C_{28}H_{34}O_{15}$	methanol, by ultrasonication	-	-	-	-	Lu et al. (2023)
47	flavonoids	6-demethoxytangeretin	$C_{19}H_{18}O_6$	methanol, by ultrasonication	-	-	-	-	Lu et al. (2023)
48	flavonoids	Poncirin	$C_{28}H_{34}O_{14}$	methanol, by ultrasonication	-	-	-	-	Lu et al. (2023)
49	carbohydrates	Mannose	$C_6H_{12}O_6$	Petroleum ether and ethyl acetate were extracted twice each	-	NR	NR	+	Xue et al. (2023)
50	carbohydrates	Glucose	$C_6H_{12}O_6$	Petroleum ether and ethyl acetate were extracted twice each	+	NR	NR	+	Xue et al. (2023)
51	carbohydrates	Sucrose	$C_{12}H_{22}O_{11}$	Petroleum ether and ethyl acetate were extracted twice each	+	NR	NR	-	Xue et al. (2023)
52	carbohydrates	Raffinose	$C_{18}H_{32}O_{16}$	Petroleum ether and ethyl acetate were extracted twice each	+	NR	NR	-	Xue et al. (2023)
53	carbohydrates	Manninotriose	$C_{18}H_{32}O_{16}$	Petroleum ether and ethyl acetate were extracted twice each	+	NR	NR	+	Xue et al. (2023)
54	carbohydrates	Fructose	$C_6H_{12}O_6$	Petroleum ether and ethyl acetate were extracted twice each	+	NR	+	+	Xue et al. (2023), Zhu et al. (2023)
55	carbohydrates	Melibiose	$C_{12}H_{22}O_{11}$	Petroleum ether and ethyl acetate were extracted twice each	-	NR	+	+	Xue et al. (2023), Zhu et al. (2023)
56	carbohydrates	Stachyose	$C_{24}H_{42}O_{21}$	Petroleum ether and ethyl acetate were extracted twice each	+	NR	-	-	Xue et al. (2023), Zhu et al. (2023)
57	carbohydrates	Verbascose	$C_{30}H_{52}O_{26}$	methanol, by ultrasonication	+	NR	+	+	Zhu et al. (2023)
58	lonones	rehmannia neoterpene B	$C_{15}H_{24}O_6$	methanol, by ultrasonication	+	+	+	+	Lu et al. (2023)
59	lonones	rehmannia neoterpene E	$C_{21}H_{34}O_{10}$	methanol, by ultrasonication	+	+	+	+	Lu et al. (2023)
60	lonones	hydroxyl wild acid	$C_{15}H_{24}O_5$	methanol, by ultrasonication	+	+	+	+	Lu et al. (2023)
61	lonones	rehmannia neoterpene F	$C_{21}H_{34}O_{10}$	methanol, by ultrasonication	+	+	+	+	Lu et al. (2023)
62	lonones	Rehmapicroside	$C_{16}H_{26}O_8$	methanol, by ultrasonication	+	+	+	+	Lu et al. (2023)

(Continued on following page)

TABLE 1 (*Continued*) Compounds in raw Rehmanniae Radix and Rehmanniae Radix praeparata.

No.	Category	Compound	Molecular formulas	Extraction method	Raw	Steamed	Wine stewed	Repeatedly steamed and sundried	References
63	lonones	oxyrehmanionoside B	$C_{19}H_{34}O_9$	methanol, by ultrasonication	+	+	+	+	Lu et al. (2023)
64	lonones	Rehmapicrogenin	$C_{10}H_{16}O_3$	methanol, by ultrasonication	+	+	+	+	Lu et al. (2023)
65	lonones	aeginetic acid 5-O-β-D quinovoside	$C_{21}H_{34}O_8$	methanol, by ultrasonication	+	+	+	+	Lu et al. (2023)
66	lonones	rehmannia neoterpene C	$C_{28}H_{40}O_{10}$	methanol, by ultrasonication	+	+	+	+	Lu et al. (2023)
67	lonones	neo-rehmannioside	$C_{21}H_{36}O_9$	methanol, by ultrasonication	+	+	+	+	Lu et al. (2023)
68	lonones	kojic acid	$C_{15}H_{24}O_4$	methanol, by ultrasonication	+	+	+	+	Lu et al. (2023), Zhu et al. (2023)
69	lonones	rehmapicroside or its isomers	$C_{16}H_{26}O_8$	methanol, by ultrasonication	+	NR	+	-	Zhu et al. (2023)
70	organic acids	malic acid	$C_4H_6O_5$	methanol, by ultrasonication	+	+	+	+	Lu et al. (2023)
71	organic acids	citric acid	$C_6H_8O_7$	methanol, by ultrasonication	+	+	+	+	Lu et al. (2023)
72	phenolic acids	protocatechuic acid	$C_7H_6O_4$	methanol, by ultrasonication	+	+	+	+	Lu et al. (2023)
73	phenolic acids	p-hydroxybenzoic acid	$C_7H_6O_3$	methanol, by ultrasonication	+	+	+	+	Lu et al. (2023)
74	phenolic acids	vanillic acid	$C_8H_8O_4$	methanol, by ultrasonication	+	+	+	+	Lu et al. (2023)
75	phenolic acids	caffeic acid	$C_9H_8O_4$	methanol, by ultrasonication	+	+	+	+	Lu et al. (2023)
76	phenolic acids	ferulic acid	$C_{10}H_{10}O_4$	methanol, by ultrasonication	+	+	+	+	Lu et al. (2023)
77	phenolic acids	dihydroferulic acid	$C_{10}H_{12}O_4$	methanol, by ultrasonication	+	NR	+	+	Zhu et al. (2023)
78	others	5-hydroxymethyl-2-furfura	$C_6H_6O_3$	methanol, by ultrasonication	-	+	+	+	Li et al. (2020), Zhu et al. (2023)
79	others	Monotropeine	$C_{16}H_{22}O_{11}$	methanol, by ultrasonication	+	+	+	+	Lu et al. (2023)
80	NR	Dunnisinoside	$C_{26}H_{30}O_{13}$	methanol, by ultrasonication	+	+	+	+	Lu et al. (2023)
81	NR	rhamnopyranosyl vanilloyl	$C_{14}H_{18}O_8$	methanol, by ultrasonication	+	+	+	+	Lu et al. (2023)
82	NR	sibirioside B	$C_{22}H_{30}O_{13}$	methanol, by ultrasonication	+	+	+	+	Lu et al. (2023)
83	NR	1-hydroxy-2,6,6-trimethylcyclohex-2-enecarboxylic acid	$C_{10}H_{16}O_3$	methanol, by ultrasonication	+	+	+	+	Lu et al. (2023)
84	NR	Diosmin	$C_{28}H_{32}O_{15}$	methanol, by ultrasonication	-	-	-	-	Lu et al. (2023)
85	NR	gionoside C	$C_{29}H_{36}O_{13}$	methanol, by ultrasonication	+	+	+	+	Lu et al. (2023)

(Continued on following page)

TABLE 1 (*Continued*) Compounds in raw Rehmanniae Radix and Rehmanniae Radix praeparata.

No.	Category	Compound	Molecular formulas	Extraction method	Raw	Steamed	Wine stewed	Repeatedly steamed and sundried	References
86	NR	jiocarotenoside A_1/A_2	$C_{21}H_{34}O_9$	methanol, by ultrasonication	+	+	+	+	Lu et al. (2023)
87	NR	nigroside I/II	$C_{30}H_{38}O_{14}$	methanol, by ultrasonication	+	+	+	+	Lu et al. (2023)

P.S: +: detected in samples; -: can't be found in samples; NR: no researches were carried out. The references cited in the table are [22-26、32] and are listed below.

3.3 Active compounds after processing

RRP undergoes numerous processing methods, each affecting its compounds and concentration differently. Modern studies focus on compounds like iridoid glycosides, phenylethanoid glycosides, carbohydrates, and 5-hydroxymethyl furfural (5-HMF). Table 1 details the extraction methods and the compounds derived from both RRR and RRP, processed respectively by steaming with water, stewing with wine, and repeated steamed and sun-dried.

3.3.1 Glycoside analysis

In RRP, the glycoside compounds most researched are iridoid glycosides, phenylethanoid glycosides, and nucleosides.

Experimental studies reveal iridoid glycosides and phenylethanoid glycosides as significant quality markers, reflecting the degree of processing in RRP (Liu et al., 2023). The experimental data showed that the content of rehmannioside D after steaming and wine stewing was lower than that before processing, and the content of rehmannioside D in wine stewing was less than that of steamed products with the same degree of processing (Jiang Y. et al., 2023). Using UPLC-PDA and HPLC methods for testing (Zhang LX. et al., 2023; Yang et al., 2024), the data shows that in the process of wine steaming, a significant decrease was observed in iridoid glycosides such as catalpol, rehmannioside D, rhinanthin, leonuride, geniposidic acid, and melittin during wine stewing. The most substantial decline was in catalpol, dropping from 44.00 mg/g in FRR to 2.192 mg/g in the wine stewed RR. Similarly, verbascoside from phenylethanoid glycosides showed a notable reduction during wine stewing. In nucleosides, adenosine and uridine levels increased, whereas guanosine decreased. Further HPLC analysis indicated that with successive steaming from one to nine times, the concentrations of catalpol, rehmannioside D, leonuride, and verbascoside diminished (Ma et al., 2023). However, during the "nine steamed and nine sun-dried" process, from "one steamed and one sun-dried" to "seven steamed and seven sun-dried," the concentration of catalpol, rehmannioside D, leonuride, verbascoside and isoverbascoside increased with the number of cycles, yet showed no significant change from "seven steamed and seven sun-dried" to "nine steamed and nine sun-dried" (Chen SQ. et al., 2023). Experimental findings (Zhu et al., 2023) suggest that compared to RRR, the total iridoid glycoside concentration decreased in three processed forms: RR stewed with wine, nine steamed and nine sun-dried RR (without Citri Reticulatae Pericarpium and Amomi Fructus), and nine steamed and nine sun-dried RR (with Citri Reticulatae Pericarpium and Amomi Fructus). Conversely, the total phenylethanoid glycoside concentration increased in the nine steamed and nine sun-dried RRP (with Citri Reticulatae Pericarpium and Amomi Fructus) while decreasing in RR steamed with wine, RR stewed with wine, and nine steamed and nine sundried RR (without Citri Reticulatae Pericarpium and Amomi Fructus). Other studies (Chen et al., 2021) have noted a general decrease in glycoside concentration after processing, particularly higher levels of rehmannioside D, heterophylloside, and leonuride in RR processed with both Citri Reticulatae Pericarpium and Amomi Fructus compared to processing with just one of these excipients.

3.3.2 Carbohydrates

Experiments demonstrate that carbohydrate components exhibit different trends over the course of processing. These variations not only distinguish between different processed RR, but also, to some extent, indicate the processing endpoint for RRP, providing a partial reference for its quality evaluation. (Zhang et al., 2020).

The ATR-FTIR method was utilized to conduct a comprehensive analysis of water extracts from FRR, RRR, and RRP, quantifying compounds such as mannose, manninotriose, stachyose, fructose, glucose, galactose, melibiose, and verbascoside. This confirms that carbohydrates are the primary differential compounds between FRR and its processed forms (Tian et al., 2022). Quantitative analysis at various processing stages shows that while sucrose, raffinose, stachyose, and verbascoside decrease, fructose, glucose, melibiose, and manninotriose increase significantly. Carbohydrate profiles in RRR and RRP thus exhibit distinct characteristics, forming a basis for quality assessment of both (Zhang et al., 2016). During wine stewing and steaming, polysaccharide concentration initially rises then falls. The polysaccharide content in wine-stewed products is higher than that in steamed products at the same processing stage (Jiang Y. et al., 2023). During the "one steamed and one sun-dried" to "seven steamed and seven sun-dried" processing, polysaccharide concentration in RRP increases with each cycle. However, from "seven steamed and seven sun-dried" to "nine steamed and nine sun-dried," the polysaccharide concentration declines. The highest polysaccharide mass fraction, 30.10%, is found in the "seven steamed and seven sun-dried" RRP (Chen SQ. et al., 2023). During nine steaming cycles, the polysaccharide concentration in RRR is lowest, peaking in the fifth cycle before sharply declining, the variation in polysaccharide content in RRP after six steaming cycles is minimal (Jia et al., 2023). By measuring the content of D-fructose, glucose, sucrose,

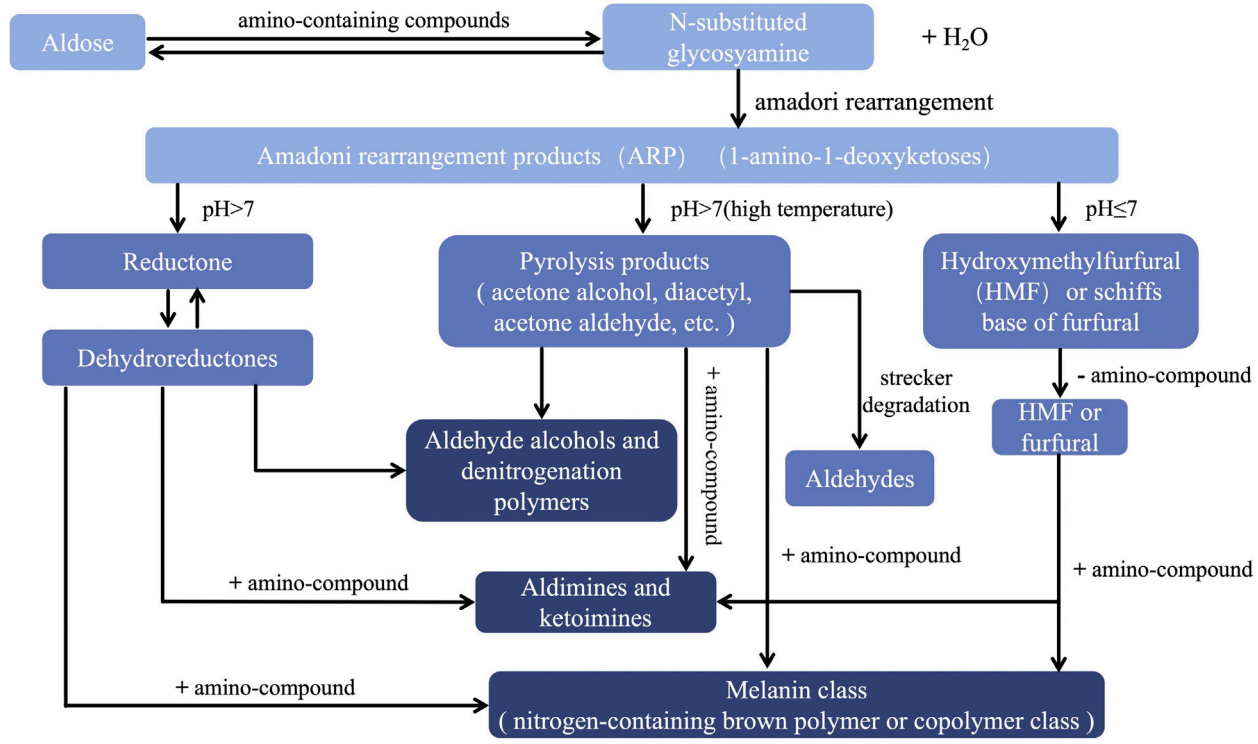

FIGURE 2
Schematic diagram of Hodge Maillard reaction process. PS: The color from light to dark corresponds to the initial stage, intermediate stage and final stage of the Maillard reaction, respectively. [40] Gong RZ, Huo XH, Zhang L, Liu C, Li SS, Sun YS. (2019). Advances in effects and regulation of Maillard reaction on quality of Chinese materia medica. Chinese Traditional and Herbal Drugs (01),243-251.

melibiose, stachyose, manninotriose, raffinose, and verbascoside, it was found that after processing trends show a decrease in oligosaccharide concentration and an increase in monosaccharide concentration. In RR processed with Amomi Fructus and Citri Reticulatae Pericarpium, the concentration of D-fructose, glucose, and manninotriose increased by 29.24%, 57.14%, and 44.65% respectively, compared to samples processed without these excipients (Chen et al., 2021).

3.3.3 Other compounds

5-HMF, a marker of the Maillard reaction (Wang et al., 2020), is a new substance formed during RR processing. The mechanism and products of the Maillard reaction are highly complex. When Hodge named this compound reaction in 1953, he summarized the process of the reaction (Shown in the Figure 2 (Gong et al., 2019; Zhou et al., 2014). It is absent in RRR but its concentration significantly increases after processing (Chen et al., 2021; Zhu et al., 2023), with its presence correlating strongly with the darkening color of RRP (Ma et al., 2023). In addition, it has also been found in the processing studies of other traditional Chinese medicines that the presence of 5-HMF can be detected after processing, but not before processing, indicating that 5-HMF can be used as an indicator to evaluate the degree of processing (Yang et al., 2023).

Trace element analysis from "one steamed and one sun-dried" to "nine steamed and nine sun-dried" shows an initial increase and then a decrease in beneficial elements like zinc, copper, and iron, while harmful elements such as cadmium, arsenic, and lead gradually decline with more steaming and sun-drying cycles, potentially reducing the accumulation of toxic substances in human soft tissues (Chen SQ. et al., 2023).

Amino acid analysis revealed that both total and free amino acid mass fractions decrease in processed RR, with basic amino acids, especially arginine and lysine, showing the most significant declines (Gao et al., 2010).

4 Application of RR and its active compounds in ovarian hypofunction diseases

RR exhibits a range of pharmacological effects. *In vivo* and *in vitro* experiments have confirmed its mechanism in enhancing granulosa cell proliferation, antioxidant and anti-aging effects, and modulation of the immune-inflammatory microenvironment. Thus, it plays a therapeutic role in ovarian hypofunction diseases, with reproductive endocrine protection function. The mechanism of Ovarian Hypofunction Diseases and the function of RR are shown in Figure 3.

4.1 Improves granulosa cell proliferation

The follicle, composed of oocytes, granulosa cells (GCs), and follicular membrane cells, is fundamental to ovarian function. The

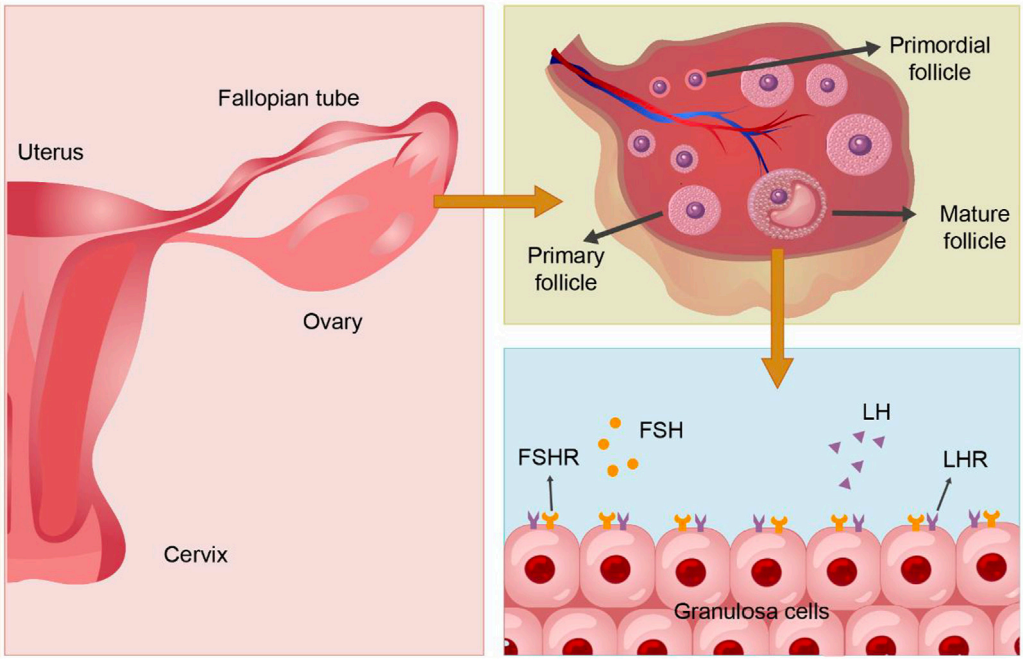

FIGURE 3
The structure and physiology of the ovary and granulosa cells. PS: Follicle stimulating hormone (FSH), Follicle stimulating hormone receptor (FSHR); Luteinizing hormone (LH), Luteinizing hormone receptor (LHR).

proliferation and differentiation of GCs signify follicle development. GCs are crucial for synthesizing, expressing, and metabolizing various hormones, serving as the primary source of ovarian estradiol, inhibin, and activin, and playing roles in oocyte reserve, maturation, and pregnancy maintenance (Kranc et al., 2017). The structure and physiology of the ovary and GCs are shown in Figure 4. GCs are central to studies on follicular growth and atresia mechanisms. Ovarian hypofunction diseases relate to GC apoptosis, follicle stimulating hormone (FSH) receptor signaling defects, autoimmunity, and other factors (Nelson, 2009). Prior studies suggest that abnormal proliferation and apoptosis of ovarian GCs may cause excessive follicular atresia (Matsuda et al., 2012). Additionally, hormones from the pituitary gland and ovaries regulate ovarian function and follicle development and atresia. FSH initiates key events in ovarian follicles: GC proliferation, estrogen synthesis, and expression of the luteinizing hormone receptor (LHR) in GCs (Liu et al., 2024), crucial for GC differentiation in antral and preovulatory follicles (Hsueh et al., 2000). The follicle stimulating hormone receptor (FSHR), a specific G protein-coupled receptor on ovarian GCs (Hunzicker-Dunn and Maizels, 2006), promotes GCs proliferation by binding to FSH, facilitates androgen conversion to estrogen, leads to follicle maturation, produces a peak in LH levels, and induces ovulation (Casarini and Crépieux, 2019) (Shown in the Figure 5). Haploinsufficiency of FSHR accelerates oocyte loss in mice, marking a significant factor in ovarian aging and estrogen deficiency (Danilovich and Sairam, 2002).

RRP is commonly used to tonify the kidney to promote follicle development and maturation, but the effects on ovaries vary with different processing methods and degrees. Researchers (Que et al., 2021) have observed varying impacts of the nine steamed and nine sun-dried RRP group, the one steamed and one sun-dried RRP group, and the RRR group on mouse ovaries. The nine steamed and nine sun-dried RRP group significantly increased preantral and sinusoid follicles and elevated FSHR levels in the ovaries, unlike the one steamed and one sun-dried RRP group and the RRR group, which did not promote follicle development. FSHR may be a target of the nine steamed and nine sun-dried RRP. Furthermore, 5-HMF, a compound formed by the Maillard reaction of sugars and amino acids during processing, was identified as potentially influencing the medicinal properties of RRP. The concentration of 5-HMF correlates closely with steaming and heating time (Yang, 2010). Enhanced expression of FSHR improves GCs function, while silencing FSHR expression leads to GCs apoptosis and follicular atresia (Du et al., 2016). It has been suggested from experimental studies that processed RR might increase 5-HMF concentration and upregulate FSHR levels, enhancing GCs proliferation, fostering follicle development, and ultimately improving ovarian function and reproductive outcomes. A new study (Lin et al., 2019) introduced the processing method of nine steamed and nine baked RRP, comparing it with three other RR preparations. Results indicated that the proliferation effect on rat ovarian GCs was associated with RR polysaccharide concentration, with the most significant effect at a mass concentration of 150 μg/mL. Among these, the total polysaccharide concentration was highest in RR processed by nine steamed and nine baked RRP, with the proliferation hierarchy as follows: nine steamed and nine sun-dried RRP polysaccharides > nine steamed and nine baked RRP polysaccharides > modern method RRP polysaccharides > RRR polysaccharides. Intriguingly, experimental studies (Liu, 2018) found that the aqueous extract of the modern steaming RRP method may hinder ovulation in normal female rats, leading to

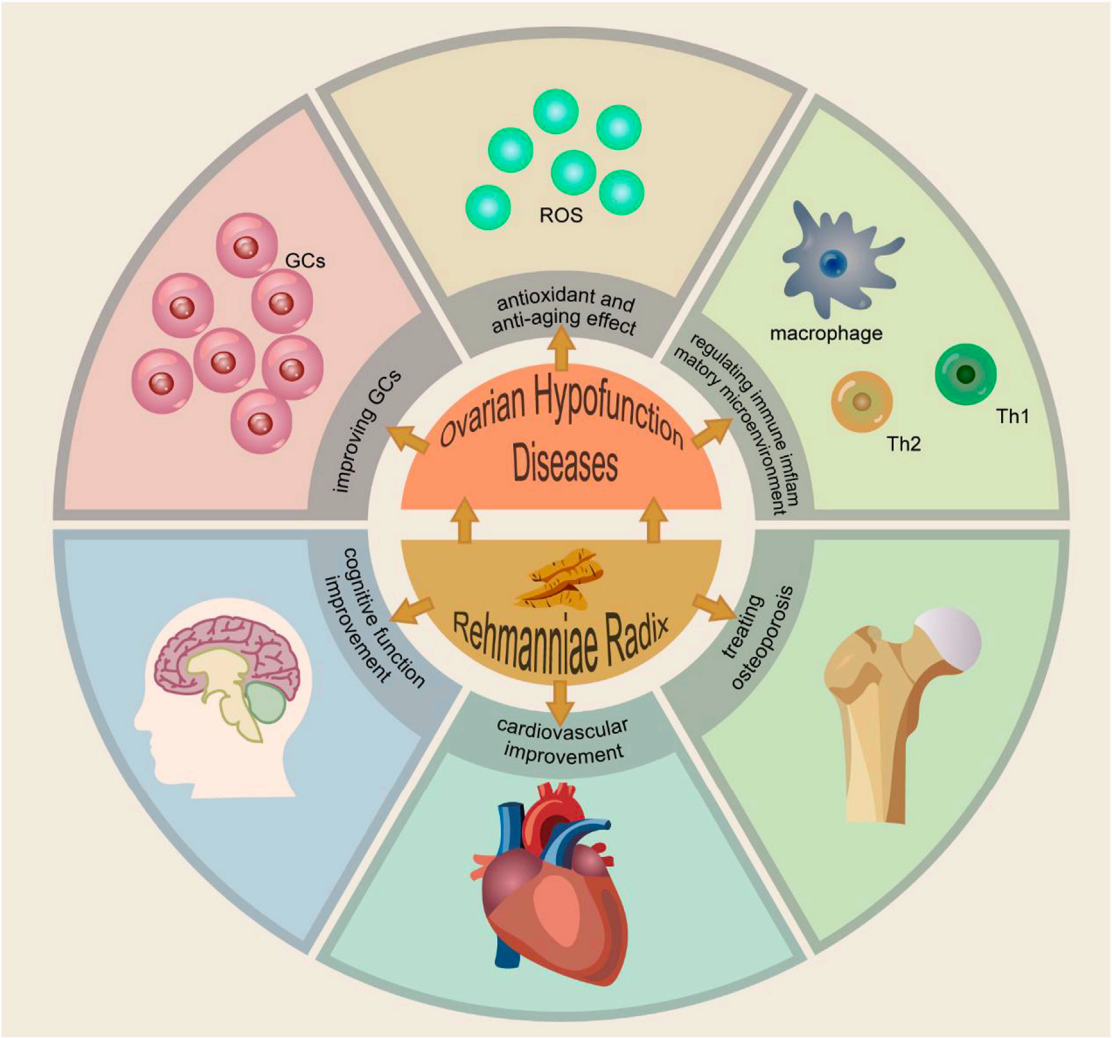

FIGURE 4
The Mechanism of Ovarian Hypofunction Diseases and the Function of Rehmanniae Radix. PS: Granulosa cells (GCs). Reactive oxygen species (ROS).

prolonged estrous cycles, increased atretic follicles, and decreased serum sex hormone (estradiol, progesterone) levels, while the aqueous extract of the nine steaming and nine sun-dried RRP may not affect ovulation in female rats with normal estrous cycle, but the specific compounds and dosage impacting ovulation require further investigation.

4.2 Antioxidant and anti-aging

Ovarian senescence, influenced by factors affecting the quantity and quality of oocytes, leads to a decline in ovarian function and gradual aging. In 1954, Harman first proposed the free radical theory of aging, suggesting that aging-related diseases are triggered by the interaction of reactive oxygen species (ROS) with cellular components, thereby inducing aging-related changes (Harman, 1956; Harman, 2006). Hence, reducing oxidative stress and the production of free radicals can decelerate aging and extend life. Oxidative stress is considered a principal pathogenesis of ovarian aging. Normally, a dynamic balance exists between ROS and antioxidants in the body. Disruption of this balance due to excessive ROS production or increased antioxidant utilization induces oxidative stress. Oxidative stress can lead to various pathological changes in cells, including mitochondrial dysfunction, DNA damage, telomere shortening, etc., all of which are key factors in aging-related diseases. Studies have shown that oxidative stress within the ovarian microenvironment can diminish oocyte quality, induce apoptosis of GCs, accelerate corpus luteum degeneration, and lead to ovarian aging and infertility (Freitas et al., 2017; Liang J. et al., 2023), affecting the success rate of ART (Oyawoye et al., 2003).

Excessive ROS can also initiate crosstalk among various signaling pathways and protein factors, contributing to the pathogenesis of ovarian aging and serving as therapeutic targets. Currently, the regulation of ovarian signaling pathways by ROS mainly focuses on important signaling pathways such as Recombinant Kelch Like ECH Associated Protein 1 (KEAP1)-Nuclear factor-E2-related factor 2 (Nrf2), NF-kB, FOXO, etc. Nrf2 is a critical transcription factor in oxidative stress, regulating the antioxidant response with KEAP1 to protect

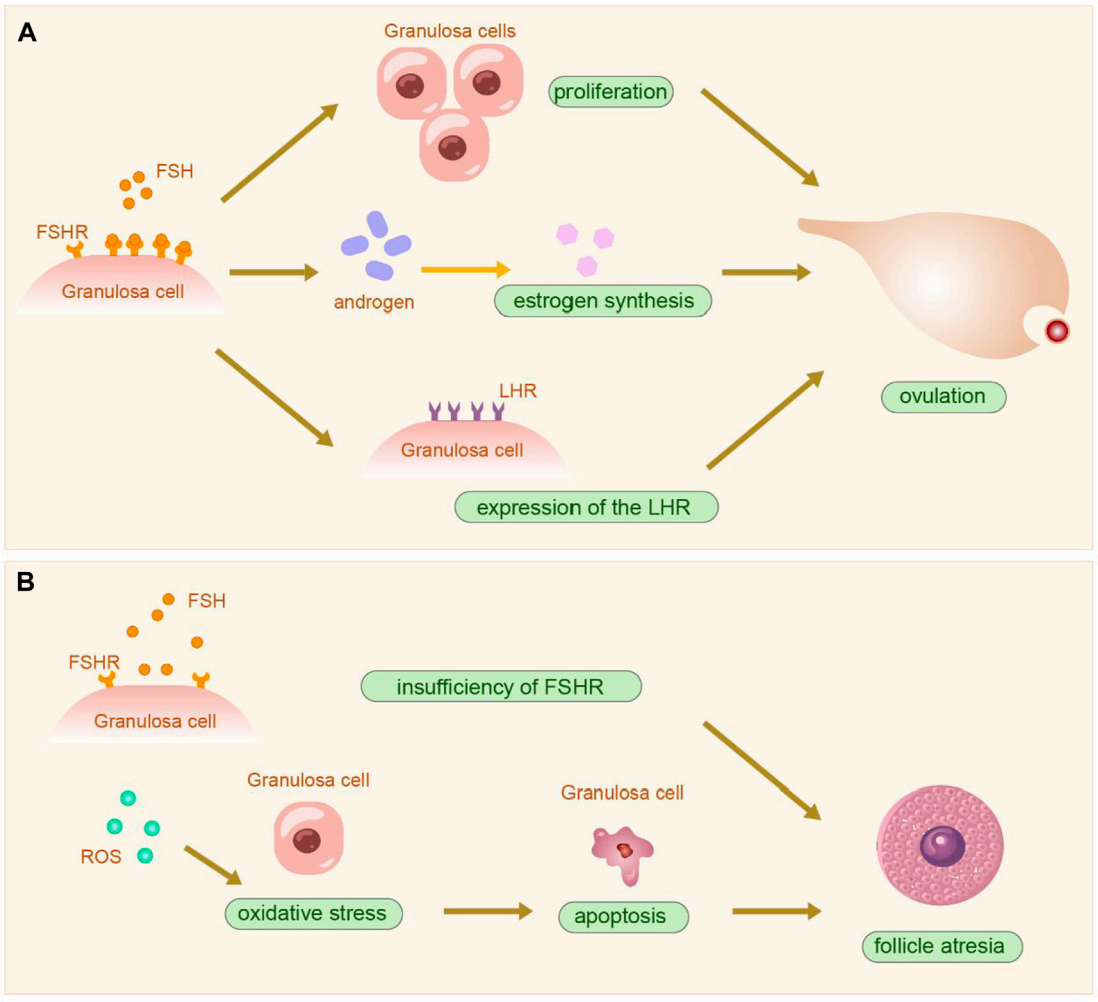

FIGURE 5
The physiopathological diagram of granulosa cells. **(A)**. The physiological process following the action of FSH on ovarian granulosa cells. **(B)**. The onset of follicle atresia after insufficiency of FSHR and oxidative stress. PS: Follicle stimulating hormone (FSH); Follicle stimulating hormone receptor (FSHR); Luteinizing hormone receptor (LHR); Reactive oxygen species (ROS).

cellular functions (Baird and Yamamoto, 2020). Nrf2 promotes the expression of downstream antioxidant enzymes such as heme oxygenase 1 (HO-1), NADP(H) quinone dehydrogenase 1 (NQO1), and glutathione-S-transferases (GSTs). This mechanism effectively mitigates intracellular oxidative stress and minimizes cellular damage from ROS(Gao X. et al., 2023). Research has shown that (Ma et al., 2018) Nrf2 expression levels in ovarian GCs correlate with women's age, highlighting Nrf2 as a key factor in oocyte aging and suggesting that a decline in Nrf2 expression may be closely linked to reduced reproductive capability in older women. Additionally, Nrf2 activity has been found to correlate positively with species longevity (Lewis et al., 2015) and improves endothelial cell senescence (Romero et al., 2019). Therefore, Nrf2 is one of the key points for treating ovarian aging. ROS induces inflammatory cells, such as macrophages, to produce TNF-α. When TNF-α binds to membrane receptors, it mediates the phosphorylation and degradation of IkB, activating the NF-kB pathway to control the transcription of anti-apoptotic and inflammation-related genes. The FOXO family, a crucial transcription regulatory factor within the PI3K-AKT signaling pathway, is involved in regulating cell proliferation, apoptosis, and differentiation. FOXO3 enhances NRF2 activity by promoting KEAP1 degradation and also increases BCL10 expression, regulating the activation of the IkB-NF-kB pathway (Shixuan, 2021).

In RR studies, processing has been found to increase the concentration of 5-HMF, a Maillard reaction product, enhancing free radical scavenging capabilities and playing an antioxidant role (Kwon et al., 2019). RR polysaccharide activates the Nrf2/Keap1 pathway and significantly increases the activity of antioxidant enzymes (Ren et al., 2023). However, Rehmannioside A notably improves oxidative stress after activating the PI3K/Nrf2/SLC7A11 signaling pathway (Fu et al., 2022). Additionally, the phenolic/phenylpropionic acid pathway, mediated by Cinnamate 4-hydroxylase (C4H), has been identified in RR phenol studies as involved in regulating oxidative stress tolerance (Yang Y. H. et al., 2021). In aging research, Rehmannia glutinosa 70 (RG70) has shown superior antioxidant activity *in vitro* (compared to RG50, RG90, and

RGB), enhancing the antioxidant enzyme system of *Caenorhabditis elegans*, reducing ROS levels, and increasing the expression of lifespan-related genes daf-16 and skn-1 and their downstream genes sdo-3 and gcs-1, thereby achieving an anti-aging effect (Liang L. et al., 2023). Another study found that RG70 reduced the expression levels of TNF-α, IL-1β, and IL-6 by modulating the ROS/NF-kB signaling pathway, thereby alleviating oxidative stress and inflammatory response (Zhang H. et al., 2023). Another aspect of the anti-aging mechanism of RR is to enhance the function of hematopoietic stem cells, downregulate aging-related proteins p53 and p16, reduce ROS levels, and achieve an anti-aging effect (Bai et al., 2018). RR polysaccharide also activates the antioxidant enzyme system under oxidative stress, thereby stimulating the daf-16 gene on the insulin/IGF-1 signaling pathway (IIS) and prolonging the lifespan of *C. elegans* (Yuan et al., 2019). Moreover, some studies have found that microplastics activate the Wnt/β-Catenin signaling pathway and oxidative stress in rats, leading to apoptosis of ovarian GCs and causing fibrosis, ultimately reducing ovarian reserve function (An et al., 2021). In a study of RR extract catalpol, it was found to regulate pulmonary fibrosis through the Wnt/β-catenin pathway and reduce oxidative stress in lung tissue (Yang F. et al., 2021). Another experiment with the RR-Cornus officinalis pair revealed that this combination could reduce pro-inflammatory cytokines IL-1β, IL-6, and TNF-α, and downregulate the expression of TGF-β1, JNK, p38, and ERK to improve renal interstitial fibrosis (Zhu et al., 2024). Future studies could also explore the pharmacological mechanism of RR in ameliorating ovarian aging from the perspective of ovarian fibrosis.

4.3 Regulates the immune inflammatory microenvironment

The ovary is frequently targeted by autoimmune attacks in both organ-specific and systemic autoimmune diseases. The precise mechanism of autoimmunity in these conditions remains unclear, potentially triggered by genetic or environmental factors (Domniz and Meirow, 2019). Studies indicate that between 10% and 55% of patients with POI also suffer from autoimmune diseases (Szeliga et al., 2021). In cases of POI with adrenal autoimmune disease, ovarian histology biopsies reveal persistent autoimmune oophoritis, with inflammatory cells particularly surrounding the pre-ovulatory follicle and corpus luteum which produce steroid hormones (Kirshenbaum and Orvieto, 2019). Research has demonstrated a disorder in T lymphocyte subsets in POI patients. Compared to healthy women, POI patients show a decreased percentage of $CD4^+$ T lymphocytes and an increased percentage of $CD8^+$ T lymphocytes in peripheral blood, with TSH levels negatively correlated with $CD4^+$ percentages and positively with $CD8^+$ percentages (Hsieh and Ho, 2021). Additionally, the expression of the fork-head transcription factor 3 (Foxp3) in peripheral blood is significantly reduced in POI patients, alongside increased levels of pro-inflammatory factors such as interferon γ (IFN-γ) and TNF-α, and decreased levels of anti-inflammatory factors like interleukin-10 (IL-10) and transforming growth factor beta (TGF-β) (Wang et al., 2022; Mao and Ji, 2023). Th1/Th2 cells, subtypes of $CD4^+$ T cells, play roles in mediating cellular immune and inflammatory responses, secreting pro-inflammatory cytokines such as IFN-γ, TNF-α, and IL-6, while Th2 cells primarily secrete anti-inflammatory cytokines like TGF-β and IL-10. These studies suggest a disturbance in the local immune inflammatory microenvironment in POI patients, with an imbalance of Th1/Th2 cells in the ovaries disrupting homeostasis, affecting follicle formation and ovulation (Boots and Jungheim, 2015), potentially leading to apoptosis and follicular atresia (Huang et al., 2019). Moreover, the local inflammatory state can induce ovarian fibrosis, making modulation of the immune inflammatory microenvironment another therapeutic approach for treating ovarian aging.

Extensive research confirms that immunity regulation and anti-inflammation are among the pharmacological effects of RR. RR polysaccharides, particularly after repeated steam drying, effectively enhance anti-inflammatory activity (Lu et al., 2022). These polysaccharides activate dendritic cells (DCs) (Huang et al., 2013) both *in vitro* and *in vivo*, increase cell proliferation and cytokine secretion, and sustain cellular and humoral immune responses (Huang et al., 2016a). They promote IFN-γ production in $CD4^+$ and $CD8^+$ T cells (Xu et al., 2017) and increase Th1, Th2, and Th17 cytokines in mice, thus improving immunity (Huang et al., 2021). RR polysaccharides also activate the non-specific immune response of macrophages by increasing nitric oxide levels, enhancing macrophage phagocytic activity (Huang et al., 2016b), and thereby bolstering immune response and anti-infection capabilities (Feng et al., 2020). Additionally, 2,5-dihydroxyacetylbenzone (DHAP), extracted from RRP, has shown potential in treating lipopolysaccharide (LPS)-stimulated macrophage inflammatory responses in RAW264.7 mice. DHAP effectively inhibited the phosphorylation of extracellular signal-related kinase (ERK) 1/2 and nuclear translocation of NF-κB p65, reducing inflammatory mediator production in activated macrophages and achieving anti-inflammatory activity (Han et al., 2012). Recent studies also link gut microbiota with POI (Wu et al., 2021), with Mendelian studies suggesting that dysbiosis of gut microbiota can lead to POI (Wang et al., 2023). Notably, research on RR oligosaccharides and polysaccharides has shown they can enhance the abundance of intestinal microbiota, reduce intestinal inflammation, and repair intestinal barrier damage by maintaining intestinal microbiota homeostasis (Li X. et al., 2023; Lv et al., 2023; Ren et al., 2023). Furthermore, RR oligosaccharides enhance the vitality of stem cells and improve the immunomodulatory efficacy of stem cells, achieving better therapeutic outcomes (Zhang et al., 2012). Interestingly, in a study of overweight women, RR was found to reduce BMI by improving gut microbiota, enriching research on RR in metabolic diseases and underscoring its potential as a prebiotic (Han et al., 2015).

4.4 Impact on long-term complications: cardiovascular and cerebrovascular diseases, osteoporosis, and cognitive dysfunction

Estrogen can inhibit macrophage oxidation of low-density lipoprotein, induce direct antioxidant effects to reduce macrophage activation through oxidized low-density lipoprotein protein and prevent the progression of atherosclerosis (Clarkson, 2018). Estrogen can also directly act on cardiomyocytes, including

activating the AKT pathway and inhibiting cardiomyocyte apoptosis and necrosis. Patients with diseases of ovarian hypofunction diseases are at increased risk of cardiovascular and cerebrovascular diseases due to decreased estrogen levels. The risk of cardiovascular and cerebrovascular diseases increases with age. A Post-menopause, women experience prolonged low estrogen levels, reducing the protective effects on blood vessels and heightening the risk of cardiovascular and cerebrovascular diseases compared to men of the same age (Bushnell et al., 2014). The ovarian hormone 17β-estradiol plays a critical role in sex differences in cardiovascular diseases due to its impact on myocardial remodeling, function, and atherosclerotic lesion management (Bourassa et al., 1996; Stewart et al., 2006). A meta-analysis (Daan et al., 2016) revealed that women with POI face higher cardiovascular risks than middle-aged premenopausal women, including increased abdominal fat, elevated chronic inflammatory markers, and tendencies towards higher blood pressure and impaired kidney function. RR extract, particularly catalpol, has been found to protect rat cardiomyocytes by regulating autophagy, inhibiting apoptosis, enhancing oxidative stress response, and modulating estrogen receptors, thereby improving myocardial ischemia (Lin et al., 2017). Catalpol also mitigates oxidative stress, inflammatory responses, and apoptosis in the heart by inhibiting NF-κB activation, reducing cardiovascular event occurrences (Nemmar et al., 2022). Hyperhomocysteinemia (HHCY), a recognized independent risk factor for atherosclerosis, is ameliorated by catalpol in human aortic endothelial cells through the inhibition of Nox4/NF-κB and endoplasmic reticulum stress (Hu et al., 2019). Additionally, the active compound puerarin from Catalpol and Pueraria lobata significantly improves cerebrovascular endothelial cell apoptosis, increases local cerebral blood flow, and reduces infarct size at a dosage of 65.4 mg/kg (Liu et al., 2017).

Premature ovarian aging leads to decreased bone mineral density and increased osteoporosis risk, partly due to the adverse effects of prolonged high FSH levels and low estrogen (Mills et al., 2021). A longitudinal study (Shea et al., 2021) indicated a higher osteoporosis incidence in women with POI compared to those with early or normal menopausal onset (21.9% vs. 16.7%). Extensive research has shown that RR extract effectively prevents and treats osteoporosis, potentially developing as a new therapeutic drug. This effect is attributed to RR extract's ability to stimulate osteoblast proliferation, inhibit osteoclast activity and production, and prevent bone loss in osteoporotic mouse models with ovarian resection (Oh et al., 2003; Lim and Kim, 2013). Inosine, a primary active molecule in RR, significantly inhibits bone marrow macrophage-derived osteoclast differentiation and formation by blocking NF-κB activation, thereby reducing bone loss (Lee et al., 2013). RR compound ajugol alleviates osteoarthritis by promoting autophagy and attenuating endoplasmic reticulum stress-induced cell death and extracellular matrix degradation at 50 μM(Wu et al., 2023). Metabolomics studies (Xia et al., 2019) reveal that RR prevents dexamethasone-induced bone loss by interfering with steroid hormone biosynthesis, upregulating cytochrome P450 17A1 (CYP17A1) and aromatase (CYP19A1), and downregulating 11β-hydroxysteroid dehydrogenase (HSD11B1).

Cognitive dysfunction and memory loss are also significant long-term risks after premature ovarian failure, closely linked to estrogen deficiency (Gibbs, 2010; Djiogue et al., 2018). Notably, a meta-analysis (Zhao et al., 2023) indicated that osteoporotic patients have a higher risk of cognitive impairment compared to non-osteoporotic patients (OR = 2.01%, 95% CI: 1.63–2.48, $p < 0.01$). Catalpol isolated from RR plays a neuroprotective role in brain tissues and improves cognitive dysfunction by enhancing endogenous antioxidant enzyme activity and inhibiting free radical production (Zhang et al., 2007). Another study (Zhang et al., 2013) found that Catalpol also offers neuroprotective effects in d-galactose-induced aging mice by regulating the cholinergic system and reducing inflammatory cytokine expression (TNF-α, IL-1β). Thus, the active compounds of RR effectively reduce long-term health risks in patients with premature ovarian aging and offer benefits for both short-term and long-term health.

5 The application of TCM compound with RR in ovarian hypofunction diseases

RR is commonly used in clinical practice in combination with other Chinese botanical drugs in recipes such as Siwu Decoction, Liuwei Dihuang Pill, Guishen Pill, Yijing Decoction, and Chinese patent medicines like KunTai Capsule. As the primary botanical drug in many TCM compounds, RR can enhance the efficacy of these formulas. The composition of TCM compounds containing RRP was shown in Table 2, and its mechanism were shown in Table 3 and Table 4.

5.1 Siwu decoction

Siwu Decoction, in which RRP is as its sovereign botanical drug, Angelicae Sinensis Radix as the minister botanical drug, and Paeoniae Radix Alba and Chuanxiong Rhizoma as assistant botanical drugs, serves to nourish and replenish blood. As a tonic formula, it was first documented in the Song Dynasty's "*Taiping Huimin Heji Ju Fang*" for treating gynecological conditions. Today, it is widely employed to address irregular menstruation and various complications during pregnancy and childbirth, including those associated with ovarian hypofunction. Each menstrual cycle involves cyclic ovarian remodeling, necessitating extensive vascular remodeling to support new follicle growth. A dense, highly permeable vascular network supplies the ovary with essential hormones and nutrients for robust metabolism and delivers matrix factors to the cumulus-oocyte complex before ovulation (Brown and Russell, 2014). Consequently, ovarian blood vessels are essential for follicles, ovarian structure, and function. Research on Siwu Decoction has demonstrated its ability to enhance ovarian angiogenesis in POF model mice by activating the STAT3/HIF-1a/VEGF signaling pathway, thus increasing the production of related pro-angiogenic factors (VEGF, bFGF). It also stabilizes new blood vessel maturation through the regulation of PDGFB, Ang1, and Ang2 expression, ensuring sufficient vascular support for follicle development and consistent proliferation, and enhancing ovarian function (Zhou, 2022). Estrogen receptors (ER), including ERα, ERβ, and G protein-coupled estrogen receptor 1 (GPER), are crucial for follicle and oocyte growth, development, and ovulation (Tang et al., 2019). Phytoestrogens, natural compounds with significant ER regulatory

TABLE 2 Basic research on traditional Chinese medicine compounds of Rehmanniae Radix.

Recipe	Disease	Animals/ Cells	Dosage	Treatment targets	Mechanisms	Reference
Siwu Decoction	POF	Mice	3.24 g/(kg·d) 12.96 g/(kg·d)	Promoting the production of VEGF and bFGF, and regulating the expression of PDGFB, Ang1, and Ang2	Enhancing ovarian angiogenesis in POF mice, maintaining the stability and maturation of newly formed blood vessels and supporting follicle development	Zhou (2022)
	NR	Rats	1.04 g/(kg·d) 2.08 g/(kg·d)	Upregulating the expression of ERα and ERβ, and reducing the ratio of ERα/ERβ	Exerting estrogen-like effects, increasing uterine tissue weight, and promoting uterine development	Lu et al. (2019)
		Human breast cancer cells MCF7	NR			
	DOR	Rats	5.4 g/(kg·d) 10.8 g/(kg·d)	increasing the abundance of Verrucomicrobia, Epsilonbacteraeota, and Christensenellaceae, and decreasing the abundance of Firmicutes and Bacteroidetes	Influencing intestinal flora, increase in beneficial bacteria, regulating energy metabolism, biological repair, and synthesis, improving ovarian function, and decreasing FSH and LH, increasing E_2	Zhu et al. (2022b)
Liuwei Dihuang Pill	DOR	Rats	1.08 g/(kg·d)	Upregulating the expression of YY1 and downregulating the expression of CYP4F3	Protecting the integrity of the mitochondrial morphology of ovarian granulosa cells, inhibiting oxidative stress, promoting follicle development, Increasing litter size and survival rate of offspring	Gao et al. (2023b)
	ODI	Granulosa cells	NR	Increase in the number of AGNORs	Proliferation of ovarian granulosa cells and promoting follicle development	Yue (2009)
	OP	Rats	0.1575 g/(kg·d)	Downregulating the expression of Caspase-1, IL-1β and TNF-α in the serum and reducing the mRNA expression of NLRP3 and GSDMD in bone tissue	Inhibiting inflammatory factors, alleviating inflammatory response, regulating cell pyroptosis, and resisting osteoporosis	Chen et al. (2023b)
Guishen Pill	DOR	Mice	21.6 g/(kg·d)	Upregulating the expression of ER, PR, MVH, Oct-4 and Egr1	Influencing the secretion of estrogen and AMH in females, improving ovarian function	Cui et al. (2015)
	DOR	Mice	1.4 g/(kg·d) 2.8 g/(kg·d) 5.6 g/(kg·d)	Upregulating the expression of LC3 and Beclin 1, Downregulating the expression of p62 in Ovarian tissue	Reversing the Cyclophosphamide -induced ovarian tissue excessive autophagy state, promoting the dynamic balance of autophagy, improving hormone levels, and restoring ovarian function	Zhu and Du (2023)
	POF	Mice	12 g/(kg·d) 24 g/(kg·d) 48 g/(kg·d)	Increasing IFN-γ and IL-2 levels significantly, elevating the number of $CD3^+$ T cells, $CD4^+$ T cells and NK cells, and raising $CD4^+$ T/$CD8^+$ T ratio	Increasing the spleen index of mice, enhancing the proliferation ability of T cells, regulating the balance of T cell subsets, and improving immune function disorders caused by premature ovarian failure	Li et al. (2018)
	POF	Rats	9.45 g/(kg·d)	Downregulating the expression of RANKL, upregulating the expression of OPG in bone tissue, promoting $CD4^+CD25^+Foxp3^+$Treg cells, and increasing the level of IL-10 and TGF-β in the serum	Inhibiting the differentiation and activity of osteoclasts, improving the bone loss and microstructural damage of femurs in POF rats, and having a therapeutic effect on osteoporosis	Ba et al. (2023)
Yijing Decoction	DOR	Rats	5.9 g/(kg·d) 11.8 g/(kg·d) 23.6 g/(kg·d)	Downregulating the expression of HIF-1α, Bnip3 and Beclin1	Improving the hypoxic state of DOR model rats, reversing the process of cellular autophagy, regulating hormone secretion, and protecting ovarian tissues	Wan and Chen (2022)
	DOR	Rats	11.79 g/(kg·d)	Downregulating the level of TNF-α and IFN-γ, downregulating the expression of SDF-1 and CXCR4, and reducing the proportion of Th17 cells and increasing the proportion of Treg cells	Regulating the Th17 cells/Treg cells balance, alleviating ovarian immune inflammation damage, decreasing the levels of FSH, LH, and IL-17 in serum, increasing the levels of E_2, AMH, and IL-10, and enhancing ovarian index and uterine index	Xie (2021)

(Continued on following page)

TABLE 2 (*Continued*) Basic research on traditional Chinese medicine compounds of Rehmanniae Radix.

Recipe	Disease	Animals/ Cells	Dosage	Treatment targets	Mechanisms	Reference
Kuntai Capsule	POI	Mice	0.4 g/(kg·d) 0.8 g/(kg·d) 1.6 g/(kg·d)	Upregulating the expression of SIRT5 and FOXO3a proteins	Reducing ROS, enhancing antioxidant enzyme activity, regulating mitochondrial oxidative stress, and participating in cell proliferation and the cell cycle	Gong et al. (2024)
	POI	Rats	0.6 g/(kg·d) 1.8 g/(kg·d)	Upregulating the expression of LC3A-II, GDF9 and Beclin-1	Regulating autophagy, inhibiting or partnering with apoptosis, eliminating damaged organelles to adapt to constantly changing internal and external environments, and promoting cell survival by delaying aging and cell death	Luo et al. (2023)
	DOR	Rats	0.21 g/(kg·d) 0.63 g/(kg·d) 1.89 g/(kg·d)	Upregulating the expression of Bcl-2 protein, downregulating the expression of Bax protein, and raising the ratio of Bcl-2 and Bax	Inhibiting the apoptosis of ovarian granulosa cells, delaying aging, downregulating FSH and LH levels, and upregulating E_2 levels	Geng and Tan (2017)

P.S: Not reported (NR); Premature ovarian failure (POF); Premature ovarian insufficiency (POI); Diminished ovarian reserve (DOR); Osteoporosis (OP); Ovulatory disorder infertility (ODI); Reactive oxygen species (ROS); Follicle stimulating hormone (FSH); Luteinizing hormone (LH); Estradiol (E_2); Anti-Müllerian hormone (AMH).

activity, offer alternatives for those unwilling or unable to undergo HRT (Yang et al., 2019). *In vitro* cell studies have shown that serum containing Siwu Decoction exhibits estrogen-like effects, potentially through regulation of ERα and ERβ expression (Lu et al., 2019). Earlier discussions highlighted the findings from Mendelian Randomization (MR) studies on the link between POI and intestinal microbiota. Studies have shown that DOR rats induced by Tripterygium glycosides exhibit reduced intestinal microbiota diversity. Yet, following treatment with Siwu Decoction, there is a significant recovery in the diversity of intestinal microbiota in model rats, with a concurrent increase in beneficial bacteria (Zhu M. et al., 2022).

5.2 Liuwei Dihuang Pill

Liuwei Dihuang Pill comprises six botanical drugs: RRP, Dioscoreae Rhizoma, Corni Fructus, Poria, Alismatis Rhizoma, and Moutan Cortex. This formula is a fundamental TCM preparation for kidney nourishment and yin reinforcement, commonly employed in treating ovarian hypofunction diseases. Clinical trials (Du et al., 2013; Du, 2016; Li et al., 2016; Qin, 2017; Gao, 2021) have demonstrated that combining Liuwei Dihuang Pill with HRT enhances clinical symptoms and sex hormone levels (FSH, LH, E_2) more effectively than HRT alone, without increasing adverse reactions and potentially boosting the therapeutic outcomes. Fundamental research has shown that Liuwei Dihuang Pill promotes the proliferation of human ovarian granulosa cells and follicle maturation, thus facilitating ovulation, making it suitable for treating ovulatory disorders diseases (Yue, 2009). Another study revealed that Liuwei Dihuang Pill protects the mitochondrial integrity of ovarian granulosa cells and ameliorates mitochondrial dysfunction in cyclophosphamide-induced DOR mouse models. This protective effect is achieved by reducing ROS accumulation, mitigating oxidative stress, and thus preventing granulosa cell apoptosis (Gao T. et al., 2023). Subsequent research on these model mice indicated that intervention with Liuwei Dihuang Pill results in a higher number of offspring and pup survival rates compared to the control group. Furthermore, studies on long-term health risks suggest that Liuwei Dihuang Pill may reduce inflammatory responses and regulate bone metabolism via modulation of the NLRP3/Caspase-1/GSDMD pyroptosis signaling pathway, offering potential anti-osteoporosis benefits (Chen ZB. et al., 2023).

5.3 Guishen Pill

The Guishen Pill contains RRP, Dioscoreae Rhizoma, Corni Fructus, Poria, Angelicae Sinensis Radix, Lycii Fructus, Eucommiae Cortex, and Cuscutae Semen. This formula nourishes kidney essence, tonifies blood, and regulates menstruation. Guishen Pill, a TCM formula for tonifying the kidney and benefiting essence, is commonly used to treat ovarian hypofunction. Clinical studies (Du and Fan, 2018; Xu et al., 2020; Hu et al., 2023) indicate that Guishen Pill, when combined with HRT, surpasses HRT alone in enhancing endometrial thickness, ovarian volume, and sex hormone levels in patients with ovarian hypofunction diseases, without exacerbating adverse effects. Oxidative stress damage is a primary aging factor. An experiment (Cui et al., 2015) developed an ovarian aging model in mice through continuous superovulation and ozone inhalation, intensifying oxidative stress and diminishing follicle quality. Post-intervention with Guishen Pill led to increased expression of Oct-4 and MVH mRNA in model mice ($p < 0.05$). Oct-4 is identified with embryonic-like stem cells and ovarian germ cells (Johnson et al., 2005; Virant-Klun, 2015). Research reveals that mice deficient in the MVH gene show arrested differentiation and apoptosis in reproductive cells, marked by reduced Oct-4 expression, resulting in compromised reproductive capacity (Tanaka et al., 2000). Therefore, it can be speculated that Guishen Pill may improve stem cell function by inhibiting oxidative stress, thereby promoting the differentiation of oocyte cells and restoring

TABLE 3 Clinical research on traditional Chinese medicine compounds of Rehmanniae Radix.

Recipe	Author & years	Disease	Samples		Intervention		Duration		Outcomes	Reference
			T	C	T	C	T	C		
Liuwei Dihuang Pill	Gao L 2021	DOR	33	33	Liuwei Dihuang Pill + HRT	HRT	3 months	3 months	FSH, LH, E_2, AMH, AFC, OV	Gao (2021)
	Qin LH 2017	POF	39	39	Liuwei Dihuang Pill + HRT	HRT	3 months	3 months	FSH, LH, E_2	Qin (2017)
	Li Q 2016	POF	61	48	Liuwei Dihuang Pill + HRT	HRT	6 months	6 months	FSH, LH, E_2	Li et al. (2016)
	Du JM 2016	POF	40	40	Liuwei Dihuang Pill + HRT	HRT	3 months	3 months	FSH, LH, E_2	Du (2016)
	Du D 2013	POF	32	30	Liuwei Dihuang Pill + HRT	HRT	3 months	3 months	FSH, LH, E_2	Du et al. (2013)
Guishen Pill	Xu JX 2020	DOR	60	60	Guishen Pill + HRT	HRT	3 months	3 months	FSH, LH, E_2, AFC, OV, Pregnancy rate, PSV, Adverse reaction	Xu et al. (2020)
	Hu XH 2023	POF	43	43	Guishen Pill + HRT	HRT	21 days	21 days	FSH, LH, E_2	Hu et al. (2023)
	Du QM 2018	POF	30	30	Guishen Pill + HRT	HRT	6 months	6 months	FSH, E_2, PSV	Du and Fan (2018)
Yijing Decoction	Li LM 2017	DOR	33	34	Yijing Decoction	HRT	3 months	3 months	FSH, LH, E_2, AMH, AFC, Adverse reaction	Li et al. (2017)
	Zhang JM 2023	POF	48	48	Yijing Decoction + HRT	HRT	6 weeks	6 weeks	FSH, LH, E_2, P, T, PRL	Zhang and Lin (2023)
	Hong YL 2019	POR	33	33	Yijing Decoction + PPOS	PPOS	3 months	-	FSH, E_2, AMH, AFC, Mature follicle rate, Embryo quality rate	Hong et al. (2019)
Kuntai Capsule	Gao P 2019	DOR	40	40	Kuntai Capsule	HRT	9 weeks	3 months	FSH, LH, E_2, PSV	Gao (2019)
	Lin XM 2021	DOR	65	65	Kuntai Capsule	HRT	3 months	3 months	FSH, E_2, AMH, AFC, PSV	Lin et al. (2021)
	Cui N 2018	DOR	33	35	Kuntai Capsule	Dehydroepiandrosterone	3 months	3 months	FSH, LH, E_2, AMH, AFC, Pregnancy rate, Adverse reaction P, T, PRL	Cui et al. (2018)
	Zhou XH 2023	POF	43	43	Kuntai Capsule + HRT	HRT	3 months	3 months	FSH, LH, E_2, AMH, AFC, OV, Endometrial thickness, Adverse reaction	Zhou et al. (2023)
	Jiang LL 2023	POF	43	43	Kuntai Capsule + HRT	HRT	12 weeks	12 weeks	FSH, LH, E_2, AMH, AFC, OV, Treg/%, Th17/%, TGF-β1, IL-21	Jiang et al. (2023b)

P.S: Not reported (NR).

Disease: Premature ovarian failure (POF); Premature ovarian insufficiency (POI); Diminished ovarian reserve (DOR); Poor ovarian response (POR).

Intervention: Hormone replacement therapy (HRT); MPA + Human menopausal gonadotropin (HMG)+ Human chorionic gonadotrophin (HCG)+ GnRH-a (PPOS).

Outcomes: Follicle stimulating hormone (FSH); Luteinizing hormone (LH); Estradiol (E_2); Anti-Müllerian hormone (AMH); Antral follicle count (AFC); Ovarian volume (OV); Peak systolic velocity (PSV); Progesterone (P); Testosterone (T); Prolactin (PRL).

10.3389/fphar.2024.1426972

10.3389/fphar.2024.1426972

TABLE 4 The composition of traditional Chinese medicine compounds containing Rehmanniae Radix Praeparata.

Recipe	Composition			Medicinal part
	Scientific name	Species name	Name in pharmacopeia	
Siwu decoction	Rehmannia glutinosa (Gaertn.) DC	Orobanchaceae	Rehmanniae Radix Praeparata	Dried tuber roots
	Angelica sinensis (Oliv.) Diels	Apiaceae	Angelicae Sinensis Radix	Dried roots
	Paeonia lactiflora Pall	Paeoniaceae	Paeoniae Radix Alba	Dried roots
	Conioselinum anthriscoides 'Chuanxiong'	Apiaceae	Chuanxiong Rhizoma	Dried rhizomes
Liuwei Dihuang Pill	Rehmannia glutinosa (Gaertn.) DC	Orobanchaceae	Rehmanniae Radix Praeparata	Dried tuber roots
	Dioscorea oppositifolia L	Dioscoreaceae	Dioscoreae Rhizoma	Dried rhizomes
	Cornus officinalis Siebold & Zucc	Cornaceae	Corni Fructus	Dried ripe pulp
	Poria cocos (Schw.)Wolf		Poria	Dried sclerotium
	Alisma plantago-aquatica subsp. orientale (Sam.) Sam	Alismataceae	Alismatis Rhizoma	Dried stem tuber
	Paeonia × suffruticosa Andrews	Paeoniaceae	Moutan Cortex	Dried root bark
Guishen Pill	Rehmannia glutinosa (Gaertn.) DC.	Orobanchaceae	Rehmanniae Radix Praeparata	Dried tuber roots
	Dioscorea oppositifolia L	Dioscoreaceae	Dioscoreae Rhizoma	Dried rhizomes
	Cornus officinalis Siebold & Zucc	Cornaceae	Corni Fructus	Dried mature pulp
	Poria cocos (Schw.)Wolf	Polyporaceae	Poria	Dried sclerotium
	Angelica sinensis (Oliv.) Diels	Apiaceae	Angelicae Sinensis Radix	Dried roots
	Lycium barbarum L	Solanaceae	Lycii Fructus	Dried ripe fruit
	Eucommia ulmoides Oliv	Eucommiaceae	Eucommiae Cortex	Dried Bark
	Cuscuta chinensis Lam	Convolvulaceae	Cuscutae Semen	Dried ripe seeds
Yijing decoction	Rehmannia glutinosa (Gaertn.) DC.	Orobanchaceae	Rehmanniae Radix Praeparata	Dried tuber roots
	Atractylodes macrocephala Koidz	Asteraceae	Atractylodis Macrocephalae Rhizoma	Dried rhizomes
	Dioscorea oppositifolia L	Dioscoreaceae	Dioscoreae Rhizoma	Dried rhizomes
	Angelica sinensis (Oliv.) Diels	Apiaceae	Angelicae Sinensis Radix	Dried roots
	Paeonia lactiflora Pall	Paeoniaceae	Paeoniae Radix Alba	Dried roots
	Ziziphus jujuba Mill	Rhamnaceae	Jujubae Fructus	Dried ripe fruit
	Paeonia × suffruticosa Andrews	Paeoniaceae	Moutan Cortex	Dried root bark
	Adenophora triphylla (Thunb.) A.DC	Campanulaceae	Adenophorae Radix	Dried roots
	Bupleurum chinense DC	Apiaceae	Bupleuri Radix	Dried roots
	Eucommia ulmoides Oliv	Eucommiaceae	Eucommiae Cortex	Dried Bark
	Panax ginseng C.A.Mey	Araliaceae	Ginseng Radix Et Rhizoma	Dried roots and rhizomes
Kuntai Capsule	Rehmannia glutinosa (Gaertn.) DC	Orobanchaceae	Rehmanniae Radix Praeparata	Dried tuber roots
	Coptis chinensis Franch	Ranunculaceae	Coptidis Rhizoma	Dried rhizomes
	Paeonia lactiflora Pall	Paeoniaceae	Paeoniae Radix Alba	Dried roots
	Scutellaria baicalensis Georgi	Lamiaceae	Scutellariae Radix	Dried roots

(Continued on following page)

TABLE 4 (*Continued*) The composition of traditional Chinese medicine compounds containing Rehmanniae Radix Praeparata.

Recipe	Composition			Medicinal part
	Scientific name	Species name	Name in pharmacopeia	
	Equus asinusl	Equine	Asini Corii Colla	Dried donkey skin or fresh skin by boiling, concentrated into a solid glue
	Poria cocos (Schw.)Wolf	polyporaceae	Poria	Dried sclerotium

PS: The "Scientific name" and "Species name" in the table were retrieved from the "Medicinal Plant Names Services" website (https://mpns.science.kew.org/mpns-portal); "Name in pharmacopeia" was retrieved from *National Pharmacopoeia Committee. Pharmacopoeia of the People's Republic of China: Volume I.* among them, the appropriate "Scientific names" and "Species name" of Poria and Asini Corii Colla could not be retrieved from the website and were searched from the pharmacopoeia instead.

ovarian function in mice. Additionally, animal experiments have demonstrated that Guishen Pill can reduce the protein and mRNA levels of LC3 and Beclin 1 in the ovarian tissues of DOR mice, increase the levels of p62 protein and mRNA, and improve ovarian function by inhibiting ovarian autophagy (Zhu and Du, 2023). Meanwhile, in studying the immune mechanisms in ovarian premature aging model mice, it was found that Guishen Pill could significantly increase the spleen index, enhance the proliferation ability of T cells, significantly increase the ratio of $CD3^+T$, $CD4^+T$, $CD4^+T/CD8^+T$, NK cells, IFN-γ and IL-2 in mice ($p < 0.05$), and significantly decrease the percentage of $CD8^+$ T cells ($p < 0.05$) (Li et al., 2018). Moreover, Guishen Pill can also improve bone mass and reduce microstructural damage in the femurs of rats with POF, thereby achieving its potential in treating osteoporosis (Ba et al., 2023).

5.4 Yijing decoction

Yijing Decoction, derived from *Fu Qingzhu's Obstetrics and Gynecology*, contains eleven medicinal ingredients: RRP, Atractylodis Macrocephalae Rhizoma, Dioscoreae Rhizoma, Angelicae Sinensis Radix, Paeoniae Radix Alba, Jujubae Fructus, Moutan Cortex, Adenophorae Radix, Bupleuri Radix, Eucommiae Cortex and Ginseng Radix Et Rhizoma. The book employs this formula to treat patients who appear amenorrhea before age 49″, which aligns with the characteristics of ovarian hypofunction diseases. Subsequent clinical studies (Li et al., 2017; Zhang and Lin, 2023) demonstrate that Yijing Decoction improves clinical symptoms and sex hormone levels of patients with ovarian hypofunction diseases, thus enhancing pregnancy outcomes. For older patients with diminished ovarian reserve undergoing IVF-ET, Yijing Decoction, used alongside controlled ovarian stimulation protocols, significantly increases the number of retrieved ova, maturity of ova, and quality of embryos, improving ovarian responsiveness and oocytes and embryo quality (Hong et al., 2019). Experimental research (Wan and Chen, 2022) shows that Yijing Decoction counteracts hypoxia-induced activation of the Bnip3/Beclin1 pathway, thereby reducing autophagy-induced damage to ovarian tissue. The SDF-1 (stromal cell-derived factor-1)/CXCR4 axis is pivotal in embryonic development and enhances vascular regeneration and the resolution of ischemic conditions in injured tissues. SDF-1 also serves as a crucial cytokine in the regulation of local inflammation and tissue repair (Cencioni et al., 2012). Research on Yijing Decoction has demonstrated that this formula can modulate the Th17/Treg balance through the SDF-1/CXCR4 pathway, decreasing IL-17 and increasing IL-10 levels. This mechanism alters the immune-inflammatory microenvironment, thereby affecting ovarian function in cyclophosphamide-induced DOR model rats (Xie, 2021).

5.5 Kuntai capsule

Kuntai capsule, derived from the HuangLian-EJiao decoction in the *Treatise on Febrile Diseases*, consist of RRP, Coptidis Rhizoma, Paeoniae Radix Alba, Scutellariae Radix, Asini Corii Colla, and Poria. The efficacy and safety has been confirmed through numerous clinical trials (Cui et al., 2018; Gao, 2019; Lin et al., 2021; Zhou et al., 2023) and systematic reviews (Shen et al., 2020; A RN et al., 2019; Zhang et al., 2024; Liu et al., 2021). A study (Gong et al., 2024) identified that a primary target of Kuntai capsule in treating POF model mice is the regulation of oxidative stress damage, primarily through the FOXO3 and SIRT5 genes. The AGE-RAGE signaling pathway plays a crucial role in managing oxidative stress and inflammation (Shi et al., 2023), and Kuntai capsule may enhance ovarian function by promoting follicular development and increasing the granulosa cell layer thickness in dominant follicles via this pathway (Huang et al., 2024). Further research (Luo et al., 2023) suggests that Kuntai capsule also boosts the expression of GDF9, a key TGF-β family member vital for granulosa cell proliferation and follicular growth. They also found that Kuntai capsule can upregulate the expression of Beclin 1, mediate cell autophagy, delay delayed cell senescence and cell death to promote cell survival. Regarding apoptosis, Kuntai capsule has been found to maintain the balance between pro-apoptotic and inhibitory proteins by adjusting the Bcl-2/Bax ratio, specifically by upregulating Bcl-2 and downregulating Bax expression, thus regulating apoptosis of ovarian granulosa cells to improve ovarian reserve function and delay aging (Geng and Tan, 2017). Moreover, the imbalance of the Th17/Treg cell ratio, a significant factor in immune disorders, is corrected in patients with ovarian hypofunction. Clinical studies have shown that Kuntai capsule increases TGF-β1 levels in the peripheral blood of POF patients, reduces IL-21 levels, and corrects the Th17/Treg cell ratio imbalance, thereby regulating the autoimmune system (Jiang LL. et al., 2023).

6 Limitations and future research prospects

Processing plays a critical role in influencing the pharmacological characteristics and effectiveness of botanical drugs. Various processing techniques can have diverse impacts on the bioactive compounds of herbal medicines, leading to modifications in their physiological effects. Consequently, the selection of an appropriate processing method to effectively manipulate the pharmacological properties of botanical drugs is essential for clinical applications. Nevertheless, regional disparities exist in the preparation methods of RRP in different regions. For example, regarding the processing method of prepared RRP, Zhu XD et al. (Zhu et al., 2023) used the "Jiangxi Provincial Standard for the Processing of Chinese Medicinal Slices (2008 Edition)," Chen QY et al. (Chen et al., 2021) used the "Jianchang Bang Processing Technique," and Tian JY et al. (Tian et al., 2022) used the Beijing 2008 edition of the Drug Processing Specification. Some experiments even opted for purchasing RRP (Zhang et al., 2016). Furthermore, inconsistencies exist in the inclusion of excipients during RR steaming processes. For instance, Chen SQ et al. (Chen SQ. et al., 2023) utilized plain water for steaming RR, whereas Ma YJ et al. (Ma et al., 2023) employed yellow rice wine in the steaming process. These variations present difficulties in conducting quantitative analysis. In terms of compound analysis, the 2020 edition of the Pharmacopoeia of the People's Republic of China only provides concentration specifications for catalpol and rehmannioside D in RRP and RR, without establishing concentration limits for other potentially bioactive compounds. Moreover, investigations into the use of RRP for conditions associated with ovarian hypofunction predominantly rely on findings from *in vitro* and *in vivo* studies, with limited incorporation of clinical research data. Clinical trials utilizing traditional Chinese medicine compounds containing RRP as the key component often exhibit small sample sizes, potentially compromising the applicability of their findings. Furthermore, the absence of blinding in many clinical studies, as well as their restricted focus on Asian populations, may introduce bias into the research outcomes.

Hence, it is imperative to enhance the following facets in forthcoming research: 1) standardizing and unifying the processing methods of RR and the addition of excipients, investigating the changes in RR compounds after adding excipients, and optimizing the storage conditions of botanical drugs according to the characteristics of processed products to guarantee their stability. 2) Conducting clinical research on the efficacious compounds of RRP for ovarian hypofunction involves integrating both basic and clinical research methodologies to substantiate their efficacy and safety, elucidating their scientific implications and mechanisms, and potentially developing RRP as pharmaceutical agents for the treatment of ovarian hypofunction. 3) Standardizing the clinical research design of traditional Chinese medicine compounds containing RRP aims to furnish high-quality evidence-based data for clinical application.

Author contributions

H-ZZ: Conceptualization, Data curation, Investigation, Methodology, Validation, Writing–original draft. JM: Data curation, Investigation, Methodology, Software, Writing–original draft. Y-XL: Data curation, Investigation, Software, Writing–original draft. M-YL: Conceptualization, Methodology, Supervision, Writing–review and editing. S-BW: Methodology, Project administration, Resources, Writing–review and editing.

Funding

The author(s) declare that financial support was received for the research, authorship, and/or publication of this article. The work were supported by the Group Standard Project of Chinese Association of Chinese Medicine (Project No: 20211220-BZ-CACM); The National Celebrated Traditional Chinese Medicine Expert Inheritance Studio of S-BW (Project No: CJJ2023062). Based on real-world research explored the efficacy and mechanism of the regulation of the P38MAPK/P53/P21 signaling pathway mediating Th1/Th2 cell homeostasis in the treatment of POI (Project No: MPRC2023009).

Conflict of interest

The authors declare that the research was conducted in the absence of any commercial or financial relationships that could be construed as a potential conflict of interest.

Publisher's note

References

An, R., Wang, X., Yang, L., Zhang, J., Wang, N., Xu, F., et al. (2021). Polystyrene microplastics cause granulosa cells apoptosis and fibrosis in ovary through oxidative stress in rats. *Toxicology* 449, 152665. doi:10.1016/j.tox.2020.152665

A Rn, L. Y. Y., Li, S. C., and Xu, L. Z. (2019). Meta-analysis of the efficacy and safety of Kuntai capsule in the treatment of early-onset ovarian insufficiency. *Chin. J. Evidence-Based Med.* 08, 953–959.

Ba, X., Chen, Z., Huang, Y., Tu, S. H., and Wang, Y. (2023). The effect of Guishen Pill on bone mineral density and bone microstructure in rats with premature ovarian failure and its mechanism. *Chin. J. Osteoporos.* 03, 390–396.

Bai, L., Shi, G. Y., Yang, Y. J., Chen, W., Zhang, L. F., and Qin, C. (2018). Rehmannia glutinosa exhibits anti-aging effect through maintaining the quiescence and decreasing the senescence of hematopoietic stem cells. *Anim. Model Exp. Med.* 1 (3), 194–202. doi:10.1002/ame2.12034

Baird, L., and Yamamoto, M. (2020). The molecular mechanisms regulating the KEAP1-NRF2 pathway. *Mol. Cell. Biol.* 40 (13), e00099-20. doi:10.1128/MCB.00099-20

Boots, C. E., and Jungheim, E. S. (2015). Inflammation and human ovarian follicular dynamics. *Seminars reproductive Med.* 33 (4), 270–275. doi:10.1055/s-0035-1554928

Bourassa, P. A., Milos, P. M., Gaynor, B. J., Breslow, J. L., and Aiello, R. J. (1996). Estrogen reduces atherosclerotic lesion development in apolipoprotein E-deficient mice. *Proc. Natl. Acad. Sci. U. S. A.* 93 (19), 10022–10027. doi:10.1073/pnas.93.19.10022

Brown, H. M., and Russell, D. L. (2014). Blood and lymphatic vasculature in the ovary: development, function and disease. *Hum. Reprod. update* 20 (1), 29–39. doi:10.1093/humupd/dmt049

Bushnell, C., McCullough, L. D., Awad, I. A., Chireau, M. V., Fedder, W. N., Furie, K. L., et al. (2014). Guidelines for the prevention of stroke in women: a statement for healthcare professionals from the American Heart Association/American Stroke Association. *Stroke* 45 (5), 1545–1588. doi:10.1161/01.str.0000442009.06663.48

Canonico, M., Plu-Bureau, G., O'Sullivan, M. J., Stefanick, M. L., Cochrane, B., Scarabin, P. Y., et al. (2014). Age at menopause, reproductive history, and venous thromboembolism risk among postmenopausal women: the Women's Health Initiative Hormone Therapy clinical trials. *Menopause* 21 (3), 214–220. doi:10.1097/GME.0b013e31829752e0

Casarini, L., and Crépieux, P. (2019). Molecular mechanisms of action of FSH. *Front. Endocrinol.* 10, 305. doi:10.3389/fendo.2019.00305

Cencioni, C., Capogrossi, M. C., and Napolitano, M. (2012). The SDF-1/CXCR4 axis in stem cell preconditioning. *Cardiovasc. Res.* 94 (3), 400–407. doi:10.1093/cvr/cvs132

Chen, Q. Y., Wang, X. P., Lei, X., Gao, Y. Z., Xu, J., Wang, L. F., et al. (2021). Effects of Amomi Fructus and Citri Reticulatae Pericarpium on chemical composition in Rehmanniae Radix and Rehmanniae Radix Praeparata. *Chin. Traditional Herb. Drugs* 20, 6168–6177.

Chen, S. Q., Yang, K. P., Kang, W. L., Zhou, Y. C., Tao, S. M., Guan, Y. C., et al. (2023a). Study on concoction and detection of active components and Trace elements of Radix Rehmanniae Praeparata. *Analysis Test. Technol. Instrum.* 04, 392–399. doi:10.16495/j.1006-3757.2023.04.008

Chen, Z. B., Zhao, J. L., Hong, S. H., and Tang, H. Y. (2023b). Role of the signal axis of NLRP3/Caspase-1/GSDMD for preventing and treating osteoporosis by Liuwei Dihuang Pill decoction in rats. *Chin. J. Osteoporos. Bone Mineral Res.* 06, 559–567.

Chen, Z. J., Tian, Q. J., Qiao, J., Liu, J. Y., Yang, D. Z., Huang, H. F., et al. (2017). Chinese expert consensus on premature ovarian insufficiency. *Chin. J. Obstetrics Gynecol.* 52 (9), 577–581. doi:10.3760/cma.j.issn.0529-567X.2017.09.001

Clarkson, T. B. (2018). Estrogen effects on arteries vary with stage of reproductive life and extent of subclinical atherosclerosis progression. *Menopause* 25 (11), 1262–1274. doi:10.1097/GME.0000000000001228

Cui, D. D., Ma, W. W., Wen, L., Song, K. K., Ding, J. H., Huang, C., et al. (2015). Effect of guishen pill on expression levels of oct-4, MVH, and egr-1 in mice with diminished ovarian reserve. *Chin. J. Integr. Traditional West. Med.* 01, 76–80.

Cui, N., Jiang, L., Yang, A. M., Zhang, J., Xu, Y. M., Wang, W., et al. (2018). Clinical observation of Kuntai jiaonang in treating 33 patients with hypofunction of ovarian reserve infertility. *J. Traditional Chin. Med.* 02, 132–136. doi:10.13288/j.11-2166/r.2018.02.011

Daan, N. M., Muka, T., Koster, M. P., Roeters van Lennep, J. E., Lambalk, C. B., Laven, J. S. E., et al. (2016). Cardiovascular risk in women with premature ovarian insufficiency compared to premenopausal women at middle age. *J. Clin. Endocrinol. metabolism* 101 (9), 3306–3315. doi:10.1210/jc.2016-1141

Danilovich, N., and Sairam, M. R. (2002). Haploinsufficiency of the follicle-stimulating hormone receptor accelerates oocyte loss inducing early reproductive senescence and biological aging in mice. *Biol. reproduction* 67 (2), 361–369. doi:10.1095/biolreprod67.2.361

Djiogue, S., Djiyou Djeuda, A. B., Seke Etet, P. F., Ketcha Wanda, G. J. M., Djikem Tadah, R. N., and Njamen, D. (2018). Memory and exploratory behavior impairment in ovariectomized Wistar rats. *Behav. Brain Funct.* 14 (1), 14. doi:10.1186/s12993-018-0146-7

Domniz, N., and Meirow, D. (2019). Premature ovarian insufficiency and autoimmune diseases. *Clin. obstetrics Gynaecol.* 60, 42–55. doi:10.1016/j.bpobgyn.2019.07.008

Du, D., Wei, J. L., and Chen, M. Y. (2013). Clinical study of Liuwei Dihuang pills combined with hormone replacement in the treatment of premature ovarian failure. *Chin. Archives Traditional Chin. Med.* 12, 2738–2740. doi:10.13193/j.issn.1673-7717.2013.12.047

Du, J. M. (2016). Clinical observation of hormone therapy combined with Liuwei Dihuang pills in the replacement treatment of premature ovarian failure. *Shenzhen J. Integr. Traditional Chin. West. Med.* 04, 51–53. doi:10.16458/j.cnki.1007-0893.2016.04.025

Du, Q. M., and Fan, L. S. (2018). Clinical study of 60 cases of premature ovarian failure treated with guishen pill combined with sequential estrogen and progesterone therapy. *Jiangsu J. Traditional Chin. Med.* 07, 39–41.

Du, X., Zhang, L., Li, X., Pan, Z., Liu, H., and Li, Q. (2016). TGF-β signaling controls FSHR signaling-reduced ovarian granulosa cell apoptosis through the SMAD4/miR-143 axis. *Cell death Dis.* 7 (11), e2476. doi:10.1038/cddis.2016.379

Ewertz, M., Mellemkjaer, L., Poulsen, A. H., Friis, S., Sørensen, H. T., Pedersen, L., et al. (2005). Hormone use for menopausal symptoms and risk of breast cancer. A Danish cohort study. *Br. J. cancer* 92 (7), 1293–1297. doi:10.1038/sj.bjc.6602472

Feng, J. C., Cai, Z. L., Zhang, X. P., Chen, Y. Y., Chang, X. L., Wang, X. F., et al. (2020). The effects of oral rehmannia glutinosa polysaccharide administration on immune responses, antioxidant activity and resistance against aeromonas hydrophila in the common carp, *Cyprinus carpio* L. *Front. Immunol.* 11, 904. doi:10.3389/fimmu.2020.00904

Freitas, C., Neto, A. C., Matos, L., Silva, E., Ribeiro, Â., Silva-Carvalho, J. L., et al. (2017). Follicular Fluid redox involvement for ovarian follicle growth. *J. ovarian Res.* 10 (1), 44. doi:10.1186/s13048-017-0342-3

Fu, C., Wu, Y., Liu, S., Luo, C., Lu, Y., Liu, M., et al. (2022). Rehmannioside A improves cognitive impairment and alleviates ferroptosis via activating PI3K/AKT/Nrf2 and SLC7A11/GPX4 signaling pathway after ischemia. *J. Ethnopharmacol.* 289, 115021. doi:10.1016/j.jep.2022.115021

Gao, G. Z., Zhou, J. W., Wang, H. Q., Rao, P. F., and Ke, L. J. (2010). Analysis of amino acids in rehmannia glutinosa Libosch during heating process. *Biot. Resour.* 03, 52–54. doi:10.14188/j.ajsh.2010.03.022

Gao, L. (2021). *Clinical observation of Liuwei Dihuang Pill combined with Fenmotong in the treatment of decreased ovarian reserve function with Kidney-yin deficiency*. Gansu University Of Chinese Medicine. doi:10.27026/d.cnki.ggszc.2021.000118

Gao, P. (2019). Effect of Kuntai capsule on reproductive endocrine and ovarian blood supply in patients with ovarian reserve deficiency. *Maternal Child Health Care China* 09, 2080–2083.

Gao, T., Zhong, J. W., Qin, L., Wang, X. Y., Li, X. R., and Luo, Y. X. (2023b). Based on proteomics technology, the mechanism of action of Liuwei Dihuang pill in the treatment of mice with diminished ovarian reserve was explored. *China J. Chin. Materia Medica* 12, 3224–3234. doi:10.19540/j.cnki.cjcmm.20230202.704

Gao, X., Wang, B., Huang, Y., Wu, M., Li, Y., Li, Y., et al. (2023a). Role of the Nrf2 signaling pathway in ovarian aging: potential mechanism and protective strategies. *Int. J. Mol. Sci.* 24 (17), 13327. doi:10.3390/ijms241713327

Geng, L. H., and Tan, Y. (2017). Effect of Kuntai capsule on the expression of ovarian apoptosis regulatory proteins Bcl-2 and Bax in rats with decreased ovarian reserve. *Chin. J. Exp. Traditional Med. Formulae* 08, 138–143. doi:10.13422/j.cnki.syfjx.2017080138

Gibbs, R. B. (2010). Estrogen therapy and cognition: a review of the cholinergic hypothesis. *Endocr. Rev.* 31 (2), 224–253. doi:10.1210/er.2009-0036

Gong, L., Hou, J., Yang, H., Zhang, X., Zhao, J., Wang, L., et al. (2024). Kuntai capsule attenuates premature ovarian insufficiency by activating the FOXO3/SIRT5 signaling pathway in mice: a comprehensive study using UHPLC-LTQ-Orbitrap and integrated pharmacology. *J. Ethnopharmacol.* 322, 117625. doi:10.1016/j.jep.2023.117625

Gong, R. Z., Huo, X. H., Zhang, L., Liu, C., Li, S. S., and Sun, Y. S. (2019). Advances in effects and regulation of Maillard reaction on quality of Chinese materia medica. *Chin. Traditional Herb. Drugs* 01, 243–251.

Gu, H., Zhao, X., Zhao, X., Yang, Y., and Lv, X. (2014). Risk of stroke in healthy postmenopausal women during and after hormone therapy: a meta-analysis. *Menopause* 21 (11), 1204–1210. doi:10.1097/GME.0000000000000227

Gu, M., Yuan, Y. P., Qin, Z. N., Xu, Y., Shi, N. N., Wang, Y. P., et al. (2021). A combined quality evaluation method that integrates chemical constituents, appearance traits and origins of raw Rehmanniae Radix pieces. *Chin. J. Nat. Med.* 19 (7), 551–560. doi:10.1016/S1875-5364(21)60056-0

Han, K., Bose, S., Kim, Y. M., Chin, Y. W., Kim, B. S., Wang, J. h., et al. (2015). Rehmannia glutinosa reduced waist circumferences of Korean obese women possibly through modulation of gut microbiota. *Food and Funct.* 6 (8), 2684–2692. doi:10.1039/c5fo00232j

Han, Y., Jung, H. W., Lee, J. Y., Kim, J. S., Kang, S. S., Kim, Y. S., et al. (2012). 2,5-dihydroxyacetophenone isolated from Rehmanniae Radix Preparata inhibits inflammatory responses in lipopolysaccharide-stimulated RAW264.7 macrophages. *J. Med. food* 15 (6), 505–510. doi:10.1089/jmf.2011.1940

Harman, D. (1956). Aging: a theory based on free radical and radiation chemistry. *J. Gerontol.* 11 (3), 298–300. doi:10.1093/geronj/11.3.298

Harman, D. (2006). Free radical theory of aging: an update: increasing the functional life span. *Ann. N. Y. Acad. Sci.* 1067, 10–21. doi:10.1196/annals.1354.003

Heinrich, M., Yao, R., and Xiao, P. (2021). 'Food and medicine continuum' - why we should promote cross-cultural communication between the global East and West. *Chin. Herb. Med.* 14 (1), 3–4. doi:10.1016/j.chmed.2021.12.002

Hong, Y. L., Tan, Y., Yin, Y. Y., and Chen, J. (2019). Application of Yijing Decoction combined with PPOS program in IVF-ET for elderly women. *China J. Traditional Chin. Med. Pharm.* 07, 3315–3319.

Hsieh, Y. T., and Ho, J. Y. P. (2021). Thyroid autoimmunity is associated with higher risk of premature ovarian insufficiency-a nationwide Health Insurance Research Database study. *Hum. Reprod. Oxf. Engl.* 36 (6), 1621–1629. doi:10.1093/humrep/deab025

Hsueh, A. J., McGee, E. A., Hayashi, M., and Hsu, S. Y. (2000). Hormonal regulation of early follicle development in the rat ovary. *Mol. Cell. Endocrinol.* 163 (1-2), 95–100. doi:10.1016/s0303-7207(99)00245-2

Hu, H., Wang, C., Jin, Y., Meng, Q., Liu, Q., Liu, Z., et al. (2019). Catalpol inhibits homocysteine-induced oxidation and inflammation via inhibiting Nox4/NF-κB and GRP78/PERK pathways in human aorta endothelial cells. *Inflammation* 42 (1), 64–80. doi:10.1007/s10753-018-0873-9

Hu, X. H., Lin, Q., and Hu, Y. H. (2023). Effect of guishen pill combined with climen on premature ovarian failure and its effect on ovarian function. *Liaoning J. Traditional Chin. Med.* 04, 97–100. doi:10.13192/j.issn.1000-1719.2023.04.027

Huang, J. G., Zhang, J., Xiang, R. J., Wu, Y. Y., He, T. Y., Zhao, M. N., et al. (2024). Mechanism of Kuntai Capsules in treatment of polycystic ovary syndrome rat models based on AGE-RAGE signal pathway. *China J. Chin. Materia Medica* 04, 1082–1090. doi:10.19540/j.cnki.cjcmm.20231115.501

Huang, Y., Hu, C., Ye, H., Luo, R., Fu, X., Li, X., et al. (2019). Inflamm-aging: a new mechanism affecting premature ovarian insufficiency. *J. Immunol. Res.* 2019, 8069898. doi:10.1155/2019/8069898

Huang, Y., Jiang, C., Hu, Y., Zhao, X., Shi, C., Yu, Y., et al. (2013). Immunoenhancement effect of rehmannia glutinosa polysaccharide on lymphocyte proliferation and dendritic cell. *Carbohydr. Polym.* 96 (2), 516–521. doi:10.1016/j.carbpol.2013.04.018

Huang, Y., Liu, Z., Bo, R., Xing, J., Luo, L., Zhen, S., et al. (2016b). The enhanced immune response of PCV-2 vaccine using Rehmannia glutinosa polysaccharide liposome as an adjuvant. *Int. J. Biol. Macromol.* 86, 929–936. doi:10.1016/j.ijbiomac.2016.02.003

Huang, Y., Nan, L., Xiao, C., Su, F., Li, K., Ji, Q. A., et al. (2021). PEGylated nano-Rehmannia glutinosa polysaccharide induces potent adaptive immunity against Bordetella bronchiseptica. *Int. J. Biol. Macromol.* 168, 507–517. doi:10.1016/j.ijbiomac.2020.12.044

Huang, Y., Qin, T., Huang, Y., Liu, Z., Bo, R., Hu, Y., et al. (2016a). Rehmannia glutinosa polysaccharide liposome as a novel strategy for stimulating an efficient immune response and their effects on dendritic cells. *Int. J. nanomedicine* 11, 6795–6808. doi:10.2147/IJN.S119108

Hunzicker-Dunn, M., and Maizels, E. T. (2006). FSH signaling pathways in immature granulosa cells that regulate target gene expression: branching out from protein kinase A. *Cell. Signal.* 18 (9), 1351–1359. doi:10.1016/j.cellsig.2006.02.011

Jia, H., Zhang, W. F., Lei, J. W., Li, Y. Y., Yang, C. J., and Fan, K. F. (2023). UV combined with MIR spectroscopy to discuss the dynamic changes of sugar during the processing of Rehmannia glutinosa. *Lishizhen Med. Materia Medica Res.* 01, 96–99.

Jiang, L. L., Tang, W. C., Kang, X. Y., Xue, L. L., Qin, J. R., Guo, Z. G., et al. (2023b). The efficacy of Kuntai capsule combined with estrogen and progesterone replacement therapy on premature ovarian failure and its effects on Treg, Th17 and VEGF. *J. Chin. Med. Mater.* 09, 2336–2340. doi:10.13863/j.issn1001-4454.2023.09.039

Jiang, Y., Luan, Y. G., Huang, R., He, X. J., Wang, X., and Tan, P. (2023a). Comparative analysis of characters and components of wine-stewed and steamed Rehmanniae Radix with different processing degrees. *Mod. Chin. Med.* 09, 1957–1965. doi:10.13313/j.issn.1673-4890.20230104006

Johnson, J., Bagley, J., Skaznik-Wikiel, M., Lee, H. J., Adams, G. B., Niikura, Y., et al. (2005). Oocyte generation in adult mammalian ovaries by putative germ cells in bone marrow and peripheral blood. *Cell* 122 (2), 303–315. doi:10.1016/j.cell.2005.06.031

Kirshenbaum, M., and Orvieto, R. (2019). Premature ovarian insufficiency (POI) and autoimmunity-an update appraisal. *J. assisted reproduction Genet.* 36 (11), 2207–2215. doi:10.1007/s10815-019-01572-0

Kranc, W., Brązert, M., Ożegowska, K., Nawrocki, M. J., Budna, J., Celichowski, P., et al. (2017). Expression profile of genes regulating steroid biosynthesis and metabolism in human ovarian granulosa cells-A primary culture approach. *Int. J. Mol. Sci.* 18 (12), 2673. doi:10.3390/ijms18122673

Kwon, Y., Yu, S., Choi, G. S., Kim, J. H., Baik, M., Su, S. T., et al. (2019). Puffing of Rehmannia glutinosa enhances anti-oxidant capacity and down-regulates IL-6 production in RAW 264.7 cells. *Food Sci. Biotechnol.* 28 (4), 1235–1240. doi:10.1007/s10068-019-00566-z

Lee, S. Y., Lee, K. S., Yi, S. H., Kook, S. H., and Lee, J. C. (2013). Acteoside suppresses RANKL-mediated osteoclastogenesis by inhibiting c-Fos induction and NF-κB pathway and attenuating ROS production. *PloS one* 8 (12), e80873. doi:10.1371/journal.pone.0080873

Leridon, H. (2004). Can assisted reproduction technology compensate for the natural decline in fertility with age? A model assessment. *Hum. Reprod. Oxf. Engl.* 19 (7), 1548–1553. doi:10.1093/humrep/deh304

Lewis, K. N., Wason, E., Edrey, Y. H., Kristan, D. M., Nevo, E., and Buffenstein, R. (2015). Regulation of Nrf2 signaling and longevity in naturally long-lived rodents. *Proc. Natl. Acad. Sci. U. S. A.* 112 (12), 3722–3727. doi:10.1073/pnas.1417566112

Li, D., Guo, H., Niu, L., Yin, Q., Zhang, Y., and Zhuang, P. (2023b). Clinical value-oriented research paradigm about inheritance and innovation development of TCM dominant diseases. *Chin. Herb. Med.* 15 (4), 476–484. doi:10.1016/j.chmed.2023.09.002

Li, L. H., Li, Z. C., and Hong, W. T. (2018). Effect of guishen pill on cellular immunity in mice with premature ovarian failure. *Chin. J. Immunol.* 08, 1178–1182.

Li, L. M., He, X. K., Tao, L. L., Sun, D. M., Chen, Y. X., Chen, X. P., et al. (2017). A clinical study on the improvement of ovarian function in patients with kidney deficiency and liver stagnation syndrome in the treat of Yijing Decoction. *Lishizhen Med. Materia Medica Res.* 12, 2943–2945.

Li, M., Zhu, Y., Wei, J., Chen, L., Chen, S., and Lai, D. (2023a). The global prevalence of premature ovarian insufficiency: a systematic review and meta-analysis. *Climacteric J. Int. Menopause Soc.* 26 (2), 95–102. doi:10.1080/13697137.2022.2153033

Li, Q., Tang, J. S., Qiu, S., Zhang, L. H., Luo, H. Y., Qiu, M., et al. (2016). The clinical effect of drug combination by Liuwei Dihuang pills and climen in treatment of POF. *Hebei Med.* 02, 339–341.

Li, X., Gui, R., Wang, X., Ning, E., Zhang, L., Fan, Y., et al. (2023c). Oligosaccharides isolated from Rehmannia glutinosa protect LPS-induced intestinal inflammation and barrier injury in mice. *Front. Nutr.* 10, 1139006. doi:10.3389/fnut.2023.1139006

Li, X., Xing, Y. D., Li, S. S., and Liu, H. (2020). Effect of different processing methods on the contents of seven chemical components in Rehmanniae Radix Preparata. *J. Bengbu Med. Coll.* 05, 634–637. doi:10.13898/j.cnki.issn.1000-2200.2020.05.021

Liang, J., Gao, Y., Feng, Z., Zhang, B., Na, Z., and Li, D. (2023a). Reactive oxygen species and ovarian diseases: antioxidant strategies. *Redox Biol.* 62, 102659. doi:10.1016/j.redox.2023.102659

Liang, L., Yue, Y., Zhong, L., Liang, Y., Shi, R., Luo, R., et al. (2023b). Anti-aging activities of Rehmannia glutinosa Libosch. crude polysaccharide in *Caenorhabditis elegans* based on gut microbiota and metabonomic analysis. *Int. J. Biol. Macromol.* 253 (8), 127647. doi:10.1016/j.ijbiomac.2023.127647

Lim, D. W., and Kim, Y. T. (2013). Dried root of Rehmannia glutinosa prevents bone loss in ovariectomized rats. *Mol. Basel. Switz.* 18 (5), 5804–5813. doi:10.3390/molecules18055804

Lin, C., Lu, Y., Yan, X., Wu, X., Kuai, M., Sun, X., et al. (2017). Catalpol protects glucose-deprived rat embryonic cardiac cells by inducing mitophagy and modulating estrogen receptor. *Biomed. Pharmacother. = Biomedecine Pharmacother.* 89, 973–982. doi:10.1016/j.biopha.2017.02.069

Lin, H., Gui, S. H., Yu, B. B., Que, X. H., and Zhu, J. Q. (2019). Analysis of polysaccharide monosaccharides of Radix Rehmanniae by different processing processes and their effects on ovarian granulosa cells. *Chin. Tradit. Pat. Med.* 12, 2958–2963.

Lin, X. M., Chen, M., Wang, Q. L., Ye, X. M., and Chen, H. F. (2021). Clinical observation of Kuntai capsule combined with Fenmotong in treatment of decline of ovarian reserve function. *World J. Clin. Cases* 6 (28), 8349–8357. doi:10.12998/wjcc.v9.i28.8349

Liu, L. Y., Ji, Y. H., Wang, G. L. F., Huang, Y., and Zeng, Z. J. (2023). Study on the characteristic specturm and color change of steamed Rehmanniae Radix preparata and optimization of processing technology. *J. Nanjing Univ. Traditional Chin. Med.* 08, 764–774. doi:10.14148/j.issn.1672-0482.2023.0764

Liu, W., Nguyen, T. N., Tran Thi, T. V., and Zhou, S. (2021). Corrigendum to "Kuntai capsule plus hormone therapy vs. Hormone therapy alone in patients with premature ovarian failure: a systematic review and meta-analysis". *Evid. Based Complement. Altern. Med.* 2021, 5737914. Erratum for: Evid Based Complement Alternat Med. 2019 Jun 26;2019:2085804. PMID: 33603817; PMCID: PMC7872766. doi:10.1155/2021/5737914

Liu, Y., Tang, Q., Shao, S., Chen, Y., Chen, W., and Xu, X. (2017). Lyophilized powder of catalpol and puerarin protected cerebral vessels from ischemia by its anti-apoptosis on endothelial cells. *Int. J. Biol. Sci.* 13 (3), 327–338. doi:10.7150/ijbs.17751

Liu, Z., Dai, L., Sun, T., Liu, Y., Bao, Y., Gu, M., et al. (2024). Massively parallel CRISPR-cas9 knockout screening in sheep granulosa cells for FSH response genes. *Animals* 14 (6), 898. doi:10.3390/ani14060898

Liu, Z. Q. (2018). *Spectral effects of two processing Radix Rehmanniae Preparata on the ovulation function of rats*. Guangzhou University of Traditional Chinese Medicine.

Lu, D., Zhao, P. W., Chen, M., Yang, Y., and Niu, J. Z. (2019). Study on estrogenic effects and its molecular mechanism of Siwu decoction via estrogen receptor subtypes. *Liaoning J. Traditional Chin. Med.* 05, 1074–1077. doi:10.13192/j.issn.1000-1719.2019.05.057

Lu, M. K., Chang, C. C., Chao, C. H., and Hsu, Y. C. (2022). Structural changes, and anti-inflammatory, anti-cancer potential of polysaccharides from multiple processing of Rehmannia glutinosa. *Int. J. Biol. Macromol.* 206, 621–632. doi:10.1016/j.ijbiomac.2022.02.112

Lu, X. M., Zhong, L. Y., Wang, S., Deng, Y. W., Liu, H., Chen, M. X., et al. (2023). Effect of processing method on chemical constituents of Rehmanniae Radix: based on UHPLC-LTQ-Orbitrap MS. *China J. Chin. Materia Medica* 02, 399–414. doi:10.19540/j.cnki.cjcmm.20220816.301

Luo, S., Ruan, X., and Mueck, A. O. (2023). The effect of Kuntai capsule on ovarian function in cisplatin-induced premature ovarian insufficiency rats. *Front. Endocrinol.* 13, 1097165. doi:10.3389/fendo.2022.1097165

Lv, H., Jia, H., Cai, W., Cao, R., Xue, C., and Dong, N. (2023). Rehmannia glutinosa polysaccharides attenuates colitis via reshaping gut microbiota and short-chain fatty acid production. *J. Sci. food Agric.* 103 (8), 3926–3938. doi:10.1002/jsfa.12326

Ma, R., Liang, W., Sun, Q., Qiu, X., Lin, Y., Ge, X., et al. (2018). Sirt1/Nrf2 pathway is involved in oocyte aging by regulating Cyclin B1. *Aging* 10 (10), 2991–3004. doi:10.18632/aging.101609

Ma, Y. J., Yao, C., Yu, L. L., Liu, P., Li, M. E., and Chen, T. C. (2023). Research on the correlation between the chroma of rehmannia glutinosa processed by "nine steaming and nine drying" and index components based on traditional experience. *Lishizhen Med. Materia Medica Res.* 06, 1366–1370.

Mao, S. Q., and Ji, D. Y. (2023). Study on the correlation between TH1/Treg cell immune imbalance and factor level changes and disease severity in patients with early-onset ovarian insufficiency. *Chin. J. Woman Child Health Res.* 06, 1065–1068. doi:10.19829/j.zgfybj.issn.1001-4411.2023.06.024

Matsuda, F., Inoue, N., Manabe, N., and Ohkura, S. (2012). Follicular growth and atresia in mammalian ovaries: regulation by survival and death of granulosa cells. *J. reproduction Dev.* 58 (1), 44–50. doi:10.1262/jrd.2011-012

Mills, E. G., Yang, L., Nielsen, M. F., Kassem, M., Dhillo, W. S., and Comninos, A. N. (2021). The relationship between bone and reproductive hormones beyond estrogens and androgens. *Endocr. Rev.* 42 (6), 691–719. doi:10.1210/endrev/bnab015

National Pharmacopoeia Committee (2020). *Pharmacopoeia of the People 's Republic of China: volume I*. 2020 Edition. Beijing: China Pharmaceutical Science and Technology Press.

Nelson, L. M. (2009). Clinical practice. Primary ovarian insufficiency. *N. Engl. J. Med.* 360 (6), 606–614. doi:10.1056/NEJMcp0808697

Nemmar, A., Beegam, S., Zaaba, N. E., Alblooshi, S., Alseiari, S., and Ali, B. H. (2022). The salutary effects of catalpol on diesel exhaust particles-induced thrombogenic changes and cardiac oxidative stress, inflammation and apoptosis. *Biomedicines* 10 (1), 99. doi:10.3390/biomedicines10010099

Oh, K. O., Kim, S. W., Kim, J. Y., Ko, S. Y., Kim, H. M., Baek, J. H., et al. (2003). Effect of Rehmannia glutinosa Libosch extracts on bone metabolism. *Clin. Chim. acta* 334 (1-2), 185–195. doi:10.1016/s0009-8981(03)00238-9

Oyawoye, O., Abdel Gadir, A., Garner, A., Constantinovici, N., Perrett, C., and Hardiman, P. (2003). Antioxidants and reactive oxygen species in follicular fluid of women undergoing IVF: relationship to outcome. *Hum. Reprod. Oxf. Engl.* 18 (11), 2270–2274. doi:10.1093/humrep/deg450

Pastore, L. M., Christianson, M. S., Stelling, J., Kearns, W. G., and Segars, J. H. (2018). Reproductive ovarian testing and the alphabet soup of diagnoses: DOR, POI, POF, POR, and FOR. *J. assisted reproduction Genet.* 35 (1), 17–23. doi:10.1007/s10815-017-1058-4

Peng, H. S., Xu, C. Q., Yuan, Y., Zha, L. P., Chen, H. W., Guan, L., et al. (2019). The earliest excipient products of Traditional Chinese Medicine:Identification and analysis of samples from wooden lacquer box unearthed from Haihunhou tomb in the Western Han Dynasty. *Chin. Sci. Bull.* 09, 935–947. doi:10.1360/n972018-01176

Peng, X. X., Wang, D. Q., and Peng, H. S. (2018). Brief discussion on evolution and changes of processing of medicinal materials in "steamed for nine times and shined for nine times" in ancient materia medica. *J. West Anhui Univ.* 02, 92–99.

Qianfeng, G. (2005). *Processing science of traditional Chinese medicine*. Beijing: Science Press.

Qin, L. H. (2017). Clinical evaluation of hormone therapy combined with Liuwei Dihuang pills in the treatment of premature ovarian failure. *Electron. J. Clin. Med. Literature* 80, 15775. doi:10.16281/j.cnki.jocml.2017.80.108

Que, X. H., Gui, S. H., Zhong, Q. Y., Yu, B. B., and Lin, H. (2021). Effects of different degrees of Radix Rehmanniae on mouse ovaries and analysis of their cold and heat medicinal properties. *Chin. Tradit. Pat. Med.* 11, 3222–3226.

Rebar, R. W. (2009). Premature ovarian failure. *Obstetrics Gynecol.* 113 (6), 1355–1363. doi:10.1097/AOG.0b013e3181a66843

Ren, H., Li, K., Min, Y., Qiu, B., Huang, X., Luo, J., et al. (2023). Rehmannia glutinosa polysaccharides: optimization of the decolorization process and antioxidant and anti-inflammatory effects in LPS-stimulated porcine intestinal epithelial cells. *Antioxidants Basel. Switz.* 12 (4), 914. doi:10.3390/antiox12040914

Romero, A., San Hipólito-Luengo, Á., Villalobos, L. A., Vallejo, S., Valencia, I., Michalska, P., et al. (2019). The angiotensin-(1-7)/Mas receptor axis protects from endothelial cell senescence via klotho and Nrf2 activation. *Aging Cell* 18 (3), e12913. doi:10.1111/acel.12913

Shea, A. K., Buwembo, A., Mayhew, A., Sohel, N., Griffith, L. E., and Raina, P. (2021). The association between primary ovarian insufficiency and osteoporosis in the Canadian Longitudinal Study on Aging. *Menopause* 28 (6), 693–698. doi:10.1097/GME.0000000000001756

Shen, Q. X., Zhang, L. L., Lin, X. Y., Liang, Y. J., Liu, G. T., and Lu, R. L. (2020). Meta-analysis of the efficacy of Kuntai capsule combined with climen in the treatment of premature ovarian failure. *Chin. J. Mod. Appl. Pharm.* 01, 78–84. doi:10.13748/j.cnki.issn1007-7693.2020.01.015

Shi, J., Wang, J., Jia, N., and Sun, Q. (2023). A network pharmacology study on mechanism of resveratrol in treating preeclampsia via regulation of AGE-RAGE and HIF-1 signalling pathways. *Front. Endocrinol. (Lausanne)* 13, 1044775. doi:10.3389/fendo.2022.1044775

Shixuan, W. (2021). *Ovarian aging*. Beijing: People's Medical Publishing House.

Stewart, J. A., Jr, Cashatt, D. O., Borck, A. C., Brown, J. E., and Carver, W. E. (2006). 17beta-estradiol modulation of angiotensin II-stimulated response in cardiac fibroblasts. *J. Mol. Cell. Cardiol.* 41 (1), 97–107. doi:10.1016/j.yjmcc.2006.04.019

Szeliga, A., Calik-Ksepka, A., Maciejewska-Jeske, M., Grymowicz, M., Smolarczyk, K., Kostrzak, A., et al. (2021). Autoimmune diseases in patients with premature ovarian insufficiency-our current state of Knowledge. *Int. J. Mol. Sci.* 22 (5), 2594. doi:10.3390/ijms22052594

Tanaka, S. S., Toyooka, Y., Akasu, R., Katoh-Fukui, Y., Nakahara, Y., Suzuki, R., et al. (2000). The mouse homolog of Drosophila Vasa is required for the development of male germ cells. *Genes Dev.* 14 (7), 841–853. doi:10.1101/gad.14.7.841

Tang, Z. R., Zhang, R., Lian, Z. X., Deng, S. L., and Yu, K. (2019). Estrogen-receptor expression and function in female reproductive disease. *Cells* 8 (10), 1123. doi:10.3390/cells8101123

Tian, J. Y., Ma, F., and Han, L. Y. (2022). Analysis of composition differences of fresh Radix Rehmanniae, crude Radix Rehmanniae and processed Radix Rehmanniae using infrared spectroscopy. *Spectrosc. Spectr. Analysis* 10, 3203–3209.

Virant-Klun, I. (2015). Postnatal oogenesis in humans: a review of recent findings. *Stem cells cloning Adv. Appl.* 8, 49–60. doi:10.2147/SCCAA.S32650

Wan, Y. H., and Chen, X. Y. (2022). The effect and mechanism of Yijing decoction on the decline of ovarian reserve in rats. *China Pharm.* 14, 1730–1735.

Wang, B., Zhang, X. Y., Lv, C. Z., He, M. J., Meng, X. L., and Zhang, S. S. (2019). Process optimization for Rehmanniae Radix Praeparata with yellow wine stewing by multi-index-response surface method. *Chin. Traditional Herb. Drugs* 09, 2065–2073.

Wang, J., Luo, R., Zhao, X., Xia, D., Liu, Y., Shen, T., et al. (2023). Association between gut microbiota and primary ovarian insufficiency: a bidirectional two-sample Mendelian randomization study. *Front. Endocrinol.* 14, 1183219. doi:10.3389/fendo.2023.1183219

Wang, M., Wang, Y. X., Wu, Y. R., Li, N., Feng, M., Zhang, W. Z., et al. (2020). Research progress on content changes of 5-hydroxymethyl furfural during processing of Chinese medicine and it's pharmacological effects. *Drug Eval. Res.* 11, 2319–2327.

Wang, R. H., Bai, Y., and Wang, H. Q. (2022). Correlation between estrogen levels and T lymphocyte subsets and PD-1 in peripheral blood in POI patients. *Chin. J. Woman Child Health Res.* 01, 60–65.

Wu, J., Yu, H., Jin, Y., Wang, J., Zhou, L., Cheng, T., et al. (2023). Ajugol's upregulation of TFEB-mediated autophagy alleviates endoplasmic reticulum stress in chondrocytes and retards osteoarthritis progression in a mouse model. *Chin. Med.* 18 (1), 113. doi:10.1186/s13020-023-00824-7

Wu, J., Zhuo, Y., Liu, Y., Chen, Y., Ning, Y., and Yao, J. (2021). Association between premature ovarian insufficiency and gut microbiota. *BMC pregnancy childbirth* 21 (1), 418. doi:10.1186/s12884-021-03855-w

Wu, S. J., Wang, L., Zhao, M. W., Zhong, S. M., Wu, W. G., and Li, W. L. (2022). Research progress in repeatedly steamed and sundried oftraditional Chinese medicine. *Cent. South Pharm.* 09, 2015–2022.

Xia, T., Dong, X., Jiang, Y., Lin, L., Dong, Z., Shen, Y., et al. (2019). Metabolomics profiling reveals Rehmanniae Radix preparata extract protects against glucocorticoid-induced osteoporosis mainly via intervening steroid hormone biosynthesis. *Mol. Basel. Switz.* 24 (2), 253. doi:10.3390/molecules24020253

Xie, P. P. (2021). *Clinical trial and experimental study of Jiajian Yijing Decoction regulating Th17/Treg immune balance through CXCR4/SDF-1 to improve the decline of ovarian reserve function*. Guangzhou University of Chinese Medicine. doi:10.27044/d.cnki.ggzzu.2021.000949

Xie, Y., Zhong, L. Y., Wang, Z., Song, J. J., Li, J. Q., Wang, Y. B., et al. (2022). Historical evolution and modern research progress of Rehmanniae Radix. *Chin. J. Exp. Traditional Med. Formulae* 02, 273–282. doi:10.13422/j.cnki.syfjx.20211546

Xu, J. X., Zhang, Y., and Mao, F. (2020). Observation of the clinical efficacy of Gui Kidney Pill on patients with ovarian insufficiency. *J. Chin. Med. Mater.* 03, 738–740. doi:10.13863/j.issn1001-4454.2020.03.043

Xu, L., Kwak, M., Zhang, W., Zeng, L., Lee, P. C., and Jin, J. O. (2017). Rehmannia glutinosa polysaccharide induces toll-like receptor 4 dependent spleen dendritic cell

maturation and anti-cancer immunity. *Oncoimmunology* 6 (7), e1325981. doi:10.1080/2162402X.2017.1325981

Xue, S. J., Chen, Y., Chen, S. Q., and Che, Q. T. (2023). Simultaneous determination of eight saccharides contents in Radix Rehmanniae and its different processed products by HPLC-ELSD. *Chin. J. Pharm. Analysis* 06, 939–949. doi:10.16155/j.0254-1793.2023.06.04

Yan, S. T., Fan, H., Li, R. L., Wang, L. P., Luo, W. J., Gao, F., et al. (2020). Historical evolution and modern research of steamed for nine times and shined for nine times for Chinese medicine. *China Pharm.* 01, 136–141.

Yang, F., Hou, Z. F., Zhu, H. Y., Chen, X. X., Li, W. Y., Cao, R. S., et al. (2021b). Catalpol protects against pulmonary fibrosis through inhibiting TGF-β1/smad3 and wnt/β-catenin signaling pathways. *Front. Pharmacol.* 11, 594139. doi:10.3389/fphar.2020.594139

Yang, J., Wen, L., Jiang, Y., and Yang, B. (2019). Natural estrogen receptor modulators and their heterologous biosynthesis. *Trends Endocrinol. metabolism* 30 (1), 66–76. doi:10.1016/j.tem.2018.11.002

Yang, J. J., Zhang, L. H., Zhang, M. Y., Yang, M. X., Zou, L., Cui, Y., et al. (2024). Exploration of the dynamic variations of the characteristic constituents and the degradation products of catalpol during the process of Radix Rehmanniae. *Mol. Basel. Switz.* 29 (3), 705. doi:10.3390/molecules29030705

Yang, P. M. (2010). Comparison of the contents of catalpa alcohol and 5-hydroxymethylfurfural at different times of Radix Rehmanniae. *China J. Traditional Chin. Med. Pharm.* 07, 1096–1098.

Yang, S. H., Zhu, J., Wu, W. T., Li, J. M., Tong, H. L., Huang, Y., et al. (2023). Rhizoma Atractylodis Macrocephalae-Assessing the influence of herbal processing methods and improved effects on functional dyspepsia. *Front. Pharmacol.* 14, 1236656. doi:10.3389/fphar.2023.1236656

Yang, Y. H., Yang, H., Li, R. F., Li, C. X., Zeng, L., Wang, C. J., et al. (2021a). A Rehmannia glutinosa cinnamate 4-hydroxylase promotes phenolic accumulation and enhances tolerance to oxidative stress. *Plant Cell Rep.* 40 (2), 375–391. doi:10.1007/s00299-020-02639-4

Yuan, Y., Kang, N., Li, Q., Zhang, Y., Liu, Y., and Tan, P. (2019). Study of the effect of neutral polysaccharides from rehmannia glutinosa on lifespan of *Caenorhabditis elegans*. *Mol. Basel. Switz.* 24 (24), 4592. doi:10.3390/molecules24244592

Yue, W. (2009). Effect of Liuwei Dihuang Pill on the protein of nucleolar composition of ovarian granulosa cells in ovulatory disorder infertility. *Shaanxi J. Traditional Chin. Med.* 09, 1253–1254.

Zhang, H., Yue, Y., Zhang, Q., Liang, L., Li, C., Chen, Y., et al. (2023b). Structural characterization and anti-inflammatory effects of an arabinan isolated from Rehmannia glutinosa Libosch. *Carbohydr. Polym.* 303, 120441. doi:10.1016/j.carbpol.2022.120441

Zhang, J. M., and Lin, Y. P. (2023). Clinical study on yijing decoction combined with sequential therapy of estrogen and progesterone for premature ovarian failure with syndrome of kidney deficiency and liver depression. *New Chin. Med.* 04, 25–29. doi:10.13457/j.cnki.jncm.2023.04.006

Zhang, L. X., Wei, Y., Li, F. F., Li, Z. N., and Zhang, T. T. (2023a). Fingerprint pattern recognition and multi-component content determination of different processed products of Rehmannia glutinosa Libosch. *Hubei Agric. Sci.* 09, 135–141. doi:10.14088/j.cnki.issn0439-8114.2023.09.025

Zhang, W. T., Yue, C., Huang, Q. W., Yuan, K., Yan, A. J., and Shi, S. M. (2016). Contents of eight saccharides in unprocessed and processed Rehmannia glutinosa and content changes at different processing time points. *Chin. Traditional Herb. Drugs* 07, 1132–1136.

Zhang, X., Jin, C., Li, Y., Guan, S., Han, F., and Zhang, S. (2013). Catalpol improves cholinergic function and reduces inflammatory cytokines in the senescent mice induced by D-galactose. *Food Chem. Toxicol.* 58, 50–55. doi:10.1016/j.fct.2013.04.006

Zhang, X., Zhang, L., Xiong, L., Liu, X., Zhang, J., Yu, F., et al. (2024). Kuntai capsule for the treatment of diminished ovarian reserve: a systematic review and meta-analysis of randomized controlled trials. *J. Ethnopharmacol.* 329, 118167. doi:10.1016/j.jep.2024.118167

Zhang, X. L., Jiang, B., Li, Z. B., Hao, S., and An, L. J. (2007). Catalpol ameliorates cognition deficits and attenuates oxidative damage in the brain of senescent mice induced by D-galactose. *Pharmacol. Biochem. Behav.* 88 (1), 64–72. doi:10.1016/j.pbb.2007.07.004

Zhang, Y. (2023). Awareness and ability of paradigm shift are needed for research on dominant diseases of TCM. *Chin. Herb. Med.* 15 (4), 475. doi:10.1016/j.chmed.2023.10.001

Zhang, Y., Sun, F. F., Yang, J. N., Zhang, J. S., and Zhang, Z. L. (2020). Establishment of thin layer chromatography identification method for different processed products of Rehmanniae Radix. *Chin. J. Exp. Traditional Med. Formulae* 15, 142–149. doi:10.13422/j.cnki.syfjx.20200849

Zhang, Y., Wang, Y., Wang, L., Zhang, Y., Qin, Y., Chen, T., et al. (2012). Effects of Rehmannia glutinosa oligosaccharide on human adipose-derived mesenchymal stem cells *in vitro*. *Life Sci.* 91 (25-26), 1323–1327. doi:10.1016/j.lfs.2012.10.015

Zhao, Y., Chen, H., Qiu, F., He, J., and Chen, J. (2023). Cognitive impairment and risks of osteoporosis: a systematic review and meta-analysis. *Archives gerontology geriatrics* 106, 104879. doi:10.1016/j.archger.2022.104879

Zhou, F. R. (2022). *Exploring the mechanisms of Siwu Tang in improving premature ovarian failure: based on the " richness or deficiency in vessel" and angiogenesis in the ovary*. Huazhong University of Science and Technology. doi:10.27157/d.cnki.ghzku.2022.002334

Zhou, X. H., Zu, Y. E., Liu, Q. Y., Liang, Y., and Huang, J. M. (2023). The effects of Kuntai capsule combined with fenmotong in the treatment of premature ovarian failure on endometrium, ovaries, antral follicles and sex hormones. *Chin. J. Fam. Plan.* 11, 2572–2576.

Zhou, Y. Q., He, F. Y., Yang, Y. T., Shi, J. L., Deng, K. W., Tang, Y., et al. (2014). Research situation of Maillard reaction and its influence on research methods for processing and preparation process of Chinese materia medica. *Chin. Traditional Herb. Drugs* 01, 125–130.

Zhu, H., Peng, H. S., Huang, L. Q., and Yuan, Y. (2021). Chinese ancient herbal processing: evidence of rice-steaming as the processing method of Rehmannia in Han Dynasty. *Sci. Bull.* 66 (4), 307–309. doi:10.1016/j.scib.2020.11.008

Zhu, J., Zhu, X. M., Shi, Y. H., Li, Q., Liu, X. D., Wang, Z., et al. (2022a). Research progress of Radix Rehmanniae and predictive analysis of its quality markers. *J. Chin. Med. Mater.* 05, 1273–1281. doi:10.13863/j.issn1001-4454.2022.05.044

Zhu, J. H., Wang, L., Ma, Z. X., Duan, J. A., and Tao, J. H. (2024). Rehmannia glutinosa Libosch and Cornus officinalis Sieb herb couple ameliorates renal interstitial fibrosis in CKD rats by inhibiting the TGF-β1/MAPK signaling pathway. *J. Ethnopharmacol.* 318 (Pt B), 117039. doi:10.1016/j.jep.2023.117039

Zhu, M., Zhou, G., and Duan, J. A. (2022b). Effect of Siwu decoction on intestinal microbiota in rats with low ovarian function. *Chin. J. Exp. Traditional Med. Formulae* 17, 25–32. doi:10.13422/j.cnki.syfjx.20221006

Zhu, W. Y., and Du, Y. F. (2023). Effect of Gui Kidney Pill on ovarian autophagy in a mouse model of hypoactive ovarian reserve. *J. Hebei Traditional Chin. Med. Pharmacol.* 04, 11–15. doi:10.16370/j.cnki.13-1214/r.2023.04.008

Zhu, X. D., Ding, Y. P., Yao, W., Wang, S., Chen, Y. H., Huang, L. P., et al. (2023). Based on UPLC-Q-TOF-MS ~ E technology combined with UNIFI software, the characteristic chromatogram method of different processed products of Radix Rehmanniae was established. *J. Chin. Med. Mater.* 01, 73–78. doi:10.13863/j.issn1001-4454.2023.01.013

frontiers | Frontiers in Pharmacology

TYPE Review
PUBLISHED 07 August 2024
DOI 10.3389/fphar.2024.1442297

OPEN ACCESS

EDITED BY
Qianfeng Gong,
Jiangxi University of Traditional Chinese Medicine, China

REVIEWED BY
Anna Kiss,
University of Szeged, Hungary
Zhaohui Liu,
Capital Medical University, China
Zhao Rui-hua,
China Academy of Chinese Medical Sciences, China

*CORRESPONDENCE
Shao-Bin Wei,
shaobinwei5620@163.com

†These authors have contributed equally to this work and share first authorship

RECEIVED 01 June 2024
ACCEPTED 22 July 2024
PUBLISHED 07 August 2024

CITATION
Wen Y, Yan P-J, Fan P-X, Lu S-S, Li M-Y, Fu X-Y and Wei S-B (2024), The application of rhubarb concoctions in traditional Chinese medicine and its compounds, processing methods, pharmacology, toxicology and clinical research. *Front. Pharmacol.* 15:1442297. doi: 10.3389/fphar.2024.1442297

The application of rhubarb concoctions in traditional Chinese medicine and its compounds, processing methods, pharmacology, toxicology and clinical research

Yi Wen[1†], Pei-Jia Yan[1†], Pei-Xuan Fan[1], Shan-Shan Lu[1], Mao-Ya Li[1], Xian-Yun Fu[2] and Shao-Bin Wei[1*]

[1]Gynecology Department, Hospital of Chengdu University of Traditional Chinese Medicine, Chengdu, China, [2]College of Medicine and Health Sciences, China Three Gorges University, Yichang, China

Objective: This study reviews the development of rhubarb processing and the current status of pharmacological research. We summarized the effects of different processing methods on the active compounds, pharmacological effects, and toxicity of rhubarb, as well as the clinical application of different concoctions, providing reference for further pharmacological research and clinical application of rhubarb.

Methods: A comprehensive literature review was conducted using databases such as Pubmed, Embase, National Science and Technology Library, Web of science, CNKI, China Science and Technology Journal Database, SinoMed, and the *Pharmacopoeia of the People's Republic of China*. Search terms included "rhubarb", "raw rhubarb", "wine rhubarb", "cooked rhubarb", "rhubarb charcoal", "herbal processing", "compounds", "pharmacological effects", "inflammation", "gastrointestinal bleeding", and "tumor".

Results: Historical records of rhubarb processing date back to the Han Dynasty, with continual innovations. Currently, the types of rhubarb used in traditional Chinese medicine have stabilized to three species: *Rheum palmatum L.*, *Rheum tanguticum Maxim.ex Balf.* and *Rheum officinale Baill*. Common concoctions include raw rhubarb, wine rhubarb, cooked rhubarb and rhubarb charcoal. The active compounds of rhubarb are known to defecation, exhibit antibacterial and anti-inflammatory properties, regulate coagulation, protect the digestive system, and possess anti-tumor activities. Guided by Chinese medicine theory, the use of different rhubarb concoctions can enhance specific effects such as purgation to eliminate accumulation, clearing heat and toxins, cooling blood to stop hemorrhages, activating blood circulation to remove blood stasis, and inducing dampness to descend jaundice, thereby effectively treating various diseases. The therapeutic impact of these concoctions on diseases reflects not only in the changes to the active compounds of rhubarb but also in the formulations of traditional Chinese medicine. Processing has also shown advantages in reducing toxicity.

Conclusion: Different processing methods alter the active compounds of rhubarb, thereby enhancing its various pharmacological effects and meeting

the therapeutic needs of diverse diseases. Selecting an appropriate processing method based on the patient's specific conditions can maximize its pharmacological properties and improve clinical outcomes.

KEYWORDS

clinical applications, compounds, pharmacology, processing, rhubarb

1 Introduction

Rhubarb, an herbaceous plant within the Polygonaceae family, comprises approximately 60 species globally (Cao et al., 2017). In China, it is primarily utilized for medicinal purposes, ranking as one of the four principal traditional Chinese medicines (Min et al., 2019). Rhubarb's roots and stems are therapeutically effective, with its medicinal application initially recorded in the *Shennong Herbal Scripture* (*Shennong Bencao Jing*). The species of rhubarb commonly employed in traditional Chinese medicine (TCM) are the dried roots and rhizomes of *Rheum palmatum L.*, *Rheum tanguticum Maxim. ex Balf.* and *Rheum officinale Baill.* These exhibit multiple pharmacological properties, including purgation, heat clearing, fire discharging, blood cooling and detoxification, stasis elimination, collateral obstruction removal and jaundice reduction (Committee, 2020). *Rheum palmatum L.* is mainly produced in Gansu and Qinghai, and is mostly cultivated, accounting for the majority of rhubarb production in China. *Rheum tanguticum Maxim. ex Balf.* is mainly produced in Qinghai and Gansu, wild or cultivated. *Rheum officinale Baill.* is mainly produced in Sichuan and Guizhou, cultivated or wild, with relatively low yield (Kang, 2013). As a multi origin traditional Chinese medicine, research has shown that there are differences in the types and contents of compounds contained in rhubarb medicinal materials with different origins, which may lead to differences in their pharmacological effects. However, such differences have not been considered in practical clinical applications.

The processing of Chinese medicines adheres to traditional theories, guided by the requirements of diagnosis, drug characteristics, and the specifics of pharmaceutical preparation (Zhang, 2009). The processing of rhubarb has a long history. Currently, the main rhubarb concoctions used in China include raw rhubarb, wine rhubarb, cooked rhubarb and rhubarb charcoal, addressing ailments across the cardiovascular (Wu et al., 2023), digestive (Hu et al., 2018), endocrine (Zeng et al., 2021), reproductive systems (Otoo et al., 2023) and more.

This study examines the alterations in active compounds of three rhubarb species listed in the *Pharmacopoeia of the People's Republic of China* after different processing methods, their impacts on traditional and modern pharmacology, clinical uses, and toxicity, providing reference for further pharmacological and clinical research on rhubarb in the future.

2 Processing of rhubarb

"Using decoction pieces from processed herbs for treatment, raw and cooked herbs have different medicinal effects" is a characteristic of TCM (Zhu et al., 2024). The processing of Chinese herbal medicine involves various procedures such as washing, cutting, soaking, boiling, stir-frying, roasting and steaming, to produce clinically applicable decoction pieces. During these processes, the addition of auxiliary ingredients like vinegar, wine, honey and salt water is often required (Zhu et al., 2016a). In clinical settings, it is imperative to consider numerous factors, including the balance of yin and yang, the state of the viscera, qi and blood, dietary habits, emotional states, climatic conditions and the daily activities of patients to ensure precise diagnosis and treatment. Thus, it is essential to modify the properties, flavors and meridians of TCM herbs through varied processing techniques to optimize efficacy, minimize toxicity and enhance palatability, thereby tailoring them to specific therapeutic requirements (Hou et al., 2023).

2.1 Origin and development of rhubarb processing

Rhubarb processing has been practiced for thousands of years. The earliest documentation, from the Han Dynasty, describes techniques such as "removing black skin" and "wine washing, wine soaking" found in Zhang Zhongjing's *Golden Chamber Jade Letter Classic* (*Jingui Yuhan Jing*) (Zhang et al., 2021). Thereafter, a detailed account from the Southern and Northern Dynasty in *Master Lei's Discourse on Drug Processing* (*Lei Gong Pao Zhi Lun*) noted that rhubarb was "carefully cut, steamed for 5 h, sun-dried, then sprinkled with melted wax and steamed for 9 h, repeated seven times and sun-dried again, and then sprinkled with diluted honey water and steamed for 24 h until the cross-section turned black, dried in the sun for optimal use". This record also profoundly influenced subsequent generations.

In the early stages, people only divided rhubarb into two categories: raw and cooked. The ancient people had a broad understanding of "cooking" rhubarb. No matter what method was used to heat the rhubarb to achieve the goal of alleviating diarrhea and side effects, it can be included in the scope of "cooking". Such as calcination, steaming, simmering, boiling, stir frying and so on (Wang Y. et al., 2018). During the Tang and Song dynasties, techniques such as "boiling with wine", "steaming with wine" and "steaming under rice" were developed. The use of vinegar in rhubarb processing was first noted in the Tang Dynasty's *Materia Medica for Dietotherapy* (*ShiLiao BenCao*). And the "nine times steaming and nine times drying in the sun" in *General Records of Holy Universal Relief* (*ShengJi ZongLu*) of the Song Dynasty can be said to be the earliest application of the method for processing "*JiuZhengJiuShai*" rhubarb.

In the Jin and Yuan dynasties, rhubarb processing methods became increasingly diverse. The *Miraculous Book of Ten Medicine* (*Shiyao Shenshu*) of the Yuan Dynasty described a method considered the official initiation of rhubarb charcoal production: "Burn until the surface is charred black on the outside, but the inner

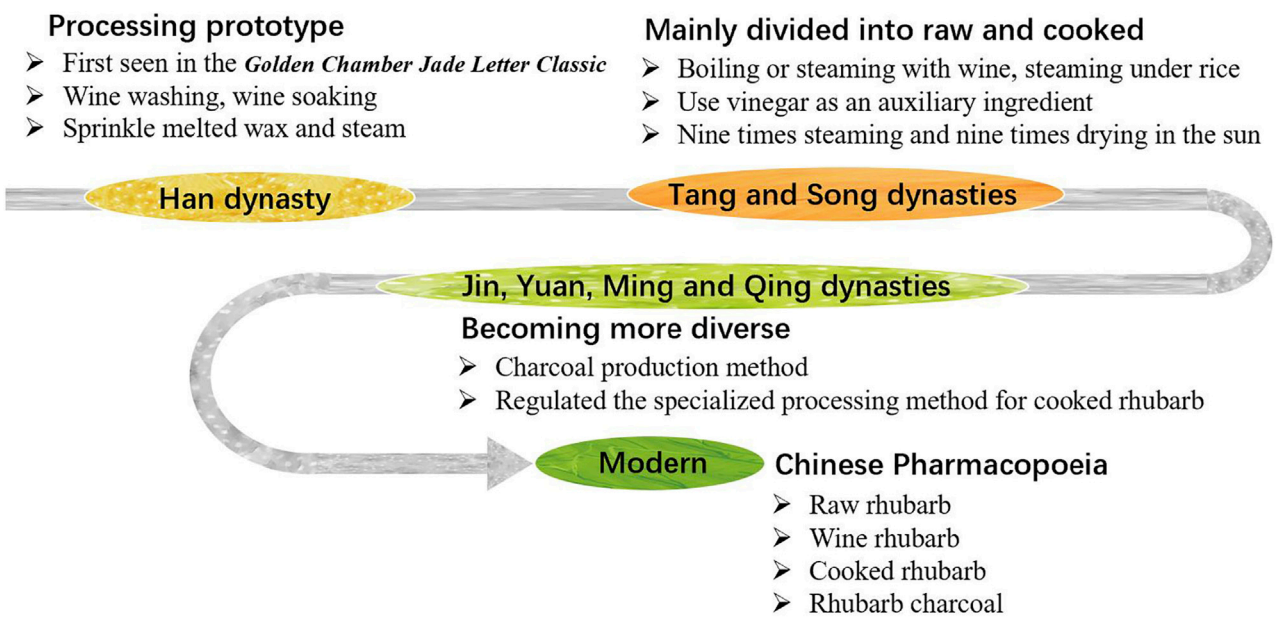

FIGURE 1
Research on the origin and development of rhubarb processing.

layer retains its original flavor, grind it into an extremely fine powder". In Ming and Qing dynasties, the processing of rhubarb with wine as an auxiliary ingredient became very popular (Ren et al., 2023). The method of wine soaking and steaming over water that emerged in this period laid the foundation for the modern sealed wine stewing method of cooked rhubarb (Wang Y. et al., 2018), and also distinguished it from the wine stir-fried rhubarb. The detailed processing methods of rhubarb used in past dynasties are documented in Supplementary Table S1.

In modern times, the processing methods of rhubarb have become gradually refined. The state has organized various traditional rhubarb processing methods, established the "*General rules of Chinese medicine processing*". In 1963, several monographs on traditional Chinese medicine processing, including *Integration of Chinese Medicine Processing Experience* were published. In the same year, for the first time, the government included raw rhubarb, wine rhubarb, cooked rhubarb and rhubarb charcoal, which renowned for their long history, extensive use and significant therapeutic effects, into the second edition of the *Pharmacopoeia of the People's Republic of China*, and have been used as official norms since 1985. In addition, the 1988 *National Standards for Traditional Chinese Medicine Processing* and subsequent processing standards for local provinces have also played crucial roles in unifying and standardizing rhubarb processing by selecting and incorporating current, practical concoctions and their techniques from all over the country (Figure 1).

2.2 Compounds in different concoctions of rhubarb

Current literature reveals that rhubarb contains over 100 compounds, primarily including anthraquinones, tannins, stilbenes, phenylbutanones (Gao et al., 2017; Yao et al., 2021). Anthraquinones, encompassing both derivatives and anthrone derivatives, are identified as the key characteristics and pharmacologically active compounds of rhubarb, offering effects such as laxative, anti-inflammatory, antibacterial, antiviral, and anticancer (Malik and Müller, 2016). These derivatives are classified into two types: free and combined. Free anthraquinones consist of compounds such as rhein, emodin, aloe-emodin, chrysophanol and physcion. Combined anthraquinones, typically glycosides, result from the linkage of free anthraquinones with glycosyl groups, and anthrone derivatives include compounds such as sennoside A–D (Cao et al., 2017). Tannins, another significant compound, display antioxidant, anti-inflammatory, antibacterial, hemostatic and anti-diarrheal effects (Qin et al., 2011; Laddha and Kulkarni, 2019; Marcińczyk et al., 2021). They are divided into hydrolyzable tannins, condensed tannins with gallic acid and catechin as structural units, and complex tannins that combine these types. Moreover, stilbene compounds such as rhapontigenin, piceatannol, and their derivatives (Wang et al., 2019) have recently been recognized for their considerable biological potential, exhibiting anti-inflammatory (Dvorakova and Landa, 2017), anticancer (De Filippis et al., 2017), antibacterial (Singh et al., 2019) and anti-aging activities (Dutta et al., 2023). Phenylbutanone, including lindleyin and isolindleyin, is noted for its anti-inflammatory and analgesic properties (Zhang K. X. et al., 2022; Figure 2).

The processing methods for rhubarb, as recorded in the *Chinese Pharmacopoeia*, include cleaning rhubarb root, removing impurities, washing, moistening thoroughly, and slicing into thick pieces or blocks, referred to as raw rhubarb. Wine rhubarb is produced by stir-frying raw rhubarb with wine. Cooked rhubarb is obtained by stewing or steaming raw rhubarb with wine until it turns uniformly black. Rhubarb charcoal is produced by stir-frying raw rhubarb without any additives until the surface is charred black

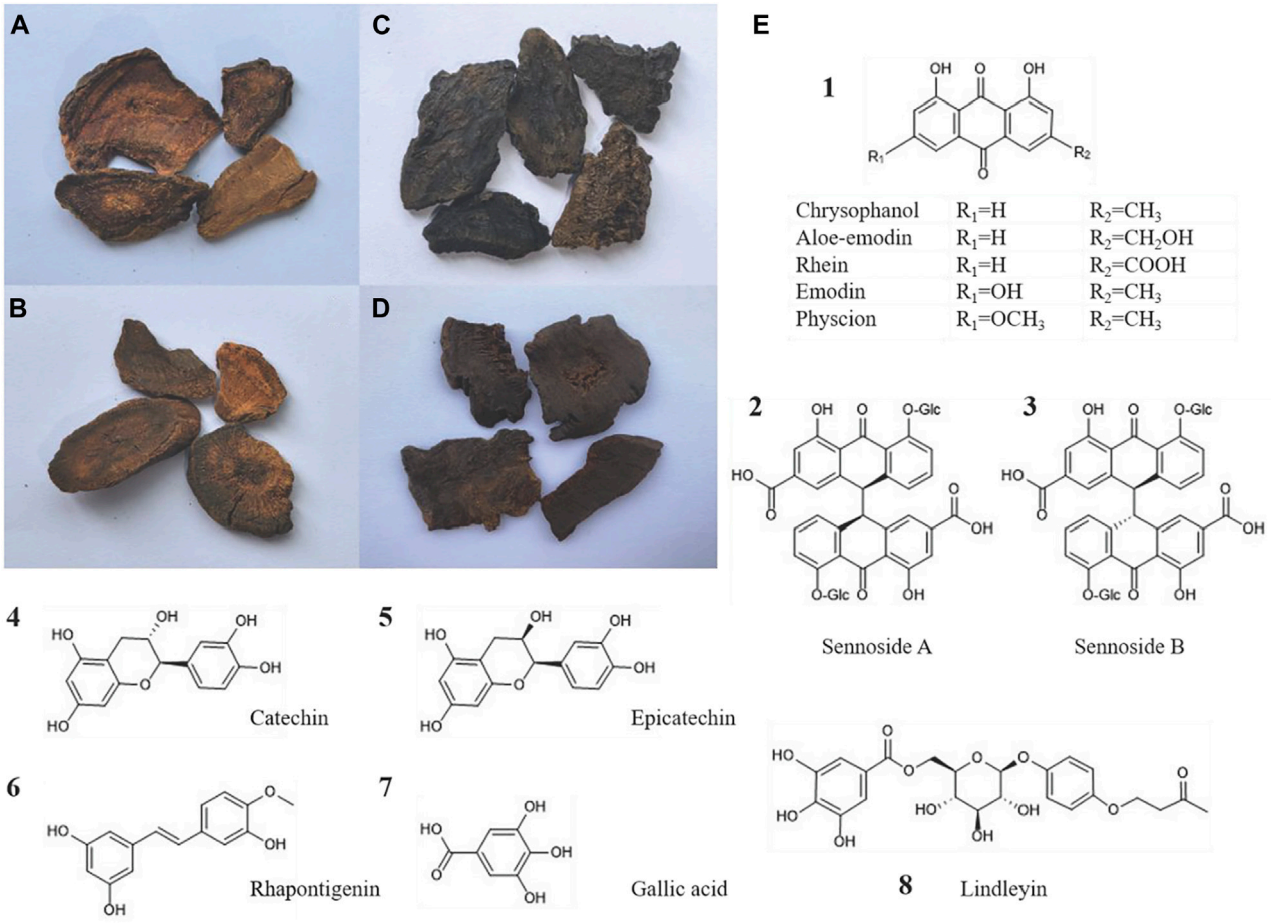

FIGURE 2
Four types of rhubarb concoctions and the chemical structural formulas of the main active compounds of rhubarb: **(A)** Raw rhubarb, **(B)** Wine rhubarb, **(C)** Cooked rhubarb, **(D)** Rhubarb charcoal. **(E)** The chemical structural formulas of the main free anthraquinones, sennoside A/B, catechins, epicatechin, rhapontigenin, gallic acid, and lindleyin in rhubarb are respectively presented.

and the interior turns burnt brown. The prevalence of glycosides in rhubarb's effective compounds, which are highly soluble in water and readily hydrolyzed under acidic conditions, explains the preference to minimize water use in processing the four officially recognized rhubarb concoctions used in clinical practice. This also underlines the need for the "less soaking, more moistening" approach during cleaning (Wen et al., 2020), avoidance of steaming or boiling with water, and exclusion of vinegar as an additive. The reactivity of tannins with iron and their ease of oxidation may account for the historical use of bamboo knives for cutting rhubarb in the Song Dynasty and the modern elimination of sun drying. The high solubility of most effective compounds in ethanol supports the traditional use of wine in processing wine rhubarb and cooked rhubarb. These varied processing methods not only emphasize different functional aspects of rhubarb but also alter its medicinal properties, creating new therapeutic effects and broadening its clinical utility.

It can be seen from the processing method of raw rhubarb that the harvested rhubarb raw materials are made into raw rhubarb decoction pieces, which mainly reflects the purifying of medicinal materials, easy to be weighed and used, increasing the contact area between medicinal materials and solvents, which is conducive to the purpose of boiling out the effective compounds when making decoctions. The compounds in it have not changed. The high content of combined anthraquinones and sennosides, known for their laxative effects impart raw rhubarb with its bitter flavor, cold and descending properties, and potent purgative and obstruction-clearing actions. Some anthraquinones are also integral to rhubarb's ability to promote blood circulation and remove blood stasis (Seo et al., 2012; Tan et al., 2018; Li et al., 2019). Current pharmacological research underscores that the heat-clearing and detoxifying effects of Chinese medicinal herbs are largely linked to their anti-inflammatory and antibacterial activities, offering a scientific basis for the attributed properties of rhubarb (Wang et al., 2019; Zhang et al., 2020).

However, the other processing methods are further processed on the basis of raw rhubarb, including different physical or chemical transformations such as hydrolysis, carbonization, oxidation, decomposition and condensation (Ni et al., 2012), which will inevitably alter the content or ratios of compounds in the medicinal material. This suggests that changes in compounds during these processing methods may be crucial for modifying properties, enhancing efficacy and reducing toxicity. To investigate these changes ulteriorly, a comprehensive literature

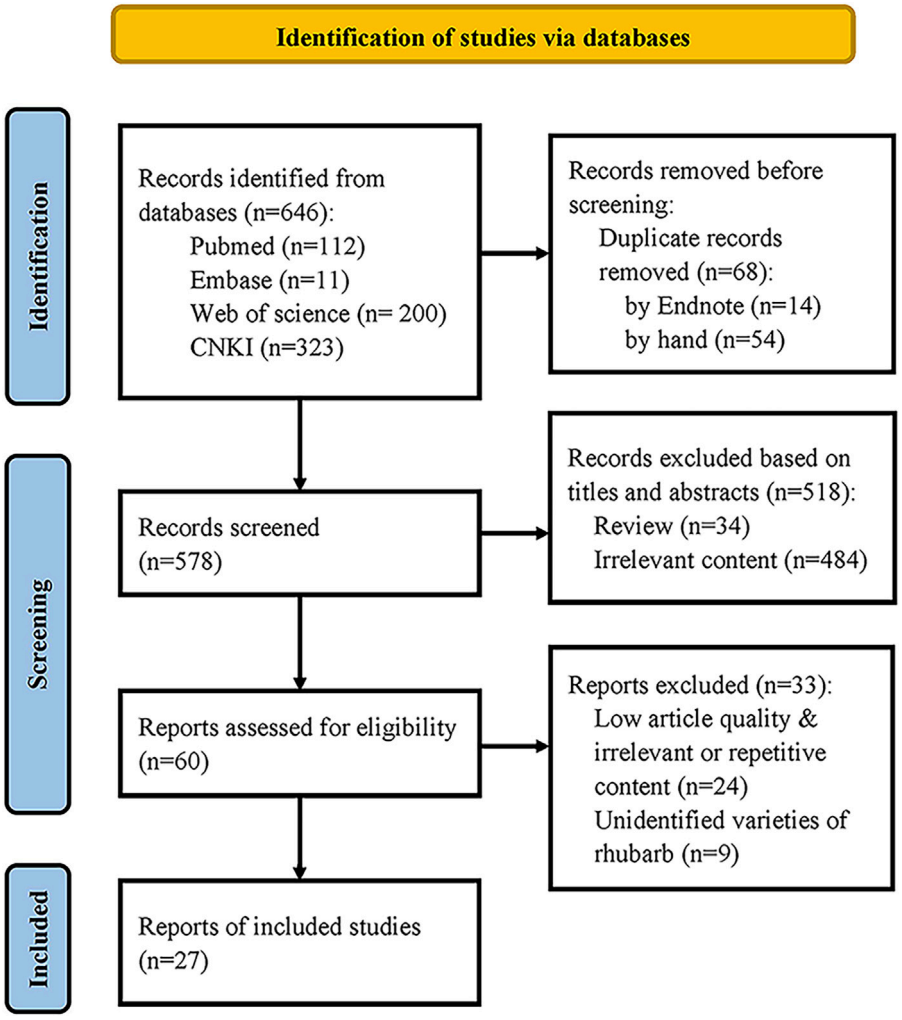

FIGURE 3
Flow chart of literature selection.

search was conducted focusing on the compounds of wine rhubarb, cooked rhubarb and rhubarb charcoal before and after processing, aimed to elucidate patterns of compound changes of three processing methods of rhubarb by sorting, analyzing and summarizing. Relevant publications published in English or Chinese from January 2010 to April 2024 were identified in databases such as PubMed, Web of Science, Embase and CNKI using search terms "rhubarb", "processing" and "composition". Two authors (Lu Shanshan and Fan Peixuan) identified studies from these databases independently, and disagreements were solved by consultation. If it cannot be resolved, it was resolved through consultation with the corresponding author professor Wei Shaobin. The search strategy is shown in Supplementary Table S2, with the last search date of 10 May 2024.

Preset inclusion criteria: (1) Study on the comparison of compounds before and after processing of wine rhubarb, cooked rhubarb and rhubarb charcoal (containing at least one of them); (2) Study published in English or Chinese; (3) The medicinal materials were identified as rhubarb species included in the *Chinese Pharmacopoeia*. Exclusion criteria: (1) Studies where full text is not available; (2) Repeated studies; (3) Non original studies. Finally, according to PRISMA statement of systematic review, there are 27 literature remained, as shown in Figure 3.

We extracted the following details from each study: (1) The first author's name and publication year; (2) The rhubarb concoctions used and the specific processing methods; (3) The method used to determine the content of the compound and the solvent used to prepare the sample; (4) The difference in compound detection between raw rhubarb and other rhubarb concoctions. Two authors (Lu Shanshan and Fan Peixuan) extracted the data independently, and disagreements were solved by consultation. If it cannot be resolved, it was resolved through consultation with the corresponding author, professor Wei Shaobin. The characteristics of the included studies are shown in Supplementary Tables S3–S5.

We applied a self-designed scale to evaluate the methodological quality of the included study: (1) Optimized the content determination method; (2) Conducted precision, stability, and repeatability tests for detection; (3) Reported the specific values

measured in the results section; (4) Reported statistical methods; (5) Potential conflict of interest Statement. Two authors (Lu Shanshan and Fan Peixuan) evaluated the quality of studies independently, and disagreements were solved by consultation. If it cannot be resolved, it was resolved through consultation with the corresponding author professor Wei Shaobin. The results showed that out of the 27 articles, 18 optimized the conditions for compound content determination, such as the mobile phase used in chromatography and the method of sample preparation; 20 conducted the precision, stability and repeatability tests; 17 articles reported numerical information on the measured compounds in the results section, while the remaining 10 articles indirectly described changes in the compounds through graphics or arrows; 16 studies did not clearly report the statistical methods used; Only two articles have made potential conflict of interest statements. Among them, there are 14 studies that meet the above three conditions, 10 studies that meet the two conditions, and three studies that meet the one condition. The research quality list is shown in Supplementary Table S6.

2.2.1 Wine rhubarb

According to our statistics, 13 articles have described the differences in the compounds between wine rhubarb and raw rhubarb. The main compounds that increased in rhubarb after being fried with wine include free anthraquinones, tannins (gallic acid, catechin, gallic acid-3-O-glucoside), phenylbutanones [4-(4′hydroxyphenyl)-2-butanone, 4′-hydroxy-phenyl-2-butanone-4′-O-β-D-(6″-galloyl)-glucoside, 4′-hydroxyphenyl-2-butane-4′-O-β-D-(6″-O-cinnamoyl)-glucoside]. Main compounds that decreased include combined anthraquinones, anthrones, tannins [(epi)catechin-O-gallate, cinnamoyl-O-glucose-O-galloyl, cinnamoyl-O -glucose-O-digalloyl], stilbenes [trans-3,5,4′-trihydroxyvinyl-4′-O-β-D-glucoside, trans-3,5,4′- trihydroxystilbene-4′-O-β-D-(6″-O-galloyl)-glucoside], phenylbutanones [4′-hydroxyphenyl-2-butanone, 4-hydroxyphenyl-2-butane-4′-O-β-D-(2″-O-galloyl-6″-O-(4″-hydroxy)-cinnamoyl)-glucoside].

2.2.2 Cooked rhubarb

There are 21 articles described the differences in the compounds between cooked rhubarb and raw rhubarb. The main compounds of rhubarb increased after steaming with wine include free anthraquinones, tannins (gallic acid, catechin, gallic acid-3-O-glucoside), 5-hydroxymethyl furfural (5-HMF), 4-(4'hydroxy-phenyl)-2-butanone. Main compounds that decreased include combined anthraquinones, anthrones, macromolecular tannins, stilbenes [trans-3,5,4′-trihydroxystilbene-4′-O-β-D-glucoside, trans-3,5,4′-trihydroxystilbene-4′-O-β-D-(6″-O-galloyl)-glucoside], phenylbutanones [4′-hydroxyphenyl-2-butanone, 4′-hydroxyphenyl-2-butanone-4′-O-β-D-(6″-galloyl)-glucoside, 4′-hydroxyphenyl-2-butane-4′-O-β-D-(6″-O-cinnamoyl)-glucoside, 4′-hydroxyphenyl-2-butane-4′-O-β-D-(2″-O-Galloyl-6″-O-(4′-hydroxy)-cinnamoyl)-glucoside].

2.2.3 Rhubarb charcoal

The compounds differences between rhubarb charcoal and raw rhubarb were compared in 18 articles. The main compounds that increased after frying rhubarb into charcoal include free anthraquinones, gallic acid-3-O-glucoside, 5-HMF, phenylbutanones [4′-hydroxyphenyl-2-butanone, 4-(4′hydroxyphenyl)-2-butanone)]. Main compounds that decreased include combined anthraquinones, anthrones, macromolecular tannins, stilbenes [trans-3,5,4′-trihydroxystilbene-4′-O-β-D-glucoside, trans-3,5,4′-trihydroxystilbene-4′-O-β-D-(6″-O-galloyl)-glucoside], phenylbutanones [4′-hydroxyphenyl-2-butanone, 4′-hydroxyphenyl-2-butanone-4′-O-β-D-(6″-galloyl)-glucoside, 4′-hydroxyphenyl-2-butane-4′-O-β-D-(6″-O-cinnamoyl)-glucoside, 4′-hydroxyphenyl-2-butane-4′-O-β-D-(2″-O-Galloyl-6″-O-(4′-hydroxy)-cinnamoyl)-glucoside].

2.2.4 The influences of stir-frying with wine, steaming with wine and stir-frying into charcoal on the compounds of rhubarb

Wine rhubarb and cooked rhubarb both incorporate yellow wine as an auxiliary ingredient. However, wine rhubarb undergoes a brief stir-frying process over slow heat after being moistened with wine. Conversely, cooked rhubarb is stewed or steamed in a sealed container with a greater quantity of yellow wine until it turns black, undergoing a more intense processing. Rhubarb charcoal is stir-fried until carbonized, involving the highest processing temperatures and longest duration, which is the most intensive. Multiple literature has demonstrated through principal component analysis that there are significant differences in the compounds of rhubarb before and after processing (Wang et al., 2014; Zhao et al., 2014; Sun et al., 2024). According to our data, processing increases the levels of free anthraquinones, tannin monomers and other small molecule compounds like 5-HMF in rhubarb. Conversely, the contents of combined anthraquinones, sennosides, tannins, stilbenes and phenylbutanones, which are larger molecules, decrease significantly, especially in cooked rhubarb and rhubarb charcoal. This reduction may result from the decomposition of macromolecular compounds into monomers at varying degrees under high-temperature conditions. Moreover, the processing of rhubarb involves not only the hydrolysis of glycosides but also complex chemical changes, including interactions among different types of compounds, which can alter the herb's efficacy and properties (Yan et al., 2016).

Studies indicate that the extent of processing affects the levels of certain compounds. For example, the compounds in raw rhubarb and wine rhubarb remains relatively similar, while significant changes occur in cooked rhubarb and rhubarb charcoal (Li et al., 2010; Tian et al., 2010). For instance, the degradation of anthraquinones in wine rhubarb is minimal, with little total change, primarily shifting between combined and free forms. However, due to prolonged heating, the total anthraquinone content in cooked rhubarb is somewhat reduced, and the compounds in rhubarb charcoal are severely degraded (Li H. F. et al., 2011; Li, 2011). As previously noted, compounds like sennoside and anthraquinone glycoside are crucial for the laxative effects of rhubarb. Most free anthraquinones are absorbed before reaching the colon, while the combined anthraquinones are significant as they metabolize into free forms in the intestine (Wang et al., 2015a). This explains why the bitter flavor, cold and descending properties, and strong purgative and blockage-removing effects of processed rhubarb are mitigated, with cooked rhubarb having a weaker effect compared to wine rhubarb, and rhubarb charcoal having the least impact. The intestinal absorption characteristics of anthraquinones in rhubarb are very important for oral traditional Chinese medicine to achieve the expected therapeutic effect. However, there is still a lack of deeper understanding of their absorption characteristics (Ta et al., 2023).

TCM posits that yellow wine, known for its fragrant aroma and rising, diverging properties, can warm and unblock blood vessels, thereby promoting blood circulation and removing blood stasis. Consequently, wine rhubarb and cooked rhubarb, which are processed with wine, are believed to enhance these effects (Zhu et al., 2010; Yang et al., 2012). Wine rhubarb significantly alters the distribution of free anthraquinones in rats, increasing their presence in heart and lung tissues (Wu et al., 2017). This provides experimental support for its use in clearing heat toxicity from the blood phase in the upper energizer. Additionally, *in vivo* experiments demonstrated that compounds such as rhein, emodin, aloe-emodin, physcion, chrysophanol and gallic acid exhibit improved absorption in pathological state of blood stasis in rats and rabbits (Dai et al., 2014; Zhu et al., 2017). Gallic acid also reduces whole blood viscosity, plasma viscosity and plasma fibrinogen levels in blood stasis model rats (Sun et al., 2022), underscoring cooked rhubarb's potent effect in promoting blood circulation and removing blood stasis due to its significantly increased content of free anthraquinone and gallic acid (Li, 2011; Yan et al., 2016). Furthermore, the carbonization at high temperatures creates many loose pore structures, beneficial for rhubarb charcoal in adsorbing and astringing (Chen et al., 2019), thereby enhancing its hemostatic effect. This aligns with other findings, who noted that rhubarb charcoal exhibits the strongest hemostatic effect among the four concoctions (Zhu et al., 2008).

In a minority of studies, some inconsistencies with the above trends were observed. For instance, the content of emodin-8-O-β-D-glucoside and two phenylbutanone glycosides in rhubarb which have larger molecular weight increased after being stir-fried with wine, likely due to the ethanol in wine may make these compounds more soluble under less intense processing conditions (Li et al., 2010; Tian et al., 2010). Several studies also reported a decrease in the content of some free anthraquinones and tannin monomers in rhubarb after processing (Wang et al., 2015b; Yan et al., 2016; Zhang Q. et al., 2022). During the process of frying rhubarb into charcoal, the content of gallic acid, 5-HMF and free anthraquinones showed a pattern of first increasing and then decreasing (Yang et al., 2020). This may be related to the sublimation of free anthraquinones (Wu et al., 2020) and the intense processing, which led to the destruction of these compounds. Given the characteristics and complexity of plant materials, any analysis of plant compounds requires the application of appropriate plant sample preparation procedures in order to extract the compounds to be analyzed from the matrix. The extraction rates of each compound vary in different solvents (Nan et al., 2019). It has also been reported that the concentration of water in the extractant can affect the accuracy of the determination of anthraquinone glycoside content (Wianowska, 2014). Therefore, different sample preparation procedures, solvents and the specific processing temperature and time used by different scholars may also be the reasons for the differences in conclusions.

The heterogeneity among included studies may affect the summary of the compound changes before and after processing of rhubarb, and we can draw some insights for further research. Optimizing the detection conditions and sample preparation methods before starting the experiment can help obtain more efficient, accurate and sensitive results. Secondly, the examination and reporting of linearity, precision, stability, repeatability and recovery rate of the methodology can reduce the risk of research result bias. The raw data and statistical methods used in studies are also important features for evaluating the quality of evidence. Optimizing the quality of experimental design and reports may be an issue that needs attention in the future.

3 Modern pharmacological effects of rhubarb

Rhubarb is extensively utilized in TCM due to a variety of effects, increasingly supported by research into its monomer compound. These effects are primarily attributed to various compounds found in rhubarb, such as anthraquinone derivatives, organic acids, volatile oils, glycosides and tannins. Recent studies have also highlighted its potential in anti-tumor applications (Supplementary Table S7).

3.1 Laxative

Modern pharmacological studies have verified that sennoside A, an anthraquinone compound in rhubarb, its laxative impact may be due to its inhibition of water transfer through decreased expression of aquaporin-3 (AQP3) in the colon. This effect is mediated by anthrone, an active metabolite of sennoside A, which activates macrophages in the colon and accelerates prostaglandin E2 (PGE2) secretion (Kon et al., 2014). Additionally, free anthraquinones facilitate stool softening and promote laxation by increasing serum levels of vasoactive intestinal peptide (VIP), motilin (MTL) and substance P (SP), up-regulating the expression of VIP, cyclase-associated protein 1 (CAP1) and protein kinase A (PKA), and the expression of epithelial sodium channels (ENaC), and Na^+/H^+ exchanger 3 (NHE3) (Lv et al., 2024). Moreover, the laxative effects of rhubarb are also linked to its regulatory impact on intestinal flora and metabolism (Yang et al., 2022; Figure 4).

3.2 Anti-bacterial

Research on the bacteriostatic properties of rhubarb's monomers shows that free anthraquinones (including emodin, rhein, aloe-emodin) possess significant bacteriostatic activity against a broad spectrum of bacteria, such as *Staphylococcus aureus*, *Lactobacillus* and *Escherichia coli* (Stompor-Gorący, 2021). Rhubarb inhibits the growth of *S. aureus* by compromising the integrity of its cell wall and cell membrane (Xu et al., 2021). Additionally, aqueous extracts of rhubarb can prevent biofilm formation by down-regulating transduction systems and altering the levels of DNA-binding proteins and transcriptional regulators (Ding et al., 2017). *Chlamydia trachomatis* is a specialised pathogen that has become an exclusive intracellular pathogen due to a drastically reduced coding capacity, resulting in its dependence on the host cell for nutrient supply (Stelzner et al., 2023). While it does not directly inactivate *C. trachomatis*, it inhibits infection by modulating pathogen-host cell interactions (Yu et al., 2022; Figure 5).

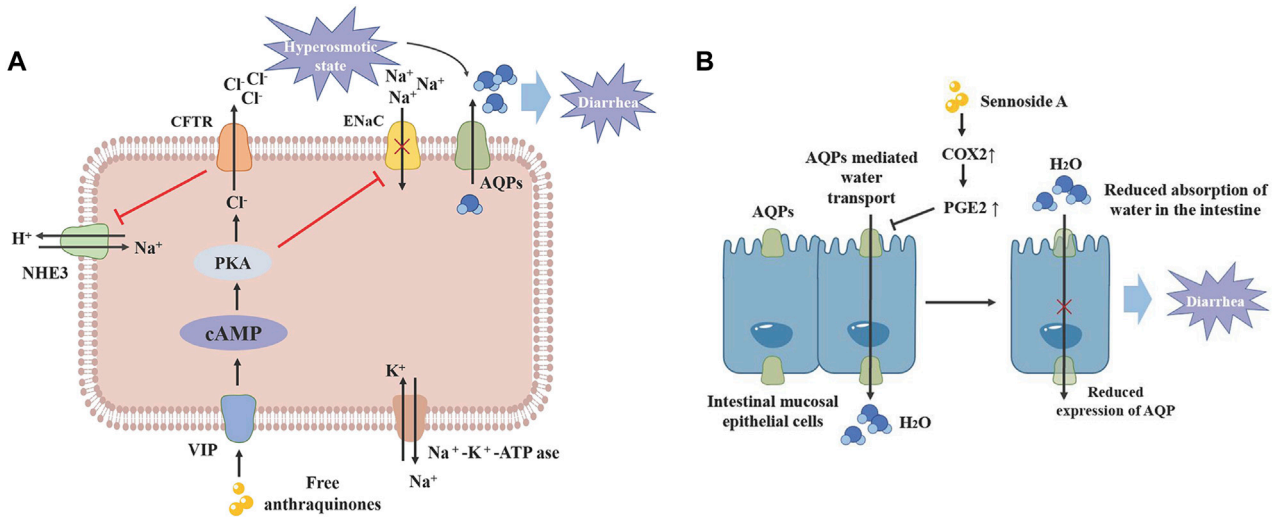

FIGURE 4
The laxative mechanism of monomer in rhubarb. **(A)** Free anthraquinone can upregulate VIP expression, promote CAMP/PKA signaling pathway transduction and CFTR expression, while inhibiting ENaC and NHE3 expression, increasing intestinal osmotic pressure and leading to diarrhea. **(B)** Sennoside A can inhibit the expression of COX2 and the release of PEG2 in macrophages, thereby reducing the expression of AQPs in the colon and inhibiting the absorption of water in the intestine, leading to diarrhea. CFTR: Cystic fibrosis transmembrane conductance regulator. AQP: Aquaporin. VIP: Vasoactive intestinal peptide. NHE3: Na*/H exchanger 3. ENaC: Epithelial sodium channel.

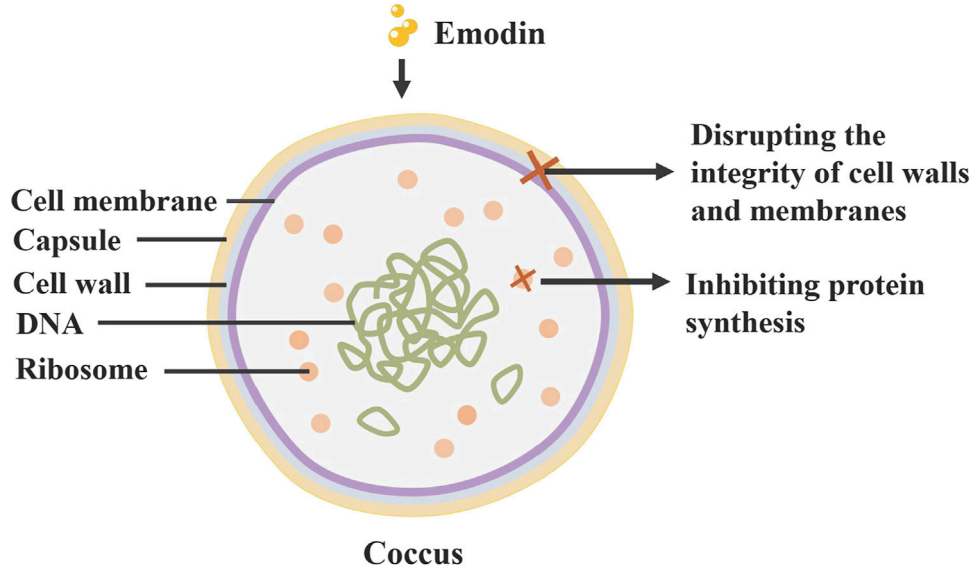

FIGURE 5
Antibacterial effect of rhubarb: Anthraquinone compounds in rhubarb can inhibit the growth of *Staphylococcus aureus* by disrupting its cell wall and membrane, and inhibiting its protein synthesis.

3.3 Anti-inflammatory

Numerous active compounds in rhubarb display potent anti-inflammatory activity, with anthraquinones like emodin, rhein, chrysophanol and aloe-emodin being particularly significant. Studies involving lipopolysaccharide (LPS)-induced RAW264.7 cells have shown that rhein inhibits the production of pro-inflammatory cytokines (interleukin-6 [IL-6], IL-1β and tumor necrosis factor-α [TNF-α]), and reduces NF-κB p65 levels. In LPS + ATP-induced RAW264.7 macrophages, rhein also diminished the expression of NALP3 inflammasome and cleaved IL-1β, suggesting that rhein's anti-inflammatory effects may stem from its ability to inhibit both NF-κB and NALP3 inflammasome pathways (Ge et al., 2017). Emodin and chrysophanol are noted to have similar effects (Zhu et al., 2016b; Wen et al., 2018). Notably, the anti-inflammatory effectiveness of aloe-emodin exceeds that of emodin and rhein at the same dosage, a difference attributed to its molecular structure (Hu, 2019; Figure 6).

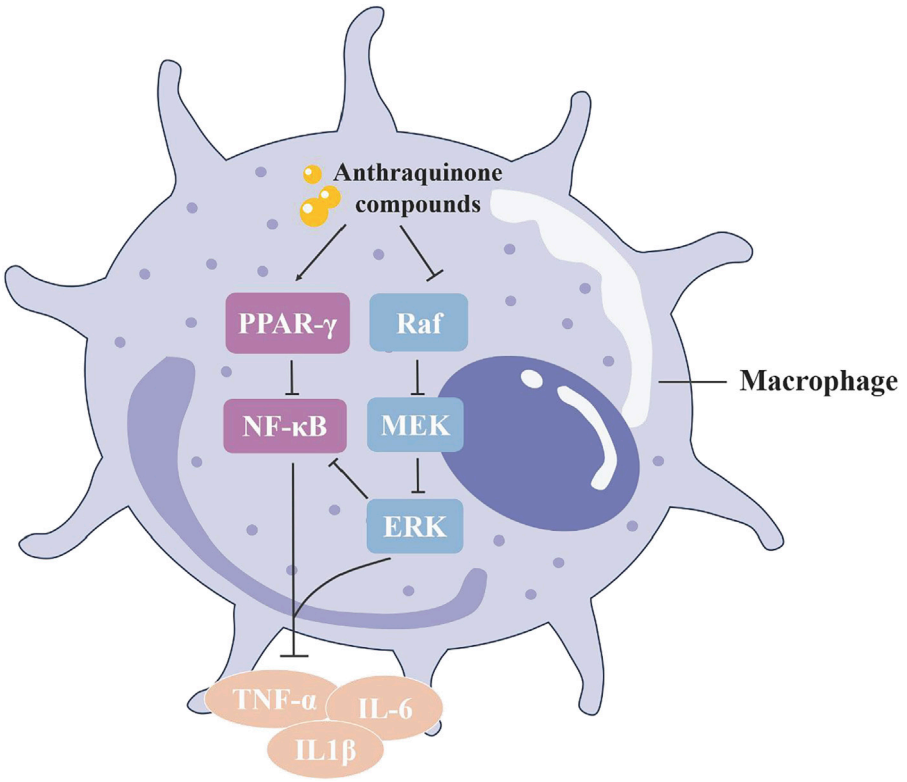

FIGURE 6
The ant-inflammatory mechanism of anthraquinone in rhubarb: The anthraquinone compounds in rhubarb can promote PPAR−y signaling in macrophages and inhibit phosphorylation of the MAPK signaling pathway, thereby inhibiting downstream NF−κ B activation and the release of inflammatory factors, reducing inflammation.

3.4 Regulation of blood coagulation

Rhubarb demonstrates a bidirectional regulatory effect on blood coagulation, capable of both activating and stopping bleeding through its diverse active compounds. Research based on network pharmacology has identified that key compounds in rhubarb, emodin-8-O-β-D-glucopyranoside, physcion-8-O-β-D-glucopyranoside and 3′-O-gallate, significantly enhance blood rheological parameters and arterial blood flow in hyperviscosity syndrome (HVS) rats, with anticoagulant effects comparable to aspirin (Gao et al., 2020). Conversely, the same compounds in rhubarb also perform hemostatic functions. Aqueous extracts of *R. palmatum L.* have shown pronounced vasoconstrictive effects on blood vessels, with d-catechin and gallic acid identified as the hemostatic active compounds through compound isolation, pharmacological screening and chemical structure identification (Du et al., 1983). Studies on *R. tanguticum Maxim.ex Balf.* from different production areas have also confirmed significant hemostatic and platelet-increasing effects in *R. tanguticum Maxim.ex Balf.* from the four main production areas of Qinghai (Wang S. W. et al., 2015). A systematic strategy based on computational simulation, biological validation and biophysical research was used in the experiment, which confirmed that gallic acid can directly inhibit thrombin and its induced platelet aggregation, and can also bind to thrombin protein and rapidly stabilize protein conformation (Zhang Y. et al., 2022). However, the current research on hemostasis of gallic acid mostly focuses on the hemostatic materials with gallic acid esterification and gallic acid compounds as raw materials (Trombetta et al., 2024; Yu et al., 2024). There is a lack of reliable experimental research on the mechanism through which d-catechin and gallic acid in rhubarb exert hemostatic effects (Figure 7).

3.5 Digestive system protective effects

Rhubarb exerts a protective effect on various organs of the digestive system. In studies examining the effects of the classic formula *Yinchenhao Decoction* (YCHD), with rhubarb as the main medication, on hepatic fibrosis, treatment with rhein in human hepatic L02 cells notably decreased the protein level of cleaved cysteine-3, and increased the expression of p-ERK1/2, PI3K and Bcl-XL proteins. *In vivo* experiments further demonstrated that treatment with YCHD not only alleviated liver fibrosis symptoms but also reduced apoptosis in hepatic parenchymal cells, confirming the decoction's ability to inhibit hepatic fibrosis in rats by regulating apoptosis (Cai et al., 2019). Moreover, emodin mitigates concurrent Concanavalin A (Con A)-induced liver injury in mice by inhibiting infiltration and activation of $CD4^+$ and F4/80+ cells, and suppressing the p38- MAPK-NF-κB pathway in $CD4^+$ T cells and macrophages (Xue et al., 2015). In addition, emodin may alleviate pancreatic injury by correcting the Treg/Th cell imbalance and inhibiting the inflammatory response, thereby mitigating severe acute pancreatitis (Wu et al., 2019; Figure 8).

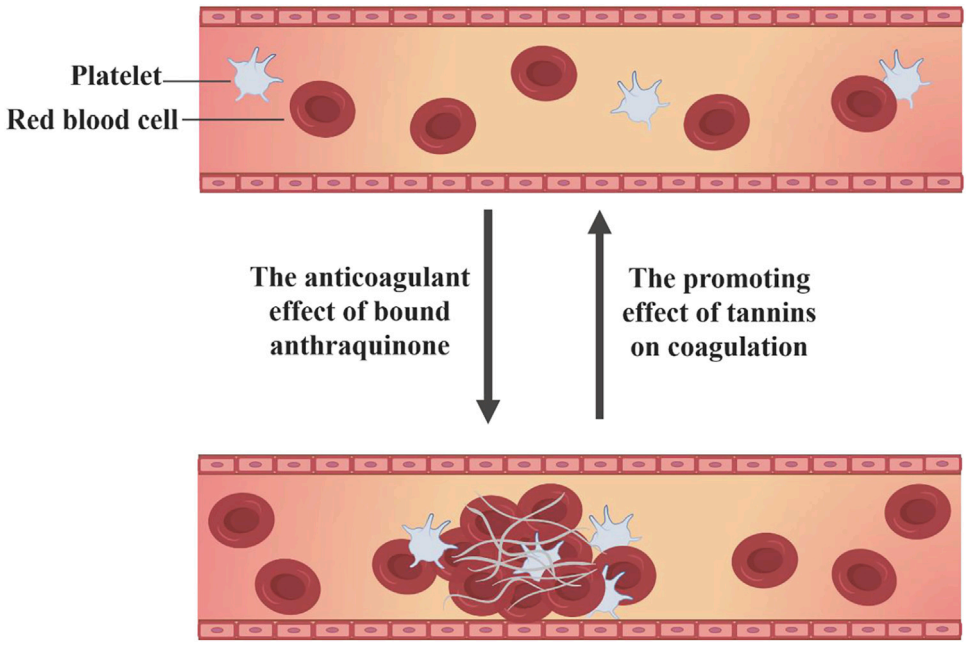

FIGURE 7
Bidirectional regulation of coagulation function by rhubarb compounds.

3.6 Anti-tumor

Rhubarb exhibits a potent inhibitory effect on various tumors across the respiratory, digestive and reproductive systems, including lung adenocarcinoma (Shia et al., 2011), gastric cancer (Chen et al., 2007), pancreatic cancer (Pan et al., 2016), cervical cancer (Liu et al., 2018) and ovarian cancer (Zhou et al., 2017). It effectively inhibits tumor cell growth (Liu et al., 2018), suppresses tumor invasion and migration (Chen et al., 2010; Zhou et al., 2017), and prevents the formation of tumor neovascularization, playing a crucial role in various stages of tumor progression by targeting different mechanisms. The anti-tumor effects of rhubarb are primarily attributed to a range of compounds extracted from it, such as emodin, rhein, aloe-emodin and stilbene (Cao et al., 2017). Rhein can regulate cyclin D1 by inducing the degradation of β-catenin, arresting the cell cycle in S-phase and inhibiting the proliferation of cervical cancer HeLa cells (Liu et al., 2018). It has been shown to induce apoptosis in human nasopharyngeal carcinoma cells through endoplasmic reticulum stress and a $Ca2^{+}$-dependent mitochondrial death pathway and to inhibit the migration and invasion of human tongue cancer SCC-4 cells and human ovarian cancer SKOV3-PM4 cells by regulating matrix metalloproteinases (MMPS) (Chen et al., 2010; Zhou et al., 2017). The Wnt/β-catenin signaling pathway, crucial in cell proliferation and invasion in lung cancer, gastric cancer, ovarian cancer and nephroblastoma, is negatively regulated by rhubarb, which promotes β-catenin protein degradation and inhibits tumor metastasis (Tsai et al., 2013). In advanced stages of cancer, TGF-β signaling has been shown to promote invasiveness and metastasis by inducing the expression of Snail and other transcription factors, leading to epithelial mesenchymal transition (EMT) (Peinado et al., 2003). Emodin can inhibit the expression of β-catenin in SiHa and HeLa cervical cancer cells, downregulate transforming growth factor-β (TGF-β), and inhibit the Wnt/β-catenin signaling pathway, and thus suppress the occurrence of EMT (Thacker and Karunagaran, 2015). These findings indicate that rhubarb's compounds can impact cancer-related biological processes through multiple signaling pathways, offering advantages over traditional cytotoxic drugs by reducing tumor drug resistance due to their multi-targeting properties. It has been demonstrated that emodin at a concentration of 10 μM can enhance the sensitivity of tumor cells to chemotherapy and radiotherapy by decreasing P-glycoprotein (P-gp) function and activating the mitochondrial apoptotic pathway *in vitro* (Liu et al., 2012; Li et al., 2016; Figure 9).

4 Influence of rhubarb concoctions on traditional pharmacological effects and clinical applications

Different concoctions of rhubarb significantly impact its traditional pharmacological actions, primarily due to changes in compounds during processing. These alterations in traditional pharmacology across various concoctions are detailed in Supplementary Table S8. Throughout years of clinical practice, medical practitioners have recognized the limitations of using single herbs due to the complexity of diseases and the diversity of patient constitutions. Consequently, they have developed a variety of Chinese medicinal herb combinations, such as pairs of herbs, angular herbs and multi-herb formulas, tailored according to the principles of Chinese medicine's diagnostic methods and the characteristics of the medicines (Wang et al., 2012). This extensive use of concoctions enhances the unique advantages and appeal of Chinese medicine in treating various diseases, as

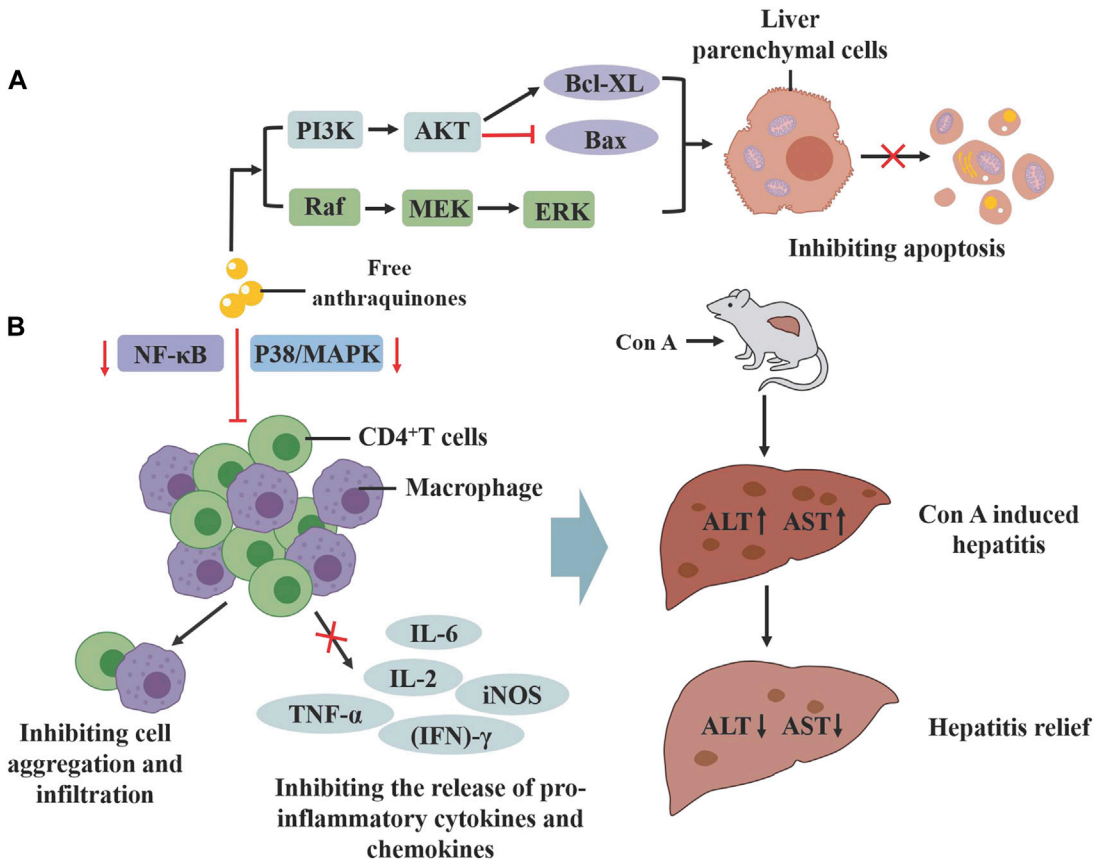

FIGURE 8
The protective effect of active compounds in rhubarb on the digestive system. **(A)** Rhein can activate the PI3K/AKT and MAPK signaling pathways, inhibiting liver cell apoptosis. **(B)** Emodin can inhibit the p38-MAPK and NF-KB signaling pathways in CD4+cells and macrophages, alleviating ConA induced liver injury.

exemplified in the traditional use of rhubarb. We have compiled the main formulas of Chinese medicine that utilize different concoctions of rhubarb (Supplementary Table S9). Given the distinct main effects of each concoction, individual concoctions of rhubarb and their compound formulas are also widely employed in treating conditions like constipation, intestinal obstruction, hepatitis, gastrointestinal bleeding, malignant tumors and other diseases (Supplementary Table S10; Figure 10).

4.1 Purgation to eliminate accumulation

"Purgation to eliminate accumulation" refers to the process by which medications clear stagnation in the stomach and intestines and alleviate constipation, thereby treating related gastrointestinal issues. Raw rhubarb is a primary agent for this effect. The laxative efficacy of raw rhubarb tends to diminish when processed, likely due to the decomposition and inactivation of anthraquinones during processing. Studies comparing the laxative effects of four rhubarb concoctions (raw rhubarb, wine rhubarb, cooked rhubarb and rhubarb charcoal) on healthy mice found that only raw rhubarb and wine rhubarb exhibited significant laxative effects, occurring approximately 3 h post-administration. Wine rhubarb slightly delayed the onset and reduced the frequency and volume of diarrheal stools compared to raw rhubarb, which showed considerably stronger laxative properties. Further experiments on intestinal motility revealed that raw rhubarb produced the most potent diarrheal effects, wine rhubarb was moderately effective, and both rhubarb charcoal and cooked rhubarb exhibited some antidiarrheal properties (Yan et al., 2010). In an experiment analyzing the effect of 75% ethanol extract of different concoctions on the propulsion rate of small intestinal charcoal and the activity of Na^+-K^+-ATPase in colon intestinal wall cells, results indicated significant inhibition of Na^+-K^+-ATPase activity in all concoctions compared to controls, with raw rhubarb showing the strongest effect. Both raw and wine rhubarb increased the propulsion rate of small intestinal charcoal in rats, while cooked rhubarb and rhubarb charcoal decreased it, aligning with previous research (Li Y. et al., 2011). The diarrhea-causing potency of different rhubarb concoctions, assessed *via* the "parallel line method of quantitative response", showed that raw rhubarb had the highest potency at 825.22 U/g, followed by wine rhubarb at 699.05 U/g, with cooked rhubarb weaker at 459.76 U/g, and rhubarb charcoal undetectable due to its low diarrheal potency (Li et al., 2012c). The comparative analysis of the laxative effects of raw and cooked rhubarb in a mouse model of heat-induced constipation revealed that the more potent effect of raw rhubarb might be induced by the stimulation of intestinal smooth muscle

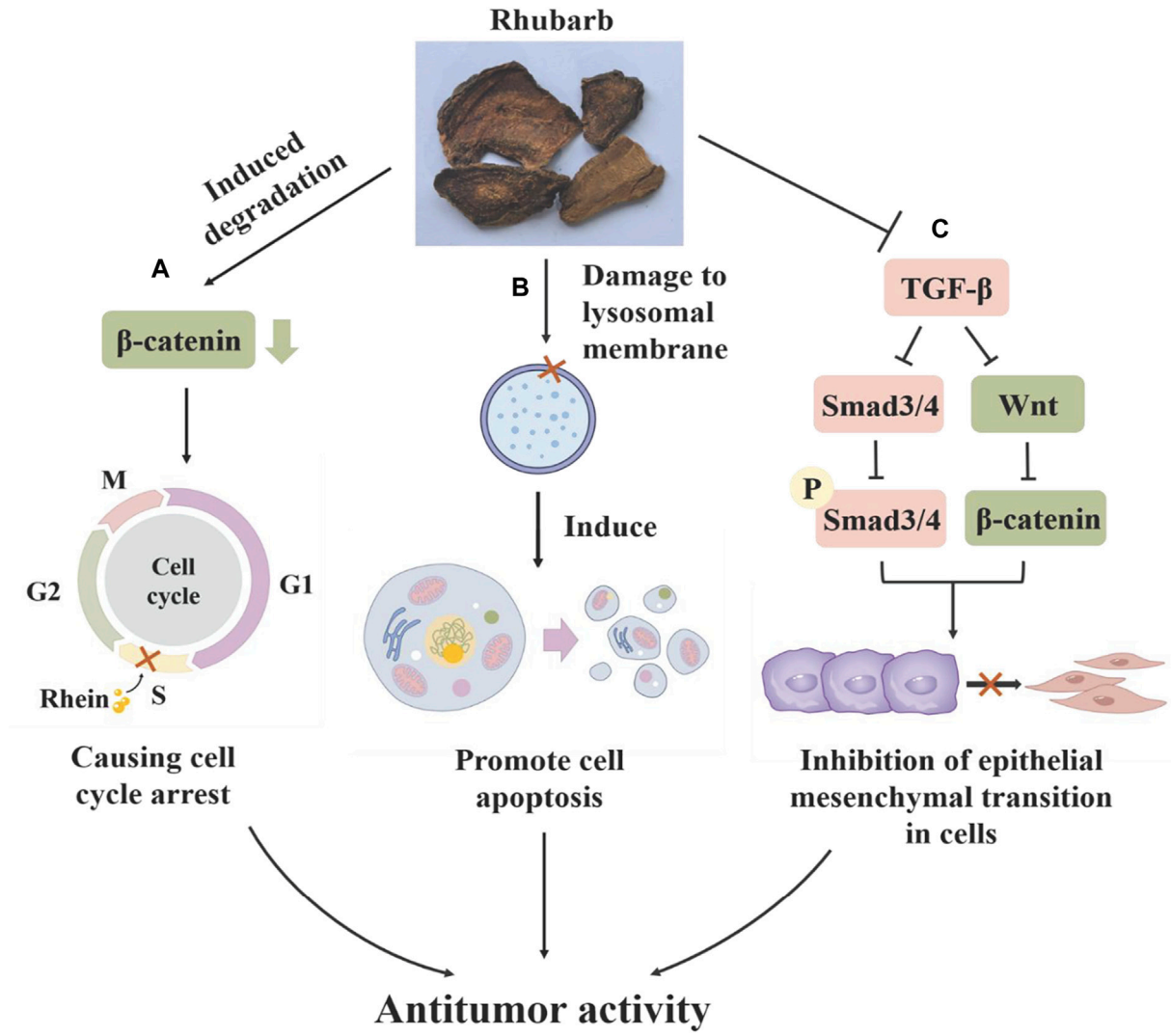

FIGURE 9
The mechanism of rhubarb in inhibiting gynecological malignant tumors: **(A)** Rhein can induce the degradation of ß-Catenin protein, causing cell cycle arrest in the S phase and inhibiting the proliferation of cervical cancer HeLa cells. **(B)** Rhubarb can damage the lysosomal membrane, increase the activity of tissue protease, and induce cell apoptosis. **(C)** Rhubarb can inhibit TGF-B/Smads and Wnt/B-catenin signaling pathways, thereby inhibiting the epithelial mesenchymal transition of tumor cells.

contractions, mediated by increased secretion of intestinal acetylcholinesterase (Ach E) and SP and the augmentation of intracellular Ca^{2+} concentration (Wu et al., 2014). Conversely, the diminished efficacy of cooked rhubarb may illustrate one mechanism behind the adage "raw rhubarb causes diarrhea, while cooked acts gradually".

Raw rhubarb and its formulations are utilized in treating constipation, gastrointestinal dysfunction and intestinal obstruction. Supplementation with raw rhubarb extract has improved stool frequency and consistency in a dose-dependent manner in middle-aged constipated patients, without impacting safety indicators, thus confirming its reliability and safety for non-severe constipation cases. This therapeutic effect is likely linked to the modulation of the intestinal microbiota by raw rhubarb (Neyrinck et al., 2022). Additionally, significant enhancements in gastrointestinal dynamics have been observed in patients with severe acute pancreatitis treated with *Da Chengqi Decoction* combined with western medicine therapy (Xiu et al., 2023). Topical application of raw rhubarb powder to the *Shenque* acupoint has effectively improved functional constipation in Parkinson's patients in terms of defecation frequency and stool character (Fan et al., 2015). External application of raw rhubarb and mirabilite powder around the umbilicus to assist in the treatment of adhesive intestinal obstruction can improve intestinal inflammation, shorten the duration of abdominal pain relief, and expedite the onset of spontaneous gas and defecation, thus proving the treatment's efficacy (Wang W. et al., 2018). *Jiawei Chengqi Decoction* can promote the recovery of gastrointestinal function, improve urodynamics, and improve the quality of life of patients after extensive hysterectomy with preservation of pelvic autonomic nerves, and the clinical efficacy is remarkable (Gao and Wang, 2015).

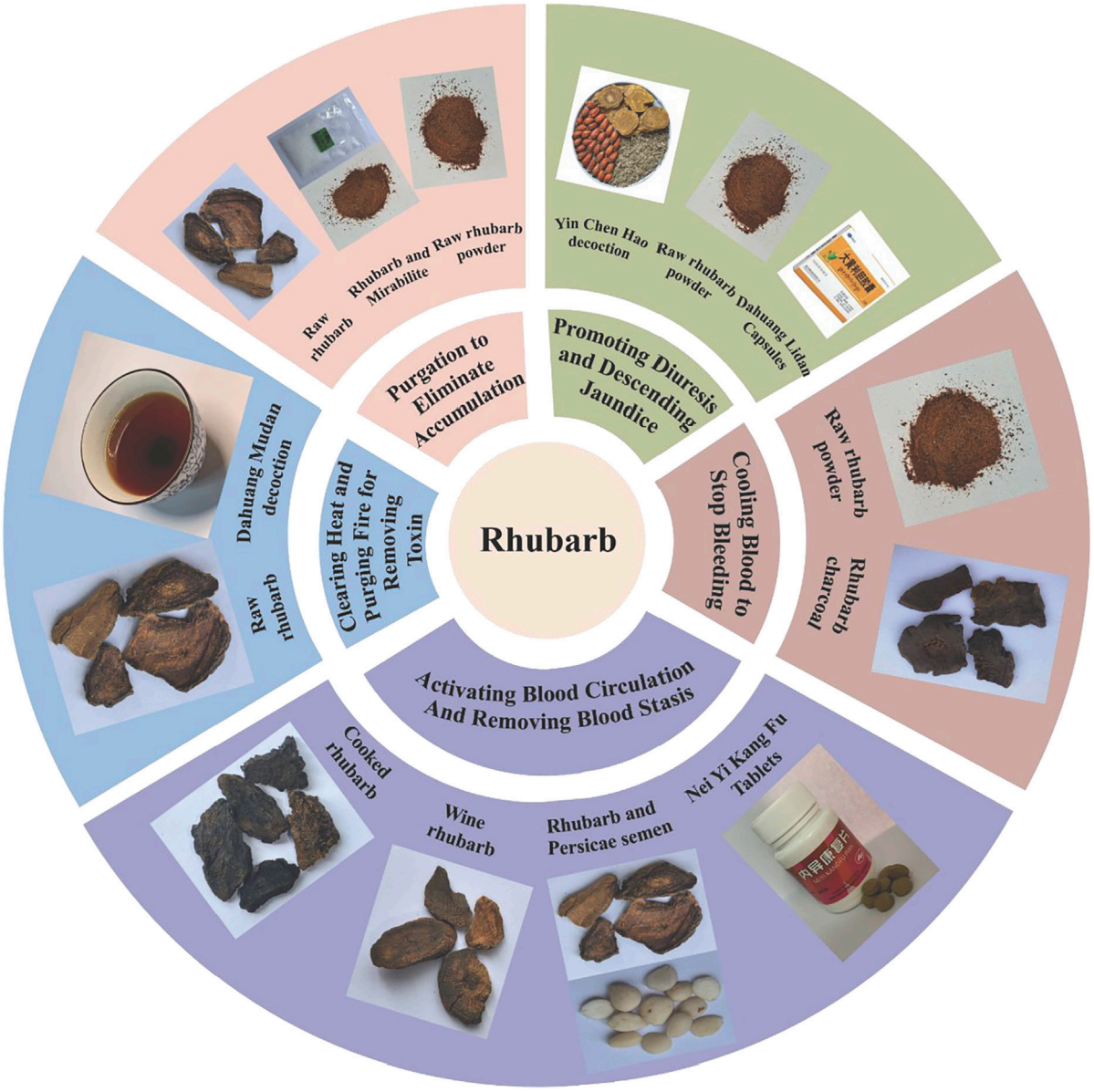

FIGURE 10
Influence of rhubarb concoctions on traditional pharmacological effects and clinical applications.

4.2 Clearing heat and purging fire for removing toxin

Rhubarb is known for its ability to clear heat, purge fire and detoxify, primarily due to its anti-pathogenic microorganism, anti-inflammatory and antitoxin pharmacological effects (Wang et al., 2019). In studies using a rat fever model and a rat foot swelling model, both raw and cooked rhubarb demonstrated an inhibitory effect on the increase of body temperature and swelling rate (Yang et al., 2011). The effects of rhubarb on inflammation were further analyzed using an oral ulcer model and a pneumonia model in rats, comparing the outcomes before and after wine-roasting (Wang Y. et al., 2015). Post wine-roasting, wine rhubarb significantly reduced the inflammation scores in rats with oral ulcers and was more effective in healing mucous membrane tissue damage. It also markedly decreased the number of leukocytes, the ratio of neutrophils and the level of TNF-α in the blood of pneumonia-afflicted rats, indicating that wine rhubarb has enhanced therapeutic effects on upper energizer diseases compared to its raw form.

In the management of inflammatory diseases, raw rhubarb is frequently used and proves effective in treating both acute and chronic inflammatory conditions. Topically applied raw rhubarb extract as an adjuvant treatment for severe periodontitis in diabetic patients improves clinical indices, demonstrates robust clinical efficacy, and maintains a favorable safety profile (Li et al., 2018). The combination of *Dahuang Mudan Decoction* (DMD) with antibiotics in treating pediatric periappendiceal abscesses significantly boosts the cure rate without causing liver injury,

underscoring the safety of this therapy (Lin et al., 2023). Many preclinical studies have shown that DMD has functions such as balancing gut microbiota, restoring intestinal homeostasis, protecting intestinal mucosa, immune suppression and anti-inflammatory effects. It is commonly used in clinical practice to treat ulcerative colitis (Yang et al., 2023). In treating chronic pelvic inflammatory disease, DMD reduces leukocyte levels in the serum and effectively mitigates the inflammatory response, enhancing clinical outcomes (Chen, 2021). Nasal feeding of raw rhubarb as an adjunct treatment for patients with severe pancreatitis complicated by abdominal cavity infection notably improves patient conditions, reduces inflammatory factors, and aids in the regression of the disease (Xiang et al., 2021).

4.3 Cooling blood to stop bleeding

Rhubarb is recognized for its ability to cool blood and stop bleeding, famously characterized as "stopping bleeding without leaving stasis" (Wang et al., 2019). The hemostatic effects of rhubarb and its various concoctions were compared using two methods: the capillary glass tube method and the mouse tail-breaking method, with a gray correlation analysis used to investigate the spectral effect relationship. The results indicated that the hemostatic times for the raw rhubarb group (13.90 ± 1.97 min) and the rhubarb charcoal group (6.40 ± 1.45 min) were significantly shorter than those of the control group (16.10 ± 1.66 min). There was no notable difference in hemostatic times between the wine rhubarb group (15.00 ± 1.94 min) and the cooked rhubarb group (15.00 ± 1.94 min). Additionally, compared to the coagulation time of the control group (3.05 ± 0.72 min), the coagulation time for the rhubarb charcoal group (1.85 ± 0.63 min) was significantly shorter (Zhu et al., 2008).

Clinically, rhubarb powder is frequently used to treat upper gastrointestinal bleeding. Gastroscopic application of ultramicro rhubarb powder for acute non-variceal upper gastrointestinal bleeding has shown significant advantages in terms of hemostasis time and rebleeding rates compared to epinephrine preparations (He and Yin, 2014; Zhou et al., 2015). In TCM, the process of "stir-fry to a charcoal" is employed to enhance the hemostatic effect, and rhubarb charcoal is commonly used to treat hemorrhagic conditions. However, there are no clinical studies evaluating the hemostatic effectiveness of rhubarb charcoal alone or in combination with compound formulas.

4.4 Removing blood stasis and dredging meridians

The term "removing blood stasis and dredging meridians" involves using medication to eliminate blood stasis, enabling *qi* and blood to flow freely through the body's meridians. A comparison of the effects of four rhubarb concoctions on activating blood circulation and removing blood stasis in an acute blood stasis rat model revealed varying degrees of improvement in fibrinogen (FIB), prothrombin time (PT), activated partial thromboplastin time (APTT), thrombin time (TT) and whole blood viscosity. The effects of wine rhubarb and cooked rhubarb were less pronounced than those of raw rhubarb, and charcoal rhubarb showed no significant impact on any indices (Sui et al., 2012). An evaluation using a blood bio-efficiency assay assessed the antiplatelet aggregation effects of 10 anthraquinone derivatives found in rhubarb. The results indicated that the blood-activating potency of rhein and emodin was significantly higher than that of aloe-emodin, chrysophanol and physcion, and was 5.02 and 5.15 times greater than that of aspirin, respectively, demonstrating a stronger antagonism to adenosine diphosphate (ADP)-induced platelet aggregation; The antiplatelet potencies of aloe-emodin-8-O-β-D-glucoside, rhein-8-O-β-D -glucoside, emodin-8-O-β-D -glucoside, chrysophanol-8-O-β-D -glucoside and physcion-8-O-β-D -glucoside were higher 4.13, 4.46, 9.31, 5.46 and 7.80 times than that of aspirin, respectively, which indicated that the five anthraquinone glucosides had a strong ability to antagonize ADP-induced platelet aggregation (Tan et al., 2018).

Among the different rhubarb concoctions, wine rhubarb and cooked rhubarb are most effective in activating blood circulation and removing blood stasis, making them commonly used in clinical settings for treating diseases associated with blood stasis. In traditional Chinese medicine processing theory, wine directs the medicine's properties to the upper energizer, making wine rhubarb particularly effective for treating blood stasis in respiratory diseases. *Jiawei Xiayuxue Decoction* combined with acetylcysteine has improved alveolar diffusion function, exercise endurance and quality of life in patients with interstitial pulmonary fibrosis, while halting the progression of lung lesions (An et al., 2017).

In TCM, one of the primary pathological factors of tumor diseases is "blood stasis". *Dahuang Zhechong Pill* (DZP), a classic formula for activating blood circulation and removing blood stasis that includes cooked rhubarb, underscores rhubarb's primary clinical application in tumor treatment. Drug research has also found that DZP can exert anti-tumor effects by inhibiting cell proliferation, inducing cell apoptosis, regulating immune function, inhibiting angiogenesis, reducing metastasis and reversing cell drug resistance (Tian et al., 2023). Transcatheter arterial chemoembolization (TACE) is recognized as a safe and effective palliative treatment for intermediate and advanced hepatocellular carcinoma, yet postoperative complications can impact therapeutic efficacy (Lv et al., 2022). The combination of DZP with TACE in treating primary liver cancer significantly enhanced the effective rate to 88.99%, improved clinical indicators, raised the benefit rate to 94.87%, and markedly reduced the incidence of postoperative adverse reactions (Dai et al., 2021). Additionally, DZP combined with paclitaxel+cisplatin and olaparib has improved lymphocyte and serum tumor marker levels in patients with advanced ovarian cancer, enhancing patient quality of life and reducing adverse reaction incidences (Chen and Zhao, 2023).

Endometriosis (EMs) and adenomyosis (AM), although benign gynecological conditions, exhibit malignant behaviors such as implantation, infiltration, metastasis and recurrence (Xia et al., 2016). And TCM theory suggests that the core mechanism is "stagnation of blood stasis". The Wine Rhubarb-Peach Seed herb pair, pivotal in many formulas for resolving blood stasis, has been studied by the author's team for its effectiveness in treating AM. As a systematic and holistic medical research paradigm, network

pharmacology helps to systematically reveal the biological basis of TCM, and has been widely applied in the research of bioactive compounds, syndromes, formulas and other topics of TCM (Wang and Li, 2022). Network pharmacology studies have suggested that this herb pair can target AM through multiple pathways, particularly through the P53 signaling and apoptosis pathways mediated by the expression of P53 and BAX (Liao et al., 2020). Additionally, this herb pair influences the kinetic characteristics of endometrial cells in mice with AM, inhibiting abnormal proliferation and reducing cell migration and invasiveness (Lei et al., 2023). The traditional hospital preparation *NeYiKangFu Tablet* (NYKF), featuring the Cooked Rhubarb-Peach Seed herb pair, has been widely used clinically to treat EMs and AM. NYKF promotes apoptosis and inhibits cell proliferation and migration in EMs by targeting the RAF kinase inhibitor protein (RKIP) to inhibit the RAF/MEK/ERK signaling pathway, as demonstrated in our animal experiments (Wen et al., 2022). DZP, whose core medication including Cooked Rhubarb-Peach Seed herb pair, has also been utilized in the treatment of EMs. Compared with mifepristone, DZP can better improve clinical symptoms and signs in patients, and its mechanism of action may be related to the regulation of prostaglandin levels (Li, 2013). On the basis of progestin therapy, the use of DZP in the treatment of EMs patients with pelvic pain can further reduce the symptoms associated with pelvic pain, improve the quality of life of the patients and clinical efficacy, and have the effect of regulating the levels of prostaglandins, matrix metalloproteinases and pro-inflammatory factors (Fan et al., 2019).

4.5 Promoting diuresis and descending jaundice

Promoting diuresis and descending jaundice are critical traditional effects of rhubarb, reflecting its therapeutic role in treating liver and gallbladder disorders. Rhubarb compound preparations have demonstrated effective treatment for common liver diseases such as jaundice hepatitis, non-alcoholic fatty liver disease and cirrhosis ascites. The combination of *Dahuang Lidan Capsule* and silymarin in treating non-alcoholic fatty liver disease has been shown to improve the liver function and lipid levels in patients, enhance clinical outcomes, and potentially regulate intestinal flora, which may be one of the mechanisms of its effectiveness (Li et al., 2021). YCHD combined with probiotics significantly ameliorates symptoms of non-alcoholic fatty liver disease, reduces levels of blood lipids and liver enzymes, prevents hepatocyte destruction, and notably decreases levels of lipopolysaccharide-binding protein (LBP), total bile acid (TBA) and TNF-α. This treatment also repairs intestinal mucosal barrier function, reduces the inflammatory response causing liver damage, and interrupts the liver-intestinal vicious cycle, thus protecting the liver (Gu, 2021). Furthermore, the oral administration of raw rhubarb powder as an adjuvant in the treatment of jaundice hepatitis significantly improved the pathological damage to the liver of patients and markedly reduces the levels of alanine aminotransferase (ALT) and total bilirubin (TB) in the liver tissue and serum, possibly through the modulation of the Fas/FasL system by rhubarb (Huang et al., 2008). However, the differences between various rhubarb concoctions in inducing diuresis and reducing jaundice have not been experimentally studied and warrant further investigation.

5 Toxicological studies

5.1 Toxicity of rhubarb

As research into the pharmacological activities of rhubarb deepens, attention has increasingly focused on its potential toxic and side effects. Current studies predominantly suggest that anthraquinones, the most abundant compounds in rhubarb, might be responsible for its toxicity, particularly causing hepatorenal issues during drug use. Emodin exhibits concentration and time-dependent cytotoxic effects on L-02 cells (Li C. L. et al., 2012) and can significantly disrupt cellular metabolism, including glutathione and fatty acid metabolism (Liu et al., 2015). *In vitro* studies have demonstrated that aloe-emodin may inhibit the proliferation of HL-7702 cells by inducing reactive oxygen species (ROS) production, leading to Fas-mediated death and mitochondrial pathway activation, thus causing cell cycle arrest, apoptosis and liver cell damage (Dong et al., 2017). Long-term, high-dose administration of rhein also shows notable toxicity to mouse kidneys, with more pronounced effects in males (Hu et al., 2019). The toxicity of total anthraquinone from rhubarb has a dose-effect relationship with HK-2 cells, directly inhibiting their proliferation, altering cell morphology, and at low dosages, causing advanced apoptosis and necrosis (Ren et al., 2015b). Total anthraquinone can also induce varying degrees of edema and necrosis in rat renal tubular epithelial cells (Ren et al., 2012).

The strong laxative effect of rhubarb frequently causes gastrointestinal reactions in clinical practice, with anthraquinone compounds primarily responsible for these effects (Qin et al., 2011). Concerns exist that excessive use of anthraquinones may lead to melanosis coli (Zhang et al., 2023) and potentially increase the risk of colon cancer. However, it has not been confirmed that long-term use of high-dose sennosides induces intestinal hyperplasia or increases the risk of melanosis coli and subsequent colon cancer (Le et al., 2021). Emodin, another compound, exhibits embryotoxic effects (Chang et al., 2012a; Chang et al., 2012b) that could damage embryonic development through caspase-dependent apoptosis, significantly reducing the maturation of oocytes, fertilization rates and *in vitro* embryo development. It may also induce apoptosis in the cell mass within the blastocyst and the trophoblast ectoderm in mice, resulting in decreased embryo development and survival rates. In addition, certain anthraquinones in rhubarb are known to cause cardiotoxicity (Li et al., 2022), phototoxicity, genotoxicity, reproductive toxicity and other adverse effects (Dong et al., 2016; Dong et al., 2020). Tannins in rhubarb also appear to demonstrate hepatorenal toxicity, evidenced by reduced liver transparency, liver atrophy, delayed absorption of the yolk sac, liver cell deformation, and apoptosis in juvenile zebrafish (Wang et al., 2022), as well as mild toxicity to HK-2 cells (Ren et al., 2015a).

Compared to anthraquinones, the toxicity of other rhubarb compounds such as tannins, stilbenes and phenylbutanones has been less studied, and most of them were *in vitro* and *in vivo*, although this is also a crucial step for the clinical application of rhubarb. Therefore, further research on compounds other than

anthraquinones and well-designed clinical studies are needed to more comprehensively understand the toxicological effects of rhubarb on the human body.

5.2 Effects of processing on toxicity

The *Jingyue's Complete Book (Jingyue QuanShu)* and *Convenient Reader on Materia Medica (Bencao Biandu)* note that rhubarb is inherently cold, with a strong smell and flavor, classified as deeply yin, and is toxic. However, it is also acknowledged that processing rhubarb or combining it with other Chinese medicinal herbs can mitigate its intense properties. Indeed, the processing of Chinese medicinal herbs has been shown to reduce toxicity to some extent. There is experimental evidence that "7 times steaming" cooked rhubarb nearly eliminates the hepatotoxicity seen in raw products (Sim et al., 2015). A study investigated the relationship between detoxification processes and changes in rhubarb's compounds, establishing a correlation sequence for major compounds associated with hepatorenal toxicity: total combined anthraquinones> total tannins> total free anthraquinones (Wang et al., 2009). While raw rhubarb can harm the liver and kidneys in mice, processed rhubarb diminishes this toxicity, likely due to reduced levels of combined anthraquinones and tannins. Further research in an acute toxicity study on zebrafish demonstrated that, compared to liver degeneration observed in the group treated with raw rhubarb, the group treated with cooked rhubarb exhibited only mild liver degeneration at the same high concentration. The maximum non-lethal concentration of cooked rhubarb was significantly higher, about nine times that of raw rhubarb, indicating a substantial detoxification effect (Wang et al., 2022). After processing, the impact of rhubarb's "bitter cold" on the stomach is significantly reduced, lessening gastric mucosa damage and gastrointestinal dysfunction in rats (Zhang et al., 2019). The study on the toxicity of different rhubarb concoctions on *Tetrahymena thermophila* BF5, found that the inhibitory effect on growth was in the order of raw rhubarb> wine rhubarb> cooked rhubarb> rhubarb charcoal, suggesting significant detoxification post-processing (Li et al., 2012b). Another research also demonstrated that both steaming and vinegar steaming effectively reduce the genotoxicity of rhubarb (Zou et al., 2011).

Multiple toxicological studies align with compounds analyses pre- and post-processing, suggesting that processing can detoxify by reducing large molecule compounds like anthraquinones and tannins. However, the increased content of free anthraquinones such as emodin, rhein, aloe-emodin, physcion and chrysophanol post-processing presents a contradiction. An *in vivo* study examined the distribution of free anthraquinones in rat tissues after administration of raw and cooked rhubarb extracts, revealing that despite higher levels of free anthraquinones in cooked rhubarb, the concentrations of rhein, emodin and aloe-emodin, particularly in liver and kidney tissues, were significantly decreased (Fang et al., 2011). This suggests that processing not only alters the content but may also modify the efficacy and reduce toxicity by influencing the distribution and action of its compounds within the body, providing a scientific foundation for "processing attenuating toxicity". Nonetheless, more pharmacokinetic studies on the compounds of rhubarb pre- and post-processing are necessary to further elucidate the mechanisms of processing.

6 Summarizing and looking forward

Rhubarb is renowned for its diverse pharmacological effects. The TCM technique of processing can alter the composition of its compounds to enhance its efficacy, modify its medicinal properties, and reduce its toxicity. The effectiveness of rhubarb and its preparations in treating diseases has been well-documented through long-standing practice in Chinese medicine, highlighting its significant clinical value. Raw rhubarb is characterized as bitter, cold and sedative, possessing strong, harsh medicinal properties with potent laxative effects. Wine rhubarb, also bitter and cold, has a slightly slower laxative effect and is effective at clearing heat and toxins from the upper energizer. Cooked rhubarb, with reduced laxative strength, enhances blood circulation and removes blood stasis, making it particularly useful in oncology. Rhubarb charcoal, with minimal laxative properties, is primarily used to cool blood and stop bleeding. Although numerous studies have investigated the changes in active compounds due to various rhubarb processing, discrepancies in processing temperature, duration, and solvents across studies introduce variability in the outcomes. This variability complicates the consistency of the changes in active compounds after processing, impacting their clinical applications. Implementing strict and standardized processing procedures and compound identification standards is crucial to address these issues. Moreover, there is a shortage of high-quality clinical studies on the active monomers, whole drug and compound formulations of rhubarb, which hampers the development of systematic medication regimens and clinical promotion for rhubarb and its concoctions. As a multi-potency, multi-targeted Chinese medicine, ongoing pharmacological research on various concoctions of rhubarb will facilitate the standardization of its processing and clinical use, enhance our understanding of its therapeutic efficacy, and broaden the spectrum of treatable diseases with rhubarb. It is also conducive to further exploration of the medicinal value of rhubarb, improve its therapeutic effect, and provide more valuable basis for clinical application.

Author contributions

YW: Formal Analysis, Investigation, Methodology, Supervision, Writing–review and editing. P-JY: Data curation, Formal Analysis, Investigation, Methodology, Writing–original draft. P-XF: Data curation, Formal Analysis, Investigation, Methodology, Writing–original draft. S-SL: Formal Analysis, Methodology, Visualization, Writing–original draft. M-YL: Formal Analysis, Methodology, Writing–original draft. X-YF: Resources, Supervision, Writing–original draft. S-BW: Conceptualization, Funding acquisition, Methodology, Resources, Writing–review and editing.

Funding

The author(s) declare that financial support was received for the research, authorship, and/or publication of this article. This work was supported by the National Natural Science Foundation of China (No. 82174431) and the National Celebrated Traditional Chinese

Medicine Expert Inheritance Studio of Shao-bin S-BW (No. CJJ2023062).

Acknowledgments

We would like to thank all the authors for their contributions to this manuscript.

Conflict of interest

The authors declare that the research was conducted in the absence of any commercial or financial relationships that could be construed as a potential conflict of interest.

Publisher's note

Supplementary material

The Supplementary Material for this article can be found online at: https://www.frontiersin.org/articles/10.3389/fphar.2024.1442297/full#supplementary-material

References

An, S. Y., Zhao, W. Q., Zheng, M. Y., and Hu, J. (2017). Clinical study of Modified Xiayuxue Decoction combined with acetylcysteine in the treatment of interstitial pulmonary fibrosis. *Shanghai J. Traditional Chin. Med.* 51 (09), 57–59. doi:10.16305/j.1007-1334.2017.09.015

Cai, F. F., Bian, Y. Q., Wu, R., Sun, Y., Chen, X. L., Yang, M. D., et al. (2019). Yinchenhao decoction suppresses rat liver fibrosis involved in an apoptosis regulation mechanism based on network pharmacology and transcriptomic analysis. *Biomed. Pharmacother.* 114, 108863. doi:10.1016/j.biopha.2019.108863

Cao, Y. J., Pu, Z. J., Tang, Y. P., Shen, J., Chen, Y. Y., Kang, A., et al. (2017). Advances in bio-active constituents, pharmacology and clinical applications of rhubarb. *Chin. Med.* 12, 36. doi:10.1186/s13020-017-0158-5

Chang, M. H., Chang, S. C., and Chan, W. H. (2012a). Injurious effects of emodin on maturation of mouse oocytes, fertilization and fetal development via apoptosis. *Int. J. Mol. Sci.* 13 (11), 13911–13925. doi:10.3390/ijms131113911

Chang, M. H., Huang, F. J., and Chan, W. H. (2012b). Emodin induces embryonic toxicity in mouse blastocysts through apoptosis. *Toxicology* 299 (1), 25–32. doi:10.1016/j.tox.2012.05.006

Chen, H. G. (2021). Observation on the effect of modified Dahuang Mudan Decoction on chronic pelvic inflammation with damp-heat stasis syndrome. *Chin. J. Mod. Drug Appl.* 15 (16), 188–190. doi:10.14164/j.cnki.cn11-5581/r.2021.16.073

Chen, L., and Zhao, W. (2023). Effect of modified Dahuang Zhechong pills combined with paclitaxel+cisplatin and Olaparib on lymphocytes in patients with advanced ovarian cancer. *Hunan J. Traditional Chin. Med.* 39 (10), 11–14+24. doi:10.16808/j.cnki.issn1003-7705.2023.10.004

Chen, S. H., Lin, K. Y., Chang, C. C., Fang, C. L., and Lin, C. P. (2007). Aloe-emodin-induced apoptosis in human gastric carcinoma cells. *Food Chem. Toxicol.* 45 (11), 2296–2303. doi:10.1016/j.fct.2007.06.005

Chen, Y. Y., Chiang, S. Y., Lin, J. G., Ma, Y. S., Liao, C. L., Weng, S. W., et al. (2010). Emodin, aloe-emodin and rhein inhibit migration and invasion in human tongue cancer SCC-4 cells through the inhibition of gene expression of matrix metalloproteinase-9. *Int. J. Oncol.* 36 (5), 1113–1120. doi:10.3892/ijo_00000593

Chen, Z., Ye, S. Y., Yang, Y., and Li, Z. Y. (2019). A review on charred traditional Chinese herbs: carbonization to yield a haemostatic effect. *Pharm. Biol.* 57 (1), 498–506. doi:10.1080/13880209.2019.1645700

Committee, N. P. (2020). *Pharmacopoeia of the People's Republic of China(Part One)*. Beijing: China Medical Science and Technology Press.

Dai, C. M., Jin, S., and Zhang, J. Z. (2021). Effect of Dahuang Zhechong Pills combined with TACE on VEGF, MMP-2, TGF-β1 and immune function of patients with primary liver cancer (blood stasis and collaterals blocking type). *China J. Chin. Materia Medica* 46 (03), 722–729. doi:10.19540/j.cnki.cjcmm.20200716.501

Dai, X. Y., Yan, Y. L., Wu, Q. F., Yu, C. H., Liu, X., and Jiang, Y. Q. (2014). Comparative pharmacokinetics of rhein and chrysophanol after oral administration of Quyu Qingre granules in normal and acute blood stasis rabbits. *J. Ethnopharmacol.* 153 (2), 338–343. doi:10.1016/j.jep.2014.02.005

De Filippis, B., Ammazzalorso, A., Fantacuzzi, M., Giampietro, L., Maccallini, C., and Amoroso, R. (2017). Anticancer activity of stilbene-based derivatives. *ChemMedChem* 12 (8), 558–570. doi:10.1002/cmdc.201700045

Ding, W. Y., Li, Y. H., Lian, H., Ai, X. Y., Zhao, Y. L., Yang, Y. B., et al. (2017). Sub-minimum inhibitory concentrations of rhubarb water extracts inhibit Streptococcus suis biofilm formation. *Front. Pharmacol.* 8, 425. doi:10.3389/fphar.2017.00425

Dong, X., Fu, J., Yin, X., Cao, S., Li, X., Lin, L., et al. (2016). Emodin: a review of its pharmacology, toxicity and pharmacokinetics. *Phytother. Res.* 30 (8), 1207–1218. doi:10.1002/ptr.5631

Dong, X., Fu, J., Yin, X., Yang, C., and Ni, J. (2017). Aloe-emodin induces apoptosis in human liver HL-7702 cells through Fas death pathway and the mitochondrial pathway by generating reactive oxygen species. *Phytother. Res.* 31 (6), 927–936. doi:10.1002/ptr.5820

Dong, X., Zeng, Y., Liu, Y., You, L., Yin, X., Fu, J., et al. (2020). Aloe-emodin: a review of its pharmacology, toxicity, and pharmacokinetics. *Phytother. Res.* 34 (2), 270–281. doi:10.1002/ptr.6532

Du, S., Dai, K. X., Li, D. Y., and Jing, W. (1983). A study on the hemostatic active constituents of rhubarb. *Chin. Tradit. Pat. Med.* (07), 29–30.

Dutta, B. J., Rakshe, P. S., Maurya, N., Chib, S., and Singh, S. (2023). Unlocking the therapeutic potential of natural stilbene: exploring pterostilbene as a powerful ally against aging and cognitive decline. *Ageing Res. Rev.* 92, 102125. doi:10.1016/j.arr.2023.102125

Dvorakova, M., and Landa, P. (2017). Anti-inflammatory activity of natural stilbenoids: a review. *Pharmacol. Res.* 124, 126–145. doi:10.1016/j.phrs.2017.08.002

Fan, Q., Wei, Y. N., Yin, L., and Chen, X. (2019). Clinical effect of Dahuang zhechong Pill on pelvic pain caused by endometriosis with qi stagnation and blood stasis syndrome. *Chin. J. Exp. Traditional Med. Formulae* 25 (12), 121–126. doi:10.13422/j.cnki.syfjx.20191231

Fan, Y. Z., Xie, Y. C., and Lin, L. (2015). Observation on the therapeutic effect of applying rhubarb powder to Shenque acupoint on functional constipation in Parkinson's disease. *Pharmacol. Clin. Chin. Materia Medica* 31 (02), 173–174. doi:10.13412/j.cnki.zyyl.2015.02.089

Fang, F., Wang, J. B., Zhao, Y. L., Jin, C., Kong, W., Zhao, H. P., et al. (2011). Tissue distribution of free anthraquinones in SD rats after orally administered extracts from raw and prepared rhubarbs. *Acta Pharm. Sin.* 46 (03), 350–354. doi:10.16438/j.0513-4870.2011.03.008

Gao, D., Wu, S. N., Zhang, C. E., Li, R. S., Liu, Z. J., Xiao, X. H., et al. (2020). Exploration in the mechanism of rhubarb for the treatment of hyperviscosity syndrome based on network pharmacology. *J. Ethnopharmacol.* 261, 113078. doi:10.1016/j.jep.2020.113078

Gao, L. L., Guo, T., Xu, X. D., and Yang, J. S. (2017). Rapid identification and simultaneous analysis of multiple constituents from Rheum tanguticum Maxim. ex Balf. by UPLC/Q-TOF-MS. *Nat. Prod. Res.* 31 (13), 1529–1535. doi:10.1080/14786419.2017.1280491

Gao, Z. H., and Wang, Q. Q. (2015). Effect of Jiawei Chengqi Decoction on the recovery of gastrointestinal function after extensive hysterectomy with preservation of pelvic autonomic nerves. *Pharmacol. Clin. Chin. Materia Medica* 31 (04), 220–222. doi:10.13412/j.cnki.zyyl.2015.04.070

Ge, H., Tang, H., Liang, Y., Wu, J., Yang, Q., Zeng, L., et al. (2017). Rhein attenuates inflammation through inhibition of NF-κB and NALP3 inflammasome *in vivo* and *in vitro*. *Drug Des. Devel Ther.* 11, 1663–1671. doi:10.2147/dddt.S133069

Gu, W. (2021). To explore the efficacy of Yinchenhao Decoction combining with intestinal probiotics in the treatment of non-alcoholic fatty liver. *Chin. J. Integr. Traditional West. Med. Dig.* 29 (10), 745–748. doi:10.3969/j.issn.1671-038X.2021.10.14

He, Y. F., and Yin, P. F. (2014). Observation on the therapeutic effect of spraying ultra-fine rhubarb powder under gastroscopy on acute non variceal upper

gastrointestinal bleeding. *Mod. J. Integr. Traditional Chin. West. Med.* 23 (23), 2574–2576. doi:10.3969/j.issn.1008-8849.2014.23.027

Hou, A., Lv, J., Zhang, S., Zhang, J., Yang, L., Jiang, H., et al. (2023). Salt processing: a unique and classic technology for Chinese medicine processing. *Front. Pharmacol.* 14, 1116047. doi:10.3389/fphar.2023.1116047

Hu, J., Li, P., and Zhang, T. (2018). Rhubarb combined with trypsin inhibitor for severe acute pancreatitis: a systematic review and meta-analysis. *Phytother. Res.* 32 (8), 1450–1458. doi:10.1002/ptr.6096

Hu, Y. F. (2019). *The study on the molecular mechanism and structure-activity relationship of rhubarb anthraquinone inhibitingthe inflammatory in LPS-stimulated macrophages*. Chengdu (China): Chengdu University of TCM. doctor's thesis.

Hu, Y. F., Huang, W. Y., Li, Y. Q., Luo, Y., Jiang, Q., Liang, Y. S., et al. (2019). Mechanism of rhein on renal toxicity of mice. *Chin. J. Exp. Traditional Med. Formulae* 25 (11), 54–59. doi:10.13422/j.cnki.syfjx.20190821

Huang, Y. q., Lin, Z. H., and Wang, C. G. (2008). The effect of rhubarb on the expression of Fas/FasL in patients with jaundice hepatitis. *Med. J. Chin. People's Liberation Army* (02), 236. doi:10.3321/j.issn:0577-7402.2008.02.039

Kang, Y. G. (2013). *Identificology of traditional Chinese medicine*. Hunan, China: Hunan Science and Technology Press.

Kon, R., Ikarashi, N., Nagoya, C., Takayama, T., Kusunoki, Y., Ishii, M., et al. (2014). Rheinanthrone, a metabolite of sennoside A, triggers macrophage activation to decrease aquaporin-3 expression in the colon, causing the laxative effect of rhubarb extract. *J. Ethnopharmacol.* 152 (1), 190–200. doi:10.1016/j.jep.2013.12.055

Laddha, A. P., and Kulkarni, Y. A. (2019). Tannins and vascular complications of Diabetes: an update. *Phytomedicine* 56, 229–245. doi:10.1016/j.phymed.2018.10.026

Le, J., Ji, H., Zhou, X., Wei, X., Chen, Y., Fu, Y., et al. (2021). Pharmacology, toxicology, and metabolism of sennoside A, A medicinal plant-derived natural compound. *Front. Pharmacol.* 12, 714586. doi:10.3389/fphar.2021.714586

Lei, Y., Mao, P., Yi, Y. L., Fu, X. Y., and Qu, Z. (2023). Regulation mechanism of"Dahuang(rhubarb) and taoren(peach kernel) "on dynamic characteristics of endometrial cells in adenomyosis mice. *Chin. Archives Traditional Chin. Med.* 41 (04), 151–156. doi:10.13193/j.issn.1673-7717.2023.04.030

Li, C. L., Ma, J., Zheng, L., Li, H. J., and Li, P. (2012a). Determination of emodin in L-02 cells and cell culture media with liquid chromatography-mass spectrometry: application to a cellular toxicokinetic study. *J. Pharm. Biomed. Anal.* 71, 71–78. doi:10.1016/j.jpba.2012.07.031

Li, F. J. (2013). Clinical study on Dahuang zhechong capsule for treating endometriosis. *Chin. J. Exp. Traditional Med. Formulae* 19 (04), 297–299. doi:10.13422/j.cnki.syfjx.2013.04.011

Li, G. M., Chen, J. R., Zhang, H. Q., Sun, C., Chen, G. R., Xiong, Q. Y., et al. (2022). Rhein activated Fas-induced apoptosis pathway causing cardiotoxicity *in vitro* and *in vivo*. *Toxicol. Lett.* 363, 67–76. doi:10.1016/j.toxlet.2022.04.006

Li, H. F., Ma, Y. G., Xiao, X. H., and Liu, Y. (2012b). Toxicity-attenuating effect of processed rhubarb products based on bio-heat activity in Tetrahymena thermophila BF5. *Chin. Traditional Herb. Drugs* 43 (01), 103–105.

Li, H. F., Sun, Q., Wang, J. B., Jin, C., and Xiao, X. H. (2011a). Analysis on change law of main chemical constituents of rhubarb after processing. *J. Shanxi Univ. Chin. Med.* 12 (06), 14–17.

Li, H. F., Wang, J. B., Qu, Y., and Xiao, X. H. (2012c). Analysis on changes of purgative biopotency in different processed products of rhubarb. *China J. Chin. Materia Medica* 37 (03), 302–304.

Li, L. (2011). *Study on the variation rules of material basis of rhubarb after processing*. Beijing (China): China Academy of Chinese Medical Sciences. doctor's thesis.

Li, L., Zhang, C., Xiao, Y. Q., Chen, D. D., Tian, G. F., and Wang, Y. (2010). Comparison of two butyrophenone constituents in 5 kinds of pieces of Dahuang (Radix et Rhizoma Rhei). *J. Beijing Univ. Traditional Chin. Med.* 33 (08), 559–561.

Li, N., Li, J. d., Li, Y., Hua, H. L., Ji, Y. Z., and Zhou, H. M. (2021). Effect of Dahuang Lidan capsule combined with Silybin capsule in treating non-alcoholic fatty liver disease and its effect on intestinal flora. *Chin. J. Integr. Traditional West. Med. Liver Dis.* 31 (01), 37–39+43.

Li, X., Wang, H., Wang, J., Chen, Y., Yin, X., Shi, G., et al. (2016). Emodin enhances cisplatin-induced cytotoxicity in human bladder cancer cells through ROS elevation and MRP1 downregulation. *BMC Cancer* 16, 578. doi:10.1186/s12885-016-2640-3

Li, Y., Sui, F., Liu, L. L., Lin, N., Xiao, Y. Q., Li, L., et al. (2011b). Comparative Study on Purgative Effect Among Different Extracts of Processed Rhez Radix et Rhizoma. *Chin. J. Exp. Traditional Med. Formulae* 17 (17), 151–154. doi:10.13422/j.cnki.syfjx.2011.17.058

Li, Y. L., Li, Y. F., Zhou, Y. Z., Yang, J. Y., and Ran, X. (2018). The curative effect of rhubarb extract on severe periodontitis in patients with diabetes mellitus. *Shanghai J. Stomatology* 27 (06), 633–636. doi:10.19439/j.sjos.2018.06.014

Li, Z., Lin, Y., Zhang, S., Zhou, L., Yan, G., Wang, Y., et al. (2019). Emodin regulates neutrophil phenotypes to prevent hypercoagulation and lung carcinogenesis. *J. Transl. Med.* 17 (1), 90. doi:10.1186/s12967-019-1838-y

Liao, Z., Zhang, J. Q., Fu, X. Y., Wang, W., and Zhuang, M. Y. (2020). Study on mechanism of Rhei Radix et Rhizoma-Persicae Semen in treatment of adenomyosis based on network pharmacology. *China J. Chin. Materia Medica* 45 (17), 4112–4119. doi:10.19540/j.cnki.cjcmm.20200520.403

Lin, Z., Zeng, H., Cai, S., Chen, F., Wang, X., Wu, D., et al. (2023). Effects of rhubarb peony decoction combined with antibiotics in treating pediatric periappendiceal abscess. *Front. Pediatr.* 11, 1112034. doi:10.3389/fped.2023.1112034

Liu, D. L., Bu, H., Li, H., Chen, H., Guo, H. C., Wang, Z. H., et al. (2012). Emodin reverses gemcitabine resistance in pancreatic cancer cells via the mitochondrial apoptosis pathway *in vitro*. *Int. J. Oncol.* 40 (4), 1049–1057. doi:10.3892/ijo.2011.1285

Liu, S., Wang, J., Shao, T., Song, P., Kong, Q., Hua, H., et al. (2018). The natural agent rhein induces β-catenin degradation and tumour growth arrest. *J. Cell. Mol. Med.* 22 (1), 589–599. doi:10.1111/jcmm.13346

Liu, X., Liu, Y., Qu, Y., Cheng, M., and Xiao, H. (2015). Metabolomic profiling of emodin-induced cytotoxicity in human liver cells and mechanistic study. *Toxicol. Res.* 4 (4), 948–955. doi:10.1039/c4tx00246f

Lv, H., Niu, J., Pan, W., Wang, Y., Wang, L., Wang, M., et al. (2024). Stool-softening effect and action mechanism of free anthraquinones extracted from Rheum palmatum L. on water deficit-induced constipation in rats. *J. Ethnopharmacol.* 319 (Pt 3), 117336. doi:10.1016/j.jep.2023.117336

Lv, Y. H., Wu, S. S., Wang, Z. C., Wen, Z. X., Duan, G. J., Fu, Y. Q., et al. (2022). Clinical effect of Rougan Huaxian Granules combined with TACE in the treatment of primary liver cancer and its effect on serum index and immune function. *China J. Traditional Chin. Med. Pharm.* 37 (04), 2386–2390.

Malik, E. M., and Müller, C. E. (2016). Anthraquinones as pharmacological tools and drugs. *Med. Res. Rev.* 36 (4), 705–748. doi:10.1002/med.21391

Marcińczyk, N., Gromotowicz-Popławska, A., Tomczyk, M., and Chabielska, E. (2021). Tannins as hemostasis modulators. *Front. Pharmacol.* 12, 806891. doi:10.3389/fphar.2021.806891

Min, C., Jing, W., XiangJie, L., JinJian, Y., Bo, Z., and Xiao, W. (2019). Advances in authentication and quality control methods of rhubarb. *China Pharm.* 30 (18), 2583–2589. doi:10.6039/j.issn.1001-0408.2019.18.24

Nan, J. H., Zhang, X. S., Hua, Y. L., and Wei, Y. M. (2019). Study on variations of five chemical compositions in raw rhubarb and charred rhubarb. *Prog. Veterinary Med.* 40 (04), 58–63. doi:10.16437/j.cnki.1007-5038.2019.04.011

Neyrinck, A. M., Rodriguez, J., Taminiau, B., Herpin, F., Cani, P. D., Daube, G., et al. (2022). Constipation mitigation by rhubarb extract in middle-aged adults is linked to gut microbiome modulation: a double-blind randomized placebo-controlled trial. *Int. J. Mol. Sci.* 23 (23), 14685. doi:10.3390/ijms232314685

Ni, Y., Song, R., and Kokot, S. (2012). Analysis of HPLC fingerprints: discrimination of raw and processed Rhubarb samples with the aid of chemometrics. *Anal. Methods* 4 (1), 171–176. doi:10.1039/c1ay05661a

Otoo, A., Czika, A., Lamptey, J., Yang, J. P., Feng, Q., Wang, M. J., et al. (2023). Emodin improves glucose metabolism and ovarian function in PCOS mice via the HMGB1/TLR4/NF-κB molecular pathway. *Reproduction* 166 (5), 323–336. doi:10.1530/rep-22-0449

Pan, F. P., Zhou, H. K., Bu, H. Q., Chen, Z. Q., Zhang, H., Xu, L. P., et al. (2016). Emodin enhances the demethylation by 5-Aza-CdR of pancreatic cancer cell tumor-suppressor genes P16, RASSF1A and ppENK. *Oncol. Rep.* 35 (4), 1941–1949. doi:10.3892/or.2016.4554

Peinado, H., Quintanilla, M., and Cano, A. (2003). Transforming growth factor beta-1 induces snail transcription factor in epithelial cell lines: mechanisms for epithelial mesenchymal transitions. *J. Biol. Chem.* 278 (23), 21113–21123. doi:10.1074/jbc.M211304200

Qin, Y., Wang, J. B., Kong, W. J., Zhao, Y. L., Yang, H. Y., Dai, C. M., et al. (2011). The diarrhoeogenic and antidiarrhoeal bidirectional effects of rhubarb and its potential mechanism. *J. Ethnopharmacol.* 133 (3), 1096–1102. doi:10.1016/j.jep.2010.11.041

Ren, H. B., Wang, Y. Y., and Wang, T. J. (2012). Rhubarb total anthraquinone to rat acute renal toxicity research. *J. Liaoning Univ. Traditional Chin. Med.* 14 (01), 69–71. doi:10.13194/j.jlunivtcm.2012.01.71.renhb.068

Ren, L., Yang, W., Zhang, S. t., Ao, H., Hu, X. K., Chen, X., et al. (2015a). The study on the toxicity and dose-response relationship of tannin extracted from Rhubarb on HK-2 cell. *Pharmacol. Clin. Chin. Materia Medica* 31 (04), 132–135. doi:10.13412/j.cnki.zyyl.2015.04.041

Ren, L., Zeng, B. Y., Zhang, S. T., Yang, W., and Dai, C. M. (2015b). Cell toxic effect of total anthraquinone in Rhubarb on human renal tubular epithelial cells and the related mechanism. *Pharmacol. Clin. Chin. Materia Medica* 31 (01), 79–83. doi:10.13412/j.cnki.zyyl.2015.01.026

Ren, Z. L., Chen, D., Chen, J. H., Li, T., Cheng, F. F., and Wang, X. Q. (2023). Literature Analysis of the Clinical Dosage of Dahuang(Radix et Rhizoma Rhei) from Easterm Han Dynasty to the Present. *J. Traditional Chin. Med.* 64 (02), 182–188. doi:10.13288/j.11-2166/r.2023.02.013

Seo, E. J., Ngoc, T. M., Lee, S. M., Kim, Y. S., and Jung, Y. S. (2012). Chrysophanol-8-O-glucoside, an anthraquinone derivative in rhubarb, has antiplatelet and anticoagulant activities. *J. Pharmacol. Sci.* 118 (2), 245–254. doi:10.1254/jphs.11123fp

Shia, C. S., Suresh, G., Hou, Y. C., Lin, Y. C., Chao, P. D., and Juang, S. H. (2011). Suppression on metastasis by rhubarb through modulation on MMP-2 and uPA in

human A549 lung adenocarcinoma: an *ex vivo* approach. *J. Ethnopharmacol.* 133 (2), 426–433. doi:10.1016/j.jep.2010.10.020

Sim, Y., Oh, H., Oh, D. S., Kim, N., Gu, P. S., Choi, J. G., et al. (2015). An experimental study on providing a scientific evidence for seven-time alcohol-steaming of Rhei Rhizoma when clinically used. *BMC Complement. Altern. Med.* 15, 388. doi:10.1186/s12906-015-0922-y

Singh, D., Mendonsa, R., Koli, M., Subramanian, M., and Nayak, S. K. (2019). Antibacterial activity of resveratrol structural analogues: a mechanistic evaluation of the structure-activity relationship. *Toxicol. Appl. Pharmacol.* 367, 23–32. doi:10.1016/j.taap.2019.01.025

Stelzner, K., Vollmuth, N., and Rudel, T. (2023). Intracellular lifestyle of *Chlamydia trachomatis* and host-pathogen interactions. *Nat. Rev. Microbiol.* 21 (7), 448–462. doi:10.1038/s41579-023-00860-y

Stompor-Gorący, M. (2021). The health benefits of emodin, a natural anthraquinone derived from rhubarb-A summary update. *Int. J. Mol. Sci.* 22 (17), 9522. doi:10.3390/ijms22179522

Sui, F., Yan, M. J., Li, Y., Lin, N., Xiao, Y. q., and Li, L. (2012). Comparision of the actions on blood stasis of rhubarb with different prepared methods. *Pharmacol. Clin. Chin. Materia Medica* 28 (06), 90–93. doi:10.13412/j.cnki.zyyl.2012.06.032

Sun, F., Wu, X., Qi, Y., Zhong, Y., Zeng, L., Wang, K., et al. (2022). Combining ultra-high-performance liquid chromatography quadruple exactive orbitrap mass spectrometry with chemometrics to identify and verify the blood-activating components of hawthorn. *J. Sep. Sci.* 45 (15), 2924–2934. doi:10.1002/jssc.202200230

Sun, J., Xu, W. J., Zhong, L. Y., Chen, J. B., and Dong, L. (2024). UPLC-QE-Orbitrap-MS combined with network pharmacology to explore differential components and mechanisms of raw and scorched rhubarb for treatment of ulcerative colitis. *China J. Chin. Materia Medica* 49 (07), 1834–1847. doi:10.19540/j.cnki.cjcmm.20231226.302

Ta, W., Yang, X., Wang, J., Han, C., Hua, R., and Lu, W. (2023). Comparison of intestinal absorption characteristics between rhubarb traditional Chinese medicine preparation and activity ingredients using *in situ* and *in vitro* model. *Chin. Herb. Med.* 15 (1), 117–122. doi:10.1016/j.chmed.2022.09.004

Tan, P., Zhang, H. Z., Li, Y., Zhang, D. K., Wu, S. N., Wang, J. B., et al. (2018). Preliminary study on antiplatelet aggregation of 10 anthraquinones in Rhei Radix et Rhizoma based on bioassay. *Chin. Traditional Herb. Drugs* 49 (04), 859–865. doi:10.7501/j.issn.0253-2670.2018.04.017

Thacker, P. C., and Karunagaran, D. (2015). Curcumin and emodin down-regulate TGF-β signaling pathway in human cervical cancer cells. *PLoS One* 10 (3), e0120045. doi:10.1371/journal.pone.0120045

Tian, G. F., Zhang, C., Li, L., Xiao, Y. Q., Chen, D. D., and Wang, Y. (2010). Variety regulation of aloe-emodin-3-CH2-O-beta-D-glucopyranoside and emodin-8-O-beta-D-glucopyranoside in five processed pieces from Rheum palmatum. *China J. Chin. Materia Medica* 35 (18), 2437–2439.

Tian, Y., Ma, B., Yu, S., Li, Y., Pei, H., Tian, S., et al. (2023). Clinical antitumor application and pharmacological mechanisms of Dahuang Zhechong Pill. *Chin. Herb. Med.* 15 (2), 169–180. doi:10.1016/j.chmed.2023.02.002

Trombetta, A., Sanson, I., Barbi, E., Zamagni, G., Fabbris, C., Dall'Amico, R., et al. (2024). Effectiveness of bismuth subgallate for preventing bleeding following adenotonsillectomy: a multicentre study. *Am. J. Otolaryngol.* 45 (2), 104194. doi:10.1016/j.amjoto.2023.104194

Tsai, K. H., Hsien, H. H., Chen, L. M., Ting, W. J., Yang, Y. S., Kuo, C. H., et al. (2013). Rhubarb inhibits hepatocellular carcinoma cell metastasis via GSK-3-β activation to enhance protein degradation and attenuate nuclear translocation of β-catenin. *Food Chem.* 138 (1), 278–285. doi:10.1016/j.foodchem.2012.10.038

Wang, J. B., Ma, Y. G., Zhang, P., Jin, C., Sun, Y. Q., Xiao, X. H., et al. (2009). Effect of processing on the chemical contents and hepatic and renal toxicity of rhubarb studied by canonical correlation analysis. *Acta Pharm. Sin.* 44 (08), 885–890. doi:10.16438/j.0513-4870.2009.08.006

Wang, M., Fu, J., Guo, H., Tian, Y., Xu, F., Song, R., et al. (2015a). Discrimination of crude and processed rhubarb products using a chemometric approach based on ultra fast liquid chromatography with ion trap/time-of-flight mass spectrometry. *J. Sep. Sci.* 38 (3), 395–401. doi:10.1002/jssc.201401044

Wang, M., Han, T., Li, C. S., Xu, W. J., Yang, L. L., Zhang, S. Y., et al. (2022). Chemical Components and Toxicity of Radix et Rhizoma Rhei before and after Processing. *World Chin. Med.* 17 (22), 3131–3138. doi:10.3969/j.issn.1673-7202.2022.22.001

Wang, M., Tian, Y., Lv, M., Xu, F., Xu, F.-G., Zhang, Z., et al. (2015b). Targeted quantitative analysis of anthraquinone derivatives by high-performance liquid chromatography coupled with tandem mass spectrometry to discriminate between crude and processed rhubarb samples. *Anal. Methods* 7, 5375–5380. doi:10.1039/c5ay01067e

Wang, S., Hu, Y., Tan, W., Wu, X., Chen, R., Cao, J., et al. (2012). Compatibility art of traditional Chinese medicine: from the perspective of herb pairs. *J. Ethnopharmacol.* 143 (2), 412–423. doi:10.1016/j.jep.2012.07.033

Wang, S. W., Zhang, F. B., Zhang, C. R., and Li, F. X. (2015c). Study on hemostasis effect of rheum tanguticum maxim from four main producing areas in Qinghai. *China J. Traditional Chin. Med. Pharm.* 30 (07), 2613–2614.

Wang, W., Xu, M. Q., Wang, H., Ge, Y., and Rui, J. (2018a). Effect of umbilical compress of rhubarb and glauber salt powder in the treatment of adhesive intestinal obstruction. *J. Nanjing Univ. Traditional Chin. Med.* 34 (02), 140–142. doi:10.14148/j.issn.1672-0482.2018.0140

Wang, Y., Rui, T. Q., Yang, J. H., Li, J. S., Zhou, L. L., and Cai, B. C. (2015d). Effects of Wine-processing on Rhei Radix et Rhizoma on Upper-energizer Disease and Effects on Activities of Energy Metabolism Enzymes in Liver. *J. Chin. Med. Mater.* 38 (01), 53–57. doi:10.13863/j.issn1001-4454.2015.01.014

Wang, Y., Yang, X., Xia, P. F., Ma, X., Yang, R. J., Hu, J. R., et al. (2019). Research progress on chemical composition and pharmacological effects of Rhei Radix et Rhizoma and predictive analysis on quality markers. *Chin. Traditional Herb. Drugs* 50 (19), 4821–4837. doi:10.7501/j.issn.0253-2670.2019.19.033

Wang, Y., Zhang, X., Ma, Y. L., and Zhang, C. (2018b). Advances in Processing, Pharmacodynamics and Clinical Application of Prepared Rhei Radix et Rhizoma. *Chin. J. Exp. Traditional Med. Formulae* 24 (24), 219–226. doi:10.13422/j.cnki.syfjx.20182408

Wang, Z., and Li, S. (2022). Network pharmacology in quality control of traditional Chinese medicines. *Chin. Herb. Med.* 14 (4), 477–478. doi:10.1016/j.chmed.2022.09.001

Wang, Z., Wang, D., Zheng, S., Wu, L., Huang, L., and Chen, S. (2014). Ultra-performance liquid chromatography-quadrupole\time-of- flight mass spectrometry with multivariate statistical analysis for exploring potential chemical markers to distinguish between raw and processed Rheum palmatum. *BMC Complement. Altern. Med.* 14, 302. doi:10.1186/1472-6882-14-302

Wen, Q., Mei, L., Ye, S., Liu, X., Xu, Q., Miao, J., et al. (2018). Chrysophanol demonstrates anti-inflammatory properties in LPS-primed RAW 264.7 macrophages through activating PPAR-γ. *Int. Immunopharmacol.* 56, 90–97. doi:10.1016/j.intimp.2018.01.023

Wen, Y., Fan, L., Pang, L., Zhao, T., Li, R., Zhang, Y., et al. (2022). NeiyiKangfu tablets control the progression of endometriosis through inhibiting RAF/MEK/ERK signal pathway by targeting RKIP. *Gynecol. Endocrinol.* 38 (12), 1136–1146. doi:10.1080/09513590.2022.2162495

Wen, Y., Yu, X. R., Wang, H. W., Hao, Z., and Xing, Z. Q. (2020). Research progress in biotransformation of rhubarb by microorganisms. *China Brew.* 39 (07), 7–10. doi:10.11882/j.issn.0254-5071.2020.07.002

Wianowska, D. (2014). Hydrolytical instability of hydroxyanthraquinone glycosides in pressurized liquid extraction. *Anal. Bioanal. Chem.* 406 (13), 3219–3227. doi:10.1007/s00216-014-7744-5

Wu, L., Wang, X., Jiang, J., Chen, Y., Peng, B., and Jin, W. (2023). Mechanism of rhubarb in the treatment of hyperlipidemia: a recent review. *Open Med. (Wars)* 18 (1), 20230812. doi:10.1515/med-2023-0812

Wu, X. Q., Hu, C. J., Zhao, L., Geng, Y. Y., Pan, X., and Hu, L. (2014). Purgative Activity Difference and Mechanism of Raw and Processed Rhei Radix et Rhizoma. *J. Chin. Med. Mater.* 37 (09), 1562–1565. doi:10.13863/j.issn1001-4454.2014.09.014

Wu, Y., Liu, Y., Liu, J. T., and Yin, D. F. (2019). Effect of emodin on regulatory T cell/T helper 17 cell balance in mice with severe acute pancreatitis and related mechanism. *J. Chongqing Med. Univ.* 44 (05), 617–621. doi:10.13406/j.cnki.cyxb.001979

Wu, Y., Peng, X. Q., Jiang, X. Y., Shi, M. Q., Yang, S. Y., Fu, Y. J., et al. (2017). Effects of wine processed Rheum palmatum on tissue distribution of aloe-emodin, rhein and emodin in rats. *China J. Chin. Materia Medica* 42 (08), 1603–1608. doi:10.19540/j.cnki.cjcmm.20170224.014

Wu, Y. Q., Yang, D. Y., Guo, Y. Y., Gao, H. W., Sun, S., and Lv, S. W. (2020). Effects of different boiling time on the content of anthraquinones and tannins in daisaikotc soup. *Lishizhen Med. Materia Medica Res.* 31 (10), 2375–2378.

Xia, H. L., Feng, Y., An, Z. Z., Jia, Y. W., and Xie, J. C. (2016). Expressions and its correlation of Survivin and E-cadherin proteins in adenomyosis. *Chin. J. Clin. Res.* 29 (10), 1311–1314. doi:10.13429/j.cnki.cjcr.2016.10.004

Xiang, B., Zhang, G. P., Cui, H. Y., Qiu, Z. F., Gu, Z. Y., and Li, Q. Y. (2021). The therapeutic effect of rhubarb nasal feeding on abdominal infection in severe pancreatitis and its impact on vascular endothelial glycocalyx. *Chin. J. Gerontology* 41 (22), 4943–4946. doi:10.3969/j.issn.1005-9202.2021.22.022

Xiu, J., Cao, Y., and Li, H. J. (2023). Clinical efficacy of Dachengqi decoction enema combined with Western medicine in the treatment of severe acute pancreatitis and its impact on gastrointestinal dynamics. *J. Emerg. Traditional Chin. Med.* 32 (03), 506–508. doi:10.3969/j.issn.1004-745X.2023.03.034

Xu, L. Q., Mo, Y. M., Jian, Y. H., Li, Z. N., He, Q. J., Wen, W. H., et al. (2021). Study on the antibacterial effect and mechanism of rhubarb and monomer on *Staphylococcus aureus*. *Int. J. Laboratory Med.* 42 (16), 1929–1934. doi:10.3969/j.issn.1673-4130.2021.16.003

Xue, J., Chen, F., Wang, J., Wu, S., Zheng, M., Zhu, H., et al. (2015). Emodin protects against concanavalin A-induced hepatitis in mice through inhibiting activation of the p38 MAPK-NF-κB signaling pathway. *Cell. Physiol. Biochem.* 35 (4), 1557–1570. doi:10.1159/000373971

Yan, M. J., Sui, F., Li, Y., Lin, N., Xiao, Y. Q., and Li, l. (2010). Comparative study on the laxative effects of various processed products of rhubarb. *Chin. J. Exp. Traditional Med. Formulae* 16 (13), 170–171. doi:10.13422/j.cnki.syfjx.2010.13.051

Yan, Y. G., Yin, L. M., Wang, H. Y., Guo, L. L., and Deng, C. (2016). Simultaneous Determination of 10 Kinds of Chemical Components in Processed Products of Rhei Radix et Rhizoma. *China Pharm.* 27 (27), 3839–3842. doi:10.6039/j.issn.1001-0408.2016.27.31

Yang, L., Wan, Y., Li, W., Liu, C., Li, H. F., Dong, Z., et al. (2022). Targeting intestinal flora and its metabolism to explore the laxative effects of rhubarb. *Appl. Microbiol. Biotechnol.* 106 (4), 1615–1631. doi:10.1007/s00253-022-11813-5

Yang, L., Wen, Y. X., Liu, Y., Cheng, Y. R., Shi, X. J., Gong, Y. T., et al. (2020). Study on relationship between color characteristics of rhubarb charcoal in heating process and contents of 14 chemical components. *China J. Chin. Materia Medica* 45 (17), 4230–4237. doi:10.19540/j.cnki.cjcmm.20200622.307

Yang, T., Hu, C. J., Li, W. B., Zhang, T., Li, Q., and Gao, Y. (2012). Comparative study on the influence of stewed rhubarb and rhubarb on hemorheological parameters in rats with blood stasis induced by high molecular dextran. *Chin. J. Exp. Traditional Med. Formulae* 18 (21), 248–250. doi:10.13422/j.cnki.syfjx.2012.21.090

Yang, W. P., Wang, Y. W., Wang, Y. L., Li, T., Dai, W. Y., and Li, X. D. (2011). Experimental study on influence of different processing methods of rhei radix at rhizoma on its effects of purgation, antipyretic and anti-inflammatory. *Chin. J. Exp. Traditional Med. Formulae* 17 (13), 117–119. doi:10.13422/j.cnki.syfjx.2011.13.053

Yang, Y., Wang, Y., Zhao, L., Wang, F., Li, M., Wang, Q., et al. (2023). Chinese herbal medicines for treating ulcerative colitis via regulating gut microbiota-intestinal immunity axis. *Chin. Herb. Med.* 15 (2), 181–200. doi:10.1016/j.chmed.2023.03.003

Yao, M., Li, J., He, M., Ouyang, H., Ruan, L., Huang, X., et al. (2021). Investigation and identification of the multiple components of Rheum officinale Baill. using ultra-high-performance liquid chromatography coupled with quadrupole-time-of-flight tandem mass spectrometry and data mining strategy. *J. Sep. Sci.* 44 (3), 681–690. doi:10.1002/jssc.202000735

Yu, C., Lu, Y., Pang, J., and Li, L. (2024). A hemostatic sponge derived from chitosan and hydroxypropylmethylcellulose. *J. Mech. Behav. Biomed. Mater* 150, 106240. doi:10.1016/j.jmbbm.2023.106240

Yu, X., Xu, Q., Chen, W., Mai, Z., Mo, L., Su, X., et al. (2022). Rhein inhibits *Chlamydia trachomatis* infection by regulating pathogen-host cell. *Front. Public Health* 10, 1002029. doi:10.3389/fpubh.2022.1002029

Zeng, J. Y., Wang, Y., Miao, M., and Bao, X. R. (2021). The effects of rhubarb for the treatment of diabetic nephropathy in animals: a systematic review and meta-analysis. *Front. Pharmacol.* 12, 602816. doi:10.3389/fphar.2021.602816

Zhang, K. X., Yao, Q. Y., Wu, F. M., and Liu, S. (2022a). Research progress on chemical constituents and pharmacological effects of medicinal plants in genus Rheum. *Chin. J. New Drugs* 31 (06), 555–566. doi:10.3969/j.issn.1003-3734.2022.06.006

Zhang, Q., Chen, Y. Y., Yue, S. J., Wang, W. X., Zhang, L., and Tang, Y. P. (2021). Research progress on processing history evolution as well as effect on chemical compositions and traditional pharmacological effects of Rhei Radix et Rhizoma. *China J. Chin. Materia Medica* 46 (03), 539–551. doi:10.19540/j.cnki.cjcmm.20201105.601

Zhang, Q., Chen, Y. Y., Yue, S. J., Wang, W. X., Zhao, C. B., Song, Y. J., et al. (2022b). Study on the content changes of 16 chemical components in Radix et Rhizoma Rhei and its different processed products. *China J. Traditional Chin. Med. Pharm.* 37 (02), 1036–1040.

Zhang, R., Huang, C., Wu, F., Fang, K., Jiang, S., Zhao, Y., et al. (2023). Review on melanosis coli and anthraquinone-containing traditional Chinese herbs that cause melanosis coli. *Front. Pharmacol.* 14, 1160480. doi:10.3389/fphar.2023.1160480

Zhang, R. S. (2009). Emphasis on Chinese medicine concoction is the key to improving clinical efficacy. *Chin. J. Mod. Drug Appl.* 3 (07), 183. doi:10.3969/j.issn.1673-9523.2009.07.181

Zhang, T., Song, H. P., Lin, Y., Liu, L. P., Dai, Z. S., Chen, X. J., et al. (2020). Research advances on pharmacological effects and mechanisms underlying heat - clearing and detoxifying effect of huanglian jiedu decoction. *Chin. Archives Traditional Chin. Med.* 38 (11), 135–139. doi:10.13193/j.issn.1673-7717.2020.11.034

Zhang, Y., Wang, X., Lu, B., Gao, Y., Zhang, Y., Li, Y., et al. (2022c). Functional and binding studies of gallic acid showing platelet aggregation inhibitory effect as a thrombin inhibitor. *Chin. Herb. Med.* 14 (2), 303–309. doi:10.1016/j.chmed.2021.09.001

Zhang, Z., Li, T. X., Xu, L., Xie, J., Kong, D. X., and Wang, G. Z. (2019). Effect of Rhei Radix et Rhizoma on Gastrointestinal Function of Normal Rats Before and After Simmering. *Chin. J. Exp. Traditional Med. Formulae* 25 (12), 140–144. doi:10.13422/j.cnki.syfjx.20190314

Zhao, N., Zhang, X. Z., Hu, C. J., Jia, T. Z., and Xiao, H. B. (2014). Metabolomics analysis revealing multiple compounds changed in rhubarb after processing. *China J. Chin. Materia Medica* 39 (09), 1607–1613.

Zhou, G., Peng, F., Zhong, Y., Chen, Y., Tang, M., and Li, D. (2017). Rhein suppresses matrix metalloproteinase production by regulating the Rac1/ROS/MAPK/AP-1 pathway in human ovarian carcinoma cells. *Int. J. Oncol.* 50 (3), 933–941. doi:10.3892/ijo.2017.3853

Zhou, J. R., Xu, L., and Luo, X. (2015). Clinical efficacy of adrenaline injection and ultramicro-rhubarb powder spraying guided by gastroscopy in the treatment of non-variceal upper gastrointestinal hemorrhage. *China J. Endosc.* 21 (10), 1069–1072.

Zhu, H., Liu, X., Zhu, T. T., Wang, X. L., Qin, K. M., Pei, K., et al. (2017). UHPLC-MS/MS method for the simultaneous quantitation of five anthraquinones and gallic acid in rat plasma after oral administration of prepared rhubarb decoction and its application to a pharmacokinetic study in normal and acute blood stasis rats. *J. Sep. Sci.* 40 (11), 2382–2389. doi:10.1002/jssc.201700166

Zhu, J., Deng, X. X., Wu, Y. G., Li, G. K., Yi, B. X., and Gong, Q. F. (2024). Discussion on the clinical application and modern research progress of cimicifugae rhizoma based on the theory of "different use of raw and processing. *Chin. Archives Traditional Chin. Med.*, 1–12.

Zhu, S. T., Lei, P., Li, X. Z., Liu, S., and Li, Q. L. (2008). Comparative study on the laxative and hemostatic effects of different processed products of Rheum palmatum. *J. Chin. Med. Mater.* (02), 199–201. doi:10.13863/j.issn1001-4454.2008.02.014

Zhu, S. T., Li, X. Z., Wen, X. L., and Lei, P. (2010). Comparative study on promoting blood circulation to remove blood stasis function of different processed rhubarb products. *J. Pharm. Pract. Serv.* 28 (05), 354–355+358. doi:10.3969/j.issn.1006-0111.2010.05.012

Zhu, T., Liu, X., Wang, X., Cao, G., Qin, K., Pei, K., et al. (2016a). Profiling and analysis of multiple compounds in rhubarb decoction after processing by wine steaming using UHPLC-Q-TOF-MS coupled with multiple statistical strategies. *J. Sep. Sci.* 39 (15), 3081–3090. doi:10.1002/jssc.201600256

Zhu, T., Zhang, W., Feng, S. J., and Yu, H. P. (2016b). Emodin suppresses LPS-induced inflammation in RAW264.7 cells through a PPARγ-dependent pathway. *Int. Immunopharmacol.* 34, 16–24. doi:10.1016/j.intimp.2016.02.014

Zou, Z. Y., Song, Y. T., Yang, L., Gao, L., Li, H., Chen, D. S., et al. (2011). Research on the reduction effect of genotoxicity of rheum pfficinale with different methods of processing. *J. Liaoning Univ. Sci. Ed.* 38 (04), 338–342. doi:10.3969/j.issn.1000-5846.2011.04.014

frontiers | Frontiers in Pharmacology

TYPE Original Research
PUBLISHED 07 August 2024
DOI 10.3389/fphar.2024.1447241

OPEN ACCESS

EDITED BY
Qianfeng Gong,
Jiangxi University of Traditional Chinese Medicine, China

REVIEWED BY
Chang Hong,
Baotou Medical College, China
Hossam M. Hassan,
Faculty of Pharmacy Beni-Suef University, Egypt

*CORRESPONDENCE
Peixin Guo,
718374546@qq.com
Yuhuan Xie,
kmkamma@163.com
Zili Yin,
362297543@qq.com

†These authors have contributed equally to this work

RECEIVED 11 June 2024
ACCEPTED 17 July 2024
PUBLISHED 07 August 2024

CITATION
Liu F, Bai Y, Wan Y, Luo S, Zhang L, Wu X, Chen R, Yin Z, Xie Y and Guo P (2024) DaiTongXiao improves gout nephropathy by inhibiting inflammatory response through the TLR4/MyD88/NF-κB pathway.
Front. Pharmacol. 15:1447241.
doi: 10.3389/fphar.2024.1447241

DaiTongXiao improves gout nephropathy by inhibiting inflammatory response through the TLR4/MyD88/NF-κB pathway

Feifan Liu[1†], Yuanmei Bai[1†], Yan Wan[1†], Shifang Luo[1], Linao Zhang[2], Xue Wu[2], Rong Chen[1], Zili Yin[1*], Yuhuan Xie[3*] and Peixin Guo[1*]

[1]College of Ethnic Medicine, Yunnan University of Chinese Medicine, Kunming, Yunnan, China, [2]College of Chinese Medicine, Yunnan University of Chinese Medicine, Kunming, Yunnan, China, [3]College of Basic Medical Sciences, Yunnan University of Chinese Medicine, Kunming, Yunnan, China

Introduction: Gouty nephropathy (GN) arises from factors like excessive purine intake, metabolic disorders or abnormal synthesis, and uric acid hypersaturation in the blood, leading to urate crystal deposition in kidney tissue. DaiTongXiao (DTX) is a remedy used by the Dai people of China. It shows efficacy in lowering uric acid levels and exhibits anti-inflammatory and kidney-protective properties.

Methods: A GN rat model was induced using adenine and potassium oxonate. Following DTX administration, various parameters were assessed in urine, serum, and kidney tissue. Western blot analysis evaluated TLR4/MyD88/NF-κB signaling proteins, while immunofluorescence examined NF-κB nuclear expression.

Results: DTX treatment improved kidney morphology, increased body weight, and kidney index and enhanced urinary levels of blood urea nitrogen (Bun), 24-h urinary protein, uric acid (UA), and allantoin in GN rats, reducing UA, Bun, creatinine (Cre), cystatin C (CysC), serum amyloid A (SAA), α1-microglobulin (MG), and β2-MG in serum analysis. Renal tissue assessments showed decreased xanthine oxidase (XOD), hydroxyproline (Hyp), α-smooth muscle actin (α-SMA), and collage type Ⅳ (COL-Ⅳ). Kidney damage severity was notably reduced. DTX lowered serum inflammatory factors like interleukin (IL) −18, tumor necrosis factor-α (TNF-α), C-reactive protein (CRP), transforming growth factor-β1 (TGF-β1), and IL-1β in the rat serum, reducing chemokine monocyte chemoattractant protein-1 (MCP-1) and adhesion factor vascular cell adhesion molecule-1(VCAM-1). Western blotting demonstrated the downregulation of TLR4/MyD88/NF-κB pathway proteins, and immunofluorescence revealed reduced NF-κB expression in renal tissue.

Abbreviations: α-SMA, α-smooth muscle actin; Bun, blood urea nitrogen; COL-Ⅳ, collage type Ⅳ; Cre, creatinine; CRP, C-reactive protein; CysC, cystatin C; DTX, DaiTongXiao; GN, gouty nephropathy; Hyp, hydroxyproline; IL, interleukin; MCP-1, monocyte chemoattractant protein-1; MG, microglobulin; MSU, monosodium urate; PASM, periodic Acid–Schiff–methenamine; SAA, serum amyloid A; TGF-β1, transforming growth factor-β1; TNF-α, tumor necrosis factor-α; UA, uric acid; VCAM-1, vascular cell adhesion molecule-1; XOD, xanthine oxidase.

Discussion: DTX exhibits significant anti-GN effects by modulating TLR4/MyD88/NF-κB pathway protein expression, reducing inflammatory factor release, and inhibiting GN progression.

KEYWORDS

DaiTongXiao, gout nephropathy, traditional Chinese medicine, TLR4/MyD88/NF-κB pathway, mechanism research

Highlights

- Revealing the effects of DTX on rats with gout nephropathy.
- Revealing that DTX has significant ameliorative effects on gout nephropathy.
- Revealing that DTX can improve gout nephropathy by inhibiting inflammatory response through the TLR4/MyD88/NF-κB pathway.

1 Introduction

Currently, gouty nephropathy (GN) prevalence has been rising annually. Findings show that clinically, around 20% of gout patients have chronic progressive renal lesions, while autopsy confirms renal lesions in up to 100% of gout cases. After 5–10 years, the condition worsens, glomerular function is impaired, and renal insufficiency occurs, leading to GN, attributable to shifts in life quality and dietary

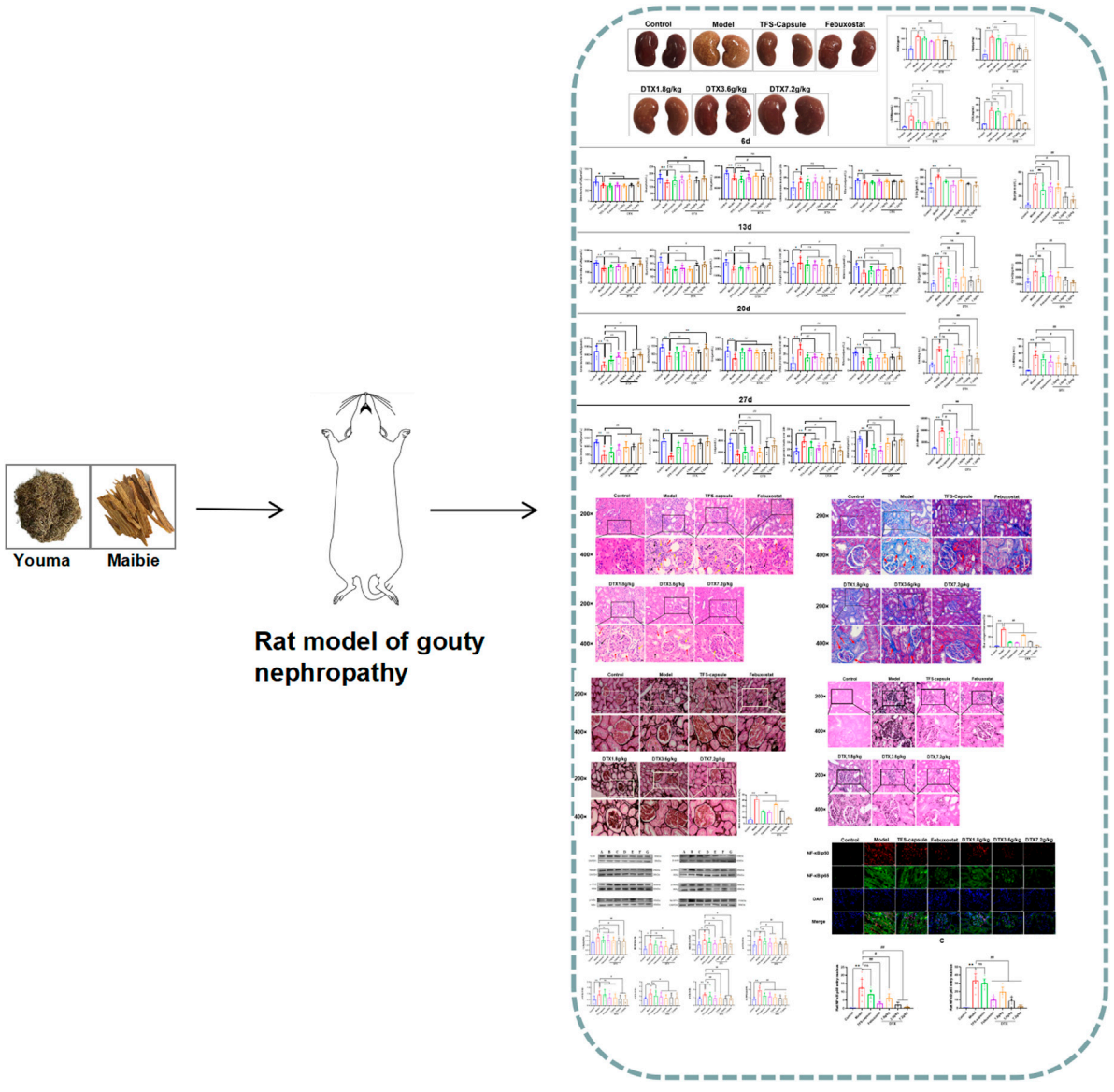

GRAPHICAL ABSTRACT

habits spurred by socioeconomic advancements (Mei et al., 2022). GN is a condition characterized by aberrant blood uric acid (UA) production or urate excretion formed in the kidney medulla, causing local inflammation and interstitial fibrosis in the kidney, also known as hyperuricemia nephropathy (Pan et al., 2021). GN is a chronic renal lesion caused by abnormal purine metabolism in the body, which leads to long-term supersaturation of blood uric acid and the deposition of excessive urate crystals in the kidneys. The pathological mechanism of the occurrence of GN may be related to the occurrence of inflammatory reactions, endothelial dysfunction, fibrosis, proliferation of vascular smooth muscle cells, activation of the renin–angiotensin system, and glomerular arteriosclerosis, among other processes. Clinical symptoms are often manifested as increased nocturia due to decreased urinary concentrating function, and manifestations of renal insufficiency, such as hypertension, edema, and anemia, appear in the late stage due to decreased glomerular filtration function. Currently, specific therapeutic agents for GN are lacking, and symptomatic treatment remains the primary approach in clinical practice. The commonly used drugs include allopurinol, febuxostat, and colchicine, all aimed at inhibiting the synthesis of uric acid (2012). However, all the aforementioned drugs have significant adverse effects; for instance, long-term application of allopurinol can cause severe liver damage (Grace and Luke, 2022), febuxostat may trigger generalized rash (H-Y et al., 2015), and colchicine is linked to cardiomyopathy and cytopenia upon prolonged application (Prasanna et al., 2020). Existing treatments have major limitations in addressing both the occurrence and development of GN. Exploring traditional prescriptions for medicines with potent efficacy and fewer adverse reactions holds profound significance. Ethnomedicines, predominantly composed of natural remedies, have demonstrated distinct advantages in combating GN.

DaiTongXiao (DTX) is a traditional remedy widely employed by the Dai community in China for treating gout, boasting a history spanning over 2,500 years (ZHENG et al., 2022). In contemporary practice, DTX is utilized to alleviate conditions stemming from elevated uric acid levels, such as gout, as detailed in the 21st-century Dai Medical Clinical Science undergraduate textbook (Wu et al., 2022; ZHENG et al., 2022). Clinical investigations involving 29 gout patients treated with DTX revealed significant improvement in 25 cases, with 4 cases showing partial recovery, yielding an overall 86.2% efficacy rate (Feng, 2015). Comprising You Ma and Mai Bie in a 3:1 ratio, the DTX formulation includes whole grass of *Elsholtzia rugulosa* Hemsl. (You Ma) in the Lamiaceae family, supported by modern research, with main components including triterpenoids, flavonoids, sterols, and their glycosides. These constituents endow it with antipyretic and detoxifying properties as well as antioxidant and uric acid-lowering effects (Zhou and Chen, 2021). Mai Bie, derived from pine (*Pinus tabuliformis* Carrière.) nodules and branch nodes, predominantly contains flavonoids, volatile oils, etc. (Zhang, 2009; Zhang et al., 2010). Renowned for its anti-inflammatory and antioxidant attributes, Mai Bie offers therapeutic potential (Shi et al., 2014). It has been shown that α-pinene and β-pinene, the active components in volatile oils, can significantly reduce the levels of inflammatory factors such as IL-6, IL-1β, and TNF-α, thus exerting anti-inflammatory effects (Jena et al., 2022). In addition, the flavonoid component of apigenin can play a role in protecting the kidneys by lowering uric acid levels and regulating the uric acid transporter group (Liao et al., 2016).

Prior research has demonstrated that DTX markedly diminishes serum blood urea nitrogen (Bun), creatinine (Cre), and uric acid (UA) in a mouse model of yeast-induced hyperuricemia, thus exerting a protective influence on renal function. Furthermore, in the monosodium urate (MSU)-induced gout rat model, DTX effectively suppresses pro-inflammatory cytokines, including tumor necrosis factor-α (TNF-α), interleukin (IL)-1β, and IL-6 secretion, mitigating inflammatory damage and exhibiting anti-inflammatory properties [9]. Further study found that through MSU injection to replicate the gout rat model, DTX substantially attenuates NLRP3 protein expression and ameliorates gout symptoms (Feifan et al., 2023). Recent research indicates that GN pathogenesis may be governed by the TLR4/MyD88/NF-κB pathway. TLR4 is situated on the cell membrane as an initiating factor of the TLR4/MyD88/NF-κB pathway. Upon recognition of MSU, pivotal adapter protein MyD88 triggers NF-κB and NLRP3 inflammasome activation. Subsequently, numerous inflammatory mediators implicated in the inflammatory immune response, such as TNF-α and IL-1β/-6, undergo further activation and regulation, instigating an inflammatory cascade amplification effect. This process culminates in GN progression. Thus, targeting the TLR4/MyD88/NF-κB pathway may represent a promising therapeutic approach for GN (Hu et al., 2020; Hosoyamada, 2021).

In this investigation, the combination of adenine and potassium oxonate was used to induce the rat GN model. The study aimed to investigate whether the mechanism underlying DTX's anti-GN effects involves TLR4/MyD88/NF-κB pathway modulation, thereby diminishing inflammatory factor release and ultimately enhancing kidney protection.

2 Materials

2.1 Drugs

DTX, formulated with a 3:1 ratio of You Ma and Mai Bie, includes herbs sourced from the Yunnan Medicinal Materials Market in China and authenticated as genuine by Professor Feng Deqiang from the Yunnan University of Traditional Chinese Medicine (Table 1). Active ingredient content adhered to standards outlined in Chinese Pharmacopoeia and local regulations. Previous investigations utilized ultraviolet spectrophotometry and gas chromatography to analyze active constituents present in DTX.

We precisely weighed 2 g of DTX extract and subjected it to reflux extraction with 50% ethanol for 2 h in a 50 mL volume. After cooling, we utilized 50% ethanol to compensate for weight loss and filtration and obtained filtrate as a test solution. The absorbance value was measured at 510 nm, and the total flavonoid content of the DTX extract was subsequently calculated. The findings revealed a strong linear relationship between total flavonoid concentrations in DTX and corresponding absorbance within 2.4–6.4 μg/mL (R^2 = 0.9993). The average recovery rate was 95.7% (RSD = 1.95%), and the total flavonoid content in DTX was determined to be 677.3 μg/mL.

TABLE 1 Drug composition of DTX.

Local name	Botanical name	Species name	Authoritative name
You Ma	*Elsholtzia rugulosa* Hemsl	Lamiaceae	-
Mai Bie	*Pinus Tabuliformis* Carrière	Pinaceae	Pini lignum nodi

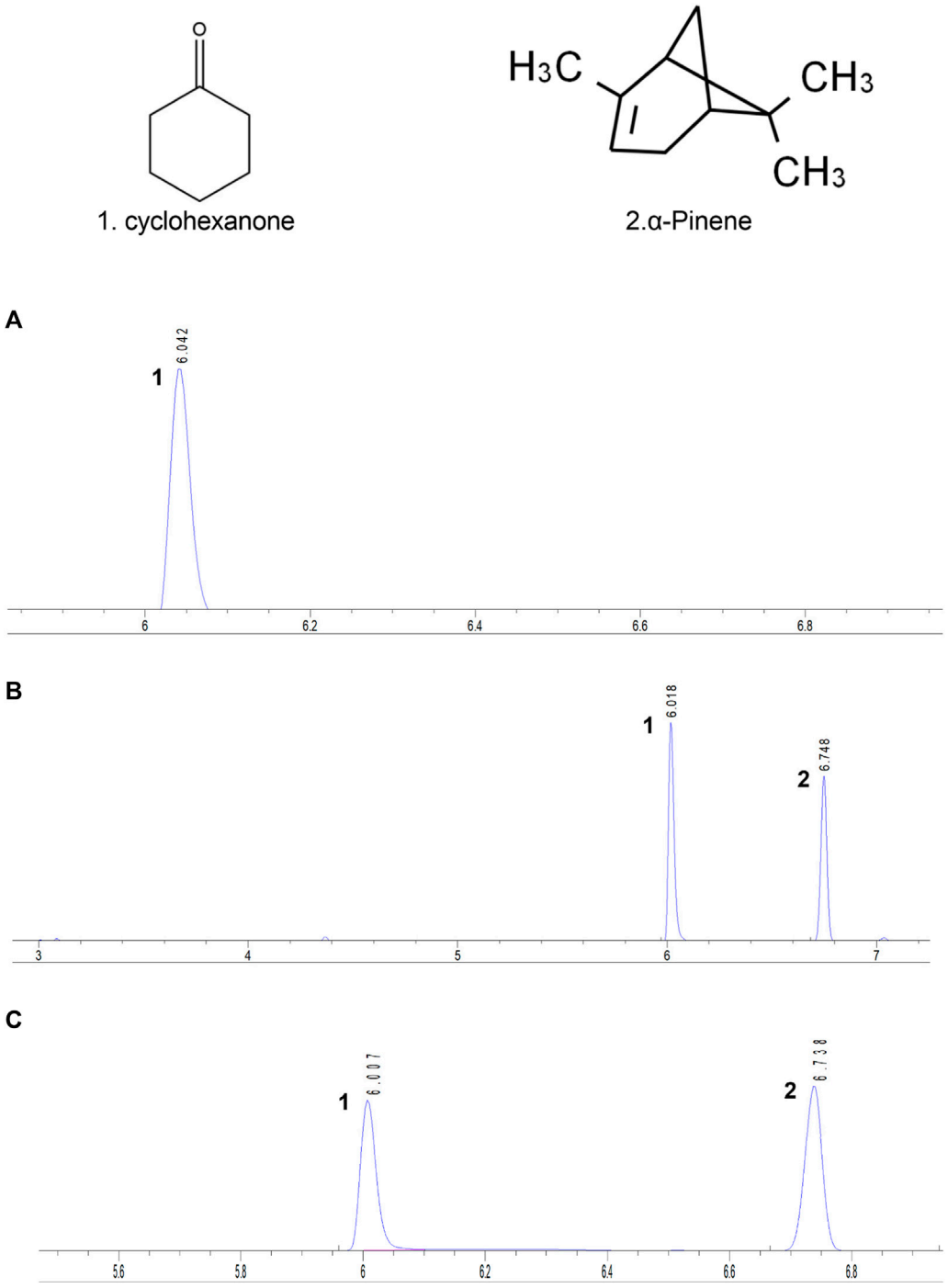

FIGURE 1
Each sample's gas chromatogram. **(A)** Control, **(B)** standard, and **(C)** testing solutions. 1. Cyclohexanone. 2. α-Pinene (Liu et al., 2024).

Furthermore, the DTX compound encompasses various volatile oil components, among which α-pinene stands out for its analgesic and anti-inflammatory capabilities, rendering it an effective ingredient for gouty arthritis treatment. Approximately 30 g of the DTX extract was accurately weighed, and DTX volatile oil of 0.1 mL was extracted according to the determination method outlined in the Appendix of the 2010 edition of the People's Republic of China Pharmacopoeia (method A). The extracted volatile oil was then quantitatively transferred into a 5-mL vial using n-hexane and diluted to the appropriate scale. Subsequently, the cyclohexanone internal standard solution (100 μL) (prepared by diluting 2 mL of cyclohexanone with n-hexane to an appropriate scale) was accurately added, followed by thorough shaking. The results demonstrated a robust linear relationship between the α-pinene injection amount within 0.08–0.4 mg (R^2 = 0.9994). The average recovery rate was determined to be 101.11% (RSD = 4.26%). The α-pinene content in DTX was quantified at 665.7 mg/mL (Figure 1) (Liu et al., 2024).

The TFS capsule, purchased from Shaanxi Panlong Pharmaceutical Group Co., Ltd (Batch No. 20220503), is renowned for its efficacy in rectifying purine metabolism disorders. It aids in restoring hepatic and renal uric acid metabolism, thereby reducing renal function impairment (Sun et al., 2023). Febuxostat was taken as a xanthine oxidase suppressor, purchased from Jiangsu Wanbang Biochemical Pharmaceutical Group Limited Liability Company (Batch No. 62212754). It impeded uric acid synthesis, thus effectively lowering serum uric acid levels while simultaneously exerting anti-inflammatory effects to reduce renal injury (Kraev et al., 2023). Both TFS capsule and febuxostat were employed as positive control drugs in this study.

To investigate DTX's impact on the kidneys of rats with GN, we induced a GN rat model using the combination of the uricogenic agent adenine and the uricase inhibitor potassium oxonate. The adenine-induced GN model primarily elevates adenine intake, resulting in increased uric acid levels and uric acid crystal formation in the kidneys, thus precipitating GN. This model exhibits a certain degree of self-healing within a short period because rats possess uricase that further metabolizes uric acid into allantoin, which is then excreted from the body. To mimic the internal biological environment in humans more accurately, this experiment introduced potassium oxonate, an inhibitor of urate oxidase, alongside adenine modeling. This addition inhibits the activity of urate oxidase, preventing the oxidative breakdown of uric acid and resulting in the accumulation of uric acid in the body, ultimately inducing GN (Zhang et al., 2023a).

2.2 Reagents

UA, Cre, Bun, urinary protein, xanthine oxidase (XOD), and hydroxyproline (Hyp) kits (Lot Nos C012-2-1, C011-2-1, C035-2-1, C013-2-1, A002-1-1, and A030-2-1, respectively) were procured from Nanjing Jiancheng Bioengineering Institute. Allantoin (Lot No. YJ059176) was sourced from Shanghai Yase Biomedical Technology Co., Ltd. Cystatin C (CysC), α1-microglobulin (MG), β2-MG, IL-1β, IL-18, TNF-α, TGF-β1, and MCP-1 kits (Lot Nos JYM0259Ra, JYM0125Ra, JYM0066Ra, JYM0419Ra, JYM0650Ra, JYM0635Ra, JYM0527Ra, and JYM0495Ra, respectively) were sourced from Wuhan Genome Biotechnology Co., Ltd. Serum amyloid A (SAA), α-smooth muscle actin (α-SMA), collage type Ⅳ (COL-Ⅳ), vascular cell adhesion molecule-1 (VCAM-1), and CRP (Lot Nos A-R00411A, A-R01271B, A-R01941A, A-R02062A, and A-R00073A, respectively) were purchased from Aidea Technology (Beijing) Co., Ltd. TLR4, MyD88, HMGB1, p-IKKα, IKKα, p-IKKβ, IKKβ, p-IKKγ, IKKγ, NLRP3, GAPDH, β-actin antibody (Lot Nos AF7017, AF5195, AF7020, AF3012, AF6014, AF3010, AF6009, AF3496, AF6495, AF4620, AF7021, and AF7018, respectively) were purchased from Affinifity Biosciences Co., Ltd. p-IκBα, IκBα antibody (Lot Nos CST2859, CST9242, respectively) were purchased from Cell Signaling Technology Co., Ltd.

2.3 Experimental animals

Seventy SPF-grade male SD rats, aged 8 weeks and with a body mass of 200 ± 20 g, were purchased from Sibeifu (Beijing) Biotechnology Co., Ltd. (License No: SCXK (Beijing) 2019–0010). They were housed at a feeding temperature of 23 ± 2°C and humidity of 50 ± 5 %, with free access to food and water. Animal management and corresponding experiments were carried out following the Animal Welfare and Management Act and Guidelines for the Care and Use of Laboratory Animals of the National Research Council of the United States and checked and approved by the Ethics Committee of the Yunnan University of Chinese Medicine (Approval number: R-062023094). Protocols for assays comply with the Declaration of Helsinki and ethical standard guidelines.

3 Methods

3.1 DTX preparation

Preparation of DTX: 12 times the volume of water was added to the prescribed botanical medicine, soaked for 0.5 h, and then transferred to a flask. A condensing tube was attached, and extraction was performed three times. Each extraction used 12 times the amount of pure water, each for 1 h (100°C). The DTX water extracts from the three extractions were combined. The solution was filtered through gauze and freeze-dried into an extract. The DTX extract was diluted using distilled water to concentrations of 0.72, 0.36, and 0.18 g raw drug/mL as DTX high/medium/low-dose solutions, respectively.

3.2 Identification of the composition of DTX

3.2.1 UHPLC-OE-MS analysis

3.2.1.1 Sample handling

A measure of 10 mL of DTX was centrifuged at 4°C at 12,000 rpm for 15 min. Using a pipette, 300 μL of the supernatant was accurately absorbed, and 1,000 μL of the extraction solution [methanol: water (4:1, v/v)] containing the internal standard of the isotope label was added. The supernatant was vortexed for 30 s, subjected to ice water bath ultrasound for

5 min, stored in the refrigerator at −40°C for 1 h, and then centrifuged at 4°C at 12,000 rpm for 15 min. Then, the supernatant was filtered through a 0.22-μm microporous filter membrane into a sample vial and was tested on the machine.

3.2.1.2 Analyzing conditions

Chromatographic conditions: A Phenomenex Kinetex C18 Column (2.1 mm × 100 mm, 2.6 μm) was used. The mobile phase consisted of two components: A, the aqueous phase containing 0.01% acetic acid and B, isopropanol: acetonitrile (1:1, v/v).

Mass spectrometry conditions: Sheath gas flow rate, 50 Arb; auxiliary gas flow rate, 15 Arb; capillary temperature, 320°C; full ms resolution. 60,000; MS/MS resolution, 15,000; collision energy, SNCE 20/30/40; and spray voltage, 3.8 kV (positive) or −3.4 kV (negative).

3.2.2 GC-MS analysis

3.2.2.1 Sample handling

DTX samples were precisely absorbed from 100-μL to 10-mL volumetric bottles, passed through a 0.22-μm microporous filter membrane, placed in the container, sealed well, and adsorbed for 50 min in a solid-phase microextraction column at a constant temperature of 60°C before directly being injected for analysis.

3.2.2.2 Analyzing conditions

Gas phase condition: Agilent HP-5MS Quartz Capillary Column (30 m × 0.25 mm × 0.25 μm) was used. Column temperature: starting temperature, 40°C; program temperature, 3°C/min to 80°C, 5°C/min to 280°C, and 10 min; inlet temperature, 250°C; and column front pressure, 100 kPa. The carrier gas was high-purity helium, the sample size was 1 μL, the shunt ratio was 2:1, and the flow rate was 1.0 mL/min.

Mass spectrum conditions: ionization mode, EI; electron energy, 70°eV; transmission line temperature, 250°C; ion source temperature, 230°C; quadrupole temperature, 150°C; scan quality range, 35–500. Wiley7n.l and NIST98.L standard spectrum libraries were used for qualitative search.

3.3 Drug dosage

To establish rat dosages equivalent to clinical DTX human dosages, a conversion based on the surface area was conducted. The clinical human dosage of DTX was a raw drug of 20 g per day. In animal experiments, doses equivalent to 1, 2, and 4 times the clinically relevant human dosage of DTX were chosen. These corresponded to small-dose (raw drug 1.8 g/kg), medium-dose (3.6 g/kg), and large-dose groups (7.2 g/kg). Doses were decided by surface area conversion between rats and humans (Formula 1). Furthermore, based on literature references, the TFS capsule was administered at 600 mg/kg (Li et al., 2022), while febuxostat was administered at 3.6 mg/kg (Shen et al., 2020).

$$\text{Dosage for rats} = X\,\text{mg/kg} \times 70\,\text{kg} \times 0.018/200\,\text{g}. \quad (1)$$

Formula 1 represents human and rat body surface area conversion formula. X is the clinical dose for humans, 70 kg is the weight of humans, 0.018 is the conversion factor, and 200 g is the weight of rats.

TABLE 2 Dosage of animals in each group.

Group	Dosage of administration
Control	Equivalent distilled water
Model	Equivalent distilled water
TFS capsule	600 mg/kg
Febuxostat	3.6 mg/kg
DTX small dose	1.8 g raw drug/kg
DTX medium dose	3.6 g raw drug/kg
DTX high dose	7.2 g raw drug/kg

3.4 Drug preparation

Preparation of adenine + potassium oxazinate solution: Adenine (100 mg) and potassium oxazinate (200 mg) powder were taken, dissolved in the 0.5% CMC-Na solution (1000 rpm/min, 20 min), and then adenine + potassium oxazinate suspension solution was obtained.

Preparation of the TFS capsule solution: Goufengshu powder of 600 mg was precisely weighed using the precision electronic balance. The powder was dissolved in 10 mL of double-steamed water (at 1000 rpm/min for 10 min) to prepare a TFS capsule solution of 60 mg/mL.

Preparation of the febuxostat solution: Using a precision electronic balance, febuxostat powder of 3.6 mg was weighed. The powder was dissolved in 10 mL of distilled water (at 1000 rpm/min for 15 min) to obtain a febuxostat solution at 0.36 mg/mL.

3.5 Modeling, grouping, and administration

A total of 70 healthy male SD rats weighing 180–220 g underwent random assignment into 8 cohorts following 1 w of acclimatization: control, model, FSS capsule, febuxostat, DTX, 1.8 g raw drug/kg, 3.6 g raw drug kg, and 7.2 g raw drug/kg groups. Except for the control group, the model was induced by intragastric administration of 100 mg/kg adenine + 200 mg/kg potassium oxazinate (solvent 0.5% CMC-Na) with intragastric 10 mL/kg across all other cohorts. After a 6 h interval, each group received corresponding intragastric drug administration according to Table 2. Rats in control and model cohorts received the administration of distilled water (10 mL/kg) once daily for 28 days. See Figure 2.

3.6 Routine state observation of rats

The body weights of the rats were measured and recorded weekly throughout the experiment. After the final induction, each group of rats was subjected to a comprehensive assessment, including the observation and recording of hair quality using a gross morphology detection scale and the observation and recording of the rat's mental state, morphology, and activity level using a behavioral rating scale.

3.7 DTX impact on UA, Bun, 24 h urinary protein, and allantoin in the urine of GN rats

On the 6th, 13th, 20th, and 27th days, rats from each group were placed individually in a metabolic cage for 24 h. After a 30-min settling period, urine samples were centrifuged (at 4°C and 4000 rpm for 10 min). After obtaining the supernatant, it was stored at −80°C for 24 h, and UA, Bun, 24-h urinary protein, and allantoin were assessed and quantified following the instructions provided with the respective kits.

3.8 DTX effects on serum UA, Cre, Bun, CysC, SAA, α1-MG, and β2-MG levels in GN rats

Following final administration, rats were deprived of water for 12 h and then weighed. For anesthesia, each rat group received an intraperitoneal injection (2 mL/kg) of 2% pentobarbital sodium. Once anesthetized, rats were secured onto the rat plate, with blood samples collected from the abdominal aorta. The blood samples were allowed to stand at room temperature for 1 h before centrifugation to separate the serum (at 4°C and 4000 rpm for 10 min). The separated serum samples were stored at −80°C. UA, Cre, Bun, CysC, SAA, α1-MG, and β2-MG levels in the serum were determined following the instructions provided with the respective kits.

3.9 Effects of DTX on the renal index in GN rats

Rat's kidney was carefully extracted, rinsed, and filter paper-dried. Its weight was recorded, and subsequently, the kidney index was calculated utilizing the formula given below. Left kidney tissues were fixed with 50 mL of 4% neutral formaldehyde at room temperature for 24 h for subsequent pathology. Meanwhile, right kidney tissues were preserved for afterward use (−80°C).

$$\text{Renal index} = \frac{\text{Bilateral renal mass}}{\text{Body mass of rats}} \times 100\%.$$

3.10 Effects of DTX on renal XOD, Hyp, α-SAM, and COL-IV levels in GN rats

Rat kidney tissue weighing 100 mg was taken and homogenized with normal saline (900 μL) using a high-speed freezing grinder for high-frequency homogenization. Following homogenization, the mixture was centrifuged at 4°C and 5,000 rpm for 15 min, yielding the supernatant. XOD, Hyp, α-SAM, and COL-IV in renal tissue homogenates were then measured.

3.11 Renal histopathological examination

The left kidney tissue was placed in 50 mL of 4% paraformaldehyde solution and fixed at room temperature for 24 h. Subsequently, paraffin sections were prepared, followed by dewaxing and dehydration processes. Staining procedures, including H&E, Masson's trichrome, periodic acid–Schiff–methenamine (PASM), and Gomori staining, were sequentially performed. Renal histopathology was observed using the automatic digital biopsy scanner.

In each group, evaluations were made regarding inflammatory infiltration, collagen fiber density, basement membrane thickening, and urate deposition.

For H&E staining, the degree of inflammatory infiltration was assessed in this study using a scoring system, with no lesions scored as 0, mild or very little scored as 1, mild or little scored as 2, moderate scored as 3, severe scored as 4, and very severe scored as 5.

For Masson's staining, the situation of collagen fiber density was analyzed in this study using Image-Pro Plus 6.0 software, and the same blue color was selected as a uniform criterion for determining the positivity of all photographs, and each photograph was analyzed to derive the ratio of positive staining to the entire area of the tissue in each photograph, i.e., the percentage of the area that was positive (%).

For PASM staining, the basement membrane thickening was analyzed in this study using Image-Pro Plus 6.0 software, and the same black color was selected as a uniform criterion for determining the positivity of all photographs, and each photograph was analyzed to derive the ratio of positive staining to the entire area of the tissue in each photograph, i.e., the percentage of the area that was positive (%).

For Gomori staining, urate deposition was analyzed in this study using Image-Pro Plus 6.0 software, and the same black color was selected as a uniform criterion for determining the positivity of all the photographs, and each photograph was analyzed to derive the ratio of positive staining to the entire area of the tissue in each photograph, i.e., the percentage of the area that was positive (%).

3.12 Effects of DTX on inflammatory cytokines, chemokines, and adhesion factors

Rat serum samples were collected, and serum MCP-1, IL-18, VCAM-1, CRP, TNF-α, IL-1β, and TGF-β1 were determined via Elisa assays.

3.13 DTX regulatory effects on renal tissue proteins were quantified by Western blotting

HMGB1, p-IKKγ/IKKγ, MyD88, NLRP3, TLR4, p-IκBα/IκBα, p-IKKα/IKKα, and p-IKKβ/IKKβ proteins in the TLR4/MyD88/NF-κB pathway were detected by Western blotting. Rat kidney tissue of uniform size was clipped on ice, and an appropriate amount of lysate was added according to the weight of the kidney: lysate (prepared by RIPA: PMSF = 100:1) = 1:10. Rat kidney tissue was homogenized using a high-speed freezing grinder at high frequency, followed by centrifugation (at 12,000 rpm for 10 min) to obtain protein supernatant. BCA was utilized to measure the total protein concentration in each sample. Subsequently, each sample was adjusted to 2 μg/μL using cracking solution, 5X loading buffer, and sample leveling. The samples were then boiled at 95°C in a metal

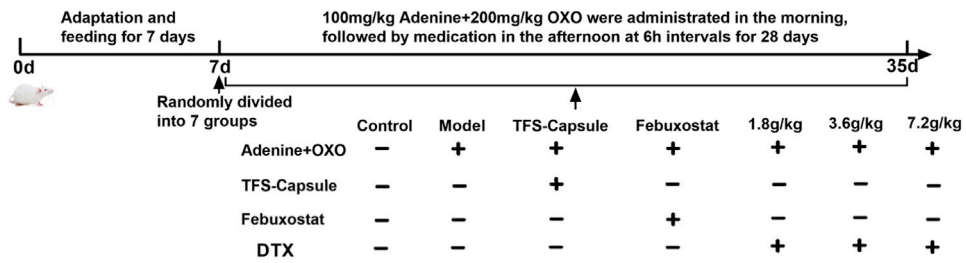

FIGURE 2
Replicating the time axis of the GN rat model.

thermostat for 5 min and rapidly cooled on ice. After subpackaging, they were stored at −80°C. Constant pressure electrophoresis (at 180 V for 40 min) was performed. Constant pressure transfer was done (at 110 V for 70 min). Milk was enclosed (at room temperature for 2 h). TLR4 (1:2000), MyD88 (1:1000), HMGB1 (1:1000), p-IKKα (1:500), IKKα (1:500), p-IKKβ (1:500), IKKβ (1:500), p-IKKγ (1:500), IKKγ (1: 500), p-IκBα (1:500), IκBα (1:500), NLRP3 (1:2000), and GAPDH (1:500) were enclosed in a refrigerator at 4°C overnight, and the goat anti-rabbit secondary anti-antibody (1:500) was added and enclosed (at room temperature for 1 h). Targeted protein/internal reference protein bands' OD value represents target protein expression.

3.14 NF-κB protein nucleation was observed using fluorescence immunoassay

Dehydrated rat kidney tissue was incubated with NF-κB p50 (1:1000) and NF-κB p65 (1:1000). NF-κB p50 and NF-κB p65 protein nucleation were observed using a fluorescence microscope after restaining the cell nucleus with DAPI and FITC (1:400) for visualization with green light.

3.15 Molecular docking

The structure of chemical compounds (*PDB/mol2 format) was downloaded from the TCMSP and PubChem databases. From the PDB database, the 3D structure of the target protein (PDB format) was downloaded for future molecular docking. PyMOL software was used to dehydrate and remove the ligand of the active center. The target protein was hydrogenated, and small drug molecule rotation bonds were established using AutoDock software and then collected in the PDBQT format. AutoDock was used to find optimal conformation. Finally, the detailed docking information was analyzed and visualized using PyMOL software.

3.16 Statistical analysis

Data analysis was performed using SPSS software (Ver. 26.0). One-way ANOVA was employed for multiple group comparisons when data followed a normal distribution. *Post hoc* analysis was performed using the LSD method for the homogeneity of variances, while Dunnett's T3 method was applied for multiple comparisons. Non-parametric tests were employed for datasets without demonstrating normal distribution. $p < 0.05$ was considered statistically significant.

4 Results

4.1 Results of UHPLC-OE-MS

In this study, the chemical composition of DTX in positive- and negative-ion modes was analyzed via UHPLC-Q-TOF MS. The mass spectrometry data were processed and analyzed using MS-DIAL software to automatically match compound fragment information and identify known components to a compound database. As a result, a total of 189 chemical components were initially identified by comparing retention times and fragmentation patterns with references, and the results are shown in Supplementary Table S1; Figure 3.

4.2 Results of GC-MS

The composition of DTX analyzed in this study was performed using GC-MS. The mass spectrometry data were processed and analyzed using Wiley7n.l and NIST98.L in order to automatically match compound fragment information and identify known constituents with the compound database. As a result, a total of 24 chemical components were initially identified by comparing the retention times with the references, and the results are shown in Table 3; Figure 4.

4.3 DTX improved general conditions of GN rats

Throughout the experiment, control rats exhibited robust activity, maintained normal hair color, consumed their diets as usual, and showed no adverse signs. Conversely, rats in the model group displayed reduced activity, lackluster hair color, and lethargy. In comparison, rats administered DTX at 1.8, 3.6, and 7.2 g/kg exhibited improved mental states, restored hair luster, normal dietary patterns, and regular stool consistency when compared to the model group.

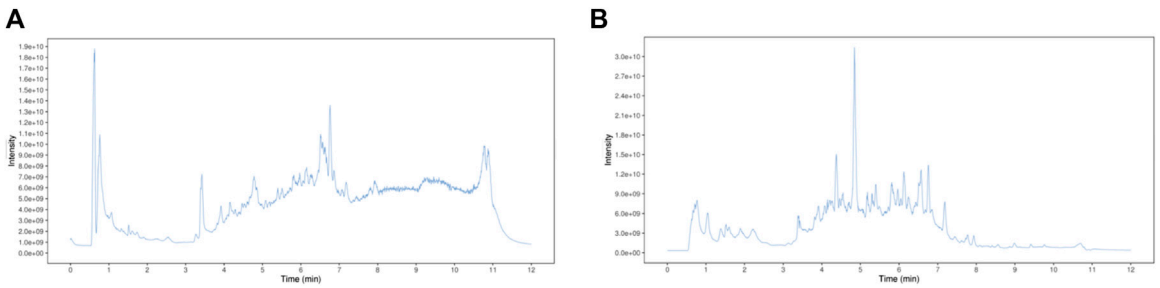

FIGURE 3
DTX chemical composition total ionogram. **(A)** Positive ion mode and **(B)** negative mon mode.

4.4 DTX improved kidney morphology in GN rats

By observing the changes in the kidney physiological structure in the GN rat model, we found that the kidney in the control group was bright red with a smooth surface and normal renal tissue shape. In contrast to the control group, kidneys in the model group appeared enlarged with uneven surfaces, exhibiting numerous white spots. However, rats administered TFS capsule, febuxostat, and DTX displayed comparatively smoother kidney surfaces, characterized by a bright red hue and a reduction in white spot areas (Figure 5).

4.5 DTX increased kidney index, body weight, and kidney weight

We investigated DTX impacts on GN by assessing the rat's kidney index, body weight, and kidney weight. In comparison to the control group, the model group presented a notable decrease in body weight on days 8, 12, 16, 20, 24, and 28 ($p < 0.05$ or $p < 0.01$) (Figure 6A). In contrast, the DTX 1.8 g/kg group displayed a significant increase in body weight on days 8, 12, 16, 20, 24, and 28 in comparison to the model group ($p < 0.05$ or $p < 0.01$) (Figure 6A). The DTX 3.6 g/kg cohort exhibited a notable increase in body weight on days 8, 24, and 28 ($p < 0.05$) (Figure 6A) while showing an upward trend on days 12, 16, and 20 ($p > 0.05$) (Figure 6C). Moreover, the DTX 7.2 g/kg group demonstrated a significant increase in body weight on days 8, 16, 20, 24, and 28 ($p < 0.05$ or $p < 0.01$) (Figure 6A).

The changes in GN rat status induced by DTX can be preliminarily assessed through renal weight and renal index. Compared to the control group, both kidney index and kidney weight in the model group exhibited significant increases with statistical significance ($p < 0.01$) (Figures 6B, C). Conversely, in comparison to the model group, both kidney index and kidney weight in the DTX groups (1.8, 3.6, and 7.2 g/kg) showed significant decreases with statistical significance ($p < 0.01$ or $p < 0.05$) (Figures 6B, C). These findings suggest that DTX may safeguard the kidneys of rats by enhancing body weight, renal weight, and renal index.

4.6 DTX improved UA, Bun, 24-h urinary protein, and allantoin in rats' urine

Urine UA, Bun, and 24 h urinary protein serve as important indicators for renal function (Kim et al., 2023). Uricase exists in most animals, facilitating uric acid breakdown into allantoin, which is then eliminated from the body (Schlesinger et al., 2023a). Reduced levels of UA, Bun, and allantoin in urine, along with the heightened levels of 24-h urinary protein, typically signify organic kidney function impairment. To explore DTX's potential in enhancing kidney excretory function, we assessed UA, Bun, 24-h urinary protein, and allantoin in rats' urine.

On day 6, we observed a notable reduction in UA, Bun, and allantoin of the model group, while 24-h urinary protein showed a significant increase compared to the control, indicating renal impairment ($p < 0.05$ or $p < 0.01$) (Figures 7A–D). Conversely, compared to the model group, DTX 1.8, 3.6, and 7.2 g/kg groups demonstrated significantly elevated Bun ($p < 0.05$ or $p < 0.01$), with Bun levels in DTX 1.8 and 3.6 g/kg groups showing significant increases ($p < 0.05$) (Figure 7B).

On day 13, experimental findings revealed that in comparison to the control group, the model group exhibited significantly reduced UA, Bun, and allantoin, along with a notable increase in 24-h urinary protein ($p < 0.05$ or $p < 0.01$). Conversely, when compared to the model group, the DTX 7.2 g/kg group displayed significantly elevated UA, Bun, and allantoin ($p < 0.05$ or $p < 0.01$). The DTX 3.6 g/kg group presented notable increases in UA and allantoin levels, along with a notable decrease in 24-h urinary protein ($p < 0.05$ or $p < 0.01$). In the DTX 1.8 g/kg group, there were decreases in UA, Bun, and allantoin levels although not statistically significant ($p > 0.05$). There was a trend toward increased Bun in the DTX 3.6 g/kg group ($p > 0.05$). The urinary protein of rats in DTX 1.8 and 3.6 g/kg groups decreased at 24 h ($p > 0.05$) (Figures 7E–H).

On day 20, in comparison to the control group, the model group presented notable decreases in UA, Bun, and allantoin, while there was a notable increase in 24-h urinary protein ($p < 0.01$). In comparison to the model group, DTX at 1.8, 3.5, and 7.2 g/kg led to significant increases in UA and allantoin levels ($p < 0.05$ or $p < 0.01$). Additionally, Bun and 24-h urinary protein were significantly decreased in the DTX 7.2 g/kg group ($p < 0.05$ or $p < 0.01$). A notable increase in Bun levels was found in the DTX 7.2 g/kg group ($p < 0.01$), while trends toward increased Bun levels were found in the DTX 1.8 and DTX 3.6 g/kg groups ($p > 0.05$) (Figures 7I–L).

10.3389/fphar.2024.1447241

TABLE 3 Results of GC-MS determination.

No.	t_R/s	Ingredient	Formula
1	7.47	α-Pinene	$C_{10}H_{16}$
2	8.47	Benzaldehyde	C_7H_6O
3	9.1	β-Pinene	$C_{10}H_{16}$
4	9.85	β-Myrcene	$C_{10}H_{16}$
5	10.57	3-Carene	$C_{10}H_{16}$
6	11.26	1-methoxy 4-methyl 2, 1-methylethyl benzene	$C_{11}H_{16}O$
7	11.46	Sabinene	$C_{10}H_{16}$
8	14.18	α-Terpinene	$C_{10}H_{16}$
9	15.27	(+)-Fenchyl alcohol	$C_{10}H_{18}O$
10	15.63	2-Cyclohexen-1-ol, 1-methyl-4-(1-methylethyl)-, trans-	$C_{10}H_{18}O$
11	15.79	3-Cyclopentene-1-acetaldehyde, 2,2,3-trimethyl-, (R)-	$C_{10}H_{16}O$
12	16.19	Bicyclo[3.1.1]heptan-3-one, 2,6,6-trimethyl-	$C_{10}H_{16}O$
13	17.44	Borneol	$C_{10}H_{18}O$
14	17.91	3-Cyclohexen-1-ol, 4-methyl-1-(1-methylethyl)-, acetate	$C_{12}H_{20}O_2$
15	18.35	Benzenemethanol, α,α,4-trimethyl-	$C_{10}H_{14}O$
16	18.48	3-Cyclohexene-1-methanol, alpha, alpha, 4-trimethyl-, 1-acetate, (1R)-	$C_{12}H_{20}O_2$
17	19.43	2-Cyclohexen-1-ol, 2-methyl-5-(1-methylethenyl)-, acetate, cis-	$C_{12}H_{18}O_2$
18	19.82	cis-Carveol	$C_{10}H_{16}O$
19	20.07	Benzaldehyde, 4-(1-methylethyl)-	$C_{10}H_{12}O$
20	20.22	2-Cyclohexen-1-one, 2-methyl-5-(1-methylethenyl)-, O-methyloxime, (+)-	$C_{11}H_{17}NO$
21	20.56	2-Cyclohexen-1-one, 3-methyl-6-(1-methylethyl)-	$C_{10}H_{16}O$
22	21.82	Benzenemethanol, 4-(1-methylethyl)-, acetate	$C_{12}H_{16}O_2$
23	23.87	Phenol, 2-methoxy-3-(2-propenyl)-	$C_{10}H_{12}O_2$
24	25.21	(+)-Longifolene	$C_{15}H_{24}$
25	25.60	β-Caryophyllene	$C_{15}H_{24}$
26	27.18	+α-Amorphene	$C_{15}H_{24}$
27	27.31	Germacrene D	$C_{15}H_{24}$
28	28.15	Phenol, 2,4-bis-(1,1-dimethylethyl), TMS	$C_{17}H_{30}OSi$
29	28.43	(+)-delta-Cadinene	$C_{15}H_{24}$
30	28.52	Phenol, 2-methoxy-4-(2-propenyl)-, acetate	$C_{12}H_{14}O_3$
31	29.98	β-Caryophyllene oxide	$C_{15}H_{24}O$
32	30.28	Hexadecane	$C_{16}H_{34}$
33	31.72	α-Cadinol	$C_{15}H_{26}O$
34	32.12	Caryophyllenol-II	$C_{15}H_{24}O$
35	32.66	Heptadecane	$C_{17}H_{36}$
36	32.91	Pentadecane	$C_{15}H_{32}$
37	34.93	Octadecane	$C_{18}H_{38}$
38	35.99	Heneicosane	$C_{21}H_{44}$
39	39.19	Isopimaradiene	$C_{20}H_{32}$

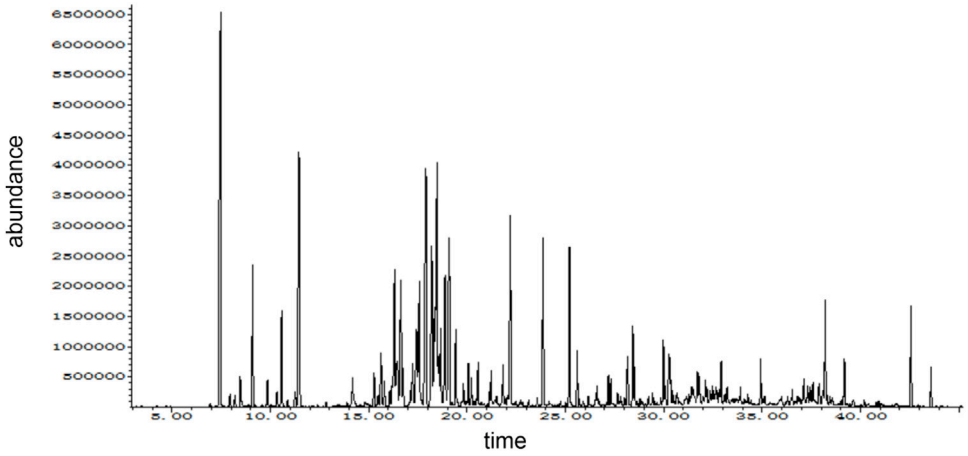

FIGURE 4
GC-MS ion map.

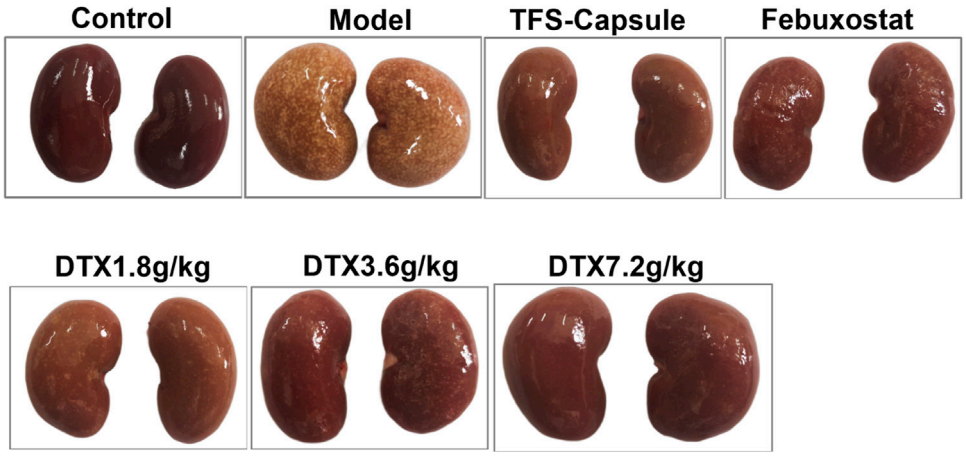

FIGURE 5
DTX improved kidney morphology in GN rats (n = 10).

On day 27, in comparison to the control group, significant decreases were found in the model group of UA, Bun, and allantoin levels, while there was a significant increase in 24-h urinary protein ($p < 0.01$). Setting the model group as a reference, DTX at 1.8, 3.6, and 7.2 g/kg led to significant increases in UA, Bun, and allantoin levels ($p < 0.01$), and a significant decrease was found in 24-h urinary protein ($p < 0.05$ or $p < 0.01$) (Figures 7M–P).

4.7 DTX decreased serum UA, Bun, Cre, CysC, SAA, α1-MG, and β2-MG in rats

Through urinary indicator analysis in rats, we observed a significant enhancement in renal excretory function following DTX administration in GN rats. To further verify the improving effect of DTX on GN, we assessed serum levels of UA, Bun, Cre, CysC, SAA, α1-MG, and β2-MG. Compared with the control group, the model group exhibited a substantial increase in serum UA, Cre, Bun, CysC, SAA, α1-MG, and β2-MG, with statistical significance ($p < 0.01$). Conversely, in the DTX 7.2 g/kg group, there was a significant reduction in UA, Bun, Cre, Cys-C, SAA, α1-MG, and β2-MG ($p < 0.01$). Decreasing indicators in the DTX 3.6 g/kg group included UA, Bun, Cre, Cys-C, α1-MG, and β2-MG ($p < 0.05$ or $p < 0.01$), while in the DTX 1.8 g/kg group, it included UA, Bun, Cys-C, SAA, and β2-MG ($p < 0.05$ or $p < 0.01$). Although SAA in the DTX 3.6 g/kg group and Cre and α1-MG in the DTX 1.8 g/kg group had decreasing trends, the differences were not statistically significant compared to the model group ($p > 0.05$) (Figures 8A–G).

4.8 DTX downregulates the levels of XOD, Hyp, α-SMA, and COL-IV in rat renal tissue

Compared to the control group, renal tissue XOD, Hyp, α-SMA, and COL-IV levels were notably increased within the model group, indicating renal impairment ($p < 0.01$) (Figures 9A–D). Conversely,

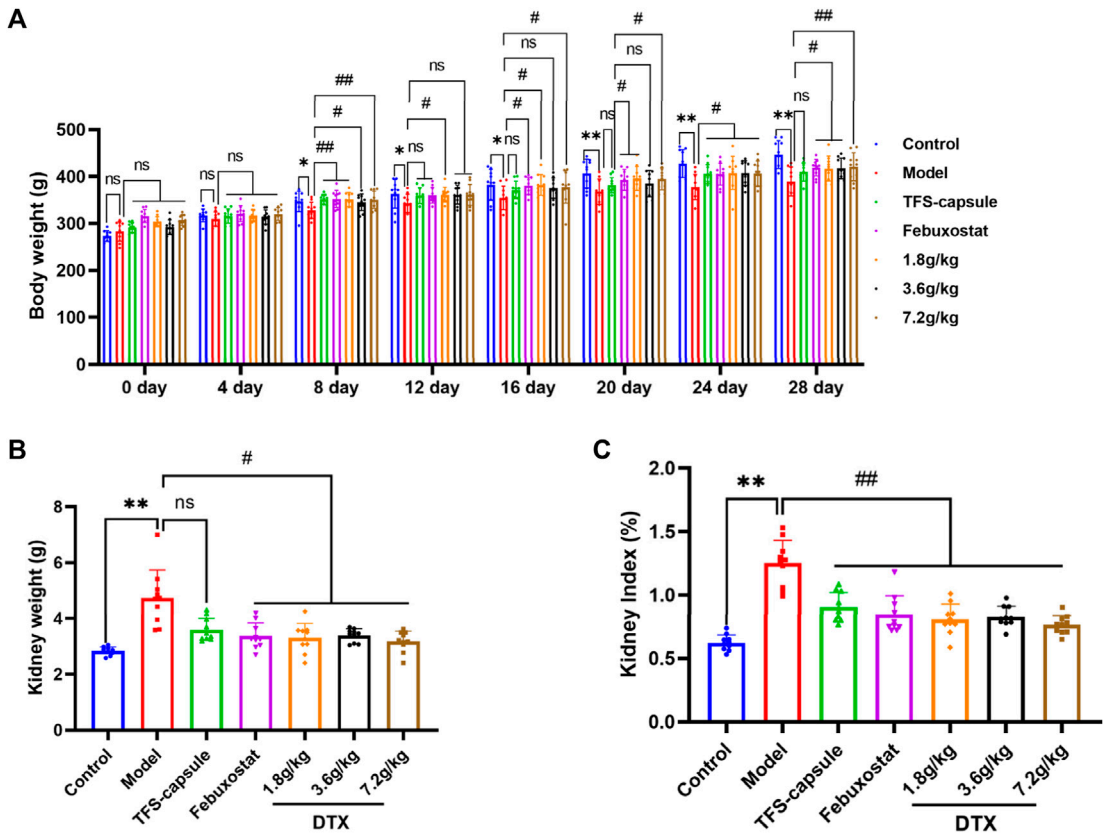

FIGURE 6
DTX improved kidney morphology in GN rats (n = 10). **(A)** Rat body weight on days 0, 4, 8, 12, 16, 20, 24, and 28; **(B)** rat kidney weight at 24 h after the last administration; **(C)** rat kidney index at 24 h after the last administration. Comparing the reference set as the control group; *$p < 0.05$ and **$p < 0.01$. Comparing the reference set as the model group, #$p < 0.05$; ##$p < 0.01$; ns: $p > 0.05$.

DTX treatment at 3.6 and 7.2 g/kg as well as 1.8 g/kg led to a substantial reduction in XOD, Hyp, α-SMA, and COL-IV levels in comparison to the model group, demonstrating significant improvements ($p < 0.05$ or $p < 0.01$) (Figures 9A–D). Although α-SMA and COL-IV in the DTX 1.8 g/kg group showed a decreasing trend, changes were not statistically significant compared to the model group ($p > 0.05$) (Figures 9C, D).

4.9 DTX ameliorated the inflammatory infiltration of GN rat kidney tissue

Renal inflammation and changes in renal cell morphology were assessed using H&E staining. In the control group, kidney morphology appeared normal, with no mesangial cell proliferation. The renal tubular epithelial cells were well-arranged with clear outlines, and there were no evident signs of degeneration, luminal expansion, inflammatory cell infiltration, or apparent pathological changes. In contrast, the model group exhibited pronounced renal tissue abnormalities characterized by extensive edema of tubular epithelial cells, cytoplasmic vacuolation, severe luminal dilation, and substantial inflammatory cell infiltration in the interstitium. However, DTX-treated groups (1.8, 3.6, and 7.2 g/kg) displayed reduced inflammatory cell infiltration in the renal interstitium, limited renal tubule dilation, absence of renal tubular epithelial cell degeneration, and overall injury severity mitigation compared to the model group (Figure 10). These findings indicate that DTX may shield the kidneys by mitigating inflammatory infiltration and bolstering renal structure.

4.10 DTX reduced collagen fiber deposition in the GN rat kidney

Masson staining revealed increased collagen fiber deposition in rats' kidneys in the model group in comparison to normal control, with statistical significance ($p < 0.01$) (Figure 11). Conversely, in DTX 1.8, 3.6, and 7.2 g/kg groups, collagen fiber deposition in renal tissue was notably reduced in comparison to the model group, with statistical significance ($p < 0.01$) (Figure 11). These findings indicate that DTX may shield kidneys by mitigating collagen fiber deposition.

4.11 DTX reduced the thickness of the basement membrane in renal tissues of GN rats

PASM staining revealed glomerular atrophy and basement membrane thickening. Compared to the control group, the

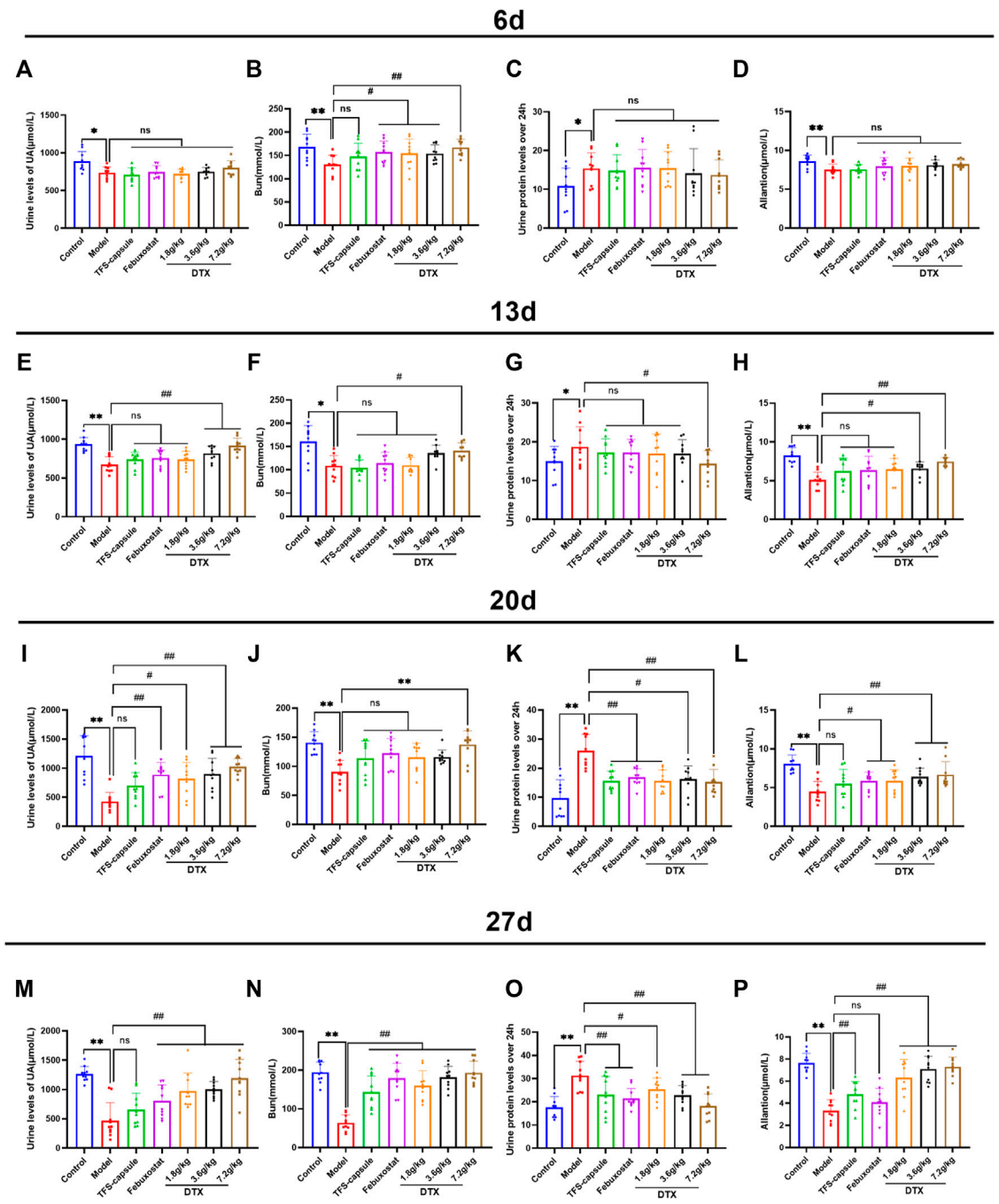

FIGURE 7
DTX elevated UA, Bun, 24-h urinary protein, and allantoin in rat urine (n = 10). **(A)** Urine UA level of rats on the 6th day, **(B)** urine Bun level of rats on the 6th day, **(C)** 24-h urine protein level of rats on the 6th day, and **(D)** urine allantoin level of rats on the 6th day. **(E)** Urine UA level of the rat on 13th day, **(F)** urine Bun level of the rat on 13th day, **(G)** urine protein level of the rat on 13th day for 24 h, and **(H)** urine allantoin level of the rat on 13th day. **(I)** Urine UA level of rats on the 20th day, **(J)** urine Bun level of rats on the 20th day, **(K)** urine protein level of rats on the 20th day, and **(L)** urine allantoin level of rats on the 20th day. **(M)** urine UA level of rats on the 27th day, **(N)** urine Bun level of rats on the 27th day, **(O)** urine protein level of rats on the 27th day, and **(P)** urine allantoin level of rats on the 27th day. Comparing the reference set as the control group; *$p < 0.05$ and **$p < 0.01$. Comparing the reference set as the model group; #$p < 0.05$ and ##$p < 0.01$; ns: $p > 0.05$.

model group presented observable thickening of the basement membrane and numerous instances of glomerular atrophy and sclerosis ($p < 0.01$) (Figure 12). However, in DTX 1.8, 3.6, and 7.2 g/kg groups, no notable tubular atrophy or thickening of the basement membrane was observed. Additionally, glomerular atrophy and sclerosis degrees were markedly improved compared to the model group ($p < 0.01$) (Figure 12). The outcomes indicated that DTX may protect kidneys by reducing basement membrane thickness and ameliorating glomerular atrophy.

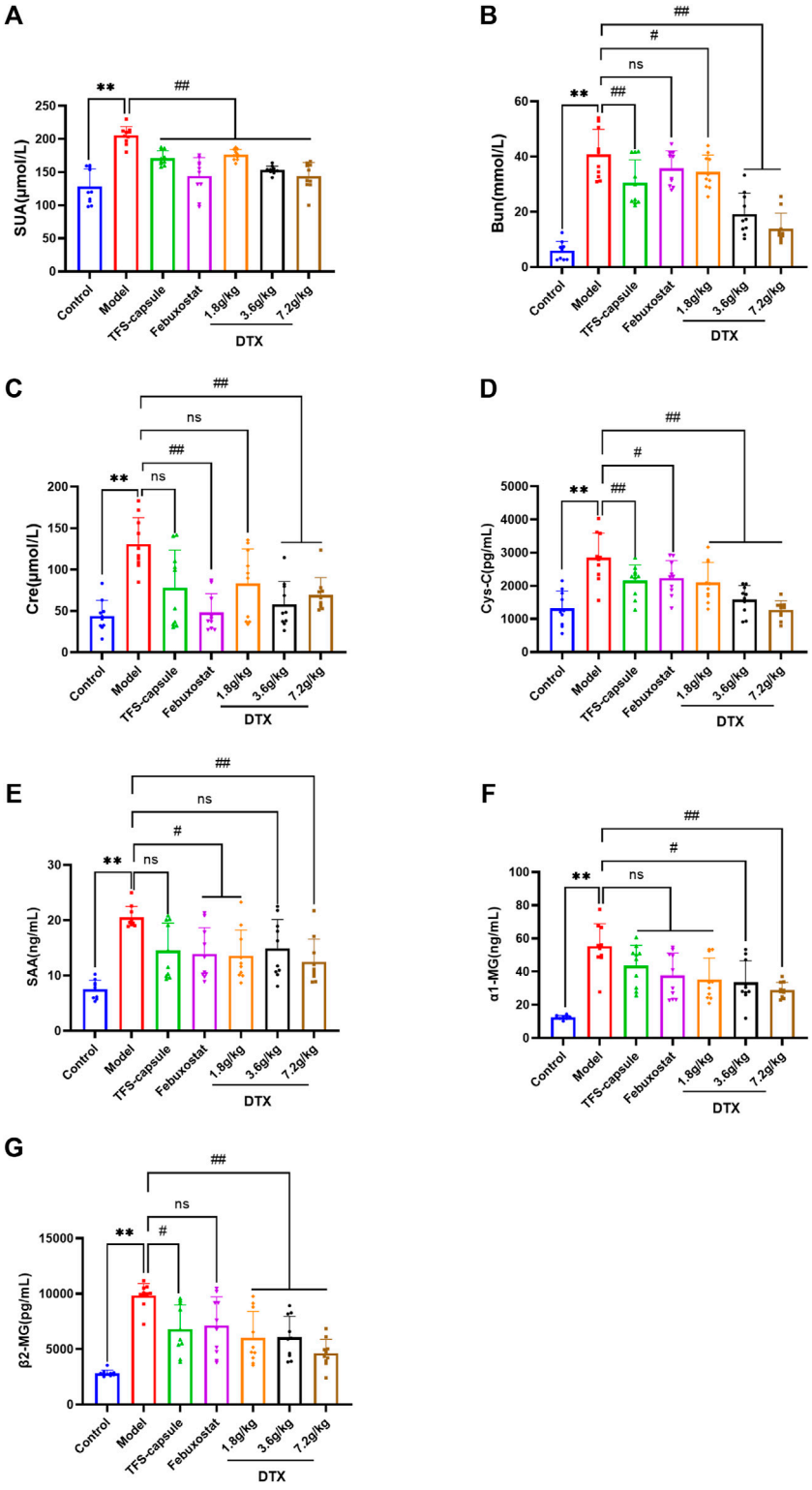

FIGURE 8
Effects of DTX on serum levels of UA, Bun, Cre, CysC, SAA, α1-MG, and β2-MG in GN rats (n = 10). **(A)** Serum UA levels. **(B)** Serum Bun level. **(C)** Serum Cre level. **(D)** Serum CysC level. **(E)** Serum SAA level. **(F)** Serum α1-MG level. **(G)** Serum β2-MG level. Comparing the reference set as the control group; *$p < 0.05$ and **$p < 0.01$. Comparing the reference set as the model group; #$p < 0.05$ and ##$p < 0.01$; ns: $p > 0.05$.

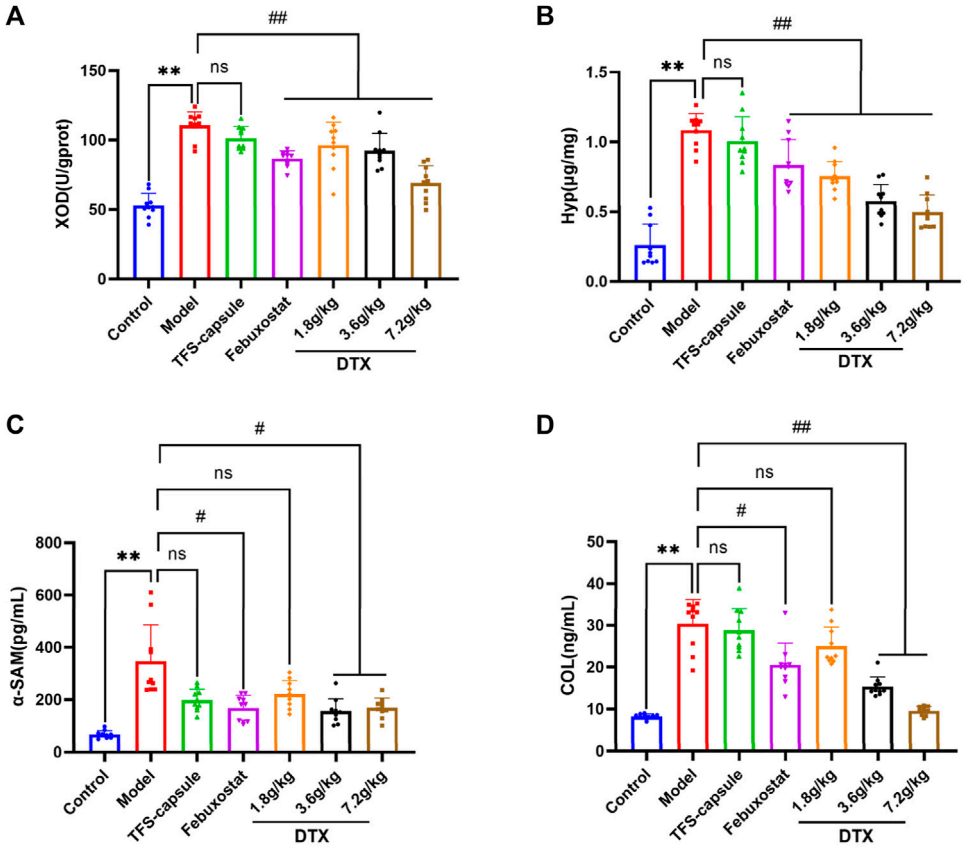

FIGURE 9
DTX reduced XOD, Hyp, α-SMA, and COL-IV levels in kidney tissues of GN rats (n = 10). **(A)** XOD in kidney tissue. **(B)** Hyp in kidney tissue. **(C)** α-SMA in kidney tissue. **(D)** COL-IV in kidney tissue. Comparing the reference set as the control group; $**p < 0.01$. Comparing the reference set as the model group; $\#p < 0.05$ and $\#\#p < 0.01$; ns: $p > 0.05$.

4.12 DTX reduced the degree of urate deposition in the renal tissues of GN rats

Gomori staining was used to observe urate deposition. The model group exhibited severe urate deposition compared to the control group. However, in DTX 1.8, 3.6, and 7.2 g/kg groups, urate deposition decreased progressively compared to the model group (Figure 13). These findings imply that DTX may safeguard the kidneys by reducing urate deposition.

4.13 Impact of DTX on serum CRP, IL-18, TGF-β1, IL-1β, and TNF-α in rats

To evaluate the potential anti-inflammatory effects of DTX, serum CRP, IL-18, TGF-β1, IL-1β, and TNF-α in rats were measured. Compared to normal control, the model group presented significantly elevated serum CRP, IL-18, TGF-β1, IL-1β, and TNF-α in rats ($p < 0.01$) (Figures 14A–D, G). Conversely, DTX treatment at 1.8, 3.6, and 7.2 g/kg resulted in a notable reduction in serum CRP, IL-18, TGF-β1, IL-1β, and TNF-α when compared to the model cohort ($p < 0.05$ or $p < 0.01$) (Figures 14A–D, G). The outcomes indicate that DTX exhibits anti-inflammatory properties and may protect kidney function.

4.14 DTX decreased the serum MCP-1 level in rats

To explore whether DTX can mitigate chemokine MCP-1 release, which plays a role in inducing renal tubule atrophy and interstitial fibrosis, thereby hastening GN progression, we measured the serum MCP-1 levels in rats. The serum MCP-1 content in the model group was markedly elevated compared to the control group ($p < 0.01$). However, in comparison to the model group, serum MCP-1 levels in the DTX 1.8, 3.6, and 7.2 g/kg groups exhibited significant decreases ($p < 0.05$ or $p < 0.01$) (Figure 14E).

4.15 DTX decreased the content of VCAM-1 in rat serum

VCAM-1 belongs to the immunoglobulin superfamily of adhesion molecules and is involved in inflammatory responses and immune regulation. Upregulated VCAM-1 expression prompts enhanced infiltration of mononuclear macrophages in kidney tissue and their adhesion to endothelial cells, resulting in increased inflammatory cells, aggravated inflammatory response, extracellular matrix deposition, and ultimately kidney injury. VCAM-1 in the rat serum was determined. Compared with the

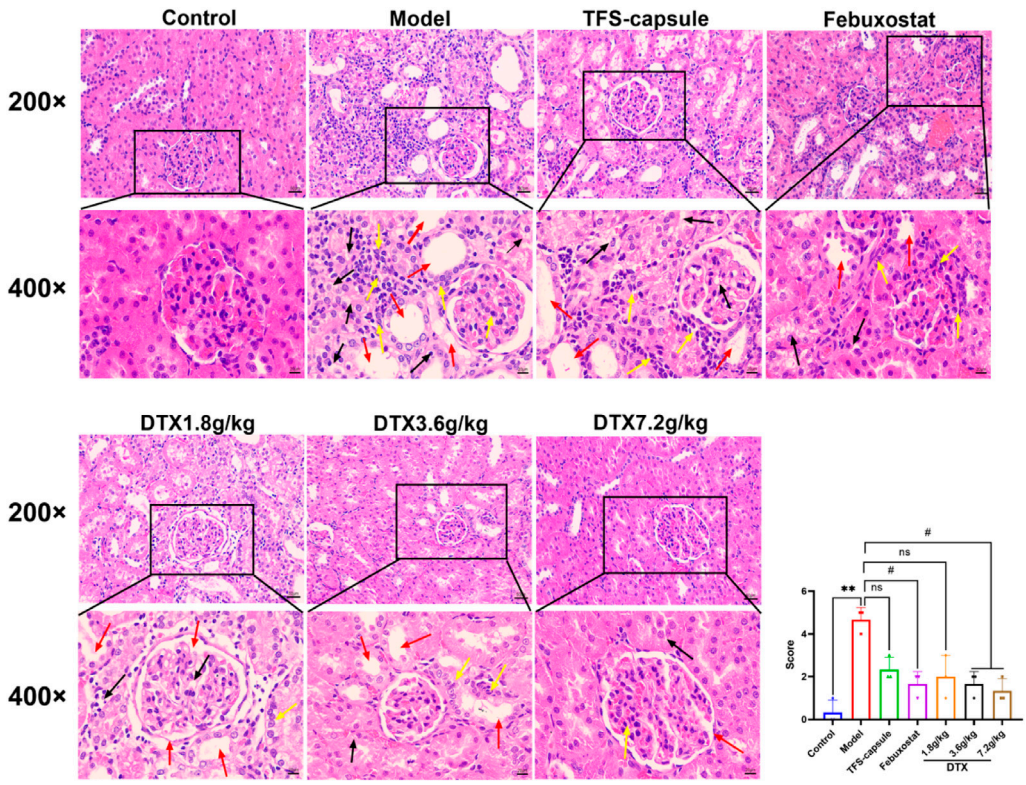

FIGURE 10
DTX suppressed inflammatory infiltration of kidney tissues in GN rats. H&E staining of rat kidneys (200× and 400×) (n = 3). Red arrow, renal tubule lumen dilation; black arrow, degeneration of renal tubular epithelial cells; yellow arrow, inflammatory infiltration. Comparing the reference set as the control group; $**p < 0.01$. Comparing the reference set as the model group; $\#p < 0.05$; ns: $p > 0.05$.

control group, serum VCAM-1 in the model group was significantly increased ($p < 0.01$). Compared with the model group, serum VCAM-1 content in DTX 1.8, 3.6, and 7.2 g/kg groups was significantly decreased ($p < 0.05$ or $p < 0.01$) (Figure 14F).

4.16 DTX suppressed the TLR4/MyD88/NF-κB pathway-related protein expression

The potential anti-GN mechanism of DTX may involve the modulation of proteins within the TLR4/MyD88/NF-κB pathway. Therefore, proteins TLR4, MyD88, HMGB1, p-IKKα/IKKα, p-IKKβ/IKKβ, p-IKKγ/IKKγ, p-IκBα/IκBα, and NLRP3 in rat renal tissue were analyzed by Western blotting (Figures 15A–G). Compared to the control group, the model group presented notable upregulation in protein expressions in TLR4, MyD88, HMGB1, p-IKKα/IKKα, p-IKKβ/IKKβ, p-IKKγ/IKKγ, p-IκBα/IκBα, and NLRP3 ($p < 0.05$ or $p < 0.01$) (Figures 15H–P). Conversely, compared with the model group, the DTX 1.8 g/kg group exhibited significant downregulation in p-IKKα/IKKα, p-IKKγ/IKKγ, p-IκBα/IκBα, and NLRP3 ($p < 0.05$ or $p < 0.01$) (Figures 15H, L, N, O). Moreover, DTX 3.6 and 7.2 g/kg groups demonstrated significant downregulation in protein expressions of TLR4, MyD88, HMGB1, p-IKKα/IKKα, p-IKKβ/IKKβ, p-IKKγ/IKKγ, p-IκBα/IκBα, and NLRP3 ($p < 0.05$ or $p < 0.01$) (Figures 15H, J, L–P). The DTX 7.2 g/kg group significantly downregulated HMGB1 protein expression ($p < 0.05$ or $p < 0.01$) (Figures 15H, K). Furthermore, MyD88, HMGB1, and p-IKKβ/IKKβ in the DTX 1.8 g/kg group and HMGB1 in the 3.6 g/kg group exhibited downward trends without statistical significance ($p > 0.05$) (Figures 15J, K, M).

4.17 DTX decreased NF-κB in renal tissues of GN rats

The NF-κB dimer plays as a mediator in the TLR4/MyD88/NF-κB pathway, contributing significantly to GN genesis. Thus, we examined the NF-κB dimer protein expression in the rat renal tissue nucleus using an immunofluorescence method. In our findings, the nucleus appeared blue under ultraviolet excitation, while NF-κB p50 was visualized in red and NF-κB p65 in green. Compared to the control group, NF-κB p50 and NF-κB p65 expressions in renal tissue nucleus were markedly elevated in the model group, demonstrating statistical significance ($p < 0.01$) (Figures 16A–C). However, in comparison to the model group, NF-κB p50 and NF-κB p65 in the renal cell nucleus of rats treated with DTX at 1.8, 3.6, and 7.2 g/kg were notably reduced ($p < 0.05$ or $p < 0.01$) (Figures 16A–C). These findings indicate that DTX may safeguard kidney function by suppressing the NF-κB dimer.

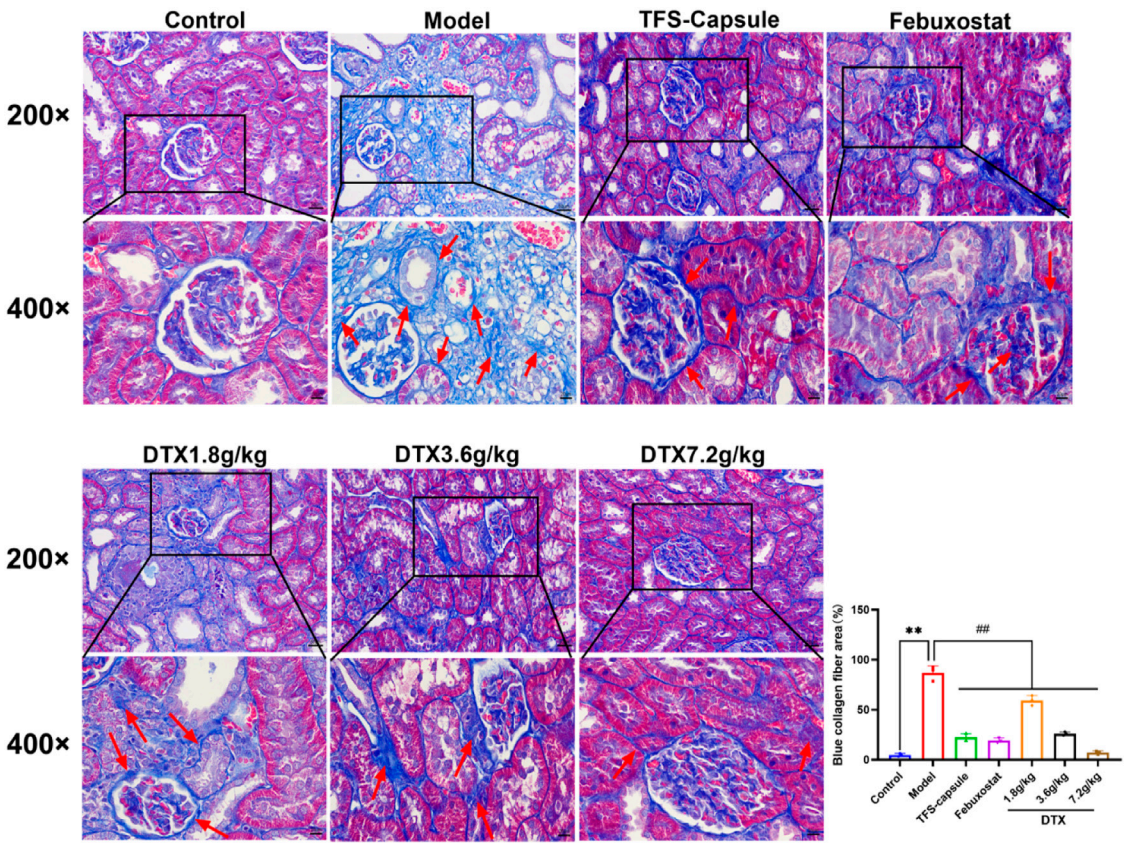

FIGURE 11
DTX improved collagen fiber deposition in the GN rat kidney (200× and 400×) (n = 3). Comparing the reference set as the control group; $^{**}p < 0.01$. Comparing the reference set as the model group; $^{\#\#}p < 0.01$. Red arrow, collagen fibrosis.

4.18 Molecular docking analysis

Apigenin, a flavonoid, promotes uric acid excretion and improves renal function. In this experiment, apigenin was found to be the main active component in DTX via UHPLC-OE-MS analysis. Therefore, this study utilized molecular docking to further evaluate the affinity between apigenin and TLR4, MyD88, and NF-κB. The results showed that the binding energies of apigenin with TLR4, MyD88, and NF-κB were −6.2 kcal/mol, −8.0 kcal/mol, and −6.1 kcal/mol, respectively, and had good affinity (Table 4; Figure 17).

5 Discussion

GN arises from excessive production or reduced excretion of UA in the body. This condition leads to a prolonged state of blood UA saturation, resulting in the deposition of uric acid crystals within the renal medulla, interstitium, and distal collecting ducts of the kidney. Over time, this deposition contributes to substantial renal lesions, including edema, urinary calculi, elevated urinary UA, and functional damage of renal tubules (Yanai et al., 2021; Shi et al., 2023). Dai medicine embodies the collective wisdom accumulated by the Dai people in China through generations of battling diseases. It amalgamates insights from ancient Indian medicine and traditional Chinese medicine, bearing distinct national and regional features (TAN et al., 2013). Among the repertoire of remedies in Dai medicine, DTX stands out as a widely employed compound for managing gout. Renowned for its potent efficacy and minimal side effects, DTX has garnered recognition (Qinghua et al., 2014a; Qinghua et al., 2014b; Feng, 2015). Some studies have shown that DTX is rich in flavonoids and volatile constituents (Feifan et al., 2023). Among them, flavonoid components inhibit the expression of TLR4, MyD88, NLRP3, and other proteins by acting on the TLR/MyD88/NLRP3 and other related protein pathways, resulting in a reduction in the release of inflammatory factors, thus producing an anti-inflammatory effect in order to inhibit the occurrence and development of gout (Xueyan et al., 2021). Volatile components such as α-pinene may play a role in protecting the kidneys by lowering plasma urea and creatinine (Noroozi et al., 2024).

In our investigation, we observed notable differences in rat kidneys treated with DTX compared to those in the model group. Specifically, DTX-treated rat kidneys appeared smoother on the surface and exhibited a brighter red color, showing reduced areas of white spots. Additionally, we assessed the renal weight and renal index of rats as indicators of changes in their kidney status induced by DTX treatment. In comparison to the model group, both kidney weight and kidney index were significantly decreased in the DTX treatment group. These findings suggest that DTX may safeguard rat kidneys with GN by

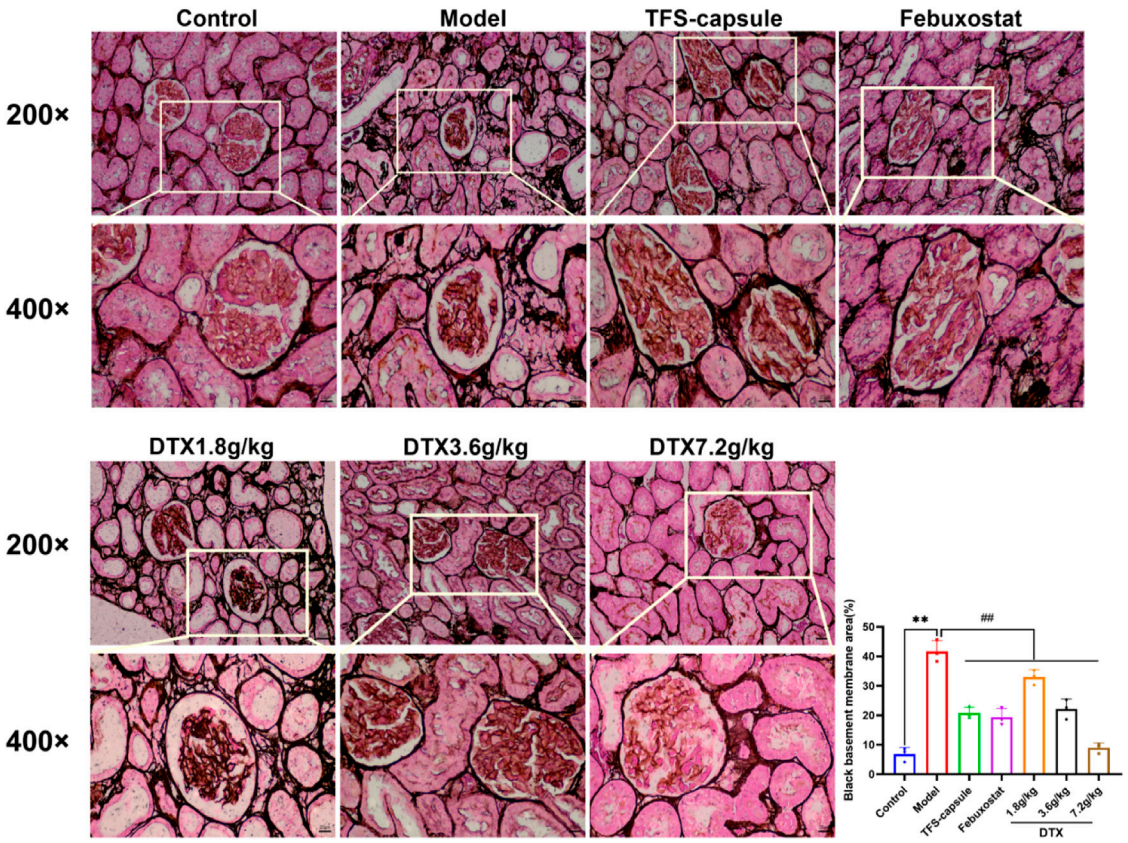

FIGURE 12
DTX reduced basement membrane thickness in kidney tissues of GN rats (200× and 400×) (n = 3). Comparing the reference set as the control group; $^{**}p < 0.01$. Comparing the reference set as the model group; $^{\#\#}p < 0.01$.

enhancing kidney morphology and reducing both kidney weight and kidney index.

UA, Cre, Bun, 24-h urinary protein, and allantoin serve as crucial evaluation indexes for assessing renal function. UA is a metabolite of purine in the body, and its accumulation leads to UA deposition in renal tubules, permanent kidney damage in renal interstitium, and finally GN (Yongsheng et al., 2022). Both Bun and Cre are primarily eliminated via glomerular filtration. When the glomerular filtration rate decreases significantly, urinary excretion of Bun and Cre decreases, resulting in elevated concentrations of Bun and Cre in the blood. Bun and Cre are primarily eliminated via glomerular filtration. When the glomerular filtration rate decreases severely, the urinary excretion of Bun and Cre decreases, resulting in elevated concentrations of Bun and Cre in the blood (Zhang et al., 2023b). Extensive proteinuria has been shown to directly harm the kidneys, exacerbating pre-existing glomerular damage and promoting glomerular sclerosis (Elsaid et al., 2024). In mammals other than the human body, urate oxidase converts uric acid into allantoin, which is then excreted from the body, mitigating renal damage caused by uric acid (Mian et al., 2021). The findings revealed notable alterations in urinary and serum parameters among experimental groups. Specifically, in the model group, urinary levels of UA, Bun, and allantoin exhibited significant reductions, whereas urinary protein levels at 24 h significantly increased. Additionally, serum concentrations of UA, Bun, and Cre were notably elevated. Conversely, DTX treatment led to elevated levels of urinary UA, Bun, and allantoin, coupled with decreased levels of urinary protein and serum UA, Bun, and Cre at 24 h. These observations suggest that DTX may mitigate GN by enhancing glomerular filtration function and renal tubular secretion and reabsorption.

In clinical studies, elevated serum levels of CysC, SAA, α1-MG, and β2-MG have been observed in patients with GN, indicating their involvement in GN pathogenesis. CysC serves as an endogenous marker that reliably reflects the glomerular filtration rate and as a marker of early renal function injury (Wang and Wang, 2024). SAA functions as an acute phase reaction protein, exhibiting increased levels in response to renal capillary endothelial injury and abnormal glomerular basement membrane function (Cai et al., 2020). Furthermore, SAA, functioning as an inflammatory mediator, can stimulate neutrophils to release a plethora of inflammatory factors, exacerbating cellular oxidative stress and contributing to the degeneration and necrosis of renal vessels and parenchymal cells (Konstandi et al., 2019). Additionally, α1-MG and β2-MG, low molecular weight proteins, primarily undergo glomerular filtration and subsequent renal tubular reabsorption. Elevated serum levels of α1-MG and β2-MG serve as effective markers for assessing renal tubular function impairment, indicating compromised glomerular filtration and tubular reabsorption functions (Yican et al., 2021). Our experimental findings revealed significantly elevated levels of

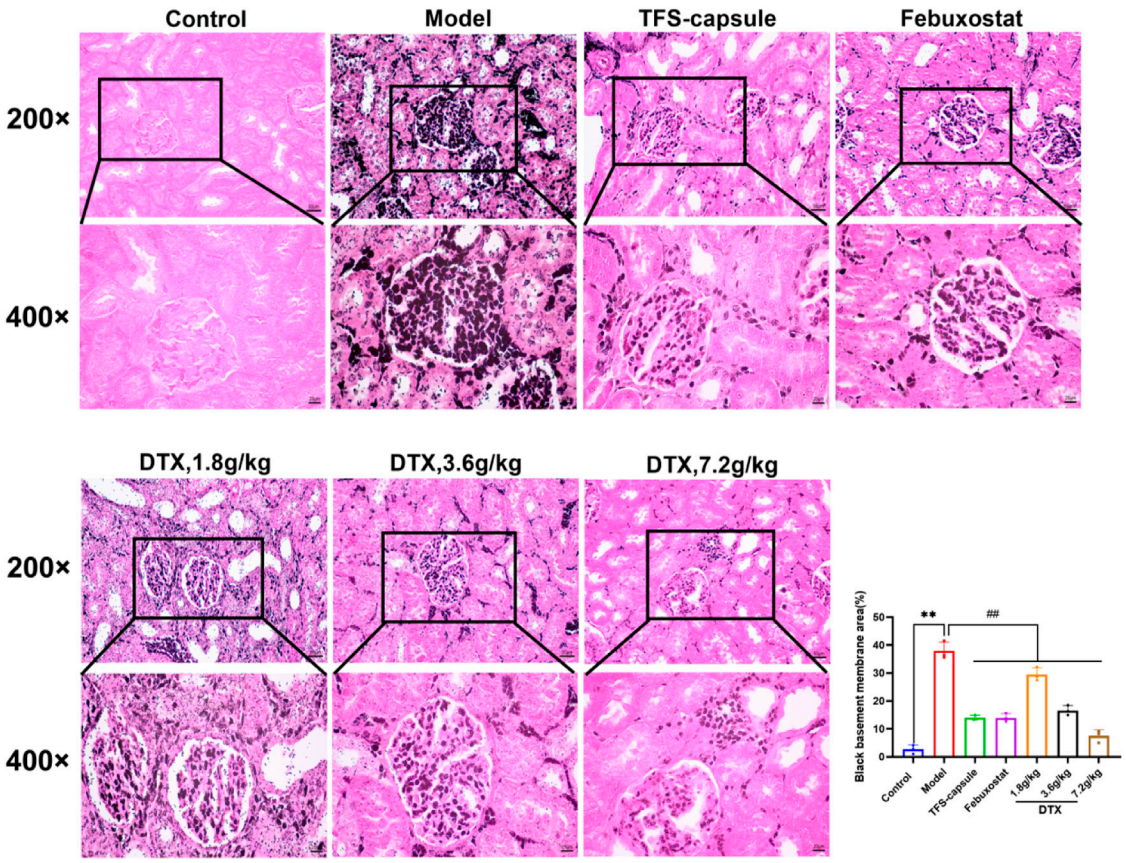

FIGURE 13
DTX reduced urate deposition in kidney tissues of GN rats. Gomori staining of rat kidneys (200× and 400×) (n = 3). Comparing the reference set as the control group; $**p < 0.01$. Comparing the reference set as the model group; $##p < 0.01$.

CysC, SAA, α1-MG, and β2-MG in the model group, whereas DTX administration effectively mitigated these levels, suggesting its potential to ameliorate GN clinical indicators. This reduction in glomerular and renal tubular damage signifies a positive impact on retarding GN progression.

XOD serves as a pivotal enzyme catalyzing the conversion of hypoxanthine to xanthine and further to uric acid (Yican et al., 2021). Elevated XOD activity signifies increased uric acid production, a primary instigator of GN (Wang et al., 2024b). Hyp is one of the characteristic components of collagen, reflecting tissue fibrosis degree. By quantifying the Hyp content in kidney tissue, the breakdown of collagen can be evaluated, providing insights into tissue remodeling processes (Haimei et al., 2022). COL-Ⅳ serves as a pivotal constituent of the extracellular matrix, while α-SMA serves as a marker for interstitial matrix formation. Excessive deposition of both entities can precipitate renal fibrosis and impede renal function (Zhou et al., 2021). The findings revealed notable elevations in XOD, Hyp, α-SMA, and COL-Ⅳ in the renal tissue of rats in the model group. Conversely, renal tissues of rats in the DTX group exhibited reduced levels of XOD, Hyp, α-SMA, and COL-Ⅳ. This suggests that DTX may mitigate renal fibrosis by suppressing uric acid production, thereby exerting a protective effect on kidneys and informing the clinical treatment of GN.

In our experiment, GN rats induced by adenine and potassium oxazinate exhibited morphological and pathophysiological alterations reminiscent of human GN. Our experimental findings confirm the successful replication of the GN model and the efficacy of drug intervention in kidney tissue. According to H&E, Masson, PASM, and Gomori staining, the model group exhibited renal inflammation, structural damage of renal tubular epithelial cells, increased collagen fiber accumulation, basement membrane thickening, massive atrophy, glomeruli sclerosis, and urate massive deposition. Conversely, DTX treatment markedly mitigated renal inflammatory responses, ameliorated the structure of renal tubular epithelial cells, attenuated collagen fiber deposition, and reduced basement membrane thickness. Meanwhile, glomerular atrophy, sclerosis, and urate deposition were also significantly improved. These observations suggested that DTX possesses anti-GN properties by enhancing the pathological state of renal tissue and mitigating urate deposition.

Kidney inflammation is intricately linked with GN (Wang et al., 2024a). IL-1β and IL-18 both belong to the IL-1 cytokine superfamily and are secreted mainly by activated macrophages, renal endothelial cells, and renal tubular epithelial cells. IL-1β prompts immune cell infiltration into damaged tissues, and studies indicate that IL-1β receptor antagonists exhibit promising therapeutic effects on gouty arthritis and GN (Schlesinger et al., 2023b). IL-18 typically resides within cells as inactive precursors,

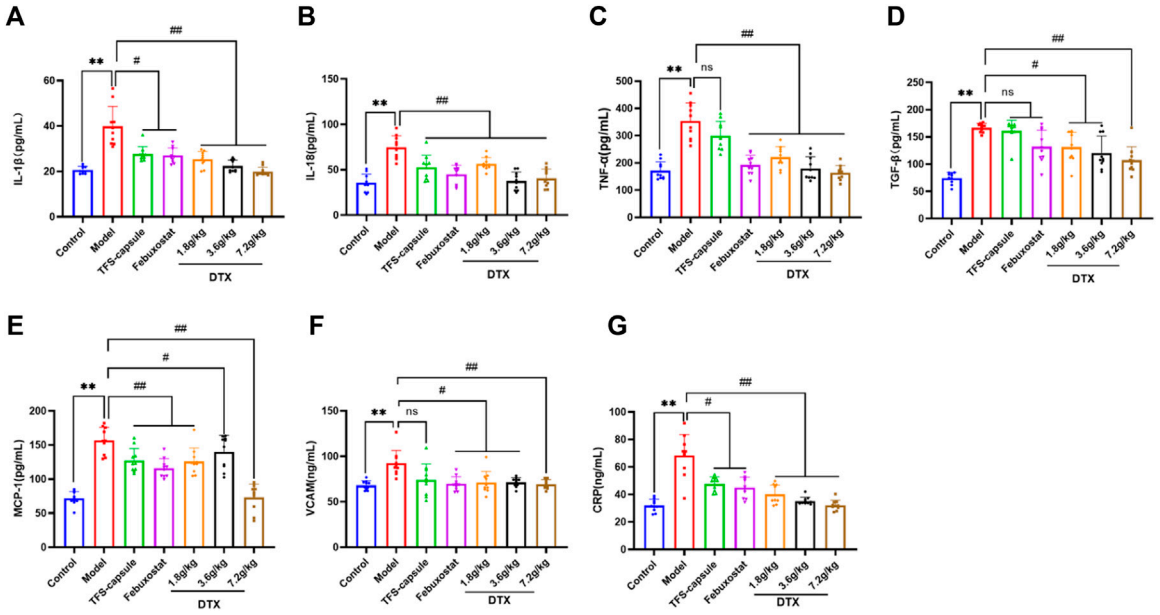

FIGURE 14
DTX alleviated inflammatory factors release in the GN rat serum (n = 10); **(A)** IL-1β in the rat serum. **(B)** IL-18 in the rat serum. **(C)** TNF-α in the rat serum. **(D)** TGF-β1 in the rat serum. **(E)** MCP-1 in the rat serum. **(F)** VCAM in the rat serum. **(G)** CRP in the rat serum. Comparing the reference set as the control group, $**p < 0.01$. Comparing the reference set as the model group; $\#p < 0.05$ and $\#\#p < 0.01$; ns: $p > 0.05$.

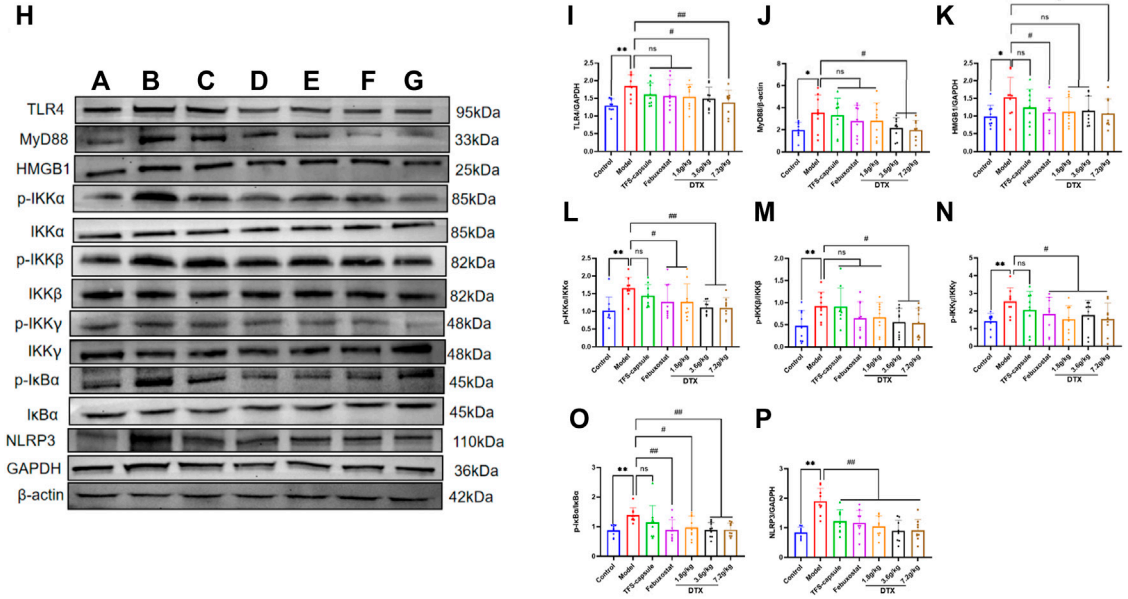

FIGURE 15
DTX modulated protein expression in GN rat kidney tissues (n = 3). **(A)** control group, **(B)** model group, **(C)** TFS capsule group, **(D)** febuxostat group, **(E)** DTX 1.8 g/kg dose group, **(F)** DTX 3.6 g/kg dose group, **(G)** DTX 7.2 g/kg dose group, and **(G)** DTX 7.2 g/kg dose group. **(H)** Protein plotting of TLR4, MyD88, HMGB1, p-IKKα/IKKα, p-IKKβ/IKKβ, p-IKKγ/IKKγ, p-IκBα/Iκbα, and NLRP3. **(I)** TLR4 protein expression. **(J)** MyD88 protein expression. **(K)** HMGB1 protein expression. **(L)** p-IKKα/IKKα protein expression. **(M)** p-IKKβ/IKKβ protein expression. **(N)** p-IKKγ/IKKγ protein expression. **(O)** p-IκBα/IκBα protein expression. **(P)** NLRP3 protein expression. Comparing the reference set as the normal group; $*p < 0.05$. Comparing the reference set as the model group; $\#p < 0.05$ and $\#\#p < 0.01$; ns: $p > 0.05$.

and upon cleavage, mature IL-18 is released into the cell, exerting immune activation effects. It induces the expression of chemokines, pro-inflammatory factors, and adhesion factors, thereby participating in the inflammatory response associated with kidney damage (Liu et al., 2023). TNF-α, originating from macrophages, plays a multifaceted role in the inflammatory

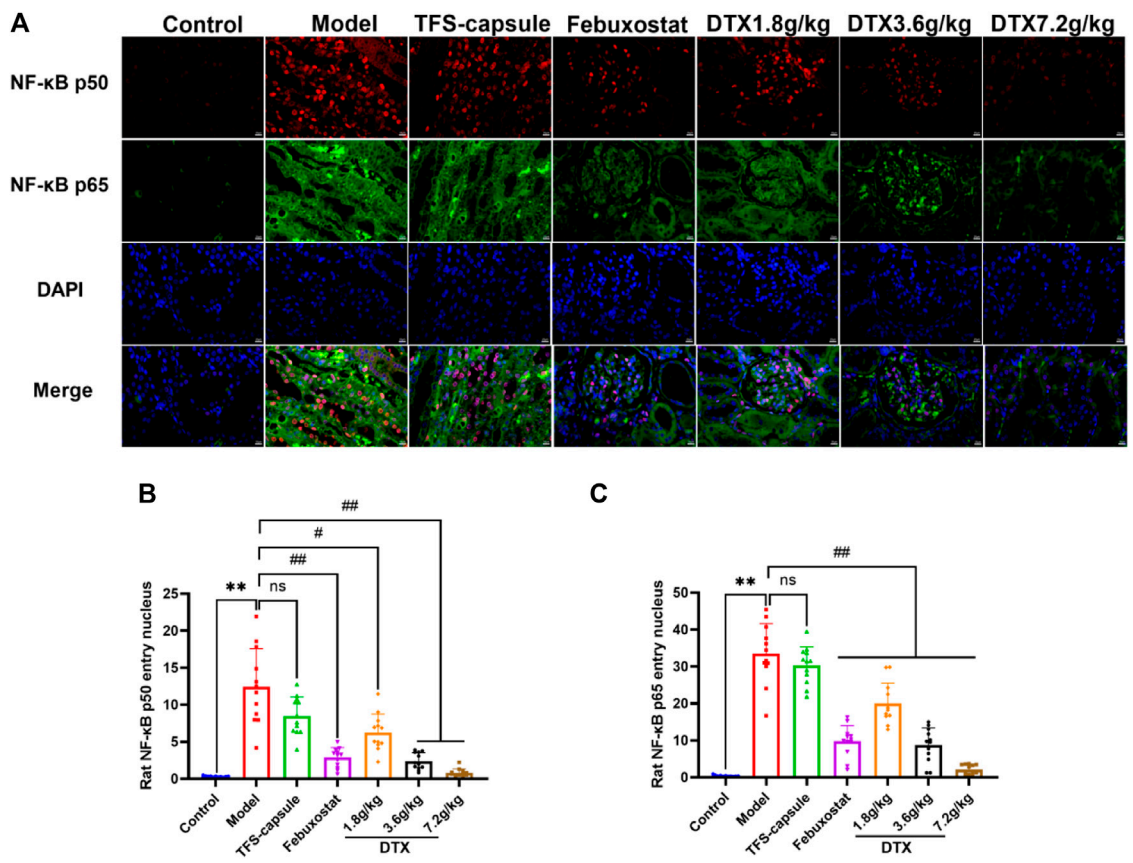

FIGURE 16
DTX reduced NF-κB expression in renal tissues of GN rats. **(A)** Rat kidney tissue (n = 3) immunofluorescence map. **(B)** Immunofluorescence surface density of the rat kidney tissue of NF-κB p50. **(C)** Immunofluorescence surface density of the rat kidney tissue of NF-κB p65. Red, NF-κB p50; green, NF-κB p65; and blue, 4, 6-diamino-2-styrenol (DAPI). Comparing the reference set as the control group; $^{**}p < 0.01$; Comparing the reference set as the model group; $\#p < 0.05$ and $\#\#p < 0.01$. ns showed no statistical significance.

TABLE 4 Molecular docking results.

Compound	Protein	Combining energy
Apigenin	TLR4	−6.2 kcal/mol
	MyD88	−8.0 kcal/mol
	NF-κB	−6.1 kcal/mol

response. Research indicates a positive correlation between TNF-α and kidney injury severity (Ye et al., 2023). As a pro-inflammatory cytokine, TNF-α aggravates the inflammatory response of neutrophils and functions as a key factor in gout generation and persistence (Chen J. et al., 2023). TGF-β1 is predominantly expressed in renal tubular epithelial cells, increasing extracellular matrix expression by stimulating myofibroblasts, enhancing adhesion between cells and matrix, and promoting the aggregation of the extracellular matrix in the renal interstitium, which is an important cytokine leading to renal fibrosis (Yang et al., 2023). MCP-1 is a prominent chemokine produced by mononuclear/macrophage cells, finding expression in various bodily tissues including vascular endothelial cells, fibroblasts, and epithelial cells. It emerges under pro-inflammatory stimuli, mobilizing immune cells to engage in the inflammatory cascade implicated in kidney damage (He et al., 2023). The adhesion of white blood cells to vascular endothelial cells, followed by their migration through the vascular endothelium to the inflammation site, constitutes a crucial step in the inflammatory process, and adhesion molecules serve as pivotal players in this process (Singh et al., 2023). VCAM-1, a member of the immunoglobulin superfamily of adhesion molecules, serves crucially in mediating adhesion and migration of immune cells like mononuclear cells/macrophages and T lymphocytes during inflammatory responses. Its interaction facilitates the recruitment of white blood cells to inflammatory sites, amplifying the inflammatory cascade and exacerbating kidney damage (Chen Z. et al., 2023). As a widely employed inflammatory indicator in clinical settings, CRP serves as a non-antibody protein and a non-specific marker reflecting chronic low-grade inflammation. It is regularly present in the human serum, albeit in minimal amounts (1 mg/L) under normal conditions. When tissues are compromised, cytokines prompt stem cells to produce substantial quantities of CRP (Nehring et al., 2024). CRP levels can surge by over 100 times during the acute response phase, making it a distinctive marker for inflammation detection (Alsogair et al., 2023). Our findings indicate that following the establishment of the GN rat model and administration of DTX, there was a significant reduction in IL-1β, IL-18, TNF-α, TGF-β1, MCP-1, VCAM-1, and CRP in the rat serum. This suggests that DTX

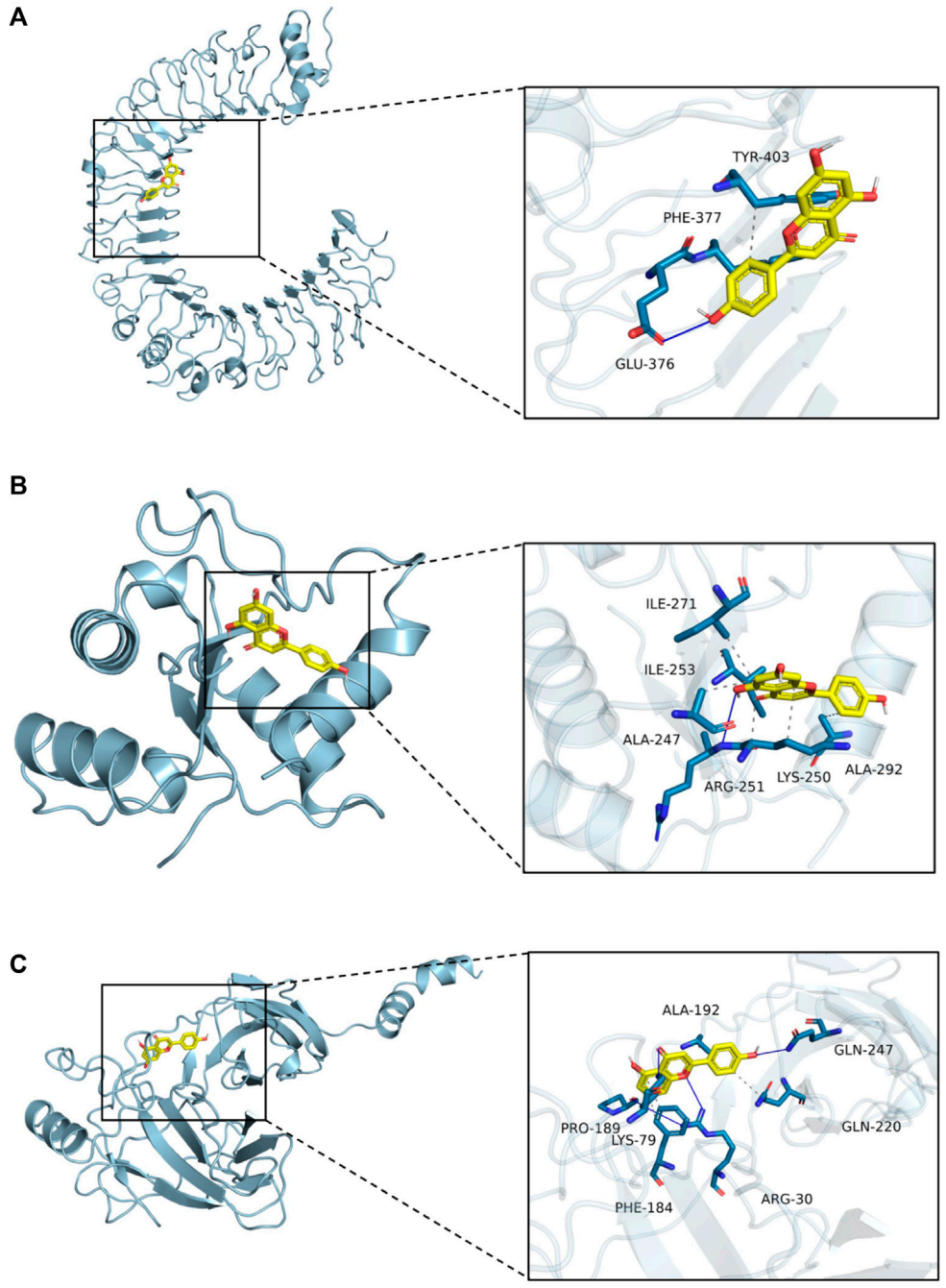

FIGURE 17
Molecular docking. **(A)** Molecular docking mode of apigenin and TLR4. **(B)** Molecular docking mode of apigenin and MyD88. **(C)** Molecular docking mode of apigenin and NF-κB.

effectively mitigates inflammatory infiltration and lowers the levels of chemokines and adhesion factors, thereby exerting its anti-GN effects.

TLR signaling is intricately linked to the activation of the immune system and the pathogenesis of GN (Luo et al., 2020). TLRs serve as pivotal protein molecules bridging both specific and non-specific immune responses (Jing et al., 2015). As an important biochemical basis for GN pathogenesis, uric acid typically precipitates in the distal tubules or collecting duct lumens as insoluble urate crystals, which in turn upregulates the expression of TLR4 on renal tubule cells (Chen et al., 2024). Upon TLR4 engagement with HMGB1 secreted by immune cells, renal tubular epithelial cells are directly activated, prompting macrophage migration to the renal interstitium and initiating a cascade where TLR4 subsequently binds to MyD88. This leads to the downstream activation of NF-κB inhibitor kinase (IKKα/IKKβ/IKKγ and IKK) (Qian et al., 2024). IKK phosphorylates serine residues on IκBα, leading to the dissociation of IκBα and

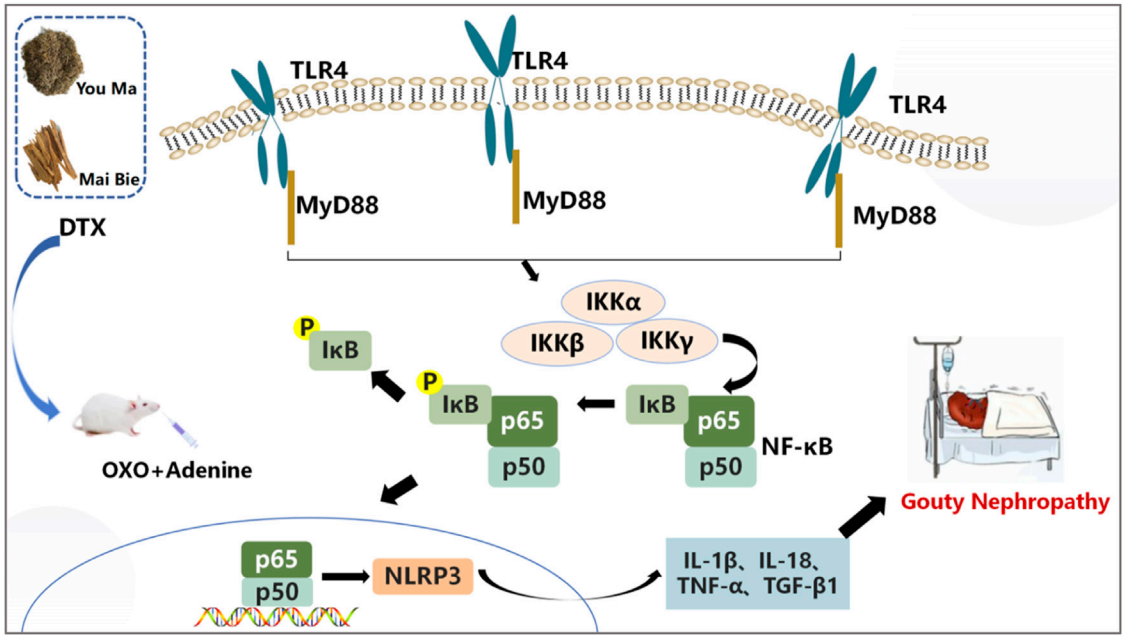

FIGURE 18
Pathogenesis of GN.

subsequent release of the NF-κB dimer composed of P50–P65 (YuanXiang et al., 2023). Following NF-κB translocation into the nucleus, the activation of the NLRP3 inflammasome occurs, resulting in the release of inflammatory factors and chemokines like IL-1β, TNF-β1, and MCP-1. This cascade recruits more inflammatory cells (Afonina et al., 2017), exacerbating inflammation and leading to severe kidney lesions in patients (Figure 18). Previous studies have shown that gouty nephropathy is associated with the TLR4/MyD88/NF-κB signaling pathway and that active substances can inhibit GN by modulating the TLR4/MyD88/NF-κB signaling pathway (Hao et al., 2023). Our study also revealed the activation of the TLR4/MyD88/NF-κB pathway in the GN rat model. Western blot analyses demonstrated significant upregulation of TLR4, MyD88, HMGB1, p-IKKα/IKKα, p-IKKβ/IKKβ, p-IKKγ/IKKγ, p-IκBα/IκBα, and NLRP3 expressions in renal tissues. Conversely, DTX treatment notably decreased protein expressions of TLR4, MyD88, HMGB1, p-IKKα/IKKα, p-IKKβ/IKKβ, p-IKKγ/IKKγ, p-IκBα/IκBα, and NLRP3 in renal tissues. This suggests that DTX might mitigate inflammatory factors by suppressing the TLR4/MyD88/NF-κB pathway, thereby enhancing the protective effect for the kidney. Additionally, in immunofluorescence findings, NF-κB expression in the nucleus was significantly reduced in the DTX-treated group. This could be attributed to IKK activation inhibition and reduced IκBα protein phosphorylation in the DTX-treated group, subsequently decreasing NF-κB release and inhibiting its nuclear expression in response to GN. The molecular docking results also showed that apigenin in DTX has a better affinity with TLR4, MyD88, and NF-κB. It is suggested that apigenin may directly act on the above targets, inhibiting the development of GN.

6 Conclusion

Our study shows the anti-GN efficacy of DTX, showcasing its ability to enhance kidney function and effectively combat kidney injury. Its mechanism of action likely involves inhibiting the inflammatory cascade by modulating the protein expression of the TLR4/MyD88/NF-κB pathway, thereby enhancing its protective effect on the kidneys. Our results reveal the previously neglected anti-GN mechanism of DTX, providing new insights and a foundation for clinical rational drug use.

Data availability statement

The raw data and image files are stored in Jianguoyun/Nutstore, available at: https://www.jianguoyun.com/p/DZj7FEEQ7_HWDBjGhckFIAA. Further queries can be directed to the corresponding authors.

Ethics statement

The animal study was approved by the Yunnan University of Chinese Medicine. The study was conducted in accordance with the local legislation and institutional requirements.

Author contributions

FL: writing–review and editing, writing–original draft, validation, supervision, software, methodology, and data curation. YB: writing–original draft, validation, software, methodology, and

investigation. YW: writing–original draft, methodology, investigation, and data curation. SL: writing–review and editing, methodology, and investigation. LZ: writing–original draft, methodology, investigation, and data curation. XW: writing–original draft, software, investigation, and conceptualization. RC: writing–review and editing, methodology, and investigation. ZY: writing–review and editing, methodology, and investigation. YX: writing–review and editing, software, resources, project administration, investigation, and funding acquisition. PG: writing–review and editing, visualization, validation, resources, project administration, methodology, and funding acquisition.

Funding

The author(s) declare that financial support was received for the research, authorship, and/or publication of this article. This work was supported by the Regional Foundation of the National Natural Science Foundation (No. 82360895, China), the Yunnan Provincial Science and Technology Department Basic Research Program of Traditional Chinese Medicine Joint Special (No. 2019FF002-028, China), the Yunnan Key Laboratory of Formulated Granules (No. 202105AG070014, China), the Yunnan Provincial Department of Education Science Research Fund Project (No. 2024Y371, China), Dai medicine Key Discipline of Pharmacy State Administration of Traditional Chinese Medicine (China), and the National Administration of Traditional Chinese Medicine High-level Key Discipline Construction Project "Dai Pharmacy" (No. zyyzdxk-2023192, China).

Acknowledgments

The authors would like to thank all the members of our group for their joint efforts to complete this paper.

Conflict of interest

The authors declare that the research was conducted in the absence of any commercial or financial relationships that could be construed as a potential conflict of interest.

Publisher's note

Supplementary material

The Supplementary Material for this article can be found online at: https://www.frontiersin.org/articles/10.3389/fphar.2024.1447241/full#supplementary-material

References

Afonina, I. S., Zhong, Z., Karin, M., and Beyaert, R. (2017). Limiting inflammation the negative regulation of NF-κB and the NLRP3 inflammasome. *Nat. Immunol.* 18 (8), 861–869. doi:10.1038/ni.3772

Alsogair, R., Altoub, H. A., Alsanad, M., Alshukr, M., AlObaid, B., Al Sayyari, A., et al. (2023). The relationship between C-reactive protein (CRP) concentrations and erythropoietin resistance, hospital admission rate, control of mineral metabolism, and comorbidity in hemodialysis patients. *Cureus* 15 (11), e48793. doi:10.7759/cureus.48793

Cai, X., Ahmad, G., Hossain, F., Liu, Y., Wang, X., Dennis, J., et al. (2020). High-density lipoprotein (hdl) inhibits serum amyloid A (SAA)-Induced vascular and renal dysfunctions in apolipoprotein E-deficient mice. *Int. J. Mol. Sci.* 21 (4), 1316. doi:10.3390/ijms21041316

Chen, J., Che, Q., Kou, Y., Rong, X., Zhang, X., Li, M., et al. (2023a). A novel drug combination of Tofacitinib and Iguratimod alleviates rheumatoid arthritis and secondary osteoporosis. *Int. Immunopharmacol.* 124 (Pt B), 110913. doi:10.1016/j.intimp.2023.110913

Chen, Y., Liu, Q., Meng, X., Zhao, L., Zheng, X., and Feng, W. (2024). Catalpol ameliorates fructose-induced renal inflammation by inhibiting TLR4/MyD88 signaling and uric acid reabsorption. *Eur. J. Pharmacol.* 967, 176356. doi:10.1016/j.ejphar.2024.176356

Chen, Z., Wang, Z., Hu, Y., Lin, H., Yin, L., Kong, J., et al. (2023b). ELABELA/APJ Axis prevents diabetic glomerular endothelial injury by regulating AMPK/NLRP3 pathway. *Inflammation* 46 (6), 2343–2358. doi:10.1007/s10753-023-01882-7

Elsaid, F. H., Hussein, A. M., Eid, E. A., Ammar, O. A., and Khalil, A. A. (2024). Effect of intermittent fasting on adriamycin-induced nephropathy: possible underlying mechanisms. *Tissue & Cell.* 88, 102360. doi:10.1016/j.tice.2024.102360

Feifan, L., Fanyi, S., Yuanmei, B., Yan, W., Lijie, Z., Jinglin, H., et al. (2023). Mechanism of DaiTongXiao in the treatment of gouty arthritis through the NLRP3 signaling pathway. *J. Ethnopharmacol.* 319 (P3), 117313. doi:10.1016/j.jep.2023.117313

Feng, Z. (2015). *Clinical observation of "Dai tongxiao" treating with "gout" due to the superabundance of wind-fire.* China: Yunnan University of Chinese Medicine.

Gout Medications (2012). "Gout medications," in *LiverTox: clinical and research information on drug-induced liver injury* (Bethesda (MD): National Institute of Diabetes and Digestive and Kidney Diseases).

Grace, L., and Luke, D. (2022). Medicinal Mishap: severe adverse drug reaction to allopurinol. *Aust. Prescr.* 45 (4), 130–131. doi:10.18773/austprescr.2022.032

Haimei, H., Wanfu, B., Hongbing, Z., Jia, W., Zhanjun, Y., Min, Q., et al. (2022). Study on the mechanism of Amygdalus mongolica oil anti-renal fibrosis based on metabolomics and transcriptomics. *Pharmacol. Res. - Mod. Chin. Med.* 5, 100166. doi:10.1016/j.prmcm.2022.100166

Hao, L., Zhiyu, C., Meng, L., Ertong, L., Juan, S., Jie, W., et al. (2023). The Terminalia chebula retz extract treats hyperuricemic nephropathy by inhibiting TLR4/myd88/NF-κb axis. *J. Ethnopharmacol.* 322, 117678.

He, S., Yao, L., and Li, J. (2023). Role of MCP-1/CCR2 axis in renal fibrosis: mechanisms and therapeutic targeting. *Med. Baltim.* 102 (42), e35613. doi:10.1097/md.0000000000035613

Hosoyamada, M. (2021). Hypothetical mechanism of exercise-induced acute kidney injury associated with renal hypouricemia. *Biomedicines* 9 (12), 1847. doi:10.3390/biomedicines9121847

Hu, N., Wang, C., Dai, X., Zhou, M., Gong, L., Yu, L., et al. (2020). Phillygenin inhibits LPS-induced activation and inflammation of LX2 cells by TLR4/MyD88/NF-κB signaling pathway. *J. Ethnopharmacol.* 248, 112361. doi:10.1016/j.jep.2019.112361

H-Y, C., C-B, C., C-Y, C., Y-A, C., Y, N. C., K-L, K., et al. (2015). Febuxostat-associated drug reaction with eosinophilia and systemic symptoms (DRESS). *J. Clin. Pharm. Ther.* 40 (6), 689–692. doi:10.1111/jcpt.12322

Jena, S., Ray, A., Mohanta, O., Das, P. K., Sahoo, A., Nayak, S., et al. (2022). Neocinnamomum caudatum essential oil ameliorates lipopolysaccharide-induced inflammation and oxidative stress in RAW 264.7 cells by inhibiting NF-κB activation and ROS production. *Molecules* 27 (23), 8193. doi:10.3390/molecules27238193

Jing, X., Xiao-Li, Z., Chensheng, F., Rui, H., Weijun, C., Yijun, L., et al. (2015). Soluble uric acid increases NALP3 inflammasome and interleukin-1β expression in human primary renal proximal tubule epithelial cells through the Toll-like receptor 4-mediated pathway. *Int. J. Mol. Med.* 35 (5), 1347–1354. doi:10.3892/ijmm.2015.2148

Kim, H. W., Lee, S. J., and Lee, D. S. (2023). 24-h urine collection in patients with urolithiasis: perspective on renal function. *Urolithiasis* 52 (1), 5. doi:10.1007/s00240-023-01500-z

Konstandi, M., Sotiropoulos, I., Matsubara, T., Malliou, F., Katsogridaki, A., Andriopoulou, C. E., et al. (2019). Adrenoceptor-stimulated inflammatory response in stress-induced serum amyloid A synthesis. *Psychopharmacology* 236 (6), 1687–1699. doi:10.1007/s00213-018-5149-4

Kraev, K. I., Popova, M. G. G., Hristov, B. K., Uchikov, P. A., Belova, S. D. P., Kraeva, M. I., et al. (2023). Celebrating versatility: febuxostat's multifaceted therapeutic application. *Life* 13 (11), 2199. doi:10.3390/life13112199

Li, B., Guangyun, L., Xiangping, W., Ning, L., Xiaoping, Z., and Mingsan, M. (2022). Total flavonoids of peony flower regulate NLRP3 inflammasome and expression of inflammatory cytokines in gouty nephropathy rats. *Chin. J. Exp. Traditional Med. Formulae* 28 (09), 43–51. doi:10.13422/j.cnki.syfjx.20220939

Liao, M., Wang, X., Lu, Y., and Wang, X. (2016). Mechanism study on effects of apigenin on reducing uric acid and renal protection in oteracil potassium-induced hyperuricemia mice. *China Pharm.* 27 (34), 4794–4797.

Liu, F., Shen, F., Bai, Y., Wan, Y., Zheng, L., He, J., et al. (2024). Mechanism of DaiTongXiao in the treatment of gouty arthritis through the NLRP3 signaling pathway. *J. Ethnopharmacol.* 319 (Pt 3), 117313. doi:10.1016/j.jep.2023.117313

Liu, Z., Xiang, H., Deng, Q., Fu, W., Li, Y., Yu, Z., et al. (2023). Baicalin and baicalein attenuate hyperuricemic nephropathy via inhibiting PI3K/AKT/NF-κB signalling pathway. *Nephrol. Carlt.* 28 (6), 315–327. doi:10.1111/nep.14159

Luo, S. F., Chin, C. Y., Ho, L. J., Tseng, W. Y., Kuo, C. F., and Lai, J. H. (2020). Monosodium urate crystals induced ICAM-1 expression and cell-cell adhesion in renal mesangial cells: implications for the pathogenesis of gouty nephropathy. *J. Microbiol. Immunol. Infect.* 53 (1), 23–32. doi:10.1016/j.jmii.2017.12.004

Mei, Y., Dong, B., Geng, Z., and Xu, L. (2022). Excess uric acid induces gouty nephropathy through crystal formation: a review of recent insights. *Front. Endocrinol. (Lausanne)* 13, 911968. doi:10.3389/fendo.2022.911968

Mian, W., Yiwen, M., Xiaoting, C., Nan, L., Shen, Q., and Haibing, C. (2021). Hyperuricemia causes kidney damage by promoting autophagy and NLRP3-mediated inflammation in rats with urate oxidase deficiency. *Dis. models Mech.* 14 (3), dmm048041. doi:10.1242/dmm.048041

Nehring, S. M., Goyal, A., and Patel, B. C. (2024). "C reactive protein," in *StatPearls. Treasure Island (FL) ineligible companies. Disclosure: amandeep Goyal declares no relevant financial relationships with ineligible companies. Disclosure: bhupendra Patel declares no relevant financial relationships with ineligible companies* (StatPearls Publishing).

Noroozi, F., Rousta, M. A., Amini, R., and Sahraeian, Z. (2024). Alpha-pinene alleviates CCl4-induced renal and testicular injury in rats by targeting oxidative stress, inflammation, and apoptosis. *Iran. J. basic Med. Sci.* 27 (6), 678–684. doi:10.22038/IJBMS.2024.73116.15890

Pan, J., Zhang, C., Shi, M., Guo, F., Liu, J., Li, L., et al. (2021). Ethanol extract of Liriodendron chinense (Hemsl.) Sarg barks attenuates hyperuricemic nephropathy by inhibiting renal fibrosis and inflammation in mice. *J. Ethnopharmacol.* 264, 113278. doi:10.1016/j.jep.2020.113278

Prasanna, M. D., Yuri, G. A., and Olena, Z. (2020). Benefits and adverse effects of hydroxychloroquine, methotrexate and colchicine: searching for repurposable drug candidates. *Rheumatol. Int.* 40 (11), 1741–1751. doi:10.1007/s00296-020-04694-2

Qian, W., Mingyuan, Z., Yuchi, C., Bingqi, Z., Fangmei, Z., Xiaoqing, Y., et al. (2024). Bletilla striata polysaccharides protect against ARDS by modulating the NLRP3/caspase1/GSDMD and HMGB1/TLR4 signaling pathways to improve pulmonary alveolar macrophage pyroptosis. *J. Ethnopharmacol.* 319 (P3), 117361. doi:10.1016/j.jep.2023.117361

Qinghua, C., Pu, C., Shihua, L., and Chao, Z. (2014a). Effect of Daitongxiao on blood uric acid, blood urea nitrogen and xanthine oxidase of mice with acute hyperuricemia. *Chin. J. Ethnomedicine Ethnopharmacy* 23 (11), 1–2.

Qinghua, C., Shihua, L., and Chao, Z. (2014b). Effect od Daitongxiao on blood uric acid and blood urea nitrogen of mice with acute hyperuricemia. *Liaoning J. Traditional Chin. Med.* 41, 2483–2484. doi:10.13192/j.issn.1000-1719.2014.11.087

Schlesinger, N., Pérez-Ruiz, F., and Lioté, F. (2023a). Mechanisms and rationale for uricase use in patients with gout. *Nat. Rev. Rheumatol.* 19 (10), 640–649. doi:10.1038/s41584-023-01006-3

Schlesinger, N., Pillinger, M. H., Simon, L. S., and Lipsky, P. E. (2023b). Interleukin-1β inhibitors for the management of acute gout flares: a systematic literature review. *Arthritis Res. Ther.* 25 (1), 128. doi:10.1186/s13075-023-03098-4

Shen, J., Yang, Q., Liu, N., Zhang, Y., and Peng, J. (2020). Effect of yishen jianpi xiezhou decoction on renal function and pathological changes in rats with gouty nephropathy. *J. Yunnan Univ. Chin. Med.* 43, 1–6. doi:10.19288/j.cnki.issn.1000-2723.2020.01.001

Shi, G., Guo, M., Li, D., Liu, X., Yang, J., and Liu, G. (2014). Chemical constituents of pinus kesiya royle ex gord. *Var. langbianensis A. Chev. Gaussen. Chin. Tradit. Pat. Med.* 36, 1467–1470. doi:10.3969/j.issn.1001-1528.2014.07.027

Shi, X., Zhuang, L., Zhai, Z., He, Y., and Sun, E. (2023). Polydatin protects against gouty nephropathy by inhibiting renal tubular cell pyroptosis. *Int. J. Rheum. Dis.* 26 (1), 116–123. doi:10.1111/1756-185x.14463

Singh, V., Kaur, R., Kumari, P., Pasricha, C., and Singh, R. (2023). ICAM-1 and VCAM-1: gatekeepers in various inflammatory and cardiovascular disorders. *Clin. Chim. Acta* 548, 117487. doi:10.1016/j.cca.2023.117487

Sun, X., Ma, J., Liu, J., Li, L. J., Zhang, L., Huang, Y. R., et al. (2023). Fc effector of anti-Aβ antibody induces synapse loss and cognitive deficits in Alzheimer's disease-like mouse model. *Syst. Med.* 8, 30–32+50. doi:10.1038/s41392-022-01273-8

Tan, Z., Chang, Y., Liu, J., Chang, X., and Zhang, Y. (2013). Ethnomedicine: fading or flowering? — Heritage and development of Dai Medicine. *J. Med. Coll. PLA* 28 (1), 54–59. doi:10.1016/s1000-1948(13)60017-9

Wang, L., and Wang, X. (2024). Diagnostic value of multi-parameter ultrasound evaluation in sepsis complicated by acute kidney injury. *Ren. Fail.* 46 (1), 2313861. doi:10.1080/0886022X.2024.2313861

Wang, L., Zhang, X., Shen, J., Wei, Y., Zhao, T., Xiao, N., et al. (2024a). Models of gouty nephropathy: exploring disease mechanisms and identifying potential therapeutic targets. *Front. Med. (Lausanne)* 11, 1305431. doi:10.3389/fmed.2024.1305431

Wang, L., Zhang, X., Shen, J., Wei, Y., Zhao, T., Xiao, N., et al. (2024b). Models of gouty nephropathy: exploring disease mechanisms and identifying potential therapeutic targets. *Front. Med.* 11, 1305431. doi:10.3389/fmed.2024.1305431

Wu, J., Chen, M., and Yu, L. (2022). Dai medicine prevention and treatment of Sha Hou (gout) expert consensus. *Chin. J. Ethnomedicine Ethnopharmacy* 31, 1–4. doi:10.3969/j.issn.1007-8517.2022.8.zgmzmjyyzz202208002

Xueyan, Z., Yingbo, L., Guangrui, D., Bisheng, H., Guoyin, K., Keli, c., et al. (2021). A purified biflavonoid extract from selaginella moellendorffii alleviates gout arthritis via NLRP3/ASC/Caspase-1 Axis suppression. *Front. Pharmacol.* 12, 676297. doi:10.3389/fphar.2021.676297

Yanai, H., Adachi, H., Hakoshima, M., and Katsuyama, H. (2021). Molecular biological and clinical understanding of the pathophysiology and treatments of hyperuricemia and its association with metabolic syndrome, cardiovascular diseases and chronic kidney disease. *Int. J. Mol. Sci.* 22 (17), 9221. doi:10.3390/ijms22179221

Yang, S., Wu, H., Li, Y., Li, L., Xiang, J., Kang, L., et al. (2023). Inhibition of PFKP in renal tubular epithelial cell restrains TGF-β induced glycolysis and renal fibrosis. *Cell. Death Dis.* 14 (12), 816. doi:10.1038/s41419-023-06347-1

Ye, H. Y., Song, Y. L., Ye, W. T., Xiong, C. X., Li, J. M., Miao, J. H., et al. (2023). Serum granulosa cell-derived TNF-α promotes inflammation and apoptosis of renal tubular cells and PCOS-related kidney injury through NF-κB signaling. *Acta Pharmacol. Sin.* 44 (12), 2432–2444. doi:10.1038/s41401-023-01128-0

Yican, W., Meng, H., Xin, D., Yiting, H., Liping, H., Yuying, D., et al. (2021). Renal tubular cell necroptosis: a novel mechanism of kidney damage in trichloroethylene hypersensitivity syndrome mice. *J. Immunotoxicol.* 18 (1), 173–182. doi:10.1080/1547691X.2021.2003486

Yongsheng, M., Bingzi, D., Zhuang, G., and Lili, X. (2022). Excess uric acid induces gouty nephropathy through crystal formation: a review of recent insights. *Front. Endocrinol.* 13, 911968. doi:10.3389/fendo.2022.911968

YuanXiang, Z., XiaoTong, Z., HongJin, L., TaoFeng, Z., AnCheng, Z., ZhengLing, Z., et al. (2023). Antidepressant-like effects of helicid on a chronic unpredictable mild stress-induced depression rat model: inhibiting the IKK/IκBα/NF-κB pathway through NCALD to reduce inflammation. *Int. Immunopharmacol.* 93 (2021), 107165. doi:10.1016/j.intimp.2020.107165

Zhang, C., Feng, W., Zheng, X., Li, H., Chen, X., and Yan, H. (2010). "Studies on chemical constituents of pinus tabuleaformis carr needles," in *Proceedings of the 2010 Chinese pharmaceutical congress and the 10th Chinese pharmacist week*, 1664–1669.

Zhang, L. (2009). *Studies on quality standard for lignum pini nodi and radix et rhizoma glycyrrhizae decoction pieces*. Peking Union Medical College.

Zhang, Y., Li, Y., Li, C., Zhao, Y., Xu, L., Ma, S., et al. (2023a). Paeonia × suffruticosa Andrews leaf extract and its main component apigenin 7-O-glucoside ameliorate hyperuricemia by inhibiting xanthine oxidase activity and regulating renal urate transporters. *Phytomedicine* 118, 154957. doi:10.1016/j.phymed.2023.154957

Zhang, Y., Wang, S., Dai, X., Liu, T., Liu, Y., Shi, H., et al. (2023b). Simiao San alleviates hyperuricemia and kidney inflammation by inhibiting NLRP3 inflammasome and JAK2/STAT3 signaling in hyperuricemia mice. *J. Ethnopharmacol.* 312, 116530. doi:10.1016/j.jep.2023.116530

Zheng, L., Bai, Y., and Guo, P. (2022). Research progress in the treatment of gouty nephropathy with Dai and western medicine. *Med. Plant* 13 (04), 99–101+104. doi:10.19600/j.cnki.issn2152-3924.2022.04.022

Zhou, Y., Chai, P., Wang, J., Li, L., and Chen, M. H. (2021). Wingless/int-1induced secreted protein-1: a new biomarker for renal fibrosis. *J. Biol. Regul. Homeost. Agents* 35 (1), 97–103. doi:10.23812/20-459-a

Zhou, Y., and Chen, G. (2021). Research progress on chemical composition, pharmacological action and comprehensive application of Yi medicine Yeba Zi. *Guid. J. Traditional Chin. Med. Pharm.* 27, 53–55+60. doi:10.13862/j.cnki.cn43-1446/r.2021.08.011

frontiers | Frontiers in Pharmacology

TYPE Original Research
PUBLISHED 16 September 2024
DOI 10.3389/fphar.2024.1440810

OPEN ACCESS

EDITED BY
Qianfeng Gong,
Jiangxi University of Traditional Chinese Medicine, China

REVIEWED BY
Xianan Sang,
Zhejiang Chinese Medical University, China
Shi-Jun Yue,
Hebei University of Chinese Medicine, China
Yi Tao,
Zhejiang University of Technology, China
Qiao Zhang,
Shaanxi University of Chinese Medicine, China

*CORRESPONDENCE
Xiaoli Wang,
792511843@qq.com

†These authors have contributed equally to this work

RECEIVED 30 May 2024
ACCEPTED 28 June 2024
PUBLISHED 16 September 2024

CITATION
Yang Z, Chen K, Zhang Y, Xu B, Huang Y, Zhang X, Liu Z, Wang T, Wu D, Peng T, Lu T, Cai H and Wang X (2024), Study on pharmacokinetic and tissue distribution of hyperin, astragalin, kaempferol-3-O-β-D-glucuronide from rats with multiple administrations of Semen Cuscutae processed with salt solution with effect of treating recurrent spontaneous abortion.
Front. Pharmacol. 15:1440810.
doi: 10.3389/fphar.2024.1440810

Study on pharmacokinetic and tissue distribution of hyperin, astragalin, kaempferol-3-O-β-D-glucuronide from rats with multiple administrations of Semen Cuscutae processed with salt solution with effect of treating recurrent spontaneous abortion

Zhitong Yang[1†], Kaiwen Chen[1†], Yuting Zhang[1†], Baiyang Xu[1], Yu Huang[1], Xue Zhang[1], Zilu Liu[1], Tongsheng Wang[1], Deling Wu[1,2,3], Tangyi Peng[4], Tulin Lu[5], Hao Cai[5] and Xiaoli Wang[1,2,3]*

[1]Anhui Province Key Laboratory of Research, Development of Chinese Medicine, Anhui University of Chinese Medicine, Hefei, China, [2]Heritage Base of TCM Processing Technology of NATCM, Anhui University of Chinese Medicine, Hefei, China, [3]Anhui Province Key Laboratory of Traditional Chinese Medicine Decoction Pieces of New Manufacturing Technology, Hefei, China, [4]The First Affiliated Hospital of Anhui University of Chinese Medicine, Hefei, China, [5]School of Pharmacy, Nanjing University of Chinese Medicine, Nanjing, China

Introduction: *Semen Cuscutae* is a traditional Chinese medicine (TCM) that tonifies the kidneys and prevents miscarriage. According to Chinese medicine theory, kidney deficiency is one of the main causes of recurrent spontaneous abortion (RSA). The previous studies showed that raw product of *Semen Cuscutae* (SP) and *Semen Cuscutae* processed with salt solution (YP) have ameliorative effects on RSA, and that YP is superior to SP. However, the active components of YP to ameliorate RSA remain unclear and require further studies. The objective of this study is to investigate the active components of YP in ameliorating RSA.

Methods: First, a rat model of RSA was established using hydroxyurea in combination with mifepristone. Aqueous decoction of YP was given by gavage to rats. Second, pregnant rats were sampled on days 5, 7, 9, 10 and 12 during the modelling period. The content of Hyperin (HY), astragalin (AS) and kaempferol-3-O-β-D-glucuronide (KA) in blood and liver, heart, spleen, lung and kidney tissues were detected by liquid chromatography-mass spectrometry (LC-MS). The pharmacodynamic indicators including progesterone (P), chorionic gonadotropin β (β-HCG), estradiol (E2), tumor necrosis factor-α (TFN-α), interleukin 4 (IL-4), and tryptophan (TRP) were

Abbreviations: AS, astragalin; AUC, area under curve; E2, estradiol; ELISA, enzyme-linked immunosorbent assay; ESI, electrospray ionization; HY, hyperin; IL-4, interleukin-4; IL-6, interleukin-6; IUA, intrauterine adhesions; KA, kaempferol-3-O-β-D-glucuronide; P, progesterone; QC, quality control samples; RSA, recurrent abortion; S, raw products of *Semen Cuscutae*; TGF-β1, transforming growth factor-β1; TNF-α, tumor necrosis factor-α; UHPLC-Q/TOF-MS, ultra-high performance liquid chromatography and quadrupole time-of-flight mass spectrometry; VEGF, vascular endothelial growth factor; YP, *Semen Cuscutae* processed with salt solution.

10.3389/fphar.2024.1440810

measured by enzyme-linked immunosorbent assay (ELISA) Pearson's correlation analysis and grey relational analysis were used to establish the relationship between the pharmacodynamic indexes and chemical constituents.

Results: The pharmacokinetic results showed that the area under curve (AUC) value of KA was the largest. The tissue distribution results showed that astragalin was widely distributed in liver, heart, spleen, lung and kidney in the RSA model rats, while HY was detected only in the uterus, and KA was detected only in the kidney. The pearson correlationl analysis showed that KA was significantly and positively correlated with the contents of E2, P, β-HCG and TRP. Both AS and HY were significantly negatively correlated with the content of TNF-α, respectively.

Discussion: This study reveals the pharmacokinetics and tissue distribution of KA, AS and HY in rats with RSA. It was elucidated that all three were involved in the regulation of progesterone levels and immune function. It initially revealed the mechanism of action of YP in enhancing the improvement of RSA, and it provided a theoretical basis for the quality assessment of YP.

KEYWORDS

recurrent spontaneous abortion, *Semen Cuscutae* processed with salt solution, correlation, UHPLC-MS/MS, active substance

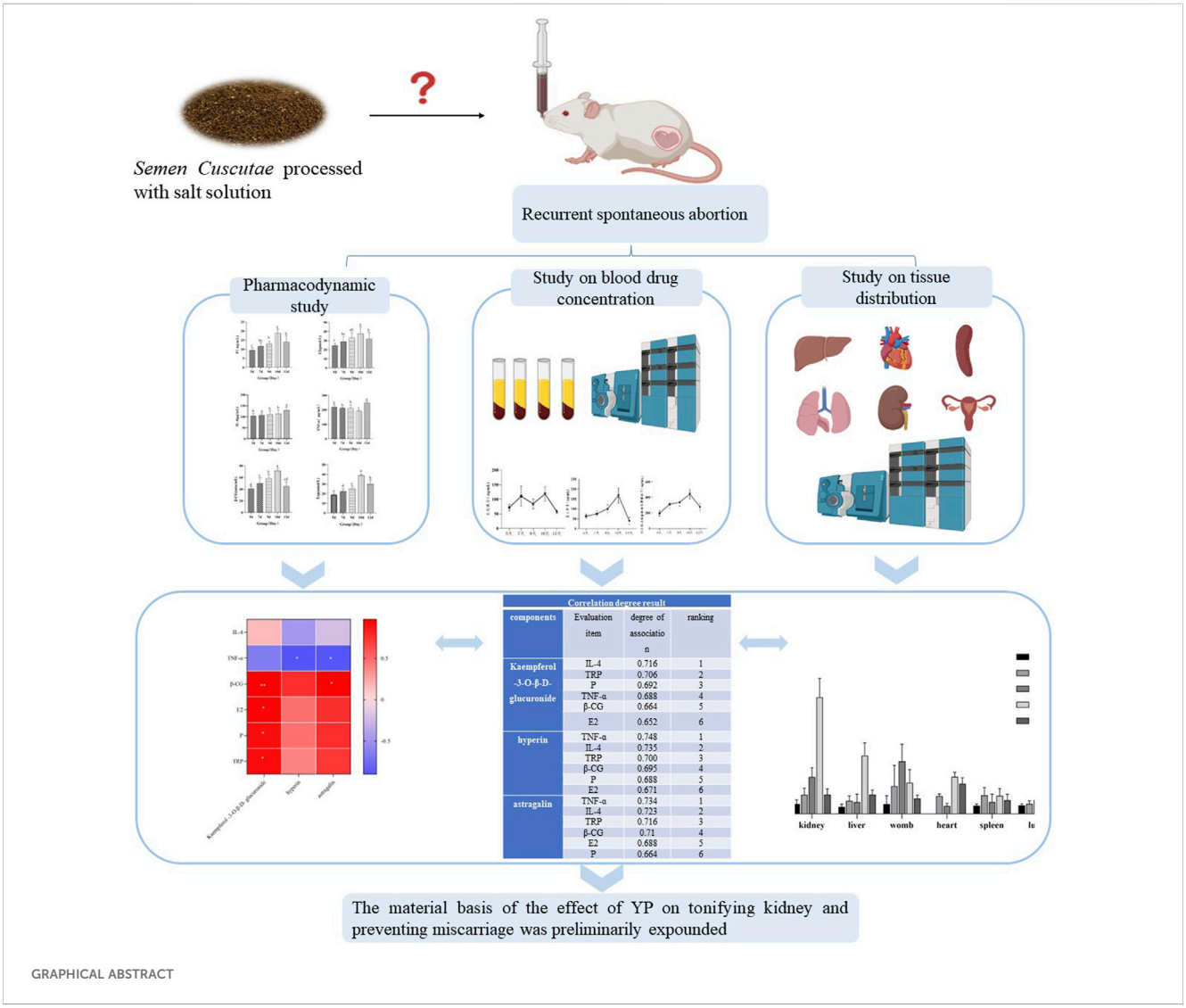

GRAPHICAL ABSTRACT

Introduction

RSA refers to spontaneous abortion that occurs at least three times in the same woman. The incidence of RSA is approximately 1%–5% in women of child-bearing age (La et al., 2021). Patients with a history of RSA have a similar chance of miscarriage. RSA belongs to the category of "sliding fetus" in traditional Chinese medicine (TCM). It is one of the most common complications of pregnancy, with the characteristics of recurrent pregnancy and abortion. The causes of RSA are complex. In addition to genetic factors such as chromosome, luteal insufficiency and other endocrine factors, infection factors, immune anticoagulant antibody syndrome, pre-thrombotic state, internal reproductive organ anatomical abnormalities, and other influencing factors, the cause of RSA is unknown in 60%–70% of patients (Deng et al., 2022). The severity of RSA not only affects the physical and mental health of women but also makes the family and society unstable to a certain extent, which has gained the attention of scholars at home and abroad. The theory of "sliding abortion" points out that the essence of innateness is hidden in the kidney and the kidney andis responsible for reproduction. The completion of pregnancy lies in the consolidation of kidney qi (Xu et al., 2023a; Wang et al., 2020). Therefore, TCM, with the effect of kidney reinforcement, has unique advantages in improving RSA.

The frequency of use of 14,169 kinds of TCM prescriptions for recurrent abortion in the obstetrics and gynecology department of the First Affiliated Hospital of Anhui University of Chinese Medicine was analyzed and studied by our research group in the early stage. The results showed that YP was used most frequently. SP has significant effect on the application of tonifying the kidney and preventing fetus (Supplementary Figures S1, S2). SP was first recorded in Shennong's Classic of Materia Medica and was listed as a quality medicine at the top grade (Xu et al., 2023b). Modern pharmacological studies have shown that SP can enhance immunity, improve reproductive function, result in anti-aging, and protect the liver (Zhang et al., 2024). The main components of SP mainly include flavonoids, glycosidic acids, alkaloids, and lignans (Liu et al., 2021). In addition, it was found that compared with SP, the total flavonoid content in YP increased (Xu et al., 2023c). As a traditional holy medicine for "tonifying kidney and preventing fetus," the efficacy of YP has long been confirmed in clinical practice (Wang et al., 2021). It was recorded in Medical Zhongzhongcan Xilu written by Zhang Xichun's that "SP has no roots and spreads on grass and trees, but the grass and trees are not lush. It is good to absorb the gasification of other things, which can be known by cultivation. The fetus is in its mother's womb, and if it absorbs the gasification of its mother well, it will not fall down. In addition, both male and female reproduction rely on the kidney for strength. SP can strengthen the kidney qi, and the body with full kidney qi can nourish the foetus." Previous research has shown that there were significant differences in the 10 components before and after salt processing with salt solution, and the flavonoids were generally increased after salt processing (Huang et al., 2022). However, the active substances of YP that treat RSA are still unclear.

Semen Cuscutae has more active components, with flavonoids being the most abundant. Modern pharmacology has shown that the total flavonoids of *Semen Cuscutae* have estrogenic effects, and KA, AS, and HY are the direct *in vivo* effectors of estrogenic effects of *Semen Cuscutae* (Sun et al., 2021). HY and KA, among others, can be used as quality markers for reproductive endocrine regulation, anti-inflammatory, immune enhancement, and inhibition of oxidative stress. The estrogenomimetic and anti-inflammatory effects of HY, AS, KA may reflect the disease state of recurrent miscarriage by regulating the hormone levels and expression of HY, AS, and KA. The estrogenomimetic and anti-inflammatory effects of HY, AS, and KA may reflect the disease state of recurrent miscarriage by regulating the hormone levels and expression of inflammatory factors in patients with RSA. Therefore, in this study, three components, HY, AS, and KA were selected as indicator components of *Semen Cuscutae*.

In the past decades, many experts and scholars have made remarkable achievements in the field of basic research on the medicinal effect of various materials. After the processing of TCM, the synergistic effect, phase system, and attenuation effect of the interaction between its components and the body is the embodiment of these comprehensive effects. Therefore, the *in vivo* study process is in line with the basic research mode of synergetic substances in TCM processing (Su et al., 2022). Pharmacokinetics study is helpful to reveal the pharmacodynamic substances of traditional Chinese medicine by studying the pharmacokinetic parameters of compounds, such as the area under the concentration–time curve (AUC), elimination half-life ($t_{1/2}$), maximum concentration (C_{max}), time to peak (T_{max}), and tissue distribution. It is also important to elucidate the interactions of various components in the body. According to the "homing in meridian" theory of the role of TCM processing excipients, each drug has its favorable site of action in the human body. In other words, each drug or compound has a target organ in the body and exerts a therapeutic effect at that site. Therefore, it is necessary to carry out pharmacokinetic and tissue distribution studies of YP to elucidate its effective substances and mechanisms of action. In this study, a sensitive, reliable, and accurate ultra-performance liquid chromatography–tandem mass spectrometry (UHPLC-MS/MS) method was established for quantitative determination of the main components of YP in rat plasma and tissues, and it was successfully applied to the pharmacokinetics and tissue distribution of YP. The association model of composition change spectrum and effect index is an important tool to study the *in vivo* process of drugs. This model has the characteristics of accuracy and dynamic change, which plays a unique role in the study of the *in vivo* process of TCM.

This paper mainly uses the correlation model of "body composition–efficacy index" to initially explore the active substances of YP in the treatment of RSA, which will help in further enriching the scientific connotation of the theory of the role of Chinese medicine processing excipients, and it has important guiding significance for the improvement of Chinese medicine quality standards and processing technology.

Materials and methods

Materials and reagents

Semen Cuscutae herbal decoction pieces were purchased from Tongling Wada Chinese Medicine Drinking Tablets Company

(Tongling, China) and confirmed as the dry matured seed of *Cuscuta australis* R. Br. or *Cuscuta chinensis* Lam. by Professor Liu Shoujin (Anhui University of Traditional Chinese Medicine). Previous studies have evaluated the quality of the characteristic profiles of S and YP (Supplementary Figures S3, S4).

Hydroxyurea tablets (Lot 1C0153D05) were purchased from Qilu Pharmaceutical Co., Ltd. (Jinan, China). Mifepristone tablets (Lot 05210302) were purchased from Jiulong Renwei Pharmaceutical Co., Ltd. (Wuhan, China). HY (Lot DJ0023-0020), AS (Lot DZ0001-0020), and KA (Lot DS0175-0005) were purchased from Chengdu Desite Biological Technology co., Ltd. (Chengdu, China), and three pure compounds were used as reference standards (purity ≥98%). Estradiol enzyme-linked immunosorbent assay (ELISA) kits were purchased from Shanghai Jianglai Biotechnology Co., Ltd. (Shanghai, China). Formic acid (R050195) was purchased from Sinopharm Chemical Reagent Co., Ltd. (Shanghai, China).

Pharmacodynamic study

YP and YP water extract preparation

YP preparation: 2 g salt was dissolved in 10 mL water, and 100 g SP was stirred with the salt solution. After the salt solution was thoroughly absorbed, they were poured into a frying pan and heated on a mild fire for 4 min. The drugs were then removed from the container for cooling. YP water extract preparation: the YP was soaked in water for 30 min. Next, it was decocted twice with boiling water (1:10 and 1:8), 30 min for each, and then filtered. The filtrate was combined and concentrated to 10.8 g/kg.

Establishment, grouping, and morphological observation of the RSA model

Female and male SPF SD rats (200–220 g) were purchased from SPF (Beijing) Biotechnology Co., Ltd., and the animal license number was SCXK (Beijing) 2019-0010. The experimental rats were given free food and water for a week of adaptive feeding. The animal experiment involved in this experiment was examined and approved by the Research Ethics Committee of Anhui University of Traditional Chinese Medicine, and the approval number was AHUCM-rats-2022097.

The female and male rats were mated (mating ratio 2: 1). Vaginal smears of female rats were examined daily in the early morning hours. The pregnancy rate of rats was 50%. Day 0 of pregnancy is defined by the presence of a large number of sperm on the vaginal smear or the dropping of a vaginal plug (Supplementary Figure S5). Finally, 30 pregnant rats were randomly categorized into five groups ($n = 6$): 5-day group, 7-day group, 9-day group, 10-day group, and 12-day group. Hydroxyurea combined with mifepristone by gavage was used to establish the RSA model. The groups were given hydroxyurea (450 mg/kg) daily in the morning, and the 10.8 g/kg water extract of YP was administered in the afternoon for the groups. The 12-day group was given mifepristone on day 11 at a dose of 3.75 mg/kg (Wang et al., 2021). After 24 h of mifepristone administration, serum, blood plasma, and tissue samples of the liver, heart, spleen, lung, kidney, and uterus were obtained from each group of rats after being anesthetized by intraperitoneal injection with pentobarbital (30 mg/kg). After anesthetizing the rats, the surrounding fat and other tissues were stripped, and the uterus and kidney were weighed. Plasma and tissues (liver, heart, spleen, lung, kidney, and uterus) taken at 5, 7, 9, 10, and 12 days were used for pharmacokinetic and tissue distribution studies, respectively.

Calculation of organ index

During the experiment, the behavior of the rats was observed daily, and their body weight was recorded. The organ index of the liver, heart, spleen, lungs, kidneys, and uterus was calculated using the following formula: organ index = organ weight (g)/body weight (g) × 100%.

Biochemical index detection

On days 5, 7, 9, 10, and 12 of pregnancy, rats were anesthetized by intraperitoneal injection of 20% Ultane, and blood was collected from the abdominal aorta. After 2 h at room temperature, the sample was centrifuged for 3,500 r/min at low temperature for 10 min, the upper serum was separated, and the levels of serum IL-4, TNF-α, P, E2, and other indexes were detected by ELISA.

Statistical analysis

The levels of serum progesterone (P), estradiol (E2), tumor necrosis factor-α (TNF-α), interleukin-4 (IL-4), rat chorionic gonadotropin (β-CG), and tryptophan (TRP) were measured and calculated according to the instructions of the kit. GraphPad Prism software (version 8.0, GraphPad Software, United States) was used to statistically analyze the experimental data. The data in the experiment were finally expressed as $\bar{x} \pm s$. Significance analysis was performed using the one-way analysis of variance (ANOVA) and was used for statistical comparison. In this experiment, $p < 0.05$ was regarded as the threshold of significance.

Pharmacokinetic study

YP and YP water extract preparation

The preparation method of YP and YP water extract was the same as that described in the part of "pharmacodynamic study/YP and YP water extract preparation" above.

Establishment, grouping, and morphological observation of the RSA model

The experiment of the establishment, grouping, and morphological observation of the RSA model was the same as that described in the part of "pharmacodynamic study" above.

Sample preparation

Rat tissue samples were homogenized with ice saline solution and centrifuged at 12,000 rpm for 15 min, and the supernatant was taken out.

In a 1.5-mL EP tube, 10 μL solution of IS was added to 100 μL of plasma samples, and 300 μL methanol was added to precipitate protein. The mixture was vortexed for 2 min and centrifuged at 12,000 rpm for 10 min at 4°C. The supernatant was transferred to a new EP tube and then dried under nitrogen at 35°C. The dried residue was re-dissolved with 100 μL methanol:water (50:50, v/v) solution. After being centrifuged at 12,000 rpm for 10 min at 4°C, a 10-μL aliquot of the supernatant was injected into LC–MS/MS for analysis.

Preparation of standards, calibration standards, and quality control samples

Appropriate amounts of KA, HY, and AS were accurately weighed and prepared with methanol with mass concentrations of 0.200 mg/mL, 0.200 mg/mL, and 0.204 mg/mL, respectively. Glipizide was dissolved in methanol and further diluted to 200 ng/mL to obtain the IS solution. Seven aliquots of 90 μL blank plasma were spiked with 10 μL of a mixed standard solution of KA, HY, and AS to yield calibration standards with concentrations in the range of 1–1,000 ng/mL KA, 1–1,000 ng/mL HY, and 1–1,000 ng/mL AS. Quality control (QC) samples were independently prepared in a similar manner to obtain three levels of samples: low, medium, and high concentrations for each analyte.

Chromatographic and mass spectrometry conditions

The chromatographic separation was performed on an ACQUITY UPLC®BEH C18 (2.1 × 100 mm, 1.7 μm) with the column temperature maintained at 35°C. Mobile phase A consisted of methanol and mobile phase B consisted of 0.1% formic acid. The flow rate was 0.3 mL/min, and the injection volume was 5 μL. The gradient elution procedure was as follows: 0–5 min, 45 %–80%A; 5–5.5 min, 80%–45%A; 5.5–6.0 min, 45%A.

For mass spectrometry conditions, the analyte and IS were ionized in the ESI negative ion mode. The ion source temperature was 500°C, the ion spray voltage was −4,500 V, Gas1 was 50 psi, Gas2 was 50 psi, and the MRM mode for quantification of KA was m/z 461.0→284.7. The MRM mode for quantification of HY was m/z 463.2→300.0. The MRM mode for quantification of AS was m/z 447.1→283.9. The MRM mode for quantification of IS was m/z 444.1→319.0 (Figure 1).

Method validation

Selectivity validation

Blank plasma and kidney samples were collected for selectivity validation, and the blank samples were mixed with KA, AS, HY, and IS solutions for further testing. Rat plasma and kidney tissues 2 h after continued dosing of YP on the fifth day were collected to determine the KA, AS, and HY. All samples were processed according to the methods described in the part of "sample preparation."

Linearity validation

The linearity of the standard curve was determined by plotting the peak area ratio (KA, AS, and HY/IS, *y*-axis) versus their concentration (*x*-axis) in plasma using a weighted linear least-squares regression model ($1/x^2$). The samples were processed according to the methods described in the part of "sample preparation."

Lower limit of quantitation validation

The lower limit of quantitation (LLOQ) was defined as the lowest concentration of three analytes that were precisely added to the blank plasma for detection. The samples were handled in the same manner as described in the part of "sample preparation." The relative standard deviations (RSDs) of the concentrations of the three analytes in the samples were calculated.

Accuracy and precision validation

The intra-day and inter-day precision and accuracy of the three analytes in the rat plasma, liver, heart, spleen, lung, kidney, and uterus tissues were obtained by analyzing the low and high concentration QC samples in six replicates on day one and three consecutive days, respectively.

Extraction recovery and matrix effect validation

The extraction recovery of KA, AS, and HY was evaluated at low, middle, and high concentration levels by comparing the peak areas of the two analytes in the blank plasma-spiked samples with those of the post-extraction spiked samples. The matrix effect was measured at three concentration levels by comparing the peak areas of the analytes from the post-extraction spiked blank samples to those of the aliquots of methanol spiked with the same standard.

Stability validation

The stability of the analytes in the rat plasma, liver, heart, spleen, lung, kidney, and uterus tissues, including short-term and freeze–thaw stability, was evaluated at low and high concentration levels in six replicates under diverse conditions: 12 h at room temperature (short-term stability), 4 weeks at −20°C (long-term stability), and after three freeze–thaw cycles (freeze–thaw stability).

Statistical analysis

Data regarding KA, AS, and HY from plasma concentration–time curves were evaluated using DAS 2.0 software (Mathematical Pharmacology Professional Committee of China, Shanghai, China). Pharmacokinetic parameters were analyzed using SPSS 21.0 software.

Tissue distribution study

A study was conducted to study the distribution of KA, AS, and HY in the liver, heart, spleen, lung, kidney, and uterus tissues. The grouping, administration, and tissue sampling of rats were the same as previously mentioned in part of "pharmacokinetic study/establishment, grouping, and morphological observation of RSA model."

Gray relationship analysis of pharmacodynamics and pharmacokinetics

Gray correlation analysis (GCA) was performed using the data processing system SPSS software (version 23.0, IBM, United States) to establish the pharmacodynamics and pharmacokinetics relationship, that is, the relationship between the components and efficacy.

Results

The therapeutic effect of YP on RSA rats

Assessments of body weight and organ index

To explore the therapeutic effect of YP on RSA, we treated RSA rats with YP decoction at doses of 10.8 g/kg for 12 days. There was a slow increase in the body weight of pregnant rats in the 5-, 7-, 9-, 10-, and 12-day groups, and the body weight of rats in the 7-day group was significantly higher than that of rats in the first day of the gestation group ($p < 0.01$). The gradual increase in uterine

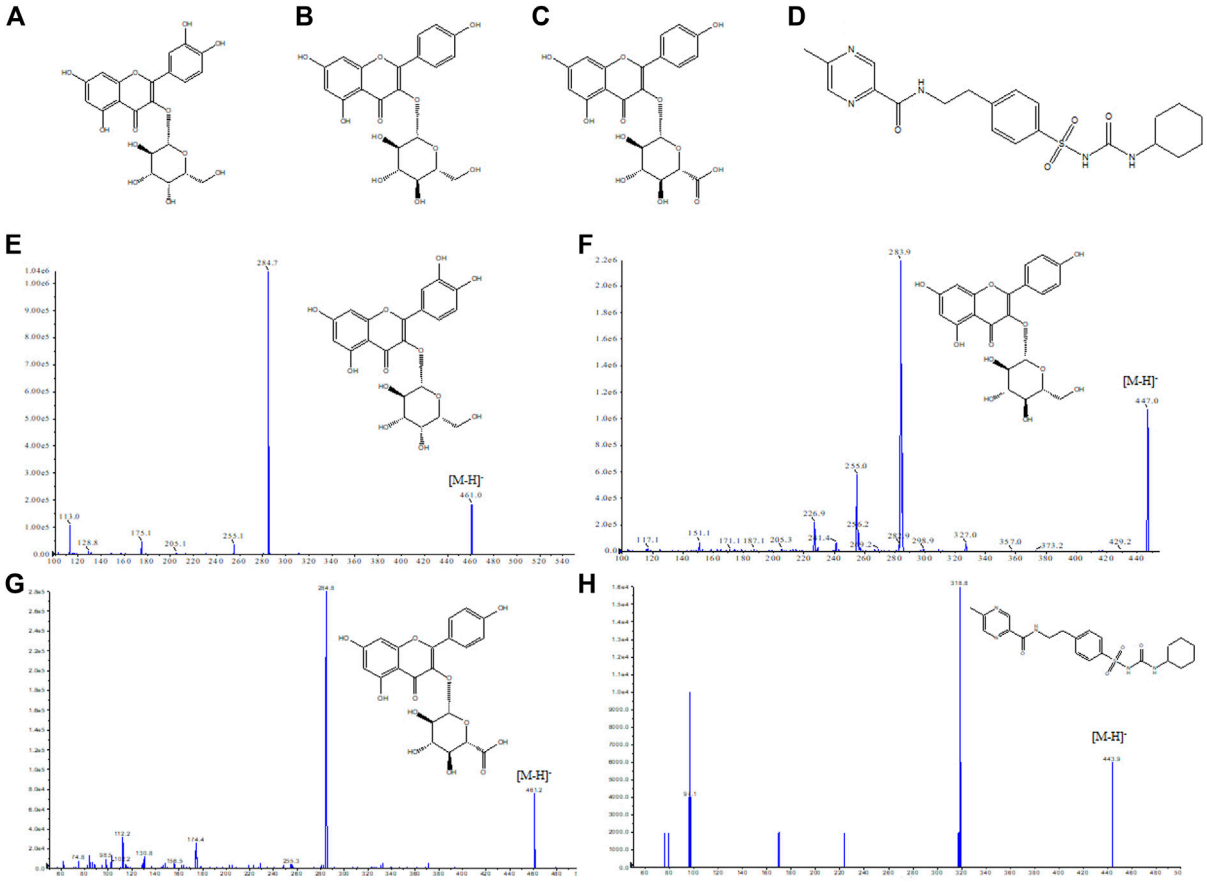

FIGURE 1
Chemical structure of three compounds and mass spectrum of each component to be detected and the internal standard compound. **(A)** Hyperin, **(B)** astragalin, **(C)** kaempferol-3-O-β-D-glucuronide, and **(D)** glipizide. **(E)** Mass Spectrometry of Hyperin, **(F)** Mass Spectrometry of astragalin, **(G)** Mass Spectrometry of kaempferol-3-O-β-D-glucuronide, **(H)** Mass Spectrometry of glipizide.

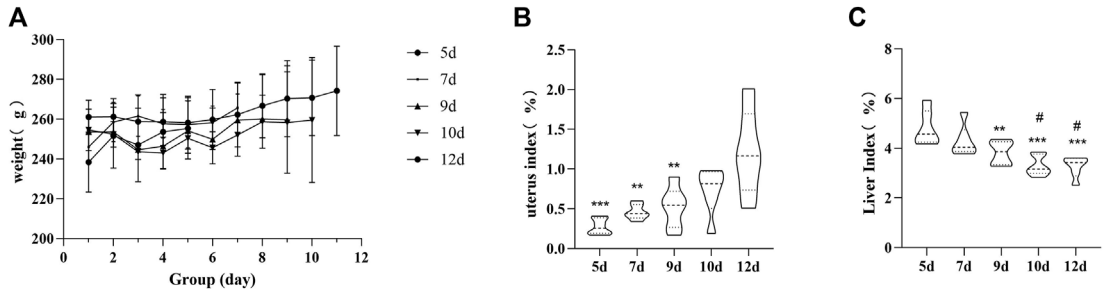

FIGURE 2
Rat body weight **(A)**, changes of uterine coefficient **(B)**, and changes of liver coefficient **(C)**. Uterus: comparison of 12-day group, $^{\#\#}p < 0.05$, $^{\triangle\triangle}p < 0.05$, $^{***}p < 0.001$.

coefficients and decrease in liver coefficients during the side modeling and administration of the drug suggest that YP has a protective effect on the fetus (Figures 2A–C).

Effects of YP on serum biochemical indicators

The results of biochemical indicators showed that compared with the 5-day group, the serum concentrations of E2, P, β-HCG, IL-4, and TRP in the 10-day group increased significantly, whereas the concentration of TNF-α decreased significantly. These results showed that YP may cause improvement in rats with RSA by regulating E2, P, β-HCG, TRP, IL-4, and TNF-α. Compared with the 10-day group, the serum concentrations of E2, P, β-HCG, and TRP in the 12-day group decreased significantly, whereas the concentration of IL-4 and TNF-α increased significantly. This shows that the establishment of RSA is successful (Figures 3A–F).

10.3389/fphar.2024.1440810

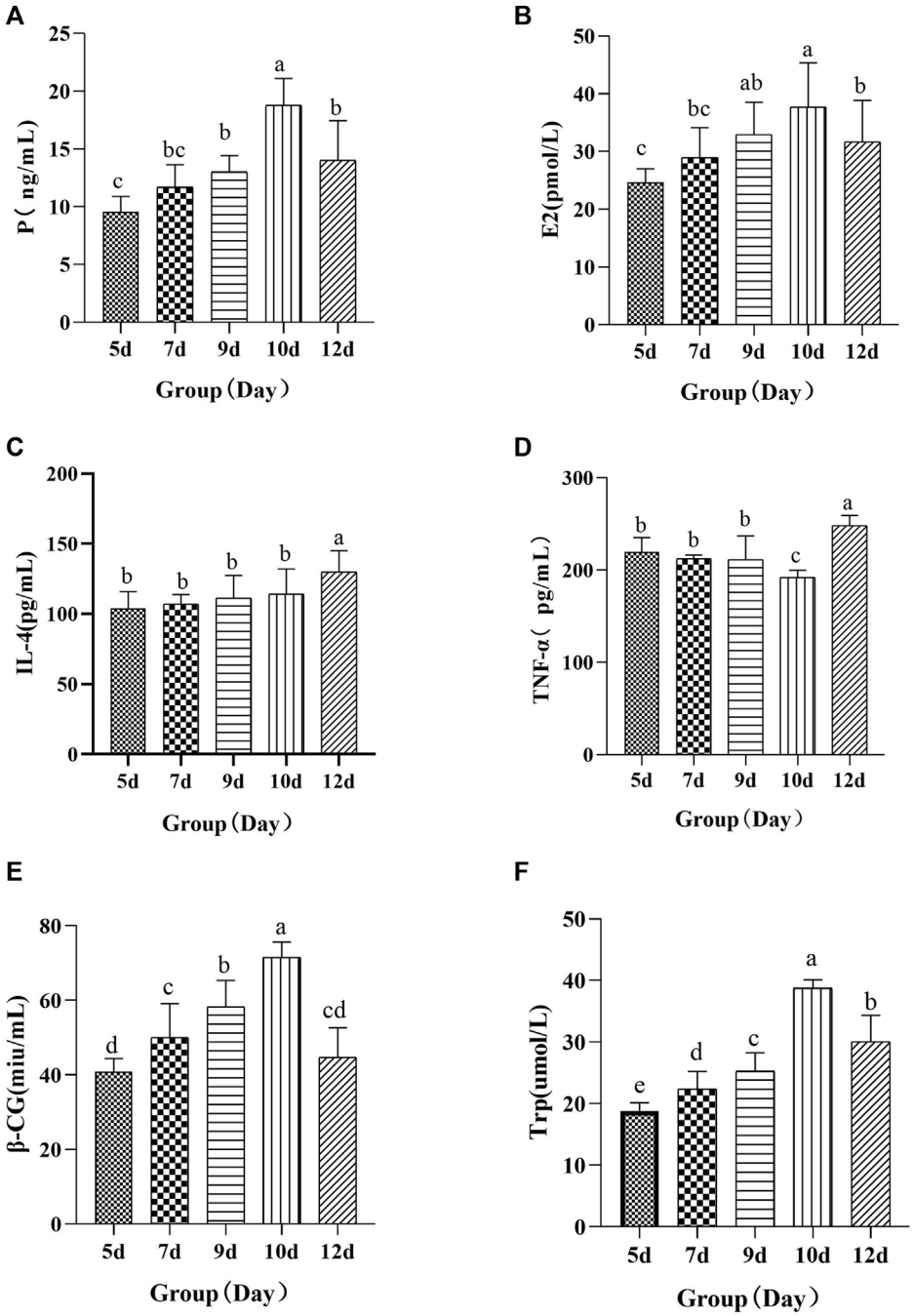

FIGURE 3
Changes of serum P **(A)**, E2 **(B)**, IL-4 **(C)**, TNF-α **(D)**, β-HCG **(E)**, and TRP **(F)**. Different letters in the figure indicate significant differences among the samples ($p < 0.05$).

Pharmacokinetic study

Optimization of UHPLC-MS/MS

To obtain appropriate retention times, good separability, and symmetrical peak shapes, 0.1% formic acid aqueous solution (methanol) was chosen as a suitable mobile phase. According to the comprehensive consideration of the matrix effect and determination efficiency, the final optimized gradient elution program was as follows: 0–5 min, 45%–80% methanol; 5–5.5 min, 80%–45% methanol; 5.5–6.0 min, 45% methanol.

To optimize the MS spectra, the positive and negative ion modes of the first-order mass spectrometry of the analytes and IS solutions were investigated. It was found that the MS detection of HY, AS, and KA was sensitive in the negative ion mode, whereas IS responded in both the positive and negative ion modes. Therefore, the negative ion mode was selected for the determination, and the optimized MS parameters to achieve maximum responses are summarized in Table 1.

TABLE 1 Mass spectrometry conditions of three components and the internal standard.

Compound	Parent ion (m/z)	Daughter ion (m/z)	DP/V	CE/V	ESI
Kaempferol-3-O-β-D-glucuronide	461.00	284.80	−102.7	−27.93	—
Hyperin	463.20	299.60	−118.86	−36.13	—
Astragalin	447.10	283.80	−102.90	−34.07	—
Glipizide	444.10	319.00	−113.25	−27.12	—

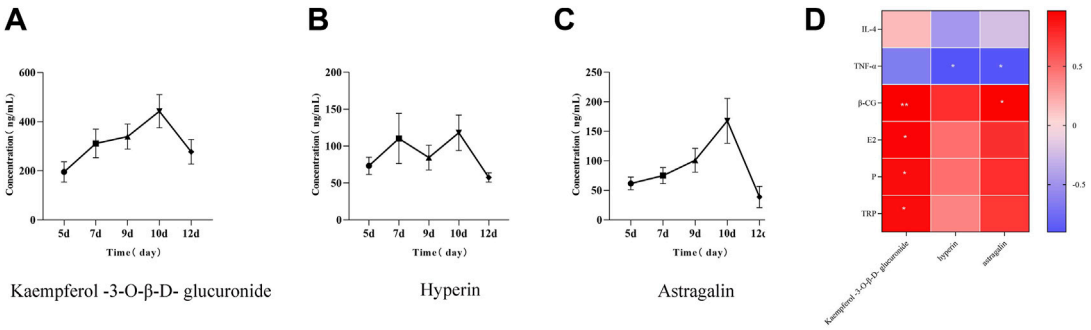

FIGURE 4
In vivo process and correlation analysis of three components in YP. **(A)** Blood concentration–time curve of KA, **(B)** blood concentration–time curve of HY, **(C)** blood concentration–time curve of AS, and **(D)** thermogram of correlation coefficient between blood components and pharmacodynamic indexes of YP.

Method validation

Specificity

The retention times of HY, AS, KA, and IS are shown in Figure 4. The chromatograms of the three analytes and IS in the blank plasma, blank plasma spiked with the analytes and IS, and plasma samples collected after oral administration of YP for 5 days 2 h were compared. The same sample treatments and comparisons were performed for kidney tissues. The results showed symmetric peaks of the analytes and IS with no endogenous substance interferences, stable baselines, and high specificity (Supplementary Figure S6).

Linearity and LLOQ

The standard curve and linear regression equation of the analytes that were established by detection of the plasma and kidney samples containing various concentrations of HY, AS, KA. HY, AS, KA, exhibited good linearity, with correlation coefficients (R^2) ≥ 0.99. The LLOQs of naringin and paeoniflorin are listed in Supplementary Table S1. The results showed that the method was suitable for the quantitative analysis of the two analytes and met the pharmacokinetic requirements.

Accuracy and precision

The results showed that the intra- and inter-day precisions of the three analytes were within 14.72%, and the accuracy ranged from −14.38% to 14.32% (Supplementary Table S2). All analysis values were within the accepted criteria, proving that the method was accurate and reliable for the target analytes.

Extraction recovery and matrix effect

The recovery of the analytes was greater than 90.87%, and the matrix effects were between 91.84% and 107.21%. The above results showed that the analysis of the three analytes in the plasma and kidney tissue had no obvious matrix effect (Supplementary Table S3).

Stability

The short-term stability and freeze–thaw stability of the analytes in the plasma and kidney tissue were evaluated and are shown in Supplementary Table S4. The results displayed RSD values less than 14.04%, indicating that the biological samples were stable during these stability tests.

Pharmacokinetic evaluation

The validated LC–MS/MS method was successfully applied to the pharmacokinetic study of HY, AS, and KA in rat plasma after oral administration of the YP decoction. As depicted in Figure 4, double peaks appeared in the concentration–time curve of HY in RSA rats administered YP. The first peak concentration of HY appeared at 7 days, and the second peak concentration appeared at 10 days. In addition, the second peak concentration was much higher than the first one. Compared with the other two compounds, the area under the curve of KA is the largest (Figures 4A–C).

Tissue distribution of the analytes in rat tissues

The tissue distribution of AS was extensive in rats, and they were examined in the liver, heart, spleen, lung, kidney, and womb tissues (Figures 5A–C). AS was detected in the heart tissue on the 7th day. The concentration of AS reached the maximum on the 9th day in womb tissue, and that of other tissues reached the maximum on the

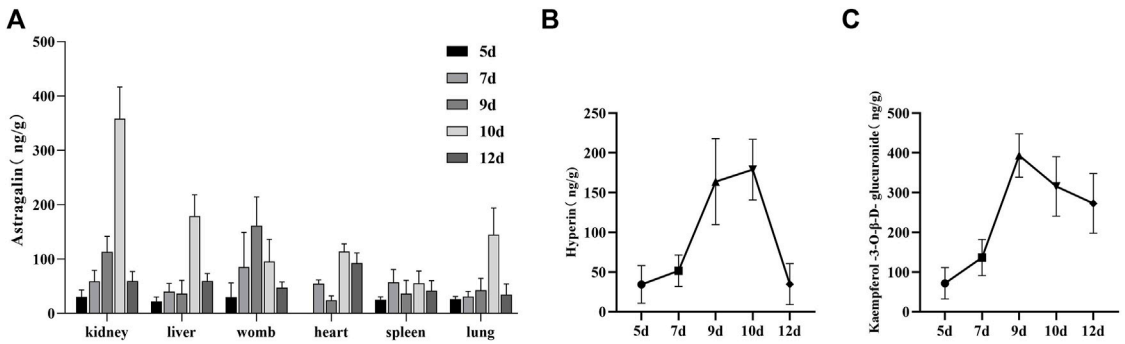

FIGURE 5
(A) Tissue distribution characteristics of AS, **(B)** tissue distribution characteristics of KA, and **(C)** tissue distribution characteristics of HY.

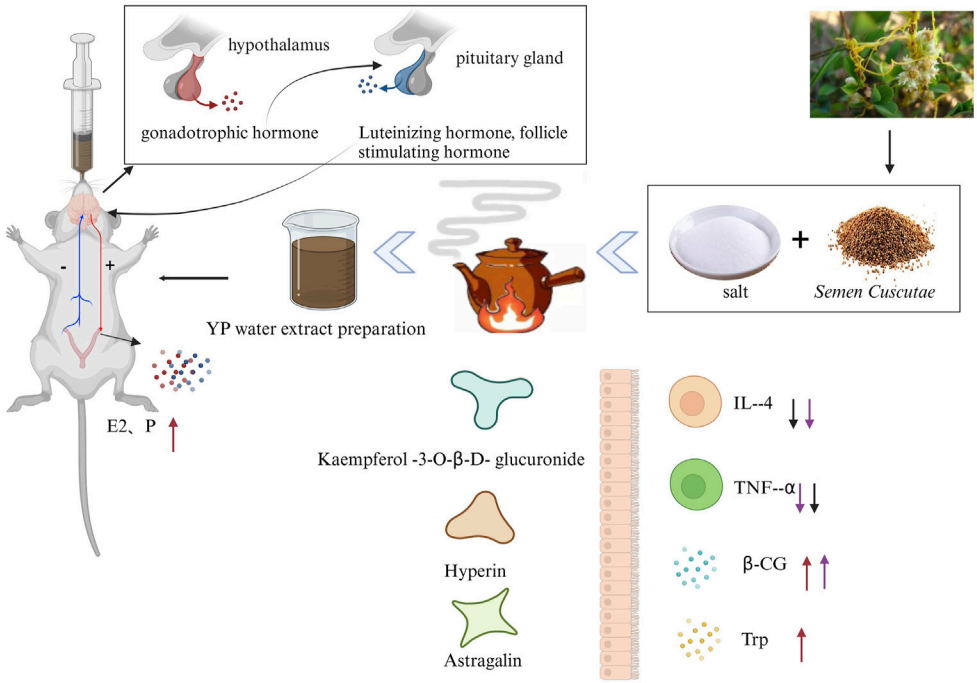

"+"Represents positive feedback regulation, "-"Represents negative feedback regulation; Purple arrow represents astragaloside, brown arrow represents kaempferol -3-O-β-D- glucuronide, and black arrow represents hyperoside.

FIGURE 6
Mechanism of *Semen Cuscutae* salted on recurrent spontaneous abortion.

10th day. Compared with the 10-day group, the concentration of AS in the liver, heart, lung, and uterus decreased rapidly in the 12-day group. HY was only detected in the womb, and the concentration reached the peak on the 10th day and decreased rapidly on the 12th day. KA was only detected in renal tissue, reaching the peak on the 9th day, and still having a high concentration on the 12th day.

Correlation analysis

To further confirm whether YP can alleviate recurrent abortion induced by gavage of hydroxyurea combined with mifepristone by regulating serum biochemical indexes, the correlation between flavonoids and serum biochemical indexes was analyzed (Figure 4D). There was a significant positive correlation among KA, E2, and β-HCG ($p < 0.05$). However, AS and HY were negatively correlated with TNF-α ($p < 0.05$), and AS was positively correlated with β-HCG ($p < 0.05$). The mechanism of this study can be seen in Figure 6.

Discussion

RSA is a complex disease caused by a variety of pathogenic factors. It is the most common complication of human pregnancy,

with a high prevalence of approximately 10%–15% (Li et al., 2021a; Li et al., 2021b). β-HCG, P, and E2 can respond to embryonic development (Mi et al., 2021; Chen, 2018; Xiang, 2018). Other studies have shown that there is also a strong association between Th1/Th2 cytokines and the development of RSA. In this study, pregnant rats in the 5-, 7-, 9-, and 10-day groups all showed the following symptoms: rats curled up and hugged, dry and dull hair, thinning, weight loss, and sticky and loose stools in the anus. In addition, the longer it goes on, the more pronounced the symptoms become. After the abortifacient was given, there was bruising in the uterus after autopsy in the group on day 12, indicating the success of the RSA model. Studies have shown that when miscarriage occurs, maternal expression of Th1-type cytokines such as TNF-α is elevated, whereas the expression of Th2-type cytokines such as IL-4 was downregulated. This dysregulation of the immune homeostasis mediated by Th1- and Th2-type cytokines is one of the mechanisms leading to the occurrence of miscarriage (Kolanko et al., 2019). In the present study, we found an overall decreasing trend in Th1 type of inflammatory factor, which was elevated by the administration of the abortifacient. Meanwhile, Th2-type inflammatory factors were generally elevated. This suggests that YP can effectively regulate the levels of pregnancy hormones and Th1/Th2 cytokines in RSA. It corrects immune dysfunction, reduces miscarriage rates, and improves pregnancy outcomes. At the same time, P, E2, β-HCG, and TRP tended to increase with the duration of gestation and decreased with the administration of mifepristone. It has been found that β-HCG is secreted and produced by syncytiotrophoblast cells of the chorionic villi. The level of β-HCG increased exponentially in the first trimester of pregnancy, and then it decreased rapidly. Its main function is to stimulate the corpus luteum of pregnancy and secrete P and E2, which is beneficial for embryo development (Zhou, 2019), which is mutually confirmed by the results of this study. Tissue distribution experiments showed that AS could be detected in the heart, liver, spleen, lung, kidney, and uterus, indicating that AS could be widely distributed and metabolized in rats. Especially in the liver and kidney tissues, the concentration is higher, indicating that the kidney, liver, and uterus are the core target organs of the active ingredients of YP distribution. It also shows that YP can improve the distribution, absorption, and metabolism of KA in the body and promote its absorption in the kidney tissue, which is consistent with the traditional theory of "salt into the kidney channel," while YP into the liver and kidney channel.

Transforming growth factor-β1 (TGF-β1) has been reported to be a secreted protein. It can induce inflammation in intrauterine adhesions (IUA) by enhancing the expression of pro-inflammatory factors such as TNF-α and IL-6 (Ai et al., 2020). HY has been shown to have anti-inflammatory pharmacological effects. In addition, as a main ingredient in Shou Zi Wan, it is widely used in the treatment of unexplained RSA. It is hypothesized that HY is closely related to uterine function, which coincides with the detection of chrysin in the uterus. Another study showed that kaempferol improves the doxorubicin-induced renal structure and function in rats by attenuating impairments in urine output, albumin/creatinine excretion, and creatinine clearance. It can also exert a nephroprotective effect by activating and upregulating SIRT 1, which in turn activates Nrf 2 and inhibits NF-κB p65 (Alagal et al., 2022). It can be hypothesized that KA has a close association with the kidneys, and therefore, this component can be detected in renal tissues.

In this study, we combined the results of gray correlation and Pearson correlation analyses to hypothesize that kaempferol, KA, AS, and HY may be the active ingredients of SP for the treatment of RSA. By reviewing the literature, the author found that kaempferol is an important flavonoid compound in S. It can promote primordial follicle activation and cell proliferation by regulating the PI3K/AKT signaling pathway. It also has the effect of promoting the diastolic effect of rat uterine smooth muscle (Santos et al., 2019). It provides theoretical support for the development of this ingredient for use in abortion-improving drugs. AS can upregulate the expression of ATP-binding transporter proteins A1 and G1 in macrophages. It promotes cholesterol efflux, inhibits inflammatory responses, and significantly reduces the secretion of inflammatory factors such as TNF-α and IL-6 (Zhao et al., 2021). HY inhibits macrophage chemotaxis, activates macrophages, and promotes macrophage differentiation from pro-inflammatory M1 subtype to anti-inflammatory M2 subtype. This mechanism is thought to be mediated by the direct regulation of NR4A1 by chrysosplenetin (Sun et al., 2021). Kaempferol has a significant inhibitory effect on COX1 and COX2. Once the cyclooxygenase pathway is activated, the membranes of the phospholipids rupture, resulting in the production of arachidonic acid, which is further converted via cyclooxygenase to prostaglandin analogs, causing inflammation. Thus, KA may prevent inflammation by inhibiting the cyclooxygenase pathway and thereby preventing inflammation. This is in keeping with the gray correlation results of this study, where all three active ingredients had a strong relationship with inflammatory factors. In addition, in angiogenesis mechanism studies, molecular docking results showed that kaempferol binds well to the target. Kaempferol promotes angiogenesis by reducing the reactive oxygen species (ROS) metabolism through the inhibition of the NF-κB pathway and upregulation of related transcriptional pathways (Imran et al., 2019). KA, HY, and AS are highly correlated with the estrogenic effects of total flavonoids from SS (Yue et al., 2023). This corroborates with the results of the present study. The results of this study provide data support and theoretical backing for further investigation of the efficacy and mechanism of these three components in the treatment of RSA.

It is innovative and feasible to investigate the molecular mechanisms of the three active components of *Semen Cuscutae*. In the future, mass spectrometry imaging technology will be used to pinpoint the target of action of KA, AS, HY, and proteomics, transteomics, transgenics, and other components of *Semen Cuscutae*. Furthermore, metabolomics will be used to study the three active ingredients from a multi-omics perspective. Relevant pathway proteins can be characterised through Western Blot experiment, and cellular experiment can be performed for the verification of the mechanism to explore the potential molecular mechanisms of the three active components of *Semen Cuscutae* to improve recurrent miscarriage using multi-omics technology.

Conclusion

In conclusion, this paper mainly uses the correlation model of "body composition–efficacy index", and we initially investigated the pharmacodynamics, pharmacokinetics and tissue distribution of HY, AS and KA in YP in the treatment of RSA. This research will help to further enrich the scientific connotation of the theory of the role of Chinese medicine processing excipients, and it has

important guiding significance for the improvement of Chinese medicine quality standards and processing technology.

Data availability statement

The original contributions presented in the study are included in the article/Supplementary Material; further inquiries can be directed to the corresponding author.

Ethics statement

The animal studies were approved by the Research Ethics Committee of Anhui University of Traditional Chinese Medicine. The studies were conducted in accordance with the local legislation and institutional requirements. Written informed consent was obtained from the owners for the participation of their animals in this study.

Author contributions

ZY: data curation, methodology, and writing–original draft. KC: writing–original draft and data curation. YZ: writing–original draft and data curation. BX: resources, software, and writing–review and editing. YH: resources, software, and writing–review and editing. XZ: data curation and writing–review and editing. ZL: data curation and writing–review and editing. TW: data curation, methodology, writing–review and editing. DW: data curation, methodology, and writing–review and editing. TP: supervision, validation, and writing–review and editing. TL: supervision, validation, and writing–review and editing. HC: data curation, formal analysis, and writing–review and editing. XW: funding acquisition and writing–review and editing.

Funding

The author(s) declare that financial support was received for the research, authorship, and/or publication of this article. This work was supported by National Key R&D Program Projects (2023YFC3504200), National Natural Science Foundation of China (NSFC) (No. 82204623), the Youth Science and Technology talents Cultivation Project of Anhui University of Chinese Medicine (No. 2021qnyc04), the Key Projects of Scientific Research in Universities of Anhui Province (2022AH050471), and the Scientific Research Team Program of Anhui Colleges and Universities (Grant no. 2022AH010036).

Conflict of interest

The authors declare that the research was conducted in the absence of any commercial or financial relationships that could be construed as a potential conflict of interest.

Publisher's note

All claims expressed in this article are solely those of the authors and do not necessarily represent those of their affiliated organizations, or those of the publisher, the editors, and the reviewers. Any product that may be evaluated in this article, or claim that may be made by its manufacturer, is not guaranteed or endorsed by the publisher.

Supplementary material

The Supplementary Material for this article can be found online at: https://www.frontiersin.org/articles/10.3389/fphar.2024.1440810/full#supplementary-material

SUPPLEMENTARY FIGURE S1
Network diagram of high-frequency drug association rules.

SUPPLEMENTARY FIGURE S2
Frequency of use of common herbs for the treatment of slippery fetus and fetal movement.

SUPPLEMENTARY FIGURE S3
HPLC characterization of 20 batches of *Semen Cuscutae* and salt-processed *Semen Cuscutae* tablets.

SUPPLEMENTARY FIGURE S4
Control characteristic profiles and HPLC plots of *Semen Cuscutae*, salt-processed *Semen Cuscutae*, and mixed controls.

SUPPLEMENTARY FIGURE S5
Micrograph of rat vaginal smear **(A)**: diestrus vaginal smear **(B)**: estrus vaginal smear (a large number of keratinised cells) **(C)**: diestrus vaginal smear (a small amount of keratinised cells) **(D)**, rat vaginal sperm smear. keratinised cells) **(C)**: diestrus vaginal smear (a small amount of keratinised cells) **(D)**, rat vaginal sperm smear.

SUPPLEMENTARY FIGURE S6
Typical chromatogram of index components and internal standard in the plasma and tissues of recurrent spontaneous abortion rat model. **(A)**: blank plasma; **(B)**: blank plasma+ astragaloside; **(C)**: blank plasma+ hyperoside; **(D)**: blank plasma+ kaempferol -3-O-β-D glucuronide; **(E)**: blank plasma+ internal standard; **(F)**: administration of plasma (astragaloside); **(G)**: administration of plasma (hyperin); **(H)**: administration of plasma (kaempferol -3-O-β-D -glucuronide); **(I)**: administration of plasma (internal standard); **(J)**: blank organization; **(K)**: blank tissue+ astragaloside; **(L)**: blank tissue+ hyperoside; **(M)**: blank tissue+ kaempferol-3-O-β-D-glucuronide; **(N)**: blank organization+ internal standard; **(O)**: administration organization (astragaloside); **(P)**: administration tissue (hyperin); **(Q)**: administration tissue (kaempferol-3-O-β-D-glucuronide); **(R)**: administration organization (internal standard).

References

Ai, Y., Chen, M., Liu, J., Ren, L., Yan, X., and Feng, Y. (2020). lncRNA TUG1 promotes endometrial fibrosis and inflammation by sponging miR-590-5p to regulate Fasl in intrauterine adhesions. *Int. Immunopharmacol.* 86, 106703. doi:10.1016/j.intimp.2020.106703

Alagal, R. I., Alfaris, N. A., Alshammari, G. M., Altamimi, J. Z., Almousa, L. A., and Yahya, M. A. (2022). Kaempferol attenuates doxorubicin-mediated nephropathy in rats by activating sirt1 signaling. *J. Funct. Foods* 89, 104918. doi:10.1016/j.jff.2021.104918

Chen, R. X. (2018). The value of serum E2, progesterone and β-hCG levels in early pregnancy in pregnant women with preeclamptic miscarriage in predicting pregnancy outcome. *Maternal Child Health China.* 33, 1371–1373.

Deng, T. Q., Liao, X. Y., and Zhu, S. M. (2022). Recent advances in treatment of recurrent spontaneous abortion. *Obstet. Gynecol. Surv.* 77 (6), 355–366. doi:10.1097/OGX.0000000000001033

Huang, Y., Yu, H. Y., Xiong, J. W., Ding, X. M., Xu, B. Y., Liu, L. N., et al. (2022). Chemical profiling of raw product of Semen Cuscuta and stir-baking Semen Cuscuta with salt solution based on UHPLC-Q/TOF-MS combined multivariate statistical analysis. *Chin. J. New Drugs* 31 (15).

Imran, M., Salehi, B., Sharifi-Rad, J., Aslam Gondal, T., Saeed, F., Imran, A., et al. (2019). Kaempferol: a key emphasis to its anticancer potential. *Molecules* 24, 2277. doi:10.3390/molecules24122277

Kolanko, E., Kopaczka, K., Koryciak-Komarska, H., Czech, E., Szmytkowska, P., Gramignoli, R., et al. (2019). Increased immunomodulatory capacity of human amniotic cells after activation by pro-inflammatory chemokines. *Eur. J. Pharmacol.* 859, 172545. doi:10.1016/j.ejphar.2019.172545

La, X. L., Wang, W. J., Zhang, M., and Liang, L. (2021). Definition and multiple factors of recurrent spontaneous abortion. *Adv. Exp. Med. Biol.* 1300, 231–257. doi:10.1007/978-981-33-4187-6_11

Li, D., Zheng, L., Zhao, D., Xu, Y., and Wang, Y. (2021a). The role of immune cells in recurrent spontaneous abortion. *Reprod. Sci.* 28 (12), 3303–3315. doi:10.1007/s43032-021-00599-y

Li, J., Feng, D., He, S., Wu, Q., Su, Z., and Ye, H. (2021b). Meta-analysis: association of homocysteine with recurrent spontaneous abortion. *Women Health* 61, 713–720. doi:10.1080/03630242.2021.1957747

Liu, Y., Liu, Y., Ding, W., and Wang, X. L. (2021). Advances in research of pharmacologic action of Cuscuta chinensis tonifying the kidney. *J. Yichun Univ.* 43 (09), 22–25.

Mi, Y. R., Li, X. Q., You, J. P., and Zhe, N. (2021). Effect of solidifying and stabilizing fetal soup combined with progesterone on serum sex hormones and MCP-1 and IL-1β levels in patients with preeclampsia. *New Chin. Med. Clin. Pharmacol.* 32, 123–127.

Santos, J. M. S., Monte, A. P. O., Lins, T. L. B. G., Barberino, R. S., Menezes, V. G., Gouveia, B. B., et al. (2019). Kaempferol can be used as the single antioxidant in the *in vitro* culture medium, stimulating sheep secondary follicle development through the phosphatidylinositol 3-kinase signaling pathway. *Theriogenology* 136, 86–94. doi:10.1016/j.theriogenology.2019.06.036

Su, L. L., Tong, H. J., Zhang, J. B., Hao, M., Fei, C. H., Ji, D., et al. (2022). Revealing the mechanism of raw and vinegar-processed Curcuma aromatica Salisb. [Zingiberaceae] regulates primary dysmenorrhea in rats via integrated metabolomics. *Front. Pharmacol.* 13, 926291. doi:10.3389/fphar.2022.926291

Sun, K., Luo, J., Jing, X., Xiang, W., Guo, J., Yao, X., et al. (2021). Hyperoside ameliorates the progression of osteoarthritis: an *in vitro* and *in vivo* study. *Phytomedicine* 80, 153387. doi:10.1016/j.phymed.2020.153387

Wang, X. L., Gao, H. Y., Tan, S., Xu, C., Xu, F. Q., Wang, T. S., et al. (2021). An integrated approach to uncover quality markers of stir-baking Semen Cuscuta with salt solution preventing recurrent spontaneous abortion based on chemical and metabolomic profiling. *J. Chromatogr. B Anal. Technol. Biomed. Life Sci.* 1177, 122727. doi:10.1016/j.jchromb.2021.122727

Wang, X. L., Jiang, Y., Fan, L. L., Wu, D. L., Han, Y. Q., and Jin, C. S. (2020). Modern research on theory of "salt-processing enhancing drug into kidney meridian" proposed by healer Jia-mo Chen from Xinan. *Chin. Tradit. Herb. Drugs* 51 (05), 1336–1342.

Xiang, H. (2018). Clinical significance of β-hCG, PROG, E2 and CA125 in patients with preeclampsia. *China Maternal Child Health* 33, 2546–2549.

Xu, B. Y., Ding, X. M., Jin, C. S., Wu, D. L., Peng, T. Y., and Wang, X. L. (2023a). Chromatogram of Chinese dodder seed unprocessedor processed with salt solutionon high-performance liquid chromatography and content determination of five main component. *J. Anhuiuniv Chin. Med.* 42 (02), 95–100.

Xu, B. Y., Yang, Z. T., Zhang, X., Liu, Z. L., Huang, Y., Ding, X. M., et al. (2023b). 16S rDNA Sequencing combined with metabolomics profiling with multi-index scoring method reveals the mechanism of salt-processed Semen Cuscuta in Bushen Antai mixture on kidney yang deficiency syndrome. *J. Chromatogr. B Anal. Technol. Biomed. Life Sci.* 1216, 123602. doi:10.1016/j.jchromb.2023.123602

Xu, Y. J., Ren, X. L., and Zeng, Q. (2023c). Experience in treating fetal leakage and fetal movement of spleen and kidney weakness of traditional Chinese medicine. *Chin. J. Ethnomed Ethnopharm* 32 (15), 89–92+100.

Yue, X., Song, H., Xu, Y., Liu, D. S., Sun, X. M., and Li, W. L. (2023). Screening of active ingredients for estrogenic effects in total flavonoids of Cuscuta chinensis. *Chin. Pharm.* 34, 569–574.

Zhang, X., Huang, Y., Yang, Z. T., Xu, B., Liu, Z. L., Ding, X. M., et al. (2024). Exploring the mechanism of Semen Cuscutae processed with salt solution in improving kidney deficiency miscarriage based on serum pharmacochemistry and network pharmacology. *Arabian J. Chem.* 17 (2024), 105456. doi:10.1016/j.arabjc.2023.105456

Zhao, Z. W., Zhang, M., Wang, G., Zou, J., Gao, J. H., Zhou, L., et al. (2021). Astragalin retards atherosclerosis by promoting cholesterol efflux and inhibiting the inflammatory response via upregulating ABCA1 and ABCG1 expression in macrophages. *J. Cardiovasc Pharmacol.* 77, 217–227. doi:10.1097/FJC.0000000000000944

Zhou, S. M. (2019). Study on the prognostic value of serum CA125, HCG and progesterone in predicting early preeclampsia. *Chin. J. Mod. Med.* 21, 84–85.

frontiers | Frontiers in Pharmacology

TYPE Original Research
PUBLISHED 11 November 2024
DOI 10.3389/fphar.2024.1425794

OPEN ACCESS

EDITED BY
José Carlos Tavares Carvalho,
Universidade Federal do Amapá, Brazil

REVIEWED BY
Bo Zhang,
Tsinghua University, China
Jinming Zhang,
Chengdu University of Traditional Chinese Medicine, China
Jiang Hai,
Heilongjiang University of Chinese Medicine, China

*CORRESPONDENCE
Ming Yang,
yangming16@126.com

RECEIVED 30 April 2024
ACCEPTED 02 September 2024
PUBLISHED 11 November 2024

CITATION
Qiu Y, Wang N, Yu Z, Guo X and Yang M (2024) Changes in the chemical composition and medicinal effects of black ginseng during processing.
Front. Pharmacol. 15:1425794.
doi: 10.3389/fphar.2024.1425794

Changes in the chemical composition and medicinal effects of black ginseng during processing

Ye Qiu[1,2,3], Nengyuan Wang[3], Zhe Yu[3], Xiao Guo[4] and Ming Yang[1,2]*

[1]Jiangxi University of Chinese Medicine, Nanchang, Jiangxi, China, [2]National Pharmaceutical Engineering Centre for Solid Preparation in Chinese Herbal Medicine, Nanchang, Jiangxi, China, [3]Department of Traditional Chinese Medicine, College of Pharmacy, Changchun University of Chinese Medicine, Changchun, China, [4]Jilin Cancer Hospital, Changchun, China

Aim of the Study: To study the changes in the chemical composition and medicinal effects of black ginseng during processing.

Materials and Methods: The contents of ginsenosides Rg1, Re, Rh1, Rb1, 20-(S)-Rg3, 20-(R)-Rg3, and Rg5 were determined using high-performance liquid chromatography (HPLC), and the percentage of rare saponins was calculated. Furthermore, changes in the contents of reducing sugars and amino acids (i.e., Maillard reaction (MR) substrates) were measured to assess the relationship between processing and the MR. Compounds were identified using HPLC-MS and their cleavage patterns were analyzed. Gene co-expression network bioinformatics techniques were applied to identify the pharmacological mechanism of black ginseng.

Results: The changes in the physicochemical characteristics of black ginseng during processing were determined based on the MR. Rare saponins accumulated during black ginseng processing. In addition, reducing sugars were produced through polysaccharide pyrolysis and the MR; thus, their content initially increased and then decreased. The amino acid content gradually decreased as the number of evaporation steps increased, indicating that both amino acids and reducing sugars acted as substrates for the MR during black ginseng processing. Thirty-one saponins, 18 sugars, and 58 amino acids were identified based on the MS analysis. Transcriptomics results demonstrated that black ginseng can regulate signaling pathways such as the TNF, IL-17, MAPK, and PI3K-Akt pathways. This finding helps us understand the observed proliferation and differentiation of immune-related cells and positively regulated cell adhesion.

KEYWORDS

black ginseng, ginsenoside, amino acids, Maillard reaction, transcriptome

1 Introduction

Black ginseng is a black or dark brown product made by repeatedly steaming and drying ginseng (*Panax ginseng* CA Mey.), a plant from the Wugangaceae family. Black ginseng is a fairly new concoction rich in rare saponins. Ginsenosides are the main active substances in black ginseng and exhibit various pharmacological effects, such as anti-tumor

(Yang D. et al., 2020; Qing et al., 2020; Zhang et al., 2019; Zheng et al., 2019), anti-oxidant (Choudhry et al., 2019; Hussain et al., 2021; Li et al., 2020; Wu et al., 2023; Wang et al., 2019), anti-inflammatory (Kim et al., 2020; Choi et al., 2021; Xu et al., 2022; Chen et al., 2021), and anti-viral (Kim et al., 2019; Zhang et al., 2023) properties. The appearance of black ginseng powder, tablets, and other products in the market indicates the potential of black ginseng as a dual-purpose product (i.e., as food and medicine) (Heinrich et al., 2022; Chen, 2023; Yang S-h et al., 2023). Therefore, research on the chemical composition and pharmacological effects of black ginseng is crucial.

Black ginseng processing involves the Maillard reaction (MR) (i.e., non-enzymatic browning), one of the most important chemical reactions that occur during food processing and storage. The MR affects food quality. First reported by French scientist L.C. Maillard in 1921, the MR involves a dehydration condensation between carbonyl-containing reducing sugars, aldehydes, ketones, and nitrogenous substances such as proteins, amino acids, and peptides with free amino groups, ultimately producing melanin-like compounds (van Boekel, 2006).

In this paper, we analyzed the changes in chemical composition during black ginseng processing, based on the MR. We investigated the compositional differences between the ginsenosides, reducing sugars, and amino acids in black ginseng and fresh ginseng, using high-performance liquid chromatography-mass spectrometry (HPLC-MS). We also used transcriptomics with gene chip technology to enrich the genes before and after processing, analyzed the differences in biological pathways, and examined changes in pharmacodynamics. This research aims to identify the key points in black ginseng preparation and provide a foundation for the in-depth study of the product's potential mechanisms. Moreover, we conducted a preliminary study on the differences in the pharmacological mechanisms of black ginseng and fresh ginseng, aiming to offer ideas for further exploration of the underlying mechanisms.

2 Materials and methods

2.1 Plant materials and reagents

Ginsenosides and glucose with purity greater than 98% were purchased from Shanghai Yuanye Biotechnology Co. Methanol and acetonitrile for chromatography were provided by Thermo Fisher Scientific (Waltham MA, United States). Other chemicals were of reagent grade.

All ginseng samples were purchased from Tonghua Tahuaxing Native Products Co. and certified according to the standards recorded in the Chinese Pharmacopoeia. The first process worked as follow: streaming samples for 1.5 h under atmospheric pressure and heating at 70°C for 18 h. After that, samples were steamed for 2 h, and baked at 60°C for 9 h,which was repeated for nine times.

2.2 Preparation of black ginseng extract

Black ginseng (0.2 g) was transferred to a test tube and 30 mL of 40% ethanol aqueous solution was added and mixed well. The sample was placed in a constant-temperature water bath at 80°C for 60 min. Then, the sample was centrifuged at 4,000 r/min for 15 min, and the supernatant was collected and stored at room temperature.

2.3 Measurement items and test methods

2.3.1 Determination of ginsenoside content

Ginseng was powdered and sieved four times. Next, 1 g of powder was placed in a Soxhlet extractor, trichloromethane was added, and the mixture was heated by reflux for 3 h. The solvent was then evaporated to dryness. The residue was dissolved with 50 mL of water saturated with n-butanol and passed through filter paper into a 100 mL conical flask, which was tightly plugged and placed overnight under ultrasonication (250 W, 50 kHz). After filtration, 25 mL of filtrate was measured and evaporated. Methanol was added to dissolve the residue, which was transferred into a 5 mL measuring flask.

2.3.2 Determination of reducing sugar content

Glucose (100 mg) was heated in an oven at 80°C to a constant weight and dissolved with water to obtain 1.0 mg/mL and 0.1 mg/mL glucose standard solutions.

To obtain the reducing sugar standard curve, 0, 0.2, 0.4, 0.6, 0.8, 1.0, and 1.2 mL of glucose standard solutions (1 mg/mL) were added to respective test tubes. Distilled water (2 mL) was added and mixed well. Then, 1.5 mL of 3,5-dinitrosalicylic acid solution was added and mixed well. The solutions were heated in a boiling-water bath for 5 min. The volume was adjusted to 10 mL with distilled water and the tubes were removed and cooled down immediately. Absorbance was measured at 520 nm, using an UV spectrophotometer. Readings were taken three times in parallel.

The black ginseng extract (1 mL, obtained as described in Section 2.2) was transferred into a test tube and its absorbance was determined. The content of reducing sugar in the sample was obtained using the standard curve.

2.3.3 Determination of amino acid content

The sample (0.1 g) was mixed with 1 mL of extraction solution at room temperature and centrifuged at 12,000 rpm for 10 min. The supernatant was collected and reagents were sequentially added according to Table 1.

2.4 High-performance liquid chromatography-mass spectrometry (HPLC-MS)

For HPLC, the mobile phase was 0.1% formic acid aqueous solution (A) and acetonitrile (B). The elution gradient was as follows: 0–2 min, 5% B; 2–6 min, 5%–30% B; 6–7 min, 30% B; 7–12 min, 30%–78% B; 12–14 min, 78% B; 14–17 min, 78%–95% B; 17–20 min, 95% B; 20–21 min, 95%–5% B; 21–25 min, 5% B. The column temperature was 30°C, the flow rate was 0.3 mL/min, the injection volume was 2 mL/min, and the autosampler temperature was 4°C.

TABLE 1 Amino acid content determination.

Reagent (μL)	Measuring tube	Blank tube
Blank tube		40
Supernatant	40	
Chemical reaction max	560	560
Reagent III	40	40
The reagents were mixed in tubes, which were then covered tightly with sealing film to prevent moisture loss and placed in a boiling-water bath for 15 min. Subsequently, the tubes were cooled down to room temperature and shaken for 1 min		
95% ethoxide	320	320
The sample was mixed well; 200 μL of clarified liquid was taken (centrifuged at 8,000 rpm for 5 min at room temperature if turbidity was present) and poured into a 96-well plate. Absorbance (value A) was read at 570 nm		

For MS, the positive and negative ion modes were used. In both cases, the source was kept at 325°C. The sheath gas, auxiliary gas, and purging gas flow rates were 45, 15, and 1 arb, respectively. The electrospray voltage was 3.5 kV, the capillary temperature was 330°C, and the S-Lens RF level was 55%.

The scanning mode was full scan (*m/z* 100~1,500) with data-dependent secondary mass spectrometry (dd-MS2, TopN = 5) and resolution of 120,000 (primary mass spectrometry) and 60,000 (secondary mass spectrometry). The collision mode was high-energy collisional dissociation (HCD).

2.5 Transcriptomics testing

The black ginseng aqueous fraction was used as the positive control. The human breast cancer cell line MCF-7 served as the model. The IC_{50} concentration of the screening drug was 5 mg/mL. MCF-7 cells were inoculated in 96-well plates at 1×10^4 cells/100 μL, and cultured for 24 h. Subsequently, the black ginseng aqueous fraction was added to the cells at three concentrations (5, 2.5, and 1.25 mg/mL). Black ginseng aqueous fraction alone was used as the negative control. Three-year-old aqueous extracts served as the negative control groups. After an additional 24 h of incubation, total RNA was extracted. Transcriptome changes were detected using a high-efficiency, high-throughput gene detection system (HISTAG), with three biological replicates per concentration.

3 Results

3.1 Chemical composition of ginseng and black ginseng

3.1.1 Changes in the ginsenoside content

Ginsenosides Rg1, Re, Rh1, Rb1, 20-(S)-Rg3, 20-(R)-Rg3, and Rg5 were used as indicators to assess the MR's progress by calculating the proportion of rare saponins within the total saponin content. The results (Figure 1A) indicate a steady increase in the proportion of rare saponins under atmospheric pressure. The conversion of ginsenosides was particularly high during the sixth steaming process, after which it slowed down again. This pattern reflects the progression of the MR.

3.1.2 Changes in the reducing sugar content

Reducing sugar, as the MR's substrate, indicates the progress of the reaction to a certain extent. During ginseng steaming, the reducing sugar content initially increases and then decreases as the number of steaming cycles increases (Figure 1B). This is primarily due to the abundance of polysaccharides in fresh ginseng, which are degraded during high-temperature processing. In the reaction's early stages, the degradation rate of these polysaccharides is faster, increasing the reducing sugar content. However, as the steaming cycles continue, the original polysaccharides in ginseng are depleted, and reducing sugar production slows down. Because reducing sugars continually react with amino compounds during the MR, their contents reach a plateau and remain stable until the end of the process.

3.1.3 Changes in the amino acid content

The basis of the MR is the condensation of amino compounds with carbonyl compounds (reducing sugars). Amino acids, as substrates of the MR, indicate the reaction's progression. The amino acid content decreased steadily during the first five evaporation cycles under atmospheric pressure (Figure 1C). The most rapid decrease was observed during the sixth evaporation. This may be explained by the reducing sugar content peaking after the fifth evaporation, leading to a higher substrate concentration and an accelerated reaction between the carbonyl and amino groups. Afterward, the decrease in the amino acid content slowed down again until the end of the steaming process. Thus, we confirmed that both amino acids and reducing sugars are substrates in the MR.

3.2 Results of mass spectrometry

The HPLC-MS analysis was conducted in both the positive and negative ion modes. The resulting total ion chromatograms are displayed in Figure 2. These chromatograms reveal notable differences in the chemical composition of fresh and black ginseng, indicating that repeated steaming of fresh ginseng affects its chemical composition.

3.2.1 Ginsenoside mass spectrometry results

Ginsenosides can be classified into dammarane-type, ocotillo-type, and oleanolic acid-type ginsenosides based on their glycoside

10.3389/fphar.2024.1425794

TABLE 2 Ginsenoside mass spectral data.

Number	RT [min]	Name	Annot. DeltaMass [ppm]	Annotation MW	Calc. MW	Ginsenoside type	Ginseng	Number	Trend of change
1	5.433	Pseudoginsenoside F11	0.04	800.49	800.49	Ocotillon	+		
2	6.025	Ginsenoside F1	0.38	638.44	638.44	PPT	+	+	↑
3	7.362	Ginsenoside Rg1	0.94	946.55	946.55	PPT	+	+	↓
4	7.400	20-O-Glucoginsenoside Rf	−0.62	800.49	800.49	PPT	+	+	↓
5	8.645	Ginsenoside Rf	1.14	962.55	962.55	PPT	+		
6	9.238	Ginsenoside Rb1	−0.71	800.49	800.49	PPT	+	+	↓
7	9.316	Ginsenoside Rb2	−1.36	1108.60	1108.60	PPD	+		
8	9.439	Ginsenoside Rb3	−0.29	1078.59	1078.59	PPD	+		
9	9.443	Ginsenoside F3	−1.13	1078.59	1078.59	PPD	+	+	↓
10	9.549	Ginsenoside Rh3	0.87	770.48	770.48	PPT	+	+	↓
11	9.556	Ginsenoside Rg2	−1.24	604.43	604.43	PPD	+	+	↑
12	9.581	Ginsenoside Rb1	0.81	784.50	784.50	PPT	+	+	↓
13	9.645	20-R-Glucoginsenoside Rh1	−0.72	1108.60	1108.60	PPD		+	
14	9.693	Ginsenoside Rc	−0.85	638.44	638.44	PPT		+	
15	9.715	Ginsenoside Rd	−0.24	1078.59	1078.59	PPD	+	+	↓
16	9.715	Ginsenoside	0.45	1078.59	1078.59	PPD	+		
17	9.716	20-S-Glucoginsenoside Rg3	−1.00	784.50	784.50	PPD		+	
18	9.716	20(R)-Protopanaxadiol	−1.39	460.39	460.39	PPD		+	
19	9.798	20-S-Glucoginsenoside Rh1	1.42	638.44	638.44	PPT		+	
20	10.242	20-O-Glucoginsenoside Rf	1.04	962.55	962.55	PPT		+	
21	10.482	Ginsenoside compound K	−0.92	622.44	622.44	PPD		+	
22	10.490	20-R-Glucoginsenoside Rg3	−0.98	784.50	784.50	PPD		+	
23	10.702	Ginsenoside Rk1	−1.12	766.49	766.49	PPD		+	
24	10.799	Ginsenoside Rg5	1.37	766.49	766.49	PPD		+	
25	10.990	Oleanolic acid	−1.14	456.36	456.36	Oleanolane	+	+	↑
26	11.029	Ginsenoside Rh4	−0.53	620.43	620.43	PPT		+	
27	11.109	Panaxytriol	−1.57	476.39	476.39	PPT		+	
28	11.145	Ginsenoside Rk3	1.05	620.43	620.43	PPT		+	
29	11.220	Ginsenoside F2	1.65	784.50	784.50	PPD	+	+	↑

(Continued on following page)

TABLE 2 (*Continued*) Ginsenoside mass spectral data.

Number	RT [min]	Name	Annot. DeltaMass [ppm]	Annotation MW	Calc. MW	Ginsenoside type	Ginseng	Number	Trend of change
30	11.891	Pseudoginsenoside F11	0.32	826.51	826.51	PPT		+	
31	12.567	Ginsenoside F1	0.64	826.51	826.51	PPT		+	

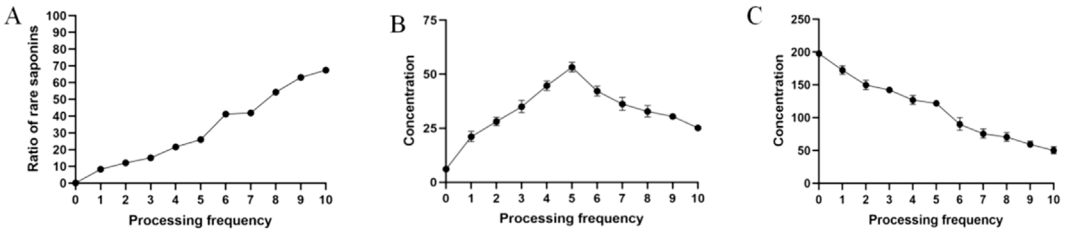

FIGURE 1
Changes in the chemical composition. **(A)** Changes in rare saponins; **(B)** changes in the reducing sugar content; **(C)** changes in the amino acid content.

structures. Most dammarane-type ginsenosides are triterpenoids and can be further categorized as protoginseng diols (PPDs) and protoginseng triols (PPTs). We used Compound Discoverer 3.3 to compare the MS of fresh ginseng with that of black ginseng (i.e., processed by high-temperature steaming). These samples were classified and analyzed to identify ginsenosides, using secondary MS data from the mzCloud and mzVault databases (Thermo Fisher Scientific). The results revealed substantial differences between the ginsenoside profiles of fresh ginseng and black ginseng. Thirty-one ginsenosides were identified: 16 from fresh ginseng and 26 from black ginseng, with 11 common saponins, most of which decreased during processing (Table 2).

The results showed that the ginsenosides' types and contents changed notably after repeated steaming. The contents of the original ginsenosides (e.g., Rg1, Re, Rb1, Rb2, Rb3, and Rc) decreased while rare saponins, such as ginsenosides 20-(R)-Rg3, 20-(S)-Rg3, Rk1, Rk3, and Rg5 appeared. The MS ion fragmentation patterns together with the ginsenoside structures helped us infer the transformation process of ginsenosides, described below.

Ginsenosides such as Rb1, Rb2, Rb3, CK, and Rc are PPDs. The presence of hydroxyl or hydroxyl substitutions at the C-3 and C-20 positions is a common structural feature of these ginsenosides. During high-temperature processing, glycosyl groups at the C-3 and C-20 positions of these ginsenosides are hydrolyzed and replaced with hydroxyl groups of varying molecular weights. For instance, when ginsenoside Rb1 is heated, the disaccharide group at the C-20 position is hydrolyzed and replaced with a hydroxyl group, generating ginsenoside 20-(S)-Rg3. This product can undergo further hydrolysis to remove a glucose molecule at C-3, resulting in ginsenoside Rh2. Dehydroxylation at C-20 releases a water molecule, converting Rh2 into ginsenoside Rh3. The hydroxyl group at C-20 of 20-(S)-Rg3 is unstable and dehydrates between C-20 and C-21 to generate ginsenoside Rk1. If dehydration occurs between C-20 and C-22, ginsenoside Rg5 is formed. Moreover, the unsaturated double bond positions in ginsenosides Rk1 and Rg5 can undergo an addition reaction, producing ginsenoside 20-(R)-Rg3 (Figure 3). These substituents can be hydrolyzed and replaced by hydroxyl groups during high-temperature processing because of the structural feature of diol-type saponins, which mainly differ by the substituents at C-20, generating the corresponding rare saponins. Therefore, the contents of 20-(S)-Rg3, 20-(R)-Rg3, Rk1, and Rg5 in black ginseng increase. In addition, the glucose molecule at C-3 of ginsenoside Rk1 can be removed to generate ginsenoside Rk2.

Ginsenosides such as Re, Rg1, Rg2, and Rf are PPTs, based on PPDs with the addition of hydroxyl or hydroxyl substitutions at the C-6 position. For instance, ginsenoside Re can be converted into Rg1 by removing the rhamnoside (Rha) at the C-6 position. During steaming, Rg1 undergoes hydrolysis at the C-6 position, where the original sugar group is replaced with a hydroxyl group, producing ginsenoside F1. If F1 loses the sugar group at the C-20 position, it forms 20-(S)-Rh1. Further dehydration of 20-(S)-Rh1 creates an unsaturated bond at the C-20 or C-22 positions, resulting in ginsenoside Rk3. If a water molecule is removed between the C-20 and C-21 positions, another unsaturated bond forms, generating Rh4. Finally, ginsenoside Rh4 can undergo addition at the C-20 or C-21 positions to form 20-(R)-Rg3 (Figure 4).

In summary, the original saponins in ginseng are transformed during high-temperature processing, which can trigger a series of chemical reactions, such as deglycosylation, dehydration, and addition, producing rare saponins unique to black ginseng, such as the ginsenosides 20-(S)-Rg3, 20-(R)-Rg3, and Rk1. When ginseng is steamed, the sugar groups are reduced, enabling these, the hydroxyl groups, and other polar groups to form complexes with cholesterol in the cell membranes. This interaction alters the permeability and function of the cell membranes, influencing ginseng's pharmacological effects. For instance, saponins from fresh ginseng cannot effectively regulate serum corticosterone and adrenocorticotropic hormone (ACTH) levels. By contrast,

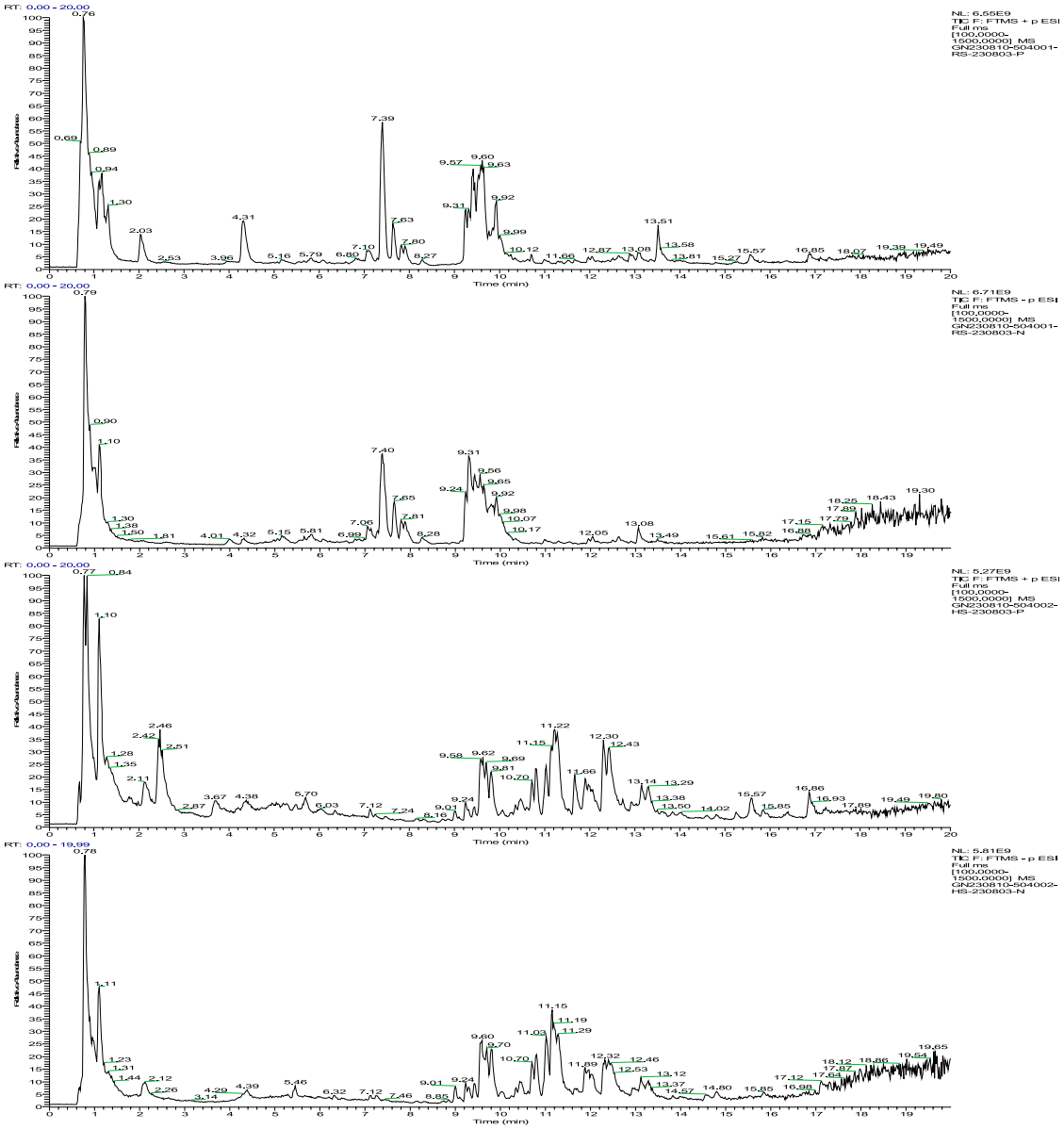

FIGURE 2
(A) Positive ion flow diagram of fresh ginseng; **(B)** negative ion flow diagram of fresh ginseng; **(C)** positive ion flow diagram of black ginseng; **(D)** negative ion flow diagram of black ginseng.

deglycosylated derivatives from black ginseng, such as Rg3 and CK, increase ACTH levels and normalize the hyperactivity of the HPA axis (Zhang et al., 2016), resulting in antidepressant effects. However, Rh2 lacks this effect, which may be due to the position of the sugar substituent, a hypothesis that requires further verification. Furthermore, black ginseng obtained through steaming (but not fresh ginseng) exhibits strong memory-enhancing effects. This effect was attributed to secondary saponins like Rg5 and Rg3 (Lee et al., 2020).

3.2.2 Sugar and amino acid mass spectrometry results

The transformation of sugars and amino acids in black ginseng was investigated. Black ginseng was prepared by steaming fresh ginseng at 117°C for 1.5 h, followed by drying at 68°C; this cycle was repeated three times. The results revealed that the sugars and amino acids in black ginseng were markedly different from those in fresh ginseng (Tables 3, 4). Eighteen sugars were detected, seven in the positive ion mode and 11 in the negative ion mode. Of these, eight compounds were found in fresh ginseng and 10 in black ginseng. Furthermore, 58 amino acids were detected, 45 in the positive ion mode and 13 in the negative ion mode. Among them, 49 compounds were detected in fresh ginseng and nine in black ginseng.

The results showed that the sugar and amino acids in black ginseng differed from those in fresh ginseng. In the latter, oligosaccharides and polysaccharides are the predominant sugars, and peptides and single amino acids are the predominant amino compounds. During high-temperature processing, the

10.3389/fphar.2024.1425794

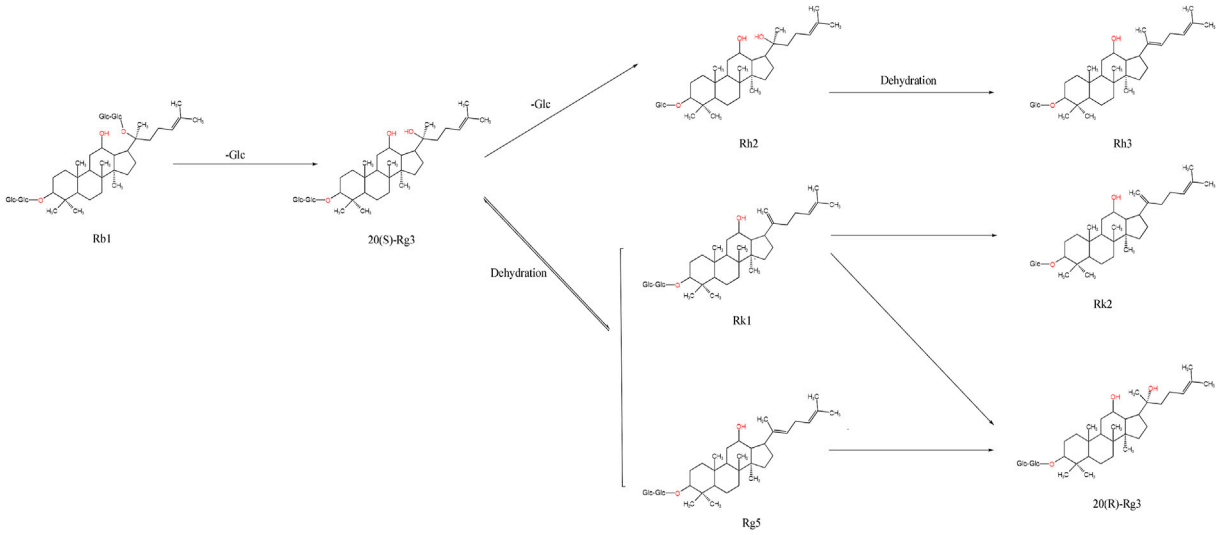

FIGURE 3
Schematic diagram of the transformation of ginsenoside Rb1.

TABLE 3 Sugars detected by HPLC-MS.

Number	RT [min]	Name	Annot. DeltaMass [ppm]	Annotation MW	Calc. MW	Ionic mode	Ginseng	Black ginseng
1	0.771	Hex-2-ulose	−1.06	180.06339	180.0632	+		+
2	0.771	Galactinol	−1.29	342.11621	342.11577	+		+
3	0.773	D-(+)-Maltose	−0.29	342.11621	342.11611	−		+
4	0.777	D-Sucrose	−1.1	342.11621	342.11583	+	+	
5	0.784	Raffinose	0.27	504.16903	504.16917	−		+
6	0.793	α,α-Trehalose	−0.33	342.11621	342.1161	−	+	
7	0.815	Trehalose-6-phosphate	0.23	422.08254	422.08264	−		+
8	0.825	D-Glucono-1,5-lactone	−4.67	178.04774	178.04691	−		+
9	0.85	1,4-D-xylobiose	−0.56	282.09508	282.09492	−		+
10	1.075	Nystose	1.21	666.22186	666.22267	−	+	
11	2.131	Glucosylisomaltol	−1.66	288.08452	288.08404	+		+
12	4.858	1-(4-Hydroxybenzoyl) glucose	−0.51	300.08452	300.08436	−	+	
13	5.038	Caffeic acid hexoside	−0.38	342.09508	342.09495	−		+
14	7.072	Polydextrose	−1.54	283.13208	283.13164	+	+	
15	7.145	Sibiricose A1	0.27	548.17412	548.17427	−	+	
16	9.313	α-Lactose	−1.83	342.11621	342.11558	+	+	
17	9.315	Maltotetraose	−1.16	666.22186	666.22109	+	+	
18	17.313	3-O-Undecyl-D-glucopyranose	1.02	334.23554	334.23588	−		+

polysaccharides in ginseng are hydrolyzed to produce monosaccharides, and the peptide chains between the amino acids are broken. Simultaneously, the amino groups of amino acids combine with the carbonyl groups of ketose sugars, generating monosaccharide and glucose derivatives. Thus, the sugars in black ginseng are mainly monosaccharides and glucose

10.3389/fphar.2024.1425794

TABLE 4 Amino acids detected by HPLC-MS.

Number	RT [min]	Name	Annot. DeltaMass [ppm]	Annotation MW	Calc. MW	Ionic mode	Ginseng	Black ginseng
1	0.684	D-(+)-Pipecolinic acid	−0.28	129.08	129.08	+	+	
2	0.695	L-Histidine	0.41	155.07	155.07	+	+	
3	0.743	N-Methylthreonine	−3.56	133.07	133.07	−	+	
4	0.761	DL-Arginine	−0.25	174.11	174.11	+	+	
5	0.799	D-(+)-Proline	1.83	115.06	115.06	+	+	
6	0.834	Acetylarginine	0.64	216.12	216.12	+	+	
7	0.910	N-Acetylhistamine	−0.31	153.09	153.09	+	+	
8	1.067	Valine	1.52	117.08	117.08	+	+	
9	1.094	L-(−)-Methionine	0.06	149.05	149.05	+	+	
10	1.118	N-Fructosyl tyrosine	−0.51	343.13	343.13	+	+	
11	1.194	L-Tyrosine	−4.87	181.07	181.07	−	+	
12	1.207	L-Isoleucine	0.3	131.09	131.09	+	+	
13	1.265	N-Fructosyl isoleucine	−1.26	293.15	293.15	+	+	
14	1.300	L-Norleucine	0.3	131.09	131.09	+	+	
15	1.309	Prolylleucine	−0.56	228.15	228.15	+	+	
16	1.404	Leucylalanine	−0.21	202.13	202.13	+	+	
17	1.443	L-Threo-3-phenylserine	−0.39	181.07	181.07	+		+
18	1.485	Valylproline	−0.27	214.13	214.13	+	+	
19	1.580	Valylvaline	−0.17	216.15	216.15	+	+	
20	1.791	Acetylproline	−0.25	157.07	157.07	+	+	
21	2.229	5-Hydroxytryptophan	−0.2	220.08	220.08	+	+	
22	2.302	Serylleucine	−0.24	218.13	218.13	+	+	
23	2.431	γ-Glutamyltyrosine	−0.83	310.12	310.12	+	+	
24	2.564	Metyrosine	−0.41	195.09	195.09	+		+
25	2.612	Ala-Ile	0.02	202.13	202.13	+	+	
26	2.629	Ala-Leu	−3.62	202.13	202.13	−	+	
27	2.637	L-Phenylalanine	0.2	165.08	165.08	+	+	
28	2.638	Threonylleucine (isomer of 809, 926)	−0.27	232.14	232.14	+	+	
29	2.687	Glycyl-L-leucine	−0.09	188.12	188.12	+	+	
30	3.757	H-LEU-VAL-OH	−0.2	230.16	230.16	+	+	
31	4.243	Ala-Phe	−0.98	236.12	236.12	+	+	
32	4.254	Leucylproline	−0.9	228.15	228.15	+	+	
33	4.305	DL-Tryptophan	−0.19	204.09	204.09	+	+	
34	4.319	D-(+)-Tryptophan	−3.08	204.09	204.09	−	+	
35	4.421	Leucylvaline	−0.8	230.16	230.16	+	+	
36	4.521	γ-Glutamylleucine	−0.47	260.14	260.14	−	+	
37	4.552	N-Acetylhomoproline	−0.82	171.09	171.09	+		+

(Continued on following page)

TABLE 4 (*Continued*) Amino acids detected by HPLC-MS.

Number	RT [min]	Name	Annot. DeltaMass [ppm]	Annotation MW	Calc. MW	Ionic mode	Ginseng	Black ginseng
38	4.664	N-Acetyl-L-tyrosine	−2.2	223.08	223.08	−	+	
39	5.037	Cyclo (Pro-Val)	−0.57	196.12	196.12	+		+
40	5.040	Glutamylphenylalanine (isomer of 1,503)	−0.63	294.12	294.12	+	+	
41	5.250	H-PHE-VAL-OH	−0.95	264.15	264.15	+	+	
42	5.571	Leucylleucine	−0.67	244.18	244.18	+	+	
43	5.576	Isoleucylisoleucine	−1.24	244.18	244.18	−	+	
44	5.696	N-Benzoyl-DL-alanine	−0.66	193.07	193.07	+		+
45	6.121	Phenylalanylisoleucine (isomer of 1,329)	−0.88	278.16	278.16	+	+	
46	6.161	N-Acetyl-L-leucine	−0.07	173.11	173.11	+	+	
47	6.166	2-(Acetylamino)hexanoic acid	−4.94	173.11	173.10	−		+
48	6.266	Glu-Val-Phe	−0.84	393.19	393.19	+	+	
49	6.359	Cyclo (leucyl-prolyl)	−1.02	210.14	210.14	+		+
50	6.680	N-Acetylphenylalanine	−0.38	207.09	207.09	+	+	
51	6.871	Malonyltryptophan	−1.72	290.09	290.09	+	+	
52	6.872	N-Acetyl-DL-tryptophan	−0.91	246.10	246.10	−	+	
53	6.923	2-Hydroxyphenylalanine	−0.62	181.07	181.07	+		+
54	7.911	L-Methionyl-L-alpha-aspartyl-L-valyl-L-asparaginyl-L-prolyl-L-phenylalanyl-L-leucyl-L-leucyl-L-phenylalanyl-L-leucyl-L-lysyl-L-valyl-L-prolyl-L-isoleucyl-L-glutamine	−1.17	1772.99	1772.99	−	+	
55	9.388	N-Acetyl-L-phenylalanyl-L-glutaminyl-L-seryl-L-cysteinylglycyl-L-asparaginyl-L-valyl-L-phenylalanyl-L-valyl-L-alpha-aspartylglycyl-L-tyrosyl-L-phenylalanyl-L-alpha-glutamyl-L-arginyl-L-leucyl-L-arginy l-L-alanyl-L-lysyl-L-leucinamide	3.26	2389.20	2389.21	−	+	
56	9.558	L-Tyrosyl-L-seryl-L-phenylalanyl-L-lysyl-L-alpha-aspartyl-L-alanyl-L-prolyl-L-leucyl-D-alanyl-N~5~-(diaminomethylene)-L-ornithine	0.02	1166.61	1166.61	−	+	
57	9.786	Glycyl-L-seryl-O-octanoyl-L-seryl-L-phenylalanyl-L-leucyl-L-seryl-D-prolyl-L-alpha-glutamyl-L-histidyl-L-glutamamide	0.63	1212.61	1212.61	−	+	
58	10.066	3-(2-Naphthyl)-L-alanine	−1.19	215.09	215.09	+		+

derivatives, while the amino acids are predominantly acetylated or phenylated derivatives. This result further confirms that black ginseng processing involves the MR.

3.3 Differential gene identification

Three concentrations (5, 2.5, and 1.25 mg/mL) of three-year-old black ginseng aqueous extract were used as controls. MCF-7 cells treated with these three concentrations served as the experimental group. The FC-t algorithm was used to identify differentially expressed genes. The thresholds were set at $P < 0.05$, and $|FC| > 1.5$, allowing for the identification of differential genes across the three groups at different concentrations.

The differentially expressed genes before and after administering the black ginseng extract were identified: 683 genes from the cells exposed to the low-concentration extract, 668 genes from the cells exposed to the medium-concentration extract, 682 genes from the cells exposed to the high-concentration extract, and 879 genes when combining the data from all three concentrations (Figure 5).

10.3389/fphar.2024.1425794

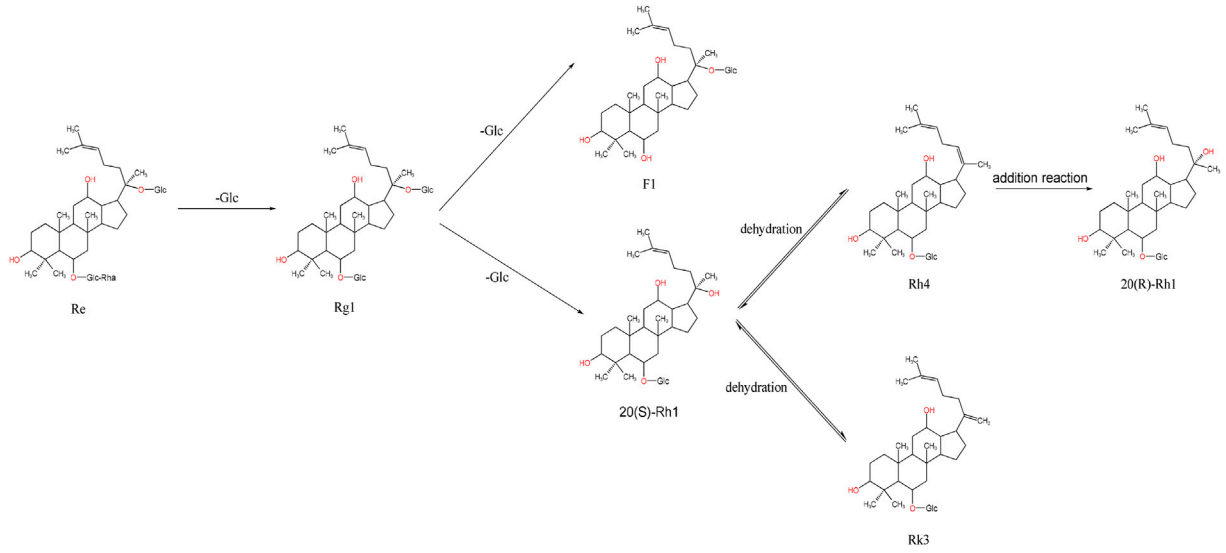

FIGURE 4
Schematic diagram of the transformation of ginsenosides Re and Rg1.

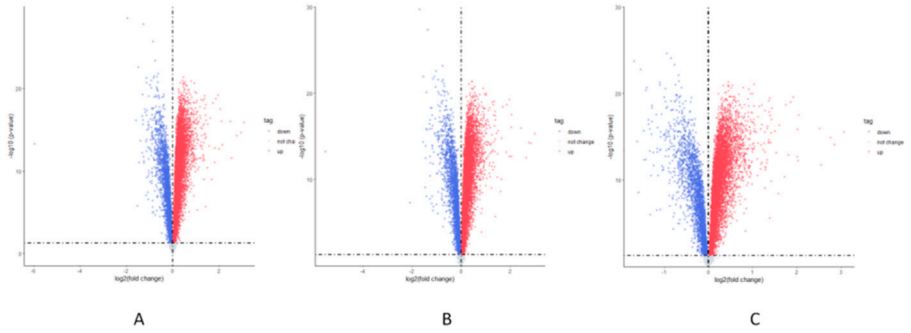

FIGURE 5
Results of differential gene analysis. **(A)** Cells exposed to the low-concentration extract; **(B)** cells exposed to the medium-concentration extract; **(C)** cells exposed to the high-concentration extract. The blue color indicates a decrease in expression, whereas red indicates an increase in expression.

TABLE 5 Number of genes in the modules.

Module number	Number of genes
1	132
2	106
3	83
4	110
5	184
6	154
7	139

3.3.1 Gene co-expression network construction and gene module delineation

Gene co-expression networks are commonly applied in transcriptomics. In this study, data from 879 genes—derived from the differential genes detected in the cells exposed to the three extract concentrations—were selected as background data. The Pearson correlation algorithm was used to construct the relationship matrix between the differential genes. Relationships with $|r| > 0.7$ and $P < 0.05$ were screened to construct the gene co-expression network.

The multilevel algorithm was used to divide the gene modules. Modules with few genes were removed while those with more genes were analyzed. As a result, seven gene modules were obtained. Table 5 shows the number of genes in each module.

3.3.2 GO and KEGG analysis of each gene module

The genes within each module were enriched and analyzed using biological pathways (BP) and the KEGG (https://www.genome.jp/kegg/) and GO (http://geneontology.org/) databases. The 20 biological processes and KEGG pathways with the smallest *P*-value for each module were selected for visualization. The GO and KEGG enrichment results corresponding to the genes in each module are presented in Figures 6, 7.

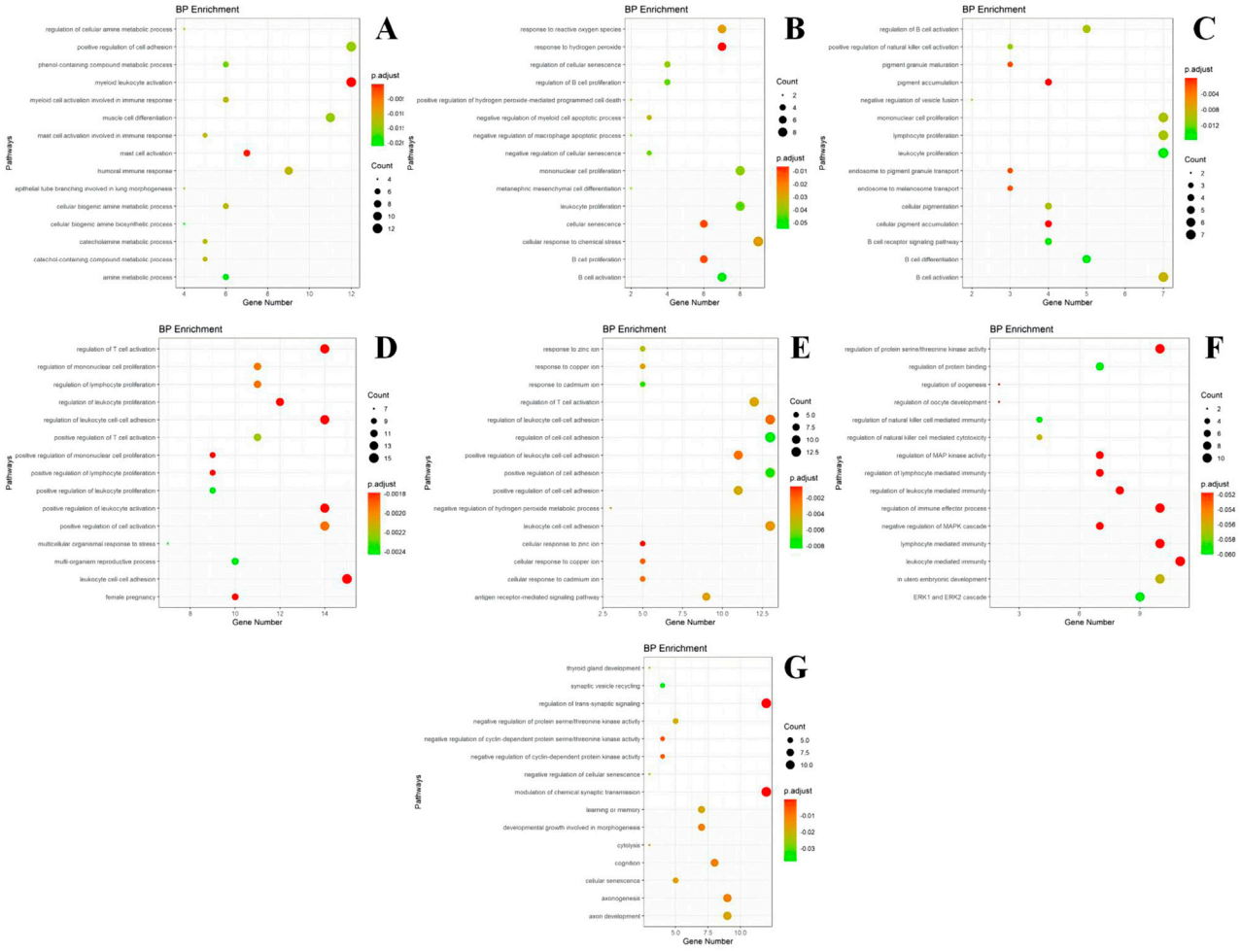

FIGURE 6
GO enrichment results of different modules. **(A)** module m1 GO enrichment analysis results; **(B)** module m2 GO enrichment analysis results; **(C)** module m3 GO enrichment analysis results; **(D)** module m4 GO enrichment analysis results; **(E)** module m5 GO enrichment analysis results; **(F)** module m6 GO enrichment analysis results; **(G)** module m7 GO enrichment analysis results. The size of the dots represents the number of genes in the entry (count value), and the color of the dots represents the degree of enrichment (*P*-value) in a gradient from yellow to red; a redder color indicates a higher degree of enrichment.

Based on the GO enrichment analysis of the differentially expressed genes, most of the enriched entries are BP. Module I is primarily involved in the positive regulation of cell adhesion, skeletal leukocyte activation, myocyte differentiation, humoral immunity, and mast cell activation. Module II is mainly associated with the cellular response to chemical stress, leukocyte proliferation, monocyte proliferation, and response to peroxides and hydrogen peroxide. Module III is primarily involved in monocyte proliferation, lymphocyte proliferation, leukocyte proliferation, and B-cell activation, differentiation, and activation regulation. Module IV participates in leukocyte cell adhesion, promotes leukocyte activation, and regulates leukocyte proliferation. Module V is involved in T-cell activation and responses to zinc and other metal ions such as copper and cadmium. Module VI participates in the regulation of immune effects, mediating the regulation of immunity by leukocytes and lymphocytes. Module VII is involved in the regulation of trans-synaptic signaling, chemosynaptic transmission, and axonal ontogeny and development.

According to the results of KEGG enrichment analysis, most of the genes in Module I are involved in pathways that regulate proteoglycan, skeletal differentiation, natural killer (NK) cell-mediated cytotoxicity in cancer, the AGE-RAGE signaling pathway in diabetic complications, and the T-cell receptor signaling pathway. Module II is implicated in the JAK-STAT signaling pathway, human immunodeficiency virus type 1 (HIV-1) infection, and NF-κB signaling pathway. Module III participates in the PI3K-Akt signaling pathway and Th17, Th1, and Th2 cell differentiation. Module IV is involved in the TNF signaling pathway. Module V is associated with the IL-17 signaling pathway, *Staphylococcus aureus* infection, B-cell receptor signaling pathway, and rheumatoid arthritis. Module VI regulates the MAPK, PI3K-Akt, and Wnt signaling pathways, as well as cellular senescence. Module VII participates in the regulation of the actin cytoskeleton.

3.3.3 Hub gene identification

The PageRank algorithm was used to calculate the importance of each gene in the protein interaction network. The 10 genes with the highest algorithm scores were identified as the module's hub genes,

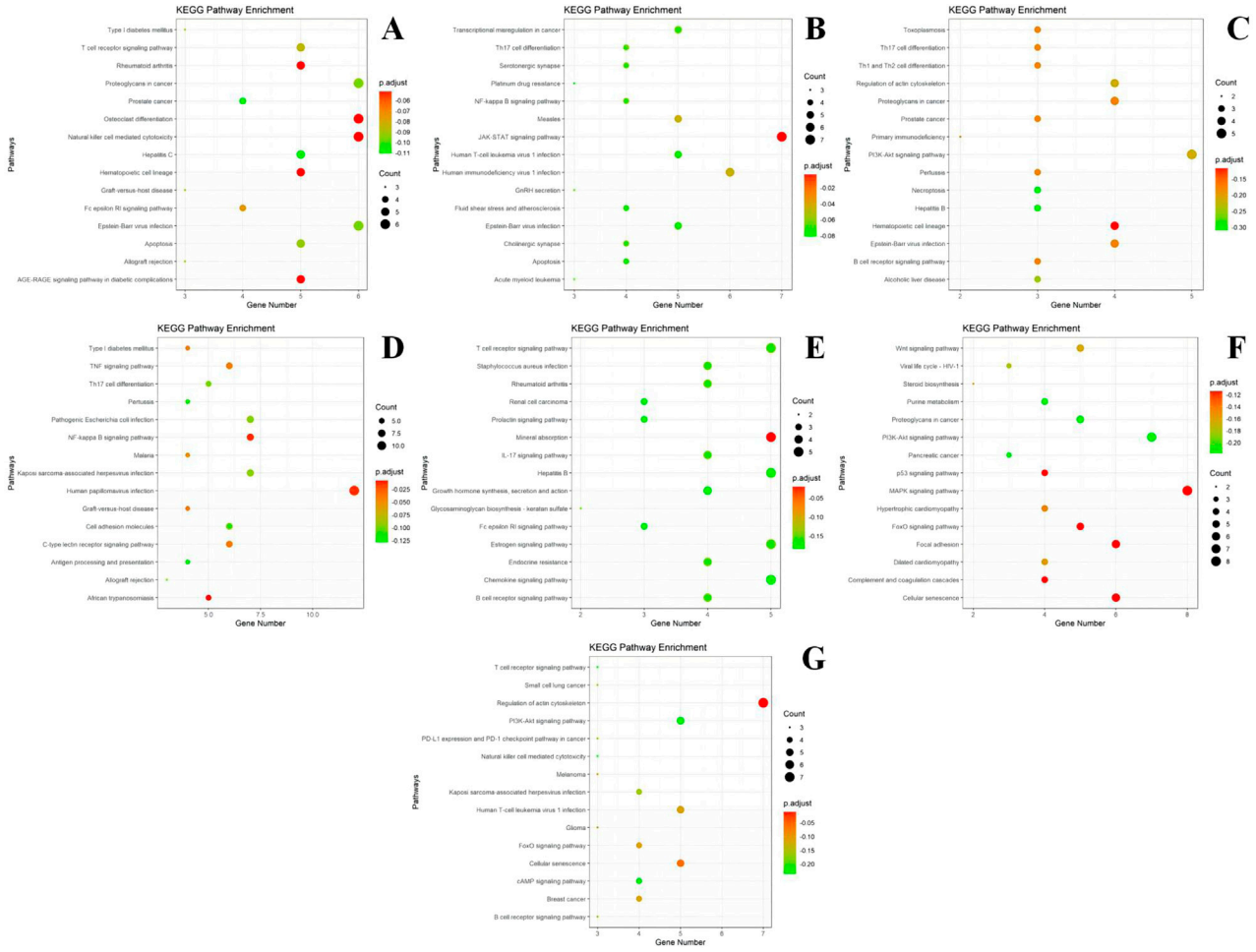

FIGURE 7
KEGG enrichment results of different modules. **(A)** module m1 KEGG enrichment analysis results; **(B)** module m2 KEGG enrichment analysis results; **(C)** module m3 KEGG enrichment analysis results; **(D)** module m4 KEGG enrichment analysis results; **(E)** module m5 KEGG enrichment analysis results; **(F)** module m6 KEGG enrichment analysis results; **(G)** module m7 KEGG enrichment analysis results. The size of the dots represents the number of genes in the entry (count value) and the color of the dots represents the degree of enrichment (*P*-value) in a gradient from yellow to red; a redder color indicates a higher degree of enrichment.

representing the most critical genes in the network. The results are displayed in Table 6.

A literature review identified several hub genes associated with biological processes and conditions. FRS2, FLRT3, RPS5, and PDLIM5 are related to cell differentiation and proliferation. INHBB, ZGPAT, MS4A6A, NNMT, LGALS1, BCL2, BCL11A, TGFB1I1, and FSCN1 are associated with tumors, with BCL2 and BCL11A noted for their anti-apoptotic effects. MBD5, OGDHL, AUTS2, EGR3, QPCT, and ITGA8 are linked to neurological diseases. Moreover, CXCL9, CD3D, DNASE1L3, CD19, ICAM3, and SPDEF are involved in immune regulation and inflammatory responses. Finally, ATF3, LMAN1L, and ACAT2 participate in metabolism.

4 Discussion

By analyzing the changes in the reducing sugar, amino acid, and ginsenoside content during black ginseng processing, we can conclude that the MR occurs during repeated steaming. This reaction consumes reducing sugars and amino acids, thereby lowering their contents. The final product of the MR, melanoidin, changes chromaticity (i.e., the color gradually deepens from an initial yellowish-white to dark brown, and, finally, to black). The repeated steaming of black ginseng is accompanied by a decrease in reducing sugars; thus, excessive steaming can result in a sour and astringent product. Therefore, the conversion rate of the active ingredients in black ginseng should be considered, while minimizing the degradation of other nutrients.

Thirty-two saponins, 18 sugars, and 58 amino acids were identified by MS. Of these, 16 saponins were found in fresh ginseng and 26 in black ginseng, including 11 common saponins. Moreover, eight sugars were found in fresh ginseng and 10 in black ginseng. In addition, 49 amino acids were identified in fresh ginseng and nine in black ginseng. These results indicate that ginseng undergoes a series of reactions during high-temperature processing, including hydrolysis, desugarization, and addition. These reactions are based on the instability of the tertiary carbonyl at the C-20 position of dammarane-type saponins, which makes the

TABLE 6 Hub genes by module.

1	2	3	4	5	6	7
FRS2	C18ORF1	LOC652493	RPS6KB1	TPST2	QPCT	HBD
INHBB	CD3D	IGKV1D-13	ATP6V1B1	AKAP17A	GNL3L	HBG1/HBG2
PAH	FLRT3	POU2AF1	GALNT3	FOXD1	ITGA8	CUX2
ZGPAT	DNASE1L3	LPHN2	PLIN2	EGR3	WSCD1	GABBR1
MS4A6A	IGHA 2 IGHG3/IGHM	AUTS2	C13ORF15	RHCG	NMU	CRABP2
POLM	BCL2	CD19	IDO1	MTUS1	HIST1H3D	PACSIN2
NNMT	OGDHL	CPLX3/LMAN1L	HIST1H2BH	ACAT2	TGFB1I1	FSCN1
MBD5	RPS5	PDLIM5	SPON1	C1ORF63	PHLDA2	STON1
CXCL9	BCL11A	IGKC/IGKV3-20	ADM	SPDEF	TPM2	MICB
LGALS1	ATF3	LOC732160/NDUFA10	ICAM3	SPARC	CYTH2	NXT1

compounds prone to hydrolysis under high-temperature conditions. This results in the cleavage of the sugar substituent at the C-20 position, the generation of hydroxyl substituents, and further hydrolysis to produce unsaturated saponins.

Ginseng primarily undergoes deglycosylation and dehydration during steaming to produce secondary saponins. The different positions and quantities of the sugar substituents affect ginseng's pharmacological activities. The anticancer effect of ginsenosides is inversely related to the number of sugar groups they contain (Sun et al., 2011; Ahuja et al., 2018). For example, the original saponins Rc and Rb1 in ginseng have almost no anticancer activity, whereas the secondary saponins Rg3 and Rh2 exhibit anticancer activity (Liu et al., 2024; Wang et al., 2021; Wu et al., 2024; Zhang et al., 2021). Furthermore, the pharmacological effect of Rg3 (two sugar groups) is weaker than that of Rh2 (one sugar group).

There are also notable differences in the pharmacological effects of Rg5 and Rh2. Both can be obtained by removing one sugar group from Rg3. When the sugar group at the C-20 position is removed, Rg5, which exhibits antidepressant efficacy, is generated. By contrast, the Rh2 generated at the C-3 position does not possess such an effect. The MR occurs concurrently during steaming, hydrolyzing polysaccharides and polypeptides to generate small-molecule compounds. The amino compounds in the system can be dehydrated and condensed with the carbonyl compounds (reducing glycosides). High-molecular-weight melanoidins are formed through a series of chemical reactions such as condensation, polymerization, decomposition, and cyclization. This process gradually deepens the color of ginseng and imparts a characteristic aroma. The conversion of secondary saponins during black ginseng processing may be closely related to the MR. Some studies have reported that the products generated by the MR in ginseng have strong free-radical-scavenging activity (Park et al., 2018). However, the structure and formation mechanism of melanoidins remain unclear. Bruhns et al. (2019) suggested that the ratio of carbohydrates to amino acids required for melanoidin synthesis could be inferred from the carbon-to-nitrogen ratio in the final product. Experimental evidence suggests that eliminating water molecules leads to the rearrangement of fragments containing unsaturated portions, resulting in the formation of a chromophore system and, ultimately, melanoidin production, changing the product's color.

A total of 879 genes were identified by comparing the genetic changes in cells exposed to ginseng extracts before and after steaming at three concentrations, using gene chip technology (Gao et al., 2023). The differential genes identified were used to construct a relationship matrix using the correlation algorithm proposed by Erskine. Relationships with $|r| > 0.7$ and $P < 0.05$ were selected to construct the gene co-expression network. Subsequently, the multilevel algorithm was applied to divide the gene modules, resulting in seven modules.

Most of the GO enrichment results were related to the BP pathway. Compared to cells exposed to fresh ginseng, the differential genes detected in cells exposed to black ginseng are more effective in regulating cell adhesion and promoting biological pathways such as signaling, cancer metastasis, and immune responses. Furthermore, the gene enrichment results in the fifth module indicate that these genes may be involved in the cellular response to metal ions such as copper, zinc, and cadmium. The cellular response to metal ions influences cellular autophagy, where the cell maintains stability by clearing deformed proteins or senescent dead cells. For example, high zinc ion concentrations promote the formation of autophagic vesicles in alcohol-induced hepatocellular carcinoma cells and are associated with dopamine-induced autophagy in PC12 cells (Hung et al., 2013). Zinc ions also promote autophagosome formation in triamcinolone acetonide-induced breast cancer cells. Similarly, in mouse macrophages, zinc ion deficiency activates caspase-1 to promote apoptosis (Summersgill et al., 2014). Thus, black ginseng powder may enhance the cellular response to metal ions and, thereby, induce cellular autophagy. This could be useful for developing new drugs for neurological diseases, tumors, and related diseases.

The KEGG results revealed that the differential genes identified after ginseng and black ginseng administration were mostly present in the TNF, IL-17, MAPK, and PI3K-Akt signaling pathways, all of which are closely related to inflammation (Liu X. et al., 2022; Zhang et al., 2022; Yang S. et al., 2020), apoptosis (Liu T. et al., 2022), immune responses, and other physiological processes. These findings align with the changes in the components during black ginseng processing. For example, the secondary saponin Rg5—produced during black ginseng processing—induces apoptosis and autophagy by inhibiting the PI3K-Akt signaling pathway and may become a promising anti-tumor drug against breast cancer (Yang D. et al., 2020; Yang S-H. et al., 2023). Lee

et al. (2019) confirmed that black ginseng inhibited the pro-inflammatory mediators iNOS and COX-2 and the pro-inflammatory cytokines IL1β, IL-6, and TNF-α. Protein expression was determined using protein blotting, which confirmed that black ginseng exhibited stronger anti-inflammatory effects compared to fresh ginseng.

The PageRank algorithm was used to calculate the importance of each gene in the protein interaction network. As a result, 10 hub genes were selected for each module, with a total of 70 key genes. Most of these genes are related to tumors and immune and neurological diseases. Some of them may serve as new therapeutic targets, providing innovative ideas for clinical applications.

5 Conclusion

This study investigated the changes in the chemical composition and pharmacological effects of black ginseng during processing. The relationship among the compositional changes of ginsenosides (the main active components in ginseng), the substrates of the Maillard reaction (MR; reducing sugars and amino acids), and the melanoidins generated was analyzed. Chromaticity measurements were performed to determine the changes in the color of black ginseng during the reaction. A higher proportion of rare saponins in the system correlates with a lower amino acid content and a higher melanoidin content. High-performance liquid chromatography-mass spectrometry (HPLC-MS) was used to identify the ginsenosides, sugars, and amino acids in the samples and determine the changes in the chemical composition during processing. The goal was to provide a basis for a more comprehensive study of the chemical composition during black ginseng processing and melanoidin formation.

In addition, differential gene analysis and GO and KEGG enrichment analyses of cells exposed to fresh ginseng and black ginseng extracts were conducted using gene chip technology and transcriptomics. We found that black ginseng regulates the proliferation and differentiation of immune-related cells and positively regulates cell adhesion, suggesting broader prospects in treating neurological diseases and tumors as well as immunotherapy. This study is a preliminary exploration of the differences between the pharmacological mechanisms of black ginseng and fresh ginseng, aiming to provide data for in-depth research into their potential mechanisms.

Data availability statement

The original contributions presented in the study are included in the article/supplementary material, further inquiries can be directed to the corresponding author.

Author contributions

YQ: Conceptualization, Writing–original draft, Writing–review and editing. MW: Writing–original draft. ZY: Validation, Writing–review and editing. XG: Data curation, Writing–review and editing. MY: Conceptualization, Supervision, Writing–review and editing.

Funding

The author(s) declare that no financial support was received for the research, authorship, and/or publication of this article.

Conflict of interest

The authors declare that the research was conducted in the absence of any commercial or financial relationships that could be construed as a potential conflict of interest.

Publisher's note

References

Ahuja, A., Kim, J. H., Kim, J.-H., Yi, Y.-S., and Cho, J. Y. (2018). Functional role of ginseng-derived compounds in cancer. *J. Ginseng Res.* 42, 248–254. doi:10.1016/j.jgr.2017.04.009

Bruhns, P., Kanzler, C., Degenhardt, A. G., Koch, T. J., and Kroh, L. W. (2019). Basic structure of melanoidins formed in the Maillard reaction of 3-deoxyglucosone and γ-aminobutyric acid. *J. Agric. Food Chem.* 67, 5197–5203. doi:10.1021/acs.jafc.9b00202

Chen, J. (2023). Essential role of medicine and food homology in health and wellness. *Chin. Herb. Med.* 15, 347–348. doi:10.1016/j.chmed.2023.05.001

Chen, W., Balan, P., and Popovich, D. G. (2021). The effects of New Zealand grown ginseng fractions on cytokine production from human monocytic THP-1 cells. *Molecules* 26, 1158. doi:10.3390/molecules26041158

Choi, W. Y., Lee, G., Kwon, D. S., Shin, H. J., and Cho, Y. (2021). Black ginseng extract attenuates TNF-α-induced inflammation via downregulation of NF-κB signaling in human keratinocytes. *J. Korean Soc. Food Sci. Nutr.* 50, 1030–1039. doi:10.3746/jkfn.2021.50.10.1030

Choudhry, Q. N., Kim, J. H., Cho, H. T., Heo, W., Lee, J. J., Lee, J. H., et al. (2019). Ameliorative effect of black ginseng extract against oxidative stress-induced cellular damages in mouse hepatocytes. *J. Ginseng Res.* 43, 179–185. doi:10.1016/j.jgr.2017.10.003

Gao, M., Huo, X., Lu, L., Liu, M., and Zhang, G. (2023). Analysis of codon usage patterns in *Bupleurum falcatum* chloroplast genome. *Chin. Herb. Med.* 15, 284–290. doi:10.1016/j.chmed.2022.08.007

Heinrich, M., Yao, R., and Xiao, P. (2022). Food and medicine continuum' - why we should promote cross-cultural communication between the global East and West. *Chin. Herb. Med.* 14, 3–4. doi:10.1016/j.chmed.2021.12.002

Hung, H.-H., Huang, W.-P., and Pan, C.-Y. (2013). Dopamine- and zinc-induced autophagosome formation facilitates PC12 cell survival. *Cell Biol. Toxicol.* 29, 415–429. doi:10.1007/s10565-013-9261-2

Hussain, F., Akram, A., Hafeez, J., and Shahid, M. (2021). Biofunctional characterization of red, black and white ginseng (*Panax ginseng* Meyer) root extracts. *Rev. Mex. De. Ing. Quimica* 20, 175–186. doi:10.24275/rmiq/bio1735

Kim, E.-H., Kim, S.-W., Park, S.-J., Kim, S., Yu, K.-M., Kim, S. G., et al. (2019). Greater efficacy of black ginseng (CJ EnerG) over red ginseng against lethal influenza A virus infection. *Nutrients* 11, 1879. doi:10.3390/nu11081879

Kim, Y. J., Lee, D. Y., Park, H.-E., Yoon, D., Lee, B., Kim, J. G., et al. (2020). Serum metabolic profiling reveals potential anti-inflammatory effects of the intake of black ginseng extracts in beagle dogs. *Molecules* 25, 3759. doi:10.3390/molecules25163759

Lee, D.-K., Park, S., Nguyen Phuoc, L., Min, J. E., Kim, H. M., Yang, E., et al. (2020). Research quality-based multivariate modeling for comparison of the pharmacological effects of black and red ginseng. *Nutrients* 12, 2590. doi:10.3390/nu12092590

Lee, Y. Y., Saba, E., Irfan, M., Kim, M., Chan, J. Y., Jeon, B. S., et al. (2019). The anti-inflammatory and anti-nociceptive effects of Korean black ginseng. *Phytomedicine* 54, 169–181. doi:10.1016/j.phymed.2018.09.186

Li, H., Chen, C., Li, Z.-M., Yang, Y., Xing, C.-Q., Li, Y., et al. (2020). Specific interaction with human serum albumin reduces ginsenoside cytotoxicity in human umbilical vein endothelial cells. *Front. Pharmacol.* 11, 498. doi:10.3389/fphar.2020.00498

Liu, T., Li, Q., Xu, X., Li, G., Tian, C., and Zhang, T. (2022b). Molecular mechanisms of anti-cancer bioactivities of seaweed polysaccharides. *Chin. Herb. Med.* 14, 528–534. doi:10.1016/j.chmed.2022.02.003

Liu, X., Wang, S., Li, J., Zhang, J., and Liu, D. (2022a). Regulatory effect of traditional Chinese medicines on signaling pathways of process from chronic atrophic gastritis to gastric cancer. *Chin. Herb. Med.* 14, 5–19. doi:10.1016/j.chmed.2021.10.008

Liu, Y., Li, G., Ning, J., and Zhao, Y. (2024). Unveiling the experimental proof of the anticancer potential of ginsenoside Rg3 (Review). *Oncol. Lett.* 27, 182. doi:10.3892/ol.2024.14315

Park, C. H., Choi, J. S., and Yokozawa, T. (2018). Increase in the hydroxyl radical-scavenging activity of *Panax ginseng* and ginsenosides by heat-processing. *Drug Discov. and Ther.* 12, 114–121. doi:10.5582/ddt.2018.01010

Qing, Y., Ning, C., Dao-Biao, C., and Xin, J. (2020). Effect of ginsenoside Rg_3 nanostructured lipid carrier modified by pullulan on promoting absorption and its anti-tumor evaluation *in vitro*. *Zhongguo Zhong yao za zhi = Zhongguo zhongyao zazhi = China J. Chin. Materia Medica* 45, 5184–5192. doi:10.19540/j.cnki.cjcmm.20200819.304

Summersgill, H., England, H., Lopez-Castejon, G., Lawrence, C. B., Luheshi, N. M., Pahle, J., et al. (2014). Zinc depletion regulates the processing and secretion of IL-1β. *Cell Death and Dis.* 5, e1040. doi:10.1038/cddis.2013.547

Sun, S., Qi, L.-W., Du, G.-J., Mehendale, S. R., Wang, C.-Z., and Yuan, C.-S. (2011). Red notoginseng higher ginsenoside content and stronger anticancer potential than Asian and American ginseng. *Food Chem.* 125, 1299–1305. doi:10.1016/j.foodchem.2010.10.049

van Boekel, M. (2006). Formation of flavour compounds in the Maillard reaction. *Biotechnol. Adv.* 24, 230–233. doi:10.1016/j.biotechadv.2005.11.004

Wang, J.-H., Wang, D., Li, W.-X., Huang, Y., Dai, Z.-B., and Zhang, X.-L. (2019). Optimization of UDP-glucose supply module and production of ginsenoside F1 in *Saccharomyces cerevisiae*. *Zhongguo Zhong yao za zhi = Zhongguo zhongyao zazhi = China J. Chin. Materia Medica* 44, 4596–4604. doi:10.19540/j.cnki.cjcmm.20190829.101

Wang, Z., Liu, R., Chen, L., Wang, H., Zhou, M., Wang, Y., et al. (2021). Pharmacokinetics of ginsenoside Rh2, the major anticancer ingredient of ginsenoside H dripping pills, in healthy subjects. *Clin. Pharmacol. Drug Dev.* 10, 669–674. doi:10.1002/cpdd.877

Wu, L., Bai, L., Dai, W., Wu, Y., Xi, P., Zheng, L., et al. (2024). Ginsenoside Rg3: a review of its anticancer mechanisms and potential therapeutic applications. *Curr. Top. Med. Chem.* 24, 869–884. doi:10.2174/0115680266283661240226052054

Wu, Y., Duan, Z., Qu, L., Zhang, Y., Zhu, C., and Fan, D. (2023). Gastroprotective effects of ginsenoside Rh4 against ethanol-induced gastric mucosal injury by inhibiting the MAPK/NF-κB signaling pathway. *Food and Funct.* 14, 5167–5181. doi:10.1039/d2fo03693b

Xu, H.-L., Chen, G.-H., Wu, Y.-T., Xie, L.-P., Tan, Z.-B., Liu, B., et al. (2022). Ginsenoside Ro, an oleanolic saponin of *Panax ginseng*, exerts anti-inflammatory effect by direct inhibiting toll like receptor 4 signaling pathway. *J. Ginseng Res.* 46, 315–319. doi:10.1016/j.jgr.2022.02.007

Yang, D., Li, X., and Zhang, X. (2020a). Ginsenoside Rh2 induces DNA damage and autophagy in vestibular schwannoma is dependent of LAMP2 transcriptional suppression. *Biochem. Biophysical Res. Commun.* 522, 300–307. doi:10.1016/j.bbrc.2019.11.026

Yang, S., Zhang, J., Yan, Y., Yang, M., Li, C., Li, J., et al. (2020b). Network pharmacology-based strategy to investigate the pharmacologic mechanisms of *Atractylodes macrocephala* Koidz. for the treatment of chronic gastritis. *Front. Pharmacol.* 10, 1629. doi:10.3389/fphar.2019.01629

Yang, S.-H., Tao, G., Yang, L., Wu, X., Liu, J.-W., Dagher, F., et al. (2023a). Dietary phytochemical and metabolic disease prevention: focus on plant proteins. *Front. Nutr.* 10, 1089487. doi:10.3389/fnut.2023.1089487

Yang, S.-H., Zhu, J., Wu, W.-T., Li, J.-M., Tong, H.-L., Huang, Y., et al. (2023b). Rhizoma Atractylodis Macrocephalae-Assessing the influence of herbal processing methods and improved effects on functional dyspepsia. *Front. Pharmacol.* 14, 1236656. doi:10.3389/fphar.2023.1236656

Zhang, H., Li, Z., Zhou, Z., Yang, H., Zhong, Z., and Lou, C. (2016). Antidepressant-like effects of ginsenosides: a comparison of ginsenoside Rb_3 and its four deglycosylated derivatives, Rg_3, Rh_2, compound K, and 20(*S*)-protopanaxadiol in mice models of despair. *Pharmacol. Biochem. Behav.* 140, 17–26. doi:10.1016/j.pbb.2015.10.018

Zhang, H., Park, S., Huang, H., Kim, E., Yi, J., Choi, S.-K., et al. (2021). Anticancer effects and potential mechanisms of ginsenoside Rh2 in various cancer types (Review). *Oncol. Rep.* 45, 33. doi:10.3892/or.2021.7984

Zhang, W., Cui, N., Ye, J., Yang, B., Sun, Y., and Kuang, H. (2022). Curcumin's prevention of inflammation-driven early gastric cancer and its molecular mechanism. *Chin. Herb. Med.* 14, 244–253. doi:10.1016/j.chmed.2021.11.003

Zhang, W.-Y., Liu, F.-G., and Zheng, Y.-N. (2019). Synthesis and anti-tumor activity of ginsenoside Rh_2 caprylic acid monoester. *Zhongguo Zhong yao za zhi = Zhongguo zhongyao zazhi = China J. Chin. Materia Medica* 44, 3758–3762. doi:10.19540/j.cnki.cjcmm.20190508.201

Zhang, Y., Zhong, X., Xi, Z., Li, Y., and Xu, H. (2023). Antiviral potential of the genus *Panax*: an updated review on their effects and underlying mechanism of action. *J. Ginseng Res.* 47, 183–192. doi:10.1016/j.jgr.2022.11.003

Zheng, S.-w., Xiao, S.-y., Wang, J., Hou, W., and Wang, Y.-p. (2019). Inhibitory effects of ginsenoside Ro on the growth of B16F10 melanoma via its metabolites. *Molecules* 24, 2985. doi:10.3390/molecules24162985

frontiers | Frontiers in Pharmacology

TYPE Original Research
PUBLISHED 09 December 2024
DOI 10.3389/fphar.2024.1489777

OPEN ACCESS

EDITED BY
Lingyun Zhong,
Jiangxi University of Traditional Chinese Medicine, China

REVIEWED BY
Junfeng Niu,
Shaanxi Normal University, China
Jianfeng Han,
Xi'an Jiaotong University, China
Lina Ji,
Zhejiang Chinese Medical University, China

*CORRESPONDENCE
Yang Liu,
liuyang3111111@163.com

†These authors have contributed equally to this work

RECEIVED 01 September 2024
ACCEPTED 25 November 2024
PUBLISHED 09 December 2024

CITATION
Zhang X, Jiang S, Sun T, Zhi W, Ding K, Qiao Z, Zhang H, Li Y and Liu Y (2024) Post-harvest processing methods have critical roles on the contents of active metabolites and pharmacological effects of *Astragali Radix*. *Front. Pharmacol.* 15:1489777. doi: 10.3389/fphar.2024.1489777

Post-harvest processing methods have critical roles on the contents of active metabolites and pharmacological effects of *Astragali Radix*

Xiaoyan Zhang[1†], Shengnan Jiang[1†], Tingting Sun[1], Wenbing Zhi[1], Kairu Ding[2], Ziyao Qiao[2], Hong Zhang[1,2], Ye Li[1] and Yang Liu[1,2*]

[1]Institute of Chinese Medicine, Shaanxi Academy of Traditional Chinese Medicine (Shaanxi Traditional Chinese Medicine Hospital), Xi'an, China, [2]College of Life Sciences, Northwest University, Xi'an, China

Background: Processing methods of traditional Chinese medicinal materials are critical in influencing the active metabolites and pharmacological effects. The fresh processing method effectively prevents the loss and degradation of metabolites, common in traditional drying and softening processes, while also reducing production costs. *Astragali Radix* (AR), a leguminous botanical drug, is widely utilized in clinical practice and functional foods. Therefore, optimizing its the post-harvest processing method is crucial for enhancing production and application.

Methods: AR samples were processed using different methods with varying moisture content, including unpretreated samples and those subjected to kneading and sweating treatments. These samples were evaluated for physical appearance and active metabolite content. The entropy weight method, combined with the technique for order preference by similarity to ideal solution (TOPSIS), was employed to optimize the fresh processing method. A comparative study between freshly processed AR (AR-F) and traditionally processed AR (AR-T) assessed active metabolites, pharmacological effects and mechanisms.

Results: The appearance and active metabolites content of AR samples were affected by moisture content, kneading, and sweating treatments. After these treatments, the content of polysaccharides and calycosin-7-O-glucoside increased compared to unpretreated samples at the same moisture level. Entropy weight-TOPSIS analysis showed that the sample with 35% moisture, 100 kneading cycles, and 12 h of sweating had the highest score. Comparative studies revealed that AR-F had significantly higher content of total polysaccharides, total flavonoids, and calycosin-7-O-glucoside compared to AR-T, along with an increased flavonoid glycoside/aglycone ratio. However, no significant differences were observed in the total saponins and their metabolites. Pharmacological studies demonstrated that total flavonoids in AR-F exhibited superior macrophage RAW264.7 activation, compared to AR-T. Furthermore, we confirmed that the enhanced immunomodulatory capacity of AR-F was linked to its ability to stimulate the release of TNF, SRC, ER-α, AKT, HSP90, and Caspase-3 in RAW264.7 cells.

Conclusion: Our study optimized the fresh processing method of AR, and conducted a systematic comparative analysis between fresh and traditional processing samples, providing a basis for post-harvest processing in the AR production areas.

KEYWORDS

Astragali Radix, fresh processing, traditional processing, active metabolites, pharmacological effects

1 Introduction

The processing of traditional Chinese medicinal materials is a crucial aspect of Traditional Chinese Medicine (TCM) theory, significantly influencing their chemical composition and pharmacological activity. The fresh processing method involves cleaning freshly harvested medicinal materials, cutting them into slices, segments, blocks, or sections, and then drying them. This approach aligns with the concept of fresh processing recorded in "Leigong's Pharmacopoeia" from the Northern and Southern Dynasties (Yang et al., 2016). In contrast to traditional processing methods, which require drying and soaking before cutting, fresh processing methods eliminate these steps. This effectively saves time and prevents the loss of volatile, water-soluble, enzyme-active, and heat-sensitive metabolites. Additionally, this method reduces the risk of quality non-conformance and lowers production costs. Studies have shown that fresh-cut processing results in different chemical profiles compared to traditional methods. For example, the total saponin and ginsenoside content in freeze-dried *Panax notoginseng* slices processed using fresh-cut methods increased by 16.5% and 22.5%, respectively, compared to traditional methods (Liu et al., 2019). Similarly, the contents of cinnamaldehyde, cinnamic acid, essential oil, and extractives in fresh-cut cinnamon slices were higher than those in traditionally processed slices (Luo et al., 2017). Differences in effective metabolite content can lead to changes in pharmacological activity. For instance, fresh-cut *Cortex phellodendri* slices demonstrated enhanced antipyretic effects in heat syndrome rats and greater anti-inflammatory effects in acute bacterial peritonitis rats compared to traditional slices. Additionally, at the same dosage, fresh-cut *Sophora* flavescens slices showed a significantly higher inhibition rate of ear swelling in mice induced by xylene compared to traditional slices (Chen et al., 2022a). These studies suggest that fresh processing may enhance efficacy through better metabolite retention, potentially reducing the required dosage to achieve the same therapeutic effects, thereby minimizing side effects and safety risks, which is of significant clinical importance.

Astragali Radix (AR), a leguminous botanical drug, encompasses both *Astragalus membranaceus* (Fisch) Bge. var. mongholicus (Bge.) Hsiao and *Astragalus membranaceus* (Fisch) Bge (China, 2020). The roots of this plant are revered as a supreme tonic for Qi and are widely used in TCM formulations and preparations. Known for their efficacy in treating tumors, enhancing immunity, and addressing pulmonary diseases, they are also commonly included in dietary supplements due to their anti-aging, antioxidant, hypoglycemic, and antihypertensive effects (Zhang et al., 2021). Research has identified polysaccharides, saponins, and flavonoids as the three primary active metabolites contributing to AR's pharmacological effects (Liu et al., 2024). Among these, polysaccharides are present in significantly higher amounts, ranging from 5% to 20%, compared to saponins (0.5%–3%) and flavonoids (0.1%–1%) (Li et al., 2022; Li et al., 2020). Notably, the Chinese Pharmacopoeia only includes the saponin Astragaloside IV and the flavonoid calycosin-7-O-glucoside as quality control markers for AR. The traditional processing steps for AR slices involve removing impurities, washing, drying, moistening, slicing, and drying again, which adds complexity to the process. During the "moistening" phase, polysaccharides and other glycosides, due to their high water solubility, may lose metabolites, potentially affecting their efficacy.

Therefore, optimizing the moisture content during fresh processing is crucial for preserving active metabolites, ensuring quality, and improving processing efficiency (Zhang et al., 2023; Yao et al., 2024). Kneading and sweating are traditional processing methods used in TCM, which has been observed that fresh roots subjected to these repeated compressions and heating conditions become more flexible and smooth, reducing microbial growth and facilitating slicing and storage. This process also fosters biochemical and chemical transformations within the material, enhancing its efficacy (Wu et al., 2021). Modern processing trends emphasize integrating processing at the production site, allowing AR to be directly sliced without the cumbersome steps of drying and moistening, resulting in more stable and standardized quality. However, the complexity of the material, the diversity of evaluation criteria, and differences in analytical methods often complicate efforts to establish a universally recognized "optimal" processing method.

Our study aims to systematically investigate the fresh processing of AR, focusing on the impact of moisture content, kneading, and sweating on quality. Indicators such as physical appearance, extractives, total polysaccharides, Astragaloside IV, and calycosin-7-O-glucoside have been evaluated. The entropy weight method combined with TOPSIS analysis was employed to determine the optimal processing conditions. Additionally, a comparative study was conducted on fresh and traditional processing AR in terms of total polysaccharides, total saponins, total flavonoids, and the content of four saponin and eight flavonoid metabolites. Furthermore, we focused on the flavonoid content differences between AR-T and AR-F, and clarified the immune-regulatory activity and mechanism of AR-F and AR-T through network pharmacology, molecular docking and *in vitro* cell experiments. This research provided a basis for the post-harvest processing in the producing area of AR.

2 Materials and methods

2.1 Materials

The fresh roots of AR were harvested from Guangji Hall Pharmaceutical Group Co., Ltd. In Shaanxi Province and

TABLE 1 Scoring criteria for the appearance of fresh-processed AR.

Evaluation indicator	Criteria	Score
Texture	Very brittle (difficult to slice)	0
	Slightly soft (easier to slice)	0.5
	Bendable without breaking (easy to slice)	1
Slicing continuity	Many continuous slices	0
	Few continuous slices	0.5
	No continuous slices	1
Color	Cut surface: pale white; Wood: pale white	0
	Cut surface: pale yellow-white; Wood: pale white	0.5
	Cut surface: yellow-white; Wood: light yellow	1
Proportion of curled slices	Many curled slices (≥20%)	0
	Few curled slices (10%–20%)	0.5
	Very few curled slices (≤10%)	1
Proportion of fragments	Many fragments (≥20%)	0
	Few fragments (10%–20%)	0.5
	Very few fragments (≤10%)	1

identified by researcher Hong Zhong from the Shaanxi Academy of Traditional Chinese Medicine. Standard reference materials, including Astragaloside IV, I, II, III, calycosin-7-O-glucoside, calycosin, mangiferin, mangiferin aglycone, and astragaloside A, B, C, and D, were purchased from Manster Technology Co., Ltd. (Chengdu, China), with purities exceeding 98%. The ABTS total antioxidant capacity assay kit (A015-2-1) was obtained from Nanjing Jiancheng Bioengineering Institute. 1,1-Diphenyl-2-picrylhydrazyl (DPPH, D861666) and p-nitrophenyl-α-D-glucopyranoside (PNPG, N814753) were purchased from Macklin (Shanghai, China), while α-glucosidase (S10050) was obtained from Shanghai Yuan Ye Bio-Technology Co., Ltd. Lipopolysaccharide (LPS, L2880) was acquired from Solarbio (Beijing, China). Nitric oxide (NO) assay kits were provided by Biyuntian Co., Ltd. (Shanghai, China). Chromatographic grade acetonitrile and formic acid were purchased from Thermo Fisher Scientific (United States). All other chemicals and reagents used were of analytical grade. TNF, SRC, ESR1, EGFR, AKT1, HSP90AA1 and CASP3 ELISA kit were obtained from FineTest (Wuhan, China).

2.2 Optimization of fresh processing method of AR

2.2.1 Sample preparation

Fresh Astragalus roots, free from damage, rot, or black spots, and of uniform size (approximately 1.0–1.2 cm in diameter and 3.5 cm below the top cut of the root) were selected. The roots were cleaned to remove soil and root hairs, then divided into 12 groups, each weighing 5 kg and consisting of three replicates. Six groups were dried at 40°C to achieve different moisture levels (X1: 55%; X2: 45%; X3: 40%; X4: 35%; X5: 25%; X6: 15%), then cut into 4 mm thick slices and further dried at 40°C until the moisture content fell below 10.0%. The other six groups were similarly dried at 40°C to different moisture levels (Y1: 55%; Y2: 45%; Y3: 40%; Y4: 35%; Y5: 25%; Y6: 15%), then kneaded 100 times, sealed, and allowed to rest for 12 h. The samples were then cut into 4 mm thick slices and dried again at 40°C until the moisture content was below 10.0%. All procedures were repeated three times to ensure consistency.

2.2.2 Appearance and scoring

The appearance of the samples was evaluated according to the Chinese Pharmacopoeia (2020). To comprehensively assess the quality of the samples, factors such as texture, slicing continuity, color, proportion of curled slices, and proportion of fragments were considered, with scoring criteria outlined in Table 1.

2.2.3 Determination of moisture, total ash, and water-soluble extract

The moisture, total ash and water-soluble extract content were assessed using methods 08323, 2,302, and 2,201 respectively, from the Chinese Pharmacopeia 2020 edition (China, 2020).

2.2.4 Determination of total polysaccharides, astragaloside IV, and isoflavone glycoside

Total polysaccharides were measured using the phenol-sulfuric acid method (Jiang et al., 2016). Astragaloside IV and Isoflavone glycoside were quantified according to the methods from the Chinese Pharmacopoeia 2020 edition (China, 2020).

2.2.5 Entropy Weight-TOPSIS analysis

The entropy weight method is an objective weighting approach that constructs a judgment matrix for each evaluation index to derive the entropy of each index. The entropy weight is determined based on these entropy values; lower information entropy indicates a higher degree of dispersion for the index and, consequently, a higher

weight. The TOPSIS method addresses multi-criteria evaluation and ranking problems by first calculating the index weights using the entropy weight method, and then identifying the best and worst solution vectors. The Euclidean distance measures the distance between each evaluation index and the positive ideal solution (D^+) or negative ideal solution (D^-). Comprehensive scores (C_i) are calculated based on these distances, ranking the samples to assess the quality of each AR fresh-cut processing method (Xu et al., 2022; Zhou et al., 2017; Wang et al., 2019; Shin et al., 2007).

2.3 Comparison of active metabolites content between AR-F and AR-T

2.3.1 Sample preparation

Fresh Astragalus roots, free from damage, rot, or black spots, and of uniform size, were selected and cleaned. The roots were divided into two groups, each weighing 10 kg and consisting of three replicates. For the fresh-cut method, the processing involved drying the fresh AR roots at 40°C until the moisture content reached 35%, followed by kneading 100 times, sealing, and piling for 12 h, and then slicing to produce AR-F. AR-T was processed adhered to the preparation guidelines outlined in the 2020 edition of the Chinese Pharmacopoeia for Astragalus, which included specific traditional methods such as steaming under atmospheric pressure for 5 min, as determined through preliminary trials.

2.3.2 Determination of total polysaccharides, total saponins, and total flavonoids

Total polysaccharides were measured using the phenol-sulfuric acid method (Jiang et al., 2016), while total saponins were assessed using the vanillin-ice acetic acid-perchloric acid method (Li et al., 2021). Specifically, 0.5 g of AR powder was mixed with 25 mL methanol and refluxed for 1 h. After filtering, methanol was recovered under reduced pressure. The residue was subsequently extracted with 25 mL water-saturated butanol in three portions, which was then reduced to dryness. The resulting residue was dissolved in methanol, and a portion was derivatized with vanillin-ice acetic acid and perchloric acid before measuring absorbance at 539 nm. Astragaloside IV served as the reference for calculating total saponin content. Total flavonoids were measured using the method outlined in the Chinese Pharmacopoeia (2020 edition). Sample preparation involved extraction with ethanol, followed by measurement at 280 nm using HPLC-DAD.

2.3.3 Monosaccharide composition analysis

Monosaccharide composition was analyzed through acid hydrolysis, acetylation, and GC methods. Initially, 15 g of AR powder was extracted with 300 mL of water at 90°C for 4 h, after which the supernatant was concentrated. Proteins were subsequently removed using enzyme and trichloroacetic acid methods, resulting in crude polysaccharides that were obtained by precipitation with ethanol. Each polysaccharide samples (5 mg) underwent hydrolysis with trifluoroacetic acid, followed by acetylation and reduction. Mixed standard samples of fucose, rhamnose, arabinose, xylose, mannose, glucose, galactose, glucuronic acid, and galacturonic acid were prepared similarly. The analysis was performed using GC under the following conditions: Rtx-50 column, a temperature gradient from 180°C to 240°C, with detection via FID.

2.3.4 Determination of saponin content

4.0 g of AR powder was extracted with 40 mL of methanol through two refluxing sessions. The filtrate was then concentrated and dissolved in water, followed by extraction with water-saturated butanol. After concentrating the butanol layer, the residue was dissolved in methanol. Saponin content was subsequently analyzed using HPLC-ELSD, utilizing an Agilent ZORBAX SB-Aq column with gradient elution using acetonitrile and water at specific detector temperatures.

2.3.5 Determination of flavonoid content

Flavonoid content was quantified using HPLC-DAD, following the sample preparation guidelines from the Chinese Pharmacopoeia (2020 edition) for isoflavone glycosides. The analysis was conducted on an Agilent ZORBAX SB-Aq column with gradient elution, measuring detection at 230 nm and 260 nm.

2.4 Pharmacological effect mechanism of AR-F and AR-T

2.4.1 Targets prediction of differential metabolites

Based on a previous study, we obtained the differentiated metabolites of AR-F and AR-T, and screened the potential metabolites using the Swiss ADME database. The metabolites were selected by applying the condition of at least two "yes" responses for Druglikeness. The 3D structures of the metabolites that met this criterion were then imported into the SwissTargetPrediction database, where potential targets were identified with a probability greater than 0.1.

2.4.2 Construction of the PPI network and identification of core targets

The potential targets were imported into the STRING database with the species set to human and the confidence level set to the highest. The protein interaction network was obtained by excluding isolated proteins, and the data were imported into Cytoscape 3.7.2 to construct the PPI network. Topological analysis was performed based on node degree, closeness, and betweenness. Targets with lower degrees were excluded, and the core targets were identified using the CentiScape plugin, selecting those with degree, closeness, and betweenness values greater than the median.

2.4.3 Enrichment analyses using GO and reactome databases

Core targets were subjected to GO and Reactome enrichment analyses using the DAVID. The enrichment results were then visualized through an online bioinformatics mapping platform and presented as a bubble chart.

2.4.4 Molecular docking analysis

The human protein structure files of the top seven core targets in the PPI network were downloaded from the PDB database. The 3D structures of the target-interacting metabolites were retrieved from

the PubChem database. The proteins were pre-treated by dehydration and hydrogenation using PyMol. Molecular docking between the ligand molecules and the proteins was calculated using AutoDock 1.5.7 software.

2.4.5 Extraction and purification of total flavonoids of AR (TFA)

Briefly, the dried slices of AR-F and AR-T were macerated in 95% ethanol and then extracted. The ethanol extraction was repeated 3–4 times and the pooled extract then was concentrated to a specific gravity of 1.35 by evaporation. The concentrated solution was extracted with ethyl acetate. The concentrated ethyl acetate extract was further separated by silica gel columns. The main chemical components of the purity of TFA exceeded 90%.

2.4.6 Immunomodulatory effects

2.4.6.1 Cell culture and viability assay

RAW264.7 mouse macrophage cells were purchased from ACTT Chinese Cell Resource Bank and cultured in high-glucose DMEM with 10% fetal bovine serum at 37°C with 5% CO_2. Cell viability was measured using the MTT assay. The cells were seeded in a 96-well plate at a density of 1×10^4 cells/well, and the supernatant was discarded after the cells adhered to the wall; 100 μL of DMEM culture medium containing different crude drug concentrations (32.5~1,000 μg/mL) of TFA was added, with DMEM culture medium as the blank control, and 6 replicate wells were set for each concentration. After incubation for 24 h, MTT (5 mg/mL) was added and incubated for 4 h, DMSO was added to dissolve the formazan crystals in the cells, and the absorbance was measured at 490 nm.

2.4.6.2 NO content measurement

The cells were seeded in a 96-well plate at a density of 1×10^4 cells/well. After cell adhesion, the supernatant was discarded, and 100 μL of DMEM culture medium containing different concentrations (32.5–125 μg/mL) of TFA was added, with DMEM culture medium as the blank control and LPS (1 μg/mL) as a positive control. Six replicate wells were established for each concentration. After 24 h of incubation, the cell supernatants were collected, and NO release was measured using the Griess method.

2.4.7 Enzyme-linked immunosorbent assay

Cells in the logarithmic growth phase were cultured. The blank control group received DMEM high glucose complete medium, the drug administration groups were treated with TFA at concentrations of 31.25, 62.5 and 125 μg/mL, and the positive control group received 10 μg/mL LPS solution. After 24 h of incubation, cell supernatants were collected, and ELISA was performed to measure TNF, SRC, and ESR1 expression. Cells were inoculated into 12-well plates, and after culturing, proteins were extracted via repeated freeze-thawing in liquid nitrogen. AKT1, CASP3, and HSP90AA1 expression in cells was also detected by ELISA (Saddiq et al., 2022).

2.5 Statistical analysis

Data are presented as mean ± standard deviation. For analytical and cell experiments, averages were based on three and six independent replicates, respectively. Statistical analysis was performed using GraphPad Prism 10 (San Diego, CA, United States).

3 Results

3.1 Optimization of fresh processing method of AR

3.1.1 Appearance of samples

The appearance of samples prepared using different methods is shown in Figure 1. When the moisture content of the material was between 45% and 55%, samples X1-X3 and Y1-Y3 often exhibited curled and peeling epidermis, separation of the bark and wood parts, and higher rates of warping and breakage. As the moisture content decreases to between 35% and 25%, these issues improved, resulting in fewer instances of warping and breakage. However, when the moisture content dropped further to 15%, samples X6 and Y6 became hardened and brittle at the ends, leading to fragmentation and affecting the yield of the medicinal slices. The kneading and sweating pretreatment had a noticeable impact on the appearance of the samples. Samples Y1-Y6, which were kneaded and sweated before cutting, showed significant improvements compared to samples X1-X6 which were cut directly. The pretreatment reduced bark-wood separation, resulting in more compact and dense slices with fewer instances of warping and breakage. Color is also a significant quality indicator for medicinal materials. According to pharmacopoeia standards, the cut surface of samples should exhibit a distinct color contrast between the yellowish wood part and the white bark, forming the characteristic “golden well and jade rail”. As shown in Figure 1, samples X1-X3 and Y1-Y3 had a lighter wood color, resulting in a less pronounced contrast with the bark. In contrast, samples X4-X6 and Y4-Y6 exhibited increasingly darker wood colors, better displaying the “golden well and jade rail” feature. Based on the scoring criteria in Table 1, the appearance of the 12 fresh-cut processing methods was evaluated (Figure 2A). Samples Y4 and Y5 received the highest appearance scores of 5 points. Across all moisture levels, the appearance scores of the pretreated group were consistently higher than those of the unpretreated group.

3.1.2 Content of moisture, total ash, and water-soluble extract in samples

The moisture, total ash, and water-soluble extract content of samples are shown in Figure 2B-D. All groups met the pharmacopoeia standard for moisture content (not exceeding 10.0%). However, Sample X1 had the highest total ash content, exceeding the pharmacopoeia limit of 5.0%, followed by X3, which was also significantly higher than Y4-Y6. Regarding water-soluble extract content, all groups met the pharmacopoeia standard (not less than 17.0%). Samples Y5 and Y6 had the highest water-soluble extract content, measuring 37.03% ± 1.72% and 38.67% ± 1.77%, respectively, which were significantly higher than those of the other fresh-cut slices.

3.1.3 Active metabolites content of samples

The content of active metabolites in samples with different moisture levels showed varying trends. The content of

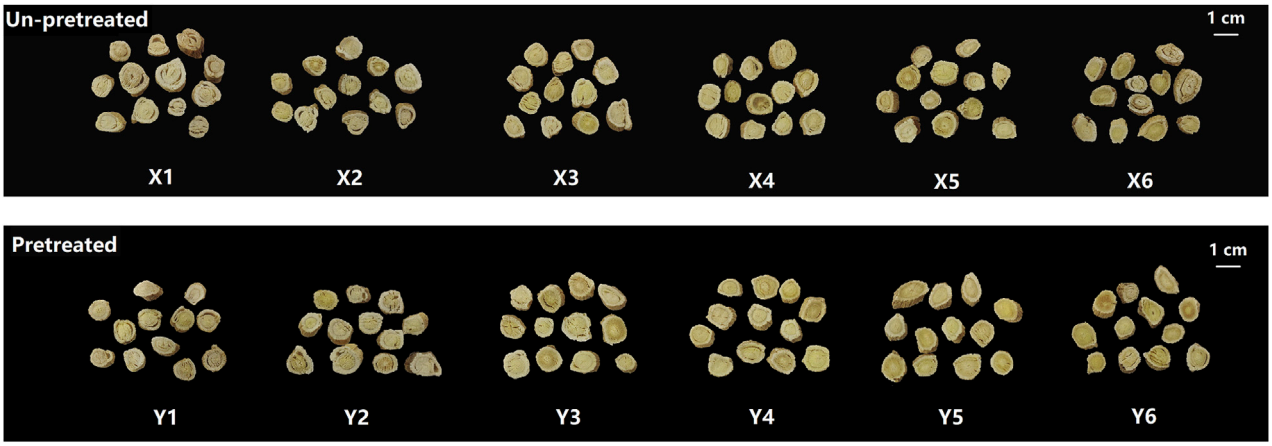

FIGURE 1
Appearance characteristics of AR with different fresh-processed methods.

Astragaloside IV (Figure 2E) fluctuated within the moisture range of 15%–55%. Except for sample X1, which had a content of 0.0813 ± 0.0085 (below the pharmacopoeia standard of not less than 0.080%), the contents in other samples were within the standard, with sample Y4 having the highest content of 0.103 ± 0.0076, with no significant differences among the samples. The content of calycosin-7-O-β-D-glucopyranoside (Figure 2F) displayed a trend of increasing and then decreasing with varying moisture content. It increased from 15% to 35% moisture content and decreased from 35% to 55% moisture content. Sample X1 had the lowest content of 0.0123 ± 0.0051, which did not meet the pharmacopoeia standard (not less than 0.020%), while sample Y4 had the highest content of 0.0388 ± 0.0061.

In samples subjected to kneading and sweating treatment, the content of calycosin-7-O-β-D-glucopyranoside increased with decreasing moisture content from 55% to 25%, reaching a maximum in sample Y5 (0.061 ± 0.0061), an increase of approximately 64%. From 25% to 15% moisture content, the content decreased. The total polysaccharide content (Figure 2G) exhibited a similar trend. Sample X1 had the lowest polysaccharide content of 4.256 ± 0.832, while sample X4 had the highest content among the untreated samples at 6.534 ± 0.657, an increase of approximately 53%. In the kneaded and sweated samples, polysaccharide content increased with decreasing moisture content from 55% to 25%, peaking at 8.998% ± 0.872% in sample Y5, an increase of approximately 43% compared to Y1. The kneading and sweating treatment had a significant impact on the content of polysaccharides and calycosin-7-O-β-D-glucopyranoside. Compared to unpretreated samples, the total polysaccharides and calycosin-7-O-β-D-glucopyranoside contents in treatment samples Y1-Y6 were significantly higher at moisture levels of 15%, 25%, and 45%. At 55% moisture content, only the calycosin-7-O-β-D-glucopyranoside content was significantly higher, while at 35% moisture content, only the polysaccharide content increased significantly. The content of astragaloside IV showed no significant difference between the treated and untreated samples. This suggests that the kneading and sweating treatment was more effective in increasing the content of polysaccharides and calycosin-7-O-β-D-glucopyranoside.

3.1.4 Entropy Weight-TOPSIS analysis

Entropy weight-TOPSIS analysis provides a more comprehensive evaluation than methods relying on a single aspect of quality. In this study, the quality of samples was influenced by a combination of appearance and intrinsic content. The entropy weight-TOPSIS analysis were performed based on appearance scores, total ash content, water-soluble extract content, total polysaccharides, astragaloside IV, and calycosin-7-O-β-D-glucopyranoside contents (Tables 2, 3). Samples Y5 and Y4 ranked first and second, respectively. Which can be attributed to their strong performance in appearance scores and extract content. The high levels of metabolites, especially total polysaccharides and astragaloside IV, significantly contributed to these results. In contrast, samples X5 and X4 ranked 6th and 8th, respectively, further confirming the efficacy of the kneading and sweating treatment methods. Therefore, cutting at a moisture content of 25%–35% after kneading and sweating treatment is identified as the optimal moisture level and processing method for AR.

3.2 Comparison of appearance between AR-F and AR-T

The appearances of AR-F and AR-T are shown in Figure 3. It can be seen that the morphologies of AR-F and AR-T are largely similar. Both are thick slices with orbicular or elliptic shapes, featuring visible longitudinal wrinkles or grooves. The cut surfaces are yellowish-white in the cortex and light yellow in the xylem, with radial textures and fissures. The main difference is the slightly lighter color of the outer skin when freshly cut, which is closer to the color of the root.

3.3 Comparison of active metabolites contents between AR-F and AR-T

3.3.1 Contents of total polysaccharides, saponins, and flavonoids

Total polysaccharides, saponins and flavonoids are the three active metabolites responsible for the pharmacological effects of AR,

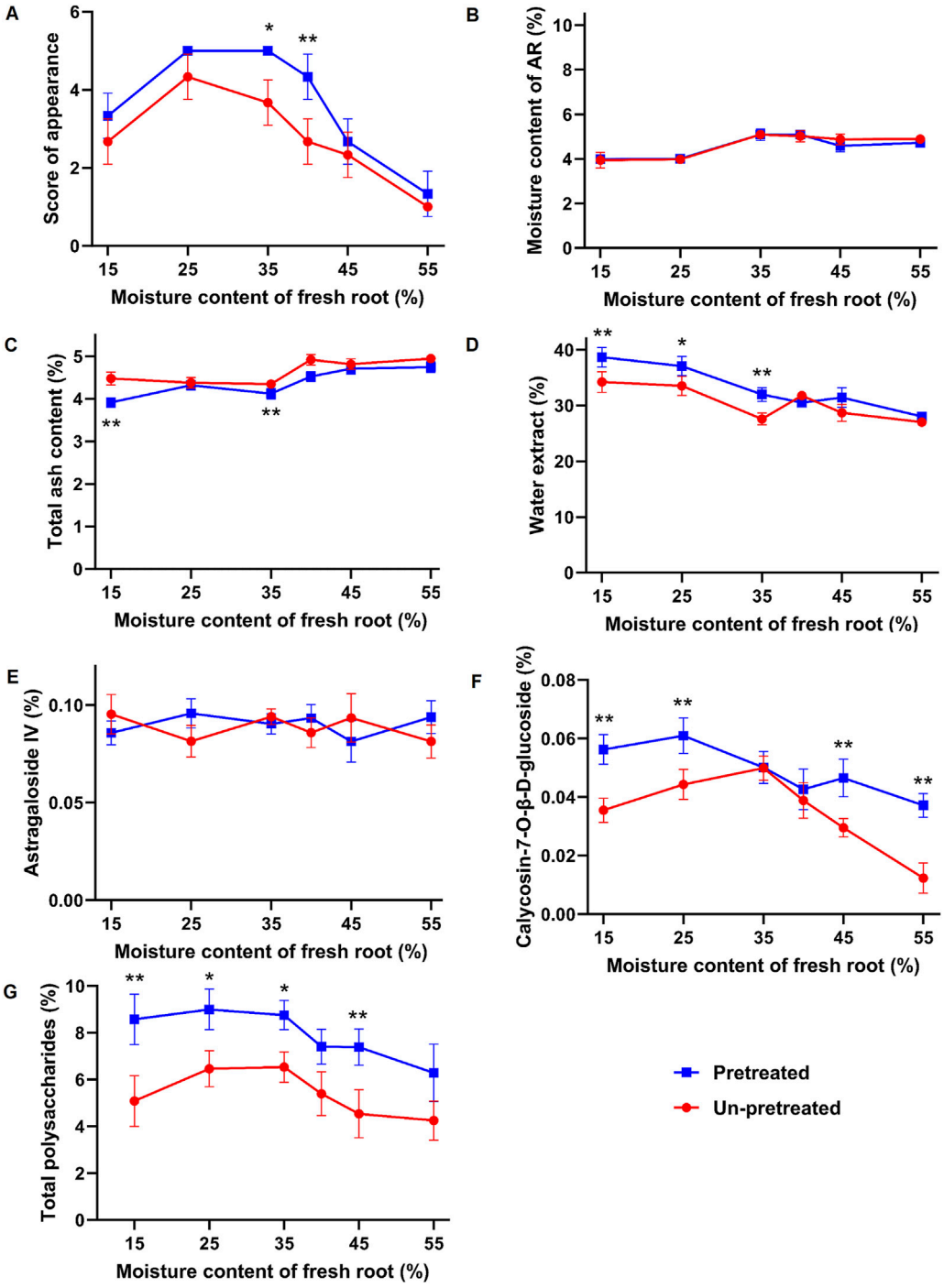

FIGURE 2
Effects of different moisture contents and processing methods on the appearance and intrinsic properties of fresh-processed AR. **(A)** Appearance score. **(B)** Moisture. **(C)** Total ash. **(D)** Water-soluble extract. **(E)** Astragaloside IV. **(F)** Calycosin-7-O-β-D-glucopyranoside. **(G)** Total polysaccharides. Compared with the un-pretreated group with the same moisture content, $*p < 0.05$, $**p < 0.01$.

including antioxidant, antiviral, antitumor activities, reduction of insulin resistance, protection against myocardial ischemia, and immune regulation (Cao et al., 2024). Their contents are shown in Table 4. The total polysaccharides and flavonoids contents in AR-F are significantly higher than those in AR-T, while the total saponins content shows no significant difference between them.

3.3.2 Monosaccharide composition analysis

The types of monosaccharides are closely related to the biological activity of polysaccharides. Monosaccharide composition analysis showed that both AR-F and AR-T polysaccharides consist of seven monosaccharides: glucose, galactose, fucose, rhamnose, arabinose, mannose, and galacturonic acid, with glucose being the major

TABLE 2 Entropy weight method for calculating weights.

Evaluation indicator	Information entropy (e)	Information utility (d)	Weight coefficient (w%)
Appearance score	0.915	0.085	14.704
Extractable content	0.872	0.128	22.133
Total polysaccharides	0.897	0.103	17.788
Astragaloside IV	0.860	0.140	24.139
Calycosin-7-O-β-D-glucopyranoside	0.945	0.055	9.440
Total ash	0.932	0.068	11.796

TABLE 3 TOPSIS evaluation results of different processing Methods for AR.

Sample	Distance to positive ideal solution (D^+)	Distance to negative ideal solution (D^-)	Relative closeness (C_i)	Ranking
Y5	0.223	0.907	0.803	1
Y4	0.439	0.691	0.611	2
Y3	0.422	0.662	0.611	3
Y6	0.511	0.732	0.589	4
X6	0.509	0.629	0.553	5
X4	0.554	0.609	0.524	6
Y1	0.635	0.559	0.468	7
X5	0.624	0.515	0.452	8
X2	0.661	0.538	0.449	9
X3	0.608	0.479	0.441	10
Y2	0.646	0.491	0.432	11
X1	0.939	0.343	0.268	12

FIGURE 3
Appearance of AR-F and AR-T.

monosaccharide. This is consistent with previous reports (Li et al., 2023a; Li et al., 2023b; Guo et al., 2024), although the relative molar ratios of the monosaccharides differ, as shown in Figure 4. Moreover, literature indicates that polysaccharides with a high proportion of glucose exhibit stronger radical scavenging and anti-inflammatory activities *in vitro* (Liao et al., 2018).

TABLE 4 Average content values and significance for AR-F and AR-T (n = 3, X±SD).

Content (mg/g)	AR-F	AR-T
Total Polysaccharides	85.152 ± 5.250**	55.640 ± 1.770
Total Saponins	14.348 ± 0.751	14.075 ± 1.099
Total Flavonoids	7.808 ± 0.015**	7.378 ± 0.129

Compared with AR-T, *$p < 0.05$,**$p < 0.01$.

3.3.3 Saponin metabolite analysis

Astragaloside I-IV are the major saponin metabolites in AR. The HPLC-ELSD chromatograms of mixed standard samples and AR samples are shown in Figure 5, and the regression equations for each metabolite are listed in Table 5. The content determination results are presented in Figure 6. No significant differences were observed in the content of each saponin between AR-F and AR-T, which is consistent with the total saponins content results.

3.3.4 Flavonoid metabolite analysis

Flavonoids are widely reported for their pharmacological activities (Cao et al., 2024). Notably, astrapterocarpan-7-O-β-D-glucoside, isomucronulatol-7-O-β-D-glucoside and isomucronulatol are unique metabolites of Astragalus (Guo et al., 2022; Lian et al., 2023). The HPLC-DAD chromatograms of the mixed standard samples and AR samples are shown in Figure 7, and the regression equations for each metabolite are listed in Table 6. The content determination results are shown in Figure 8. In AR-F, calycosin-7-O-β-D-glucoside, formononetin-7-O-β-D-glucoside, and astrapterocarpan are present at higher levels, while in AR-T, higher levels of calycosin, formononetin, astrapterocarpan-7-O-β-D-glucoside, isomucronulatol-7-O-β-D-glucoside, and isomucronulatol are observed. The cumulative content of these eight flavonoids is higher in AR-F compared to AR-T, which aligns with the total flavonoid content results. These flavonoids can be categorized into glycosides (calycosin-7-O-β-D-glucoside, formononetin-7-O-β-D-glucoside, astrapterocarpan-7-O-β-D-glucoside, and isomucronulatol-7-O-β-D-glucoside) and aglycones (calycosin, formononetin, astrapterocarpan, and isomucronulatol). The glycoside/aglycone ratio is a good indicator of AR's growth, developmental status, and stress resistance (Chen et al., 2022b). In AR-F and AR-T, the glycoside/aglycone ratios are 6.33 and 5.04, respectively, indicating a higher trend of glycoside synthesis in AR-F compared to AR-T.

3.4 Comparison of pharmacological mechanism between AR-F and AR-F

3.4.1 Targets prediction of flavonoid metabolites

Fresh processing and traditional processing do not result in differences in the types of metabolites (Sun et al., 2024). However, preliminary studies revealed that the total flavonoid content in AR-F was significantly higher than that in AR-T. Based on this, flavonoid metabolites were selected as a focus to explore the mechanism underlying the differences in pharmacological effects. A total of 35 flavonoid metabolites were identified through preliminary studies, literature review, and screening through SwissADME database (Table 7). Additionally, 460 potential targets were predicted through SwissTargetPrediction database.

3.4.2 Construction of the PPI network and identifcation of core targets

PPI network analysis and core target screening of the 460 potential targets revealed that the core targets of flavonoid metabolites were primarily AKT1, TNF, EGFR, SRC, ESR1, HSP90AA1, and CASP3 (Figure 9).

3.4.3 Enrichment analyses using GO and reactome databases

The potential targets of the flavonoid metabolites were analyzed through GO enrichment, which identified 136 biological processes, 77 cellular components, and 150 molecular functions. The main biological processes included protein autophosphorylation, response to xenobiotic stimulus, and positive regulation of phosphatidylinositol 3-kinase/protein kinase B signal transduction. The main cellular components included the cytosol, plasma membrane, and cytoplasm, while the primary molecular functions included protein serine/threonine kinase activity, histone deacetylase activity, and enzyme binding (Figure 10A). These findings indicated that the main biological processes involved were protein autophosphorylation and response to xenobiotic

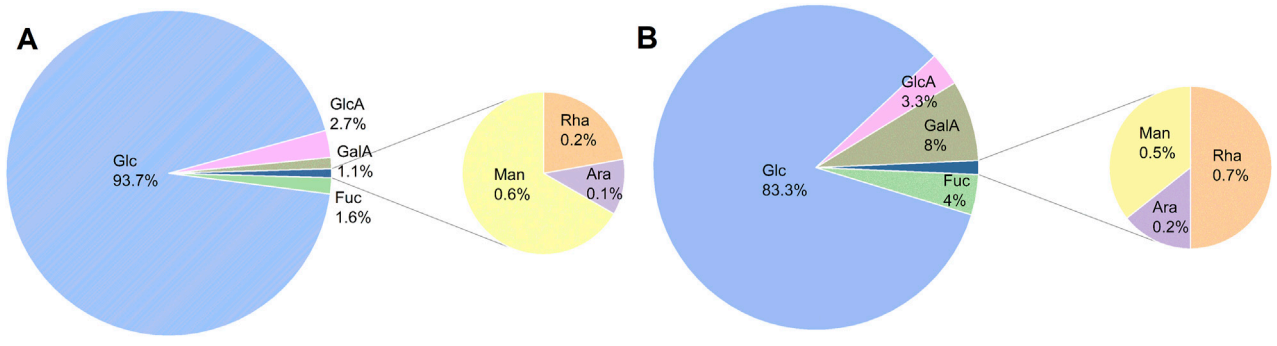

FIGURE 4
Monosaccharide composition analysis of AR. **(A)** AR-F. **(B)** AR-T.

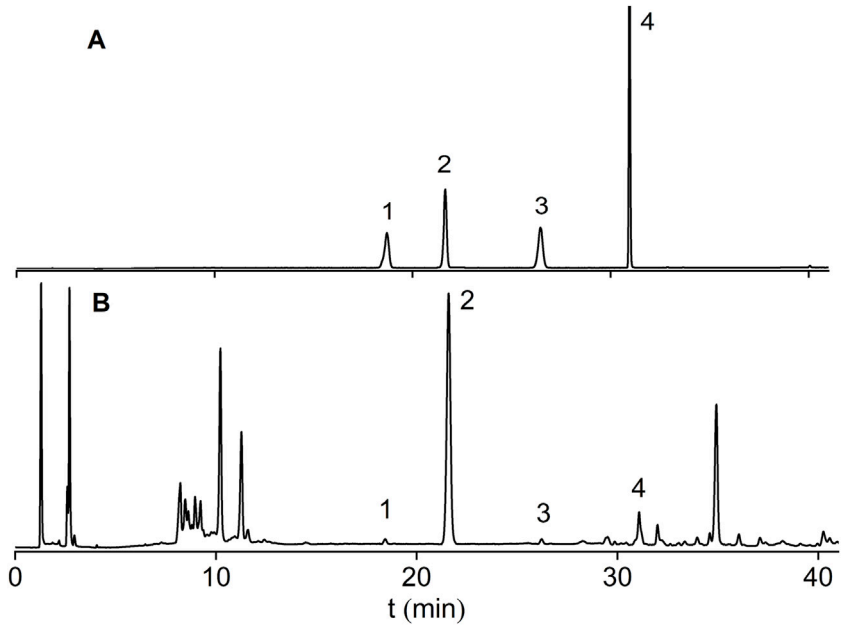

FIGURE 5
HPLC-ELSD chromatograms of saponin standards and AR. **(A)** Mixed Standards. **(B)** AR Samples; Peaks:1 Astragaloside III; 2 Astragaloside IV; 3 Astragaloside II; 4 Astragaloside I.

TABLE 5 Linear regression equations for saponin standards in AR.

Metabolite	Linear regression equation	R^2	Linear range (μg/mL)
Astragaloside IV	$\ln Y = 1.1785 \ln X - 0.1987$	0.9999	8.3360 ~ 1,042.0000
Astragaloside I	$\ln Y = 1.4270 \ln X - 1.7119$	0.9994	7.6160 ~ 952.0000
Astragaloside II	$\ln Y = 1.6145 \ln X - 2.6153$	0.9995	7.3920 ~ 824.0000
Astragaloside III	$\ln Y = 1.0790 \ln X - 0.1688$	0.9992	8.5920 ~ 1,074.0000

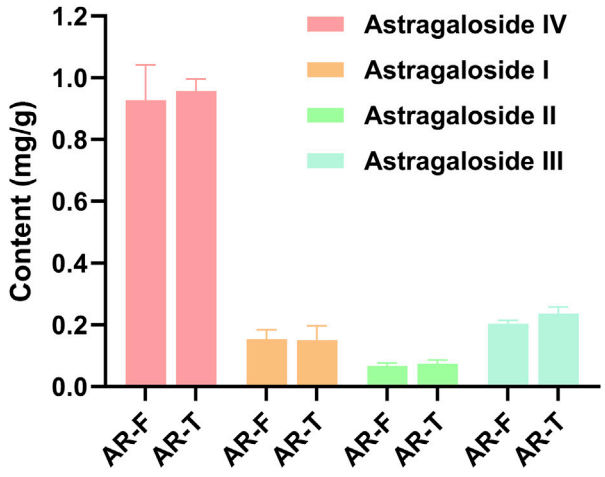

FIGURE 6
Content of four saponin metabolites in AR-F and AR-T Compared with AR-T, *$p < 0.05$, **$p < 0.01$.

stimulus. GO chord maps revealed that the targets AKT1, EGFR, TNF, ESR1, and SRC were enriched in these processes (Figure 10B). REACTOME pathway enrichment analysis identified a total of 304 signaling pathways enriched for the 460 potential targets of flavonoid metabolites. Clustering analysis showed that these pathways were primarily involved in signal transduction and immune system functions. The bubble diagrams indicated that key pathways within these categories included signaling by receptor tyrosine kinases, cytokine signaling in the immune system, and constitutive signaling by aberrant PI3K in cancer (Figure 10C).

3.4.4 Molecular docking analysis

The molecular docking results revealed that the binding energies between the seven core targets and the flavonoid metabolites were all greater than 5 kcal/mol, with Pratensein showing the highest binding energy to SRC (−9.6 kcal/mol). These findings suggest that the flavonoid metabolites bind well to the core targets (Figure 11A). Additionally, the highest scoring results for each target were visualized (Figures 11B–H).

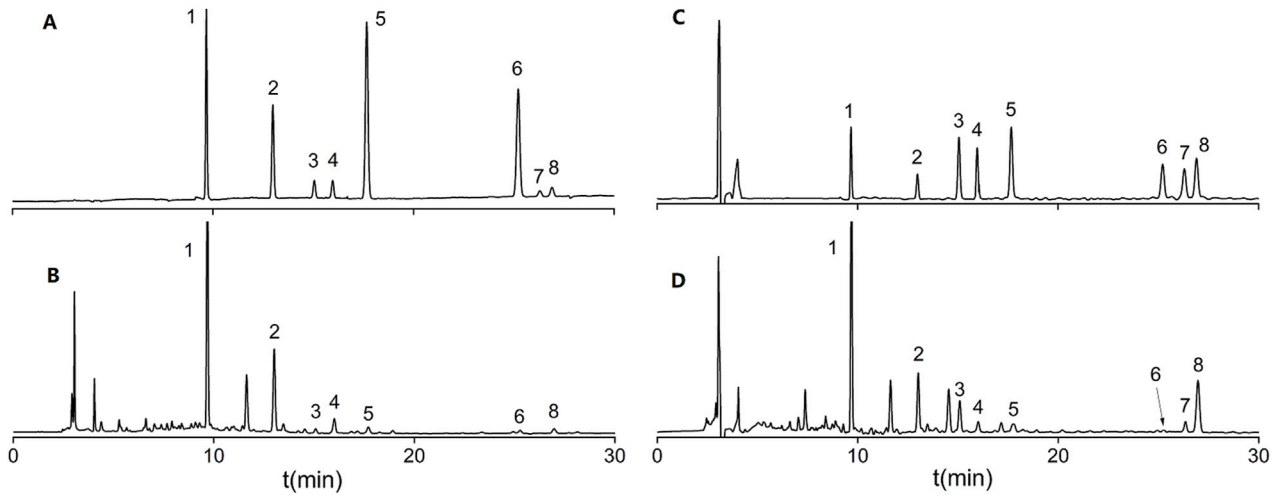

FIGURE 7
HPLC-DAD chromatograms of flavonoid standard mixtures and AR. **(A)** Mixed standard at 260 nm. **(B)** AR at 260 nm. **(C)** Mixed standard at 230 nm. **(D)** AR at 230 nm; Peaks:1 Calycosin-7-O-β-D-glucoside; 2 Formononetin-7-O-β-D-glucoside; 3 Astrapterocarpan-7-O-β-D-glucoside; 4 Isomucronulatol-7-O-β-D-glucoside; 5 Calycosin; 6 Formononetin; 7 Astrapterocarpan; 8 Isomucronulatol.

TABLE 6 Linear regression equations for flavonoid standards in AR.

Metabolite	Linear regression equation	R^2	Linear range (μg/mL)
Calycosin-7-O-β-D-glucoside	$Y = 27.865X + 13.501$	0.9998	20.040 ~ 200.400
Calycosin	$Y = 43.641X + 19.567$	0.9997	1.080 ~ 43.200
Formononetin-7-O-β-D-glucoside	$Y = 24.533X - 2.993$	0.9999	4.106 ~ 60.584
Formononetin	$Y = 36.367X + 7.222$	0.9999	2.100 ~ 42.000
Astrapterocarpan-7-O-β-D-glucoside	$Y = 15.141X + 24.077$	0.9995	12.250 ~ 122.500
Astrapterocarpan	$Y = 28.775X + 51.599$	0.9999	8.800 ~ 176.000
Isomucronulatol-7-O-β-D-glucoside	$Y = 15.618X + 6.137$	0.9998	10.400 ~ 208.000
Isomucronulatol	$Y = 32.854X + 28.166$	0.9999	10.204 ~ 102.040

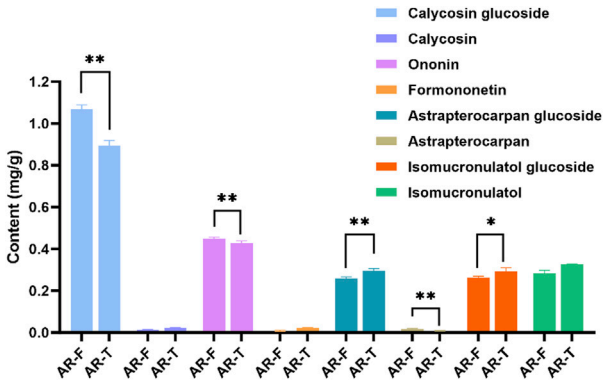

FIGURE 8
Content of eight flavonoid metabolites in AR-F and AR-T. Compared with AR-T, *$p < 0.05$, **$p < 0.01$.

3.4.5 Immunomodulatory effects

The impact of different concentrations of TFA on RAW264.7 cell viability is shown in Figure 12A. Within the concentration range of 31.25–125 μg/mL, neither AR-F nor AR-T significantly affects cell viability. However, at concentrations of 500–1,000 μg/mL, both AR-F and AR-T promote cell proliferation. The effect of TFA on NO secretion of cells is shown in Figure 12B. At concentrations of 62.5 and 125 μg/mL, both TFA in AR-F and AR-T significantly promote NO secretion compared to the control group, with AR-F showing higher NO levels than AR-T at the same concentrations. These results suggest that AR-F has better immunomodulatory activity compared to AR-T.

3.4.6 Enzyme-linked immunosorbent assay

The effect of TFA in AR-F and AR-T on the secretion of core target proteins in RAW264.7 cell is presented in Figure 13. Both AR-F and AR-T significantly increased the protein contents of TNF,

TABLE 7 Potential medicinal metabolites of flavonoids in AR.

No.	Metabolite	No.	Metabolite
1	Calycosin	19	7,3′-dihydroxy-8,4′-dimethoxyisoflavone
2	Calycosin-7-O-β-D-glucoside	20	3′,7-Dihydroxy-5′-methoxyisoflavone
3	Formononetin	21	4′,5,7-Trihydroxy-3′-methoxyisoflavone
4	Formononetin7-O-glucoside	22	Afrormosin
5	Astrapterocarpan	23	3,9,10-Tri-methoxypterocarpan
6	Astrapterocarpan-7-O-β-D-glucoside	24	Daidzein
7	Isomucronulatol	25	8,2′-Dihydroxy-7,4′-dimethoxyisoflavane
8	4′,7-dihydroxyflavone	26	7-O-methylisomucronulatol
9	3′,4′,7-trihydroxyflavone	27	7,2′,3′-Trihydroxy-4′-methoxy-isoflavane
10	Oroxylin-A	28	Pendulone
11	Wogonin	29	LicochalconeB
12	Liquiritigenin	30	isoliquiritigenin
13	Quercetin	31	2′-Methoxyisoliquiritigenin
14	Kaempferol	32	4,4′,6′-Trihydroxychalcone
15	Genistein	33	4-Methoxy-4′,6′-dihydroxychalcone
16	Pratensein	34	4,4′-Dimethyl-6′-hydroxychalcone
17	3′,7,8-trihydroxy-4′-methoxyisoflavone	35	Sophorophenolone
18	8,3′-dihydroxy-7,4′-dimethoxyisoflavone		

SRC, ER-α, AKT, Caspase-3 and HSP-90 compared to the control group, with AR-F exhibiting higher levels than AR-T.

Specifically, compared to the AR-T group, TNF, SRC and HSP-90 content in the AR-F group was significantly elevated within the concentration range of 31.25–125 μg/mL (Figures 13A, B, F). Similarly, ER-α and AKT contents in the AR-F group were significantly increased in the concentration range of 31.25–62.5 μg/mL and 62.5~125 μg/mL specifically (Figures 13C–D) compared to the AR-T group. For Caspase-3, a significant increase was observed in the AR-F group at concentrations of 62.5 μg/mL (Figure 13E) compared to the AR-T group.

4 Discussion

The color, shape, and content of active metabolites in medicinal slices are crucial indicators of the quality of TCM. Our study revealed that moisture content, as well as kneading and sweating treatment, significantly affect these indicators during fresh processing. Specifically, slicing fresh medicinal materials with high moisture content results in a whiter cross-section, while materials with lower moisture content yield a yellower cross-section. This difference may be related to the fact that high moisture content slows down the oxidation of polyphenolic metabolites and enzymatic browning in AR (Bai et al., 2020). Furthermore, as moisture content decreases, the levels of polysaccharides and calycosin-7-O-glucoside in Astragalus initially increase and then decrease. This could be due to high moisture content in fresh materials maintaining enzyme activity and cellular metabolism, which continues to participate in biosynthesis and increase the content of polysaccharides and flavonoids. However, as the AR continues to dry, enzyme activity gradually diminishes, halting the biosynthesis process. Prolonged drying may also lead to oxidation and degradation of effective metabolites, causing a decrease in their content (Bai et al., 2020). Kneading and sweating treatments can improve the morphology of AR-F. This may be because these processes make the fibrous tissue of the material more pliable, facilitating the connection between the skin and wood, and reducing the separation of the skin and flesh in slices. Additionally, sweating can redistribute the moisture within the semi-dried AR, reducing the moisture difference between the interior and the surface, and thereby decreasing the rate of fragment formation. Furthermore, the significantly increased contents of polysaccharides and calycosin-7-O-glucoside observed in the kneading and sweating treatment group compared to the unpretreated group may be due to the disruption the cell wall structure by these processes, which accelerates enzymatic reactions and promotes the release and transformation of polysaccharides and flavonoids (Dai et al., 2018). Comparing the content of various metabolites between AR-F and AR-T, we found that total polysaccharides and total flavonoids in AR-F were significantly higher than those in AR-T, consistent with findings for fresh processing of *Ophiopogon japonicus* (Cai et al., 2023). This could be attributed to the fact that fresh materials, compared to traditional drying processes, undergo less thermal degradation,

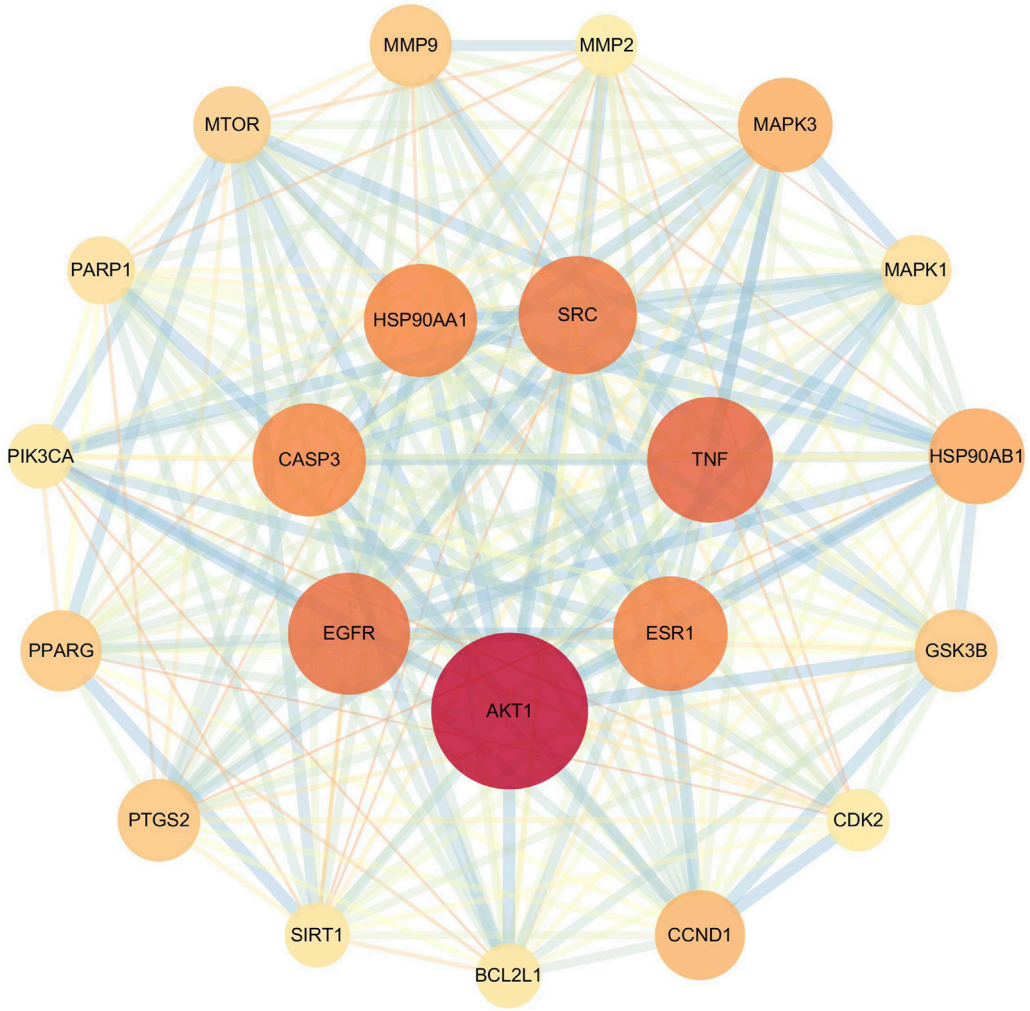

FIGURE 9
PPI network of core targets of flavonoid metabolites in AR.

oxidation, and loss of water-soluble metabolites. Notably, the content of calycosin-7-O-glucoside, a key quality control metabolite, was significantly higher in AR-F, indicating that the fresh processing method is an important way to improve the quality of AR. These findings provide valuable guidance for production and processing of AR in the pharmaceutical industry.

AR contains polysaccharides, flavonoids, and saponins as its major bioactive compounds. We conducted a comparative analysis of the chemical profiles of AR-F and AR-T. The results showed a significant increase in polysaccharides and flavonoids in AR-F compared to AR-T. Notably, the contents of calycosin-7-O-β-D-glucoside, ononin, and astrapterocarpan in AR-F increased by approximately 19.5%, 5.4%, and 77.8%, respectively.

Calycosin-7-O-β-D-glucoside, formononetin-7-O-β-D-glucoside, and astrapterocarpan are natural compounds predominantly found in legumes, especially in AR. Studies have demonstrated that calycosin-7-O-β-D-glucoside and formononetin-7-O-β-D-glucoside exhibit bidirectional immunomodulatory effects, benefiting inflammatory conditions. Calycosin-7-O-β-D-glucoside enhances macrophage phagocytosis and immune activity, promotes T and B cell proliferation, and strengthens host defense against pathogens. Additionally, it suppresses the excessive release of inflammatory cytokines such as TNF-α, IL-1β, and IL-6, alleviating inflammation caused by hyperactive immune responses. This compound also modulates the Th1/Th2 and Treg/Th17 balance, maintaining immune tolerance and controlling chronic inflammation and autoimmune diseases (Gao et al., 2014).

Formononetin-7-O-β-D-glucoside promotes B cell proliferation and antibody production, regulates cytokine secretion by T cells, and balances Th1/Th2 responses. It inhibits NF-κB and MAPK signaling pathways, reducing pro-inflammatory cytokine production and mitigating inflammation. Furthermore, it supports intestinal barrier integrity and modulates gut microbiota, indirectly enhancing immune functions (Che et al., 2024). As an antioxidant, it reduces reactive oxygen species (ROS)-induced damage to immune cells and increases anti-inflammatory cytokine expression. Astrapterocarpan interferes with NLRP3 inflammasome activation, suppressing the release of pro-inflammatory cytokines like IL-1β and IL-18, thereby attenuating inflammation. Research suggests that it may regulate the Treg/Th17 balance, modulating immune tolerance and inflammation.

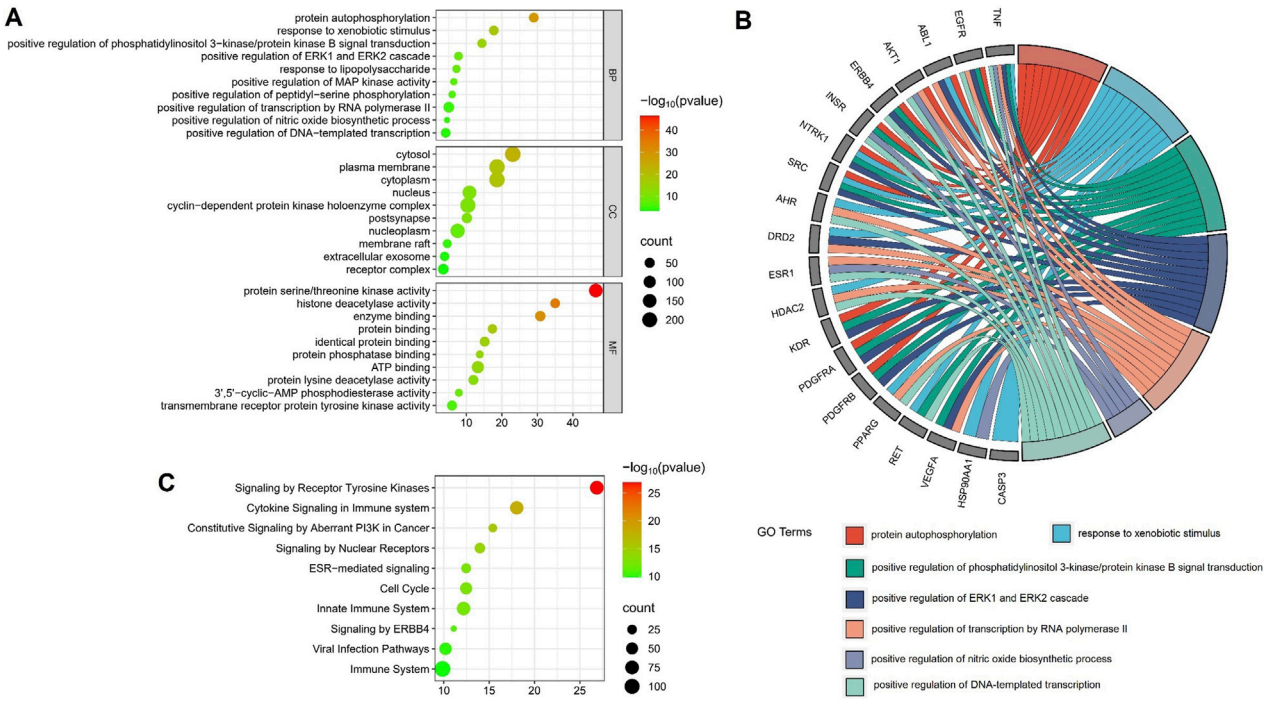

FIGURE 10
GO **(A, B)** and REACTOME Pathway **(C)** enrichment analysis.

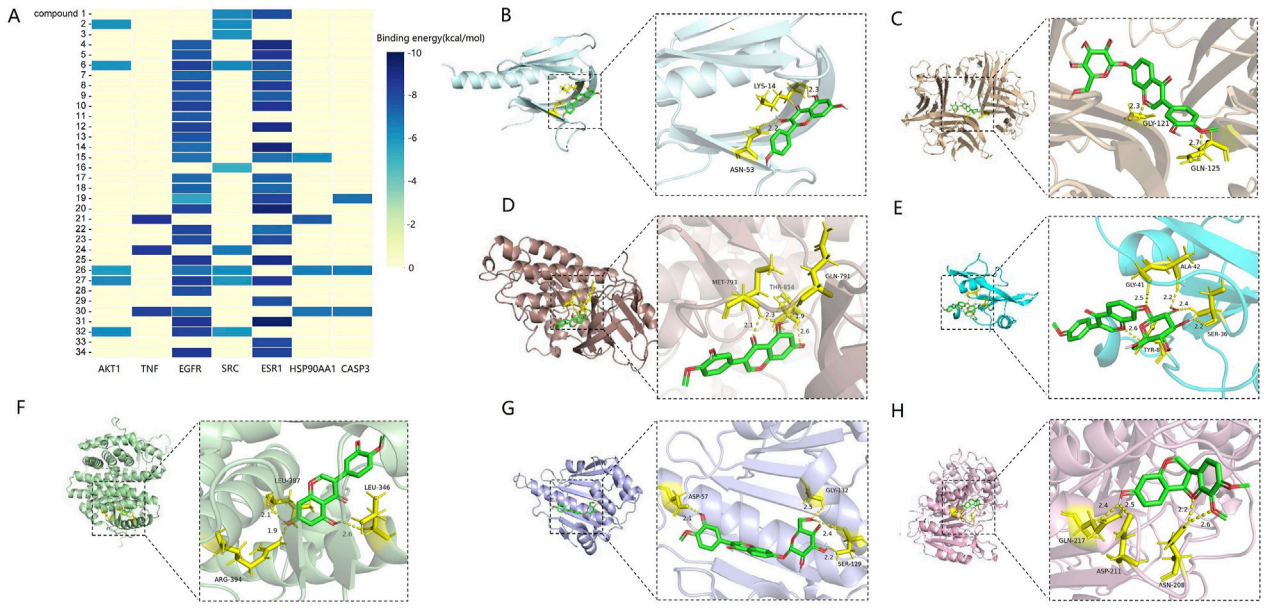

FIGURE 11
Molecular docking results **(A)** heatmap of binding energy between flavonoids and core targets. **(B)** 3D binding conformation of AKT1 and kaempferol. **(C)** 3D binding conformation of TNF and calycosin-7-O-β-D-glucoside. **(D)** 3D binding conformation of EGFR and pratensein. **(E)** 3D binding conformation of SRC and formononetin-7-O-β-D-glucoside. **(F)** 3D binding conformation of ESR1 and pratensein. **(G)** 3D binding conformation of HSP90AA1 and calycosin-7-O-β-D-glucoside. **(H)** 3D binding conformation of CASP3 and astrapterocarpan.

Additionally, it decreases oxidative stress markers (e.g., malondialdehyde, MDA) and enhances antioxidant enzyme activity, protecting immune cells from damage.

Existing studies indicate that the fresh-cutting and traditional drying processes do not alter the chemical composition of AR but affect the relative contents of specific compounds. To elucidate the

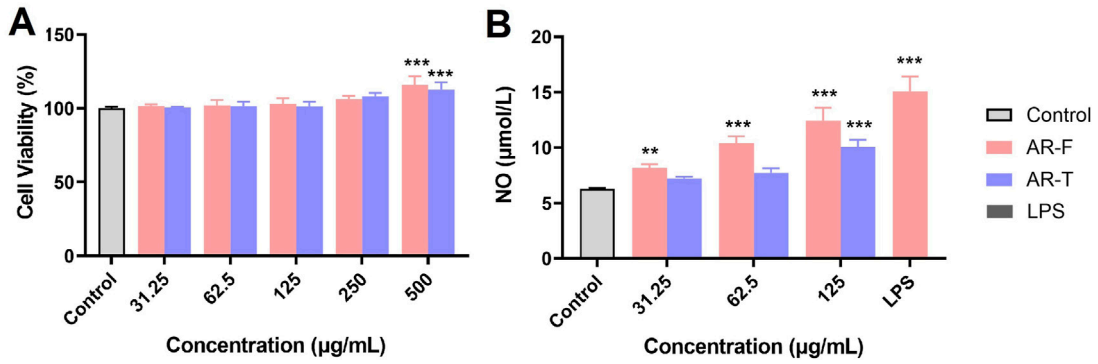

FIGURE 12
Immunomodulatory activity measurements of TFA in AR-F and AR-T. **(A)** RAW264.7 cell viability. **(B)** NO secretion by RAW264.7 cells. Compared with control, $^{**}p < 0.01$.

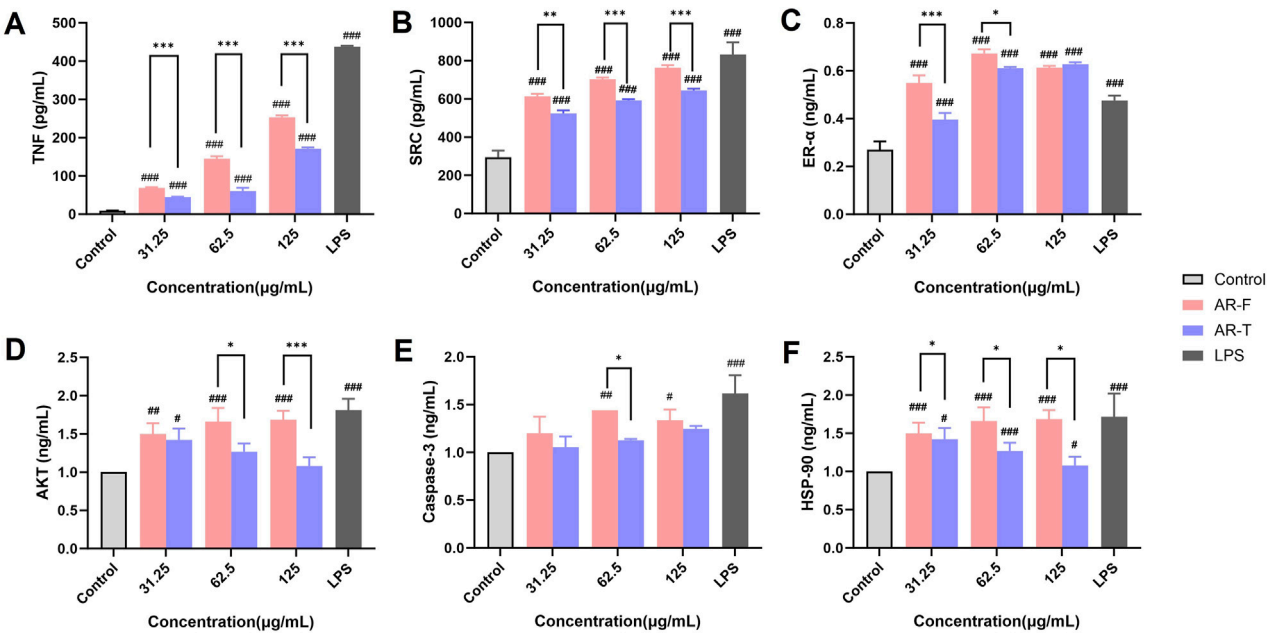

FIGURE 13
Enzyme-linked immunosorbent (ELISA) assay. **(A)** Tumor necrosis factor (TNF) **(B)** Proto-oncogene tyrosine-protein kinase Src (SRC) **(C)** Estrogen receptor (ER-α) **(D)** Protein kinase B (AKT) **(E)** Caspase-3 **(F)** Heat shock protein HSP 90-α (HSP-90) Compared with control, $^{\#}p < 0.05$, $^{\#\#}p < 0.01$, $^{\#\#\#}p < 0.001$; compared with AR-T, $^{*}p < 0.05$, $^{**}p < 0.01$, $^{***}p < 0.001$.

pharmacological differences between AR-F and AR-T, we conducted a network pharmacology analysis focusing on total flavonoids, which differ significantly in content between the two. PPI network analysis identified seven core targets for total flavonoids in AR (TFA): AKT1, ESR1, TNF, SRC, HSP90AA1, CASP3, and EGFR. These core targets are closely related to cytokine signaling and receptor tyrosine kinase pathways in the immune system. Among these targets, AKT1 is a central node influencing immune responses by regulating T cell activation and proliferation. It also participates in modulating inflammation and phagocytosis in macrophages and dendritic cells. ESR1, TNF, SRC, HSP90AA1, and CASP3 further contribute to immunoregulation via distinct mechanisms: ESR1 influences the activity of T and B cells and plays a role in the treatment of sex-related autoimmune diseases, such as rheumatoid arthritis and systemic lupus erythematosus. TNF regulates inflammatory responses, including cytokine secretion, leukocyte recruitment, and angiogenesis. Its overexpression is associated with autoimmune diseases such as Crohn's disease and psoriasis. SRC, a tyrosine kinase, is involved in signal transduction, cell migration, and proliferation. It regulates T and B cell receptor signaling and functions in natural killer cells and dendritic cells. HSP90AA1 modulates inflammatory responses by affecting type I interferon and NF-κB signaling pathways and serves as a chaperone for key molecules in antigen presentation.

CASP3 regulates immune cell apoptosis and maintains immune homeostasis. In autoimmune diseases, aberrant CASP3 activity may lead to insufficient or excessive apoptosis.

To validate the effects of AR-F and AR-T total flavonoids on these core targets, we performed cell-based experiments using RAW264.7 macrophages. At concentrations of 31.25–125 μg/mL, AR-T significantly increased TNF secretion compared to the control group, consistent with literature reports (Guo et al., 2016). Notably, AR-F further enhanced TNF secretion compared to AR-T. Molecular docking results revealed that calycosin-7-O-β-D-glucoside exhibited the highest binding energy with TNF and HSP, ononin with SRC, and astrapterocarpan with CASP3. These findings suggest that the enhanced immunomodulatory activity of AR-F relative to AR-T is associated with the increased content of these three compounds, acting through targets such as TNF, HSP, SRC, and CASP3.

5 Conclusion

Fresh processing of medicinal materials offers certain advantages, including better retention of effective metabolites, reduced storage and processing steps, lower production costs, and improved processing efficiency. Our study optimized the fresh processing method of AR, and compared the differences in active metabolite content and pharmacological effects between fresh cutting and traditional methods. It was found that fresh cutting has advantages in retaining polysaccharide and flavonoid contents, and demonstrates better immune modulation activities. This study provides scientific evidence for the quality control and rational application of fresh processing AR.

Data availability statement

The original contributions presented in the study are included in the article/supplementary material, further inquiries can be directed to the corresponding author.

Author contributions

XZ: Writing–original draft. SJ: Formal Analysis, Writing–original draft. TS: Methodology, Writing–review and editing. WZ: Data curation, Writing–original draft. KD: Investigation, Writing–original draft. ZQ: Software, Writing–original draft. HZ: Investigation, Writing–review and editing. YeL: Supervision, Writing–review and editing. YaL: Writing–review and editing.

Funding

The author(s) declare that financial support was received for the research, authorship, and/or publication of this article. This research was funded by study of Key Research and Development Program of Shaanxi (Program No. 2021ZDLSF04-06 and No. 2022ZDXM-SF-06), Special Project of Shaanxi Administration of Traditional Chinese Medicine (Program No. 2021-QYZL-01), Natural Science Foundation of Shaanxi Province (Program No. 2023-JC-QN-0820), Project of Shaanxi Administration of Traditional Chinese Medicine (Program No. 2022-QCYZH-030).

Conflict of interest

The authors declare that the research was conducted in the absence of any commercial or financial relationships that could be construed as a potential conflict of interest.

Publisher's note

References

Bai, C., Yang, J., Cao, B., Xue, Y., Gao, P., Liang, H., et al. (2020). Growth years and post-harvest processing methods have critical roles on the contents of medicinal active ingredients of Scutellaria baicalensis. *Ind. Crops Prod.* 158, 112985. doi:10.1016/j.indcrop.2020.112985

Cai, X., Deng, H., Li, W., Li, H., and Li, M. (2023). Study on fresh processing key technology and quality influence of Cut *Ophiopogonis Radix* based on multi-index evaluation. *Open Life Sci.* 18, 20220638. doi:10.1515/biol-2022-0638

Cao, L., Zhao, J., Wang, M., Khan, I. A., and Li, X. C. (2024). Rapid preparation and proton NMR fingerprinting of polysaccharides from *Radix Astragali*. *Carbohydr. Res.* 536, 109053. doi:10.1016/j.carres.2024.109053

Chen, F. Y., Li, Q., Wang, J. L., and Jiao, P. Z. (2022a). Research status of fresh cutting of Chinese medicinal materials. *Chin. Tradit. Pat. Med.* 44, 3953–3958. doi:10.3969/j.issn.1001-1528.2022.12.035

Chen, X., Chen, C., and Fu, X. (2022b). Hypoglycemic activity *in vitro* and vivo of a water-soluble polysaccharide from *Astragalus membranaceus*. *Food Funct.* 13, 11210–11222. doi:10.1039/d2fo02298b

Che, Y., Li, L., Kong, M., Geng, Y., Wang, D., Li, B., et al. (2024). Dietary supplementation of Astragalus flavonoids regulates intestinal immunology and the gut microbiota to improve growth performance and intestinal health in weaned piglets. *Front. Immunol.* 15, 1459342. doi:10.3389/fimmu.2024.1459342

China (2020). *Pharmacopoeia of the people's Republic of China*. Beijing: China Medical Science and Technology Press.

Dai, H., Li, Y., Zhang, L., Xiang, X., Wang, F., and Xiong, H. (2018). Effects of kneading process on *codonopsis polysaccharides*. *Pharm. J. Chin. PLA* 34, 232–235. doi:10.3969/j.issn.1008-9926.2018.03.010

Gao, J., Liu, Z. J., Chen, T., and Zhao, D. (2014). Pharmaceutical properties of calycosin, the major bioactive isoflavonoid in the dry root extract of Radix astragali. *Pharm. Biol.* 52 (9), 1217–1222. doi:10.3109/13880209.2013.879188

Guo, Y., Wang, L., Liu, K., Li, M., Jin, Y., Gu, L., et al. (2024). A rapid and accurate UHPLC method for determination of monosaccharides in polysaccharides of different sources of *Radix Astragali* and its immune activity analysis. *Molecules.* 29, 2287. doi:10.3390/molecules29102287

Guo, Z., Xu, H. Y., Xu, L., Wang, S. S., and Zhang, X. M. (2016). *In vivo* and *in vitro* immunomodulatory and anti-inflammatory effects of total flavonoids of Astragalus. *Complementary Altern. Med.* 13 (4), 60–73. doi:10.21010/ajtcam.v13i4.10

Guo, Y., Li, R., Qin, X., and Li, Z. (2022). Characteristic metabolites of *astragali Radix* from hengshan mountains based on multi-index metabolites determination. *Mod. Chin. Med.* 24, 1473–1480. doi:10.13313/j.issn.1673-4890.20211214002

Jiang, Y., Qi, X., Gao, K., Liu, W., Li, N., Cheng, N., et al. (2016). Relationship between molecular weight, monosaccharide composition and immunobiologic activity of *Astragalus polysaccharides*. *Glycoconj J.* 33, 755–761. doi:10.1007/s10719-016-9669-z

Lian, T., Wei, S., Feng, Z., Yu, F., Zhao, T., Liu, F., et al. (2023). Patterns of identifying the production area of *Astragali Radix* from Zizhou based on the flavonoid content characteristics. *J. Beijing Univ. Traditional Chin. Med.* 46, 281–288. doi:10.3969/j.issn.1006-2157.2023.02.022

Liao, J., Li, C., Huang, J., Liu, W., Chen, H., Liao, S., et al. (2018). Structure characterization of honey-processed *Astragalus polysaccharides* and its anti-inflammatory activity *in vitro*. *Molecules* 23, 168. doi:10.3390/molecules23010168

Li, C., Lv, Y., Gao, W., Mao, K., Shan, W., Tong, S., et al. (2023a). A comprehensive strategy for prediction and quality evaluation of standardized planting herbs based on plant metabolomics coupled with extreme learning machine: *astragali Radix* as an example. *Phytochem. Anal.* 34, 606–616. doi:10.1002/pca.3241

Li, H., Li, K., Lv, W., Feng, S., Wen, Y., Li, Z., et al. (2023b). Analysis on sugar spectrum difference between wild-simulated and transplanted *astragali Radix*. *Chin. J. Exp. Traditional Med. Formulae* 29, 141–148. doi:10.13422/j.cnki.syfjx.20230663

Li, J., Luo, J., Chai, Y., Guo, Y., Tianzhi, Y., and Bao, Y. (2021). Hypoglycemic effect of *Taraxacum officinale* root extract and its synergism with Radix Astragali extract. *Food Sci. Nutr.* 9, 2075–2085. doi:10.1002/fsn3.2176

Li, K., Cao, Y. X., Jiao, S. M., Du, G. H., Du, Y. G., and Qin, X. M. (2020). Structural characterization and immune activity screening of polysaccharides with different molecular weights from *astragali Radix*. *Front. Pharmacol.* 11, 582091. doi:10.3389/fphar.2020.582091

Liu, Y. X., Song, X. M., Dan, L. W., Tang, J. M., Jiang, Y., Deng, C., et al. (2024). Astragali Radix: comprehensive review of its botany, phytochemistry, pharmacology and clinical application. *Arch. Pharm. Res.* 47, 165–218. doi:10.1007/s12272-024-01489-y

Liu, Y., Chen, J. F., Xu, N., Lin, W. G., Liu, Y. M., Chen, M. L., et al. (2019). Effects of fresh-cut on drying rate and quality of *Panax notoginseng*. *Zhongguo Zhong Yao Za Zhi* 44, 1381–1391. doi:10.19540/j.cnki.cjcmm.20181221.002

Li, X., Guo, X., Sha, M., Gao, W., and Li, X. (2022). Combining network pharmacology with chromatographic fingerprinting and multicomponent quantitative analysis for the quality evaluation of *Astragali Radix*. *Biomed. Chromatogr.* 36, e5319. doi:10.1002/bmc.5319

Luo, S., Wang, Y., Li, W., Zhang, Y., Sun, Z., and Nie, R. (2017). Feasibility study on fresh *cinnamon* cutting. *J. Chin. Med. Mater.* 40, 2836–2838. doi:10.13863/j.issn1001-4454.2017.12.020

Saddiq, A. A., El-Far, A. H., Mohamed Abdullah, S. A., Godugu, K., Almaghrabi, O. A., and Mousa, S. A. (2022). Curcumin, thymoquinone, and 3, 3'-diindolylmethane combinations attenuate lung and liver cancers progression. *Front. Pharmacol.* 13, 936996. doi:10.3389/fphar.2022.936996

Shin, H. S., Shyur, H. J., and Lee, E. S. (2007). An extension of TOPSIS for group decision making. *Math. Comput. Model.* 45, 801–813. doi:10.1016/j.mcm.2006.03.023

Sun, X., Song, Z., Tang, Z., Yu, J., Fan, X., Yang, Y., et al. (2024). Effects of different post-harvest processing methods on changes in the active ingredients of licorice based on LC-MS and plant metabolomics. *Phytochem. Anal.* doi:10.1002/pca.3419

Wang, L., Fan, S., Wang, X., Wang, X., Yan, X., Shan, D., et al. (2019). Physicochemical aspects and sensory profiles as various potential factors for comprehensive quality assessment of nü-Er-cha produced from rhamnus heterophylla oliv. *Molecules* 24, 3211. doi:10.3390/molecules24183211

Wu, H., Li, D., Bian, T., Song, Q., Li, X., Li, G., et al. (2021). Study on integrative technology of primary processing for Astragali Radix based on response surface method combined with entropy weight method. *Chin. Traditional Herb. Drugs.* 52, 5854–5861. doi:10.7501/j.issn.0253-2670.2021.19.008

Xu, J., Yang, B., Li, M., Li, Z., Tu, Y., Tang, L., et al. (2022). Research on germplasm diversity of Amomum villosum. Lour in genuine producing area. *PLoS One* 17, e0268246. doi:10.1371/journal.pone.0268246

Yang, J., Li, L., Ji, D., Mao, C., Wu, Q., and Lu, T. (2016). Research on history and present situation of integration of habitat processing and processing of Chinese herbal medicine. *Chin. Traditional Herb. Drugs* 47, 2751–2757. doi:10.7501/j.issn.0253-2670.2016.15.026

Yao, Y., Xu, M., Zhang, X., Lu, M., Liu, X., Cai, G., et al. (2024). The influence of fresh cutting and traditional cutting methods on the quality of licorice slices. *J. Chin. Med. Mater.* 47, 342–347. doi:10.13863/j.issn1001-4454.2024.02.013

Zhang, C. H., Yang, X., Wei, J. R., Chen, N. M., Xu, J. P., Bi, Y. Q., et al. (2021). Ethnopharmacology, phytochemistry, pharmacology, toxicology and clinical applications of Radix astragali. *Chin. J. Integr. Med.* 27, 229–240. doi:10.1007/s11655-019-3032-8

Zhang, A., Lin, M., Duan, G., Wu, H., Wu, Y., Gong, L., et al. (2023). Optimization of fresh-cuting process of smilacis chinae rhizoma Chinese traditional and herbal. *Drugs* 54, 3834–3841. doi:10.7501/j.issn.0253-2670.2023.12.010

Zhou, S., Liu, B., and Meng, J. (2017). Quality evaluation of raw moutan cortex using the AHP and gray correlation-TOPSIS method. *Pharmacogn. Mag.* 13, 528–533. doi:10.4103/0973-1296.211029

frontiers | Frontiers in Pharmacology

TYPE Original Research
PUBLISHED 19 December 2024
DOI 10.3389/fphar.2024.1468237

OPEN ACCESS

EDITED BY
Michael Heinrich,
University College London, United Kingdom

REVIEWED BY
Lei Chen,
Guangdong Ocean University, China
Wang Lingchong,
Nanjing University of Chinese Medicine, China

*CORRESPONDENCE
Aiwu Zhang,
zhangaiwu@jlau.edu.cn

RECEIVED 21 July 2024
ACCEPTED 04 December 2024
PUBLISHED 19 December 2024

CITATION
Chen S, Li Y, Yang Y, Zhao S, Shi H, Yang C, Wu M and Zhang A (2024) Comparison of the composition, immunological activity and anti-fatigue effects of different parts in sika deer antler.
Front. Pharmacol. 15:1468237.
doi: 10.3389/fphar.2024.1468237

Comparison of the composition, immunological activity and anti-fatigue effects of different parts in sika deer antler

Siqi Chen, Yidan Li, Yichun Yang, Shibo Zhao, Huali Shi, Chengkai Yang, Min Wu and Aiwu Zhang*

College of Animal Science and Technology, Jilin Agricultural University, Changchun, China

Background: Sika deer (*Cervus nippon Temminck*, 1838) antler is a highly esteemed tonic renowned for its abundant assortment of polypeptides, polysaccharides, amino acids, and minerals, and is recognized for its multifarious pharmacological properties. However, limited research has been conducted regarding the variation in composition of deer antlers between the upper and basal sections, as well as their pharmacological effects on immunological activity and anti-fatigue in mice. The objective of this study was to conduct a comprehensive analysis on the appearance, chemical composition, and pharmacological effects of different components within sika deer antlers. This investigation aims to elucidate the disparities in quality among various parts of antlers and establish a theoretical foundation for the precise utilization of sika deer antlers.

Methods: The contents of protein, amino acids, polysaccharides, phospholipids, minerals and nucleotides in wax, powder, gauze and bone slices were determined by different nutrient assays. Then, 100 mice were randomly divided into 5 groups. The mice in control group were administered 0.3 mL of saline solution per day. The mice in experimental groups were administered 0.3 mL enzymatic hydrolysate of the wax slice, powder slice, gauze slice, bone slice separately per day, continuously for 14 days from the first day. The effect of antler on boosting immunity was evaluated by testing organ indices and assessing immunoglobulin levels by ELISA. Anti-fatigue effects were assessed by a mouse swimming test. Finally, the correlation between composition and pharmacological effects was analysed.

Results: The content of each marker substance gradually decreases from the upper to the basal of deer antler. The protein and uracil content in the wax slice were significantly higher than the other three groups ($p < 0.05$), and the phospholipid and inosine content were strongly significantly higher than the other three groups ($p < 0.01$). The content of polysaccharides and hypoxanthine in the wax slice group and powder slice group was significantly higher than that in the gauze slice group and bone slice group ($p < 0.05$). The amino acid content decreases from the upper to the basal section. Among, the content of Glu, Gly, His, and Pro wax slice was significantly higher than the other three groups ($p < 0.01$). The content of other minerals except Fe and Mg in the wax slice group was significantly higher than the other three groups ($p < 0.01$), and the content of Fe and Mg in the bone slice was the highest. Additionally, the immune organ index, immunoglobulin, and glycogen contents displayed a significant increase in

comparison to both the control group and the other experimental groups ($p < 0.05$). And the swimming endurance of mice in the wax slice group was significantly prolonged ($p < 0.01$). The skeletal muscle state of the wax group mice exhibited superior characteristics, characterized by distinct horizontal stripes and tightly arranged muscle fibers. In contrast, the bone group displayed noticeable yet relatively less compact horizontal stripes. Among the organic and inorganic compositions of deer antler, the highest degree of correlation with the content of IgA, IgM, and IgG was found to be protein ($r^2 = 0.999$), uracil ($r^2 = 0.987$), and inosine ($r^2 = 0.999$), respectively. The proteins ($r^2 = 0.997$) appear to exert a significant influence on the anti-fatigue effect, while polysaccharides ($r^2 = 0.865$) demonstrate the least relevance.

Conclusion: These outcomes indicated that the wax slice yielded optimal results among the tested parts and demonstrated the highest efficacy.

KEYWORDS

sika deer antler, composition, immunological activity, anti-fatigue effect, traditional medicine

1 Introduction

Deer antler refers to the immature horn of male deer, a member of the Cervidae family, characterized by densely packed antler hair that has not yet undergone ossification. The investigation of deer antler has long been a prominent subject in the realm of traditional pharmacological research, with prior studies demonstrating its diverse array of inorganic and organic compounds. The former primarily consists of various micronutrients (Dong et al., 2004), whereas the latter predominantly encompasses polysaccharides, phospholipids, nucleosides, lipid-soluble and water-soluble compounds, as well as insoluble proteins. These chemical constituents are intricately associated with the pharmacological properties of deer antler (Liu et al., 2020).

Two millennia ago, ancient medical literature provided a comprehensive account of the therapeutic application of sika deer antlers (*Cervus nippon Temminck*, 1838) for treating a diverse range of 52 ailments (Kawtikwar et al., 2010). In recent years, the application of genomics, proteomics, and other molecular biology techniques has significantly broadened the scope of research on marker substances and medicinal mechanisms associated with deer antler. However, despite the continuous expansion of this scope, there remains a limited focus on evaluating the efficacy of different components within deer antler. The minimal dosage, rapid therapeutic effects, and positive health outcomes of Sika deer antler and its derivatives have garnered significant attention from researchers both domestically and internationally. In terms of immune enhancement, Zheng (Zheng et al., 2017) demonstrated that oral administration of deer antler in mice resulted in an increased proportion of T cells and a decreased proportion of B cells in peripheral blood. Scientific evidence has demonstrated the significant impact of deer antler on augmenting cellular immunity within the human body.

Meanwhile, Liu and college (Liu et al., 2023) elucidated the potential regulatory mechanism of deer antler in enhancing immunity through network pharmacology and molecular docking technology, and identified four substances and 130 core targets that may exert immune regulatory effects. Deer antler extract also exerts a significant impact on the process of fracture healing. The findings reported by Wang (Wang et al., 2022) demonstrate that deer antler extract effectively stimulates fracture healing through the activation of the BMP-2/SMAD4 signaling pathway. Deer antler also exhibits a notable anti-fatigue effect. The findings of Zhang (Zhang et al., 2020) demonstrated a direct correlation between the levels of eight nucleotides in deer antler, spanning from the upper to basal section, and the forced swimming test performance in mice. Therefore, it can be inferred that deer antler exhibits a significant anti-fatigue effect. Undoubtedly, deer antler exhibits potent pharmacological properties with anti-inflammatory effects. Widyowati (Widyowati et al., 2023) established a mouse model of arthritis and demonstrated the efficacy of orally administered ethanol extract of deer antler in reducing IL-1β cytokine levels. The present study aims to demonstrate the efficacy of deer antler in reducing the levels of inflammatory factors, thereby highlighting its significant potential in combating inflammation. The diverse chemical composition of deer antler serves as the foundation for its multifaceted medicinal properties. The intricate chemical

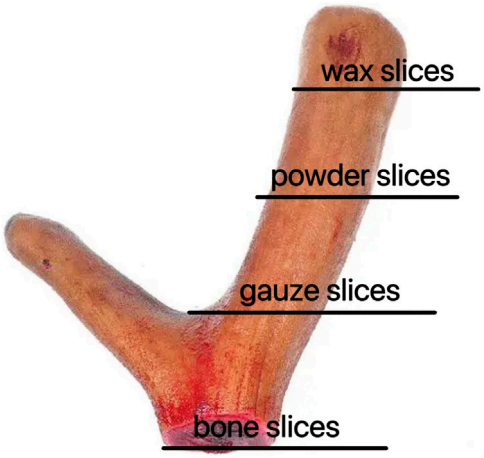

FIGURE 1
Different parts of deer antler in sika deer (from the upper to the basal section).

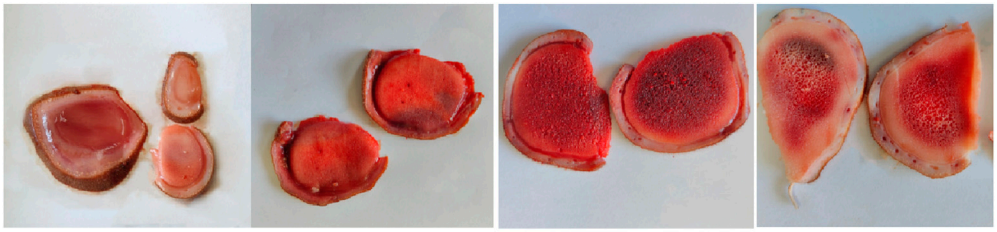

FIGURE 2
Appearance of different parts of deer antlers slice [In the panel **(A)** wax slice, **(B)** powder slice, **(C)** gauze slice, **(D)** bone slice].

composition of deer antler underscores the intricacy of its pharmacological potential. Furthermore, the intricate interplay between deer antler quality, marker substances, and concentration underscores the multifaceted relationship between the quality of deer antler and its pharmacological effects.

To date, numerous studies have been conducted to investigate the comprehensive pharmacological effects of deer antler. However, limited research has been conducted on the fractionation of deer antler to investigate its chemical composition and pharmacological variations. Hence, the objective of this study is to conduct a comparative analysis on the composition of four distinct segments of deer antlers, namely, wax slice, powder slice, gauze slice, and bone slice (Figure 1). Furthermore, we endeavored to assess the immunomodulatory activity and anti-fatigue efficacy of deer antler hydrolysate in mice. Through this study, our objective is to provide valuable insights into the pharmacological effects and therapeutic mechanisms of deer antler, facilitating a comprehensive exploration in line with the rigorous standards set by Nature journal.

2 Materials and methods

2.1 Sample collection

Sika deer antlers in the early stages of growth and development were provided by the Dongda Deer Farm in Changchun, Jilin Province, China. The deer was first placed under general anesthesia and the antler was then removed proximally using a surgical hand saw (Shi et al., 2021). The studies were approved by the Experimental Animal Welfare and Ethics Committee of Dongda Deer Farm (permit number: 20230810001). The studies were conducted in accordance with the local legislation and institutional requirements.

2.2 Reagents and antibodies

Copper sulfate (CAS: 7758-98-7), potassium sulfate (CAS: 7778-80-5), sulfuric acid (CAS: 7664-93-9), 2% boric acid solution, nitric acid (CAS: 7697-37-2), methyl red bromocresol green mixed indicator, 40% sodium hydroxide solution (CAS: 1310-73-2), boric acid (CAS: 10043-35-3), ethanol (CAS: 64-17-5), phenol (CAS: 108-95-2), high-purity nitrogen gas, sodium citrate (CAS: 68-04-2), elution buffer solution, indanone solution (CAS: 485-47-2), amino acid standard, Sodium molybdate (CAS: 7631-95-0), potassium dihydrogen phosphate (CAS: 7778-77-0), 50% potassium hydroxide solution (CAS: 1310-58-3), hydrochloric acid (CAS: 7647-01-0), zinc oxide (CAS: 1314-13-2), 0.015% hydrazine sulfate solution (CAS: 10034-93-2), analytical pure glucose, trichloroacetic acid (CAS: 76-03-9) Potassium borohydride (CAS: 13762-51), ammonium molybdate (CAS: 13106-76-8), hydroquinone (CAS: 123-31-9), all reagents are analytical grade and come from Beijing Chemical Plant; Uracil (batch number TM0313XB13), hypoxanthine (batch number TM0313XC13), inosine (batch number TJ0623XA13) were procured from Shanghai Yuanye Biotechnology Co., Ltd. (Shanghai, China).; The mass concentration of the multi-element mixed standard reserve solution of Zn and Fe, as well as the single element standard reserve solution of K, Na, and Mg, are both 1,000 $\mu g \cdot L^{-1}$, provided by the National Nonferrous Metals and Electronic Materials Analysis and Testing Center. Pepsin: 1:3,000, purchased from Changchun Huayi Biotechnology Co., Ltd. Paraformaldehyde (4%), hematoxylin and eosin were supplied by Biosharp, Hefei, China.

2.3 Appearance of different parts of sika deer antlers slice

Six two-branched fresh deer antlers were cut from the upper to the basal section into four separate parts: wax slice, powder slice, gauze slice and bone slice. The fresh two-branched sika deer antlers were meticulously examined to assess variations in hue, texture, and fragrance following precise slicing using a specialized slicer, facilitating a comprehensive comparison across different sections of the antlers.

2.4 Sika deer antler powder and its enzymatic hydrolysate preparation

The wax slice, powder slice, gauze slice and bone slice of each deer antler were ground and mixed together separately to pass through a 250 mm screen and stored for subsequent analysis. Twelve grams of different parts of deer antler powder were weighed and dissolved in 50 mL of distilled water. Subsequently, a 1% hydrochloric acid solution was added, and the pH was adjusted to between 1.5 and 2. Following this, 0.24 g of pepsin was added in

accordance with a 1:50 ratio of enzyme to substrate to initiate the enzymatic hydrolysis. The enzymatic digestion process was consistently maintained in a 37°C constant temperature water bath. After 6 h of enzymatic digestion, a 1% sodium hydroxide solution was introduced to adjust the pH of the enzymatic digestion solution to 6.5–7.0. Once the enzymatic digestion was complete, the solution was subjected to boiling for 10 min, followed by cooling to room temperature. Subsequently, centrifugation was carried out for 15 min at 3,500 rpm, and the resulting supernatant was collected and stored at 4°C for future use.

2.5 Chemical composition analysis of different parts in sika deer antlers

2.5.1 Determination of protein content

The protein was determined using the Bradford method and the absorbance was measured using a UV spectrophotometer. Make a suspension of deer antler powder and set it aside. Extract water-soluble protein using a 200W ultrasonic cleaner, centrifuge the supernatant after ultrasonic treatment at a speed of 4000r/min. Prepare a standard solution using bovine serum albumin (BSA) and create a standard curve. Add the extracted supernatant to Coomassie Brilliant Blue-250, mix well, and measure the absorbance after 10 min. Based on the absorbance of the sample to be tested, calculate the protein concentration of the sample from the standard curve.

2.5.2 Evaluation of phospholipids content

Phospholipids were measured according to the method of Nation Standards of the People's Republic of China GB/T 5537-2008. A precise 10 g of different parts of deer antler powder was meticulously weighed and subjected to ashing with zinc oxide. Subsequently, the resulting ash was dissolved in 10 mL of hot hydrochloric acid (1:1) and meticulously filtered. The filtrate was then neutralized with a 50% potassium hydroxide solution until turbidity appeared. Following this, hydrochloric acid was cautiously added dropwise to ensure the dissolution of all zinc hydroxide precipitates. Two drops were added, and the sample was ultimately diluted with water to the specified scale and thoroughly shaken. The phospholipid content was then determined using a UV spectrophotometer (SPECORD 205, Germany).

2.5.3 Assessment of polysaccharides content

Polysaccharides were measured according to the method of Nation Standards of the People's Republic of China GB/T 40632-2021. Weigh 1.000 g of deer antler powder, add 1 mL of a 15% trichloroacetic acid solution and a small amount of a 5% trichloroacetic acid solution, and mix thoroughly. Centrifuge three times at 3,000 rpm, collecting the supernatant each time. Add 2 mL of 6 mol/L hydrochloric acid to the supernatant, mix well, and then place in a 96°C water bath for 2 h. After the water bath, add 2 mL of 6 mol/L sodium hydroxide solution to a 25 mL volumetric flask, then add 6% phenol solution and concentrated sulfuric acid, and mix them well. Prepare the test solution, measure the absorbance at 490 nm using a UV spectrophotometer, and calculate the polysaccharide content based on the standard curve.

2.5.4 Evaluation of nucleosides content

The nucleosides were measured according to the method established by Sun et al. (2018). A precise 100 mg of different parts of deer antler powder was extracted using ultrasonic extraction with distilled water, and the resulting supernatant was filtered through a 0.22 μm aqueous filtration membrane. The content of nucleosides was determined using the UPLC method.

2.5.5 Determination of amino acid content

Amino acid were measured according to the method of Nation Standards of the People's Republic of China GB 5009.124–2016. For the analysis of amino acids, 30 mg of samples was accurately weighed following the hydrolysis of different parts of deer antler powder. The resulting samples were then meticulously filtered using a syringe filter (0.22 μm) and subjected to analysis using an amino acid autoanalyzer (Pharmacia Biotech Biochrom 20, Ninhydrin Method). The determination of amino acids was conducted based on absorbances recorded at 440 and 570 nm.

2.5.6 Assessment of mineral content

The determination of mineral content was conducted following the method outlined by Wang et al. (2018). The concentrations of potassium (K), sodium (Na), and iron (Fe) were analyzed using atomic absorption spectrometry, while magnesium (Mg) and zinc (Zn) were determined using ICP-MS.

2.6 Animal experiment

2.6.1 Animals

One hundred mice used in the experiment were procured from Liaoning Changsheng Biotechnology Co., Ltd. (Changchun, China) and were identified with license number SCXK (Liaoning) 2020-0001, as well as an experimental animal quality certificate number: NO.210726230101468567. Throughout the experiment, the mice were maintained in an environment with a constant temperature of 23°C, adequate humidity, access to abundant water and food, and 12-h light-dark cycle. The experimental protocol, which was meticulously crafted to alleviate pain and discomfort for the animals, received approval from the Animal Experiment Ethics Committee of Jilin Agricultural University (permit number: 20240703001). Mice were individually housed and underwent a 12-h fasting period prior to the experiments. All co-authors were in complete agreement with the plans and procedures of the animal experiments.

2.6.2 Experimental design

One hundred 8-week-old KM male mice were adaptively raised for 1 week, and then randomly divided into 5 groups (n = 20) including 1 control group and 4 experimental groups. The mice in control group were administered 0.3 mL of saline solution per day. The mice in experimental groups were administered 0.3 mL enzymatic hydrolysate of the wax slice, powder slice, gauze slice, bone slice separately per day, continuously for 14 days from the first day. 10 mice were used to compare the effects of different parts of deer antler on immunological activity in mice, and other 10 mice were used to compare the effects of different parts of deer antler on anti-fatigue in mice. Fourteen days later, blood samples were

TABLE 1 Reagents to be added to each tube.

Reagents	Measuring tube (μL)	Standard tube (μL)	Empty tube (μL)
Sample	60	—	—
Standard liquid	—	60	—
Distilled water	—	—	60
Colour liquid	240	240	240

Boiling water bath for 10 min (sealed to prevent water loss) Cool to room temperature.

procured from the ocular region, and the mice were euthanized through cervical dislocation. Subsequently, tissue samples including the spleen, thymus, and muscle were harvested from the deceased mice (Lu Y et al., 2024). Serum was obtained after the collected blood sample was centrifuged at 3,500 rpm at 4°C for 10 min and stored at −20°C for subsequent immunoglobulins analysis experiments.

2.6.3 Immune organ index analysis

The overall health of the mice, including their appearance, activity, and feeding behavior, was meticulously monitored throughout the experiment. Following the treatment period, the mice were humanely sacrificed, and their spleens and thymuses were promptly excised and weighed to determine the thymus index and spleen index. The index were calculated using the following formula:

$$\text{Index}\,(\text{mg/g}) = \frac{\text{weight of thymus or spleen}}{\text{body weight}}$$

2.6.4 Immunoglobulins analysis

The levels of immunoglobulin A (IgA), immunoglobulin G (IgG), and immunoglobulin M (IgM) in the blood were quantified using commercially available kits obtained from Nanjing Jiancheng Institute of Biotechnology (Nanjing, China) in accordance with the manufacturer's instructions.

2.6.5 Anti-fatigue analysis

After the completion of the intragastric administration regimen, on the 15th day, lead blocks weighing 8% of the mice's body weight were affixed to their tails. Subsequently, the mice were subjected to a forced swimming test in a water tank while carrying additional weight load. The swimming pool had a depth of approximately 35 cm, while the water temperature was maintained at (25 ± 2)°C throughout the study period. The duration of swimming under the imposed weight, from the initiation of swimming until the mice submerged and succumbed, was recorded to assess the impact of anti-fatigue.

2.6.6 Glycogen levels analysis

2.6.6.1 Sample preparation

After the completion of the intragastric administration regimen on the 15th day, mice were euthanized and their livers were excised. The skeletal muscles from the thighs of the mice were meticulously dissected in a circular fashion using a scalpel. Subsequently, 0.2 g of liver/muscle tissue was accurately weighed and transferred into a 10 mL centrifuge tube for subsequent homogenization. A 1 mL aliquot of the resulting homogenate was subsequently subjected to centrifugation at a speed of 8000 × g for a duration of 10 min at room temperature, and the resultant supernatant was collected as the test sample.

The reagents listed in Table 1 were then added sequentially to the centrifuge tube.

2.6.6.2 Measure of absorbances

Pipette 200 μL of the reaction solution into a 96-well plate or microglass cuvette and measure the absorbance value at 620 nm, which is recorded as the A assay, A standard and A blank; calculate ΔA assay = A assay-A blank and ΔA standard = A standard-A blank.

2.6.6.3 Establishment of standard curve

The standard curve was plotted with 0.30, 0.25, 0.20, 0.15, 0.10, 0.05 mg/mL as the horizontal coordinate (x) and its corresponding ΔA standard as the vertical coordinate (y) to obtain the standard equation y = kx + b, and the ΔA measurement was brought into the formula to obtain x (mg/mL).

2.6.6.4 Formula for calculating glycogen

$$\text{Glycogen}\,(\text{mg/g}) = \left(x \times V_{\text{sample total}} \times 0.9\right) / W = (4.5 \times x) / W.$$

($V_{\text{sample total}}$: total volume of sample to be measured, 5 mL; W: sample mass, g).

2.6.7 Pathological and histological examination

To prepare the histological slices, samples of leg muscle were first fixed in 4% paraformaldehyde, then embedded in paraffin and subsequently sectioned. The resulting tissue slices were stained with hematoxylin and eosin (H&E) from Biosharp, China, and captured under anoil microscope (Nikon Eclipse 80i, Tokyo, Japan).

2.7 Generation of correlation heat maps

The correlation heat map was generated by the Lianchuan BioCloud platform, with the Pearson method selected for the correlation analysis. The color gradient ranging from blue to red signifies the continuum of correlation, spanning from negative to positive values, while the numerical representation on the graph denotes the r^2 (correlation coefficient).

2.8 Statistical analysis

Statistical analysis was conducted using least-squares analysis of variance (ANOVA) in accordance with the general linear model

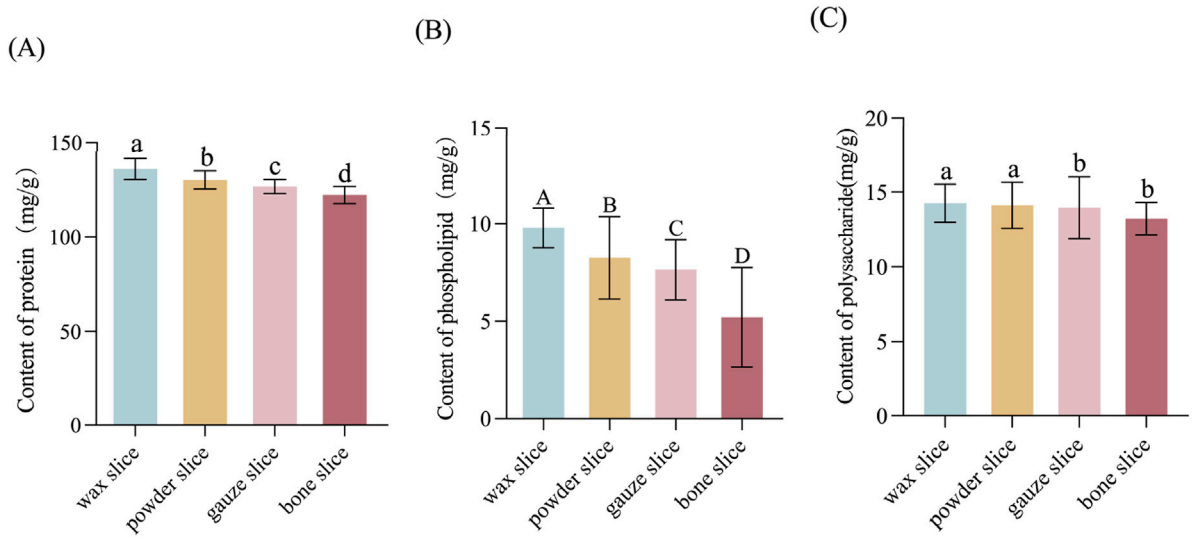

FIGURE 3
The protein, phospholipid and polysaccharide contents in different parts of deer antler **(A)** Content of protein in different parts of deer antler. **(B)** Content of phospholipid in different parts of deer antler. **(C)** Content of polysaccharide in different parts of deer antler. Note: Means for different lowercase letters were significantly different ($p < 0.05$). Means for different capital letters were extremely significantly different ($p < 0.01$).

procedure of SPSS (SPSS 26.0 for Windows; SPSS Inc., Chicago, IL, United States). Each experiment was replicated at least three times. Descriptive statistics were presented as mean ± standard deviation ($\bar{x} \pm SD$), and comparisons were made using one-way ANOVA followed by the Duncan test. A significance level of $p < 0.01$ was considered highly significant, while $p < 0.05$ was deemed significant.

3 Results

3.1 Assessment of visual characteristics

Wax slice: The slices are cut into circular or elliptical shapes. They display a light reddish-brown hue, translucency, a subtle gloss, and a reddish-brown rim along the periphery. They lack osseous structures and exhibit a resilient, compact, lipid-rich, and moist constitution reminiscent of adipose tissue. The color of the substance is a waxy yellow, exhibiting a crystalline appearance reminiscent of beeswax, which signifies its exceptional quality (Figure 2A).

Powder slice: The slices are uniformly round and slightly thick, exhibiting a neat surface texture. The specimens exhibit a smooth texture, devoid of any bony structures, and are characterized by a distinctive yellow-brown peripheral ring. Recurring instances of residual deer antler may occasionally be observed. The fishy flavor is subtly present, accompanied by a subtle hint of salinity, suggesting a lower quality in comparison to wax slices (Figure 2B).

Gauze slice: The slices are circular and substantial, showcasing a meticulous surface adorned with densely distributed honeycomb perforations and delicate filamentous apertures. The specimens demonstrate no yarn leakage and exhibit a seamless integration between the cortex and deer antler tissues. Possessing a slightly granular texture and exhibiting a yellow-brown ring at the periphery, they are comparatively coarser than powdered slices, indicating inferior quality (Figure 2C).

Bone slice: The slice exhibits a white, honeycomb-like structure with substantial interstices. The outer layer exhibits an osseous structure, contributing to a robust and brittle characteristic, rendering them susceptible to fracturing (Figure 2D).

3.2 Determination of protein, phospholipid, and polysaccharide levels

The data indicate a sequential decrease in protein content from wax slice to bone slice, with a significant variance among the four parts ($p < 0.05$, Figure 3A). Similarly, the phospholipid content exhibited a sequential reduction from wax slice to bone slice, with a highly significantly variance among the four parts ($p < 0.01$, Figure 3B). Furthermore, the polysaccharide content was notably higher in wax slice and powder slice compared to gauze slice and bone slice, the difference was significant ($p < 0.05$, Figure 3C).

3.3 Determination of nucleosides contents

The Figure 4 illustrates the levels of uracil, inosine and hypoxanthine in various parts of deer antlers. It is evident from the data that the concentration of uracil was greater in the wax slice compared to the other three parts ($p < 0.05$). There was no significant difference among the other three groups ($p > 0.05$). Additionally, the inosine content in the wax slice was strongly significantly greater than other three parts ($p < 0.01$), while both the powder slice and gauze slice exhibited significantly higher levels of inosine than the bone slice ($p < 0.01$). Moreover, the hypoxanthine content was significantly elevated in both the wax

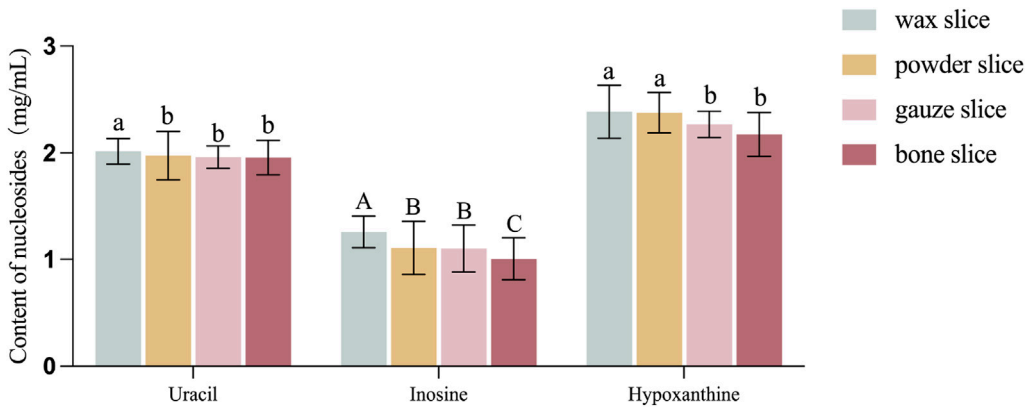

FIGURE 4
Content of nucleosides in different parts of deer antler. Note: Means for different lowercase letters were significantly different ($p < 0.05$). Means for different capital letters were extremely significantly different ($p < 0.01$).

TABLE 2 Content of amino acid in different parts of deer antler.

Item	Wax slice	Powder slice	Gauze slice	Bone slice
Asp	56.35 ± 2.74^{a}	53.77 ± 1.89^{b}	53.27 ± 1.20^{b}	52.74 ± 1.54^{c}
Thr	21.39 ± 2.11^{a}	21.38 ± 1.45^{a}	19.58 ± 1.24^{b}	18.75 ± 1.81^{b}
Ser	47.06 ± 3.14	47.05 ± 1.25	47.00 ± 1.07	46.97 ± 1.54
Glu	76.65 ± 2.19^{A}	70.56 ± 2.74^{B}	64.25 ± 4.32^{C}	60.57 ± 3.18^{D}
Gly	137.89 ± 9.24^{A}	130.52 ± 5.21^{B}	124.28 ± 5.27^{C}	123.14 ± 3.33^{C}
Ala	53.65 ± 2.78	53.44 ± 1.20	53.01 ± 1.44	52.97 ± 1.01
Cys	46.48 ± 3.24	46.12 ± 2.19	46.10 ± 1.87	46.02 ± 3.74
Val	21.99 ± 1.20	21.39 ± 1.98	21.02 ± 1.57	20.99 ± 2.10
Met	8.85 ± 0.87^{a}	8.21 ± 1.24^{b}	8.19 ± 1.27^{b}	7.64 ± 1.33^{c}
Lle	43.61 ± 4.65	43.57 ± 2.58	43.21 ± 2.11	43.01 ± 1.98
Leu	70.59 ± 7.25^{a}	65.24 ± 5.21^{b}	61.24 ± 3.57^{c}	59.24 ± 1.68^{c}
Tyr	20.13 ± 2.14	20.11 ± 1.24	20.01 ± 1.08	19.95 ± 1.57
Phe	21.2 ± 1.20^{a}	19.25 ± 2.45^{b}	19.04 ± 1.56^{b}	17.24 ± 2.00^{c}
Lys	52.01 ± 3.67^{a}	50.11 ± 2.65^{b}	48.27 ± 3.14^{c}	47.52 ± 2.14^{c}
His	41.32 ± 2.24^{A}	35.74 ± 3.51^{B}	29.57 ± 1.34^{C}	22.10 ± 1.88^{D}
Arg	34.66 ± 2.17^{a}	31.25 ± 1.25^{b}	31.00 ± 1.17^{b}	30.85 ± 1.55^{b}
Pro	48.48 ± 3.25^{A}	39.21 ± 1.27^{B}	39.07 ± 2.47^{B}	38.99 ± 2.40^{B}

Note: Means with different lowercase letters within a row differ significantly ($p < 0.05$). Means with different uppercase letters differ extremely significantly ($p < 0.01$).

slice and powder slice in comparison to the gauze slice and bone slice ($p < 0.05$).

3.4 Determination of amino acids contents

The Table 2 presents the amino acid compositions of different parts of deer antlers. It reveals a gradual decline in the levels of 17 amino acids from the upper to the basal section. Notably, the wax slice exhibited significantly higher concentrations of Asp, Met, and Phe compared to the powder slice, gauze slice, and bone slice ($p < 0.05$). Furthermore, the powder slice and gauze slice displayed significantly higher levels of these amino acids than the bone slice ($p < 0.05$). Additionally, the Thr content was significantly elevated in both the wax slice and powder slice compared to the gauze slice and bone slice ($p < 0.05$).

The levels of Glu and His in different parts were strongly significantly differences ($p < 0.01$). Moreover, the Gly content

TABLE 3 Content of mineral elements in different parts of deer antler.

Item	Wax slice	Powder slice	Gauze slice	Bone slice
K	7.62 ± 0.119^{aA}	6.48 ± 0.163^{bA}	5.00 ± 0.130^{B}	3.17 ± 0.121^{C}
Na	8.66 ± 0.115^{a}	8.15 ± 0.140^{b}	7.84 ± 0.132^{c}	7.23 ± 0.140^{d}
Mg	3.54 ± 0.11^{d}	3.77 ± 0.56^{c}	4.06 ± 0.38^{b}	4.29 ± 0.19^{a}
Zn	0.074 ± 0.001^{a}	0.071 ± 0.003^{a}	0.068 ± 0.002^{a}	0.064 ± 0.002^{b}
Fe	0.087 ± 0.008^{C}	0.113 ± 0.008^{bB}	0.128 ± 0.007^{aB}	0.156 ± 0.011^{A}

Note: Means with different lowercase letters within a row differ significantly ($p < 0.05$). Means with different uppercase letters differ extremely significantly ($p < 0.01$).

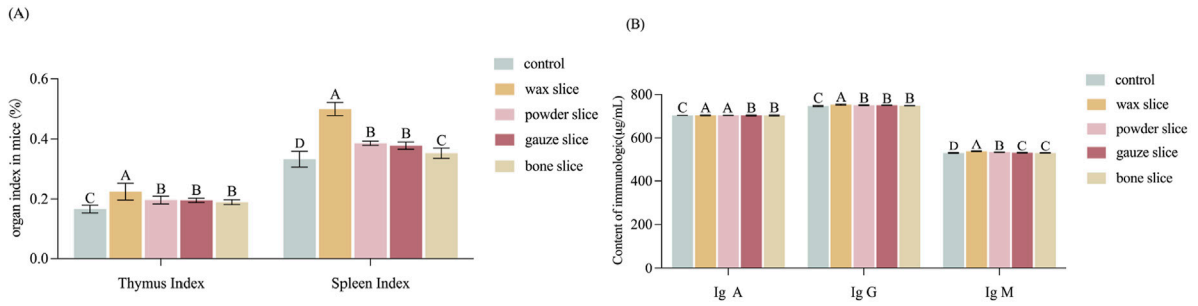

FIGURE 5
Effect of different parts of deer antler on immunological activity in mice **(A)** Effect of different parts of deer antler on organ index in mice (n = 20). **(B)** Effect of in different parts of deer antler slice on immunologic (n = 20) Note: Means with different uppercase letters differ extremely significantly ($p < 0.01$). Control: The mice in control group were administered 0.3 mL of saline solution per day, continuously for 14 days from the first day. Wax slice: The mice in wax slice group were administered 0.3 mL of wax slice enzymatic hydrolysate per day, continuously for 14 days from the first day. Powder slice: The mice in powder slice group were administered 0.3 mL of powder slice enzymatic hydrolysate per day, continuously for 14 days from the first day. Gauze slice: The mice in gauze slice group were administered 0.3 mL of gauze slice enzymatic hydrolysate per day, continuously for 14 days from the first day. Bone slice: The mice in bone slice group were administered 0.3 mL of bone slice enzymatic hydrolysate per day, continuously for 14 days from the first day (The following figure is the same.).

was notably higher in the wax slice than in the remaining three parts ($p < 0.01$), and significantly higher in the powder slice than in the gauze slice and bone slice ($p < 0.01$). Likewise, both Leu and Lys contents were significantly higher ($p < 0.05$) in the wax slice than in the other three parts, and also significantly higher ($p < 0.05$) in the powder slice than in the gauze slice and bone slice. The Arg content was significantly elevated ($p < 0.05$) in the wax slice compared to the other three parts. Lastly, the Pro content in the wax slice was highly significantly higher than the remaining three parts ($p < 0.01$).

3.5 Analysis of mineral element composition

Table 3 presents the mineral element composition in different parts of deer antlers. The data reveals that the potassium (K) content in the wax slice and powder slice was significantly higher than that in the gauze slice and bone slice ($p < 0.01$). Furthermore, the gauze slice exhibited a significantly higher K content than the bone slice ($p < 0.01$), and the wax slice group had a notably higher K content than that in the powder slice ($p < 0.05$). The sodium (Na) and magnesium (Mg) contents across different antler parts demonstrated significant variations ($p < 0.05$), with Na content declining gradually from the upper to the basal section of deer antlers, while Mg content exhibited an opposite trend. Additionally, the zinc (Zn) content in the wax slice, powder slice and gauze slice was significantly higher than the bone slice ($p < 0.05$). Conversely, the iron (Fe) content was markedly lower in the wax slice compared to the other three parts ($p < 0.01$), and it was notably lower in the powder slice and gauze slice than in the bone slice ($p < 0.01$), with a significant difference also observed between the powder slice and gauze slice ($p < 0.05$).

3.6 Effect of different parts of deer antler on immunological activity in mice

The index of thymus and spleen serve as indicative measures of the organism's immune function. Figure 5A illustrates that the organ index of mice administered with the enzymatic hydrolysate of different parts of deer antler were all significantly higher than those of the control group ($p < 0.01$). Notably, the thymus index exhibited a gradual decrease from the upper to the basal sections and was significantly higher in the wax slice group compared to the powder slice, gauze slice and bone slice groups ($p < 0.01$). Conversely, there was no significant difference observed between the powder slice, gauze slice, and bone slice groups ($p > 0.05$). Similarly, the spleen index also displayed a gradual decrease from the upper to the basal sections and was significantly higher in the wax slice group compared to the powder slice, gauze slice, and bone slice groups ($p < 0.01$). Moreover, there was no significant difference observed between the powder slice and gauze slice groups ($p > 0.05$);

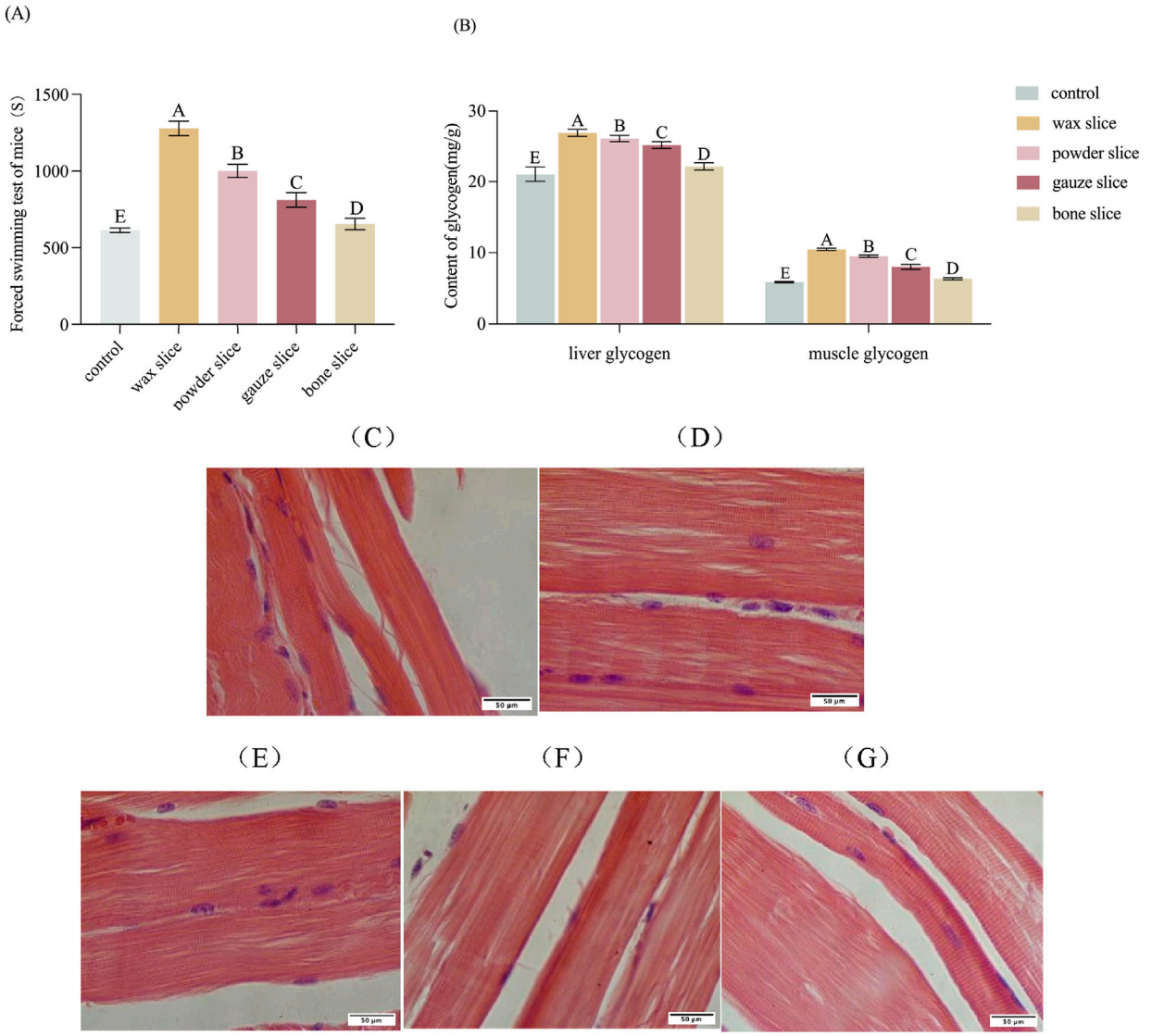

FIGURE 6
Effect of different parts of deer antler on anti-fatigue in mice. **(A)** Effect of different parts of deer antler on the swimming time of loading mice (n = 20). **(B)** Effect of different parts of deer antler on glycogen content of mice (n = 20). **(C)** Hematoxylin and Eosin (H&E)-stained of muscle sections after saline solution treatment (n = 20). **(D)** Hematoxylin and Eosin (H&E)-stained of muscle sections after wax slice enzymatic hydrolysate treatment (n = 20). **(E)** Hematoxylin and Eosin (H&E)-stained of muscle sections after powder slice enzymatic hydrolysate treatment (n = 20). **(F)** Hematoxylin and Eosin (H&E)-stained of muscle sections after gauze slice enzymatic hydrolysate treatment (n = 20). **(G)** Hematoxylin and Eosin (H&E)-stained of muscle sections after bone slice enzymatic hydrolysate treatment (n = 20). Note: Means for different lowercase letters were significantly different ($p < 0.05$). Means with different uppercase letters differ extremely significantly ($p < 0.01$).

however, both were significantly higher than the bone slice group ($p < 0.01$).

The impact of deer antler enzyme digest on the immunological activity of mice was assessed by measuring the secretion of cytokines IgA, IgG, and IgM. As depicted in Figure 5B, the serum levels of IgA exhibited a gradual decrease from the upper to the basal sections. The levels of IgA, IgG, and IgM in the experimental group were all strongly significantly than those in the control group ($p < 0.01$). Furthermore, the IgG levels in the wax slice group was strongly significantly than those in the control group and the other experimental groups ($p < 0.01$). Similarly, the IgM levels in the wax slice group was strongly significantly than those in the powder slice, gauze slice and bone slice groups ($p < 0.01$). Additionally, The serum IgA content in the wax slice and powder slice was significantly greater than that in the gauze slice and bone slice group ($p < 0.01$), while there was no significant difference between the gauze slice group and the bone slice group ($p > 0.05$).

3.7 Effect of different parts of deer antler on anti-fatigue in mice

The impact of different parts of deer antler on the forced swimming endurance of mice is displayed in Figure 6A. The forced swimming duration of mice in the experimental groups was significantly longer than that of the control group ($p < 0.01$).

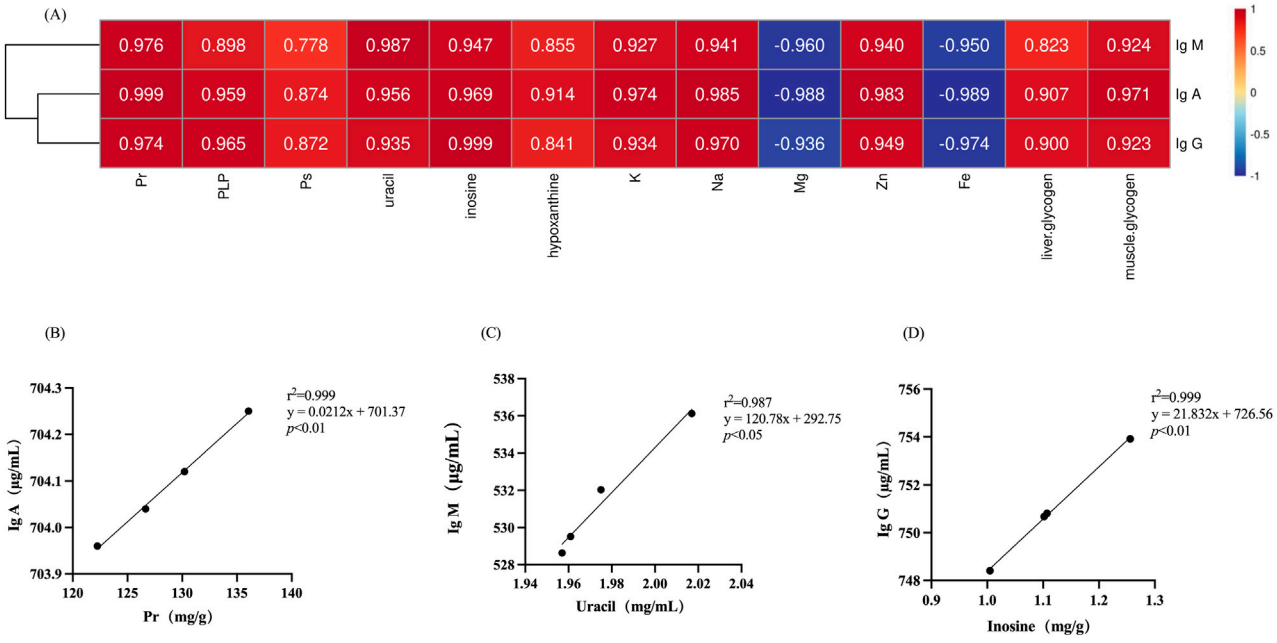

FIGURE 7
Correlation of chemical compositions in deer antlers with immunological indicators. **(A)** Heatmap of the correlation between chemical compositions in deer antler and immune indicators. **(B)** Simple linear regression analysis of protein versus IgA. **(C)** Simple linear regression analysis of uracil versus IgM. **(D)** Simple linear regression analysis of inosine versus IgG. Note: Different lower case letters indicate significant differences ($p < 0.05$) and different upper case letters indicate highly significant differences ($p < 0.01$). (Pr, protein; PLP, phospholipid; PS, polysaccharide; same as follow).

There was a significant difference observed among deer antler groups ($p < 0.01$), with the endurance ranking in the following order: wax slice > powder slice > gauze slice > bone slice.

The impact of different parts of deer antler on the glycogen content of mice is presented in Figure 6B. The hepatic and muscular glycogen levels in the experimental groups were significantly elevated compared to those in the control group ($p < 0.01$). Furthermore, there were significant differences in the levels of hepatic and muscular glycogen among the deer antler groups ($p < 0.01$), with the following ranking from highest to lowest: wax slice > powder slice > gauze slice > bone slice.

To evaluate the impact of enzymatic hydrolysate administration of different parts of deer antler on the morphology of skeletal muscle in mice, the histology of skeletal muscle was assessed through H&E staining (Figures 6C–G). The muscle fibres and transverse striations appeared more relaxed in the control group and tighter in the test group. The wax slice group displayed the most favorable skeletal muscle condition in mice, characterized by distinct transverse striations and taut muscle fibre. There was no significant difference between the powder slice group and the gauze slice group, while the transverse striations of the bone slice group were apparent but less taut.

3.8 Correlation between chemical composition and immune-enhancing effects

Correlation analysis was employed to ascertain the correlation between various types of compositions in deer antler and immune-enhancing effect. As depicted in Figure 7, among the organic and inorganic compositions of deer antler, the highest degree of correlation with the content of IgA, IgM, and IgG was found to be protein ($r^2 = 0.999$), uracil ($r^2 = 0.987$), and inosine ($r^2 = 0.999$), respectively.

3.9 Correlation between chemical composition and anti-fatigue effects

Figure 8 illustrates the correlation between chemical composition and the anti-fatigue properties. It is evident that proteins ($r^2 = 0.997$) appear to exert a significant influence on the anti-fatigue effect, while polysaccharides ($r^2 = 0.865$) demonstrate the least relevance.

4 Discussion

Deer antler, a traditional animal medicine, possesses diverse medicinal properties. The immunomodulatory and anti-fatigue properties of antler have been unequivocally demonstrated; however, limited research has investigated the effects of different parts of antler when administered separately. In consideration of the intricate composition of marker substances in animal medicines, this study initially examined the protein, amino acid, polysaccharide, phospholipid contents in wax, powder, gauze and bone slices respectively. Subsequently, the effects of enzymatic hydrolysate derived from different parts of antlers on immune

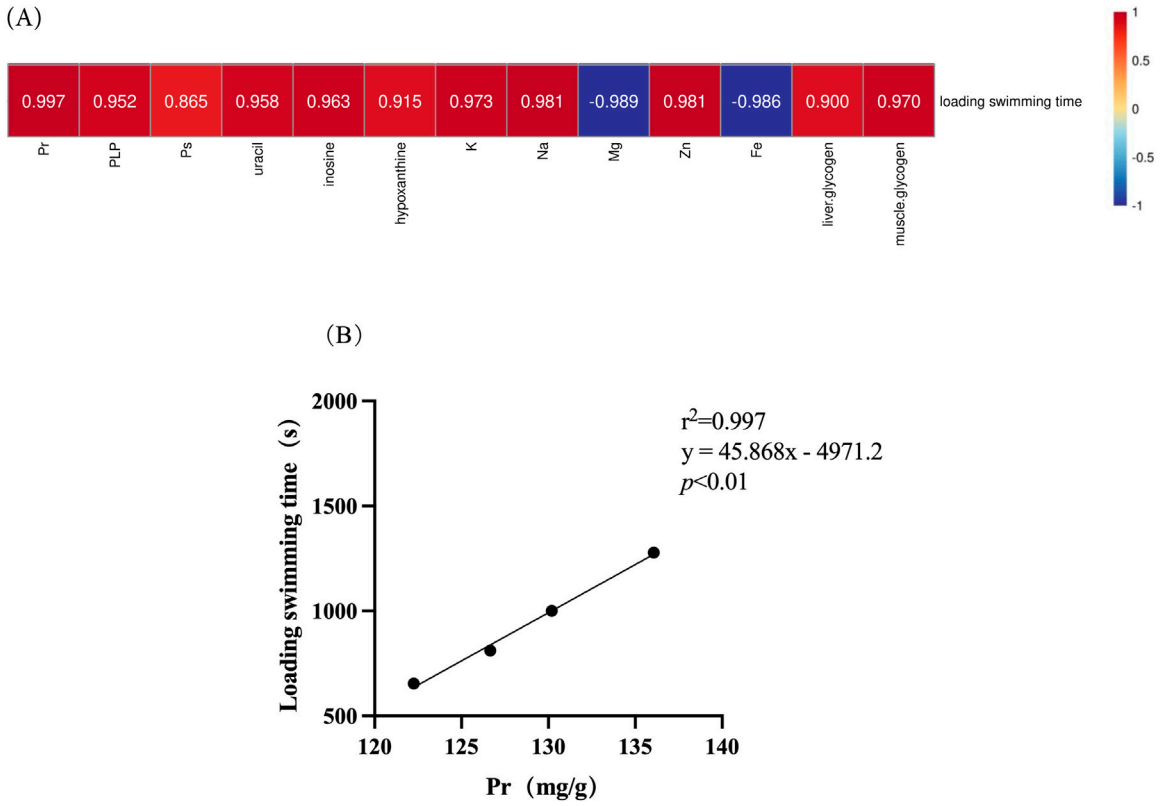

FIGURE 8
Correlation of chemical composition in deer antlers with endurance swimming duration. **(A)** Heatmap of the correlation between chemical compositions in deer antler and endurance swimming duration. **(B)** Simple linear regression analysis of protein levels versus endurance swimming duration. Note: Different upper case letters indicate highly significant differences ($p < 0.01$).

enhancement and anti-fatigue properties in mice were investigated. Finally, the composition and efficacy were examined through correlation analysis to provide a comprehensive evaluation in accordance with academic standards.

The assessment of visual qualities in deer antler slices typically relies on subjective evaluations based on sensory perception and experience, lacking quantitative criteria and being susceptible to individual biases. The inconsistent quality of deer antler slices in the market poses a challenge in distinguishing genuine products from counterfeit ones, highlighting the limitations associated with relying solely on subjective assessment. Therefore, this study conducted a comparative analysis of the morphological characteristics observed in different sections of deer antler slices, aiming to provide a more comprehensive and visually accessible approach for identifying specific parts of deer antlers. Consequently, this research facilitates the precise application and utilization of distinct components within deer antlers.

The utilization of deer antler as a raw material for the enzymatic hydrolysis-based production of deer antler polypeptide has been predominant in recent years. The deer antlers were partitioned into four segments, namely, wax slice, powder slice, gauze slice, and bone slice, and subsequently subjected to enzymatic hydrolysis to obtain the deer antler enzymatic hydrolysate. The potency of the pharmacological effects of deer antler is directly influenced by the concentration of marker substances it contains.

The pricing of various parts of deer antler in the market is, to a certain extent, determined by this factor. Therefore, it is imperative to ascertain the content of marker substances in each component of deer antler. The protein, phospholipid, and polysaccharide contents in the enzymatic hydrolysate of different deer antler parts were subsequently quantified. The results revealed a declining trend in the protein, phospholipid, and polysaccharide contents across the wax slice to the bone slice of deer antler enzymatic hydrolysate.

Deer antlers are abundant in proteins, amino acids, and polypeptides, which serve as essential biomarkers in the field of deer antler research (Jeon et al., 2008). The results of a comprehensive analysis revealed that proteins exhibited the strongest correlation with IgA levels and endurance swimming time, highlighting the pivotal role of proteins in mediating the diverse pharmacological effects of deer antler. Kim and colleagues (Kim et al., 2003) identified a total of 16 amino acids in deer antler through hydrolysis, with Asp, Glu, Pro, Gly, and Arg collectively accounting for approximately 32.5%–37.2% of the overall amino acid composition. In the present study, a total of 17 amino acids were identified, and there were no significant disparities observed in the overall amino acid composition among different parts of deer antlers. The predominant amino acids, namely, Aspartic acid (Asp), Glutamic acid (Glu), Leucine (Leu), Glycine (Gly), and Alanine (Ala), collectively accounted for approximately 50% of the total amino acid composition. Additionally, the relative

proportion of individual amino acids displayed a gradual decrease from the upper to basal sections, despite constituting a smaller fraction within deer antler. The evidence presented fully substantiates the superior nutritional value of wax slices.

The amino acids play a pivotal role as the fundamental building blocks of polypeptides. The amino acid content and peptide content in each part exhibit a consistent trend. Zha E and colleagues (Zha et al., 2013) reported the isolation of a 3.2 kDa polypeptide, nVAP32, from deer antler, which exhibited a dose-dependent modulation of immune activity in mice. Organisms are comprised of a diverse array of substances, with phospholipids emerging as a prominent class of lipid compounds characterized by the presence of phosphoric acid, playing a crucial role in the constitution of biological membranes. The results of this investigation revealed a declining trend in phospholipid levels across different sections of deer antler, from the wax slice to the bone slice. These findings suggest that the wax slice may possess superior wound-healing properties compared to the bone slice. The wax slice is situated atop the deer antler, which is recognized as the tissue exhibiting the highest growth rate and lowest cancer incidence (Li et al., 2023). This can be attributed to the continuous phosphorylation of stromal cells during the antler's growth process. Hence, the pivotal role of protein and phosphate in the pharmacological effects of deer antler cannot be overstated.

In recent years, the continuous advancement of research methodologies has propelled peptides and polysaccharides to the forefront of animal and plant medicine pharmacology investigations, garnering significant attention from both domestic and international scholars. Polysaccharides, as a class of biologically active macromolecules devoid of toxicity, have gained significant attention in recent years for their potential in the development of health products. Multiple studies have demonstrated the therapeutic potential of deer antler polysaccharides in augmenting human immune function (Li et al., 2002). Although the correlation results in this experiment indicate a modest association between polysaccharides and immune indicators, the observed trends in polysaccharide content and immune indicators across the four experimental sections consistently demonstrated a gradual decrease from the upper to basal regions. Therefore, it is widely acknowledged that polysaccharides can serve as suitable indicators for assessing the quality of various components of deer antler.

The minerals present in deer antler can be categorized into major elements and trace elements, both of which play crucial roles in facilitating the medicinal properties of deer antler. In this experiment, the concentrations of three inorganic substances, namely, potassium (K), sodium (Na), and magnesium (Mg), were analyzed across distinct sections of deer antlers. Potassium (K) and sodium (Na) play pivotal roles in maintaining the acid-base balance and osmotic pressure within the animal organism, being actively transported via the Na-K pump. The concentrations of these ions are higher both intracellularly and extracellularly, particularly in regions of active substance exchange, such as the rapidly growing tissues found at the apex of deer antlers with a wax slice. Consequently, the uppermost segment of deer antlers demonstrates the highest concentrations of Na and K, exhibiting a gradual decline in levels towards the basal section. Previous studies have demonstrated that sodium possesses the ability to modulate other subsets of T-lymphocytes associated with autoimmune diseases and allergies. CD8-positive T-lymphocytes play a pivotal role in the adaptive immune system, and it has been demonstrated that sodium ions augment the activity of the sodium-potassium pump in T-lymphocyte membranes, thereby bolstering the immune response of CD8 T-cells (Soll et al., 2024). Hence, the presence of Na and K exerts a direct influence on augmenting immune functionality. The populations of osteoblasts and osteoclasts gradually emerge in the central and basal regions of deer antler, with calcium (Ca), phosphorus (P), and magnesium (Mg) serving as the primary constituents of the bone slice (Zuo and Yu, 2013). The levels of these three elements will progressively increase during the process of ossification. Despite their minute presence within the body, trace elements play an indispensable role in the development of living organisms.

The pharmacological effects of deer antlers are diverse, with the enhancement of the body's immune activity being one of its primary impacts. The thymus and spleen function as crucial immune organs, with their organ indices serving as direct indicators of the body's level of immune functionality (Zhu et al., 2019). The impact of drugs on the spleen and thymus indices can serve as an initial indicator for investigating immunopharmacological mechanisms in animal models. A higher organ index substantiates a stronger immune response, and in conjunction with the findings of this study, it is evident that wax slices exhibit the most pronounced effect, followed by powdered slices, gauze slices, and bone slices in descending order. All these treatments significantly surpass the control group. The immunoglobulin is a type of immunoreactive substance predominantly found in serum. The immunoglobulin content level of the organism is positively associated with the efficacy of diverse biological functions, including antiviral and antibacterial activities within the animal body (Li, 2018).

In our investigation, we observed a significant increase in the levels of IgG and IgM in the wax slice group compared to all other experimental groups. Moreover, the concentration of IgA in both the wax slice and powder slice groups exhibited a significantly higher level compared to that observed in the gauze slice and bone slice groups. The results strongly support the superior efficacy of wax slice of deer antler in boosting the immune system.

Additionally, the continuous administration of enzymatically hydrolyzed deer antler extract to mice resulted in a significant augmentation in weight-bearing swimming duration, along with heightened levels of liver glycogen and muscle glycogen content within the murine hindlimb muscles. The research findings have indicated that deer antler peptides demonstrate anti-fatigue effects through the enhancement of skeletal muscle troponin-related mRNA expression, upregulation of muscle contraction-related genes to augment muscle strength, and improvement in various fatigue indicators such as blood glucose, blood urea, and lactic acid levels (Chen et al., 2014).

Nucleosides, although present in relatively low quantities, constitute a class of biomarkers in deer antler with multifaceted functions encompassing immunomodulation, anti-cancer properties and hepatoprotection. The biological functions of deer antler are intricately linked. Revised sentence: Consequently, the nucleoside content can serve as an indicator for assessing the quality of deer antler (Zhao et al., 2020). The levels of three nucleosides, namely, uracil, inosine, and hypoxanthine, were determined in this study. Remarkably, the concentrations obtained were consistent with those reported by Zhou and Li (2009). The correlation analysis revealed a robust association between uracil, inosine, and the *in vivo* levels of IgM

and IgG. This implies an inherent connection between the immunomodulatory pharmacological effects of deer antler and its nucleoside composition, suggesting a potential interdependence. Some studies have demonstrated that deer antler possesses the ability to inhibit triple-negative breast cancer through certain pathways in the immune system, indicating that specific marker substances within deer antler not only regulate immune function but also modulate cancer response via immunomodulation (Li et al., 2022). Additionally, Zhao et al. (2020) identified a total of eight nucleosides in deer antler and conducted a weight-bearing swimming experiment in mice to evaluate the anti-fatigue activity of different components of deer antler. Their findings revealed a gradual increase in the swimming duration of mice, highlighting the potential fatigue-reducing properties of deer antler.

In general, clinical trials have consistently demonstrated the profound impact of deer antler on augmenting immune response and mitigating fatigue, establishing it as a highly effective dietary supplement. The identification of the specific marker substances responsible for these effects necessitates further investigation. Furthermore, our study exclusively employed the enzymatic hydrolysate of deer antler for experimentation. Relevant future research endeavors may encompass the investigation of alternative formulations of deer antler to augment our comprehension of its pharmacological properties.

5 Conclusion

The results of this study indicate that the concentration of marker substances in wax slices of deer antler gradually decreases from the upper to the basal sections, with the highest concentration observed in the former. The protein exhibited the highest correlation coefficients with Ig A and anti-fatigue, uracil showed the strongest association with Ig M, and inosine demonstrated a significant correlation with Ig G. The data presented in this study provides evidence for the immunomodulatory and anti-fatigue properties of deer antler, supporting its potential as a valuable therapeutic agent.

Data availability statement

The original contributions presented in the study are included in the article/supplementary material, further inquiries can be directed to the corresponding author.

Ethics statement

The animal study was approved by the Experimental Animal Welfare and Ethics Committee of Jilin Agricultural University (permit number: 20240703001). The study was conducted in accordance with the local legislation and institutional requirements.

Author contributions

SC: Data curation, Formal Analysis, Investigation, Methodology, Writing–original draft. YL: Conceptualization, Investigation, Methodology, Writing–original draft. YY: Conceptualization, Data curation, Writing–original draft. SZ: Methodology, Visualization, Writing–original draft. HS: Investigation, Methodology, Writing–original draft. CY: Formal Analysis, Visualization, Writing–original draft. MW: Data curation, Supervision, Writing–review and editing. AZ: Conceptualization, Supervision, Writing–review and editing.

Funding

The author(s) declare that financial support was received for the research, authorship, and/or publication of this article. This work was financially supported by Science and Technology Development Plan Project of Jilin Province (No. 20200404012YY).

Conflict of interest

The authors declare that the research was conducted in the absence of any commercial or financial relationships that could be construed as a potential conflict of interest.

Publisher's note

All claims expressed in this article are solely those of the authors and do not necessarily represent those of their affiliated organizations, or those of the publisher, the editors and the reviewers. Any product that may be evaluated in this article, or claim that may be made by its manufacturer, is not guaranteed or endorsed by the publisher.

References

Chen, J. C., Hsiang, C. Y., Lin, Y. C., and Ho, T. Y. (2014). Deer antler extract improves fatigue effect through altering the expression of genes related to muscle strength in skeletal muscle of mice. *Evidence-Based Complementray Altern. Med.* 2014, 540580. doi:10.1155/2014/540580

Dong, W. C., Liu, C. H., Zhao, L. B., Zhao, W. G., Zhang, B. X., Zhang, X. L., et al. (2004). Determination and analysis of inorganic element content in different parts of horse antler and plum deer antler. *Special Wild Econ. Animal Plant Res.* (03), 32–36. doi:10.16720/j.cnki.tcyj.2004.03.010

Jeon, B., Kim, S., Lee, S., Park, P., Sung, S., Kim, J., et al. (2008). Effect of antler growth period on the chemical composition of velvet antler in sika deer (Cervus nippon). *Mamm. Biol.* 74 (5), 374–380. doi:10.1016/j.mambio.2008.07.005

Kawtikwar, P. S., Bhagwat, D. A., and Sakarkar, D. M. (2010). Deer antlers—traditional use and future perspectives. *Indian J. Tradit. Knowl.* 9, 245–251. doi:10.1007/s11627-010-9286-7

Kim, M. H., Moon, S. H., Lee, C. H., and Jeon, B. T. (2003). A study on the change of blood constituents during growth period of velvet antler in Korean spotted deer. *Korean J. Pharmacogn.* 34 (3), 263–268. doi:10.5187/jast.2003.45.6.1031

Li, C., Clark, D. E., Lord, E. A., Stanton, J. A., and Suttie, J. M. (2002). Sampling technique to discriminate the different tissue layers of growing antler tips for gene discovery. *Anat. Rec.* 268 (2), 125–130. doi:10.1002/ar.10120

Li, C., Li, Y., Wang, W., Scimeca, M., Melino, G., Du, R., et al. (2023). Deer antlers: the fastest growing tissue with least cancer occurrence. *Cell Death Differ.* 30 (12), 2452–2461. doi:10.1038/s41418-023-01231-z

Li, J. J. (2018). A brief discussion on the role of immunoglobulins in immunization. *Chin. Livest. Poult. Breed.* 14 (2), 85.

Li, M., Li, Q., Dong, H., Zhao, S., Ning, J., Bai, X., et al. (2022). Pilose antler polypeptides enhance chemotherapy effects in triple-negative breast cancer by

activating the adaptive immune system. *Int. J. Biol. Macromol.* 222 (Pt B), 2628–2638. doi:10.1016/j.ijbiomac.2022.10.045

Liu, C. X., Xu, L. W., and Li, G. Y. (2020). Research progress on extraction technology and pharmacological effects of antler ActiveIngredients. *Special Wild Econ. Animal Plant Res.* 42 (03), 86–89. doi:10.16720/j.cnki.tcyj.2020.03.018

Liu, L., Jiao, Y., Yang, M., Wu, L., Long, G., and Hu, W. (2023). Network pharmacology, molecular docking and molecular dynamics to explore the potential immunomodulatory mechanisms of deer antler. *Int. J. Mol. Sci.* 24 (12), 10370. doi:10.3390/ijms241210370

Lu, Y., Xiong, Y., Zhang, S., Wang, B., Feng, Y., Pu, Z., et al. (2024). D-mannose reduces oxidative stress, inhibits inflammation, and increases treg cell proportions in mice with ulcerative colitis. *Front. Pharmacol.* 15, 1454713. doi:10.3389/fphar.2024.1454713

Shi, H., Zhao, T., Li, Y., Xiao, X., Wu, J., Zhang, H., et al. (2021). Velvet antler ameliorates cardiac function by restoring sarcoplasmic reticulum Ca2+-ATPase activity in rats with heart failure after myocardial infarction. *Front. Pharmacol.* 12, 621194. doi:10.3389/fphar.2021.621194

Soll, D., Chu, C. F., Sun, S., Lutz, V., Arunkumar, M., Gachechiladze, M., et al. (2024). Sodium chloride in the tumor microenvironment enhances T cell metabolic fitness and cytotoxicity. *Nat. Immunol.* 25 (10), 1830–1844. doi:10.1038/s41590-024-01918-6

Sun, Y. S., Wang, Y. H., Wang, Y. F., Chen, B., Chen, L. X., et al. (2018). Simultaneous determination of nucleosides and nucleobases in Cervi Cornu Pantotrichum ofsika deer (Cervus nippon) with different processing methods by UPLC. *Chin. Traditional Herb. Drugs* 49 (04), 840–846. doi:10.7501/j.issn.0253-2670.2018.04.014

Wang, J., Wei, Y., Zhou, Z., Yang, J., Jia, Y., Wu, H., et al. (2022). Deer antler extract promotes tibia fracture healing in mice by activating BMP-2/SMAD4 signaling pathway. *J. Orthop. Surg. Res.* 17 (1), 468. doi:10.1186/s13018-022-03364-2

Wang, Y. H., Jiang, Y., Sun, Y. S., Shang, Y. S., Li, Y., Chen, B., et al. (2018). Comparative analysis of inorganic elements in antlers with different processing methods. *Chin. J. Pharm. Analysis* 38 (01), 104–111.

Widyowati, R., Suciati, S., Hariyadi, D. M., Chang, H. I., Ipg Suryawan, N., Tarigan, N., et al. (2023). The pro-inflammatory cytokine IL-Iβ alteration by deer (*Rusa unicolor*) antler extract on osteoarthritis rat model. *Saudi Pharm. J.* 31 (6), 1109–1114. doi:10.1016/j.jsps.2023.03.022

Zha, E., Li, X., Li, D., Guo, X., Gao, S., and Yue, X. (2013). Immunomodulatory effects of a 3.2 kDa polypeptide from velvet antler of Cervus nippon Temminck. *Int. Immunopharmacol.* 16 (2), 210–213. doi:10.1016/j.intimp.2013.02.027

Zhang, P., Guo, Z. H., Ma, L., Wang, G., and Zhao, Y. (2020). Investigation of anti-fatigue effect and simultaneous determination of eight nucleosides in different parts of velvet antler in red deer and sika deer. *Chem. Biodivers.* 17, e1900512. doi:10.1002/cbdv.201900512

Zhao, Y., Zhang, P., Guo, Z., and Wang, G. (2020). Investigation of anti-fatigue effect and simultaneous determination of eight nucleosides in different parts of velvet antler in red deer and sika deer. *Chem. and Biodivers.* 17 (2), e1900512. doi:10.1002/cbdv.201900512

Zheng, K., Fan, Y., Ji, R., and Ma, S. (2017). Distinctive effects of pilose antler on mouse peripheral blood immune cell populations. *Food Agric. Immunol.* 28 (6), 1181–1195. doi:10.1080/09540105.2017.1332011

Zhou, R., and Li, S. (2009). Supercritical carbon dioxide and co-solvent extractions of estradiol and progesterone from antler velvet. *J. Food Compos. and Analysis* 22 (1), 72–78. doi:10.1016/j.jfca.2008.07.008

Zhu, G., Jiang, Y., Yao, Y., Wu, N., Luo, J., Hu, M., et al. (2019). Ovotransferrin ameliorates the dysbiosis of immunomodulatory function and intestinal microbiota induced by cyclophosphamide. *Food Funct.* 10 (2), 1109–1122. doi:10.1039/c8fo02312c

Zuo, Q., and Yu, X. K. (2013). Effect of swimming on bone mineral density and the levels of six bone elements in mice. *Chin. J. Osteoporos.* 19 (07), 670–674.

Frontiers in Pharmacology

Explores the interactions between chemicals and living beings

The most cited journal in its field, which advances access to pharmacological discoveries to prevent and treat human disease.

Discover the latest Research Topics

See more →

Frontiers

Avenue du Tribunal-Fédéral 34
1005 Lausanne, Switzerland
frontiersin.org

Contact us

+41 (0)21 510 17 00
frontiersin.org/about/contact